The Atomisation of Detergent Slurries

by

Colin Anthony Sudlow

Doctor of Philosophy

Department of Chemical Engineering
The University of Aston in Birmingham

November 1991

The Atomisation of Detergent Slurries

Colin Anthony Sudlow **PhD** **November 1991**

Summary

A study was made to determine the conditions under which the optimum droplet size distribution (ie, narrowest size range with a minimum of fines and over-sized agglomerates), is generated in sprays from centrifugal pressure nozzles. A range of non-Newtonian detergent slurries were tested but the results are of wider application and parallel work was undertaken with water, ionic solutions and chalk slurries. Six centrifugal pressure nozzles were used and the drop-size distributions correlated as a function of fluid properties, pressure, flowrate, feed temperature, and nozzle characteristics.

Measurements were made using a Malvern Particle Size Analyser slung across a specially-designed transparent tower section of approximately 1.2 m diameter in order to reduce obscuration caused by the spray and improve existing droplet sizing techniques. The results obtained were based upon the Rosin-Rammler distribution model and the Size Analyser provided a direct print-out of size distribution and the parameters characterising it. A Spraying Systems nozzle, AAÁSSTC8-8, produced the optimum spray distribution with the detergent slurry at a temperature of 60°C whilst operating at 1200 psi. With other fluids the Delevan 2.2SJ nozzle produced the optimum spray distribution operating at 1200 psi but with the Spraying Systems nozzles there was no clear-cut optimum set of conditions, ie the nozzle and pressure varied depending upon the fluid being sprayed.

The mechanisms of liquid sheet break-up and droplet dispersion were investigated in specially-constructed, scaled-up, transparent nozzles. A mathematical model of centrifugal pressure nozzle atomisation was developed based upon fundamental operating parameters rather than resorting to empirical correlations. This enabled theoretical predictions to be made over a wide range of operating conditions and nozzle types. The model predictions for volumetric flowrate, liquid sheet length and air core diameter showed good agreement with the experimentally determined results. However, the model predicted smaller droplet sizes than were produced experimentally due to inaccuracies identified in the initial assumptions.

Key words: Spray Drying, Atomisation, Droplet Size-Distribution, Detergent.

To my family, for their continual encouragement,

support and inspiration.

Acknowledgements

The Author would like to express his gratitude to the following people:

Dr C.J. Mumford for his valued guidance throughout the course of this research programme.

Dr E.L. Smith for his guidance during the development of the mathematical model.

Mr I. Murkett, Mr W. Curtis, Mr P. Green and Mr M. Santoro for their assistance during the construction and commissioning of the experimental apparatus.

Dr S. Sharma for his assistance in the compilation of the background literature for Chapter 2.

Mr A. Crowcombe for his valued expertise in photography.

Mr G. Guest and Lodge-Cottrell for their useful advice in the design of the experimental apparatus.

Colgate-Palmolive for their financial support of the research programme.

The rediscovery of a fact in the library is often a more difficult and uncertain process than the first discovery in a laboratory.

Lord Rayleigh - 1884

Contents

List of Figures

List of Figures (continued)

List of Figures (continued)

List of Tables

List of Plates

Introduction

Atomisation is used in many areas of chemical engineering in processes which are dependent upon, or controlled by, the surface area of exposed liquid. Thus spray drying, combustion of liquid fuels, humidification, dehumidification, water cooling and gas absorption are all operations in which the flow of heat or mass transfer is increased by the break-up of the liquid into a spray or mist. However the fundamental physics involved in atomisation, particularly when viscous liquids are concerned, are not well-defined. Hence the droplet size range likely to be produced in a given situation is difficult to predict from first principles.

Spray drying is a form of 'convection' drying, ie where all the heat transfer is from a hot gas to the material being dried. The majority of this transfer is by forced convection, although, in applications with high gas temperatures, radiation also plays some part. It involves a sequence of operations which can be investigated independently within the confines of the laboratory, but which mutually interact to such a degree that it is difficult to isolate them for design purposes. The feed is first dispersed by some form of atomisation device; the spray is then mixed with a heated gas and dried by a process of simultaneous heat and mass transfer. Finally the dry product is removed from the dryer. The distribution of droplet sizes is crucially important since it determines the residence time in the dryer and, since it is area dependent, the drying rate.

A wide variety of materials have been successfully spray dried including: milk, coffee, detergents, plasma, drug products, industrial dyes, starch mixtures, and inorganic salts [1]. These examples serve to illustrate how widely the physical properties of feed may vary. In combustion, the range of variance of the physical properties of the spray is not as great as that encountered in spray drying and in most other processes the physical properties of the liquid do not differ greatly from those of water.

A review of the most common types of commercially available atomisation devices is given in Chapter 1. Although, a considerable amount of experimental data has been presented in the literature on the characteristics of sprays as a function of the operating conditions and atomiser dimensions, the majority of the work is restricted to water as the spraying medium or, in the case of centrifugal pressure nozzles, liquid fuels such as kerosene. However, with the notable exception of McIrvine [2], little work has been done on the effect of liquid properties using non-Newtonian fluids.

A variety of techniques have been presented in the literature for the measurement of droplet sizes in atomisation work. Many methods have been developed for work with liquid jets (for example, coated glass slides), consequently they are often rendered virtually useless in the measurement of sprays. Other methods are limited to particular fluids being studied (for example, molten wax). This study made use of a Particle Size Analyser based upon the theory of light diffraction and the theory behind its operation, along with a review of the droplet sizing techniques used in previous work, is presented in Chapter 3.

The mechanisms of atomisation are complex and several different theories have been presented in the literature to describe the phenomena of droplet dispersion, as reviewed in Chapter 4. Much of the previous work has been in the form of empirical correlations which generally limit the theory to specific nozzles and/or feed conditions. This work comprised an investigation into the atomisation of detergent slurries and other Newtonian and non-Newtonian fluids using both experimental and numerical methods. Additionally it included a study of the mechanisms and droplet size distributions relevant to the atomisation of viscous and non-viscous fluids by centrifugal pressure nozzles.

Chapter 1: Spray Drying Fundamentals

Introduction

Spray drying is the transformation of a slurry, solution, or paste into a dried particulate product by spraying the feed into a hot drying medium, usually air. It is a one-step continuous process where the combination of high heat and mass transfer coefficients with large surface areas, results in short drying times which are often in the order of a few seconds. Consequently the process has significant advantages over other drying methods.

Spray drying is used extensively in many industries. The most familiar uses are in the food industry for heat sensitive materials such as milk and coffee, and in the domestic chemical industry for washing powders; less common uses within the chemical industry include pharmaceuticals and high-tonnage throughputs in the fields of mineral ores and clays. Generally it is the requirement to obtain a particulate product close to specification which favours the selection of spray drying over other processes that are also capable of taking a liquid feed, for example drum drying.

Although spray dryers take many forms, dictated by the nature of the feed, the basic stages involved in the drying process are similar, as illustrated in Figure 1.1. The material to be dried is converted into a fine particulate spray by an atomisation device before being introduced into the drying tower. The hot drying medium is fed into the top of the tower and passes co-currently with the droplets through the tower. Alternatively the drying air can be introduced at the bottom of the tower to pass counter-currently to the droplets (Variations in the different types of spray-air contact are discussed in Section 1.2). The droplets are dried during their residence in the tower and the dried particulate product is separated from the air-stream using a standard particulate recovery method, for example a cyclone. Fines are recovered in a separate stage, often using a hydro-cyclone, and may be recycled or processed separately.

Figure 1.1: *Process Stages in Spray Drying*

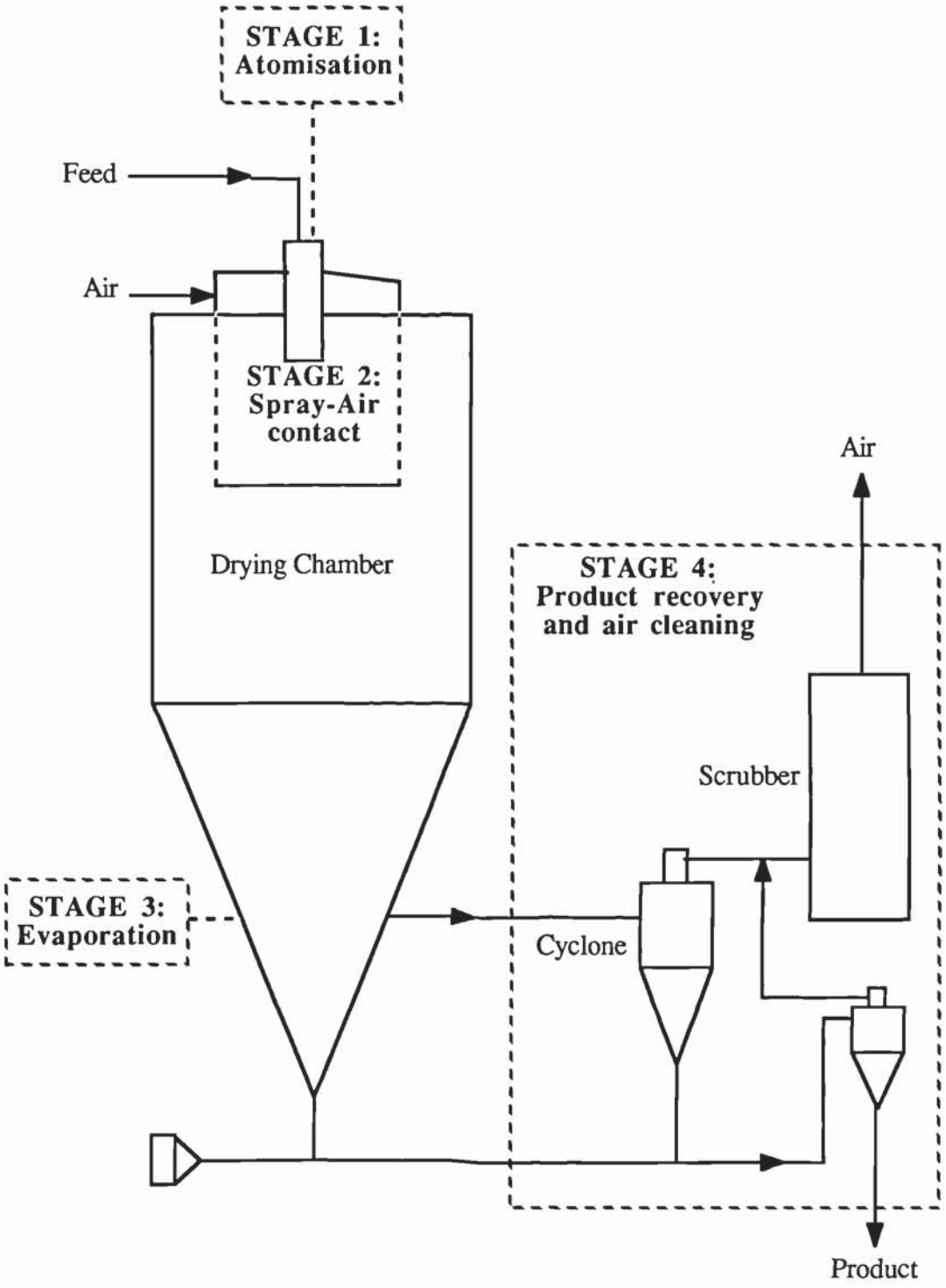

1.1 Methods of Atomisation

Atomisation is the first important stage of the spray drying process. The aim of atomisation is to break a continuous liquid jet into a multitude of droplets in order to increase the total surface area of the liquid to aid subsequent evaporation and to result in a particulate product. The initial size of a droplet does not necessarily represent the size of resultant dried particle at the end of the drying process since particles may shrink, swell or fragment. However, the droplet residence time, drying mechanism (after the 'constant rate' period) and drop trajectory are all size dependent. The latter is important in the design of the drying tower if wall impingement is to be avoided, or if inter-spray contact, which may cause agglomeration, is undesirable.

Table 1.1: *Methods of Atomisation*

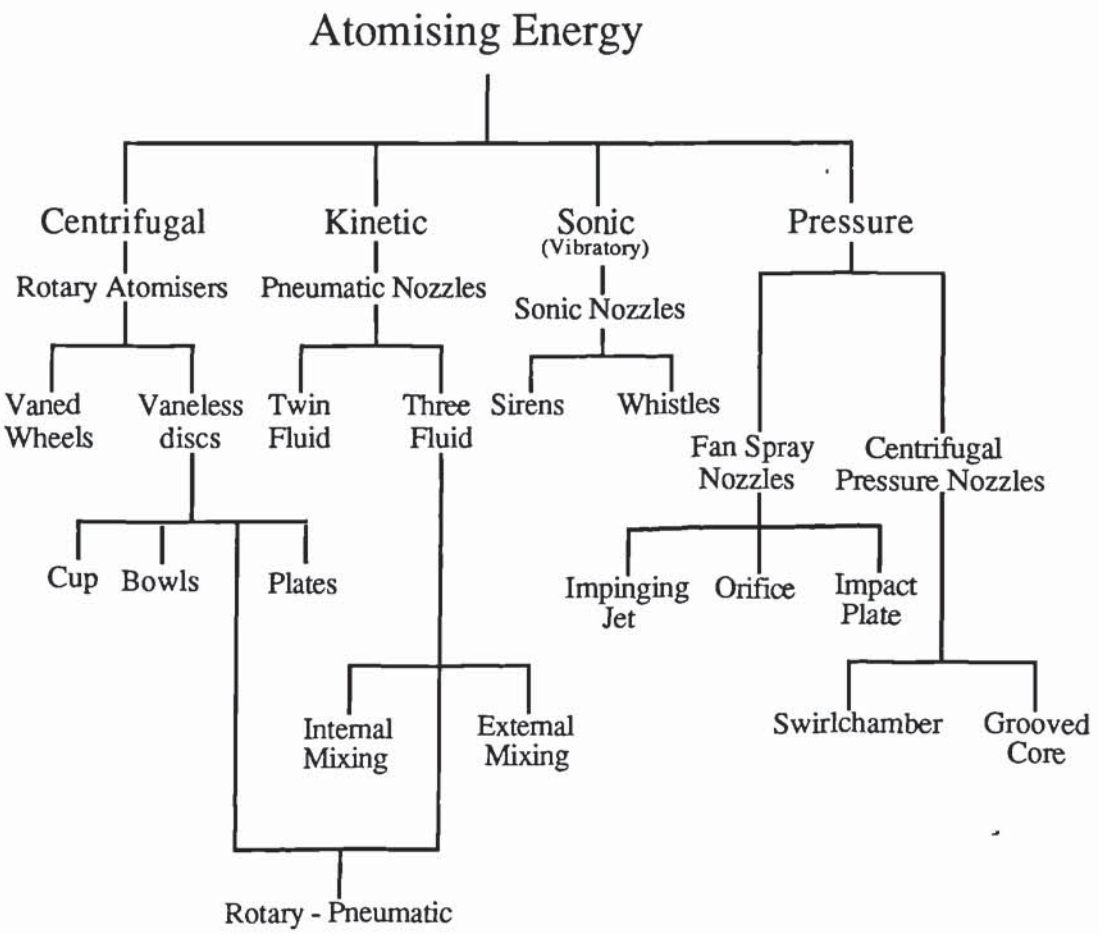

There are a multitude of atomisation devices available which all fall into one of four main categories, as illustrated by Table 1.1. Each category is based upon the type of energy used to promote the disintegration of the bulk liquid. The common forms of classification for atomisation devices are centrifugal, pressure and kinetic energy. Sonic and vibratory atomisers are less common and their applications are still in an early stage of development [1].

The majority of the atomisers employed in the chemical and process industries were designed for low viscosity Newtonian liquids. Consequently when they are employed for slurries, pastes or liquids with Non-Newtonian properties there is often a significant deterioration in performance. This is due to the change in atomisation mechanisms with increasing viscosity; erosion and damage may also occur to the highly machined surfaces of the atomiser, such as the outlet orifice of a nozzle, subsequently leading to a loss in product quality. It is therefore important to select the most suitable atomiser for the duty to be performed.

1.1.1 Rotary Atomisation

In rotary atomisation, the feed liquid is fed onto a rotating surface and centrifugally accelerated to high velocity before being discharged. Under normal operating conditions the liquid extends from the periphery of the surface in the form of a thin sheet which subsequently breaks up at some distance away, either freely by aerodynamic effects or by disturbance caused by air movement close to the atomiser.

A rotary atomiser is extremely versatile since the accelerating (or atomisation) force can be controlled independently from the liquid feed by variation of the rotation speed and it can successfully handle a wide range of feed rates with liquids having a wide range of properties. The rotating surface within the atomiser may be a simple flat disc, a bowl (or cup), a vaned disc or a type of slotted wheel. A full review of the effect of liquid feed rates, the speed of rotation of the disc and other variables on the

mechanism of liquid disintegration caused by rotary atomisers is given by Masters [1]; a brief description of the main types of rotary atomiser is given below.

Flat Smooth (or Vaneless) Disc Atomiser

The degree of disintegration obtainable from this type of atomiser depends upon the magnitude of the feed acceleration over the surface of the disc. The velocity of the liquid leaving the disc is governed by the degree of slippage between the liquid and the rotating surface. The extent of slippage depends upon the feed rate and the physical properties of the liquid, ie the viscous drag and the surface wetting property of the liquid.

The mechanism of disintegration depends upon the physical properties of the liquid (ie viscosity and surface tension) and the speed of rotation of the disc [3]. At low disc peripheral speeds, ie below 500 rpm, when liquid viscosity and surface tension dominate the atomisation process, the spray is formed by individual formation and release of droplets from the edge of the disc. This is illustrated in Figure 1.2a. An increase in the disc speed, ie greater than 700 rpm, and an increase in the feed rate causes the mechanism to change to one of ligament break-up. These ligaments begin to extend out from the edge of the disc before disintegrating into sprays of parent and satellite droplets as shown in Figure 1.2b. Increases in the viscosity of the feed will increase the proportion of satellite droplets and produce larger parent droplets in the spray. The transition between the predominance of the physical properties of the liquid and inertial forces occurs at disc speeds in excess of 3,000 rpm, when the ligaments join to form a sheet extending from the edge of the disc (See Figure 1.2c). Smooth vaneless discs have no industrial applications in the field of spray drying. Interest in the flow and droplet formation lies in relationships between droplet size and operating conditions which also hold for industrial rotary atomisers.

Figure 1.2: *Mechanisms of Rotary Atomisation*

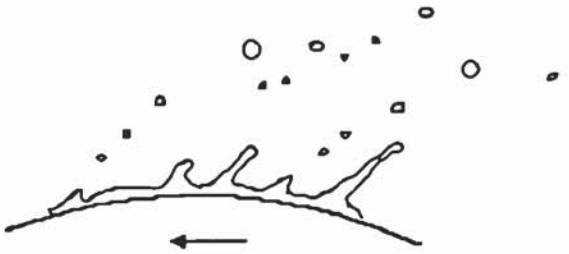

a) Direct Droplet Formation (Low disc speeds)

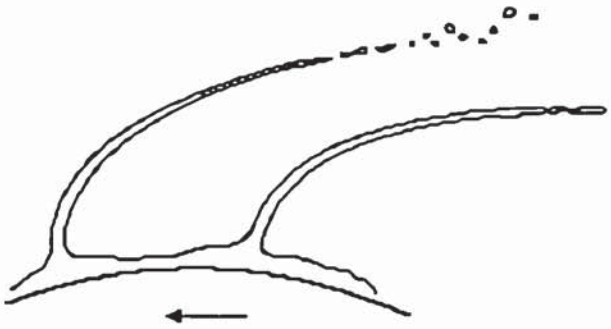

b) Ligament Formation (Above 700 rpm)

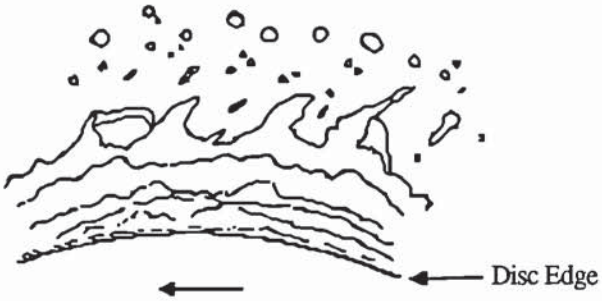

c) Sheet Formation (Above 3,000 rpm)

Wheel or Vaned Disc Atomisers

The mechanism of atomisation applicable to the wheel or vaned atomiser is similar to that of a smooth vaneless disc. However, unlike the vaneless disc there is no liquid slippage on the wheel once the liquid has contacted the vanes. The vanes, which may be either straight, radial or curved, serve to prevent the transverse flow of liquid across the surface. The atomisation mechanism does not allow for the formation of a homogeneous spray, although sprays of small mean droplet sizes, for example 20 to

30 μm, can be produced. An increase in liquid viscosity or surface tension of the feed liquid has the effect of producing a more uniform spray, with a lowering of the mean droplet size. However, for general operating conditions it is not possible or desirable to adjust the physical properties of the feed liquid.

A photograph of a turbine driven, vaned wheel atomiser that has been used for work within the Department is shown in Plate 1. Alternative forms of drive for these atomisers include belt or direct drive from an electric motor with fixed or variable speed control.

Commercial use of this type of atomiser tends to favour high liquid feed rates at high wheel peripheral speeds, ie above 30,000 rpm; under these conditions the liquid disintegration occurs at the edge of the wheel due to frictional effects between air and the liquid film surface as it emerges from the vane.

Atomisation by Vaneless Bowls, Cups and Plates

Inverted bowls, cups and plates are effectively classified as vaneless disc atomisers. However, unlike wheel atomisers, friction between the liquid and the surface of the disc is increased to prevent slippage of the liquid. The liquid is fed onto the underside of the plate or the internal surface of the cup or bowl and is forced against the surface by centrifugal action.

The mechanism of atomisation is similar to that of the vaneless disc atomiser. The final disintegration of the liquid is governed by disc design, speed of rotation, feed rate and liquid physical properties.

1.1.2 Nozzle Atomisation

The purpose of the nozzle atomiser is to provide acceleration and disintegration of the bulk liquid flow leading to dispersion of the resulting droplets to form a spray. A single orifice or ejector cannot be considered as an atomiser, although the liquid is disintegrated if the jet is turbulent enough, since the droplets are not dispersed by the

Plate 1 : *Turbine-Driven, Vaned Rotary Atomiser (Niro Atomisers Ltd.)*

The atomiser consists of a 66 mm diameter vaned wheel, fitted with 8 mm slots, which is driven by compressed air (supplied in the pressure range of 70 to 90 psig) to produce wheel speeds between 25,000 to 35,000 rpm.

action of the nozzle.

The energy transfer occurring during nozzle atomisation is extremely inefficient [4]. Attempts to improve the degree of atomisation, nozzle flexibility and spray trajectory have resulted in the development of several types of nozzle.

Pneumatic Nozzle Atomisation

Pneumatic, twin-fluid or blast atomisation involves the impaction of the bulk liquid with a high velocity gas stream, usually air or steam. Atomisation occurs due to the relatively high velocity gas stream creating high frictional forces upon the liquid surface which leads to disintegration of the liquid into droplets. These conditions are generated by either accelerating the gas to sonic or supersonic velocities prior to liquid contact, or directing the gas stream onto unstable thin sheets of liquid which are formed by rotating the liquid within the nozzle. The break-up of the liquid is so rapid and effective that sprays of low mean droplet size are formed.

Various nozzle designs are suitable for this type of atomisation but they generally fall into one of four categories:

1) Internal Mixing - The gas to liquid contact occurs within the nozzle.
2) External Mixing - The gas to liquid contact occurs just outside the nozzle.
3) Three-Fluid Atomisation - This involves a combination of internal and external mixing by using two separate gas streams.
4) Pneumatic Cup Atomisation - This is not a type of nozzle atomisation but involves the combination of a rotating cup atomiser and an external high velocity gas stream. This type of atomiser has been developed to produce a very fine spray from a low viscosity feed or a spray of coarse mean droplet size from high viscosity liquids

The advantage of the pneumatic atomiser lies in its ability to produce a spray of high homogeneity and small mean droplet size, ie in the range of 10 to 30μm, over a wide range of operating conditions, whilst handling low or high viscosity feeds. With more viscous feeds homogeneity is not as good and the mean droplet size tends to increase

[5]. Pneumatic nozzles do not require high pressure pumping equipment, a notable advantage over other types of pressure nozzle with which high pressure working can lead to operational or maintenance problems. However, filtration of the gas stream is essential and foreign matter must be prevented from reaching the nozzle head to avoid blockage of the gas flow orifice, although the presence of a liquid orifice larger than those in centrifugal pressure nozzles reduces the possibility of clogging.

Pneumatic atomisers are used mainly to form very fine sprays of low viscosity Newtonian liquids. The nozzles can also be used in the atomisation of highly viscous Newtonian or non-Newtonian liquids. Such feeds include slurries or pastes, gelatine, plastics, glues and pre-gelatinised corn starches. Pneumatic nozzles are suitable for products where flow properties cause a sharp increase in viscosity with shear. Such products cannot be atomised in pressure nozzles due to the occurrence of high shear rates within the nozzle but can be handled successfully by pneumatic nozzles due to the application of very low shear stresses.

Pressure Atomisation

The principle of a pressure nozzle is the conversion of pressure energy within the bulk liquid into kinetic energy of a thin moving sheet. The sheet breaks up under the influence of the physical liquid properties and by frictional effects with the medium (usually air) into which the liquid sheet is discharged. The sheet rapidly becomes unstable due to disturbances on the sheet surface promoting disintegration into ligaments and droplets [6].

The size and shape of the liquid sheet can be controlled by varying the direction of flow and the velocity of the fluid entering the nozzle. Conical or flat liquid sheets can be produced by this method.

Fan Spray Nozzles

The impingement of two streams of liquid behind a single-hole orifice produces a sheet of liquid in a plane perpendicular to that of the streams. The principle is illustrated in

Figure 1.3, which shows liquid flowing through a rectangular orifice at the end of a rectangular tube. These conditions constrict the flow through the orifice to only one plane and the streamlines converge to form a region of pressure behind the orifice. The flat sheet that is produced as the liquid freely spreads out is dependent only upon the orifice configuration [4]. Hence the spray angle can vary from a straight stream to over one hundred degrees.

Figure 1.3: *The Principle of the Fan Spray Nozzle*

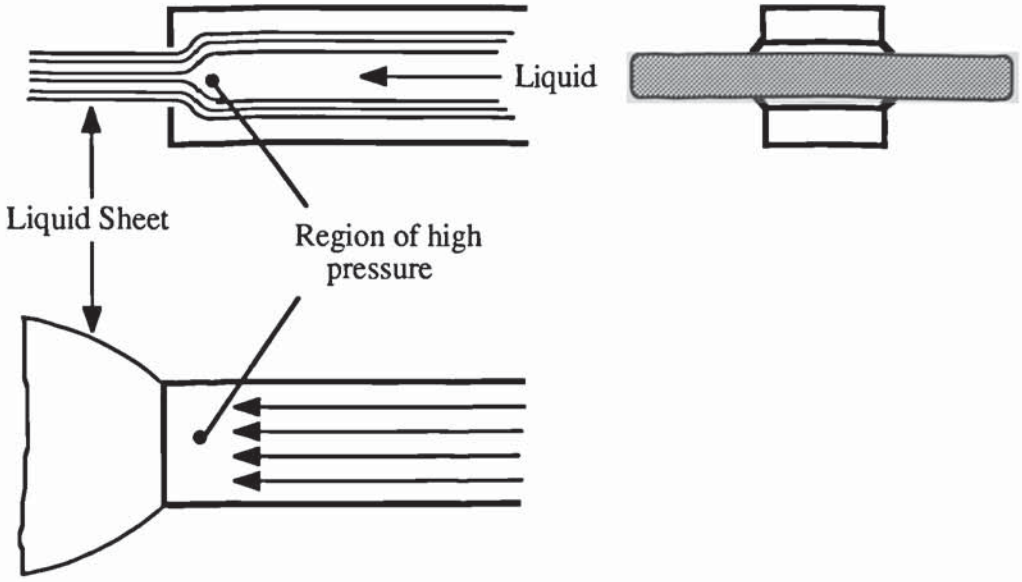

Under ambient conditions the mechanism of disintegration is promoted by the formation of waves on the surface of the liquid sheet which increase until the sheet becomes unstable [7]. In this region of instability the sheet breaks up into ligaments which, in turn, rapidly form parent and satellite droplets. Thorough experimental and theoretical investigations of this type of atomisation have been conducted by Dombrowski and numerous co-workers [7-10].

The directional and controllable nature of the resultant liquid spray renders the fan spray nozzle extremely popular for coating work and use in paint spraying.

Figure 1.4 : *Droplet Population Profiles in Solid and Hollow Cone Sprays*

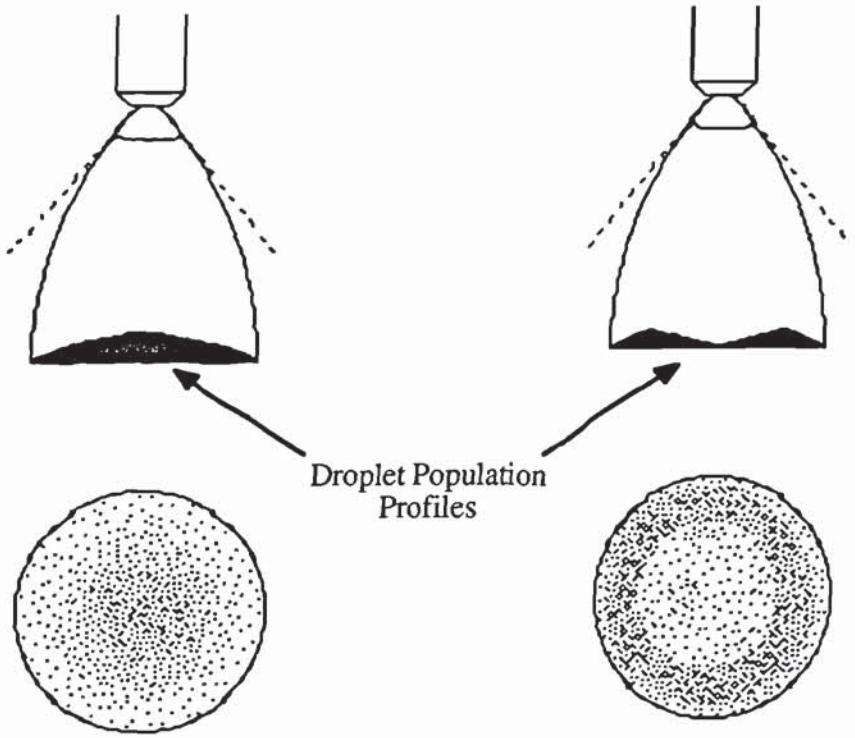

a) Solid Cone Spray

b) Hollow Cone Spray

Centrifugal Pressure Nozzles

When a liquid flows through a narrow divergent annular orifice a conical sheet of liquid is produced in which the liquid is flowing in radial lines. This type of nozzle may be used to produce either hollow or solid cone sprays. In a solid cone spray, illustrated in Figure 1.4a, the entire volume of the spray cone is filled with droplets with the highest concentration in the centre. However, in the hollow cone, illustrated in Figure 1.4b, the highest concentration of droplets exists around the periphery of the cone. The absence of droplets in the centre is due to the formation of an air core caused by liquid rotation within the nozzle. For equal feed rates and feed pressures, the droplet size is more homogeneous in the hollow cone than the solid cone. This accounts for the popularity of the hollow cone nozzle or swirl nozzle in spray drying and similar operations where homogeneity of the liquid spray is critical to the production of a reasonably homogeneous product.

The mechanism of flow through a swirlchamber atomiser producing a hollow cone spray, and its effect upon the atomisation of liquids, are discussed in detail in Chapter 4.

1.1.3 Sonic or Vibratory atomisation

Interest in sonic atomisation for possible use in spray drying has increased in recent years. This has arisen due to the requirement for an atomisation technique to deal with numerous liquids that cannot be successfully atomised by conventional nozzles and rotary atomisers. These liquids include products that are non-Newtonian, highly viscous liquids with long-chain molecular structures which form only filaments (not individual droplets) from rotary atomisers, and liquids that require excessive pressures for effective atomisation in pressure nozzles.

Attention was first drawn to the use of sonic energy as the likely atomisation mechanism suggested the formation of uniformly sized droplets. To date sonic nozzle development has not reached the stage at which such nozzles are a real alternative to more conventional methods of atomisation already in use. However, the advantages of sonic nozzles operating at low pressures and having wide liquid channels suggests that they may be suitable for abrasive and corrosive materials. Development work has centred around four main types of device: the Hartman monowhistle nozzle [11], stem jet nozzle [12], vortex whistle nozzle [13], and the mechanical vibratory nozzle. It has been reported [1] that small-sized spray dryers have been fitted with multi-whistle liquid atomisers and ultrasonic sources placed in the dryer walls in the region of the drying zone which produced a marked improvement in dryer capacity. However, the low volumetric throughput of these types of nozzle severely limits there commercial applications.

1.1.4 Electrostatic Atomisation

Electrostatic atomisation is essentially the enhancement of the electrostatic field that is produced when a liquid disintegrates into a spray. It can be achieved by the

application of a charge to a standard type of atomisation device (for example, rotary atomisers and pneumatic nozzles), which creates a unipolar electrostatic field substantially greater than that occurring solely by liquid disintegration. In these cases of atomisation the liquid disintegration is dominated by the mechanical forces within the 'hybrid' nozzle, with the field charge dependent upon the applied electrostatic charge. There are also nozzle arrangements in which liquid disintegration into a highly-charged spray is caused solely by the application of an electrostatic charge. In this type of atomisation the drop size distribution and field charge are determined by the initial size of the applied electrostatic charge.

This type of atomisation is used extensively in the spraying of paints and pesticides, which require the droplets to be deposited upon target areas at specified application rates. Although useful in situations where over-spray of the target area is both undesirable and uneconomical, it has little potential at present in the field of spray drying due to the requirement of complex and costly electrical insulation equipment in order to avoid build-up of charged particles on the drying tower walls. A review of the principles involved and of the progress in this field is given by Bailey [14].

1.2 Spray-Air Contact

The prediction and control of air and spray movement within the spray dryer is an important requirement for dryer design and performance. The manner in which the liquid spray contacts the drying air determines the optimum residence time of the droplets, the extent of wall deposition and often has an effect upon the evaporation mechanisms of the spray droplets. Thus the properties of the final dried particle are heavily influenced by the spray-air contact within the dryer.

1.2.1 Types of Drying Chamber

Spray-air contact within the spray dryer is classified according to the drying chamber layout, ie as a co-current, counter-current or mixed flow dryer. However, such designation of co-current, counter-current or mixed flow to the spray-air contact does not actually represent the true conditions within the drying chamber. For example, in the case of a co-current dryer with a rotary atomiser the spray is initially contacted by the air entering obliquely, and there are regions within the dryer where localised eddies cause the spray-air contact to be practically counter-current [1].

Co-current Drying Chambers

The air dispenser and the atomiser are located together at either the top, base or end of the drying chamber. The two dryers illustrated in Figure 1.5a are the most common. In this type of dryer the wettest droplets are in contact with the hottest air which has the advantage of not over-heating the partially dried product. This arrangement is therefore favoured with thermally sensitive materials, for example coffee.

Counter-current Drying Chambers

In counter-current flow dryers, illustrated in Figure 1.5b, the atomiser and air dispenser are generally located at opposite ends of the drying chamber, although one major detergent manufacturer employs three atomiser ring mains spaced along the chamber. Counter-current flow is mainly restricted to nozzle atomisation in tall, narrow diameter towers. This enables coarser sprays to be dried due to greater mixing of the spray and air within the chamber and wall impingement is often reduced due to a decrease in the radial trajectory of the spray. This fractionally increases the residence time of the droplets but this advantage is often offset by a tendency for more deposition of solid upon the atomiser.

Swirling flow is induced in some detergent drying towers by arranging for tangential entry of the air via a series of angled nozzles [15].

Figure 1.5: *Product-Air Flow in Spray Dryers*

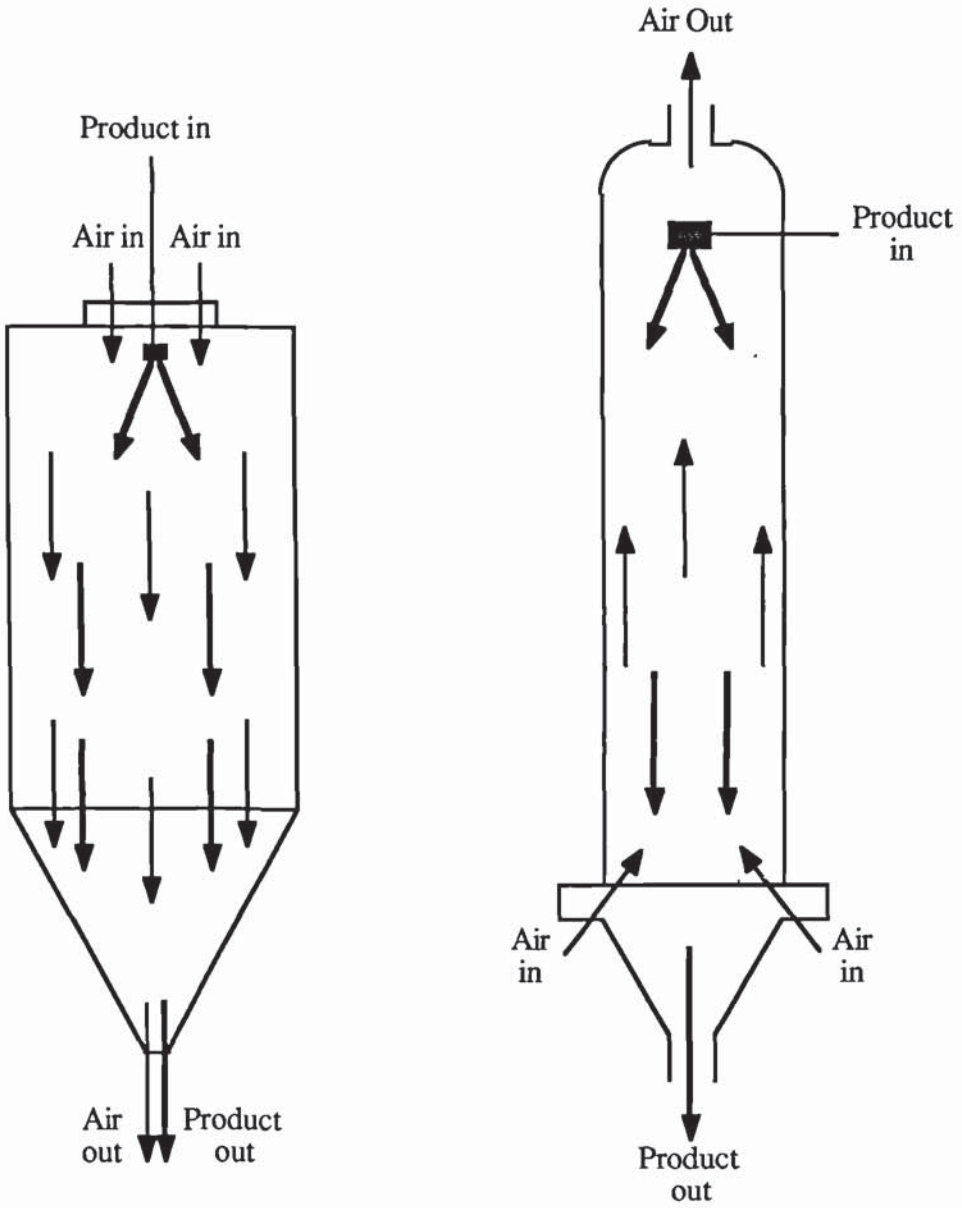

a) Co-current Dryer

b) Counter-current Dryer

Mixed Flow Drying Chambers

In this type of dryer the air and spray are subjected to a mixture of co-current and counter-current flow conditions during their passage through the drying chamber. This can be accomplished by the following methods:

a) The air flows in two directions whilst the product flows one way. The air inlet and outlet ducts are situated at the top of the drying chamber along with the

atomiser as illustrated in Figure 1.6a. The high velocities developed within the dryer promote conditions of high evaporation rates and produce short residence times. However, due to a high powder to air ratio within the drying chamber a high percentage of the product remains entrained in the air and is carried out of the top of the dryer.

Figure 1.6: *Mixed Flow in Spray Dryers*

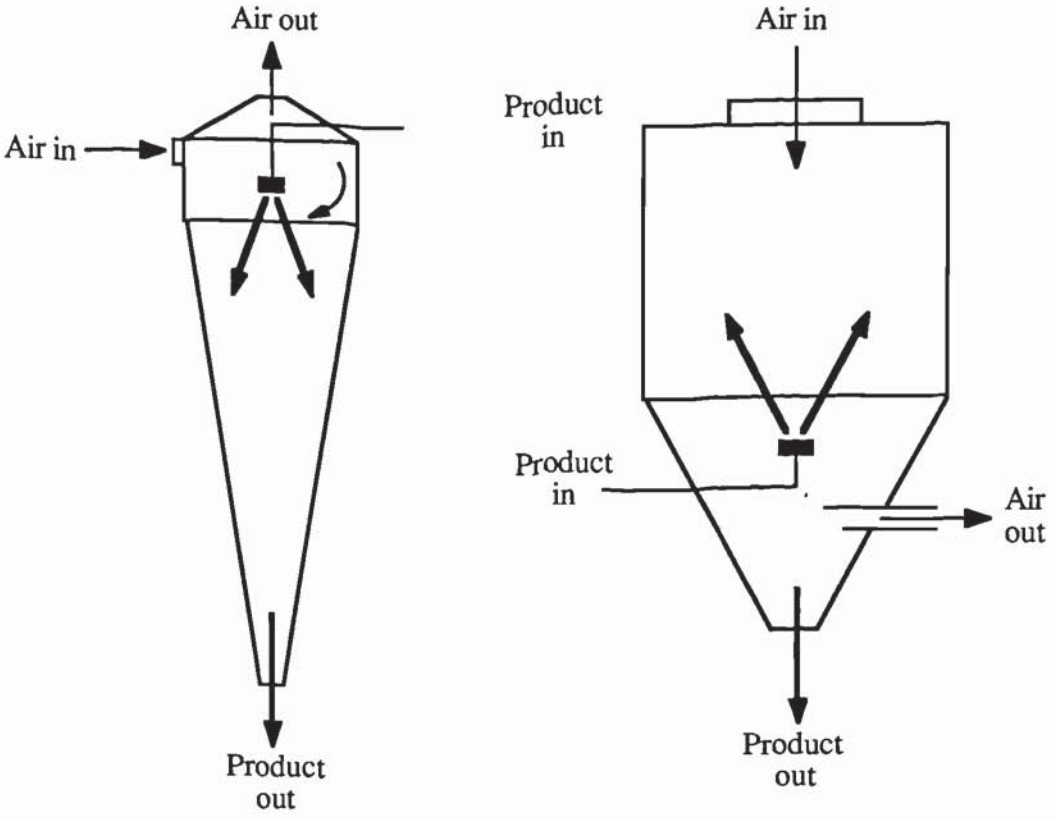

a) Cyclone Dryer

b) Fountain Dryer

b) The product flows in two directions whilst the air flows one way. The atomiser sprays up from the base of the drying chamber into the down-coming drying air and the product is discharged at the base, as illustrated by Figure 1.6b. This type of dryer is often referred to as a 'Fountain Spray Dryer'. The product from the dryer can either be carried away in the exhaust air or undergo separation at the base of the drying chamber to be discharged separately.

1.2.2 General Principles

Irrespective of the mode of atomisation, the droplets in the resulting spray are ejected at a velocity far greater than the air velocity within the drying chamber. However, direct penetration of the droplets is limited to short distances from the atomiser due to rapid dissipation of the kinetic energy of the individual droplets by friction from the drying air. The droplets are heavily influenced by the surrounding air flow, and the design of the air dispenser governs their movement.

Droplet travel from the time of injection to the point of contact with the drying chamber wall can be considered in several ways, either as one- or two-dimensional motion in the case of nozzle atomisers in non-rotary air flow, or as three-dimensional motion in the case of a rotary atomiser operating in rotary air flow. Droplet motion can be represented by theoretically derived correlations. However, certain assumptions are usually introduced to reduce the complexity of the correlations. These include,

(a) heat transfer between the droplet and air is by forced convection.

(b) the spray consists of homogeneous, spherical droplets.

(c) droplet agglomeration and break-up along the trajectory is disregarded.

(d) in rotary air flow dryers, the air flow is considered as a forced vortex; in non-rotary air flow dryers the air flow is considered as parallel streamline flow.

The work of Lapple & Shepherd [16] is often cited in the literature. They solved the dynamic equations for spherical particles undergoing no mass transfer in a uniform flow field. Masters [17], in a study of rotary disc atomisation applied these equations, and those for heat and mass transfer developed by Ranz & Marshall [18], to illustrate the three-dimensional motion of a droplet with regard to wall impingement. A critical droplet diameter was found that affected the extent of wall impingement. However, no solutions were given for a rotating flow field because of the complexity of the air flow patterns, moreover in practice the situation is more complex due to the use of multiple atomisers.

The movement of a decelerating droplet is normally very small and its path of travel can be considered to be that of the air flow pattern in the drying chamber. For

rotary disc atomisation in large diameter drying chambers local effects around the atomiser are negligible. However, in small diameter drying chambers, ie less than 0.9m diameter, it has been shown that the air movement caused by the atomiser is the controlling factor determining droplet trajectory paths [19].

Katta & Gauvin [20] studied droplet residence times and developed a model to predict the three-dimensional motion of droplets in a pilot plant spray dryer. They showed that the droplet motion was dependent upon both the atomising device and the air flow pattern within the drying chamber.

Gauvin *et al* [21] identified two drying zones, a 'nozzle' zone and a 'free entrainment' zone, within the spray drying towers they studied and concluded that the presence of such zones must be considered in residence time analysis. Flow visualisation studies and residence time distributions in a counter-current pilot plant spray dryer by Ade-John & Jeffreys [22] identified the volumes of the various drying zones. The overall flow pattern within the dryer was simulated by a combination of well defined flows such as completely mixed well-stirred tank reactor zones, plug flow zones and by-pass zones. Their work identified the presence of a thin by-pass layer around the walls of the tower that was present under all experimental conditions. From smoke pulse experiments they identified three other zones, a well-mixed section at the air entry region, a well-mixed section around the spray nozzle and a plug flow zone connecting them. The changes in volume of these zones caused by the air flow and tower dimensions were correlated by dimensional analysis.

Subsequently Sharma [23] studied the air flow patterns in a 1.2m diameter transparent counter-current spray tower by flow visualisation. Smoke was introduced into various zones within the tower to trace the direction, and gauge the intensity, of the air flow. A variety of air entry configurations were investigated, by means of a set of variable-angle air inlet nozzles. This confirmed the existence of a core of high rotational and axial velocity channelling up the axis of the tower. The stability of the flow within the core was strongly dependent upon the air entry arrangement. An incorrect balance of flow between the air inlet nozzles caused the core to move from

the tower axis resulting in a flow reduction and, in the extreme case, the creation of a wall by-pass.

Therefore, it is possible from this type of work to obtain a better estimate of droplet residence time. This is an important factor in spray dryer design. It is useful to know the influence of air entrainment upon droplet motion from nozzles as the relative velocity between the droplets and air is an important factor in the calculation of the rate of moisture evaporation during the saturated surface drying period. However it is less important following crust formation when mass transfer within the particle becomes rate controlling. Entrainment of the air within the spray maintains the droplet velocity at a significantly greater level than the terminal velocity of the droplet over the entire time period when the majority of the evaporation occurs. This causes deposition upon the drying chamber walls due to faster droplet trajectories producing shorter trajectory times for droplets which are not sufficiently dry to avoid adhesion upon impact.

1.3 Drying of Droplets

The evaporation of liquid from a spray involves simultaneous heat and mass transfer. Heat is transferred by convection from the drying medium (usually air) and converted into latent heat during moisture evaporation. The vaporised moisture is then transferred into the drying medium. The mechanism of moisture transport within a particle has been described by several theories, but it is generally recognised that the mechanism involves some combination of diffusion, capillary action and evaporation-condensation.

The rate of heat and mass transfer are dependent upon the temperature and humidity of the drying air, the droplet diameter and the relative velocity between the droplet and the air. For a droplet under constant environmental conditions the drying

process can be divided into a constant rate and a falling rate period. A idealised drying curve is illustrated in Figure 1.7.

Figure 1.7: *Typical Drying Rate Curve*

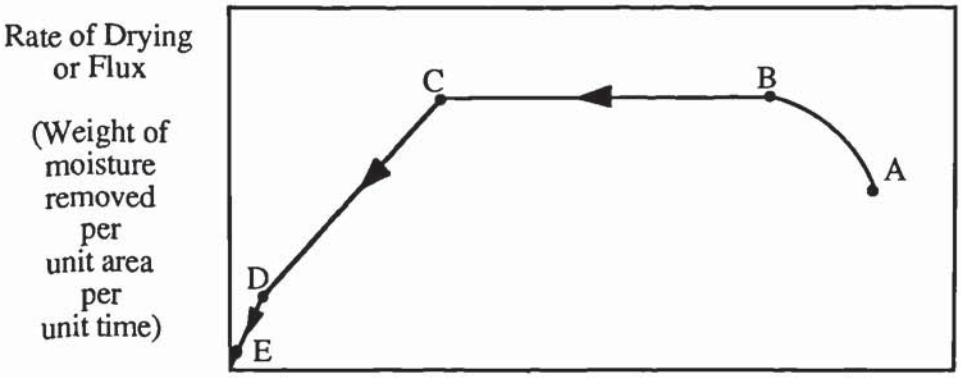

In the region A to B, the droplet has contacted the drying air and the drying rate increases as the heat transfer across the droplet-air interface establishes an equilibrium.

In the region B to C, the drying proceeds at a constant rate as the conditions of dynamic equilibrium are present. The droplet surface remains saturated due to the migration of internal moisture to the surface.

In the region C to D, the drying rate starts to fall as the critical point (C) is reached. This period can form more than one phase due to the presence of local areas of surface wetness and will continue until the entire droplet surface has been dried (ie, a crust has formed).

In the region D to E, the solid layer or crust of the partially dried droplet resists further mass transfer. Evaporation will now proceed at a continually decreasing rate until the droplet moisture content is in equilibrium with the drying air. Generally the approach to the equilibrium position, E, is slow and, in spray drying, the product is usually removed from the dryer before this condition is reached. This sequence is however idealised, for example, in some cases C to E comprises of a continuous curve with no transition point D.

1.3.1 Evaporation of Pure Liquid Droplets

Understanding of the mechanisms of evaporation in spray drying have been brought about by conclusions drawn from the study of the evaporation of pure liquids. This ideal case of evaporation can be modified to compensate for any deviation from basic theory that is caused by the presence of dissolved or insoluble solids.

Dimensional analysis of the heat and mass transfer for a spherical particle moving in a fluid reveals,

$$\text{Nu (Nusselt Number)} = \frac{\text{Total Heat Transfer}}{\text{Conductive Heat Transfer}} = \frac{h_c\, d}{k_i} = f(\text{Re, Pr}) \qquad - 1.1$$

$$\text{Sh (Sherwood Number)} = \frac{\text{Mass Diffusivity}}{\text{Molecular Diffusivity}} = \frac{k_g\, d}{D_v} = f(\text{Re, Sc}) \qquad - 1.2$$

where,

$$\text{Re (Reynolds Number)} = \frac{\text{Inertia Force}}{\text{Viscous Force}} = \frac{\rho_l V d}{\mu_l} \qquad - 1.3$$

$$\text{Pr (Prandtl Number)} = \frac{\text{Kinematic Diffusivity}}{\text{Thermal Diffusivity}} = \frac{C_p \mu_a}{k_i} \qquad - 1.4$$

$$\text{Sc (Schmidt Number)} = \frac{\text{Kinematic Viscosity}}{\text{Molecular Diffusivity}} = \frac{\mu_a}{\rho_a D_v} \qquad - 1.5$$

The form of equations (1.1) to (1.5) has been investigated by many workers. One of the earliest expressions, derived by Frössling [24], considered the solution of the simultaneous equations for continuity and heat and mass transfer across the boundary layer. Frössling gave solutions in the forms,

$$Nu = 2.0 + \varphi\, Re^{0.5} Pr^{0.33} \qquad - 1.6$$

$$Sh = 2.0 + \varphi\, Re^{0.5} Sc^{0.33} \qquad - 1.7$$

For the case of a droplet in still air the Reynolds Number term is reduced to zero, thus

$$Nu = 2.0 \qquad - 1.8$$

$$Sh = 2.0 \qquad - 1.9$$

Experimental work has produced several values for the constant φ, but work by Ranz & Marshall [18] has produced the most widely quoted value of 0.6.

Equations (1.8) and (1.9), for heat and mass transfer, are limited by the assumptions that the droplet remains spherical, the internal structure of the droplet remains stable, and the neglect of any heat transfer to the evaporated moisture.

Pure Liquid Sprays

The characteristics of evaporation of droplets in a spray differs from those of a single droplet. Although the basic theory still applies, several new variables need to be introduced in order to analyse the evaporation of the spray . The spray must be defined in terms of a representative diameter and size distribution, the average relative velocity between the droplets and the drying air, droplet trajectory, and the population density of the spray at any given time.

Sprays with a large size distribution of droplets initially evaporate rapidly due to the higher rate of evaporation of the smaller droplets. However, the overall rate is reduced due to the slower evaporation of the larger droplets. Consequently the droplet size distribution will vary with time; an initial increase in the mean diameter is subsequently off-set by an overall decrease until moisture evaporation is complete.

Pham & Keey [25] investigated the transition period or jet zone of the spray as it emerges from the nozzle. The temperature, velocity, and concentration profiles were simplified to enable the prediction of evaporation within this zone. They concluded that severe errors would occur if jet dynamics were neglected.

1.3.2 Evaporation of Liquid Droplets Containing Solids

The presence of dissolved solids in a liquid droplet reduces its rate of evaporation. The vapour pressure of the droplet is generally reduced and thus the rate of mass transfer decreases. Initially a free liquid surface is created between the drying air and the liquid contained within the droplet, and evaporation proceeds as in the case of the pure liquid. Once the liquid has been concentrated beyond saturation, a crust is

formed that separates the air from the liquid at the interface resulting in a particle with a core consisting of saturated liquid.

Once the crust has been formed, the heat and mass transport mechanisms depend upon the nature of the crust. With many materials, for example detergents, skim milk and coffee, there is also a resistance to heat and mass transfer due to a film or skin which exists prior to crust formation. Figure 1.8 illustrates the effect of crust properties upon the evaporation of residual moisture. With a specific material dried under conditions yielding an impervious crust, the initial rate of evaporation may be greater but the time for complete evaporation is extended. However, the evaporation time will be reduced if the crust is fractured by the production of a blow-hole. The creation of a porous crust enables the vapour to easily diffuse to the surface but the drying rate gradually falls until complete evaporation is achieved.

Figure 1.8: *Effect of Crust Properties on Evaporation Times*

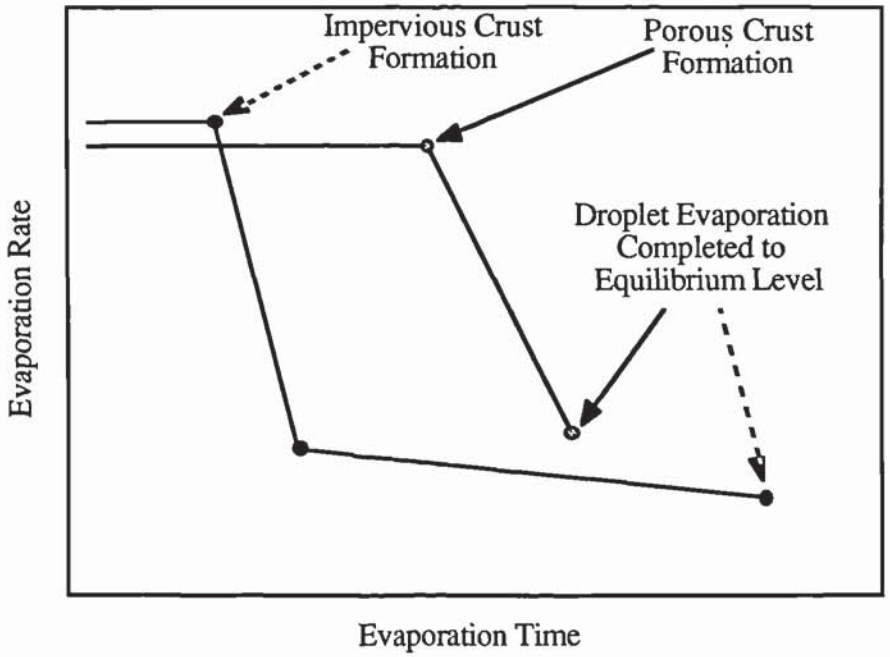

Charlesworth & Marshall [26] studied the drying of stationary droplets containing dissolved solids suspended on a glass filament vertically in a hot air stream. For a range of materials and drying conditions, they investigated crust formation upon

the droplet surface and weight changes due to evaporation. Figure 1.9 illustrates the most common shape and composition changes that occur in spray dried particles. Different phenomena were observed based upon whether the temperature of the drying air was above or below the droplet boiling point.

The drying of droplets of particulate slurries was studied by Audu [27]. He observed single droplets suspended from a slowly rotating nozzle in a horizontal wind tunnel (thus providing simulated conditions to those in the vicinity of a droplet in a spray dryer) and forming crusts of uniform thickness. Values of φ for water droplets were obtained that differed from that of Ranz & Marshall [18] which were found to vary with air temperature. A further correlation was proposed for mass transfer as the coefficient φ, being temperature dependent, was found to vary over a wider range than that found by previous workers,

$$Sh = 2.0 + 0.44\left(\frac{T_a - T_d}{T_{am}}\right)^{-0.008} Re^{0.5} Sc^{0.33} \qquad - \ 1.10$$

It can be seen that the temperature correction term in equation (1.10) would approximate to zero for all but the most extreme cases and Ali [28] stated that it did not take into account heat transfer by conduction from the filament attached to the droplet. He revised the correlation to include saturated surfaces and obtained the following expression,

$$Sh = 2.0 + \varphi\left(\frac{T_a - T_d}{T_{am}}\right)^{b} Re^{0.5} Sc^{0.33} \qquad - \ 1.11$$

For suspended droplets in the size range 2mm to 8mm he stated that the values of the two constants were: $\varphi = 0.501$, $b = -0.03$, and, for free-flight droplets in the size range of 1.5mm to 6mm the values of the constants were: $\varphi = 0.62$, $b = -0.01$.

In a study of droplets evaporating whilst suspended in free-flight in a vertical wind tunnel, the rate of mass transfer was found to be increased by droplet oscillation [29]; conditions which pertain immediately following atomisation. However, once a

Figure 1.9: *Characteristics of Droplets undergoing Drying [26]*

(a) The temperature of the drying air below the boiling point of the liquid

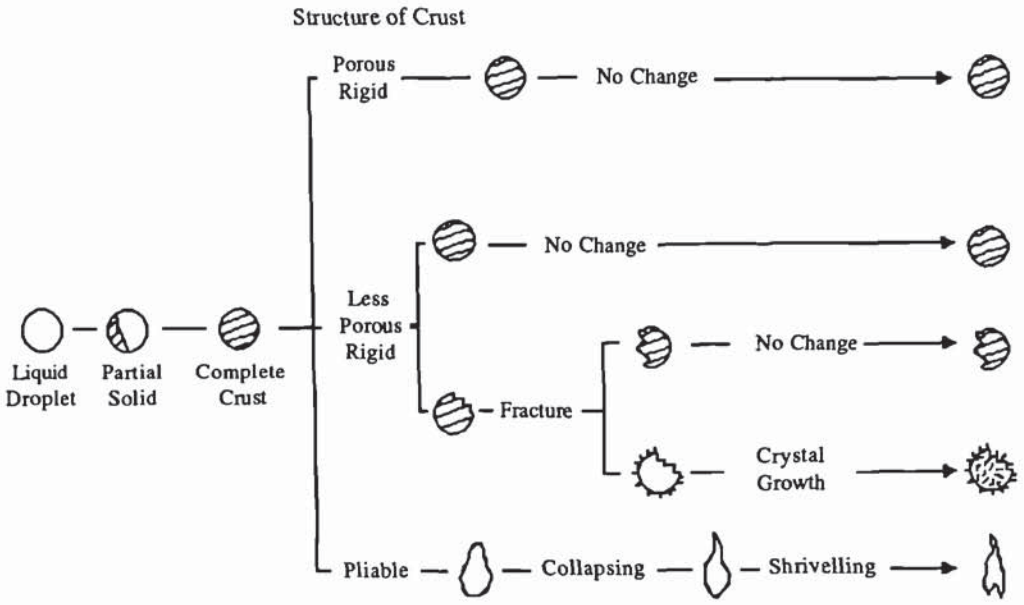

(b) The temperature of the drying air above the boiling point of the liquid

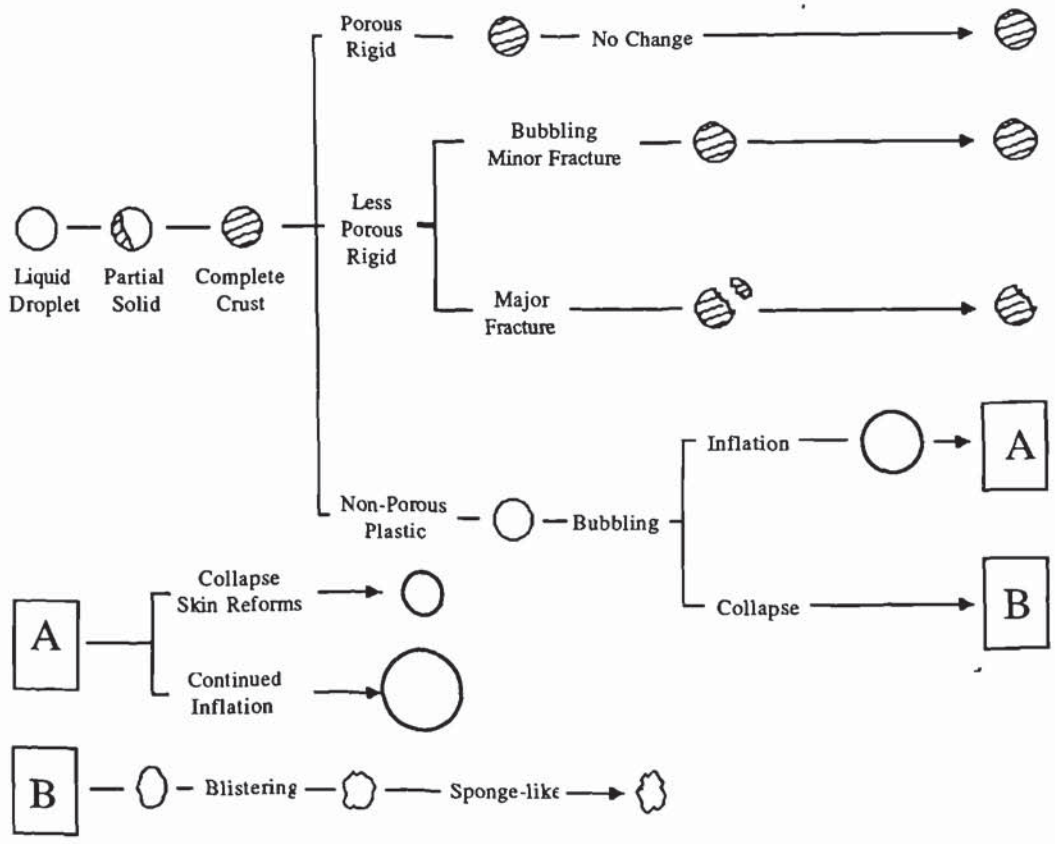

crust has been formed these oscillations dampen out and the rate of mass transfer is reduced, falling into line with predicted values.

For slurry droplets, the overall mass transfer coefficient was found to decrease with an increase in droplet size and drying temperature and is determined by equation (1.12),

$$\frac{1}{K_G} = \frac{1}{H' k_g} + \frac{1}{k_c} \qquad - 1.12$$

where: H ' is a constant of proportionality, ie Henry's constant, and is determined by the ratio of the molar concentrations of the diffusing species in the bulk or interface phase on either side of the phase boundary.

For small droplets the mass transfer coefficient for the crust (k_c) was found to control the drying process [30], and is defined by equation (1.13),

$$k_c = \frac{D_v P_o^{1.5}}{C_T} \qquad - 1.13$$

where, P_o is the porosity of the crust

C_T is the crust thickness

Audu & Jeffreys [30] found that the crust resistance to mass transfer accounted for as much as 62.4% of the total resistance for sodium sulphate droplets and 97.5% for detergent droplets. The disadvantage of their experimental technique was that the droplets were suspended from a stainless steel nozzle of the same diameter as the droplet (approximately 2mm) and no allowance was made for heat conduction into the droplet from the suspension device which would be quite substantial. They proposed a crust thickness model based upon a mass balance of the moisture in the surrounding air. However the model predicted values that were as much as 20% higher than experimental results.

Thus, knowledge of the controlling mass transfer coefficient for the crust, k_c, and that of the liquid mass transfer coefficient, k_g (determined by equation (1.11))

enables the calculation of the overall mass transfer coefficient for use in the design of spray drying equipment from equation (1.12).

Sprays of Droplets Containing Solids

The above theoretical considerations of heat and mass transfer in single droplets also applies to sprays. However, the degree of reduction of the vapour pressure is dependent upon the size of the individual droplets and the surface area to volume ratio; consequently crust formation does not appear simultaneously throughout the spray. Thus analysis of spray drying is highly complex and very few investigations have been conducted in this field. Dlouhy & Gauvin [31] studied this type of evaporation and showed that the time for the evaporation of the entire spray could be predicted with a reasonable degree of accuracy using a step-wise calculation method.

Sharma [32] developed a model that enabled the prediction of droplet trajectories and residence times for a given size distribution. The work was based upon the assumption that the droplets were spherical and underwent no change in shape, agglomeration or break-up during the course of drying. Although his later work [23] showed the presence of droplet agglomeration in the later stages of drying, the predictions obtained from his model were found to be in reasonable agreement with experimental data available from industrial scale dryers.

1.3.3 Drying in Media other than Air

It is becoming more frequent for spray drying operations to be carried out in an inert atmosphere. In the case of explosion hazards due to the presence of solvents in the feed nitrogen or superheated steam is used. Use of an inert atmosphere requires the spray drying to be performed in a closed-cycle system to limit gas usage and recover feed solvents.

The effect upon the evaporation of the spray in the drying chamber will depend upon the properties of the gaseous atmosphere that is employed. For a gas in which there is a higher diffusivity than air, there will be an increase in the rate of droplet

evaporation in the constant rate period. For a low viscosity gas the Prandtl Number will decrease accordingly.

Drying in Gases

The rate of surface evaporation in a gas lighter than air (for example, helium) is much higher due to the higher rates of diffusion and thermal conductivity. The advantage of a light atmosphere is counteracted by a more extensive droplet trajectory than in air. Even though the evaporation time may be considerably faster this is largely off-set by correspondingly higher terminal velocities, resulting in little change in overall dryer dimensions for a given evaporative capacity. The economics are also probably unfavourable.

Drying in Superheated Vapours

The droplet evaporation mechanism in a superheated drying medium is one of negligible resistance to mass transfer and the droplet temperature approximating to that of the saturated vapour, related to the operating pressure of the dryer. The mechanism is different to that occurring in a gaseous medium, where droplet temperatures are initially lower.

Superheated vapours may be used instead of gases or air in spray drying because there is a definite improvement in the thermal efficiency of the drying operation and also the provision of an inert atmosphere, where product oxidation and explosion hazards are prevented. The use of a superheated vapour also provides a reduction in the volume of the drying medium leaving the dryer.

Drying in Superheated Steam

The rate of evaporation of aqueous droplets into superheated steam is determined by the heat transfer to the droplets. There is no diffusional mass transfer in the gas phase [33]. The rate of heat transfer is the limiting factor for the removal of volatiles and the droplet surface temperatures are much higher than when drying is taking place in air,

although the actual temperatures depend upon the steam pressure. The heat transfer rate is somewhat lower than in air.

The main problem involved in the application of superheated steam concerns condensation, especially in the outlet to the dryer and inside the product handling equipment. Operational difficulties often outweigh the improvements in the properties of the dried product obtained from employing a drying atmosphere of superheated steam.

1.4 Product Recovery

The final stage of any spray drying operation is the separation of the dried product from the air leaving the drying chamber. This stage should enable economic recovery of the dried product and result in an exhaust air stream free from entrained particles. The requirement of an economic recovery method is that the product is obtained in its most usable or saleable form and, in an open-cycle dryer, the discharge of airborne particles to the atmosphere must be below the statutory limits of local pollution standards. In a closed-cycle dryer the requirement of a clean exhaust is to avoid the chance of overheated airborne particles when the drying medium is returned to the system heating unit. Any 'scorching' can often lead to ignition or the passage of dark particles into the drying chamber with consequent product contamination.

The product removal stage of a spray dryer can be based on either a single-point discharge or a two-point discharge system. In the single-point system the entire product is conveyed to the collecting equipment for removal from the air stream. The two-point system involves primary separation at the base of the drying chamber where the majority of the dried product is removed and secondary separation where the fines are recovered from the air stream by the collecting equipment.

The degree of primary product separation is dependent upon the chamber design, the atomisation of the product and the drying air flow. The product is separated from

the exhaust air by either the formation of cyclonic air flows at the base of a conical drying chamber, or the particles falling out of the air flow onto a flat chamber base. Whatever separation method is employed some form of collection equipment is still required after the drying chamber. Typical examples of collection equipment employed are cyclones, bag filters, scrubbers, and electrostatic precipitators. The choice of equipment is generally based upon cost, collection efficiency and the treatment of the product undergoing separation [1].

Table 1.2: *Efficiencies of Collection Equipment at Various Particle Sizes [34]*

Collection Equipment	Percentage Efficiency at		
	50 μm	5 μm	1 μm
Cellular Cyclone	98	42	13
Tubular Cyclone	100	89	40
Medium-efficiency Cyclone	94	27	8
High-efficiency Cyclone	96	73	27
Irrigated Cyclone	100	87	42
Electrostatic Precipitator	> 99	99	86
Irrigated Electrostatic Precipitator	> 99	98	92
Low-velocity Bag Filter	100	> 99	99
Shaker-type Fabric Filter	> 99	> 99	99
Reverse-jet Fabric Filter	100	> 99	99

Selection of Collecting Equipment

Many of today's spray drying applications are so established that certain types of separating equipment are connected with particular products. Operational experience has shown the equipment which is capable of meeting the required demands for cost and separation performance. Although rules for equipment selection do exist they can,

at times be rather general. Typical efficiencies of the main types of collection equipment are given in Table 1.2.

Separation efficiency is generally based upon the value of the product, cost of recovery and environmental pollution standards. The type of equipment employed is often not capable of removing all the product from the exhaust air but is found to be acceptable due to operational convenience and maintenance and other costs. It is also possible to rectify limitations in collection efficiency by installing secondary equipment, whereas limitations in other aspects are not easily rectified. To justify the installation of any separation equipment, it must have an acceptable level of separation efficiency, it must be able to fit into the plant layout, and the investment and operational costs must be offset by the value of the product.

Chapter 2: Spray Drying and the Detergent Industry

Introduction

The production volume of today's detergent industry is enormous and combined sales in the household cleaning market (ie, sales of both soap and detergent products) exceeded £2200 million in recent years [35]. The industry is dominated by three giant conglomerates: Proctor & Gamble Co. which claims 45% of the total market share, Lever Brothers Inc. and Colgate-Palmolive who command 24% and 14% market shares respectively [36].

The industry is essentially a complex balancing act with manufacturers facing environmental concerns, escalating raw material costs and critical product shortages in a highly competitive business climate. Additionally it is currently undergoing one of its biggest and most radical changes for at least twenty-years with major swings towards non-phosphate and heavy-duty liquid detergents.

The increase in low or non-phosphate detergents has mainly been prompted by legislation and voluntary agreements concerning phosphate content in response to pressure from politicians and environmental pressure groups. Phosphate content has also been reduced as manufacturers search for more cost-effective formulations with research being conducted into citrate builders as one possible alternative [36].

The sale of liquid detergents has increased in many countries where powders have traditionally been dominant, as consumers give more priority to convenience. This growth has been heavily influenced by the introduction of the 'wash ball' in the late 1980's which consumers perceived took the detergent to the 'heart of the wash' [37] and despite the fact that liquids do not contain bleaches, which in Europe are incorporated into most powders.

The beginnings of the detergent industry are not as difficult to identify ás those of the soap industry, although it is not easy to pinpoint exactly when the industry came into being. The major problem is that of determining what is being referred to as 'synthetic detergent' as many definitions have been proposed. Although the term surfactant is increasingly being used throughout the world it is possible to find

references to syndet in some American journals and tenside (short for tensio-active material) in European journals. It was therefore after much discussion and deliberation that the industry came to agree upon the following definitions [38]:

Detergent: A product which has been specially formulated to promote detergency. A detergent formulation consists of essential constituents (ie, surface active agents) and subsidiary constituents (ie, builders, boosters, fillers and auxillaries).

Surface active agent: A chemical compound which includes at least one group with an affinity for markedly polar surfaces (hydrophylic), in most cases ensuring water solubility, and a group which has little affinity for water (hydrophobic). A surface active agent is also referred to as an amphiphyllic product and detergent compositions generally contain a mixture of such compounds.

2.1 History of the Industry

The first synthetic detergents appeared during the First World War due to development work in Germany to allow fats to be released for other purposes. These early detergents consisted of a type of short-chain alkyl naphthalene sulphonate molecules and proved to be only moderately good in the role of a detergent. However, they were found to be good wetting agents and are still being produced for use as textile auxiliaries [38].

In the late nineteen-twenties and early 'thirties long-chain alcohol molecules were sulphonated and sold as neutralised sodium salts after the addition of sodium sulphate, as an extender. The early nineteen-thirties saw the introduction of long-chain alkyl aryl sulphonate molecules with benzene providing an aromatic nucleus sold as the sodium salts extended with sodium sulphate. By the end of the Second World War the alkyl aryl sulphonates were outselling the alcohol sulphonates in the general cleaning market, but the alcohol sulphonates were finding greater suitability in the field of shampoos. By the end of the nineteen-forties condensed phosphates had been introduced onto the market to solve the problem of 'heavy-duty' (cotton) washing. The initial use of tetra sodium pyrophosphate, followed by that of sodium

tripolyphosphate, in detergent formulations was found to be extremely successful in this field.

Up until the early nineteen-sixties the major ingredient in detergent formulations had been propylene tetramer benzene sulphonate, but the increasing amounts of foam on rivers and other effluent treatment problems were then linked to the molecule. Further investigation revealed that the propylene based alkyl benzene sulphonates were not completely degraded by bacterial action; this attribute arose because the narrow branched-chain structure of alkyl benzene hinders bacterial attack. This problem was solved by the introduction of the straight-chained alkyl benzene molecule after it was found that the straight chain fatty acid sulphonates were readily degraded.

Figure 2.1: *Segments of the U.K. Fabric Washing Products Market (£m)*

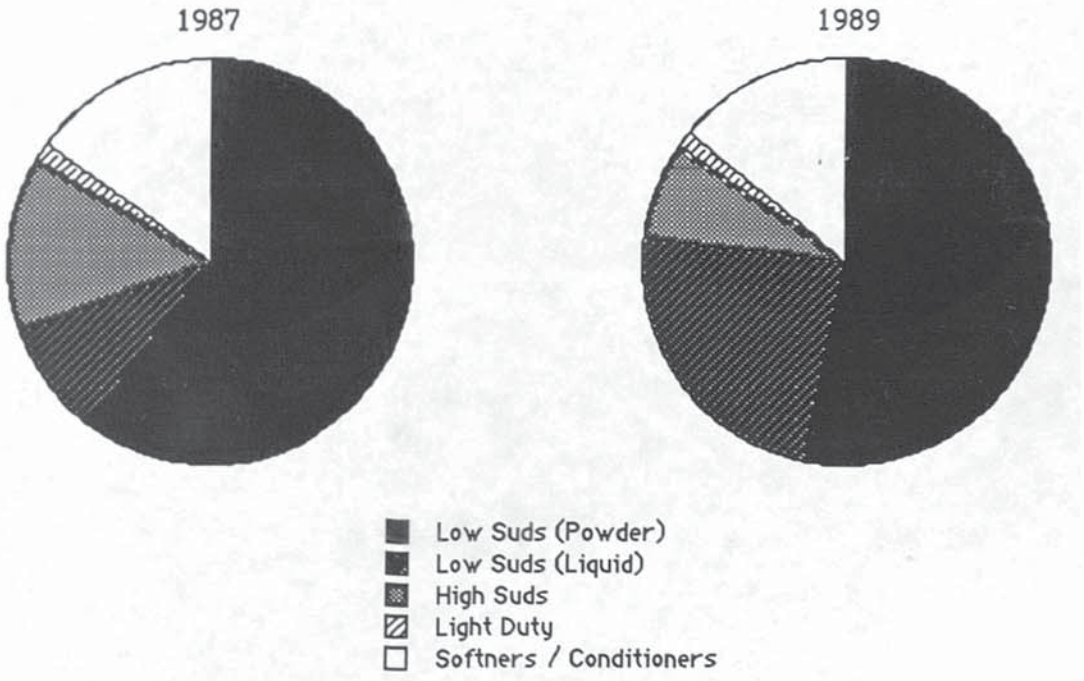

The nineteen-seventies saw the biggest single revolution within the industry with the introduction of enzyme additives to produce 'biological' washing powders. The use of enzyme additives in detergent formulations was not a new idea as proteolytic enzymes had been used in both Germany and Switzerland as early as the nineteen-twenties but with only a moderate degree of success [38]. However, there was some

reaction against the biological formulations causing problems for people with sensitive skin. This forced the manufacturers to 're-introduce' the non-biological formulation and by the nineteen-eighties both formulations were being sold side-by-side.

The late nineteen-eighties saw an increase in the demand for heavy duty low-suds liquid detergents which now account for 34% of the detergent market [37]; this trend is illustrated in Figure 2.1. The total sales of soaps and detergent products throughout the nineteen-eighties is given in Table 2.1 which also shows a relative increase in the sales of washing powders. The same period saw pressure from environmental groups beginning to affect the market with the successful launch of several 'green', phosphate-free formulations, products, such as Ark and Ecover.

Table 2.1: *Sectors of the U.K. Soaps and Detergents Market (£m)*

Detergent Product	**1981**	**1985**	**1987**	**1989**
Soap Products	168.1	183.7	120.0	124.0
Fabric Washing Products	278.7	426.2	530.0	670.7
Liquid Detergents	*6.0*	*4.0*	*48.0*	*186.0*
Dish Washing Products	73.6	98.0	167.0	162.0
Household Cleaners	32.3	38.2	75.0	104.0
Total Sales	552.7	746.1	892.0	1171.1

At the beginning of the nineteen-nineties the industry trends from the late nineteen-eighties look set to continue with the phosphate content of both liquids and powders continuing to decrease and manufacturers already looking for viable alternatives [36]. Although liquid detergents look set to increase their market share through out the forthcoming decade it is unlikely that they will start to outsell washing powders for sometime to come [37].

2.2 The Principle Detergent Groups [38]

Detergents, like soaps, are materials which dissolve, or tend to dissolve, in water and in non-aqueous materials under certain conditions. This tendency is induced by the inclusion of two distinct groups within the molecule. One group is termed as the hydrophile, readily soluble in water, whilst the other is termed the hydrophobe, which on its own would be insoluble in water.

The hydrophilic group is usually synthetically combined with the hydrophobic molecule to produce a compound that is soluble in water; however, this process does not necessarily produce a detergent. Detergency is actually based upon the ratio of the molecular weights of the hydrophobic and hydrophilic portions of the molecule. Consider the dodecane molecule, $C_{12}H_{26}$, as an illustration. It is completely insoluble but if an -OH group replaces one of hydrogen atoms at either end of the chain, then the resultant lauryl alcohol molecule, $C_{11}H_{23}CH_2OH$, is still virtually insoluble but a tendency towards solubility has been introduced. Sulphonation of the lauryl alcohol to a sulphuric ester, $C_{11}H_{23}OSO_2OH$, produces a molecule that is totally miscible in water in all proportions and if the ester is subsequently neutralised the compound becomes completely soluble (and is, in this instance, a very good detergent).

All types of detergent can be classified as either Anionic, Cationic, Non-Ionic, or Amphoteric.

Anionic Detergents

This is the largest class of detergents. In these compounds the detergency is based upon the anion, which must be neutralised by an alkaline or other basic material before full detergency is reached. With the exception of any specialised or proprietary detergents, anionic detergents fall into the following groups:

Alkyl Aryl Sulphonates - This is by far the largest group in general use, since dodecyl benzene sulphonate (the leading member of the group) is present in some form in over sixty-percent of all the detergents used throughout the world.

Long-chain (Fatty) Alcohol Sulphates - These tend to be the most expensive detergents in this category and are only generally available in the neutralised form with a

concentration of 60%. Spray drying makes it is possible to produce concentrations of up to 90% but significant production costs rule out anything but specialised usage.

Olefine Sulphates and Sulphonates - These are usually good wetting agents and moderately good detergents but suffer from the disadvantage that they are only available as the sodium salt in solutions with a concentration of 40% and have a very penetrating odour.

Sulphated Monoglycerides - These were used in the late nineteen-forties as heavy-duty household powders but, because of the base, were found to be expensive and difficult to supply. The sulphated monoglycerides are difficult to manufacture in the powder form, although they are occasionally used as liquids.

Sulphated Esters - These are non-ionic detergents in the form of ethylene oxide condensates and are generally excellent detergents. However, they have the disadvantage of producing weak, unstable forms and a cloudy solution, which under extreme conditions can consist of two phases.

Cationic Detergents

In this form, detergency is based upon the cation, and although no neutralisation is involved in their manufacture, the material is effectively neutralised by a strong acid. The cationic detergents are of little interest as cleaning agents. Compared with other detergents their detergency is rather poor and production costs are high. There is also an inherent incompatibility between the cationic and anionic detergents due to their mutual precipitation upon contact. Consequently there is no advantage in the use of cationic detergents, although they tend to be powerful germicides and act as fabric softeners. For these reasons, there has been little investigation into the optimum detergency of cationic molecules.

Non-Ionic Detergents

The vast majority of all non-ionic detergents are the condensation products of ethylene oxide with a hydrophobe and consequently show non-ionic properties. The

hydrophobe is generally a material with high molecular weight containing an active hydrogen atom, and the non-ionic material can be one of four main reaction products:

a) Condensation with a long-chain (fatty) alcohol;

b) Condensation with a fatty acid;

c) Condensation with an amine;

d) Condensation with an amide.

Another group of non-ionic detergents are those that fall into the category of fatty acid alkylolamides, which are made by reacting fatty acids with alkylolamides. The alkylolamides are rarely used as detergents on their own, but are frequently used as additives for other detergent materials, for example, dodecyl benzene sulphonate. In this form they act as foam boosters and increase detergency of the host material.

Figure 2.2: *General Amphoteric Detergent Groups*

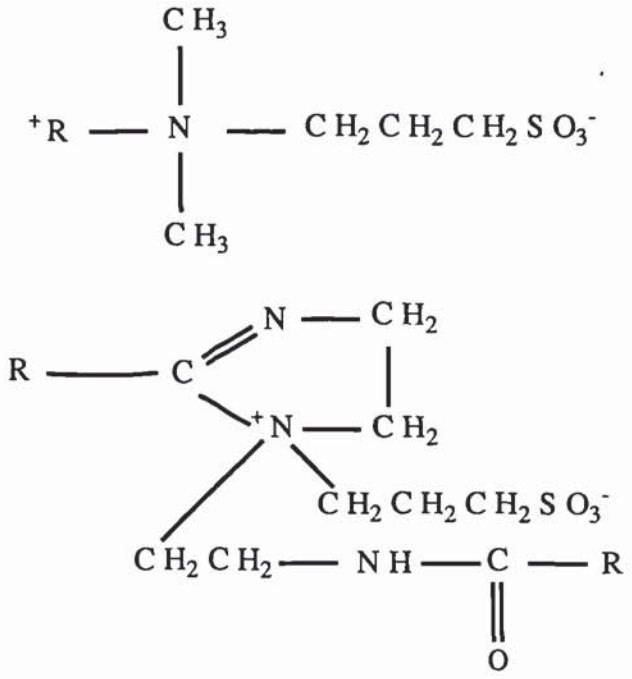

A further type of non-ionic detergent is the fatty amine oxide group which is basically made by treating tertiary amines with hydrogen peroxide. They are good detergents, but their main use is in the role of foam boosters, viscosity increasers and skin protecting agents in liquid detergents.

Amphoteric Detergents

These detergents contain both acidic and basic groups within the same molecule as illustrated by the general amphoteric detergent groups shown in Figure 2.2. The amphoteric detergents are not generally used as the raw materials for detergent formulations because their structure is complicated and often considered to be beyond the capability of most manufacturers. However, they remain of interest because of the presence of both quaternary ammonium and anionic radicals, the anionic radical being that of either a carboxyl, sulphonate, or sulphate; consequently the group has the characteristics of both anionic and cationic fabric softeners.

2.3 The Manufacture of Detergents

Industrial and domestic detergents are generally marketed in three forms, powders, liquids or pastes. The most common domestic formulation is found in the form of a powder although, through successful marketing, liquids are becoming increasingly popular. The actual ingredients of a detergent formulation varies between the various manufacturers but essentially the formulation will contain a surface active agent, a builder and a booster [38]. The formulation and synthesis of the detergent slurry used in the present study [39] is discussed in detail in Chapter 6.

A typical industrial plant layout is shown in Figure 2.3; it consists of a feed preparation stage, detergent formulation drying stage, blending and finally the packaging of the final product [1].

Powdered Detergents

The majority of the detergent formulations are still converted into a particulate form during their manufacture. There are two types of washing powder on the market, low-suds or 'automatic' powders and high-suds powders, but the method of production is essentially the same. The low-suds powders are designed for use at all temperatures in modern front-loading washing machines and the sales of these powders are forecasted

Figure 2.3: *Flow Diagram for Spray Drying of Detergent Formulations*

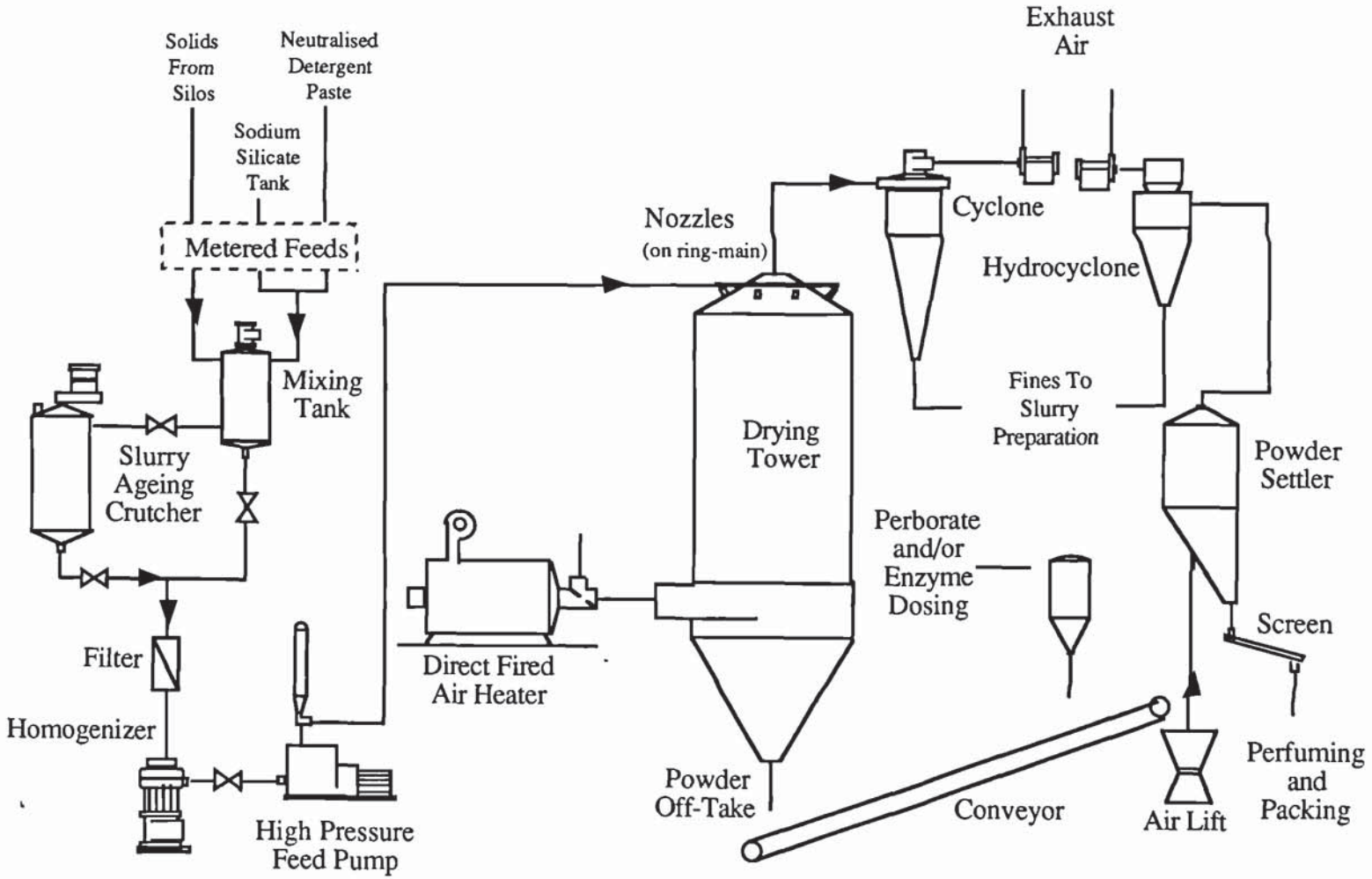

to remain static as liquid sales increase their market share [37]. The high-suds powders are designed for use in top-loading or twin-tub machines and the market has declined in real terms since 1987 but is likely to remain for the forseeable future [37].

A problem associated with the production of powders is that most of the active detergent materials used in the formulation process are not solids. Therefore, it is necessary to combine them with the builders and filling materials in such a way as to produce a final particulate form that is dry to the touch without a tendency to form cakes or lumps. Each detergent material has its own limit to the amount of active material that can be incorporated into a powder; the active material content is also limited by the method of producing the powder. The principal methods of producing powders are as follows [38]:

Simple Absorption

This application is the most limited, and the amount of active material in the finished powder is governed by the physical form of the active ingredient. If the detergent is in a solution with a concentration not exceeding 40% (ie, relatively low viscosity), then the final powder will contain between 8% to 12% of active material; whereas, if the detergent is more concentrated, for example, a non-ionic detergent (usually available in concentrations up to 100%), the practical limit is a powder containing 5% of active material.

Combined Absorption and Neutralisation [40][41]

This a more versatile method than that of simple absorption. The process is based upon neutralising alkyl benzene sulphonic acid with a dry mixture of soda ash and the other ingredients required for the formulation. The actual concentration of the acid can be anywhere in the region of 90% to 100%, but if the manufacturer conducts his own sulphonation it is more economical to use acid that does not require any intermediate handling and is anhydrous, to reduce freight costs.

This method does not involve a lower limit for the amount of active material present in the powder, but the upper limit is usually between 20% to 24%. An

advantage of this method is that powders incorporating solvents can be manufactured safely, which if produced by other methods, for example, spray drying, could constitute fire and explosion hazards due to the presence of solvent in the exhaust air stream.

Dry Mixing of Powders

It is possible to obtain dried detergent powders containing between 40% to 60% active material, from either spray or drum drying. These powders can be blended with the other required ingredients in a powder mixer, dry blender, or similar equipment.

The characteristics of, for example, a spray dried powder can be retained by ensuring that more than half of the ingredients in the mix have been spray dried, for example, using spray dried sodium tripolyphosphate in addition to the spray dried detergent concentrate.

A slight variation in this method of production of powders is the granulation plant which consists of a vertical chamber installed with a variable speed rotating turbine giving 900 to 3500 rpm. This process is cheaper than spray drying because it requires less water to be present in the mix, consequently the energy saving of the plant is in the region of 50% [42]. Although the bulk density of the finished product is generally higher, ie 0.4 to 0.7 kg/l compared to 0.2 to 0.3 kg/l, for that from a spray dryer it is possible to reduce the bulk density using special formulations.

Spray Drying of Powders [43]

The majority of the detergent powders produced for household use are manufactured by the spray drying process, because spray dried powders have many advantages over other types of powder. These advantages can be summarised as,

i) There is no limit to the formulation. It can contain relatively high amounts of active material and soda ash is not an essential ingredient. The moisture content and the bulk density of the final powder can be varied within the limits set by tower design.

ii) The spray dried powders are free-flowing, dust-free and do not tend to form lumps. The final product is available in a convenient form and being light has a

higher sales appeal. Consequently there are no special requirements necessary for packaging normal formulations.

iii) The powders will dissolve instantly when added to water due to the final particulate material consisting of hollow beads with a large surface area. This is an important factor if the final product is to be used in automatic machines utilizing a limited washing time.

iv) The spray dryers are capable of successfully handling heat-sensitive materials.

Most of the dryers employed for drying detergent powders tend to be counter-current operated with a nozzle atomiser but for more viscous formulations a rotating disc is generally favoured over a nozzle atomiser [1].

A more detailed review of the spray drying of detergent slurries is given in Section 2.4.

Combination of Spray Dried and Dry Mixed Powders

The introduction of non-ionic detergents into powders has led to problems of stickiness. If the percentage of non-ionic detergent in a formulation rises above a certain level, dependent upon the type of detergent in use, then the spray drying of the formulation introduces practical difficulties. The problems that are generally encountered are those of build-up on the tower walls, clogging of product removal systems, and other problems caused by product stickiness; thus product development can often be hindered by technical problems.

It is possible to overcome the above problems by mechanical means, for example, using wet scrubbers and automatic cleaning rings, but this can lead to other problems especially with the more heat-sensitive materials. A method that was introduced to overcome this problem was to dose the spray dried powder with the powdered non-ionic detergent. This is achieved by a combination of dry mixing and spray drying.

Drum Drying of Powders

Occasionally detergents are manufactured by drum drying. This is probably the least useful process as large flakes are produced which have a relatively small surface area. By comparison even with powders produced by the simultaneous absorption and neutralisation process the drum dried powders are extremely slow to dissolve in water.

The operation of a drum dryer is expensive and there is risk of scorching the final product; however, they have one advantage over spray dryers in that they can be stopped and started in a relatively short time, allowing for the possibility of short runs.

The Finished Product [38]

The bulk of the household powders are perfumed. The perfume can be added either as a powder, or as a fine spray. In order to spray the perfume it must be diluted with a volatile solvent to allow for a better dispersion over the powder and not build-up in localised areas, which may cause lumping of the powder.

The quality of the finished product is determined by its manufacturing process, but an acceptable powder is characterised by:

Good colour properties - Off-colour ingredients in the slurry, such as a dark-coloured active material, may cause undesirable colouring of the powder. Discolouration caused by an inorganic component cannot be easily rectified; however, if the component at fault is organic it can be corrected by bleaching the slurry with sodium hypochlorite or hydrogen peroxide solution.

Desirable particle size and spread - A narrow particle size distribution is desirable from the viewpoint of product appearance. A wide spread of particles will increase the number of oversize particles, slowing down the time for the powder to dissolve, and increase the number of fines produced by the process. These fines cause 'dustiness' and therefore have to be disposed of, or be recycled into the process, often uneconomically.

Correct bulk density - This is the key factor in the economics of washing powder production, in particular those produced by spray drying. The containers for powders are a standard size and shape; it is not practical to sell a half-empty carton if the powder

is too heavy, or if the powder is too light the carton may be unlikely to hold the correct weight.

For any particle size distribution the bulk density is dependent upon the 'hollowness' of the particle (assuming all particles are the same size) and is given by the formula,

$$\text{Bulk Density} = \sum \frac{\left(r_e^3 - r_i^3\right)}{r_e^3} \rho_d$$

where: r_e is the external radius of the particle,

r_i is the internal radius of the particle,

ρ_d is the density of the solid particle.

Thus the thinner the wall of the bead the lower the bulk density. This would suggest that lower feed concentrations will give thinner walls and lower bulk densities. This relation does hold for solutions but for slurries changes in the feed concentration will affect its density and viscosity and influence atomisation.

Correct residual moisture content - A certain amount of water, between 4% to 8%, must be retained within the powder for economic reasons and to comply with E.E.C. regulations. However, since the powder must be free-flowing, any water can only be present as water of crystallisation and not as surface moisture.

Absence of stickiness - This is a phenomenon that is difficult to define but 'stickiness' is unacceptable in the final powder. It may be caused by poor drying, by some ingredient (or the lack of it) in the formulation or, in the case of spray drying, poor atomisation causing the presence of oversized particles which are subsequently incompletely dried. Addition of sodium silicate will substantially improve a sticky product. However, as a rule certain products have a tendency to yield a sticky product, for example, the linear alkyl benzene sulphonates are somewhat stickier than the branched-chain materials.

Uniform composition and appearance - Careful adjustment of all the process variables may produce all the desired characteristics in a product, but these optimum conditions must be established, maintained and repeated throughout the process runs. Accurate

measuring instruments must be located at all vital points in the process and sampling and analytical equipment is required to ensure that the quality of the product remains within the necessary process limits.

Some of these characteristics are interrelated. For example, if the colour is bad due to scorching then the powder will also be extremely dry with very little water content. Excessive moisture in the powder might cause it to be sticky.

Liquid Detergents

The first detergents sold for household use were basically solutions of anionic detergents in water with a concentration in the range of 5% to 20%. In recent years these light-duty detergents have become more sophisticated and now appear, with builders, for use in more heavy-duty applications, for example, household washing machines [44].

The production of liquid detergents has two advantages for the manufacturer in that they can be produced in a relatively simple plant and the diluent, being water, is extremely cheap compared with sodium sulphate or soda ash. However, one disadvantage of the production is that not all the ingredients are blended with the formulation in the liquid form which can lead to mixing problems. The advantages to the consumer are that the liquids are instantaneously dispersed in water. The material can be perfumed and be given an attractive appearance.

The choice of active ingredient depends upon the requirement of the finished liquid. The versatility of alkyl benzene sulphonic acid made by sulphonating with sulphur trioxide is of particular value, but other anionic raw materials are available as the already neutralised salt with or without the presence of various non-detergent material.

Solid and Paste Detergents

In some parts of the world the detergents are used in the form of pastes with varying concentrations. Some of the raw materials for the detergent are sold as a paste, for

example, the sodium salt of lauryl alcohol sulphate in a concentrated form without the presence of an inorganic filler.

Solid detergents are usually manufactured in three forms for use in the following applications [38]:

Detergent Toilet Bars

The production of a detergent toilet bar that is comparable with soap has many difficulties; consequently it is the subject of numerous patent applications. One major problem is that to be sold in the same price range as soap a detergent bar can not contain more than 40% active material. In order to achieve this the mass needs to be filled to 100% with relatively inexpensive material and this causes the problem. Many of the common inorganic salts cannot be used due to problems of weight, efflorescence, and surface hardness.

This problem can be overcome with the use of a soap/detergent mixture. However, although this improves detergency it does not affect any of the disadvantages of soap.

Household Scrub Bars

The first attempts to produce household scrub bars were based upon a detergent which had been available as a water solution. The water was bound with such materials as bentonite and sodium stearate, but because the starting material usually contained equal quantities of water and active material the final product contained the same ratio. This limited the amount of active material that could be used. However, this problem was overcome by the use of alkyl benzene sulphonic acids.

Tablets ('One-Shot' additions to washing machines)

This type of tablet is generally high in active material and filler content but low in inert builders. The tablets are produced so that they dissolve quickly; for this reason they are made from binders which disintegrate on contact with water.

Abrasive Cleaners

This class contains the abrasive hand-cleaners and scouring powders that are used for saucepans as well as household surfaces. The vast majority are available in the form of powders or pastes, but bars and liquids are also available.

The powders, pastes and solids are manufactured in a similar way to the non-abrasive product but with the addition of an abrasive material. In liquids the abrasive material has a tendency to settle out; in order to prevent it compacting, a gelling agent is incorporated into the mixture. This increases the viscosity, so that the abrasive can be redispersed upon agitation.

The choice of abrasive material is important and depends upon cost and the use of the final product. The following materials are listed in the order of fineness and are generally used in a size of 75μm (200 mesh) and below [38]:

Talc - Hydrous magnesium silicate. Soft. Used as a special scouring agent but not for a general household product.

Diatomaceous Earth - Siliceous skeletons of small aquatic plants. Expensive and not recommended in general household products.

Whiting - Washed chalk. Used in tile cleaners, etc. but not for general household products.

Marble - Calcium carbonate. A mild abrasive not generally used in household cleaners.

Volcanic Ash - Suitable for household cleaners.

Feldspar - Mixture of various metal aluminium silicates. It is of equivalent hardness to volcanic ash, and it is usually of a whiter colour, so it is a very desirable product when available.

Quartz - Crystalised silicon dioxide. It is abrasive on the softer metals such as copper and aluminium. Not recommended where milder abrasives are available.

Sand - Fine grains of disintegrated siliceous rock, mainly quartz which it resembles in hardness.

In many cases the soap or detergent element plays a minor role in the cleaner. It has been found that abrasive powders containing as low as 5 to 10% active detergent have very good foaming and detergent properties [38].

2.4 Spray Drying of Detergent Slurries

The spray drying of soaps and detergents has been practised for many years. The first spray dryer was patented as early as 1865 but its large scale introduction did not occur until the nineteen-twenties [45]. At the turn of the century soaps were air dried by atomising a molten mass of soap into a counter-current flow of cold air. The air cooled the droplet below its crystallisation point and the bulk of the moisture present in the original droplet remained in the powder. This is unlike spray drying in which the moisture in the droplets is either completely removed or evaporated to a predetermined degree. This process, known as spray cooling, is still used extensively [43].

In recent years the soap and detergent industry has seen an increase in the production of liquid detergents for domestic use. However, the detergent powder market is still bouyant with an increasing demand for high bulk density powders. High density powders can be produced by careful control of the atomisation and drying conditions of the detergent slurry or by grinding the dried powder into a uniform particle size. Post-drying size reduction has the disadvantage that it involves a secondary unit operation and hence added expense.

The alternative method, of controlling the atomisation and drying conditions, is more difficult to accomplish satisfactorily and requires laboratory and pilot-plant investigation to achieve the specific requirements of the final product. The general effects of changes in operating conditions, slurry characteristics and nozzle dimensions can be predicted. For example, dilution of the slurry will usually reduce the size of the droplets and narrow the distribution spread; within certain limits an increase in pressure or a decrease in the nozzle orifice diameter has the same effect. However, no generalisations are possible concerning other relevant factors, for example, solids content and drying mechanisms, since they depend upon the individual slurry and the design of the drying tower.

2.4.1 Atomisation of Detergent Slurries

Many standard atomisation devices are unsuitable for use with detergent slurries since they produce a large percentage of droplets less than 100μm which would result in a

very dusty product. Generally the industry employs either centrifugal pressure nozzles or rotary atomisers in spray drying towers; the centrifugal pressure nozzle is preferred as it allows for higher through-put and easier maintenance.

Centrifugal pressure nozzles are, for most industrial spray drying applications, attached to a ring main system with several nozzles, often as many as six, spraying into the same tower. Each nozzle can be individually isolated should it become clogged with slurry and it is standard practice to have a spare nozzle in the ring main to replace the blocked one. Alternatively nozzles may be on individual feed lines fed from the tower circumference and facilitating withdrawal for manual cleaning. The major disadvantage with centrifugal pressure nozzles is that they are very susceptible to erosion caused by abrasion of the solids suspended in the slurry. Theoretically, the erosion should be annular, but in practice it rarely is; generally nozzle wear is irregular, sometimes only minutely, which results in a product that is off specification. Therefore, each nozzle must be frequently checked for signs of wear or irregularities in its operation.

2.4.2 Detergent Spray-Air Contact

Both co-current and counter-current drying towers are used to produce detergents and many drying towers are flexible enough to use either type of air flow in order to handle special formulations or achieve a specific bulk density for the dried product [1]. The use of counter-current air flow with pressure nozzle atomisation is the preferred condition for producing high bulk density detergents. Hot air from direct-fired air heaters enters at the base of the tower and the exhaust air is drawn from the top of the tower. The inlet temperature varies according to the product, with up to 400°C being used for some detergents. Lower temperatures are used for fine washing agents, the exact value being determined by the organic content of the feed. Co-current dryers are generally used to produce low bulk density detergents, ie 0.2 to 0.3 kg/l but some spray drying towers rely upon counter-current swirling flow to encourage particle agglomeration and increase the overall bulk density of the finished product.

2.4.3 Drying of Slurry Droplets

Investigation of the morphology of the dried particles reveals that the particles are hollow. This indicates that an impervious crust forms on the surface of the droplet, the thickness of which will depend upon the nature of the slurry and the drying conditions. As the internal moisture vaporises the droplet generally tends to expand to create a hollow shell and eventually the crust fractures, creating a 'blow hole', through which the vapour escapes. However, this form of expansion does not occur when the crust thickness equals the droplet radius. This latter case was assumed by Audu [46], who showed that droplet drying mechanisms were unaffected by the formulation of the detergent slurry and concluded that after crust formation the vapour-liquid interface receded into the droplet with evaporation occuring by diffusion of water through pores in the crust.

Table 2.2: *Typical particle size distributions of detergent powders [1]*

Particle Size	Light-duty Detergent	Heavy-duty Detergent
1500 μm	0 %	2 - 3 %
500 μm	10 - 15 %	10 - 20 %
250 μm	40 - 60 %	40 - 60 %
120 μm	70 - 80 %	70- 80 %
60 μm	95 -100 %	95 - 100 %

The final particle size is slightly affected by the formulation and usage of the detergent. Typical dried particle sizes of two detergent formulations are given in Table 2.2; this demonstrates that heavy-duty detergents are generally coarser than light-duty detergents.

Chapter 3: The Measurement of Sprays, Droplets and Particles

Introduction

Many processes involve, at some stage, the formation, transfer and/or recovery of a particulate material, as either a powder, emulsion or liquid droplets in a spray. Often the particle or droplet size determines the process efficiency or affects the product performance. Spray drying is one of the many industrial processes where knowledge of the initial droplet or particle size is critical for the maintenance of product quality.

Particle size analysis is the quantitative determination of the size, shape and poly-dispersity of particles in the system under investigation. One common phenomenon with systems of this type is the presence of a particle size distribution, ie the occurrence of a range of particle sizes. Consequently a knowledge of the characteristics of a single particle is of limited importance but the mean characteristics of a large number of particles has more practical use and can be studied statistically. However, knowledge of these characteristics is of no practical value unless an adequate correlation can be established based upon the physical properties of the system or the controllable process variables.

3.1 Particle Size Analysis

In order to successfully determine the nature and characteristics of a spray it is necessary to establish and define the conventional terminology used throughout this analysis:

Feed - This is the initial state of the fluid before its disintegration into a spray. It is usually a slurry, liquid or paste under specific conditions for a particular experiment or production run. The sample is generally characterised by feed temperature, concentration, viscosity, surface tension and density.

Spray - The spray is the sample in its disintegrated or atomised state. It is characterised by the operating conditions and design parameters of the nozzle and the physical properties of the sample medium.

Droplet - A droplet is an individual unit of the spray after atomisation. The spray will consist of droplets whilst surface moisture is present (ie, no crust has formed on the surface of the droplet). In this analysis it is assumed that a droplet remains spherical from conception until an entire crust has formed around the droplet. Once a crust or skin has been formed upon the surface of the droplet its elasticity is severely restricted and it is less likely to return to its original spherical shape after deformation.

Particle - A particle is an individual unit of the spray after the formation of a crust upon the surface of the droplet. At this stage a particle can no longer be assumed to be spherical as its shape is now determined by the type of surface crust formed (for example, plastic, rigid or forming a skin) and phenomena in its drying history, ie shrinkage, expansion or rupturing.

Agglomerate - An agglomerate is the resultant form when two or more droplets or particles coalesce during their passage through the drying tower. Generally any form of agglomeration is undesirable in spray drying, since it results in a wider size distribution and the agglomerates take longer to dry and often result in the presence of partially-dried particles at the exit of the drying tower. However, the principle of agglomeration can be used to coat partially-dried droplets whilst they are being dried. Furthermore in some spray drying processes the gas flow pattern may be arranged such that it promotes agglomeration of fines into particles, to result in a shift in the size distribution of the product [23].

Particle Shape - It is assumed, in the course of this analysis that all the droplets are spherical. In reality many spray dried products consist of non-spherical particles because of droplet/particle distortion during drying. In these cases shape is defined as the ratio of the maximum and minimum measured diameters. Alternatively a shape factor can be used to express divergence from sphericity; it is defined as the ratio between the actual surface (or volume) of the particles and the surface (or volume)

obtained from size measurement (for example, sieving) assuming the particles are spherical.

Size - Size describes the representative dimension of the droplet or particle. For spherical bodies this dimension is usually the diameter. In the case of a non-spherical body the dimension is given by a line drawn between two external points passing through the centre of gravity in a linear plane. As the latter will lead to the possibility of an infinite number of non-equivalent diameters capable of satisfying this definition, the size of an irregular body is a statistical average of all the non-equivalent diameters. Since it is assumed that the droplets are spherical then the representative dimension will be taken as the droplet diameter. However, the representative dimension for the dried particles will be more difficult to determine experimentally unless it is assumed that there is very little deviation from sphericity.

Size-Distribution - The disintegration of a liquid into a spray by an atomiser does not produce droplets of a uniform size. The atomisation mechanism inevitably produces a series of droplets which fall within a maximum and minimum to produce a distribution of sizes. The droplet size distribution in the spray is related to the operating parameters of the nozzle and the physical properties of the feed (This will be discussed in more detail in Chapter 6). The size distribution can be represented as number, diameter, area or weight/volume and the data are usually presented as a frequency or cumulative distribution curve. For convenience all size distributions will be measured as a volume distribution unless otherwise specified.

3.1.1 Distribution Functions

A number of mathematical relationships have been developed by various authors [47-49] to represent size distributions. The most common distribution models are described below.

Normal Distribution

This has limited use in modelling distributions by weight as physical processes tend to give particle distributions which are normal in number. However, it may be used in

situations of a narrow size distribution. A plot of the number of droplets or frequency against droplet size results in a 'bell-shaped' curve. The droplet frequency is given by,

$$d(N) = \frac{1}{S_N\sqrt{2\pi}} \exp\left[\frac{-(D - D_m)^2}{2 S_N^2}\right] \qquad - 3.1$$

where: d(N) is the relative frequency at size d,

S_N is the standard deviation of particle sizes,

D_m is the sample mean.

Log-Normal Distribution

This model has a theoretical basis for droplet formation and comminution processes such as grinding. The distribution is based upon two parameters, the geometric mean size (D_{GM}) and the geometric standard deviation (S_G). The geometric standard deviation is the ratio of the corresponding oversize values of 50% and 15.9% (or undersize values of 84.1% and 50%). The droplet frequency is given by,

$$d(N) = \frac{1}{D S_G\sqrt{2\pi}} \exp\left[\frac{(\log D - \log D_m)^2}{2 S_G}\right] \qquad - 3.2$$

Table 3.1: *Mean Diameter Transformation*

Mean Diameter	**Transformation** (Natural Logarithms)
D_{AM} (Linear or Arithmetic mean)	$\ln D_{GM} + 0.5 \ln 2S_G$
D_{SM} (Surface mean)	$\ln D_{GM} + 1.0 \ln 2S_G$
D_{VM} (Volume mean)	$\ln D_{GM} + 1.5 \ln 2S_G$
D_{VS} (Volume-Surface mean)	$\ln D_{GM} + 2.5 \ln 2S_G$

The Log-Normal distribution permits the determination of the geometric mean size and deviation, and with this data other mean diameters (illustrated in Table 3.1)

can be calculated. This is possible since the nature of the Log-Normal distribution law means that the geometric standard deviations on number, weight, surface and area bases are equal. The Log-Normal distribution is applicable to represent sprays from rotary (vaned-wheel) atomisers.

Square Root Normal Distribution

This distribution is similar in form to the Log-Normal distribution. Both distributions have a mean and standard deviation. The Square Root distribution is often used to characterise centrifugal pressure nozzles, as the distribution represents the spray droplet size data with more accuracy than the Log-Normal distribution. The droplet frequency distribution is given by,

$$d(N) = \frac{1}{\sqrt{8\pi D S_G}} \exp\left[\frac{-\left(\sqrt{D} - \sqrt{D_m}\right)^2}{2 S_G}\right] \qquad - 3.3$$

Upper Limit Distribution

This is a development of the Log-Normal distribution proposed by Mugele & Evans [47]. It contains a third parameter, the stable maximum droplet size, which allows more flexibility in fitting experimental data. The basis for the distribution is the fact that all sprays are made-up of droplets that have a maximum size (ie, the upper limit) and practical limits are placed upon the maximum and minimum droplet sizes (unlike the Square Root distribution, which gives meaningless values in the maximum size range). The droplet frequency distribution is as follows,

$$d(N) = \frac{1}{D S_G \sqrt{2\pi}} \exp\left[\frac{-\log\left(d_{max} - \frac{D}{D_{GM}}\right)^2}{2 S_G^2}\right] \qquad - 3.4$$

Nukyama-Tanasawa Distribution

This distribution [48] is proposed as suitable for representation of sprays from pneumatic nozzles. For the distribution to apply, a plot of (log $1/D^2$ d(N)) against D^q

the pressure nozzles. In normal circumstances both models would be tested under similar conditions to determine the one most suitable for this particular work. However, one limitation of the Malvern Particle Size Analyser and similar systems is that a distribution model is required as part of the data interpretation stage (ie, in transforming the light energy data into particle size data - see Section 3.3). This severely limits the distribution models available for use to those included in the program software which, based upon the arguments listed above, effectively means the Rosin-Rammler distribution.

However, although Malvern Instruments recommend that the Rosin-Rammler distribution model should be used for particle size determination involving centrifugal pressure nozzles [50], recent work [51] has discovered that a Model Independent analysis is more suitable for this type of work. As the name suggests this 'model' is independent of a distribution, which has the advantage that no 'smoothing' of the raw data occurs due to force-fitting of experimental data. Although, as mentioned previously, it is usual practice to test both models under experimental conditions to find the most suitable, the Rosin-Rammler distribution was used as a basis of this work. This was done since the mathematical model predicts the Rosin-Rammler parameters and knowledge of these parameters from the experimental work was required in order to test the computer simulation.

3.1.3 Mean Diameters

A mean diameter is a mathematical value intended to describe the entire spray. The values can be a measure of number, length, area or volume and are defined by the following equation,

$$D(F,G) = \left\{ \frac{\int_{d_{min}}^{d_{max}} D^F n(D)\, dD}{\int_{d_{min}}^{d_{max}} D^G n(D)\, dD} \right\}^{\left[\frac{1}{(F-G)}\right]} \qquad - 3.7$$

where: D is the mean diameter,

F, G are integers (or zero),

n(D) is the number distribution.

The mean diameters computed by the Size Analyser are given in Table 3.2. The most significant of these diameters is the Sauter Mean Diameter or Surface-Volume mean diameter, D(3,2), which is generally taken as the representative diameter of the entire spray.

Table 3.2: *Definition of Mean Diameters*

Mean Diameter		Field of Application
D(1,0)	Number, Length Mean Diameter	Comparison, Evaporation
D(2,0)	Number, Surface Mean Diameter	Absorption
D(2,1)	Length, Surface Mean Diameter (Hydraulic Mean Diameter)	Settling, Sedimentation
D(3,0)	Number, Volume Mean Diameter	Hydrology
D(3,1)	Length, Volume Mean Diameter	Evaporation, Diffusion
D(3,2)	Surface, Volume Mean Diameter (Sauter Mean Diameter)	Process Efficiency, Mass Transfer
D(4,0)	Number, Moment Mean Diameter	
D(4,1)	Length, Moment Mean Diameter	
D(4,2)	Surface, Moment Mean Diameter	
D(4,3)	Volume, Moment Mean Diameter (Debroukier Diameter)	Combustion Equilibrium

Most Frequent Diameter

An alternative method of characterising the spray is to use the most frequent diameter, D_f. This size can be found from tabular results and, when presented graphically, it

corresponds to the highest value on a frequency curve or a point of inflection on a cumulative curve (See Figure 3.1).

Figure 3.1: *Droplet Size Distribution Frequency and Cumulative Curves*

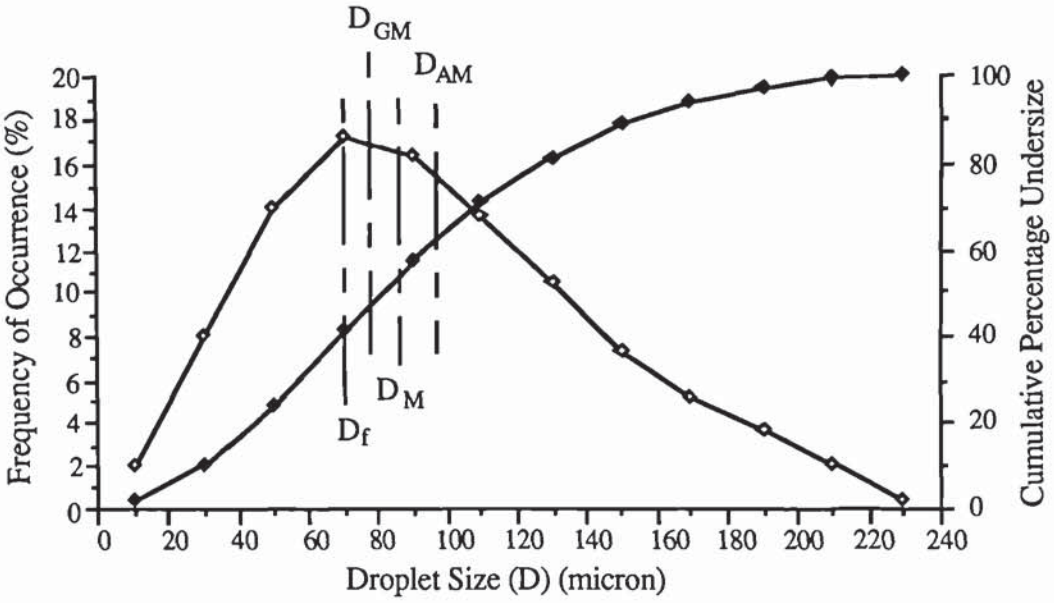

Arithmetic Mean Diameter

This is defined as the sum of the diameters of the individual droplets divided by the number of droplets. This mean diameter is most significant when the size distribution is not overbalanced by either very large or very small droplets. The Arithmetic mean can be defined in terms of a frequency curve, where

$$D_{AM} = \frac{1}{100}\int_{d_{min}}^{d_{max}} D\, n(D)\, dD \qquad - 3.8$$

Geometric Mean Diameter

This is defined as the *n*th root of the product of the diameters of the *n* droplets analysed. The Geometric mean is always smaller than the Arithmetic mean. The Geometric mean for droplets according to their sizes D_1 D_2 .....D_n (where n(D) is the percentage occurrence of a given size) is represented by,

$$D_{GM} = \sqrt[100]{\left[D_1^{F_N(D_1)} D_2^{F_N(D_2)} \ldots\ldots\ldots D_n^{F_N(D_n)}\right]} \qquad - 3.9$$

Median Diameter

The median diameter is defined as the diameter above, or below, which fifty percent of the total number of droplets lie and divides the area under the frequency curve into two equal parts. The median diameter is particularly useful when a wide size-distribution is present and is represented by the fifty percent line on the cumulative curve (Figure 3.1).

The arithmetic mean and median diameters are divergent and the relationship between them follows no definite rule, as any relation depends upon the skewness or bias of the distribution. The parameter selected is appropriate to the circumstances of sampling. In general the arithmetic mean diameter is greater than (or, at best, equal to) the median diameter.

3.2 Measuring Techniques

The droplet size distribution is the most important fundamental characteristic of a liquid spray. It is also one of the most difficult properties to determine experimentally or predict theoretically. Despite this, much attention has been given to experimental methods for determining the droplet size distribution in a spray. However, the droplet sizing techniques are often limited to particular operating conditions; consequently it is difficult to recommend a definitive method. Reviews of the various techniques employed in the literature have been given by Azzopardi [52], Marshall [53] and Dombrowski & Munday [4]. The methods illustrated below have been used by workers conducting investigations in the field of atomisation and are grouped together in terms of the phenomena employed (ie, photographic, impact, thermal, etc.).

3.2.1 Impaction Methods

Sampling Slides

One of the most popular methods of droplet sizing has been by the examination of the results of their impaction on solid surfaces or in thin, viscous liquid films. In the

course of their studies on atomisation workers have developed and utilised several types of sampling slide.

The use of a magnesium oxide coated slide has been the most favoured method used by previous workers [54-57]. This method was first used extensively in the 1940's. It has been discussed in detail by May [58], who stated that it could be used for droplets of any liquid, was convenient and easy to use, and that no errors arose due to droplet coalescence after impact, although it had little use in cases when droplets were less than 10μm.

Other workers have used greased films [48][59-61] and soot [62] as the collection medium on the sampling slide.

In all of these methods the impacting droplet produces a crater which is drop-size dependent. Several relationships have been proposed for drop-size in terms of crater diameter, they are usually of the form:

$$D = I_c C_t \qquad - 3.10$$

where: D is the diameter,

I_c is the impression coefficient,

C_t is the crater diameter.

May determined values for I_c to be 0.86 for droplets in the range 20 to 200μm and 0.75 for droplets in the range of 10 to 15μm. Clearly, however, the relationship in equation (3.10) is velocity dependent and Stoker [63] used an empirically derived relationship to determine the impression coefficient based upon the droplet Weber number,

$$I_c = 0.77\, We^{0.2} \qquad - 3.11$$

The major limitation of this method is that of 'over-sampling', ie of dense sprays either obliterating the initial crater or by-passing the sample slide, and an unrepresentative result being obtained. The latter problem can be resolved by the use of multiple slides or a cascade sampler as described below.

Cascade Sampler (or Impactor)

Two versions of this instrument have been presented in the literature [64][65]. In each a series of microscope slides are positioned in front of directional jets with decreasing orifice sizes (See Figure 3.2) and the droplet flow through the impactor is assisted by a vacuum pump attached to the outlet of the instrument. This set-up causes an increase in the momentum of the droplets by decreasing the by-pass area in the impactor. This enables the momentum of the smaller droplets to gradually increase until they achieve impaction on the slide.

May specified that his instrument [64] was for use with droplet sizes in the range of 1.5 to 50μm, although the minimum drop size could be lowered with the addition of more slides. He stated that it was possible to use either a coated slide (as described above) or a plain glass slide, carefully cleaned, with a correction factor to account for 'spreading' of the droplet on the slide. After collection the droplets were counted microscopically using a specially developed reticule.

The version developed by Mitchell & Pilcher [65] was for use with smaller particles (ie, less than 25μm, as larger particles would be included in the material impacting on the first slide). After an initial calibration by microscopic counting, to obtain the cut-off ranges for each slide, no further calibration was required and the results were presented as a mass distribution. They reported that problems arose due to 'wall loss' (ie, droplets impacting within the impactor) and presented an equation to account for it,

$$\eta_w = \left[e^{-\left(0.00428\, D_s^2 \times Q^{1.5}\right)}\right] \times \left[\frac{D_p^2 Q^2}{10800\, D_j^3}\right] \qquad - \ 3.12$$

where: η_w is the fraction impacted on the wall

D_{ws} is the wall to slide distance, cm

D_j is the diameter of the impactor jet, cm

D_p is the diameter of the aerosol particle, μm

D_s is the diameter of the impactor slide, cm

Q is the volumetric flowrate, l/min

Figure 3.2: *Cascade Impactor (Mitchell & Pilcher [65])*

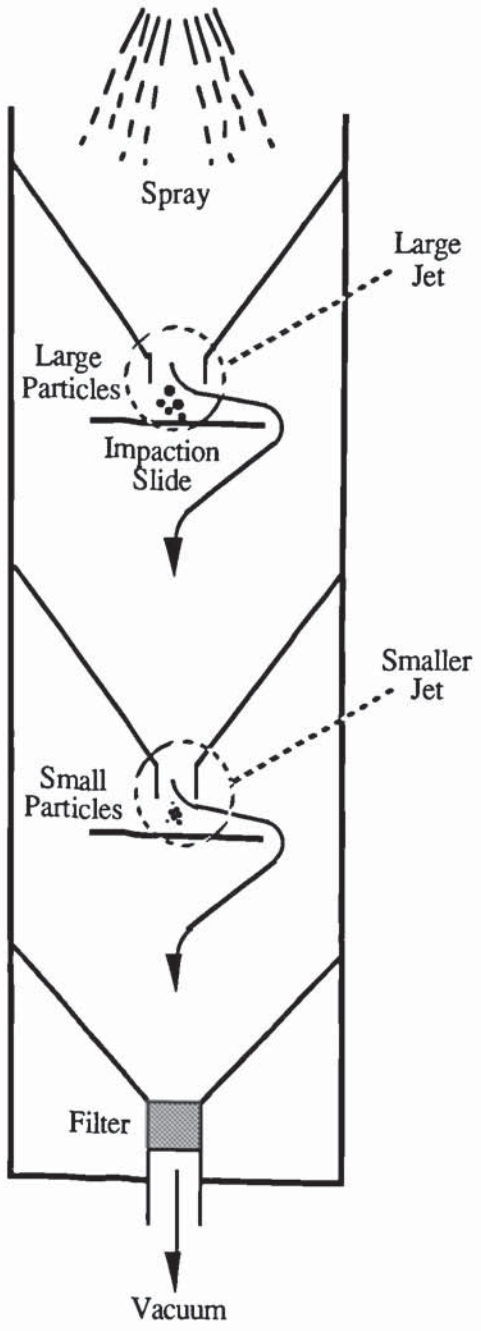

In a more recent paper May [66] updated his earlier work by reviewing the cascade designs subsequently developed and developed a new impactor which was able to sample the entire size range of airborne particles in eight stages (twice as many stages as in his earlier design). He concluded that internal losses in the new design had been reduced to negligible quantities.

Collection Baths

This method of droplet size determination involves spraying one liquid into a bath containing another immiscible liquid. This has the advantage that a sample of the spray can be captured and subsequently photographed to determine the droplet size. A variety of collection media have been used by previous workers; the most common are summarised in Table 3.3. Although there has been no definitive choice of liquids given in the literature, it is important that the collection liquid fulfils the following requirements [67]:

(i) the two liquids must be immiscible;

(ii) the collection liquid should prevent the droplets from coalescing;

(iii) the drop-liquid aggregate should remain stable for a time sufficient for photography or microscopic examination.

Rupe [68] presented a detailed review of this technique and developed a method based upon one previously used by Doble [69].

Table 3.3: *Various Types of Collection Bath*

Spraying Liquid	Collection Liquid	Authors
Dyed Water	Stoddard Solution	Rupe [68], Tate [70], Darnell [71], McIrvine [2], Tate & Marshall [72].
Water	Castor Oil	De Juhasz *et al* [67], Doble [69], Straus [73], Fraser & Eisenklam [74]

Tate & Marshall [72] modified Rupe's original method and introduced a brass collection cell with an optically flat glass bottom. The glass was coated to ensure that the droplets did not spread along the surface upon contact and the entire cell was housed in a shuttered enclosure to enable a sample to be obtained at any desired position from the nozzle. Tate [70] used the same type of cell in later work, which updated the method and introduced a mathematical prediction of the number of droplets

caught in the cell from the physical dimensions of the cell, the shutter speed and Volume-Mean Diameter of the sample.

The inherent problems of this sampling method are of droplets shattering upon striking the surface of the collection liquid and the coalescence of droplets in the bath caused by 'over-sampling'. It was therefore important to sample a small amount of the spray by using some form of sampling lid for the bath and carefully restricting the impact velocity of the spray to avoid the droplets shattering.

Stained Paper

A variation of the impaction slide method is to spray dyed water, or similar colour-inducing substances, onto absorbent paper. The drop size can then be determined by measuring the diameter of the stain produced on the paper. This method was used by Dorman [75] in his work using fan spray nozzles. He initially used a microburette to obtain a calibration of stain size against drop size. The work was conducted at temperatures around 12°C so that the evaporation loss could be considered to be negligible. Dorman stated that this method was not very accurate for sizing droplets below 100μm. This was due to the inaccuracy caused by measuring small stain sizes and also the production of non-spherical stains as the fibrous structure of the paper caused the dye to run. However, the results obtained were reproducible and the errors caused by measuring small droplets were reduced by using the relevant statistical diameters.

Schweitzer [76] used a variation of this method in his work, although he was not measuring the droplet size distribution but the dispersion of liquid jets at various distances from the nozzle. He collected liquid on blotting paper arranged in a series of concentric rings and subsequently weighed each ring to determine the extent of liquid dispersion. If it is assumed that the smaller (lighter) drops are dispersed further than larger (heavier) drops, then rather crude size distribution results can be obtained from his work.

3.2.2 Thermal Methods

Drop size can be determined by forcing the spray droplets to undergo a change of state. The two most common methods involve the correlation between droplet evaporation time and size [77] [78] and direct freezing of the spray by collection at low temperature [79] [80]. A variation of the latter method has been developed by previous workers [81] [82] using a substitute liquid, such as molten wax, that will solidify at room temperature to give a representative distribution.

Droplet Evaporation

This method involves the impingement of the droplet(s) onto a hot surface to yield an evaporation time that is drop-size dependent. Leonchik *et al* [77] used a heated mica sheet for this purpose and weighed and photographed droplets on the mica sheet during evaporation. The initial problem they had to overcome was avoiding coalescence of the droplets; this was achieved by coating the mica sheet with a hydrophobic material, such as dimethyl-dichloro silane, and taking care to ensure that individual droplets remained at least two diameters apart. The method was considered suitable for obtaining a drop size distribution in a localised area but a knowledge of the spray density is required in order to determine the distribution of the entire spray. An alternative technique was employed by Van Passer [78], who used a thin hot wire to avoid the problem of retaining droplets on a flat surface. In this method heat was continuously dissipated, by forced convection, into the surroundings and when a droplet impinged on the wire it caused a notable deflection in the readings that was proportional to droplet volume. Good correlations were obtained between droplet radius and temperature, although problems arose due to the requirement that the wire must be strong enough to withstand droplet impact and a tendency for smaller droplets to by-pass the wire.

Gretzinger & Marshall [83] combined the principle of evaporation and particle collection in an oil bath during their work involving pneumatic atomisers. They evaporated an aqueous dye solution and determined the size of the resulting dye

aerosol particles. This was then related to the initial drop size of the spray by the concentration of the original dye solution.

Droplet Freezing

This technique enables the entire spray to be collected and sized, using a standard solid particle sizing method (for example, sieving), whilst the droplets are maintained at a low temperature. The most popular freezing media are alcohol or hexane in a dry ice bath [79][84] or liquid nitrogen [80].

Taylor & Harmon [79] sprayed water into a bath containing liquid hexane, cooled by dry ice and determined the droplet sizes by applying Stoke's Law as they fell onto a weigh-pan. An average value was used for the Stoke's drag coefficient which caused a 6% error in the mean droplet diameter calculation. A similar method was employed by Longwell [84] in his work on fuel oil atomisation. He collected a sample of the oil spray, taken across the radius of the spray cone, in a bath containing a mixture of alcohol, glycerine and water which was cooled by dry ice. The contents of the bath were then sieved in a cascade unit consisting of four sieves in a vacuum flask cooled by dry ice; each sieve was then weighed to obtain the droplet distribution.

Nelson & Stevens [80] froze a variety of liquids using liquid nitrogen. This was achieved by spraying directly into a cold atmosphere and collecting the partially frozen spray in liquid nitrogen; this procedure reduced droplet fracture upon contact with the liquid. The frozen droplets were sieved and subsequently weighed whilst still frozen. This method is not suitable when liquids are in equilibrium with their own vapour and is limited to freezing temperatures between those of carbon dioxide and water, to prevent errors occurring due to the solidification of the carbon dioxide.

Solidification (or Substitute Liquid Method)

This technique was originally developed in World War II in conjunction with research into fuel atomisers for the Whittle jet engine [85]. The method was further developed by Joyce [81] as part of his work on liquid fuel atomisation and has subsequently been used by Clare & Radcliffe [86] and Turner & Moulton [87]. Later work presented by

Hasson & Mizarhi [82] compared particle sizes obtained by this method to the droplet sizes determined by spray impaction on a glass slide [58], as described above.

The most common choice of substitute liquid, especially for work on fuel oils, is paraffin wax [81] [82] [86]; although other workers [87] have used organic materials such as beta-naphthtol or benzoic acid. The main criterion for the type of liquid employed is that it should solidify at above ambient temperature. In all cases the method basically involves spraying the 'liquid' in its molten state, where-upon it solidifies at ambient temperature and the resultant wax droplets are then classified by sieve analysis.

Hasson & Mizrahi [82] concluded that the droplet sizes obtained by the solidifying wax method were generally larger than those determined by the impaction method due to the contraction of the wax particles caused by cooling/solidification. This, they reasoned, represented the droplets in the initial part of the disintegration zone and the method was best suited for spray drying and combustion applications.

3.2.3 Photographic Methods

It is inherently difficult to photograph small, rapidly moving droplets with enough clarity to obtain an accurate measurement of their particle size. Nevertheless photographic methods are one of the most popular measurement techniques employed in the field of atomisation research. This is mainly because, with the correct type of lighting, successful results can be obtained using relatively simple techniques and equipment. Generally, workers have opted to use either of the two methods discussed below.

Illumination Methods

Three major forms of illumination are used to create the effect of 'stopping' the droplets for the purpose of photography:

Strobe - This is probably the most convenient method of illumination in that the strobe can be manually adjusted to match the droplet velocity. It has been used extensively for work involving the break-up of liquid jets, for example, as in reference [88]. A

typical high speed photograph will use a strobe speed in the region of 1000 cycles per second, although it is often necessary to employ two synchronised strobescopes to provide sufficient lighting for photography.

Flash - This method of illumination can either be used as a single unit to measure the droplet size from the liquid jets, for example, as in reference [89], or from sprays, for example as in reference [90]. Alternatively a double flash unit, employing a time delay in the range of micro-seconds, or even nano-seconds, can be used to obtain the velocity and size of the liquid droplets, for example, as in reference [91].

Spark - This method was superseded by the introduction of the flash unit. It involved the creation of a spark which was subsequently focused onto the liquid droplets to provide illumination for photography, for example, as in reference [92].

Extensive use has also been made of these photographic methods in the investigation of liquid sheet disintegration and atomisation mechanisms. Numerous work has been presented in the literature containing photographs that illustrate wave propagation. A classic example is that of Dombrowski & Fraser [6] who extensively photographed fan sprays in their investigation into liquid sheet break-up. In later work Dombrowski & Hooper [7] used a similar method to measure the wavelength of the disturbances on flat liquid sheets to provide data for their theoretical evaluation.

Light Absorption Method

This method relates the droplet diameter to the amount of light the spray absorbs from a light beam intersecting the spray. It was first introduced by Sauter [93] and was later adapted by Fraser *et al* [94] for their work.

The method is limited only to the determination of a mean droplet diameter (Sauter Mean Diameter) but is favoured over other photographic methods because it is quicker, since it does not require knowledge of the number of droplets present in the sample. In the apparatus developed by Fraser *et al* [94] the light beam initially passed through a slot of known dimensions before intersecting the spray, the resultant beam then striking a photomultiplier. A second photomultiplier was used to record the

incident light from the source in order to counteract any variations in the light output. It was then possible to determine the surface-volume mean diameter from the equation:

$$D_{VS} = 1.5\left[\frac{Q_l}{V_{ds}\, c \ln\left(1 - A'/100\right)}\right] \qquad - 3.13$$

where, D_{VS} is the surface-volume mean diameter,

Q_l is the liquid flowrate through the plane of the light beam,

V_{ds} is the mean droplet velocity,

c is the width of the light beam,

A' is the uncorrected light absorption term.

The mean droplet velocity was determined by dual flash photography and the flowrate passing through the beam was calculated by determining the inner and outer diameter of the spray from the expression:

$$Q_l = \frac{4\, c\, Q}{\pi\left(d_{so} + d_{si}\right)} \qquad - 3.14$$

where, d_{so} is the inner diameter of the spray,

d_{si} is the outer diameter of the spray,

Q is the total liquid volumetric flowrate.

Dombrowski & Wolfsohn [95] adapted the method for use with swirl chamber pressure nozzles which resulted in a modified form of equation (3.13):

$$D_{VS} = 1.5\left[\frac{Q_l}{V_{ds}\, c \ln\left(1 - A'/100\right)^{-1} \cos\theta/2}\right] \qquad - 3.15$$

where, θ is the cone angle of the spray.

In later work [96] they compared drop sizes determined by this technique with comparative sizes determined by a standard photographic method. The results showed reasonable agreement with the photographic results obtained, being approximately 11% greater than those obtained by other methods.

3.2.4 Optical Methods

Three major optical techniques are commonly employed for the determination of particle size. The basic apparatus for all three methods is a low-powered laser that acts as a constant monochromatic light source.

Light Scattering Methods

The intensity of light scattered by a particle depends upon the intensity of the illuminating radiation, the diameter and refractive index of the particle, the wavelength and polarisation of the light and the direction of observation relative to that of illumination. The theory of light scattering was formalised by Mie [97] who, on the basis of electromagnetic theory obtained a solution for the diffraction of a plane monochromatic wave-form by a sphere of any diameter and of any composition situated in a homogeneous medium.

Swithenbank *et al* [98] developed this theory into a particle sizing technique based upon laser diffraction. This technique has subsequently been used in an instrument that has been marketed commercially for several years by Malvern Instruments. A review of this sizing technique is given later in Section 3.3.

Laser-Doppler Anemometry

Laser-Doppler anemometers use the frequency information contained in light scattered by particles passing through an interference pattern to determine their velocity. As the intensity of the scattered light depends upon particle size, the instrument can also be used for particle size determination. An example of this type of equipment has been reviewed by Farmer [99] who stated that it could successfully measure particles in the range 10 to 120μm, but could not explain why the size range could not be extended beyond these limits.

Holography

A hologram is an interference pattern formed by light scattered by an object and light that is unaffected by it. This produces a three-dimensional scene which can be

recreated at any time. Figure 3.3 indicates the requirements to create a hologram. A beam of coherent light, after being split in two, illuminates the object. The light reflected by the object arrives at the 'target' position (for example, a photographic plate) at the same instant as the reference beam that has by-passed the object and remained unchanged in phase.

In order to examine the hologram it must be illuminated by the reference beam from the same direction as at the time of recording. The hologram acts a diffraction screen for the reference beam and a wave pattern is formed, behind the hologram, which appears to an observer similar to the original object.

Figure 3.3: *Double-beam Holography*

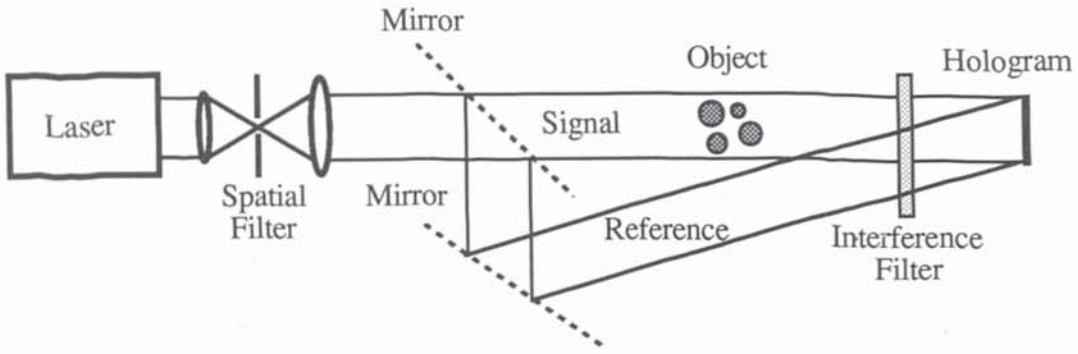

This theory has been transformed into a particle sizing technique, although problems have been reported with submicron particles [100]. Thompson [101] stated that the minimum size which can be measured by this technique is 2μm with an upper limit in the millimetre size range. Webster [102] used the technique to measure particle size and concluded that it offered considerable advantages over photography with measurement conducted in a fraction of the time.

3.2.5 Other Methods of Drop-size Determination

Electrical Charge Methods

Electrical charge techniques generally work on the principle that the droplet completes an electrical circuit as it passes between two needles. The distance between the needles

can be altered and therefore the range of droplets in a spray can be determined. This technique was used by Pye [103] to determine droplet sizes in the range 15μm to 1mm. He concluded that the technique was ideally suited for any fluid that has an electrical conductivity that could produce a measurable pulse and had the advantage that variations in the size distribution within the spray could be determined. However, his system could only determine local size distributions and several electrodes would be required to obtain a representative sample of the entire spray.

Image Analysis

Image analysis is not a separate method of drop-size determination but it has been used in conjunction with photographic methods to assist with the interpretation of results. An early instrument for image analysis is discussed in a paper by Ramshaw [104]. This instrument used the image of a 'flying spot' on a cathode ray tube to scan the photographic negative of the droplets and assigned a diameter to each which was equal to its maximum dimension of the line of scan. Using this method it was even possible to measure droplets that were slightly out of focus, although the technique was subject to hysteresis so that the intensity of the transmitted light had to fall significantly below the triggering level before the spot ceased to record the droplet diameter. This problem was overcome by 'clipping' the light signal at the mean of the extremes where the picture began to clear and to 'smear' (ie, when the droplets cast shadows in the line of scan).

Recent instruments that have been developed (for example, reference [105]) use image enhancement to assist with droplet sizing. This process, not only allows a droplet diameter to be determined by scanning the entire droplet but allows determination of the size of partially obscured droplets by enhancing the droplet image.

3.3 Laser Diffraction Technique

3.3.1 Theory

The illumination of a spherical particle by a parallel beam of monochromatic, coherent light will cause a diffraction pattern to be superimposed on the geometric image. The resultant pattern will be large when compared to the image. When a Fourier Transform Lens is placed in the light path after the particle and a screen placed at the focal plane, the undiffracted light will be focused to a point on the axis of the lens and the diffracted light will form a ring around the central spot. Movement of the particle through the illuminating beam will not cause any shift in the diffraction pattern since light diffracted at angle, θ, will give the radial displacement in the focal plane irrespective of the particle's position (See Figure 3.4). Similarly it does not matter where the particle passes in the beam as its diffraction pattern is always constant at any distance from the lens. The 'far field' diffraction pattern that is produced is termed the Fraunhofer Diffraction Pattern, for which the intensity distribution is given by the equation,

$$I(\theta) = \left[\frac{D J_1\left(\frac{D \pi \theta}{\lambda_i}\right)}{\left(\frac{D \pi \theta}{\lambda_i}\right)} \right] \qquad - 3.16$$

where: J_1 is the Bessel function of the first order 1,

λ_i is the wavelength of the incident light,

θ is the angle at which the scattered light is observed,

D is the particle diameter.

This light distribution would appear as a series of alternating light and dark concentric rings on the screen. These rings represent the maximum and minimum values from equation (3.16) and the diameter of the pattern is inversely proportional to the particle diameter (Figure 3.5). The presence of several particles will produce a summed light distribution from which it should be possible to separate the data to obtain the particle size distribution. The analysis of this process can be found in any

Figure 3.4: *Properties of the Range Lens*

standard text on optics (for example, reference [106]). Swithenbank *et al* [98] replaced the screen with a detector consisting of concentric annular rings of increasing mean radius. Thus the area of the ring detectors increases with increasing mean

Figure 3.5: *Properties of the Scattered Light from Particles*

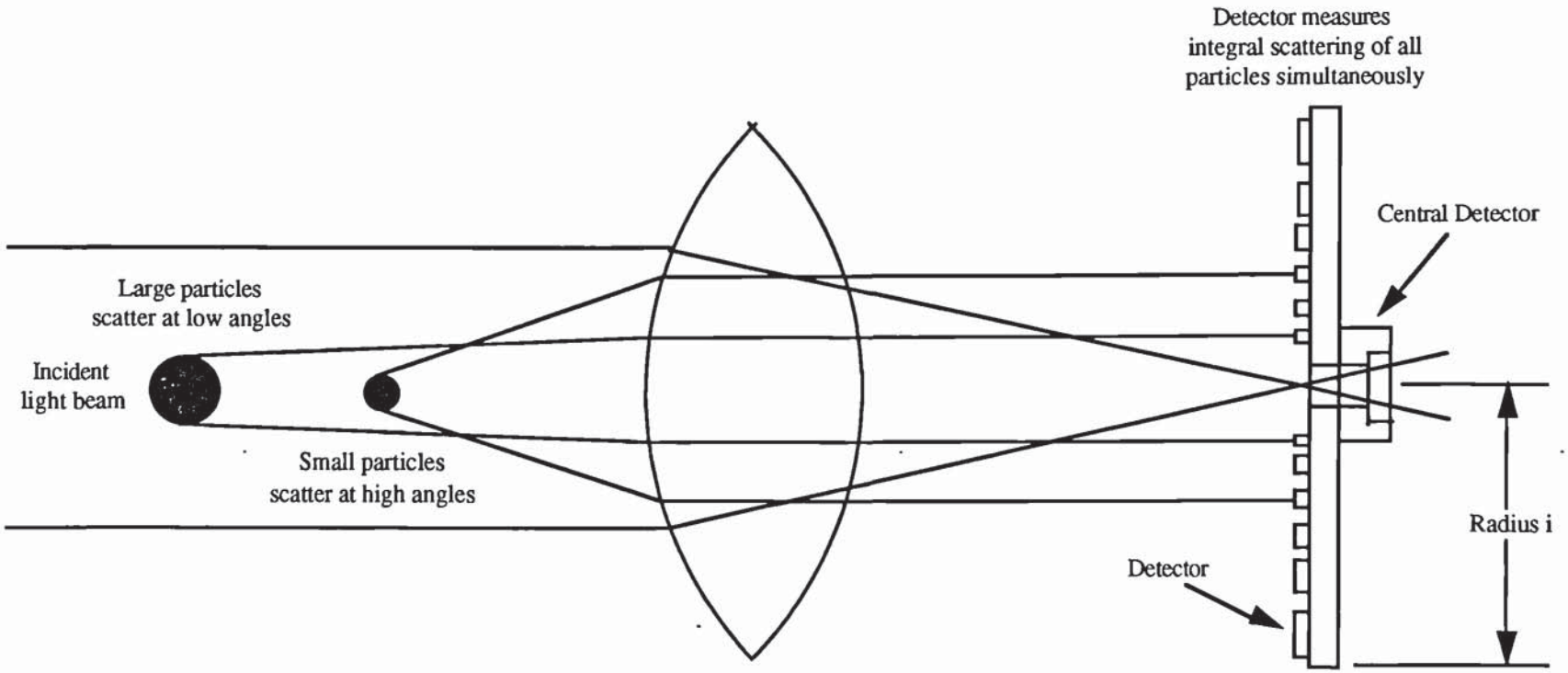

radius. Consequently the total energy detected by each ring does not suffer the extreme intensity variations indicated by equation (3.16).

The energy diffracted into a ring by a single particle is given by equation (3.17),

$$E_{ij} = C^* \frac{\pi\left(\frac{D}{2}\right)^2}{4} \left\{ J_1^{\,2}\left(\frac{D\pi\theta}{\lambda}\right) + J_o^{\,2}\left(\frac{D\pi\theta}{\lambda}\right) \right\}_j - C^* \frac{\pi\left(\frac{D}{2}\right)^2}{4} \left\{ J_1^{\,2}\left(\frac{D\pi\theta}{\lambda}\right) + J_o^{\,2}\left(\frac{D\pi\theta}{\lambda}\right) \right\}_i \quad - 3.17$$

where: i and j refer to the inside and outside radius of the ring respectively,

J_o is the Bessel function of the first kind of order 0,

C* is a constant.

For a distribution of sizes this equation becomes:

$$E_{ij} = \sum_{k=0}^{m} C' N_k d_k \left[\left\{ J_1^{\,2} z + J_o^{\,2} z \right\}_{j_k} - \left\{ J_1^{\,2} z + J_o^{\,2} z \right\}_{i_k} \right] \quad - 3.18$$

where: C' is a constant,

N_k is the number of particles with diameter d_k,

$$z = \left(\frac{D\pi\theta}{\lambda}\right)$$

or, in terms of a weight (or volume) distribution,

$$E_{ij} = \sum_{k=0}^{m} C'' \frac{W_k}{d_k} \left[\left\{ J_1^{\,2} z + J_o^{\,2} z \right\}_{j_k} - \left\{ J_1^{\,2} z + J_o^{\,2} z \right\}_{i_k} \right] \quad - 3.19$$

where: C'' is a constant,

W_k is the weight (volume) fraction of droplets with diameter d_k.

As a similar equation exists for each ring, a matrix equation can be constructed to represent the diffraction pattern,

$$E(I) = W(J) \,.\, T(I,J) \quad - 3.20$$

where: E(I) is the light energy distribution,

W(J) is the droplet weight (volume) distribution,

T(I,J) contains the coefficients that define the light energy distribution for each droplet

However, equation (3.20) can be rewritten as:

$$W(J) = E(I) \cdot T^{-1}(I,J) \qquad - 3.21$$

Then, if the inverse matrix $T^{-1}(I,J)$ is calculated for the detector, the weight distribution can be calculated from the measured light energy E(I).

However, in practice, this approach is not used because of the large dynamic range of the coefficients which can result in considerable computation difficulties leading to non-physical solutions (ie, negative weight fractions in some size ranges). The method used is to assume a form for W(J), for example, the Rosin-Rammler distribution, and itteratively adjust the parameters until the sum of the squared errors, from equation (3.22), is a minimum.

$$\sum [E(I) - W(J) \cdot T(I,J)]^2 \rightarrow 0 \qquad - 3.22$$

The ratio of the light intensity measured at the central diode, before and after the sample medium intersects the light beam gives the fraction of light transmitted through the sample. The transmission is related to the particles' total projected area by the Beer-Lambert law:

$$\ln\left\{\frac{I}{I_o}\right\} = -2L \sum_{S=1}^{m} N_S A_S \qquad - 3.23$$

where: L is the optical path length,

N_S is the number of droplets per unit volume,

A_S is the cross-sectional area of the particles in size class S,

I/I_o is the transmission (or obscuration of light).

This principle is incorporated in an instrument produced commercially by Malvern Instruments Ltd. A number of models are produced but a 2600 series unit was used to conduct work on this project.

3.3.2 Obscuration

The major limitation of this method of analysis is the problem of obscuration. This is the effective 'blocking' of the laser beam by the sample medium. Discrete samples, for example, a calibration reticule, can be positioned at the focal length of the lens with the production of only a negligible amount of obscuration. However, spray samples (for example, from pressure nozzles) intersect the laser beam across a wider range and it is the diffraction of the beam outside the focal length of the receiver lens that causes obscuration. The value of obscuration produced by the sample is determined by the following formula,

$$\text{Obscuration} = 1 - \frac{\text{Light Energy Transmitted by Sample (I)}}{\text{Incident Light Energy } (I_o)} \qquad - \ 3.24$$

Ideal values for the obscuration during sample measurement lie in the region of 0.3 to 0.4; although results have been obtained with reasonable accuracy with obscuration values in the region of 0.8 to 0.9 [50]. However, it is usually assumed that results obtained with more than 50% of the incident light obscured by the sample medium must be treated with caution [107].

Recent work by Felton *et al* [108] has produced correction factors for use when this type of particle size analysis is employed with dense (high obscuration) sample mediums. They first obtained correction factors using glass beads suspended in water as the sample medium; these values were then found to be applicable for use with diesel oil spray. When the correction factors were applied to the results obtained using a laser diffraction instrument it was found to be comparable with results obtained by Dodge [109] using a different method of analysis. They computed correction factors for several distribution models but it is the Rosin-Rammler distribution model that has

the most relevance to this project. The correction factors for the X and N parameters are as follows:

$$C_X = 1.0 + \left[0.036 + 0.4947\,(Ob)^{8.997}\right] N_{App}^{\{1.9 - 3.437\,(Ob)\}} \quad - 3.25$$

$$C_N = 1.0 + \left[0.035 + 0.1099(Ob)^{8.65}\right] N_{App}^{\{0.35 - 1.45\,(Ob)\}} \quad - 3.26$$

where: N_{App} is the apparent value of 'N' determined from the experiment,

Ob is the obscuration measured in the experiment.

These equations were subsequently found to be valid for obscuration in the region of 0.65 to 0.98 and for N_{App} in the range 1.2 to 3.8. For obscuration less than 0.65 the correction factors were comparable with experimental results and were therefore limited by convergence uncertainty.

There are physical solutions to the problem of obscuration. The most common method is to reduce the amount of the sample medium 'blocking' the laser beam. This can be accomplished by surrounding the incident beam of light by a baffle. The length of the baffle is determined so that a representative sample of the spray can still be measured whilst most of the sample medium is prevented from obscuring both the incident and resultant light beams. The details of such a method are described in Chapter 6.

3.3.3 Malvern Series 2600 Particle Size Analyser

The Optical Measurement Unit (Malvern Particle Size Analyser) comprises of two major components: a 2mW He-Ne (Type IIIb) Laser (Optical Transmitter or monochromatic, coherent light source); an Optical Receiver unit consisting of a 300mm Fourier Transform Lens and a detector with 31 concentric ring elements. The unit is linked to an IBM-PC compatible Desk Top Computer to run the software and produce a result print-out via a printer. The basic experimental equipment is illustrated in Figure 3.6.

There are four basic stages involved in the particle size analysis of a sample medium using the Size Analyser;

(i) Alignment: This is the initial stage of the experiment. The detector is positioned to ensure that the laser is hitting it with maximum possible intensity.

(ii) Measure Background: This is the calibration stage of the experiment. The amount of background light that is striking the detector elements is determined and eliminated from further calculations.

(iii) Sample Inspection: This stage computes the amount of obscuration caused by the sample medium.

(iv) Sample Measurement: The particle size distribution is computed from the Fraunhofer Diffraction Pattern using the distribution model chosen for the analysis.

Figure 3.6: *The Malvern Particle Size Analyser*

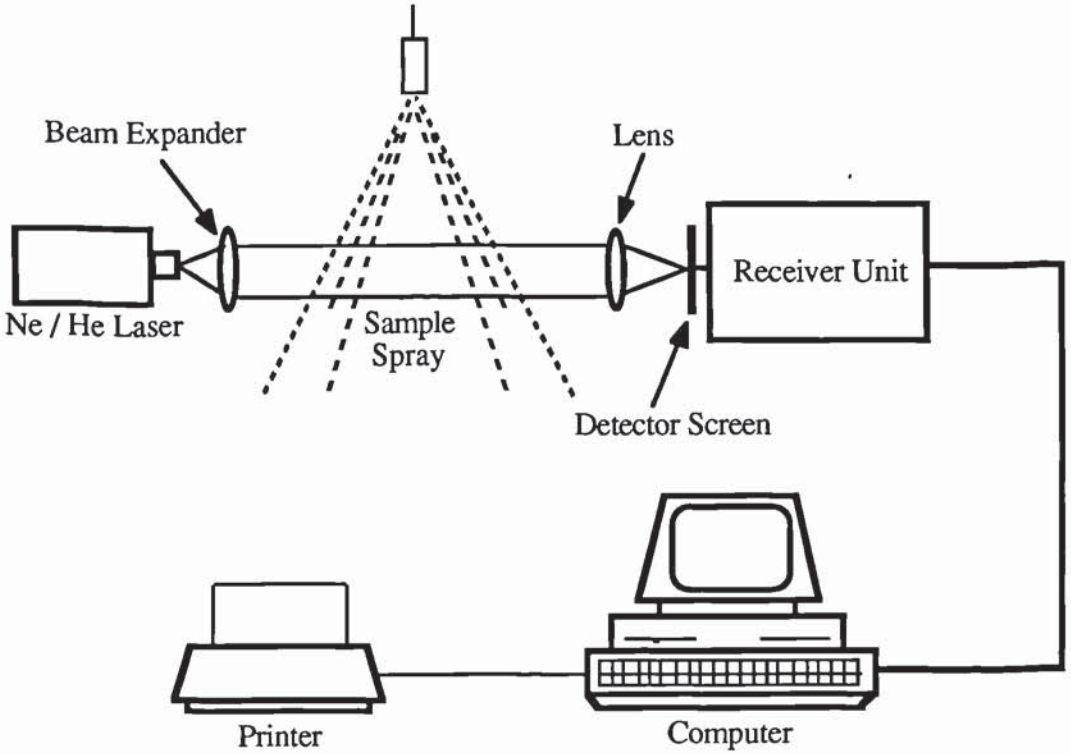

The result of the measurement analysis is a Volume Distribution characterised, in the case of the 300mm lens, between 5.8 and 564.0μm. The results may then be presented and printed in a number of different ways.

As part of the results presentation the Size Analyser compares the measured light energy with the calculated light energy based upon the distribution model. It then calculates the logarithmic difference of the 'fit'. The log. difference is defined by the following equation and an interpretation of the results is given in Table 3.4.

$$\text{Log. Difference, Ld} = \log \sum_{j=1}^{m} \left[Le_{Cal} - Le_{Mea} \right]_j^2 \qquad - \ 3.27$$

Where: Le_{Cal} is the calculated light energy hitting the detector element,

Le_{Mea} is the actual light energy hitting the detector element.

Table 3.4: *Interpretation of Log. Difference Results [50]*

Log. Difference	Definition
Ld > 6.0	Model not appropriate or experiment has been incorrectly performed.
5.5 < Ld < 6.0	Poor fit. May be adequate for trend analysis only.
5.0 < Ld < 5.5	Adequate fit but look for evidence of systematic misfitting of data.
4.0 < Ld < 5.0	Good fit. Well presented sample.
Ld < 4.0	Very unlikely with experimental data but normal with analytical data.

Chapter 4: Mechanisms of Atomisation

Introduction

Numerous theories describing atomisation mechanisms have been proposed in the literature, each supported by experimental data. However, vast areas of uncertainty remain in current knowledge on the subject and much work remains controversial. One of the most useful papers is a report by Lapple *et al* [110] which reviewed the work of over 150 researchers in the field of atomisation up to 1967. Lapple found that there were notable disagreements throughout the literature concerning the effects of the principle variables and that some investigators had reported contradictory roles for these variables with similar atomisers. The major discrepancies were attributed to the following factors:

a) Investigations tended to study the effect of a variable over a narrow range only and consequently had a limited precision in assessing the resulting variation in atomisation performance.

b) Whilst some investigations did not actually study the effect of a particular variable, they introduced it into a correlation for either a rational or arbitrary reason.

There is no similar review of any post-1967 work but more recent work in the field has been presented at a series of ICLASS Conferences (International Conference on Liquid Atomisation and Spraying Systems) [111-113]. The appropriate conference notes cover recent work in all aspects of atomisation.

This chapter will follow the development of atomisation models from the early conceptual work based upon liquid jets pioneered by Rayleigh [114] to the latest theories presented by authors at the 3rd International Conference on Liquid Atomisation and Spray Systems (ICLASS-85) [113]. In addition the current theory of centrifugal pressure nozzle atomisation will be reviewed leading on to the development of a mathematical model to predict the droplet-size distributions produced by this type of atomisation.

It is not the purpose of this chapter to review the empirical expressions used for design work. These expressions are generally multipurpose, being applicable to virtually any type of atomisation device; their sole aim is to provide a rough estimation of droplet size. An example of such an expression for predicting the mean droplet size, based upon the Upper-limit function [47], has been presented in the literature by Murty [115],

$$d_p = \frac{d_{max}}{1.8803} = \frac{D_{VS}}{0.85} \qquad - 4.1$$

where d_{max} is defined by,

$$\frac{d_{max}}{D_o} = 57\left[\frac{\rho_l V D_o}{\mu}\right]^{-0.48}\left[\frac{\mu V}{0.8739}\right]^{-0.18} \qquad - 4.2$$

4.1 History and Development of Atomisation Theory

The study of liquid atomisation has been based either upon the disintegration of liquid jets or liquid sheets. Although these are two separate fields of study, the principles involved in each case are similar and expressions have often been found to be valid for both forms of atomisation.

4.1.1 Investigations into the Break-up of Liquid Jets

The disintegration of liquid jets has been the subject of much experimental and theoretical study for over a hundred years. The first recorded work was presented in 1833 by Savart [116], who represented jet break-up in the form of a stability curve. Later work by Plateau [117] demonstrated that a cylindrical column of liquid was unstable when its length exceeded its circumference and would eventually break-up under the influence of any disturbance, even one of an arbitrarily small amplitude. However, he did not pursue any investigation into the time required for jet break-up to

occur and, as disturbances are always present in a column of liquid, then jet disintegration is inevitable under any conditions.

Rayleigh [114] took Plateau's work a stage further and proposed an idealised system, illustrated in Figure 4.1, based upon the assumption that the liquid jet is an inviscid column undergoing irrotational flow. A small disturbance or distortion in the liquid column will produce an 'imbalance' in the internal forces in the liquid which, under certain conditions will be self-perpetuating, causing the disturbance to increase exponentially until jet break-up occurs. The force required to maintain the 'imbalance' is surface tension, which Rayleigh referred to as 'capillarity', and the growth of the disturbance can be represented by the expression given in equation (4.3).

Figure 4.1: *Idealised Break-up of an Inviscid Liquid Jet [114]*

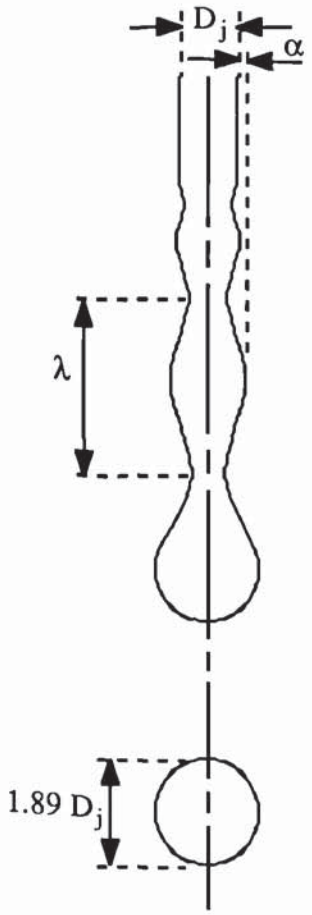

$$\alpha = \alpha_o e^{qt} \qquad - 4.2$$

where, α is the amplitude of the disturbance at time t,

α_o is the initial amplitude,

q is the growth rate of the disturbance,

t is the time factor.

Thus jet break-up will occur for all cases when the exponetial term in equation (4.2) is positive. Consequently the stability of the jet is determined by the value of q, which Rayleigh determined to be given by equation (4.3):

$$q = \sqrt{\frac{\sigma}{\rho_l R_j^3}}\, f\left(\frac{2R_j}{\lambda}\right) \qquad - 4.3$$

where, σ is the surface tension of the liquid,

ρ_l is the liquid density,

R_j is the radius of the jet orifice,

λ is the wavelength of the disturbance.

The function $(2R_j/\lambda)$ has a maximum value; therefore differentiation of q with respect to λ will yield the maximum possible growth rate of the disturbance,

$$q_{max} = 0.345\sqrt{\frac{\sigma}{\rho_l R_j^3}} \qquad - 4.4$$

The initial disturbance in the jet will consist of an infinite number of waves, each of a different wavelength. However, an optimum wavelength (λ_{opt}), usually that of the most rapidly growing disturbance, will over-run any other disturbance; the wavelength of this disturbance can be determined by equation (4.5):

$$\lambda_{opt} = 4.51(2R_j) = 9.02\,D_o \qquad - 4.5$$

Thus the wavelength of the optimum disturbance is dependent upon the diameter of the liquid jet and is not influenced by the effects of liquid physical properties or those of the surrounding medium. The droplet diameter can be determined from a mass balance, based on the assumption that one droplet is formed per disintegration wavelength,

$$d_p = 1.89\, D_o \qquad - 4.6$$

Although Rayleigh's analysis does not account for the formation of satellite droplets, numerous workers , for example Tyler [92] and Castleman [118], have found it to be in excellent agreement with experimental data for low velocity inviscid liquid jets.

A more general mathematical analysis was conducted by Weber [119], who developed a differential equation for the disintegration of a slow speed viscous jet when both viscous and inertial forces significantly affect the break-up of the jet. Weber expanded the coefficients in Rayleigh's dimensionless growth rate equation into a Fourier series and showed that the series was constant for conditions when the wave number was less than one. From this simplified equation Weber derived an expression for the wavelength of the most rapidly growing disturbance,

$$\lambda_{opt} = \pi D_o \sqrt{2\left(3\frac{We}{Re} + 1\right)} \qquad - 4.7$$

Thus for the case of an inviscid liquid (ie, when We/Re = 0),

$$\lambda_{opt} = 8.89\, D_o \qquad - 4.8$$

Comparison of equation (4.8) with equation (4.5) confirms the surprisingly good agreement with Rayleigh's analysis.

Expansion of equation (4.7) provides an expression for the break-up length of the liquid jet ,

$$\frac{l_b}{D_o} = \ln\left(\frac{R_j}{\alpha_o}\right)\left[\sqrt{We} + 3\frac{We}{Re}\right] \qquad - 4.9$$

In order to solve equation (4.9) the parameter (R_j/α_o) must be experimentally determined and Weber demonstrated that it was a constant with the value of e^{12} based upon Haenlein's data [120].

Stability Curve

The jet stability curve is the most convenient method of representing experimental stability data. Generally stability is represented by a plot of jet length at break-up, l_j, against the jet velocity. The first stability curve was constructed by Savart [116] from experimental data and demonstrated a linear increase in break-up length with velocity (region B to C in Figure 4.2).

Figure 4.2: *Schematic Diagram of the Jet Stability Curve*

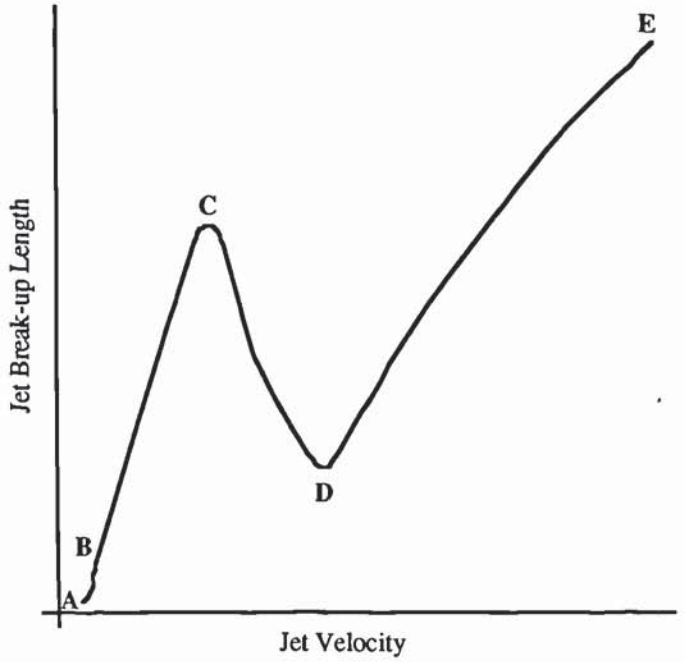

A typical stability curve showing the variation in the break-up length caused by an increase in jet velocity (pressure) is represented in Figure 4.2. The region A to B represents drip flow, where the velocity of the jet is so low the jet length is virtually negligible. At the lower critical point, B, (of minor significance) the jet changes from drip flow to jet flow and the region B to C is where the theories of Weber and Rayleigh apply. At the upper critical point, C, the jet length undergoes a sharp decrease for an increase in velocity and Haenlein [120] reported that the break-up mechanism began to change from varicose to helicoidal. Beyond point D the jet break-

up lengths begin to increase with velocity again, although experimental data indicates a decrease in break-up time for an increase in jet velocity. The exact position of point E is uncertain as the experimental data for this region is largely contradictory [121].

Smith & Moss [122] plotted L/D against the square root of the Weber number for several systems and obtained a straight line which passed through the origin. They found that the ratio of initial to final jet disturbance was the same at corresponding critical points and determined the value of the constant, ln (R_j/α_o), as 13. Similar behaviour was observed by Grant & Middleman [123] who reported a value of 13.4 from experimental data using solutions of glycerol and water, whilst Weber had obtained a value of 12 from Haenlein's data.

Tyler & Richardson [124] reported a critical point (C); until reaching this point the jet length increased with velocity but subsequently diminished rapidly. Surface tension was found to be important in the first stage but viscosity was the dominating factor in the second stage. A dimensionless formula was derived to cover both stages.

Grant & Middleman [123] modified Weber's theory to include the influence of the ambient medium, turbulence in the flow and the velocity profile of the jet. This was accomplished by treating ln (R_j/α_o) as a variable instead of a constant as in Weber's investigation. A correlation was introduced from a plot of ln (R_j/α_o) against the Ohnesorge number, Z:

$$\ln\left(\frac{R_j}{\alpha_o}\right) = -2.66 \ln(Z) + 7.68 \qquad - 4.10$$

where, Z is the ratio of the Weber and Reynolds numbers and is defined by,

$$Z = \frac{\sqrt{We}}{Re} = \frac{\mu}{\sqrt{\sigma \rho_l D_j}} \qquad - 4.11$$

The modified theory predicted jet stability with good agreement to experimental data except in the cases of liquid jet break-up at subatmospheric pressures. Consequently, they concluded that the modified theory failed to account for the effect of the ambient medium except in the case of jet break-up at atmospheric pressure.

Fenn & Middleman [125] found that aerodynamic pressure forces had no effect upon the jet break-up when the Weber number was less than 5.3. Above this value the pressure forces are more influential and jet stability became increasingly less dependent upon the viscosity ratio of the two phases; thus the jet was less stable which caused a reduction in its break-up length.

Phinney [126] assumed that the amplification rate given by Weber's theory was correct but treated the initial disturbance level as a variable. Data from a number of previous workers [123][125] was used to test his hypothesis and ln (R_j/α_o) was plotted against the Reynolds number of the flow through the orifice. A critical Reynolds number existed for each curve, above which the disturbance level was no longer constant and increased with an increase in Reynolds number. Later work [127], examined the effect of ambient density on the stability of a liquid jet compared theoretical predictions to experimental results and introduced a modified Weber number, based upon ambient density:

$$We_{\rho_a} = \frac{V^2 \rho_a D_o}{\sigma} \qquad - 4.12$$

This gave an improvement of Weber's theory, especially at low values of the Ohnesorge number, and yielded a value for the disturbance level, given by ln (R_j/α_o), equal to 13.96; this fitted the data of Fenn & Middleman [125] reasonably well and was close to values quoted by other workers.

Haenlein [120] demonstrated that jet break-up was caused by several distinct mechanisms each affected by variations in surface disturbance and aerodynamic effects. At low jet velocities there was a negligible influence of the air upon the jet; thus for inviscid jets the results for the initial disturbance ratio of wavelength to jet diameter agreed with those of Rayleigh. However, for the more viscous jets the ratio was considerably greater than the value of 4.42 predicted by Rayleigh. At higher jet velocities the wave motion was intensified by localised differences in air velocity between the wave crests and troughs. A further increase in jet velocity caused the initial disturbance to take on the form of asymmetric waves which rapidly developed

under the influence of air. Under these conditions the development of the wave motion was found to be heavily influenced by surface tension and viscosity. Reasonable agreement was obtained when comparing experimental data to those determined from Weber's analysis [119]. The only major discrepancy was for the case of a highly viscous liquid.

These break-up regions were also investigated by Ohnesorge [128], who introduced a dimensionless expression to generalise experimental results based upon the principle of mechanical similarity (ie, orifice dimensions and physical properties of the fluid). This expression, known as the Ohnesorge number (Z), is defined by equation (4.11).

Figure 4.3: *Break-up regions for liquid jets [128]*

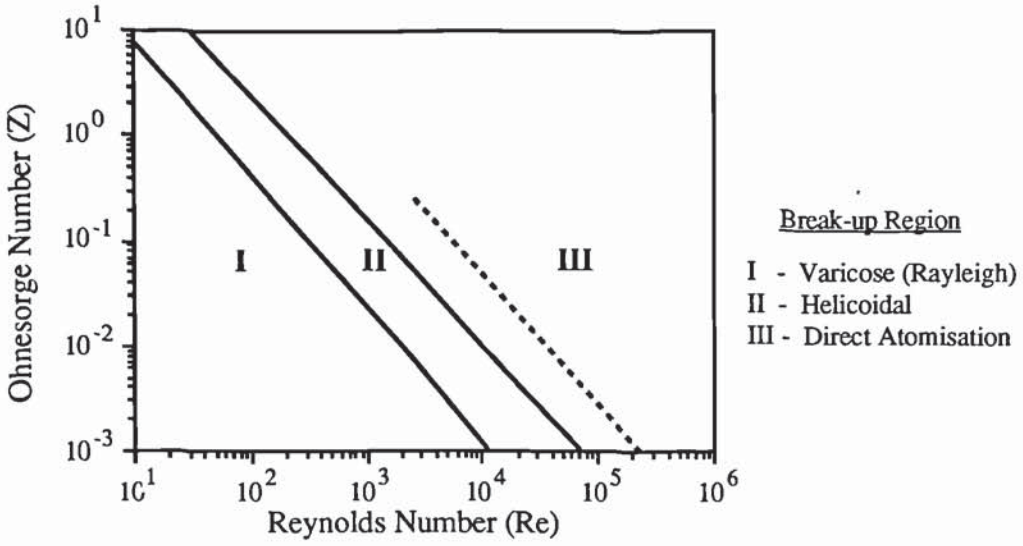

Ohnesorge stated that, for constant values of the Ohnesorge number, jet stability was merely a function of the Reynolds number. The results of his analysis indicated that jet break-up could be classified into one of three regions on a plot of the Ohnesorge number against Reynolds number, illustrated in Figure 4.3. These regions are defined as follows:

I) At low Reynolds number, the jet break-up occurred by the action of varicose vibrations into large droplets (as defined by Rayleigh);

II) At intermediate Reynolds number, jet break-up occurred by the action of helicoidal vibration producing a distribution of droplet sizes;

III) At high Reynolds number, jet break-up occurred directly upon leaving the nozzle by the action of aerodynamic forces.

McCarthy & Molloy [121] reported that it was possible for liquid jets to exhibit the complete spectrum of disintegration mechanisms, although all were represented by the same point on Ohnesorge's graph. However Miesse [129] presented data for liquid nitrogen and water which did not follow the criteria presented on Ohnesorge's graph; all the data fitted into the region of secondary atomisation (region III), whereas only the data for liquid nitrogen should have fallen into that region. Miesse transposed the boundary line between helicoidal break-up (region II) and secondary atomisation into the region of higher Reynolds number, as indicated by the dotted line on the Ohnesorge graph, thus segregating the data of primary and secondary atomisation into distinct regions on the graph. However, Schweitzer [76], in an investigation of the effect of liquid turbulence on jet break-up, found that disintegration was not solely influenced by Reynolds number but was also affected by injection pressure, viscosity, surface tension and ambient air density. Lee & Spencer [130] found that liquid turbulence was not a major factor influencing the jet break-up mechanism. In a study of the disintegration of fuel jets in low pressure air, they noted that jet break-up was caused by aerodynamic forces and concluded that, under constant operating conditions, jet disintegration was more pronounced with an increase in the distance from the nozzle, air density, or fuel velocity (or turbulence); conversely jet disintegration decreased with an increase in fuel viscosity, surface tension, or nozzle orifice diameter.

The transition from a 'wavy' jet (region II) to a spray jet disintegration mechanism (region III) was investigated by Sakai *et al* [131]. They introduced an empirical, dimensionless formula, relating Weber and Reynolds number to the discharge coefficient of the nozzle.

$$(Re)_t^{0.2} (We)_t^{0.4} = 750\, C_D^{1.4} \qquad - \ 4.13$$

where, $( )_t$ denotes transitional conditions.

Relatively coarse droplets were produced during 'wavy' jet atomisation whilst much finer droplets were produced, after the transformation into spray jet atomisation. They proposed the use of equation (4.13) to simplify the design procedures for spray operations that require either coarse or fine droplets.

Holroyd [132] applied dimensional analysis to the mean angular fluid velocity leaving the nozzle orifice, based upon the assumption that jet break-up was caused by liquid turbulence. He obtained an expression for the mean droplet diameter as a function of the Reynolds number,

$$d_p = \left[\frac{\sigma D_o^{\,2}}{\rho_l V^2}\right]^{0.33} f\left(\frac{D_o V \rho_l}{\mu}\right) \qquad - \ 4.14$$

where: V is the velocity of flow,

Holroyd stated that theoretical predictions were in fairly good agreement with the experimental results of Lee [62] but, as it was difficult to define the exact mean diameter determined by equation (4.14), the exact accuracy of the expression was dependent upon which value of mean diameter was used for comparison.

Holroyd also postulated that neglect of the Reynolds number term in equation (4.14), by considering it constant, should mean that the product of the mean droplet diameter and the cube root of injection pressure would remain constant for any given orifice and liquid. A reasonable agreement for this hypothesis was obtained using Lee's data.

Merrington & Richardson [133] developed a relationship for drop size in terms of viscosity and the relative velocity of the jet in air for both stationary and moving nozzles. At low velocity they found that the drop size reached a limiting value and their relationship no longer applied. They confirmed the work of Tyler & Richardson [124] but also discovered an anomaly for highly viscous liquids where the jet length depended significantly upon the shape and method of manufacture of the nozzle.

Duffie & Marshall [134] reported that liquid jet break-up was caused by surface tension forces which produced droplets with a diameter approximately twice that of the jet capillary diameter. The results of their work correlated approximately with Rayleigh's theory, with a ratio of wavelength to jet diameter equal to 4.6 compared to Rayleigh's value of 4.51, but a distribution of droplets was present. This droplet distribution was also acknowledged by MacDonald [135], who stated that the small satellite droplets (or Plateau's spherules), associated with main droplet formation, could be predicted using a variation of Rayleigh's analysis. Measurements using high speed photography demonstrated that the ratio of the diameters of the main droplets to those of the satellite droplets was 2.8, which compared favourably with a theoretical prediction of 2.6. La France [136] developed a third-order computer simulation program to account for the presence of satellite droplets in the break-up of a liquid jet. The experimental results presented by several authors [88][89][137] were used to test his model and the predicted surface wave profiles, disturbance amplification rates and drop sizes were found to be in agreement with the previous work.

Rutland & Jameson [89] determined the wave profile at the point where the maximum amplitude of the disturbance coincides with the jet axis, ie where break-up is assumed to occur, and predicted the volume of the 'main' droplets (from the crests of the primary disturbance) and that of the satellite droplets (from the remainder). They found their results to be in good agreement with available experimental data.

In cases of large wavelength disturbances the satellite droplets were larger in total volume than the main droplets whilst, when the value of the wave number was less than 0.35, the theory predicted that the main drop was larger than the satellite. At values of wave number greater than 0.7 the theory predicted that no satellite droplets would be formed; however, experimental evidence showed that satellite droplets were always formed, although they were very small when the wave number was large.

Non-Newtonian Jets

Goldin *et al* [138] examined the stability of laminar jets of non-Newtonian fluids by means of a linearised stability analysis. It was shown that the growth rate of disturbances for fluids without a finite yield stress was always larger than for non-Newtonian fluids which possess similar zero shear viscosities and that fluids that had a finite yield stress produced a stable jet. However, this theory assumes that the properties of the fluid leaving the nozzle are those of the fluid in its equilibrium state. This is incorrect since the fluid in the nozzle is under high shear and stress conditions which causes the gel-like structure of high viscosity fluids to break-down. A finite time is required for the internal fluid structure to reform; consequently allowance must be made for this in any calculation. In later work, Goldin *et al* [139] investigated the break-up of capillary jets of various viscous non-Newtonian fluids. Inelastic liquids with high shear-dependent viscosities were found to exhibit similar instabilities to those of a Newtonian fluid of comparable viscosity. The nature of the instability was found to be related to the reformation time of the liquid structure. Elastic fluids with similar viscosities were found to be stable under the same conditions.

Krosser & Middleman [140] extended Weber's theory for Newtonian jets to include linear viscoelastic fluids. Experimental data for poly-isobutylene in tetralin confirmed their theoretical prediction that viscoelastic jets have shorter break-up lengths than Newtonian jets at constant Reynolds and Ohnesorge numbers. Their theory did not account for the effect of internal stress within the capillary but the experimental results indicated that break-up length did have a dependency upon capillary length, a phenomenon which may be caused by the presence of an internal stress effect.

Gordon *et al* [141] studied the instability of laminar jets consisting of various solutions of Carbopol and Separan under the influence of externally controlled disturbances. Jets of 0.1% Carbopol solution exhibited break-up patterns similar to those of water. There were no sinusoidal wave formations present on jets of 0.1% Separan solution with a ligament-droplet formation being formed from the outset. They observed an initial region of exponential sinusoidal wave growth on jets of the

less elastic 0.05% Separan solution but this growth was suppressed resulting in a ligament-droplet configuration. In the initial region the growth rates of the disturbances were approximately equal to those of a Newtonian fluid with similar zero shear viscosity and the ligaments that formed on jets of Serepan were found to exhibit a stretching motion which accounted, in part, for their unusual stability.

Production of Uniform Droplet Size

Roth & Porterfield [142] investigated methods of producing a more uniform drop size in jets and sprays. Their initial work was with liquid jets where they induced an A.C. voltage across an orifice in a piezoelectric crystal. By careful manipulation of the voltage frequency and the operating pressure satellite drops could be eliminated from the spray.

The delicate nature of the crystal and the difficulty in maintaining a stable electric circuit caused them to develop another system which involved a process of magnetostriction (ie, the creation of a dimensional change in an object due to magnetism). A rod and a coil were arranged in a liquid pressure system with one end of the rod near the discharge orifice. A longitudinal vibration of the rod, caused by an A.C. voltage, was imparted into the liquid passing through the orifice and by manipulation of the operating conditions produced a stream of uniform droplets. The disappearance of the satellite drops could not be satisfactorily explained but they did appear to move towards the large drops and coalesce. These workers also investigated control of the uniformity of spray droplets by using a counter-current airflow of varying flowrate; however, they were unable to obtain a satisfactory determination of the drop size in order to assess the efficiency of the apparatus.

Sakai *et al* [143] investigated the operating conditions required to produce uniform-sized droplets by means of a longitudinally-vibrating capillary nozzle with low viscosity Newtonian liquids and non-Newtonian slurries. They proposed non-dimensional empirical formulae to predict the operating conditions required to produce uniform-sized droplets; this defined the upper and lower limits of the vibration frequency and liquid velocity. They concluded that it was possible to produce

uniform-sized droplets by the vibration, at an appropriate frequency and amplitude, of a smooth liquid jet.

4.1.2 Investigations into the Break-up of Liquid Sheets

The fundamental principle behind the disintegration of a liquid sheet involves an increase in its overall surface area resulting in instability and eventual break-up. Dombrowski & Fraser [6] established that the mechanism of sheet break-up depended upon the physical properties of the liquid and could be classified into three categories:

(i) Rim break-up: This mechanism is common for liquids where the effects of surface tension predominate over those of density and viscosity. In flat sheets of liquid the edge or rim of the sheet is generally thicker than the rest of the sheet due to the effect of surface tension and disintegration of this region of the spray is analogous to that of a free jet. When surface tension is the predominating factor the liquid is pulled out to the rim of the sheet before breaking-up into virtually uniform-sized droplets. At increased flow rate this effect gradually diminishes until eventually a sheet is formed; however, ligament formation is irregular and consequently there is a wide droplet distribution. This form of disintegration does not occur in conical sheets, due to the absence of edge effects, unless the sheet is ruptured.

(ii) Perforated Sheet: This mechanism is most pronounced in a liquid with high density or surface tension, or when the liquid is sprayed into a low density ambient gas. In these cases small holes appear in the sheet which rapidly expand until the rims of adjacent holes coalesce to form ligaments. Although the ligaments tend to break-up uniformly, the irregularity of the initial perforations causes the size of the ligaments, and consequently those of the resultant droplets, to vary considerably.

(iii) Wave-form disturbance: As with jets, liquid sheets can disintegrate by the action of a wave-form disturbance on the liquid surface. The initial disturbance is generally enhanced by aerodynamic and internal pressure effects until the amplitude is large enough to cause disruption of the sheet. At this stage sections

of the sheet, corresponding to approximately half the wavelength of the disturbance, will break away and contract under the influence of surface tension to form ligaments. These ligaments may break-up further under the action of liquid turbulence or aerodynamic effects.

Subsequently, irrespective of which break-up mechanism predominates, the sheet disintegrates into ligaments which form droplets in a method analogous to Rayleigh's theory for circular liquid jets. Garner *et al* [144] demonstrated for viscoelastic gels, which are in a semi-solid form at no applied shear, that the intermediate ligaments may not break down any further into droplets.

Dombrowski & Fraser [6] found that when solid or liquid particles were suspended in the liquid, the stability of the sheet was dependent upon the type of suspended particle. If the particles were wetted by the liquid then, irrespective of size, they had no effect upon the method of disintegration of the sheet but when suspensions of unwettable particles were involved there was a marked effect, causing perforations in the sheet. Mathematical analysis [145] of the random disturbances that produce perforations revealed that their origin was up-stream of the orifice within the nozzle. The initial cause of these disturbances was unknown; Fraser *et al* [145] proposed that it might be vibration phenomena within the nozzle but recommended further work should be done to determine the actual cause.

At low ambient density Dombrowski & Hooper [7] demonstrated that the liquid sheet was stable and droplet formation only occurred at the edges. Perforations of the liquid sheet were almost certainly caused by disturbances created by already-formed droplets impinging on the sheet. At higher ambient densities the sheet was, as demonstrated by previous workers [8][74], disrupted by aerodynamic waves. These workers extended the previous theory that predicted wavelength and growth to show that the controlling equation was dependent upon the operating conditions.

The origin of sheet perforations was investigated by Fraser *et al* [8] who presented a theoretical analysis to predict the position of the initial hole formation,

$$r_i^{1.5} = r_d^{1.5} - \frac{3}{2} r_p V_s \sqrt{\frac{\rho_l k}{2\sigma}} \qquad - 4.15$$

where: r_i is the radial distance from the orifice to the origin of the perforation,

r_d is the radial distance from the orifice to the centre of the perforation,

r_p is the radius of the perforation,

V_s is the sheet velocity,

k is the sheet thickness parameter.

Since no two photographs, taken under similar conditions, gave the same number and distribution of perforations, it was only possible to interpret the experimental data in terms of ranges and averages; however, equation (4.15) gave good agreement with these limited results. As in earlier work [7] it was deduced that the initial cause of the perforations was droplet impingement upon the sheet but no mechanism was proposed to explain the phenomenon.

Clark & Dombrowski [146] found that at temperatures above 300°C liquid sheets broke down by a combination of high frequency symmetric waves and localised disturbances which caused perforations in the sheet. It was demonstrated that the new type of wave growth was electro-hydrodynamic in origin with the electric field being generated by charged species present in the gas and the drop size was critically dependent upon the nature of the disintegration process.

Under ambient conditions sheet break-up is normally effected by wave disturbances and Squire [147] investigated the growth of sinuous waves on an inviscid liquid sheet of constant thickness by assuming a two-dimensional system. Instability of the sheet was analysed by a similar method to that given by Lamb [148] and, for conditions of large wavelengths (compared to film thickness), yielded the wavelength of the maximum instability by differentiation of the growth rate equation presented by Lamb,

$$\lambda_{max} = \frac{4 \sigma \pi}{\rho_a V_s^2} \qquad - 4.16$$

when, $\frac{1}{We} << 1$

where: λ_{max} is the wavelength of the maximum instability,

Squire obtained reasonable agreement with experimental results but noted that the theory did not give an indication of how sheet disruption actually occurred.

Dombrowski & Hooper [7] applied this theory to the case of an attenuating sheet and obtained a similar expression for the optimum wavelength of the disturbance, differing only in the magnitude of the constant. They also investigated the nature of the wave-form on the sheet and stated that both dilational and sinuous waves were theoretically present. The initial, rapid, decrease in the sheet thickness near the orifice indicated that sinuous waves were unlikely to be generated and random disturbances were likely to be dilational waves. In the case of the larger wavelength disturbances sinuous waves were found to have a larger growth rate and were more likely to predominate; however, in the case of smaller wavelength disturbances the growth rate of both types of wave were similar and dilational waves predominated. It was concluded that the discrepancies between theory and experimental data probably arose from the nature of the assumptions made in the derivations, ie the relative velocity between the sheet and ambient atmosphere would be smaller than the assumed value of the sheet velocity. Therefore the ligaments will be affected by a more complex mechanism than assumed by Rayleigh's analysis; however, no allowance was made for the effect of the ambient density.

Hagerty & Shea [149] considered the appearance of sinous waves on liquid sheets to be attributable to the fact that under normal conditions the wavelength was relatively large in comparison to the sheet thickness and consequently their growth rates were greater than those of the alternative dilated form.

Clark & Dombrowski [150] conducted a second order analysis on the aerodynamic growth of sinuous waves on parallel-sided inviscid sheets by a method of successive approximation. They extended the work of Hagerty & Shea [149] and Squire [147] to derive an equation for sheet break-up length. Good agreement was obtained with experimental results for the case of conical sheets but they found that flat sheets were larger than expected, a fact which it was implied was due to an over-large value of the initial disturbance employed in the equation.

$$l_b^{1.5} = \sqrt{\frac{9\rho_l^2 V_s^2 k}{32\left(\rho_a V_s n - \sigma n^2\right)}} \cosh^{-1}\left\{8\left(\alpha_o v\right)^{-2} + 1\right\} \qquad - 4.17$$

where: l_b is the sheet break-up length,

n is the wave number,

Crapper *et al* [151] found that, contrary to two-dimensional theory, wave growth was critically dependent upon sheet velocity and the distance from the origin of the liquid sheet. This was attributed to boundary layer separation within the nozzle and the formation of a vortex in the air surrounding the sheet. They extended their previous work [152] to obtain a better prediction of wave growth by applying large amplitude Kelvin-Helmholtz Wave theory to parallel flat sheets based on vortex formation in each wave trough. It was concluded that their theory was not entirely successful but did reveal that it was possible for large amplitude waves to be maintained by the effect of surface tension, with an internal pressure gradient in the liquid but with no corresponding large pressure differences in the ambient gas.

Crapper *et al* [153] employed a linearised analysis to investigate the wave growth on flat sheets of Newtonian and Non-Newtonian liquids and presented a first order analysis that took into account the viscosity of both the liquid and the ambient air. In order that their work should have wider applications, a 'complex' viscosity term was created which allowed both Newtonian and Non-Newtonian flow to be examined. Ambient air viscosity was found to be an important parameter in the formation of surface waves and, for conditions where the wavelength was large in comparison to the sheet thickness, liquid viscosity had no effect on the initial wave growth. However, when the amplitude of the waves had increased sufficiently, slight discrepancies occurred in their predictions.

An analysis of the stability of thin, viscous, attenuating sheets was presented by Weihs [154], who obtained an analytical equation for the amplification factor of unstable waves as a function of kinematic viscosity, wave number, sheet thickness and sheet velocity. Solution of this equation produced values for the wave number of the same order as those predicted by Squire's linearised theory.

York *et al* [155] presented a mathematical analysis to explain the disintegration of a liquid sheet based upon instability theory. They derived an equation to predict the conditions of maximum instability based upon four dimensionless groups: Weber number, wave number, growth-rate number and the dimensionless ratio of the disturbance wavelength to half the sheet thickness. They also presented an approximation for the size of the resulting droplets by assuming the ligament to be a complete ring of liquid and applying Rayleigh's analysis for cylindrical jet instability. Although their theory was limited by the initial simplifying assumptions, the results from the analysis were in reasonable agreement with experimental data obtained from swirl spray nozzles.

The variation in sheet thickness from the orifice to the break-up position was investigated by Dombrowski *et al* [156], who found that the thickness of the sheet at any point was inversely proportional to its distance from the orifice. For any given operating conditions this proportionality could be expressed by the thickness parameter, the nature of which was determined by the injection pressure. Based upon experimental data, at low injection pressures the thickness parameter was expressed by the following function,

$$k = f\left\{\sigma, \left(\frac{\sqrt{P\,\rho_l}}{\mu}\right)\right\} \qquad - \ 4.18$$

At high injection pressures it was expressed by,

$$k = f\left\{\frac{\sqrt{P\,\rho_l}}{\mu}\right\} \qquad - \ 4.19$$

Taylor [157] defined the sheet thickness parameter for an expanding conical sheet as a function of the volumetric flow and the sheet velocity:

$$k = h'l' = f\left(\frac{Q}{2\,\pi\,V_s}\right) \qquad - \ 4.20$$

A theory of break-up of the conical sheet was based upon a mechanism similar to that described by Dombrowski & Fraser [6]. For low ambient densities, where the sheet breaks-up by perforations in the surface, the expression for droplet diameter as a function of the ligament diameter was similar to Rayleigh's,

$$d_p = 1.9\sqrt{\frac{2Q\tau}{\pi^2 y}} \qquad - 4.21$$

where: τ was defined to be of the order $\pi D / V_s$,

$$y = We\left(\frac{\rho_l Q V_s}{4\sigma\pi}\right)$$

However, the effect of the air core in the nozzle was not taken into account in the calculation of the volumetric flowrate and since no experimental data was presented it is difficult to determine the accuracy of equation (4.21).

Fraser *et al* [8] developed an expression for the prediction of the break-up thickness of a flat liquid sheet from an extension of earlier work [147][149],

$$h_b = \sqrt[3]{\frac{1}{2f^2}\left(\frac{\rho_a{}^2 V_s{}^2 k^2}{\rho_a \sigma}\right)} \qquad - 4.22$$

where: h_b is the break-up thickness of the liquid sheet,

$$f = \ln\left(\frac{\alpha_b}{\alpha_o}\right)$$

α_o is the initial disturbance amplitude of the liquid sheet,

α_b is the disturbance amplitude of the liquid sheet at break-up.

Weber had found with liquid jets that the condition for break-up was that the amplitude ratio (α_b/α_o) reached a universally constant value, and Fraser *et al* confirmed from experimental data that a similar assumption was correct for liquid sheets. For a given nozzle, the amplitude ratio was also constant. There was, however, a tendency for a slow decrease in the amplitude ratio as the sheet thickness parameter (k) increased but this factor was neglected due to insufficient data to establish a more accurate criteria. Later work by Briffa & Dombrowski [158] showed that the amplitude ratio was also affected by surface tension. A comparison of equation (4.22) with experimental data gave good agreement with any data scatter due mainly to the irregularity of the wave contours at break-up.

Fraser *et al* [8] noted that the mode of disintegration was critically dependent upon the ambient density and found that liquid sheet disintegration was caused by

surface perforations at low ambient density with the absence of any form of wave disturbance. Droplet sizes produced when perforation of the liquid sheet occurred were generally larger than those obtained when disintegration was by surface waves. This was due to the fact that the thickness of the ligament produced during liquid sheet perforation was independent of the sheet thickness and generally larger than a corresponding ligament formed during wave-form disintegration. Dombrowski *et al* [9] studied the disintegration of a range of viscoelastic petroleum gels, characterised by their Gardner consistency, using single-hole fan spray nozzles. All the gels disintegrated into ligaments but the manner in which a ligament broke down depended upon the consistency of the gel. The ligaments formed by high consistency gels were further fragmented; those of intermediate consistency gels remained unbroken and those of a very low consistency gels (below 25 Gardner) produced ligaments carrying spherical droplets. This mechanism is contrary to that observed for Newtonian liquids. Measurements of the liquid sheet indicated constant velocity during its initial period of expansion which was in agreement with the behaviour of Newtonian liquids. This is due to the fact that the sheet is under the effect of continuous shear forces during expansion and no recovery to initial consistency can occur during that period.

Arai & Hashimoto [159] observed that the disintegration of liquid sheets correlated closely to vibration of the sheet up-stream of the break-up point. The mean break-up length of the sheet was determined by the conditions in the region of the gas/liquid interface (ie, governed by the sheet thickness, Weber and Reynolds number, etc.) and could be calculated from the empirical expression,

$$\frac{l_b}{\left(\frac{h_i}{2}\right)} = 3.88\left(\frac{Re_l^{0.6}}{\sqrt{\left(\frac{h_i}{h_b}\right)We_{gl}}}\right) \qquad - \ 4.23$$

where: h_i is the sheet thickness at the nozzle exit,

$$We_{gl} = \frac{\rho_g (U_\infty - U_l)^2 h_i}{\sigma}$$

U is the horizontal component of velocity (relative to the sheet),

Subscripts: g - gas

l - liquid

∞ - upstream of nozzle

Comparison of equation (4.23) and experimental data, gave a correlation coefficient of 0.995.

Dombrowski & Johns [10] conducted a mathematical analysis of the aerodynamic instability and disintegration of viscous liquid sheets produced by fan spray nozzles. An expression was developed for droplet size which compared favourably with previous experimental data. Break-up of the sheet was idealised so that it could be represented by a series of mathematical expressions which on combination yielded a relationship for droplet size,

$$d_p = \sqrt[3]{\frac{3\pi d_l^3}{\sqrt{2}}\sqrt{1 + \frac{3\mu}{\sqrt{\rho_l \sigma d_l}}}} \qquad - 4.24$$

where d_l, the ligament diameter, is given by,

$$d_l = 0.9614\left(\frac{k^2\sigma^2}{\rho_a \rho_l V_s^4}\right)^{0.17}\left[1 + 2.60\,\mu_l\sqrt[3]{\frac{k\rho_a^4 V_s^7}{72\rho_l^2\sigma^5}}\right]^{0.2} \qquad - 4.25$$

Comparison of the results obtained from equation (4.24) with the experimental data of Hasson & Mizrahi [82] yielded a relationship between calculated droplet diameter and Sauter mean diameter:

$$D_{VS} = 0.676\, d_p \qquad - 4.26$$

However, the droplets measured experimentally included those produced at the sheet edge which are generally coarser than those produced towards the centre of the sheet. Dombrowski & Johns therefore concluded that, since the results obtained from equation (4.24) only dealt with droplets produced in the central region of the sheet, the constant in equation (4.26) should be reduced to 0.63 to account for this factor.

They noted that the measured smaller droplets fell below a straight line plot of measured vs calculated diameters due to the ligaments stretching before disintegration.

Since droplet diameter is directly related to ligament diameter, as in equation (4.27), smaller droplets will therefore be produced than predicted by equation (4.24). This effect was greatest at high velocities when the disintegration time of the sheet becomes comparable to that of the ligament.

$$d_p^{\,3} = \frac{3\pi d_l^{\,2}}{n} \qquad - 4.27$$

Dorman [75] used dimensional analysis to derive an empirical equation for an inviscid liquid which related mean droplet diameter to the operating conditions of the nozzle:

$$d_p = C\frac{\sqrt[3]{\left(\frac{Q}{\theta}\right)\sigma\sqrt{\rho_l}}}{\sqrt{P}} \qquad - 4.28$$

where: d_p is the mean diameter (cm),

P is the operating pressure (psi).

C is an empirical constant.

This equation had apparently been applied to experimental data from agricultural fan spray nozzles with satisfactory results. The value of the empirical constant depended upon which mean diameter was being calculated. Dorman assigned a value of 4.4 to the constant for calculations involving the Sauter Mean Diameter obtained from a plot of equation (4.28) in the form: $y = m\,x$.

Sellens & Brzustowski [160] conducted a theoretical prediction of droplet-size distribution from the principles of conservation of mass, momentum, and energy. The analysis was based upon treating the spray as a system continuous in droplet diameter with negligible evaporation. The results obtained were considered promising but no experimental results were available to test their theory.

Gordon [161] presented a theory for the break-up of liquid drops in an air stream from which to predict a critical drop diameter for a particular velocity below which all drops were stable, and to determine the drop disintegration time. Reasonable agreement (within a factor of two) was obtained with available results. Dombrowski

& Munday [4] stated that the maximum droplet size that can remain in equilibrium during free-fall was between 0.7 and 0.8 cm, that minimum sizes had been reported less than 1μm, but that in practice droplet diameters produced by pressure nozzles were generally in the range of 10 to 1000μm.

4.2 Atomisation by Centrifugal Pressure Nozzles

The centrifugal pressure nozzle is a simple and relatively inexpensive form of atomiser which has widespread applications in combustion processes, agriculture and the chemical industries. Consequently it has attracted considerable attention from research workers and been the subject of numerous experimental and theoretical studies [4]. However, to date, little is known about atomisation mechanisms and the design engineer must rely upon general guidelines for the prediction of performance characteristics and droplet sizes.

The basic principle employed in the centrifugal pressure nozzle is the transformation of pressure energy into kinetic energy. The transfer of energy during nozzle atomisation is extremely inefficient [4] and less than 0.5% of the applied energy is actually used to break up the liquid [162]. Virtually all the remainder is converted into kinetic energy and, in the centrifugal pressure nozzle, this is carried out by the creation of a natural free vortex upstream of the nozzle orifice. This arrangement permits greater energy transfer which leads to improved atomisation [1]. As the tangential velocity is increased an air core is created in the centre of the vortex and the spray pattern takes on the form of a hollow cone. The liquid initially leaves the nozzle in the form of a liquid sheet which breaks down into droplets. The sheet velocity is constant and the thickness of the sheet diminishes as the the cone develops.

The major influences upon the atomisation of a liquid by a centrifugal pressure nozzle are due to the following factors: inertial forces of the liquid; surface tension of the liquid; viscosity of the liquid and the inertial force of the surrounding medium, as summarised in Table 4.1. Much of the work involving the effects of the above factors

upon the performance of centrifugal pressure nozzles has been concerned with the atomisation of liquid fuels.

Table 4.1: *The Effect of Physical Properties on Liquid Sheet Length*

Effect Increasing	Liquid Sheet Length
Pressure	Decrease
Viscosity	Increase
Surface Tension	Decrease
Liquid Density	Increase
Air Density	Decrease

4.2.1 Hydrodynamics of Flow within the Nozzle

Longwell [84] studied the atomisation of fuels from oil burners to establish the effect of variations in liquid properties. A notable finding was that an increase in viscosity produced a decrease in the cone angle of the spray. For an inviscid fluid the cone angle was correlated in terms of a series of dimensionless groups involving the nozzle dimensions. Under identical conditions, nozzle performance could be classified in terms of the ratio of swirlchamber height to orifice radius; a smaller ratio gave better atomisation performance, with the ideal ratio being three. Hayashi & Takeda [163] reported that the loss in atomisation efficiency caused by increasing orifice size could be off-set by reducing the orifice length to diameter ratio. It was then possible to design a nozzle with a high throughput without any loss in performance. They concluded that ratios in the region of 0.125 produced the best performance with flowrates as great as 5600 l/h.

A correlation between nozzle dimensions and performance was presented by Doble [164]. A series of nomograms were presented which related the critical dimensions of the nozzle to throughput, operating pressure and spray cone angle. This information was used to determine the nozzle throughput in the range of 4 to 1800 gallons per hour for any pressure between 20 and 100 psi. The cone angle was

determined by the dimensions of the exit orifice and the number, size and shape of the distribution channels within the nozzle. This work was extended by Doble & Halton [165], who drew an analogy between the nozzle swirlchamber and a regular cyclone. Their theory assumed the presence of a free vortex and introduced a velocity ratio term (Φ), representing the ratio of outlet and inlet velocities, which had previously been defined by Stairmand [166] as,

$$\Phi = \frac{\sqrt{\frac{r_o}{2 D_i} + \frac{4 F A_N}{A_i}} - \sqrt{\frac{r_o}{2 D_i}}}{\frac{2 F A_N}{A_i}} \qquad - 4.29$$

where, F is the friction factor = 0.02

A_i is the cross-sectional area of the inlet port

A_N is the internal surface area of the swirlchamber in contact with the fluid,

or,

$$A_N = \pi\left[\left(r_n^2 - r_{ac}^2\right) + 2\left(r_n l_s + r_o l_o\right) + A_1\right]$$

and,

$$A_1 = \left[\left(r_o^2 - r_n^2 - \left(l_n - l_s\right)^2\right)\left\{r_n\left(\frac{1}{\left(\frac{r_n^2}{r_o^2} - 1\right)}\right) - r_o\left(\frac{1}{\left(1 - \frac{r_n^2}{r_o^2}\right)}\right)\right\}\right]$$

where l_n, l_s, and r_n are defined in Figure 4.4.

The volumetric flowrate through the swirlchamber can be defined by,

$$Q = \frac{A_I U_I}{\Phi} = \int_{r_{ac}}^{r_o}\left\{2\pi r U_I \sqrt{2 D_I\left(\frac{1}{r_{ac}} - \frac{1}{r}\right)}\right\} dr \qquad - 4.30$$

Using the assumptions of free vortex flow within the swirlchamber and conservation of momentum, equation (4.30) was expanded into an expression to determine the air core diameter. Given the air core diameter it was possible to

Figure 4.4: *Principal dimensions of the Swirlchamber*

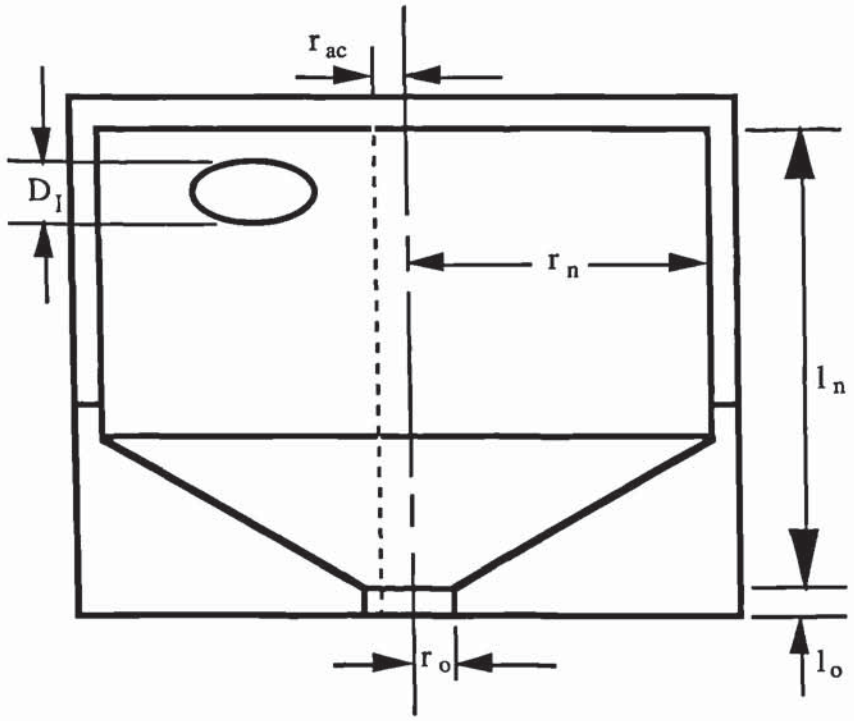

determine the cone angle and nozzle discharge coefficient from mass balance and co-ordinate geometry. Reasonable agreement was obtained with experimental data, but the theory was severely limited by the requirement for prior knowledge of the internal surface area of the swirlchamber.

Nieukamp [167] extended the standard mathematical expression for the flow within the nozzle to include an expression for flow at the exit that drew analogies from flow over a weir. This avoided the use of empirical values in the calculation of the air core diameter, sheet velocity and the cone angle. The work was based upon the assumption of rotationally symmetric flow neglecting the influences of gravity and viscosity. The expression involved a centrifugal potential term, G, which replaced the gravitational term in the weir flow equation,

$$V_o = \sqrt{g\,h^*} = \sqrt{G\,h^*} = \sqrt{\frac{U_o^{\,2}}{r_{ac}}\,h^*} \qquad - \ 4.31$$

The term for the height of flow, h*, was equivalent to the film thickness at the orifice, h_i, which upon substitution gives

$$V_o = \sqrt{\frac{U_o^2}{r_{ac}} h_i} = \sqrt{\frac{U_o^2}{r_{ac}} \left(\frac{D_o}{2} - r_{ac}\right)} \qquad - 4.32$$

An expression was derived for the air core diameter in terms of nozzle dimensions and, in agreement with Doble & Halton [165], the cone angle was found to be independent of the flow conditions. Good agreement was obtained with experimental data for water but it was concluded that the expression only applied to inviscid liquids as an increase in viscosity would reduce the centrifugal potential and consequently the air core diameter.

From tests with perspex nozzles, Darnell [71] showed that the air core diameter for any given nozzle remained relatively constant. The ratios of air core diameter to orifice diameter were generally in the range 0.6 to 0.8, except for the case of small orifice diameters when it was approximately 0.3. Marshall [53] introduced expressions for predicting the air core diameter within the swirlchamber and the nozzle orifice. The air core diameter within the orifice was found to be larger than in the swirlchamber because in the latter the effect of the radial velocity component could be ignored.

The air core in the region of the swirlchamber is determined by,

$$R_{ac} = \sqrt{\frac{\Omega^2 \rho_l}{2 g P}} \qquad - 4.33$$

The air core diameter in the orifice is determined from knowledge of the discharge coefficient:

$$C_D = \sqrt{\frac{a^3}{(2 - a)}} \qquad - 4.34$$

where,

$$a = 1 - \left(\frac{r_{ac}}{r_o}\right)^2$$

Sankarankutty *et al* [168] studied the effects of pressure and nozzle geometry upon the air core diameter. There was a tendency for the air core within the nozzle to become more uniform as the pressure increased. Under the test conditions no increase in the size of the air core occurred beyond 50 psi; the air core was not co-axial with respect to the nozzle axis but exhibited a slight offset in its size towards the rear of the swirlchamber. However, there was initially poor definition of the air core in the region near the orifice; this was resolved by viewing the air core via the exit of the nozzle with a series of baffles installed to prevent the spray impinging on the camera lens. This experimental set-up resulted in high definition pictures of the air core in the orifice and the method was considered capable of registering minute variations in the size of the air core.

Taylor [169] presented a model of the flow within the nozzle and showed, from mathematical reasoning, that the radius of the air core was smaller in the swirlchamber than the nozzle orifice. However, measurements of real fluids indicated that the air core diameter was virtually the same throughout the nozzle. It was deduced from this that perfect fluid theory had no application in the hydrodynamics of swirlchamber atomisers. The work was extended [170] to apply boundary layer theory to the flow within the nozzle in an attempt to explain discrepancies between theoretical and experimental discharge coefficients. Viscous drag at the surface of the swirlchamber was considered to retard the rotating liquid causing a current to be created towards the orifice acting through a surface boundary layer. Taylor went on to develop an expression for the thickness of this boundary layer, δ_1:

$$\frac{\delta_1}{r_o} = \frac{\delta_2}{R_D \operatorname{Sin} \varpi} \sqrt{\frac{\upsilon \operatorname{Sin} \varpi}{\Omega}} \qquad - 4.35$$

where δ_2 and R_D are dimensionless variables defined by,

$$\delta_2 = \frac{\delta_1}{r_o} \sqrt{\frac{\Omega}{\upsilon \operatorname{Sin} \varpi}} \qquad - 4.36$$

$$R_D = \frac{R_1}{r_o} \qquad - 4.37$$

The circulation constant for vortex flow within the nozzle is defined by,

$$\Omega = V_\theta r^f \qquad - 4.38$$

Equation (4.35) was modified to account for frictional drag,

$$\Omega' = C_D \frac{r_o^2}{R_I} U_s r_n \qquad - 4.39$$

where,

$$U_s = \left(\frac{2P}{\rho_l}\right)^{\frac{1}{2}}$$

Free vortex flow (ie, when f = 1) and a negligible axial velocity component were assumed in order to obtain an expression for the boundary layer thickness due to rotational flow. Based on these assumptions a large proportion of the total flow through the orifice was shown to travel through the boundary layer, even in the case of low viscosity liquids. An increase in liquid viscosity would cause the boundary layer to increase even in the absence of an air core. McIrvine [2] presented a comparison of the boundary layer thickness predicted by Taylor's theory with experimental data from a study of air core diameter by high speed photography. The results verified that, for viscous liquids, a substantial part of the film thickness was occupied by the boundary layer. Ashton [171] extended Taylor's derivation for swirlchamber atomisers and developed a model which predicted fluid flow through the nozzle. The model was expressed in terms of Cartesian coordinates which enabled a numerical solution to be obtained for any swirlchamber geometry. It was found that when the fluid viscosity exceeded 0.03 Ns/m^2 all of the fluid passed through the boundary layer.

Doumas & Laster [172] obtained an empirical correlation between the dimensions of the nozzle and the physical properties of the liquid being atomised. Based upon their theoretical analysis, a series of empirical equations were presented that predicted the cone angle, air core diameter, liquid sheet velocity and nozzle discharge coefficient. Comparison of experimental data from forty different nozzles

gave good agreement with the calculated results with a discrepancy in many cases of less than 7%.

Tate & Marshall [72] stated that the primary parameters of nozzle design influencing spray characteristics were the size of the orifice, which affected nozzle capacity and air core diameter, and the internal construction of the nozzle which affected the magnitudes of the velocity components and, hence, the degree of atomisation. Liquid viscosity was considered the most important of all the liquid physical properties influencing both the air core diameter and the final droplet size. An increase in viscosity reduced the air core diameter resulting in an increase in the mean droplet size and a decrease in spray uniformity. The influence of orifice surface finish upon liquid atomisation was studied by observing atomisation from a straight-edged and a rounded orifice with the same applied pressure. A larger cone angle, slightly greater capacity and smaller droplet size were obtained from the latter. The increase in capacity was attributed to a lower resistance to flow due to the rounded orifice; this also caused an increase in the tangential velocity component resulting in a larger cone angle and smaller droplet size.

The atomisation performance of a range of swirlchamber atomisers was investigated by Radcliffe [173], who included a study of the effect of nozzle dimensions on flow number and spray cone. Unfortunately many of the nozzles tested were not of the standard design, and often had inlet ports which were not truly tangential. Spray cone angle was found to increase with an increase in outlet orifice diameter and decreased with an increase in the inlet orifice diameter; an increase in both diameters caused an overall increase in the spray cone. However, Carlisle [174] criticised Radcliffe's work and highlighted the non-standard design of the nozzles tested and pointed out that their inclusion may have obscured many useful empirical relations. Nevertheless it was concluded that, with slight corrections to allow for non-standard design, Radcliffe's results were useful in the design, and prediction of performance, of swirlchamber atomisers.

Elkotb *et al* [175] found that atomisation was affected by the number of swirlchamber inlet ports. An improvement in the uniformity of the spray was

observed when the number of inlet ports was increased. This was attributed to a more regular fluid momentum within the swirlchamber and three inlet ports was recommended as the optimum number for sufficient spray uniformity. The mean droplet size decreased as the swirlchamber length to diameter ratio was increased until a minimum was achieved at 2.75; there was then a gradual increase in droplet size. The mean droplet size was also affected by the orifice length to diameter ratio, an increase in the ratio causing a decrease in droplet size.

Rizk & Lefebvre [176] investigated the effects of atomiser dimensions and operating conditions upon the cone angle and discharge coefficient. By adopting a theoretical approach to relate orifice film thickness to cone angle and discharge coefficient, they found that film thickness was totally independent of surface tension but was influenced by the viscosity and, to a lesser extent, the density of the liquid. Their calculated results were shown to be in reasonable agreement with experimental data reported in the literature [177].

Giffen & Massey [178] found that the discharge coefficient for centrifugal pressure nozzles was considerably less than for plain nozzles because tangential velocity is not taken into account. The nozzle discharge coefficient was found to increase with an increase in liquid viscosity due to greater frictional losses causing a reduction in tangential velocity within the swirlchamber and a relative increase in the axial velocity. An increase in liquid viscosity required a greater pressure to initially produce the air core and a reduction in its diameter, whereas, an increase in surface tension had little effect on the discharge coefficient and no effect upon the air core diameter. Over the range of viscosities tested, an increase in viscosity caused a reduction in the cone angle. An increase in surface tension caused a slight decrease in the cone angle of the spray, due to a corresponding decrease in the tangential velocity, with no significant effect upon the axial velocity.

Dombrowski & Hasson [177] studied the flow of low viscosity liquids through swirl spray nozzles and proposed a relationship between discharge coefficient and spray cone angle which was dependent only upon the orifice length to diameter ratio.

The nozzle parameter Δ, defined by equation (4.41), and the ratio of the mean vortex diameter to the orifice diameter could therefore be included in one parameter, β,

$$\beta = \left\{ \Delta \left(\frac{D_{MV}}{D_o} \right)^{1 - f} \right\} \qquad - 4.40$$

where,

$$\Delta = \frac{A_i}{D_o D_{MV}} \qquad - 4.41$$

and f is the index of fractional decay defined by equation (4.38).

The exponent f was taken to be 0.5 and deviation from ideal flow within the nozzle caused the nozzle parameter to be modified, as in equation (4.42), to include a correction factor for spray angle (C_θ) which was dependent upon the orifice length to diameter ratio.

$$\Delta' = C_\theta \left[\Delta \sqrt{\frac{D_{MV}}{D_o}} \right]^{0.67} \qquad - 4.42$$

This modified parameter was then used to obtain a modified discharge coefficient which was related to the true discharge coefficient by the empirical expression,

$$C_D = C_d C_D' - 0.05 \qquad - 4.43$$

The values for C_θ and C_d were determined by a correlation given in the source reference [177].

Ranganadha Babu *et al* [179] developed empirical expressions for air core diameter, discharge coefficient and cone angle based upon the expression for vortex flow, given by equation (4.38). Exponent f was a function of pressure and atomiser geometry at pressures below 400 psi and for any given atomiser geometry the variation of f with pressure was almost linear. However, for pressures above 400 psi f was independent of pressure and purely a function of atomiser geometry. The principle parameters of geometry were identified as orifice diameter, inlet port diameter and swirlchamber diameter. Droplet size was affected by atomiser geometry with increases

in orifice diameter and inlet port diameter causing an increase in the mean droplet diameter, with the inlet port diameter having the greater influence.

A correlation was proposed for the Sauter Mean Diameter when the discharge pressure was in the range of 100 to 1000 psi,

$$D_{VS} = f\left(A_i, A_o, A_{sc}, P\right) \qquad - \ 4.44a$$

or,

$$D_{VS} = f\left(h_i, D_o, V_o, U_o, P\right) \qquad - \ 4.44b$$

Their results showed good agreement (within 10%) of experimental data in the regions both above and below 400 psi. In subsequent work [180] the droplet size was found to decrease rapidly with an increase in pressure up to 400 psi; beyond 400 psi the effect of pressure upon droplet sizes diminished continuously. Earlier work was extended [181] to design swirlchamber nozzles that were able to achieve specified discharge rates, cone angles and mean droplet sizes. However, it was possible that several combinations of the main geometrical parameters could achieve a particular set of design criteria and the most suitable combination could only be determined from previous experience.

Non-Newtonian Fluids

Kawase & Shirotsuka [182] investigated the effects of fluid elasticity upon the break-up of viscoelastic liquid sheets. Their theoretical analysis indicated that liquid elasticity increased the number of ligaments generated during the disintegration of the sheet. They concluded that the diameter of the ligaments and hence of droplets decreased due to the liquid elasticity and, in the absence of strong non-Newtonian liquid characteristics, good comparison was obtained between experimental and theoretical results for power law fluid systems.

In an investigation into the spray characteristics of detergent slurries Nakamura *et al* [183] reported that an increase in the air content of the slurry caused a decrease in the droplet size but had no appreciable effect upon the discharge coefficient of the

nozzle. They approximated the rheological properties of the detergent slurry to those of a Bingham plastic represented by the generalised equation,

$$\tau = \tau_o + A\gamma^B \qquad - 4.45$$

where A and B are experimentally determined constants.

The slurry viscosity was found to be considerably lower under the conditions of atomisation (less than 0.1 Pa s) than that determined by the usual method (between 2 to 5 Pa s).

4.2.2 Conical liquid Sheets

Hodgkinson [184] investigated the influence of surface tension upon the formation and subsequent break-up of a conical liquid sheet. The analysis predicted several critical stages in the development of the conical sheet which were similar to those found in swirlchamber nozzles. However, this work could not be justifiably applied to swirlchamber nozzles due to the initial assumptions that the sheet does not rotate and that all the kinetic energy from the expansion of the sheet is transferred to the droplets produced. It was concluded that in the case of these nozzles the conical sheet had both tangential and axial velocities which varied due to their relative position on the sheet. Additionally the sheet must vibrate at a frequency that is determined by the swirl velocity at the air core and the influence of aerodynamic forces.

Dombrowski & Tahir [185] investigated the atomisation of oils with viscosities in the range of 0.0053 to 0.021 kg/ms and found that for a given sheet velocity the mean droplet size was unaffected by liquid viscosity. This conclusion was contrary to that reported for other forms of atomiser. Viscosity discrepancies reported by previous investigators were found to only occur when correlations were based upon constant injection pressure, where the reduction in sheet velocity caused by an increase in viscosity had not been taken into account. Empirical correlations were presented which satisfactorily expressed mean droplet size, size distribution and sheet velocity in terms of the operating variables. However, since the experiments were conducted at

normal atmospheric temperature and pressure the results were only applicable to nozzles operating under similar conditions.

Johnson [186] investigated the hydrodynamics of flow within the nozzle as part of a more detailed study into the simulation of spray drying towers. A model was derived which allowed for the effect of wall friction within the nozzle and took into account the fact that the air core is not entirely uniform within the nozzle. Two mechanisms of sheet break-up were examined:

a) that caused by irregularities within the air core, and,

b) that caused by aerodynamic forces acting upon the sheet.

An expression was developed to estimate the initial amplitude of the disturbance in both cases. The mechanism caused by aerodynamic forces was favoured and extended to include droplet formation with a prediction of a maximum and minimum sizes. The mass median diameter could be estimated from,

$$\text{Mass Median Diameter} = 0.4\left(d_{max} - d_{min}\right) + d_{min} \qquad - \ 4.46$$

Good agreement was obtained between computed results and those published by the Spraying Systems [187] and Delevan companies [188].

Dombrowski & Wolfsohn [96] reported a general trend which indicated that the sheet velocity decreased with increasing spray cone angle. Several different types of swirl nozzle were tested; the droplet sizes were found to be independent of nozzle design, although generally smaller than reported by previous workers. In a further investigation [189] a wide variation was observed in the break-up length of the liquid sheets (in the order ±30%) produced by different nozzles. This effect was deduced to be either due to disturbances in the air core as postulated by Taylor [190], or to wave formation on the conical sheet caused by pump pulsations. The latter hypothesis was tested by replacing the pump with a pressure vessel and injecting water through the nozzle using compressed air. Since the variations in the liquid sheet were of the same order as before it was inferred that disturbances in the air core were the main cause of wave formation.

A correlation was therefore introduced to predict the break-up length of a conical sheet, adapted from a similar expression for a flat inviscid liquid sheet [8],

$$l_b = \left[\frac{9}{2}\frac{\rho_l}{\rho_a}\sigma\right]^{0.33} \frac{(Q)^{0.33}}{V_s(\text{Sin }\theta)^{0.33}} \qquad - \ 4.47$$

From equation (4.47) the break-up length was predicted to be independent of nozzle design and the best correlation of experimental data was obtained when the empirical constant was assigned the value 133, with the rest of the terms expressed in imperial units. Dombrowski & Tahir [185] also investigated the hypothesis that sheet disturbances were caused by the flow disturbances in the air core as suggested by Taylor. High speed photographs revealed the presence of complex wave forms in the air core which suggested that the disintegration of the conical sheet was significantly influenced by the nature of the flow within the air core.

Som [56] noted that for both Newtonian and Non-Newtonian liquids the ratio of mean droplet diameter to the liquid sheet thickness at the orifice was inversely proportional to the Weber number which was based upon sheet thickness and velocity at the orifice. The discrepancy between the results of theoretical and experimental work were considered to be due to the nature of the liquid sheet produced by a centrifugal pressure nozzle. The theoretical analysis was based upon a flat sheet, generally of uniform thickness, whereas in reality the sheet was conical with decreasing thickness and, thus, differed in both curvature and uniformity of thickness. This reduction in the sheet thickness was determined by the spray cone angle, liquid sheet velocity and the break-up length of the sheet. York & Stubbs [155] reported typical values of the reduction ratio for liquid sheets between 0.1 to 0.3.

4.2.3 Droplet Size Predictions

Novikov [191] presented an expression for droplet formation which showed that the droplet diameter was proportional to the cube root of surface tension and inversely proportional to the cube root of pressure. The droplet diameter was independent of density and the outlet orifice dimensions but was influenced by the dimensions of the inlet orifice and swirlchamber. The results were concluded to be in good agreement with the limited amount of experiment data available with even the significant discrepancies being within the limits of experimental error.

In his work based upon Taylor's analysis, Ashton [171] obtained an expression for droplet size, based upon the cone angle, liquid sheet length and velocity:

$$d_p = 0.524\left[\frac{Q}{V_s^{\,3}\, l_b \sin\theta}\right]^{0.5} \qquad - \ 4.48$$

A comparison of the predicted droplet size from equation (4.48) and measured Sauter mean diameter produced the straight-line relationship given by equation (4.49),

$$D_{VS} = 0.547\, d_p + 76.8 \qquad - \ 4.49$$

Although this expression predicts droplet sizes of a similar magnitude to those determined by Dombrowski & Johns [10] it clearly does not pass through the origin. This can either be accounted for by measurement inaccuracies or by discrepancies in the predicted droplet sizes at higher injection pressures (small droplet size). However, the measured mean droplet sizes in this investigation were generally greater than those determined by previous workers. For example, the data of Dombrowski & Tahir [185] gave droplet sizes approximately 26% smaller than those measured by Ashton which seems to indicate that some measurement errors may have arisen.

Hasson [192] stated that although Joyce [81] reported that for swirl spray nozzles the Sauter Mean Diameter varied as a function of $\mu^{0.2}$, in the absence of comparable work for fan sprays, it appeared that the effect of viscosity on the droplet size was not as great. In swirlchamber atomisers the effects of viscosity influenced sheet break-up and affected the air core diameter; however, it had been shown that in

fan spray nozzles viscosity only affects sheet break-up, with a negligible effect on liquid sheet thickness. The overall effect of viscosity on drop sizes for fan sprays was therefore smaller, as indicated by experiments conducted by Dorman [75] which indicated that the variation was less than $\mu^{0.1}$.

However, because of a similarity between the expressions for droplet size for all types of spray created from an attenuating liquid sheet, the theoretical evidence seemed to indicate that the mean droplet size produced by pressure atomisers varied according to the expression,

$$d_p \propto \frac{1}{P^n}\left(\frac{\rho_l}{\rho_a}\right)^{\frac{1}{2n}} \qquad - \ 4.50$$

where: n has a theoretical value of 1/3 but varied experimentally between 1/2 and 1/4.

Table 4.2 summaries the numerous empirical and mathematical expressions for determining droplet diameter that have been proposed in the literature. The merits and deficiencies of each expression are often difficult to determine because many define entirely different droplet diameters. It is therefore difficult to compare the individual expressions, especially when the operating conditions and the type of the nozzle used vary significantly. Generally the main disadvantage of the expressions shown in Table 4.2 and the work described above lies in the limited range of conditions for which the expressions remain valid and their inability to predict any form of droplet size distribution. Although knowledge of the principal diameters is useful for droplet evaporation or combustion purposes, it is important that a droplet size distribution is defined in order to determine the maximum and minimum operating conditions for the process under investigation. Chapter 5 describes the development of such a model.

Table 4.2: *Correlations for Droplet Diameters Produced by Swirlchamber Atomisers*

Author	Droplet Size Equation	Application and Limits
Longwell [84]	$D_{VM} = \frac{D_o K_L e^{0.705 \frac{\mu}{P}}}{2 \sin \theta \, \Delta P^{0.375}}$	Fuel Oils: $K_L = 0.72$
Novikov [191]	$D = 1.89 \sqrt[3]{\frac{\sigma r_i^4}{P r_n^2}}$	No limits or applications quoted in the text.
Joyce [81]	$D_{VS} = K_{JO} \left(\frac{D_o^{0.5} \mu^{0.2}}{\Delta P^{0.4} \rho_l^{0.2}} \right)^{0.5}$	Fuel wax K_{JO} = constant
Darnell [71]	$D_{VM} = \frac{2760}{\Delta P^{0.5}}$ $D_{VS} = \frac{2400}{\Delta P^{0.5}}$	Water Pressure: 5 to 1500 psi FN: 0.45 to 3.0

Table 4.2 (continued)

Author	Droplet Size Equation	Application and Limits
Tate & Marshall [72]	$D_{VS} = 286\left(D_o + 0.17\right) e^{\left(\frac{13}{V_o} - 0.0094\, U_o\right)}$	Water U_o = 7 to 50 ft/s V_o = 40 to 150 ft/s D_o = 0.0135 to 0.04 in
Turner & Moulton [87]	$\overline{D} = 41.4 \frac{D_o^{1.389}\, \sigma^{0.594}\, \mu^{0.220}}{Q^{0.537}}$ Where: $\ln \overline{D} = \frac{\sum n D^3 \ln D}{\sum n D^3}$	Naphthol and Benzoic acid Pressure: 33 to 125 psi Viscosity: 0.81 to 2.02 cP Surface Tension: 26.9 to 37.2 Dynes/cm
York et al [155]	$D = 2.12 \sqrt{\frac{h\, \sigma\, We^*}{\rho_a V_a^2}}$ where: $We^* = \frac{\lambda V_a^2 \rho_a}{\sigma}$	Water, typical values: V_a = 1910 cm/s ρ_a = 0.00112 gm/cc σ = 74 dynes/cm

Table 4.2 (continued)

Author	Droplet Size Equation	Application and Limits
Radcliffe [173]	$D_{VS} = 325 \frac{Q^{0.318}}{\Delta P^{0.530}}$	Fuel oil mixtures Pressure: 6 to 125 psi FN: 0.5 to 4.15
Knight [174]	$D_{VS} = 220 \frac{Q^{0.209}}{\Delta P^{0.458}} \upsilon_l^{0.215}$	Fuel wax Pressure: 50 and 1000 psi Kinematic viscosity: 2.3 cS Volumetric Flowrate: 2 and 200 lb/h
McIrvine [2]	$D_{VM} = K_{MI} \frac{D_o^{1.28} \mu^{0.19} \sigma^{0.24}}{\Delta P^{0.33}}$	Sucrose/Water solutions K_{MI} = constant
Fraser *et al* [193]	$D_{VS} = 335 \frac{Q^{0.209}}{\Delta P^{0.036}} \upsilon_l^{0.215}$	Fuel wax Pressure: 12 to 300 psi Kinematic viscosity: 2.0 to 18.5 cS FN: 0.5 to 2.0

Table 4.2 (continued)

Author	Droplet Size Equation	Application and Limits
Nelson & Stevens [80]	$\log_{10}\frac{D_{VM}}{D_o} = -0.0811\,Y^2 + 0.124\,Y - 0.186$ Where: $Y = \log_{10}\left(Re\left(\frac{We}{Re}\right)^{0.55}\left(\frac{U_o}{V_o}\right)^{1.2}\right)$	Organic Liquids Pressure: 100 to 1500 psi
	$\log_{10}\frac{D_{VM}}{D_o} = -0.144\,Y^2 + 0.702\,Y - 1.260$ Where: $Y = \log_{10}\left(Re\left(\frac{We}{Re}\right)^{0.2}\left(\frac{U_o}{V_o}\right)^{1.2}\right)$	Water Pressure: 100 to 1500 psi
Dombrowski & Wolfsohn [95]	$D_{VS} = 332\frac{Q^{0.333}}{\Delta P^{0.5}}$	Water Pressure: 50 to 350 psi Volumetric Flowrate: 1 to 724 gal/h
Dombrowski & Tahir [185]	$D_{VS} = 2774\frac{Q^{0.248}\mu^{0.152}}{P^{0.499}}$	Lubricating Oils Pressure: 50 to 600 psi Viscosity: 0.0053 to 0.0207 kg/ms

Table 4.2 (continued)

Author	Droplet Size Equation	Application and Limits
Abou-Ellail *et al* [194]	$D_{VS} = \frac{188}{\Delta P^{0.35}} \frac{1}{\left[P_a^{0.26} \left(\frac{T_{am}}{T_a} \right)^{0.56} \right]}$	Kerosene Pressure: 1 to 17 atm Air Pressure: 1 to 5 atm Air Temperature: 300 to 700 K
Ashton [171]	$D_{VS} = 0.459 \left(\frac{Q}{V_s l_b \sin \theta} \right)^{0.5}$	Chalk slurry Pressure: 483 to 1103 kN/m^2 Mass flowrate: 11.8 to 14.9 kg/s Slurry Density: 1165 to 1429 kg/m^3
Ranganadha Babu *et al* [181]	Pressure < 400 psi: $D_{VS} = 170 \frac{Q^{0.642}}{\Delta P^{0.547}}$ Pressure ≥ 400 psi: $D_{VS} = 134 \frac{Q^{0.753}}{\Delta P^{0.576}}$	Kerosene Pressure: 100 to 1000 psi Volumetric flowrate: 6 to 200 cc/s

Chapter 5: Mathematical Model

Introduction

Three factors affect the size of droplets produced during liquid atomisation: the atomiser design, which determines the way in which the liquid is discharged; the liquid properties which influence the behaviour of the disintegrating sheet, and the spraying atmosphere which affects the mode of disintegration.

In the atomiser potential energy of the fluid is converted into kinetic energy and applied to the process of disintegrating the bulk liquid. There is a substantial energy loss involved in this process [4] and the efficiency of the ensuing liquid atomisation will depend to a large extent upon the design and manufacture of the atomiser [162]. In many processes the atomiser also has the additional function of distributing the liquid droplets throughout the drying chamber by controlling the trajectory of the spray.

Liquid properties affect spray characteristics in two ways: through their role in the break-up of the liquid sheet and due to their influence upon the liquid hydrodynamics occurring within the nozzle. The properties of most relevance to the atomisation process are density, surface tension and viscosity. It has been shown in previous work [195] that the effect of liquid density upon the droplet size distribution is quite small but it has a significant influence upon liquid flow within the swirl-chamber. Surface tension forces have a negligible influence upon the internal liquid flow [162] but will tend to impede atomisation by resisting the formation of any disturbances in the liquid; consequently ligament formation will be delayed. Viscous forces also have a tendency to suppress the formation of wave disturbances upon the liquid sheet [195] and Giffen & Muraszew [162] showed that viscosity affected liquid flow within the swirlchamber by introducing frictional forces in the bulk liquid and at the boundary between the liquid and chamber wall.

The spraying atmosphere encompasses the combined effects of temperature, humidity and the relative spray-air velocity and affects the liquid sheet in two ways.

Firstly it influences the primary mechanism of sheet disintegration, ie whether sheet break-up occurs as a result of wave formation, sheet perforation or another form of mechanism. The second effect is that of air entrainment into the liquid sheet caused by wave disturbances increasing the frictional drag of the air [6]. In regions of high disturbance, ie close to sheet break-up, the air will flow perpendicularly into the sheet enhancing liquid turbulence and subsequently affecting sheet disintegration. There is an additional effect of air entrainment caused by the conical sheet; the pressure inside the conical sheet near the nozzle is reduced by continual entrainment and the surrounding air moves inwards towards the nozzle axis in a direction normal to the surface of the sheet. This will enhance any wave motion present upon the surface of the conical sheet.

Figure 5.1: *Break-up of a Conical Liquid Sheet*

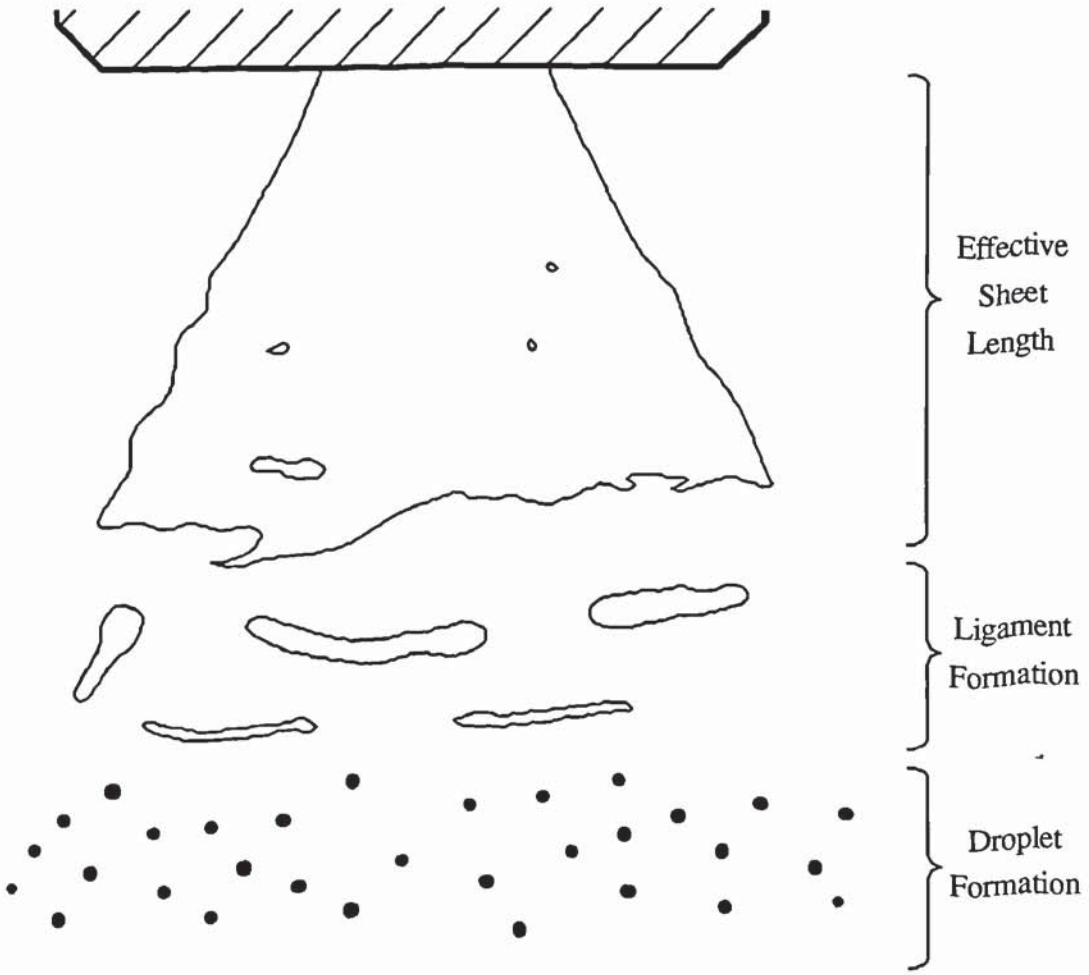

Figure 5.1 illustrates the three fundamental stages associated with the break-up of a conical liquid sheet. The conical sheet is produced by the tangential entry of the liquid into the nozzle swirlchamber. Upon leaving the orifice the sheet gradually expands and its thickness decreases until a point where break-up occurs, initially into a series of ligaments and then into a myriad of droplets.

In this chapter consideration is given to the centrifugal pressure nozzle and the mechanism of atomisation associated with this type of nozzle. The case of the swirlchamber or simplex-swirl nozzle is studied in detail. There are many designs commercially available [187][188]. However all essentially consist of a cylindrical upper-section, where the liquid enters tangentially, and a conical section through which the liquid passes to create the characteristic conical sheet.

5.1 Liquid Flow in the Swirlchamber

Liquid flow in the swirlchamber can best be described by analogy to a free spiral vortex, as illustrated in Figure 5.2. In this type of motion, an element of liquid entering the swirlchamber, although maintaining its position relative to the surrounding liquid, will be subjected to motion in the radial, axial and tangential directions during its passage through the swirlchamber. Therefore both tangential and radial velocity components can be represented as functions of the radial distance from the swirlchamber axis, ie

$$V_r = f\left(\frac{1}{r}\right) = \frac{\chi}{r} \qquad - 5.1$$

$$V_\theta = f\left(\frac{1}{r}\right) = \frac{\Omega}{r} \qquad - 5.2$$

where, χ is the radial proportionality constant,

Ω is the circulation constant.

The vortex is created by cavitation of the spinning liquid caused by its tangential entry into the chamber. An increase in the swirling motion will cause the vortex to expand

along the axis of the chamber to form an air core. The presence of an air core is explained by the condition of infinite velocity at the chamber axis, ie when r = 0.

Figure 5.2: *Free Spiral Vortex Flow*

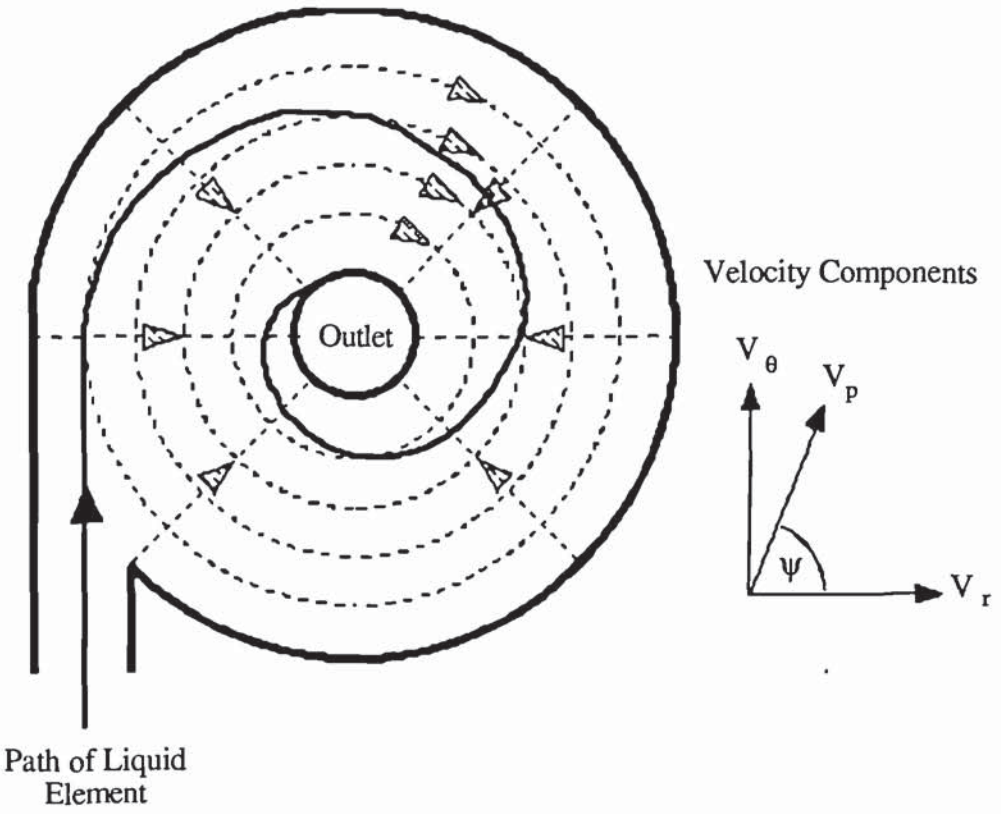

The resultant velocity of the vortex at any point in the chamber (V_p) can be defined by equation (5.3) and its trajectory (ψ) by equation (5.4).

$$V_p = \sqrt{V_r^2 + V_\theta^2} = \frac{\sqrt{\chi^2 + \Omega^2}}{r} \qquad - 5.3$$

$$\psi = \text{Tan}^{-1}\left(\frac{V_\theta}{V_r}\right) = \text{Tan}^{-1}\left(\frac{\Omega}{\chi}\right) = \text{constant} \qquad - 5.4$$

It is not within the scope of this model to undertake a detailed investigation of liquid hydrodynamics within the swirlchamber and, indeed without employing a three-dimensional computer modelling package, for example Phoenics [196], the accurate prediction of internal flow mechanisms is virtually impossible. However, it is

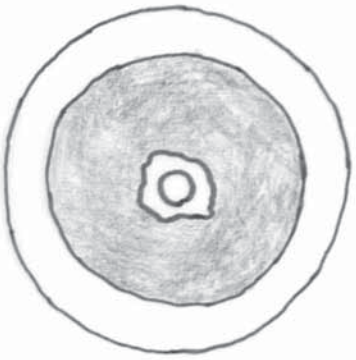

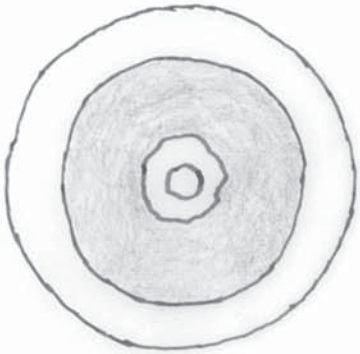

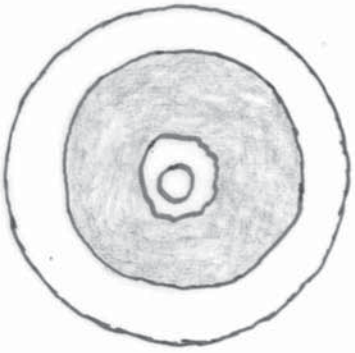

Region of Swirlchamber occupied by dye

Plate 2: *Flow Regimes in the Swirlchamber*

a) t = 0: Dye entering the chamber

b) t = 2: Most of dye has left chamber

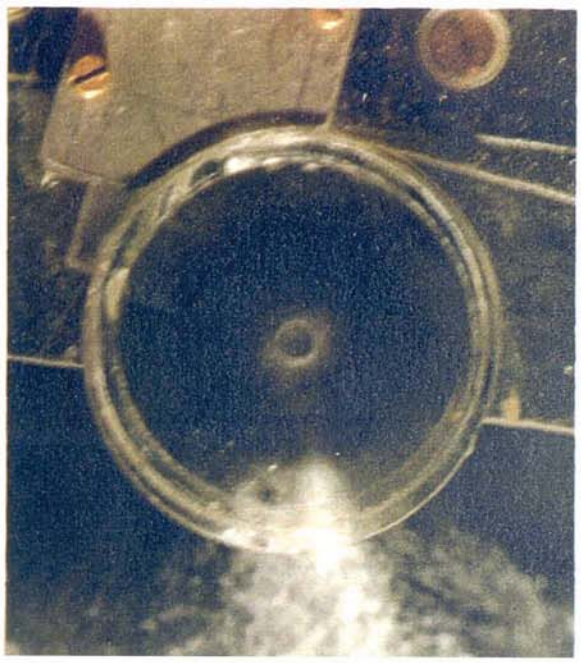

c) t = 4: A stagnant zone is visible

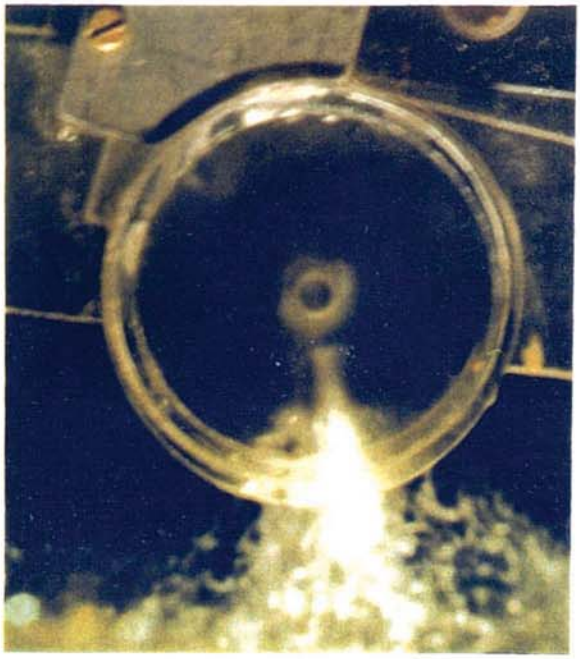

d) t = 6: Stagnant zone still visible

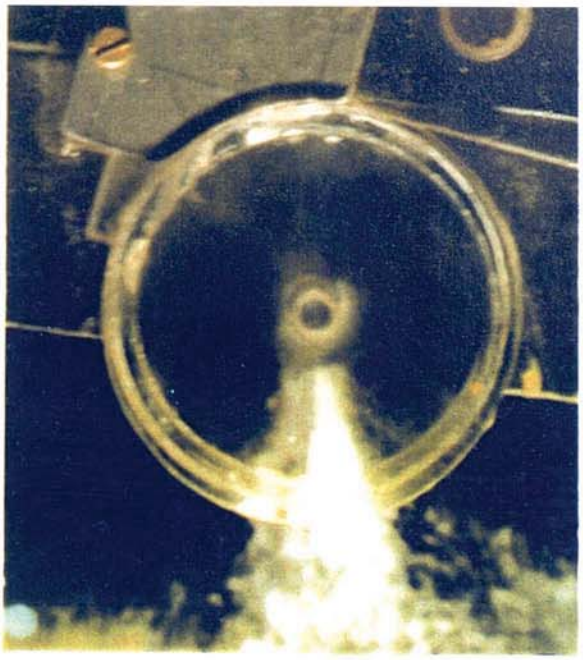

Plate 2: ***Flow Regimes in the Swirlchamber***

a) t = 0: Dye entering the chamber

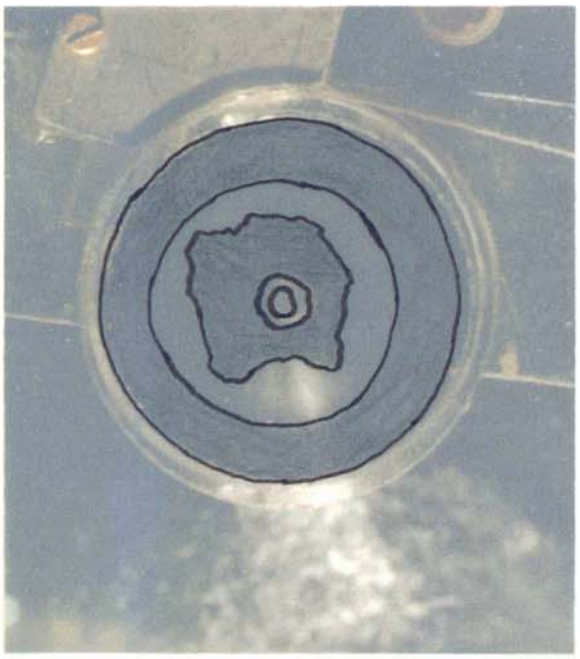

b) t = 2: Most of dye has left chamber

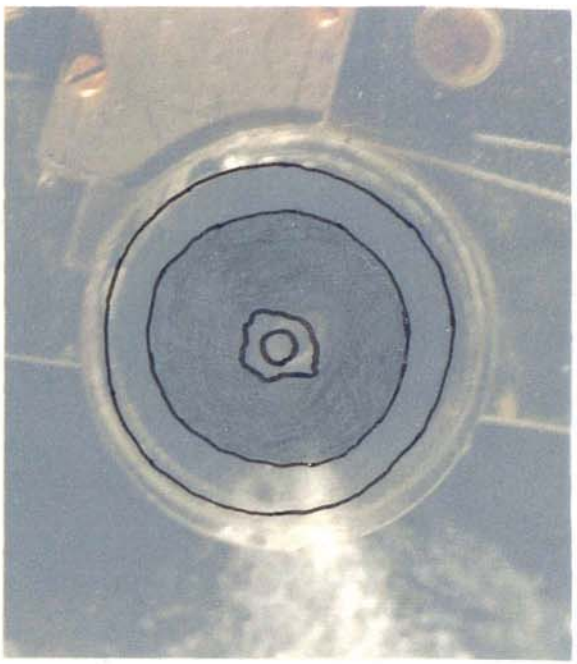

t = 4: A stagnant zone is visible

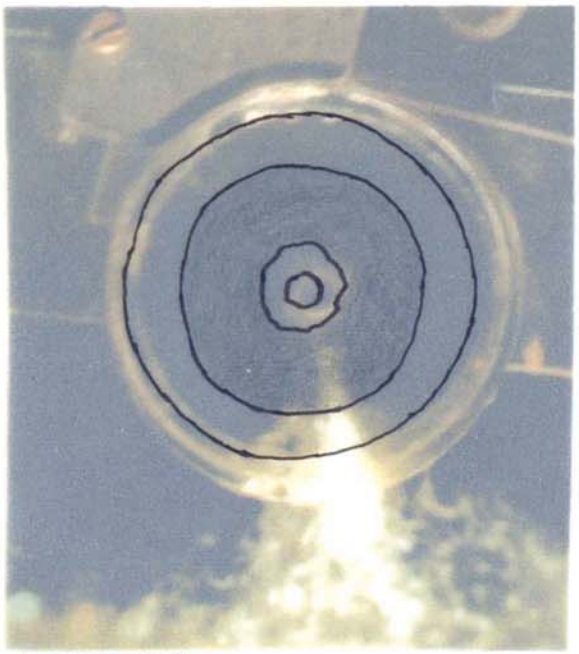

d) t = 6: Stagnant zone still visible

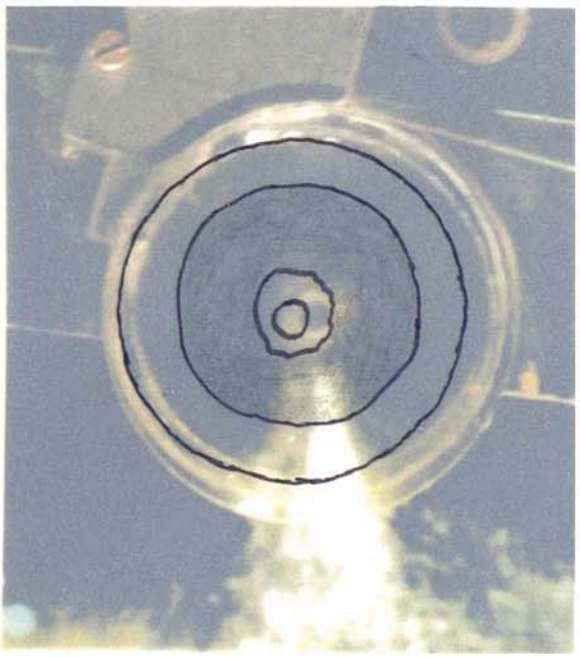

Region of Swirlchamber occupied by dye

possible to obtain some indication of the internal flow regimes from the photographs shown in Plate 2.

These photographs show the flow patterns highlighted when 5 ml of dye was injected into the inlet of a perspex nozzle (The design and purpose of the perspex nozzle are discussed in Section 5.5). Plate 2a shows the existence of three distinct zones: i) the initial entry zone around the swirlchamber wall; ii) a stagnant zone where the dye had not yet entered; iii) an asymmetrical zone surrounding the air core through which the dye appeared to be diffusing into the stagnant zone. Plate 2b, taken two seconds later, shows that the dye has now entered the stagnant zone and completely left the inner and outer zones. As illustrated by Plates 2c and 2d, the dye then gradually diffused out from the stagnant zone over a period of four to five seconds.

It is therefore necessary to idealise the liquid flow within the swirlchamber for modelling purposes. A suitable simplification in this case will be to base the internal liquid flow upon the conditions of a free vortex, which is in agreement with previous work (for example, [165][167][169][170]. Therefore equation (5.3) can be simplified to,

$$V_p \approx V_\theta = \frac{\Omega}{r} \qquad - 5.5$$

Under most conditions in the swirlchamber a boundary layer will exist close to the chamber wall, where the liquid velocity is retarded by the action of viscosity and surface friction. The radial pressure gradient accompanying the tangential swirling motion will act upon the boundary layer driving it along the wall towards the orifice and a condition could arise where a substantial portion of the flow through the orifice has passed through the boundary layer [170]. Although Taylor [170] calculated the thickness of the boundary layer by taking into account liquid viscosity, generally the treatment of the problem is based upon the simplifying assumption that viscosity can be neglected [162]. A similar assumption made for the course of this work will have the most noticeable effect of causing the prediction of over-large spray cone angles.

Figure 5.3: *Variables Affecting Liquid Flow in the Swirlchamber*

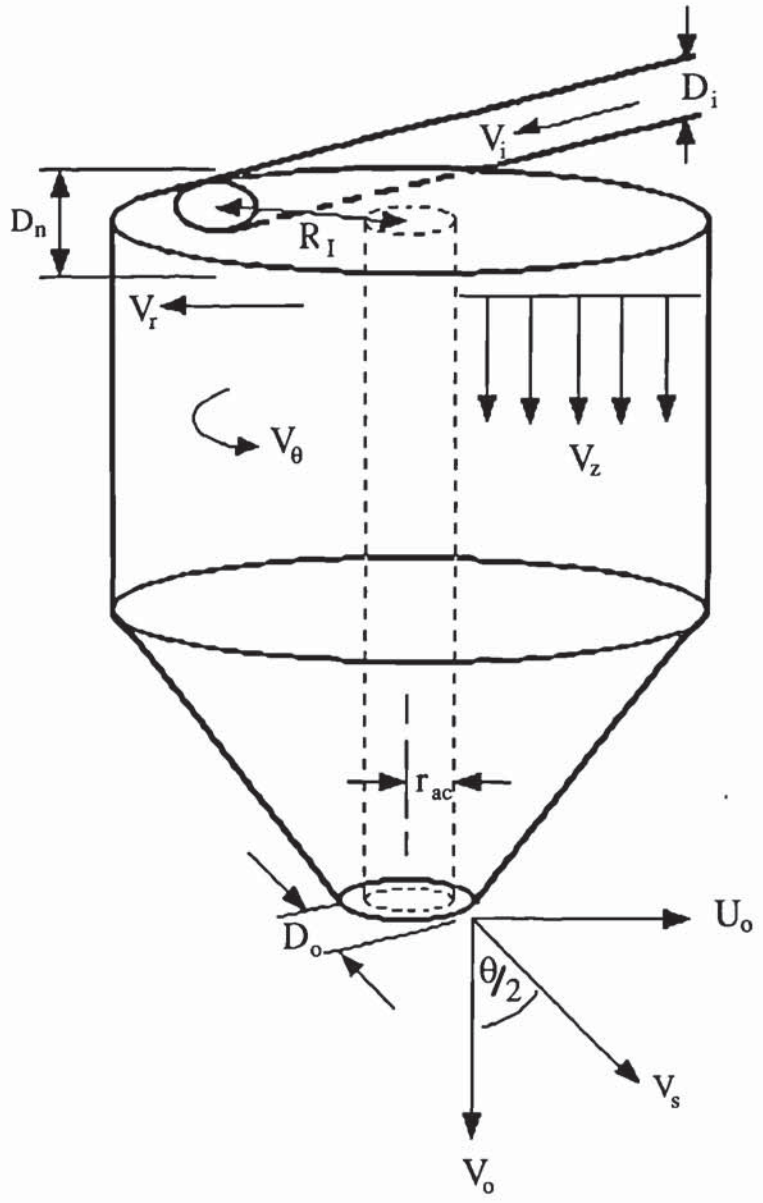

Figure 5.3 illustrates the geometry of a typical nozzle swirlchamber and the major variables influencing the liquid flow. It is assumed that the liquid has constant density (ρ_l) and constant viscosity (μ_l) under the conditions present within the nozzle. Therefore, based upon cylindrical coordinates, the continuity equation and the three equations of motion can be defined by,

Continuity Equation:

$$\frac{\partial \rho_l}{\partial t} + \frac{1}{r}\frac{\partial}{\partial r}\left(\rho_l r V_r\right) + \frac{1}{r}\frac{\partial}{\partial \theta}\left(\rho_l V_\theta\right) + \frac{\partial}{\partial z}\left(\rho_l V_z\right) = 0 \qquad - 5.6$$

Equations of Motion:

Radial Direction,

$$\rho_l\left\{\frac{\partial V_r}{\partial t} + V_r\frac{\partial V_r}{\partial r} + \frac{V_\theta}{r}\frac{\partial V_r}{\partial \theta} - \frac{V_\theta^2}{r} + V_z\frac{\partial V_r}{\partial z}\right\} = \rho_l g_r - \frac{\partial P}{\partial r} + \mu\left\{\frac{\partial}{\partial r}\left(\frac{1}{r}\frac{\partial}{\partial r}\left(r V_r\right)\right) + \frac{1}{r^2}\frac{\partial^2 V_r}{\partial \theta^2} - \frac{2}{r^2}\frac{\partial V_\theta}{\partial \theta} + \frac{\partial^2 V_r}{\partial z^2}\right\} \qquad - 5.7$$

Tangential Direction,

$$\rho_l\left\{\frac{\partial V_\theta}{\partial t} + V_r\frac{\partial V_\theta}{\partial r} + \frac{V_\theta}{r}\frac{\partial V_\theta}{\partial \theta} - \frac{V_r V_\theta}{r} + V_z\frac{\partial V_\theta}{\partial z}\right\} = \rho_l g_\theta - \frac{1}{r}\frac{\partial P}{\partial \theta} + \mu\left\{\frac{\partial}{\partial r}\left(\frac{1}{r}\frac{\partial}{\partial r}\left(r V_\theta\right)\right) + \frac{1}{r^2}\frac{\partial^2 V_\theta}{\partial \theta^2} - \frac{2}{r^2}\frac{\partial V_r}{\partial \theta} + \frac{\partial^2 V_\theta}{\partial z^2}\right\} \qquad - 5.8$$

Axial Direction,

$$\rho_l\left\{\frac{\partial V_z}{\partial t} + V_r\frac{\partial V_z}{\partial r} + \frac{V_\theta}{r}\frac{\partial V_z}{\partial \theta} + V_z\frac{\partial V_z}{\partial z}\right\} = \rho_l g_z - \frac{1}{r}\frac{\partial P}{\partial z} + \mu\left\{\frac{\partial}{\partial r}\left(r\frac{\partial V_z}{\partial r}\right) + \frac{1}{r^2}\frac{\partial^2 V_z}{\partial \theta^2} + \frac{\partial^2 V_z}{\partial z^2}\right\} \qquad - 5.9$$

Under steady-state conditions, the flow within the swirlchamber can be described as rotationally symmetrical; therefore there is no variation in any component with respect to its tangential position (θ). There is also no variation in the axial velocity component (V_z) radially across the chamber and, compared to the tangential velocity component (V_θ), the radial velocity component (V_r) is negligible.

The pressure is dependent upon the radial distance (r), because of centrifugal force, and upon the axial distance (z), because of the gravitational force (g). Therefore, if the boundary layer is considered to be thin in comparison to the bulk liquid then, the variation in pressure through its thickness can be considered to be negligible. Hence the above equations (5.6 - 5.9) can be simplified as follows,

Continuity Equation:

$$\frac{\partial V_z}{\partial z} = 0 \qquad - \ 5.10$$

Radial Direction:

$$\rho_l\left(\frac{V_\theta^{\,2}}{r} + V_z\frac{\partial V_r}{\partial z}\right) = -\frac{\partial P}{\partial r} \qquad - \ 5.11$$

Tangential Direction:

$$\rho_l\left(V_r\frac{\partial V_\theta}{\partial r} - \frac{V_r V_\theta}{r}\right) = \mu_l\left\{\frac{\partial}{\partial r}\left(\frac{1}{r}\frac{\partial}{\partial r}(r\,V_\theta)\right)\right\} \qquad - \ 5.12$$

Axial Direction:

$$\rho_l V_r\frac{\partial V_z}{\partial z} = \rho_l g - \frac{1}{r}\frac{\partial P}{\partial z} \qquad - \ 5.13$$

Now, as $V_\theta >> V_z$ then equation (5.11) can be simplified as follows,

$$\rho_l\frac{V_\theta^{\,2}}{r} = -\frac{\partial P}{\partial r}$$

or,

$$-\frac{V_\theta^{\,2}}{r} = \frac{1}{\rho_l}\frac{\partial P}{\partial r} \qquad - \ 5.14$$

Substitution of equation (5.2) into equation (5.12) enables further simplification of the equation, since,

$$\frac{\partial}{\partial r}\left(\frac{1}{r}\frac{\partial}{\partial r}(\Omega)\right) = 0$$

Therefore,

$$\frac{\partial V_\theta}{\partial r} - \frac{V_\theta}{r} = 0$$

or,

$$\frac{\partial V_\theta}{\partial r} = \frac{V_\theta}{r} \qquad - 5.15$$

Substitution of equation (5.10) into equation (5.13) also enables the equation to be simplified, ie

$$0 = \rho_l g - \frac{1}{r}\frac{\partial P}{\partial z} \qquad - 5.16$$

Substitution of equation (5.2) into equation (5.14) yields an expression relating the circulation constant to the pressure drop in the swirlchamber, ie

$$-\frac{\Omega^2}{r^3} = \frac{1}{\rho_l}\frac{dP}{dr} \qquad - 5.17a$$

or,

$$\int -\frac{\Omega^2}{r^3} dr = \int \frac{dP}{\rho_l} \qquad - 5.17b$$

Solution of equation (5.17) can be accomplished by using the boundary conditions that at the air core radius (r_{ac}) the pressure is equivalent to that of the datum or ambient pressure, ie when $r = r_{ac}$, $P = 0$. Thus,

$$\int_{r_{ac}}^{r} -\frac{\Omega^2}{r^3} dr = \frac{1}{\rho_l}\int_0^P dP$$

Hence,

$$P = \frac{\rho_l \Omega^2}{2}\left[\frac{1}{r_{ac}^2} - \frac{1}{r^2}\right] \qquad - 5.18$$

Therefore, the tangential velocity within the swirlchamber can be represented by equation (5.19):

$$V_\theta^2 = \frac{\Omega^2}{r^2} = \frac{2P}{\rho_l}\left[\frac{r_{ac}^2}{r^2 - r_{ac}^2}\right]$$

or,

$$V_\theta = \sqrt{\frac{2P}{\rho_l}\left[\frac{r_{ac}^2}{r^2 - r_{ac}^2}\right]} \qquad - 5.19$$

From the initial assumptions, the radial velocity approximates to zero, ie $V_r \approx 0$, and the axial velocity at any point in the swirlchamber is determined from the ratio of volumetric flowrate to flow area, ie

$$V_z = \frac{\text{Volumetric Flowrate}}{\left[\begin{matrix}\text{Swirlchamber}\\ \text{Area}\end{matrix}\right] - \left[\begin{matrix}\text{Air Core}\\ \text{Area}\end{matrix}\right]} \qquad - 5.20$$

Equation (5.20) can be adapted to define the inlet conditions for the liquid entering the swirlchamber. Thus,

$$Q_{In} = V_i \pi \left(\frac{D_i}{2}\right)^2 \qquad - 5.21$$

And similarly at the nozzle outlet, the volumetric flowrate is determined by,

$$Q_{Out} = V_o \pi \left(r_o^2 - r_{ac}^2\right) \qquad - 5.22$$

By mass balance equations (5.21) and (5.22) may be equated to produce an expression for the inlet velocity, ie

$$V_i = \frac{4 V_o}{D_i^2}\left(r_o^2 - r_{ac}^2\right) \qquad - 5.23$$

Now, from the integration of equation (5.15) using the boundary conditions: $r = R_I$ when $V_\theta = V_i$; $r = r_{ac}$ when $V_\theta = U_o$. Then,

$$\int_{U_o}^{V_i} \frac{dV_\theta}{V_\theta} = \int_{r_{ac}}^{R_I} -\frac{dr}{r} \qquad - 5.24$$

Thus,

$$\ln V_i - \ln U_o = -\left[\ln R_I - \ln r_{ac}\right]$$

or,

$$V_i = U_o \frac{r_{ac}}{R_I} \qquad - 5.25$$

After substitution for V_i from equation (5.21) then,

$$U_o = \frac{4Q}{\pi D_I^2} \frac{R_I}{r_{ac}} \qquad - 5.26$$

Nieukamp [167] introduced the analogy between conditions at the nozzle outlet to those present at the overflow of a weir, as illustrated in Figure 5.4. He used an expression derived from an equation that was originally introduced by Tietjens [197], which related maximum wave velocity (V*) to the height of the weir (h*), ie

$$V^* = \sqrt{g\, h^*} \qquad - 5.27$$

Figure 5.4: *Weir Flow at the Nozzle Outlet [167]*

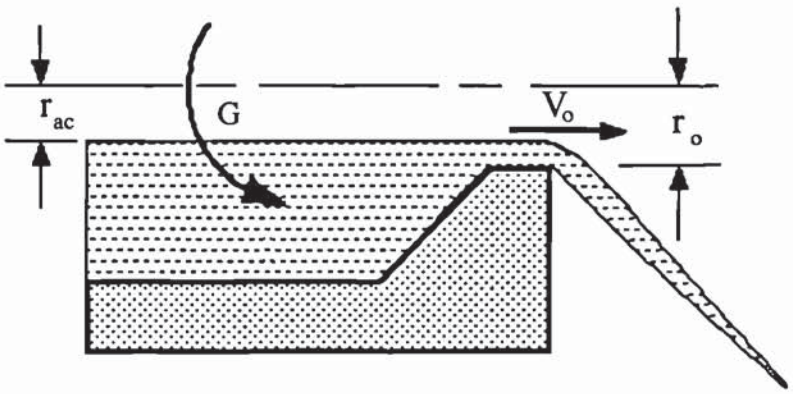

The gravity term in equation (5.27) can be replaced by the centrifugal potential, G, where:

$$G = \frac{U_o^2}{r_o} \qquad - 5.28$$

and since h* is given by $(r_o - r_{ac})$ and $V^* \equiv V_o$. Then,

$$V_o = \sqrt{G(r_o - r_{ac})} = \sqrt{\frac{U_o^2}{r_o}(r_o - r_{ac})} \quad - 5.29$$

Substitution of equation (5.22) into equation (5.28) produces an expression for the volumetric flowrate, ie

$$Q = \pi U_o\left(r_o^2 - r_{ac}^2\right)\sqrt{\frac{(r_o - r_{ac})}{r_o}} \quad - 5.30$$

Substitution for U_o from equation (5.26) produces an expression for the air core radius:

$$r_{ac} = \frac{4 R_I}{D_i^2}\left(r_o^2 - r_{ac}^2\right)\sqrt{\frac{(r_o - r_{ac})}{r_o}} \quad - 5.31$$

Hence the initial thickness of the sheet (h_i) can be calculated from,

$$h_i = r_o - r_{ac} \quad - 5.32$$

Substitution of equation (5.19) into equation (5.30) using the boundary conditions: $V_\theta = U_o$ when $r = r_o$, determines the volumetric flowrate,

$$Q = \pi\left(r_o^2 - r_{ac}^2\right)\sqrt{\frac{2P}{\rho_l}\left(\frac{r_{ac}^2}{r_o^2 - r_{ac}^2}\right)\frac{(r_o - r_{ac})}{r_o}} \quad - 5.33$$

It is now possible to determine the inlet velocity (V_i) from equation (5.21), the vertical component of the outlet velocity (V_o) from equation (5.22), and the horizontal component of the outlet velocity (U_o) from equation (5.26). Therefore, from Pythagoras' theorem based upon the velocity components at the nozzle outlet, it is possible to determine the liquid sheet velocity (V_s), ie

$$V_s = \sqrt{V_o^2 + U_o^2} \quad - 5.34$$

The cone angle of the conical sheet can be calculated from equation (5.35):

$$\mathrm{Tan}\left(\frac{\theta}{2}\right) = \frac{U_o}{V_o} \qquad - 5.35a$$

or,

$$\theta = 2\,\mathrm{Tan}^{-1}\left(\frac{U_o}{V_o}\right) \qquad - 5.35b$$

The actual area covered by the spray cone will be considerably less than the area predicted by the above equation. This is due to the combined action of internal surface friction in the nozzle, gravity and surface tension contracting the conical sheet and reducing the actual spray cone angle as the sheet moves away from the nozzle. Therefore equation (5.35) predicts the maximum cone angle of the spray.

5.2 Sheet Break-Up and Ligament Formation

It has been shown from the work of Dombrowski & Fraser [6] that a flat liquid sheet establishes two principal modes of disintegration. The most common mode of disintegration is due to the interaction of the surrounding air upon disturbances in the liquid sheet caused by irregularities in the air core [185][186]. These disturbances generally take the form of surface waves upon the sheet and when the wave amplitude reaches a critical value, disintegration occurs with 'fragments' of liquid torn-off the sheet which contract into unstable ligaments under the influence of surface tension. However, under some conditions (most commonly occurring at low atmospheric density) the sheet will remain undisturbed and disintegration occurs by the action of sheet perforation. This causes a series of thin, strand-like, filaments to be produced which break-up into droplets by the action of fluid turbulence induced by aerodynamic interaction with the surrounding air [8]. Both disintegration mechanisms are influenced by similar factors and, if sheet stability is indicated by sheet length (l_b), then

$$l_b = f\left(\rho_l, \mu_l, \sigma, \rho_a, P\right) \qquad - 5.36$$

Dombrowski & Wolfsohn [96][187] noted similar behaviour in the break-up of conical liquid sheets. Under most conditions a conical sheet disintegrates by aerodynamic wave disturbances. However, it has been recorded [4][196] that sheet perforation does occur, albeit in the presence of wave disturbances. It is therefore possible to draw an analogy between the mechanisms of disintegration for conical and flat liquid sheets.

5.2.1 Break-up of a Conical Liquid Sheet

In this study a segment of the conical sheet, width δ, will be examined using previously developed theory for flat sheets [7][10] and as with the theory behind the work of Dombrowski & Johns [10] it will be assumed that the major influence of the viscous forces is upon the growth of surface waves. Therefore, the length of a flat liquid sheet which is undergoing disintegration due to aerodynamic wave disturbances at normal atmospheric density can be determined from equation (5.37) [7],

$$l_b^2 = \frac{3}{2}\frac{\rho_l}{\rho_a} k f \sqrt{We}\,\frac{(We + 1)}{(We - 1)^2} \qquad - 5.37$$

where, $$We = \frac{\rho_l V_s^2 h_i}{\sigma} \qquad - 5.38$$

$$k = h'l' \qquad - 5.39$$

$$f = \ln\left(\frac{\alpha_b}{\alpha_o}\right)$$

The break-up length determined by equation (5.37) is strictly measured from the point where the stream-lines appear to diverge. However, the distance from this 'origin' to the orifice is negligible when compared to the total length of the sheet; therefore the break-up length can effectively be measured from the nozzle orifice.

Now for cases when the Weber number is considerably larger than unity (ie, when We >> 1), it is possible to simplify equation (5.37) as follows:

$$l_b^2 = \frac{3}{2}\frac{\rho_l}{\rho_a}\frac{k f}{\sqrt{We}} \qquad - 5.40$$

Before equation (5.37) or (5.40) can be solved it is necessary to determine the sheet thickness parameter (k) and the amplitude ratio (f) for the liquid sheet under investigation.

Determination of the Amplitude Ratio

It was reported [119], during Weber's investigation into liquid jets disintegrating by rotationally symmetrical oscillations, that the condition for break-up was when the amplitude ratio reached a universally constant value Fraser *et al* [8] assumed that similar criteria applied to the disintegration of liquid sheets and tested the assumption with flat sheets of known thicknesses at varying air densities and liquid velocities. They confirmed that, for a given nozzle, the amplitude ratio remained constant (There was a tendency for a slow decrease in the amplitude ratio with an increase in sheet thickness parameter but this was neglected due to insufficient data.).

Dombrowski & Hooper [7] established that the amplitude ratio could be assigned the value of 12, ie the same value as determined by Weber. However later work by Briffa & Dombrowski [158] determined the amplitude ratio as equivalent to 50 , ie they found that the sheet lengths were noticeably longer than those measured by Dombrowski & Hooper; whilst Clark & Dombrowski [150] reported that the amplitude ratio could be determined from the 'best-line' relationship between l' and $(\rho_l \sigma k / \rho_a^2 V_s^2)^{0.5}$. They re-examined both sets of data and found that Dombrowski & Hooper had worked under conditions where the Reynolds number was above 9000, whilst Briffa & Dombrowski had worked below that value. Therefore, it will be assumed that the amplitude ratio is influenced by the Reynolds number as follows,

$$f = 12 \qquad \text{when Re} > 9000 \qquad - 5.41a$$

$$f = 50 \qquad \text{when Re} < 9000 \qquad - 5.41b$$

where,

$$Re = 2\frac{\rho_l V_s r_o}{\mu_l} \qquad - 5.42$$

Determination of the Sheet Thickness Parameter

It is well documented [4][7][8][10][151][157] that the thickness of an attenuating flat liquid is related to its position from the orifice, as defined by equation (5.39). A corresponding relationship can be obtained for a conical sheet and, if it is assumed that the underlying theory behind equation (5.37) [147] can be applied to the mathematical investigation, then a value for the sheet thickness parameter can be derived from continuity as shown in Figure 5.5.

Figure 5.5: *Variation of Liquid Sheet Thickness with Distance*

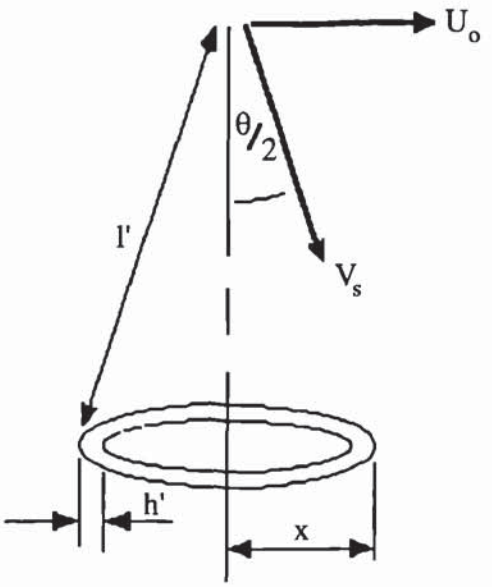

The area (A_s) subtended by the sheet in the vertical direction is given by the equation,

$$A_s = \pi\left[(x - h')^2 - x^2\right] = 2x h' + h'^2 \qquad - 5.43$$

Now,

$$x = U_o t$$

Therefore,

$$A_s = \pi\left(2 U_o h' t + h'^2\right) \qquad - 5.44$$

The volumetric flowrate is given by $Q = V_s A_s$ and since $h'^2 \rightarrow 0$, then:

$$\frac{Q}{V_s} = 2 \pi U_o h' t \qquad - 5.45$$

but $l' = V_s t$ and $U_o = V_s \text{Sin}\, \theta$. Therefore,

$$Q = 2 \pi h' l' V_s \text{Sin}\, \theta \qquad - 5.46$$

Combining equation (5.39) and (5.46) gives,

$$k = \frac{Q}{2 \pi V_s \text{Sin}\, \theta} \qquad - 5.47$$

Equation (5.47) has been quoted by several previous workers [96][187] and is in agreement with the relationship proposed by Taylor [157]. However, Dombrowski *et al* [156] reported that for a flat liquid sheet, at relatively low injection pressures, the sheet thickness parameter was a function of surface tension and equation (5.48). The surface tension effect would clearly be important with detergents, where a reduction occurs from 72 dynes/cm to around 30 dynes/cm; however at high injection pressures they found that the sheet thickness parameter was merely a function of equation (5.48):

$$k = f\left(\frac{\sqrt{\rho_l P}}{\mu_l}\right) \qquad - 5.48$$

A comparison of equations (5.47) and (5.48) shows that the latter is more influenced by the parameters that are known to affect the liquid sheet length (ie, pressure and viscosity). Equation (5.47) accurately produces a constant value for the thickness parameter over a wide range of conditions for a particular nozzle. It is therefore better described as a nozzle parameter, similar to that introduced by Rizk & Lefebvre [176], Dombrowski & Hasson [177] and Ranganadha Babu *et al* [179].

An expression for the thickness parameter for a conical liquid sheet can be derived using similar theory to that used by Dombrowski *et al* [156]. In Figure 5.6 a

the liquid surface. As the sheet is gradually attenuating away from the orifice a particle of liquid travelling along the stream-line, illustrated in the diagram, will undergo a change in momentum at point A. The rate of change of momentum experienced by the particle, defined by $\rho_l h' V_c^2$ per unit length, is equal to the surface tension at the free edge, defined by σ, ie

$$\sigma = \rho_l V_c^2 h' \qquad - 5.49$$

Figure 5.6: *Velocity Components Influencing the Trajectory of a Liquid Sheet*

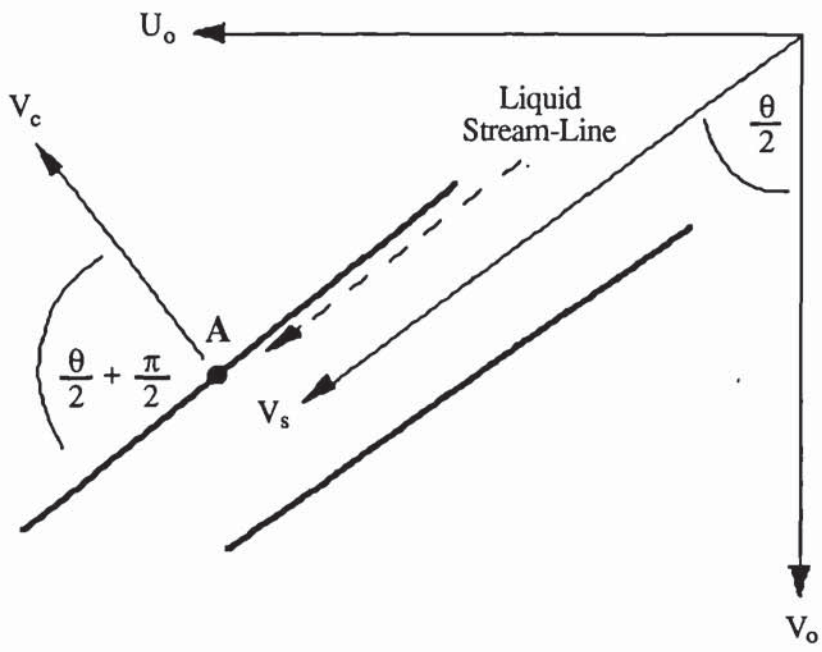

or, after substitution for k from equation (5.39):

$$k = \frac{\sigma l'}{\rho_l V_c^2}$$

Now, the velocity component, V_c, can be defined by $V_c = U_o \text{Cos}(\theta/2)$. Therefore,

$$k = \frac{\sigma l'}{\rho_l \left(U_o \text{Cos}\left(\frac{\theta}{2}\right)\right)^2} \qquad - 5.50$$

Determination of the Sheet Thickness at the Break-up Point

The liquid sheet thickness at the break-up point can now be determined from an expression derived from equations (5.39), (5.40), (5.41) and (5.50). The first stage of the derivation is to combine equations (5.40) and (5.50) in order to determine the break-up length of the liquid sheet, ie

$$l_b = \frac{3f}{2\rho_a}\sqrt{\frac{\rho_l \sigma h_b}{V_s^2}} \qquad - 5.51a$$

or,

$$l_b = \frac{3f}{2\rho_a}\sqrt{\frac{\rho_l \sigma k}{V_s^2 h_b}} \qquad - 5.51b$$

Thus, after substitution for k:

$$l_b = \frac{3}{2}\frac{f\sigma}{\rho_a V_s U_o \mathrm{Cos}\left(\frac{\theta}{2}\right)} \qquad - 5.52$$

Once the break-up length has been calculated, the sheet thickness parameter may be determined from equation (5.50). The sheet thickness at the break-up point can then be determined from equation (5.39).

5.2.2 Ligament Formation

Fraser *et al* [8] introduced the principle that the liquid sheet disintegrates to produce a ligament with a length equivalent to half the optimum wavelength at the break-up point (λ_{opt}), as shown in Figure 5.7. Assuming that the length of the ligament remains equal to the width of the original sheet segment (δ), the volume of the ligament is then given by,

$$\text{Ligament Volume} = h_b \frac{\lambda_{opt}}{2}\delta \qquad - 5.53$$

Now surface tension and atmospheric forces will cause the ligament to contract into an unstable tubiform. The volume of this tubiform is defined by,

$$\text{Tubiform Volume} = \pi \frac{d_l^2}{4} \delta \qquad \text{- 5.54}$$

Figure 5.7: *Stages in the Idealised Break-up of a Liquid Sheet*

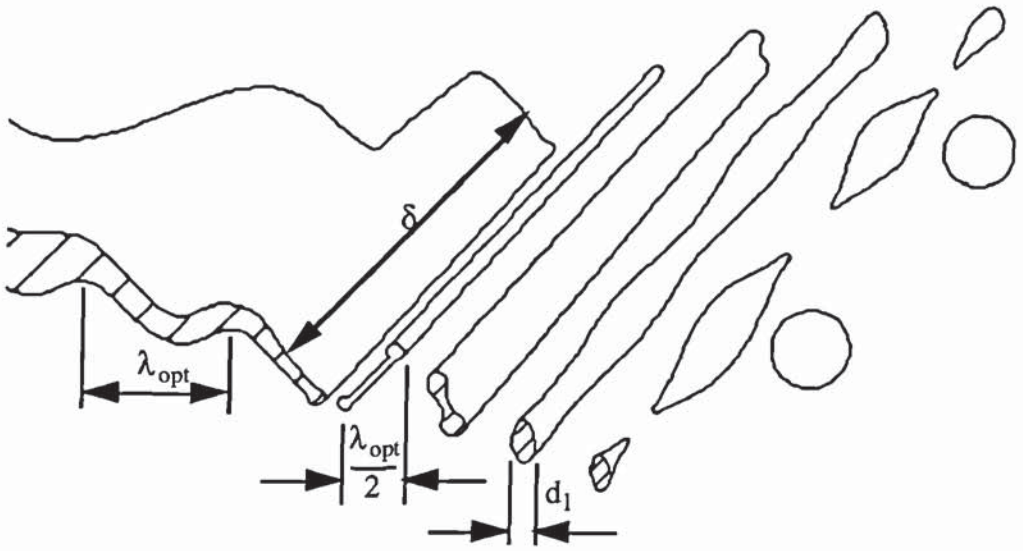

Consequently, by mass balance, equations (5.53) and (5.54) can be combined to obtain an expression for the ligament diameter, ie

$$d_l = \sqrt{\frac{2 \lambda_{opt} h_b}{\pi}} \qquad \text{- 5.55a}$$

or,

$$d_l = \sqrt{\frac{4 h_b}{n}} \qquad \text{- 5.55b}$$

where, n is the wave number of the disturbance $= \frac{2\pi}{\lambda_{opt}}$

It has previously been observed [6] that the ligaments break down by the action of symmetrical wave disturbances. Weber [119] analysed the properties of this type of wave disturbance in which surface tension forces predominate and aerodynamic action assists the disintegration. In this type of disintegration the ligaments move transversely through the air and under these conditions the surrounding air has no

effect upon the wavelength. Therefore, it can be assumed that Weber's results for surface tension break down can be applied to the mechanism of ligament formation, ie

$$n\,d_l = \sqrt{\frac{1}{2} + \frac{3\mu_l}{2\sqrt{\rho_l \sigma d_l}}} \qquad - 5.56$$

Substituting for n using equation (5.55a) produces an expression for the ligament diameter:

$$d_l = \sqrt{\frac{32\,h_b^{\,2}}{\left[1 + \frac{3\mu_l}{\sqrt{\rho_l \sigma d_l}}\right]}} \qquad - 5.57$$

5.3 Droplet Formation and Droplet Size Distribution

As previously mentioned there are two possible mechanisms of droplet formation from conical liquid sheets. It is virtually impossible to determine which mechanism is likely to predominate under the prevailing conditions in any investigation, and therefore extremely difficult to predict a droplet size distribution. However, it is possible to look at each mechanism separately and combine them to estimate the sizes of the maximum and minimum droplet produced under any conditions.

5.3.1 Maximum Droplet Diameter

The maximum droplet diameter is produced when a ligament breaks up to form a droplet. This process is illustrated in Figure 5.8, where the ligament disintegrates due to wave disturbances created by liquid turbulence induced during its formation. The wave disturbance will increase until its amplitude is equal to the radius of the ligament, at which point it disintegrates into droplets [10]. If it is assumed that one droplet is produced per disturbance wavelength, then by mass balance:

$$\pi \frac{d_l^2}{4} \lambda'_{opt} = \frac{4}{3} \pi \frac{d_p^3}{8}$$

Figure 5.8: *Droplet Formation after Ligament break-up*

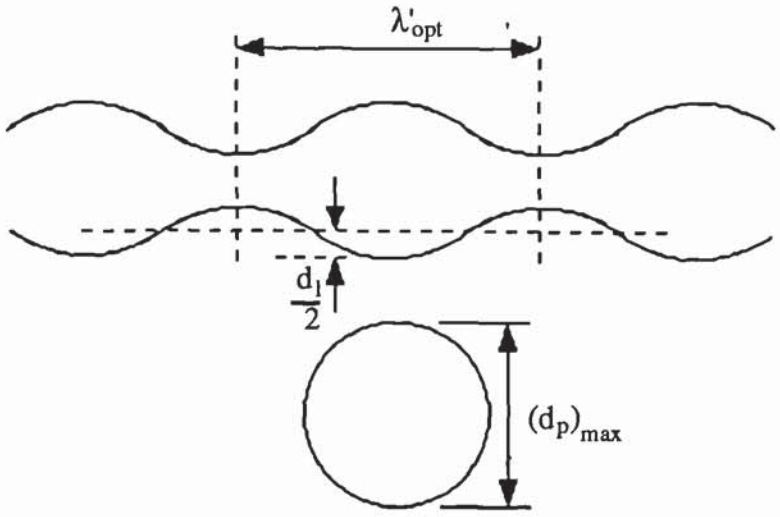

Therefore,

$$d_p^3 = \frac{3\pi}{n} d_l^2 \qquad - 5.58$$

which upon combination with equation (5.55b) gives,

$$d_p^3 = \frac{3\pi d_l^3}{4 h_b} \qquad - 5.59$$

Substitution of equation (5.57) into equation (5.59) produces an expression for the maximum possible droplet diameter, ie

$$(d_p)_{max}^3 = \frac{3\pi}{4 h_b} \left(\frac{32 h_b^2}{\left[1 + \frac{3\mu_l}{\sqrt{\rho_l \sigma d_l}} \right]} \right)^{\frac{3}{2}}$$

or,

$$(d_p)_{max} = \sqrt[3]{\frac{3\pi}{4 h_b}} \sqrt{\frac{32 h_b^2}{\left[1 + \frac{3\mu_l}{\sqrt{\rho_l \sigma d_l}}\right]}} \quad - 5.60$$

5.3.2 Minimum Droplet Diameter

The minimum droplet diameter is produced when the sheet disintegrates directly into droplets, as illustrated in Figure 5.9. This is due to liquid turbulence causing the sheet to perforate or tear in the absence of wave disturbances upon the sheet [6] [8]. In this case the sheet break-up can also be represented by Weber's equation,

$$n_T h_b = \sqrt{\frac{1}{2} + \frac{3\mu_l}{2\sqrt{\rho_l \sigma h_b}}} \quad - 5.61$$

where, n_T is the turbulence wave number.

Figure 5.9: *Droplet Formation after Sheet Break-up*

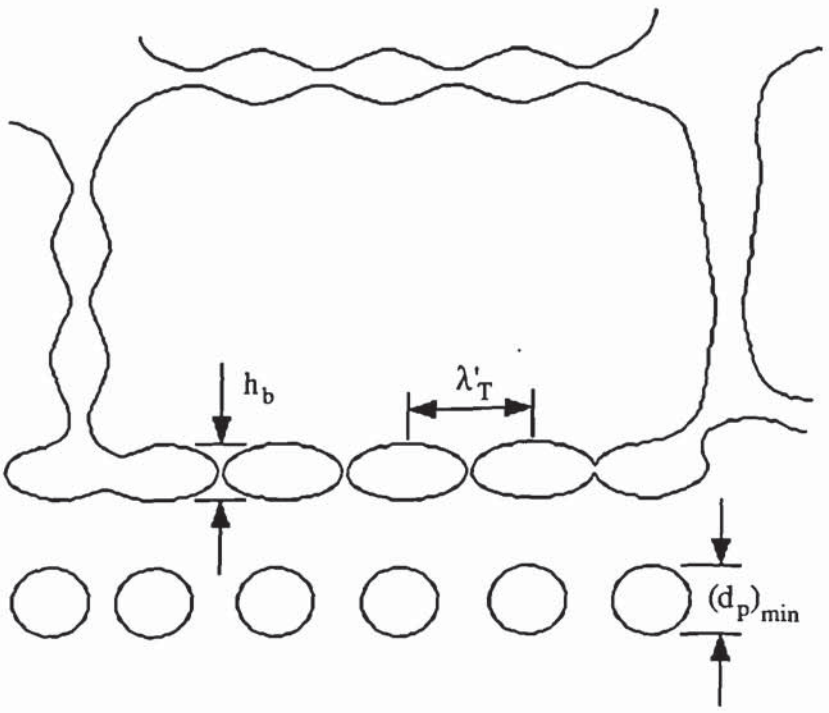

Thus the minimum droplet diameter can be determined from the following equation, derived in a similar way to equation (5.58),

$$(d_p)_{min}^{\ 3} = \frac{3\pi h_b^{\ 2}}{n_T} \qquad - 5.62$$

Substitution of equation (5.61) into equation (5.62) enables the elimination of the turbulence wave number, ie

$$(d_p)_{min}^{\ 3} = \frac{3\pi h_b^{\ 3}}{\sqrt{\frac{1}{2} + \frac{3\mu_l}{2\sqrt{\rho_l \sigma h_b}}}}$$

or,

$$(d_p)_{min} = \sqrt[3]{\frac{3\pi h_b^{\ 3}}{\sqrt{\frac{1}{2} + \frac{3\mu_l}{2\sqrt{\rho_l \sigma h_b}}}}} \qquad 5.63$$

5.3.3 Volume and Sauter Mean Diameters

As these two extreme cases are only just possible, with a very low frequency of occurrence, very little of the total volume of a spray would actually be represented by either of these droplet sizes. Therefore, the droplet size distribution that can be represented by the Volume Mean Diameter results from a combination of break-up mechanisms.

Johnson [186] used the following empirical expression to represent the Mass (Volume) Mean Diameter based upon a typical distribution curve:

$$D_{VM} = 0.4\left[(d_p)_{max} - (d_p)_{min}\right] + (d_p)_{min} \qquad - 5.64$$

Dombrowski & Johns [10] established an empirical relationship for the Sauter Mean Diameter based upon the experimental work of Hasson & Mizarhi [82]. The expression was based upon the maximum droplet diameter, ie

$$D_{VS} = 0.63(d_p)_{max} \qquad - 5.65$$

An alternative relationship between the Sauter Mean and Volume Mean Diameters can be determined from the 'best-line' relationship, illustrated in Figure 5.10, obtained from experimental data using the perspex nozzles described in Section 5.5:

$$D_{VS} = 0.71\, D_{VM} \qquad - 5.66$$

Figure 5.10: *Plot of Volume Mean Diameter against Sauter Mean Diameter*

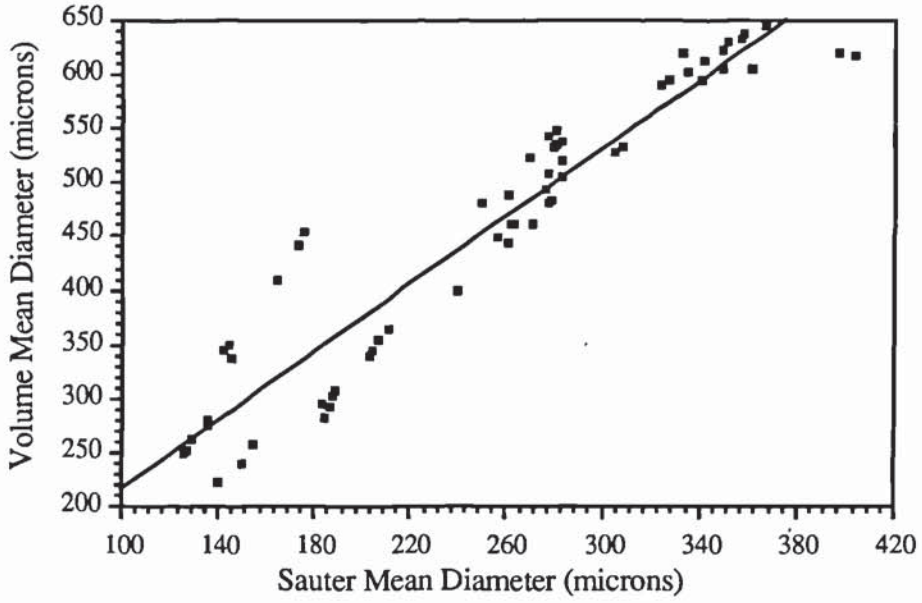

5.3.4 Determination of the Rosin-Rammler Parameters

As mentioned in Chapter 3, the Rosin-Rammler distribution model is the most suitable model for use in the representation of the droplet size distribution produced by centrifugal pressure nozzles. The two parameters of the distribution equation can thus be found from knowledge of the Volume and Sauter Mean Diameters. Therefore from the Rosin-Rammler distribution equation [49]:

$$V_D = 1 - \exp\left[-\left(\frac{D}{X}\right)^N\right] \qquad - 3.6$$

which can be rearranged as follows,

$$\ln\left\{\ln\left[\frac{1}{(1 - V_D)}\right]\right\} = N \ln\left(\frac{D}{X}\right) \qquad - 5.67$$

Now the Sauter Mean Diameter is given by the expression [180]:

$$D_{VS} = X\left(\Gamma\left[1 - \frac{1}{N}\right]\right)^{-1} \quad - 5.68$$

where, Γ is the Gamma Function.

Equation (5.68) can be simplified as follows,

$$D_{VS} = X\left(\Gamma(\phi)\right)^{-1} \quad - 5.69$$

$$\text{where,} \quad \phi = \left[1 - \frac{1}{N}\right] \text{ or, } N = \frac{1}{(1 - \phi)} \quad - 5.70$$

Combining equations (5.67) and (5.69). Then,

$$\ln\left\{\ln\left[\frac{1}{(1 - V_D)}\right]\right\} = \left[\frac{1}{(1 - \phi)}\right]\ln\left(\frac{D}{D_{VS}(\Gamma(\phi))}\right) \quad - 5.71$$

Now, when $V_D = 0.5$, then $D = D_{VM}$. Hence,

$$\ln[\ln(2)] = \left[\frac{1}{(1 - \phi)}\right]\ln\left(\frac{D_{VM}}{D_{VS}(\Gamma(\phi))}\right) \quad - 5.72$$

Solution of equation (5.72) will determine ϕ; consequently N can be obtained from equation (5.70) and then X can be determined from equation (5.68). Therefore, with knowledge of the values of X and N, the other principal diameters ($D_{v,0.1}$, $D_{v,0.2}$, $D_{v,0.3}$, etc) can be calculated from equation (5.67).

5.4 Computer Programs

The main computer program was developed in order to solve the complex equations of the mathematical model and represent the atomisation of a liquid by a swirlchamber nozzle. A second program was written for use in conjunction with the experimental results; it was designed to employ Felton's correction factors [108] for experiments conducted at high obscuration.

Figure 5.11: *Flowsheet of the Computer Program - NOZZLE.FOR*

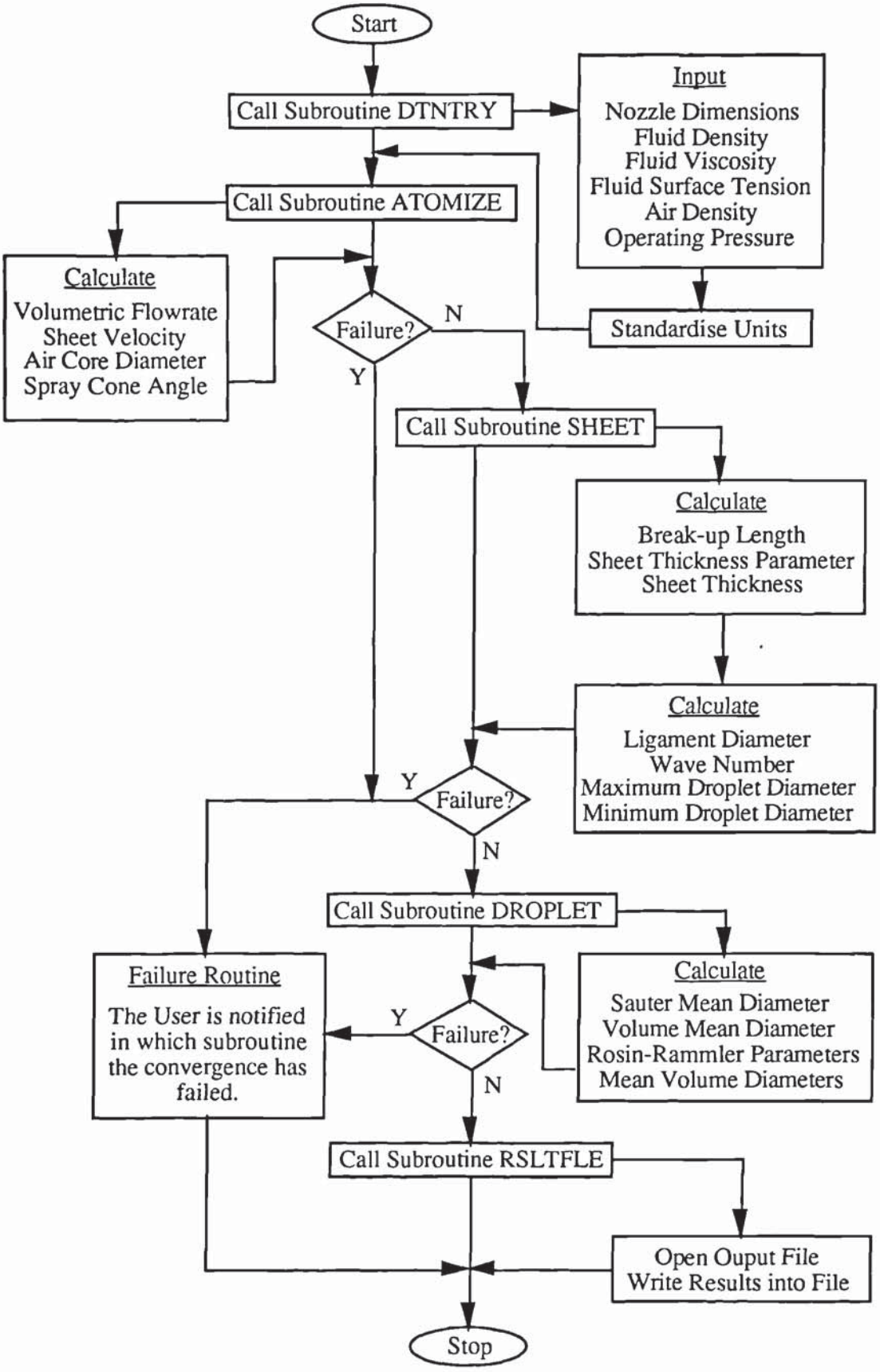

5.4.1 Mathematical Model

The flowsheet of the computer program based upon the mathematical model is illustrated in Figure 5.11. The full listing of the program, written in Fortran 77, entitled 'Nozzle.For' is shown in Appendix 3.

The program, consisting of a master segment and six subroutines, requires the input of data for physical properties of the fluid, the operating pressure and the geometry of the nozzle under investigation. The six subroutines are split up into two data handling routines and three calculation routines written around the Secant numerical algorithm, illustrated in Figure 5.12.

Figure 5.12: *The Secant Algorithm [199]*

```
      Dimension B(2), P(2)
      Tol = 10 12
      I = 2
      Itt = 50
      B(1) = First Guess
      B(2) = Second Guess
      Do 10  N = 1, I
        P(N) = f(B(N))
10    Continue
      Do 20  L = 2, Itt
        PF = B(2)-P(2)x(B(2)-B(1))/(P(2)-P(1))
        If(Abs(PF-P(2)).LT.Tol) then Return
        B(1) = B(2)
        P(1) = P(2)
        B(2) = PF
        P(2) = f(PF)
20    Continue
      End
```

The master segment is essentially the overseer of the calculation routines. It is designed to inform the user in the event of a convergence failure in any of the subroutines. Any other calculation failures (for example, division by zero, negative

logarithm value, etc) are not covered by the master segment, and, in the rare event of their occurrence (usually due an error in the input data), will cause the program to crash.

Data Handling Subroutines

The program contains two data handling routines, one to convert the input data into consistent units and the other to write the results into an output file. The input subroutine, called 'Dtntry', also acts as a filter to stop any spurious data from entering the program and refuses the input of any 'impossible' nozzle geometry, for example, orifice diameter bigger than swirlchamber diameter.

The output subroutine, called 'Rstlfle', formats the results and writes them into a data file. This data file is named by the user so that the prospect of accidental over-write of data can be avoided. The results are written into the file in the format that they were originally entered and the droplet sizes converted into microns for ease of comparison with experimental results.

Calculation Subroutines

There are three calculation subroutines which each represent a major stage in the mathematical model. A brief summary of each subroutine is given below along with a flowsheet for each subroutine.

Atomize - This subroutine determines the initial sheet thickness, cone angle and sheet velocity by modelling the flow conditions in the swirlchamber. The flowsheet is shown in Figure 5.13a.

Sheet - This subroutine determines the break-up length and final sheet thickness by modelling sheet disintegration by aerodynamic wave disturbances. It also predicts the maximum and minimum droplet sizes along with the Sauter and Volume Mean Diameters. The flowsheet for the subroutine is shown in Figure 5.13b.

Droplet - This subroutine uses the Nag library routine S14AAF for the Gamma Function in order to determine the Rosin-Rammler distribution

Figure 5.13: *Program Subroutines for NOZZLE.FOR*

a) Atomize

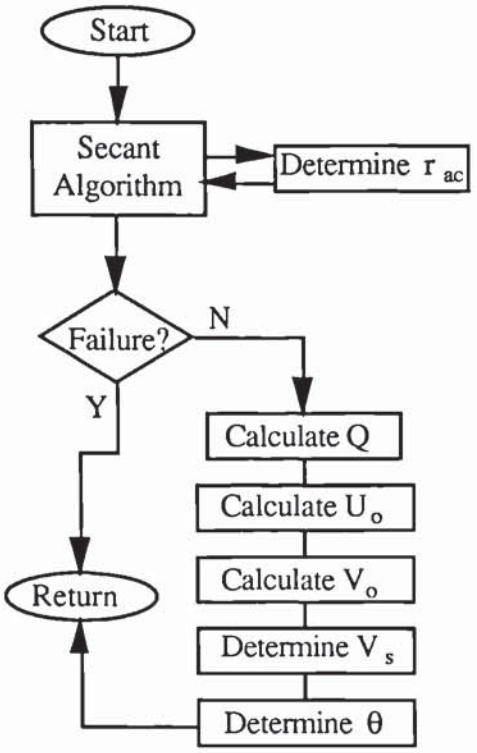

b) Sheet

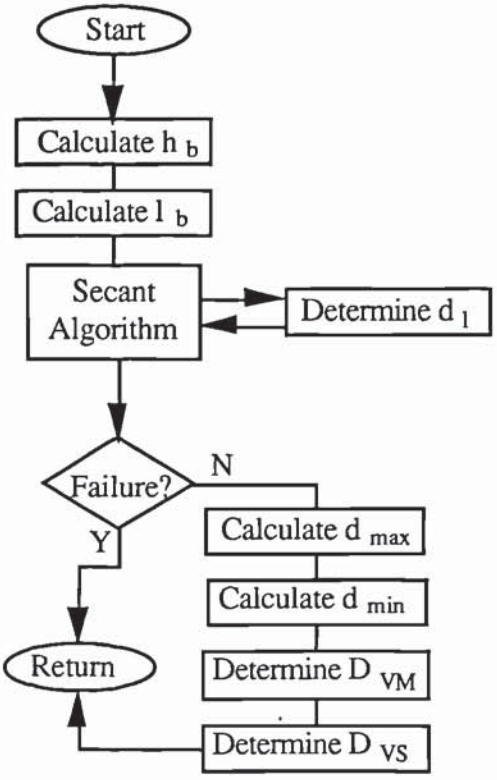

c) Droplet

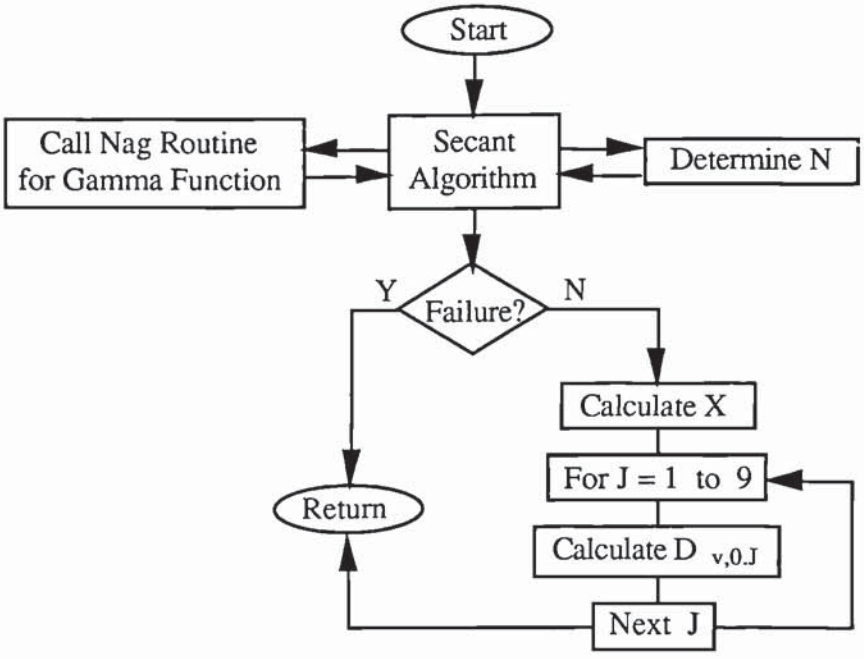

parameters. It then calculates the mean volume diameters based upon these parameters. The flow sheet for the subroutine is shown in Figure 5.13c.

Figure 5.14: *Flowsheet of the Computer Program - RRPARCO.FOR*

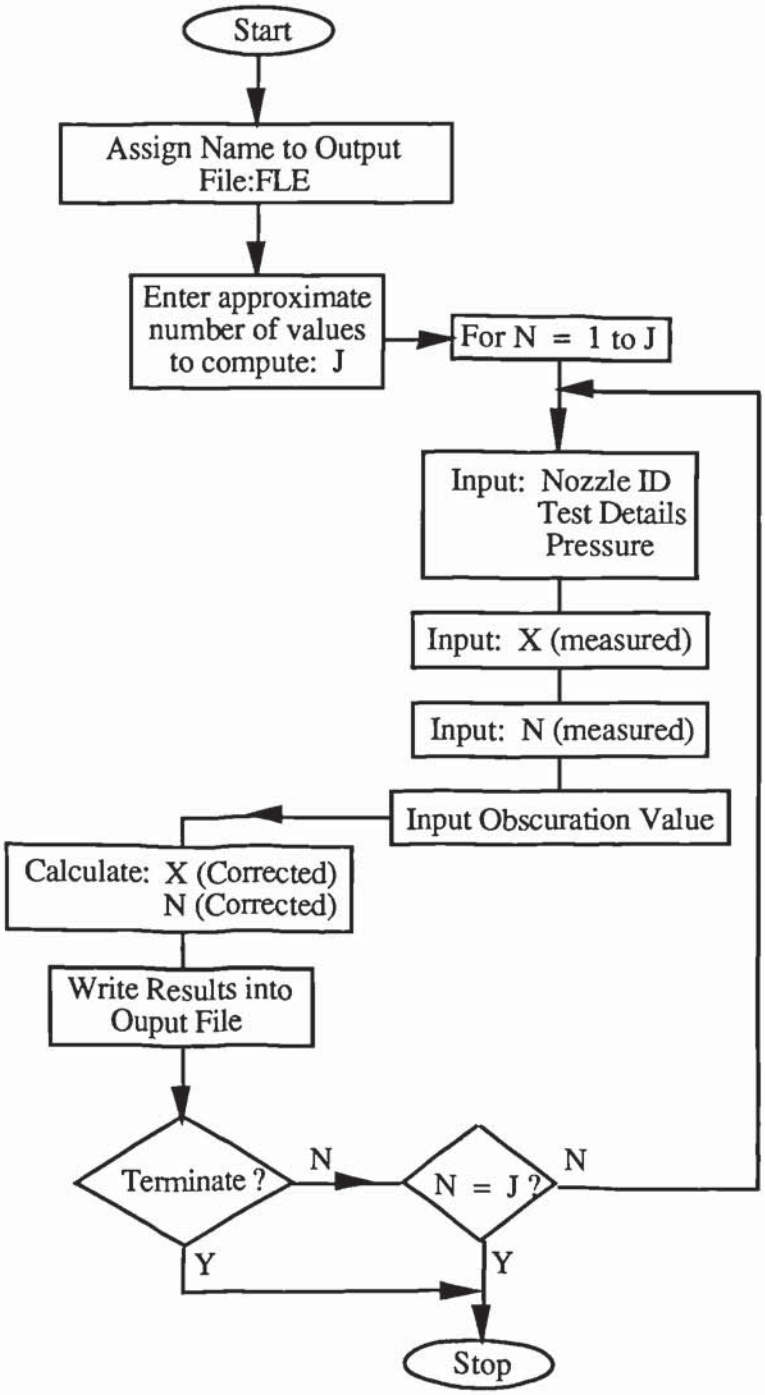

To run the problem it must first be linked to the Nag library in order to achieve access to the special library routine S14AAF. Once this has been accomplished the program can be run as normal.

5.4.2 Felton's Correction Factors

Figure 5.14 illustrates the flowsheet of the computer program written to process the experimental results obtained at high obscuration levels. The full listing of the program entitled 'Rrparco.For' is shown in Appendix 3.

The program requires the input of the Rosin-Rammler distribution parameters obtained from the experiment along with the obscuration value and experimental details. The results are written into an output file, named by the user and can be interrupted at any time without affecting the contents of the results file.

5.5 Comparison with Experimental Results

The theory behind the mathematical model was tested by comparing the calculated results with the experimental data obtained from six perspex nozzles using water as the spraying medium. Plate 3 illustrates the type of nozzle used in the experimental work and the dimensions of the six nozzles are given in Figure 5.15. The perspex nozzles were geometrically scaled-up from their industrial counterparts in order to study the flow within the swirlchamber and to enable the measurement of the air core diameter, spray cone angle, the liquid sheet length and sheet velocity.

An experimental rig, shown in Plate 4, was built specifically to test the perspex nozzles and was designed to be used in conjunction with the Malvern Particle-Size Analyser. A schematic diagram of the apparatus is shown in Figure 5.16. The volumetric flowrate was determined during the period that the Size Analyser was in operation by collecting the spray droplets in a two-litre measuring cylinder.

The experimental results were obtained from operation of the nozzles at five different pressures. However, due to the fragile nature of the perspex nozzles the

Figure 5.15: *Dimensions of the Perspex Nozzles*

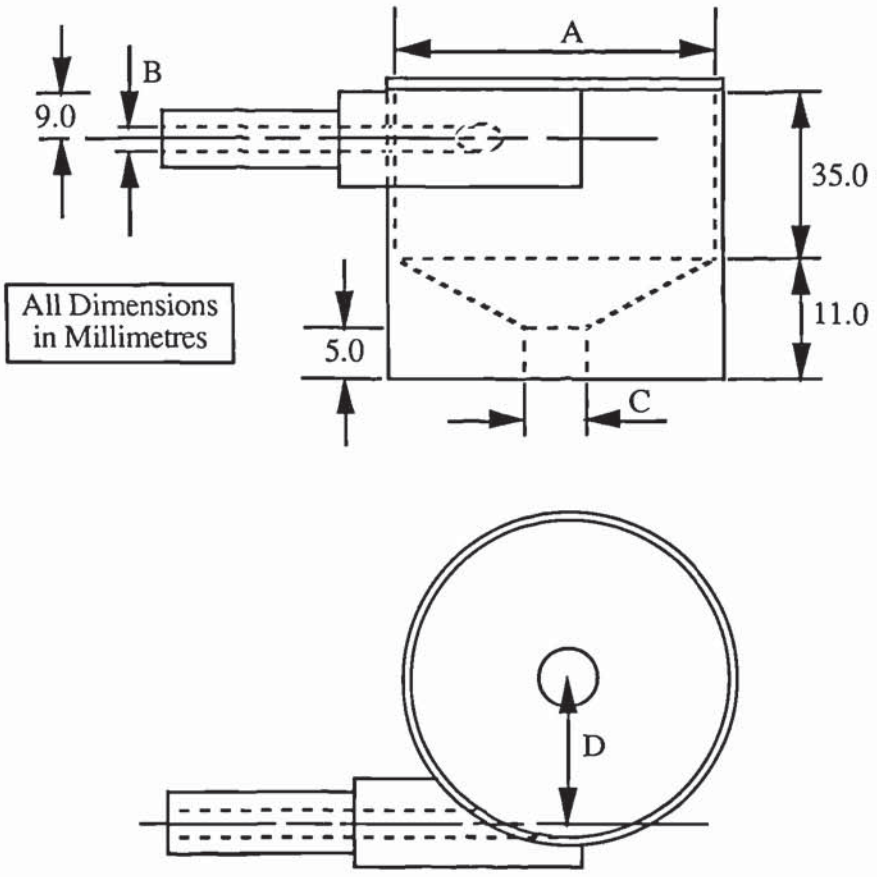

Dimension	Nozzle Number					
	1	2	3	4	5	6
A	43.71	43.87	43.51	43.76	43.89	43.59
B	4.0	4.0	6.0	6.0	6.0	4.0
C	10.0	12.0	8.0	10.0	12.0	8.0
D	41.71	41.87	40.51	40.76	40.89	41.59

Plate 3: *Perspex Centrifugal Pressure Nozzles*

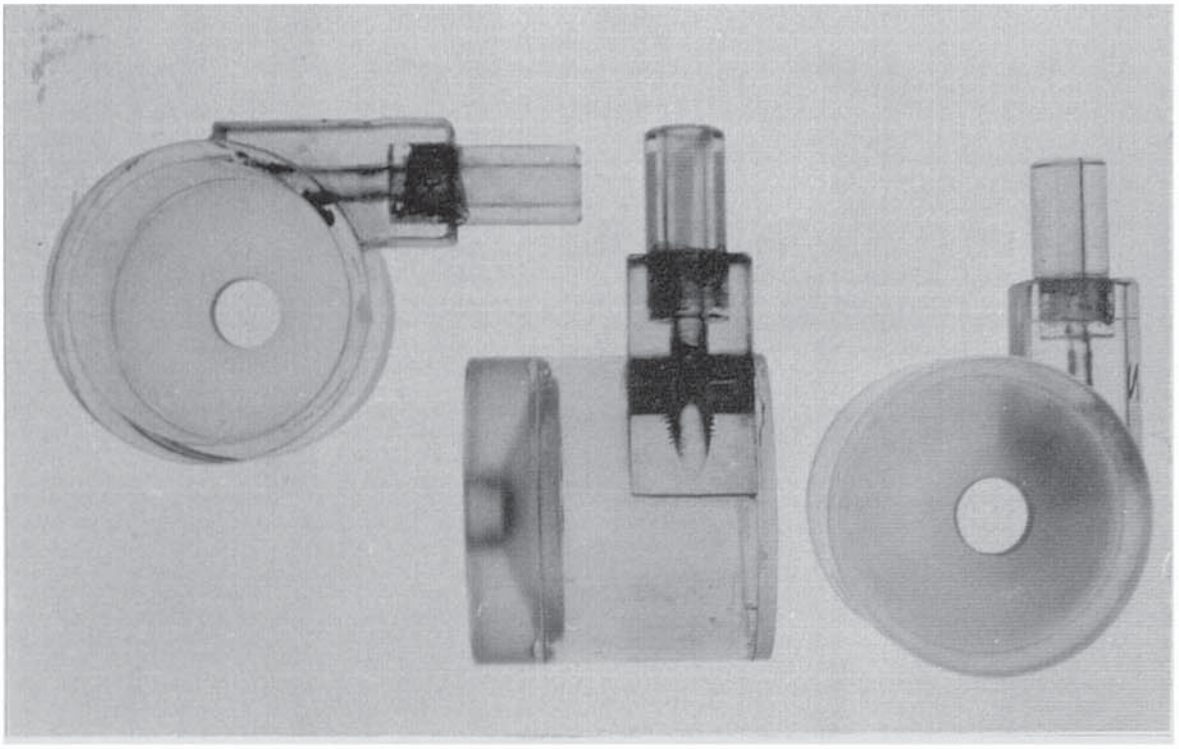

Plate 4: *The Perspex Nozzle Test Rig*

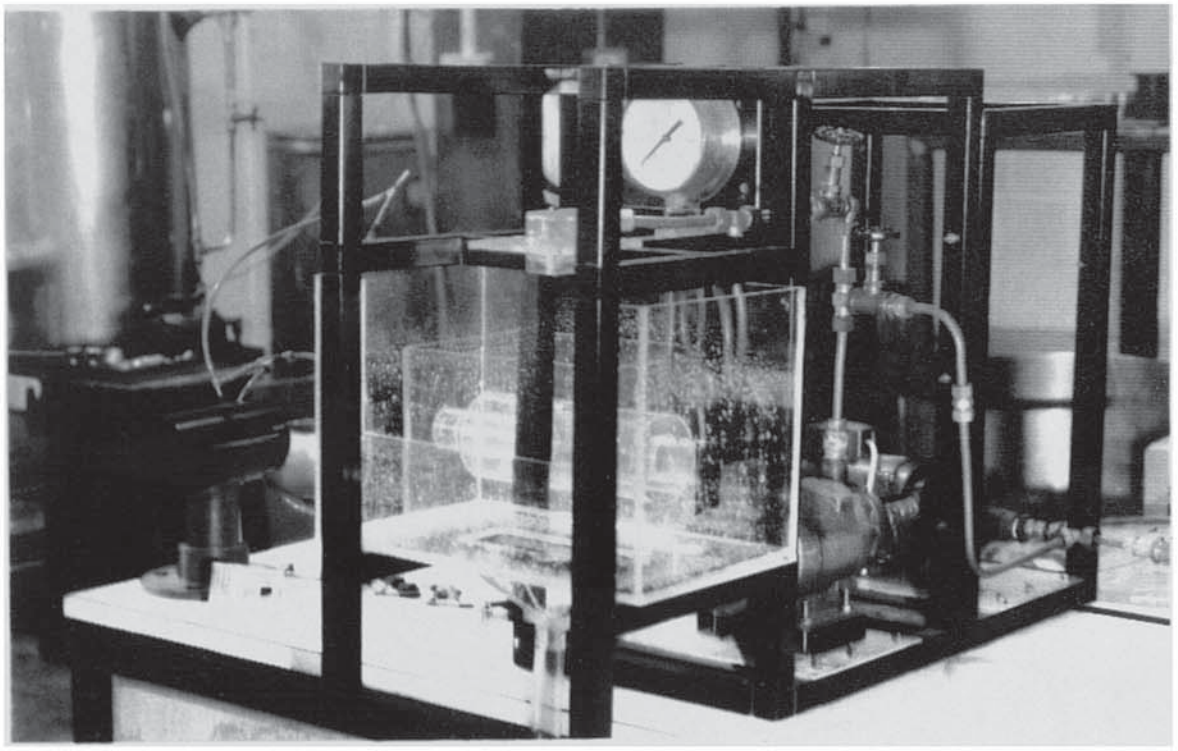

Figure 5.16: *Schematic Diagram of the Perspex Nozzle Test Rig*

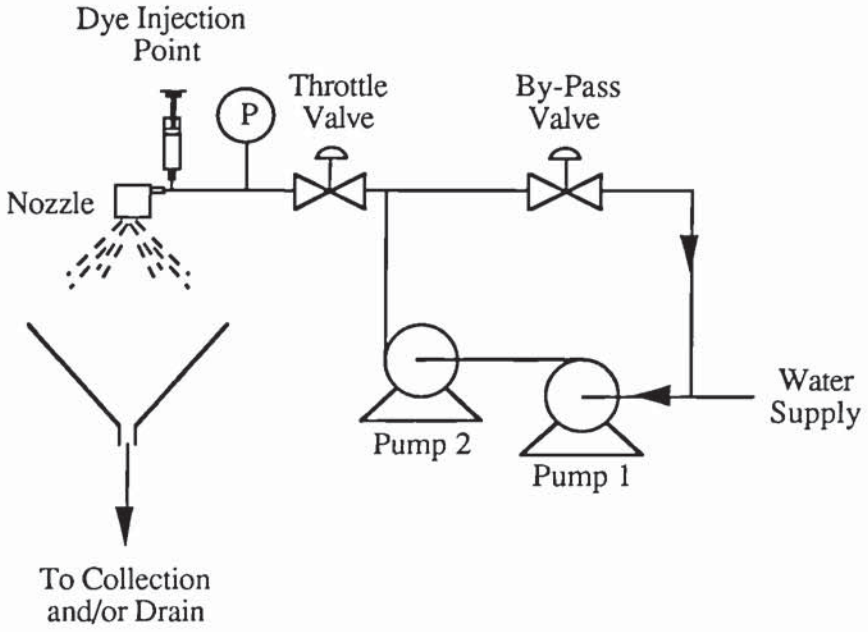

maximum operating pressure of the system had to be kept below 30 psi for safety reasons. This limited operation to pressures of 5, 10, 15, 20, and 25 psi and meant that the obscuration caused by the spray could be kept below 60%. The basic experimental methods that were used during this experimental work are described below and typical photographs obtained during the study are shown in Appendices 4, 5 and 6. Additionally a complete set of photographs obtained during the course of this study has been submitted as unbound material [200].

5.5.1 Measurement of the Droplet Size Distribution

As mentioned above the droplet size distribution was measured using the Size Analyser. The droplets produced by the perspex nozzles under test conditions were considerably larger than those produced by the Spraying Systems and Delevan nozzles; consequently the 300mm lens normally used was not suitable for the measurement of droplet sizes in the range of 1500μm. It was therefore necessary to use an 800mm lens to measure the droplet size distribution which meant that the Size Analyser had to be based on an optical bed.

Figure 5.17: *Comparison of Droplet Size Distribution Results for Nozzle P1*

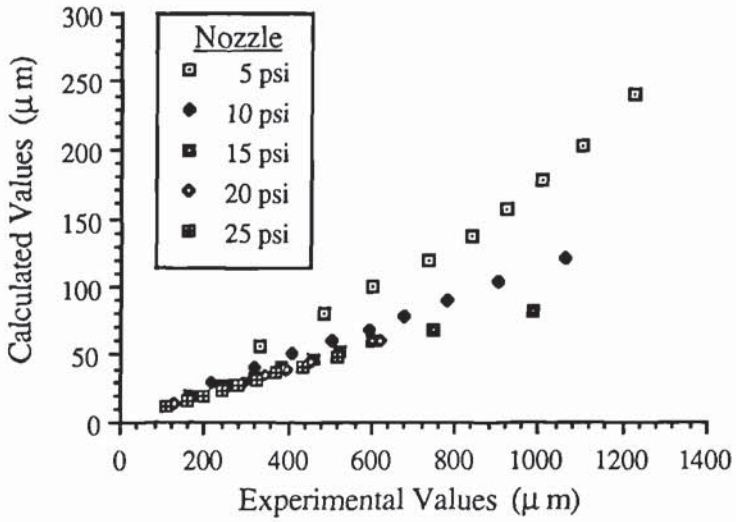

Figure 5.18: *Comparison of Droplet Size Distribution Results for Nozzle P2*

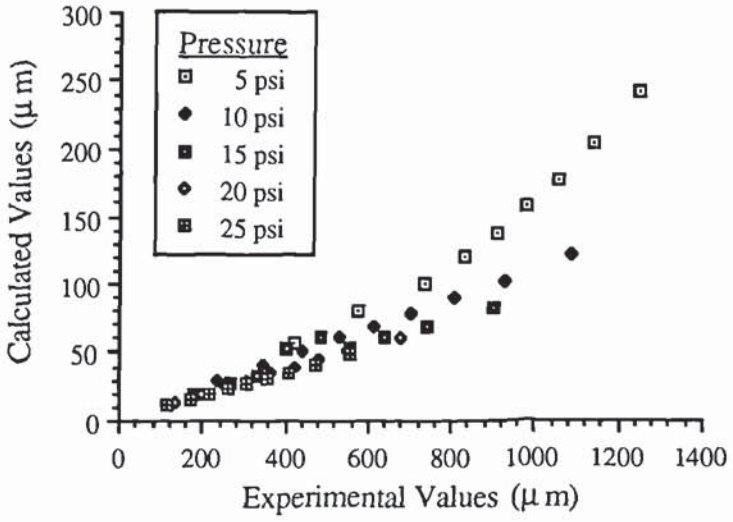

Figure 5.19: *Comparison of Droplet Size Distribution Results for Nozzle P3*

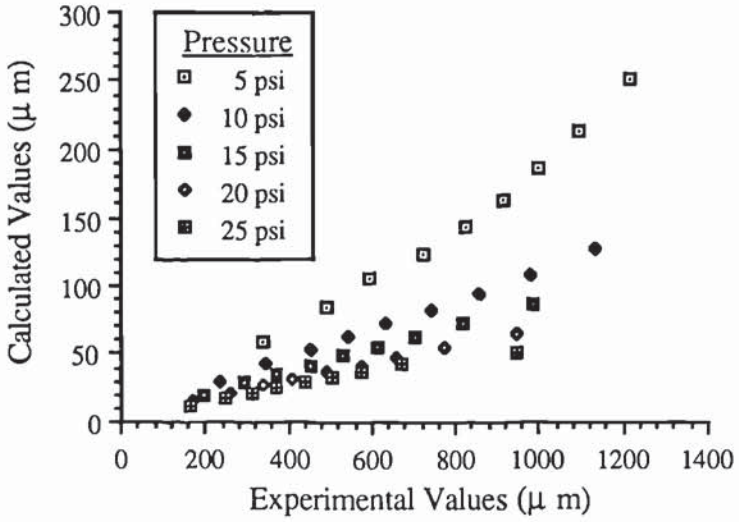

Figure 5.20: *Comparison of Droplet Size Distribution Results for Nozzle P4*

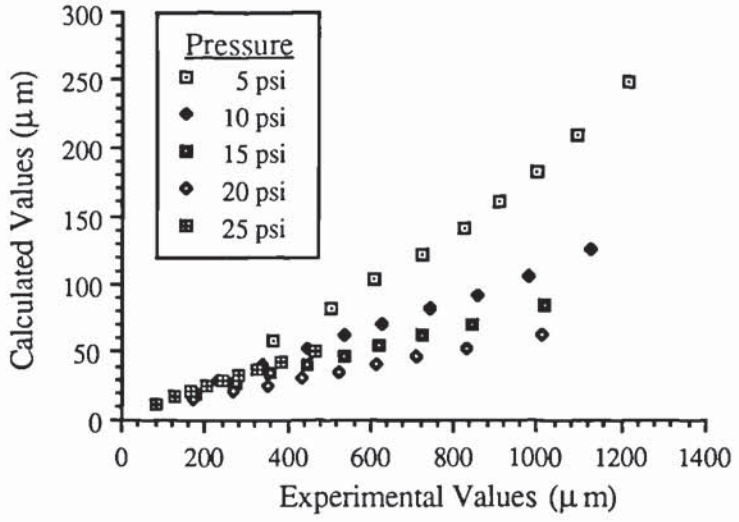

Figure 5.21: *Comparison of Droplet Size Distribution Results for Nozzle P5*

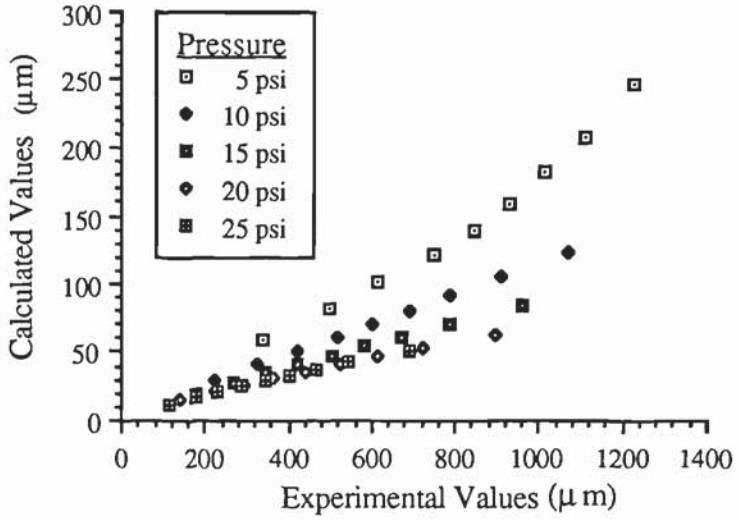

Figure 5.22: *Comparison of Droplet Size Distribution Results for Nozzle P6*

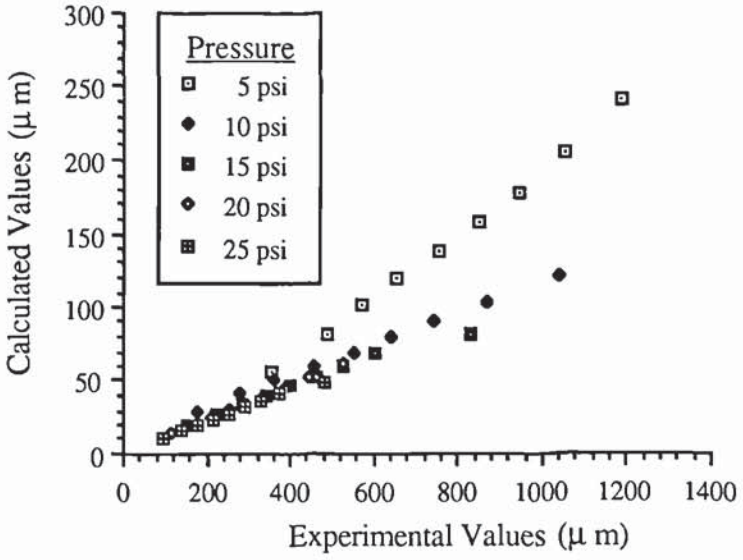

Although there were no significant problems caused by obscuration of the spray cone, there was a tendency for droplets to hit the 800mm lens and cause severe problems due to multi-scattering of the laser beam. This was eliminated by using compressed air to direct the spray away from the lens in a similar method to that employed on the large-scale rig described in Chapter 6.

The results from these experiments are presented in Appendix 2 and a comparison with the results from the mathematical model for each nozzle are illustrated in Figures 5.17 to 5.22.

5.5.2 Measurement of the Air Core Diameter

The main purpose of constructing the perspex nozzles was to allow convenient measurement of the air core. This is usually accomplished by positioning a camera vertically above the nozzle to obtain a photograph of the air core at the top of the swirlchamber [69][168]. An alternative method is to use some form of baffle arrangement to protect the camera from the spray and photograph the air core in the orifice [156] [172]. Sankarankutty *et al* [156] concluded the latter method enabled minute changes in the air core to be recorded and reported a slight reduction in the air core diameter towards the top of the swirlchamber. However, this reduction in the diameter was not as large as that reported by Johnson [186] from photographs taken perpendicular to the nozzle. Johnson also reported that the air core was slightly off-set at the top of the swirlchamber due to slight asymmetry of the vortex and stated that this was a major contributing factor to the initial cause of the liquid sheet disturbances.

In this study the camera was positioned above the nozzle and no appreciable variation in the air core diameter was observed throughout the swirlchamber (See Plate 2). Typical photographs of the air core formed in a nozzle are shown in Appendix 4 and Figure 5.23 illustrates the comparison between experimental and predicted results.

5.5.3 Measurement of the Liquid Sheet Length

The break-up length of the liquid sheet was taken to be the position at which ligament formation was visible, as illustrated in Figure 5.1; although it is possible for

Figure 5.23: *Comparison of Theoretical Prediction and Experimental Results for the Air Core Diameter*

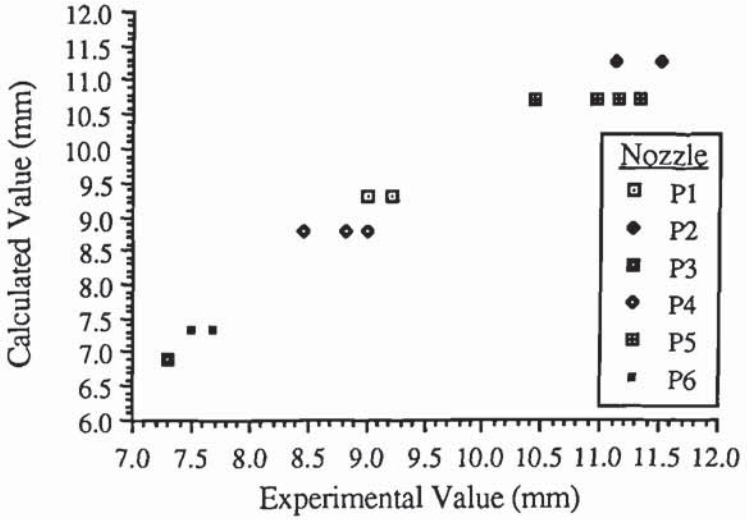

Figure 5.24: *Comparison of Theoretical Prediction and Experimental Results for the Liquid Sheet Length*

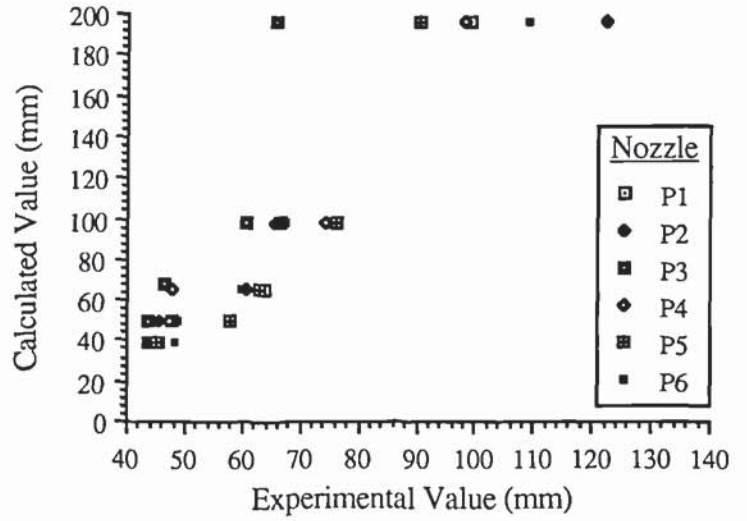

perforations in the sheet to occur much closer to the orifice [8]. Ashton [171] reported that the break-up length of the liquid sheet was subject to variations of the order of ±20%. His findings agreed with those of Wolfsohn [200], who initially attributed the variation in sheet length to pulsations from the pump supplying the nozzles. However, when the pump was replaced with a pressure vessel he was able to eliminate this hypothesis and postulated that anomalies in the air core were the primary cause of the variation in sheet length.

To account for the wide variation in sheet length, a series of flash photographs were taken of the nozzles at each operating pressure [200] and several measurements were obtained of the sheet length under similar conditions. A typical set of photographs for nozzle P1 is shown in Appendix 5 (Plates 5.1 to 5.5) and a comparison between experimental and predicted results is shown in Figure 5.24.

5.5.4 Measurement of the Spray Cone Angle

A typical method for determining the spray cone angle is illustrated in Figure 5.25. This method was used by Doumas & Laster [172], although other authors have used variations of the same principle. This version consisted of a series of precision tubes with an internal diameter of 5/16 inch placed in a semi-circle 10 inches away from the nozzle so that the centre lines of the tubes were 3 degrees apart. The overall result was a distribution of the spray over a particular spread and a value for the mean spray angle was calculated from the liquid volume distribution in each tube.

However, photography is the most common and convenient method presented in the literature for determining the spray cone angle. In this study the spray cone angle was determined from the same series of photographs that were used to determine the break-up length of the liquid sheet (See Appendix 5 and reference [200]) and the results obtained from experiment are given in Figure 5.26.

5.5.5 Measurement of the Liquid Sheet Velocity

Previous workers (for example, reference [96]) calculated sheet velocity from measurements of the thrust exerted on the nozzle by the spray. They measured the

Figure 5.25: *Spray Cone Angle Measuring Apparatus [172]*

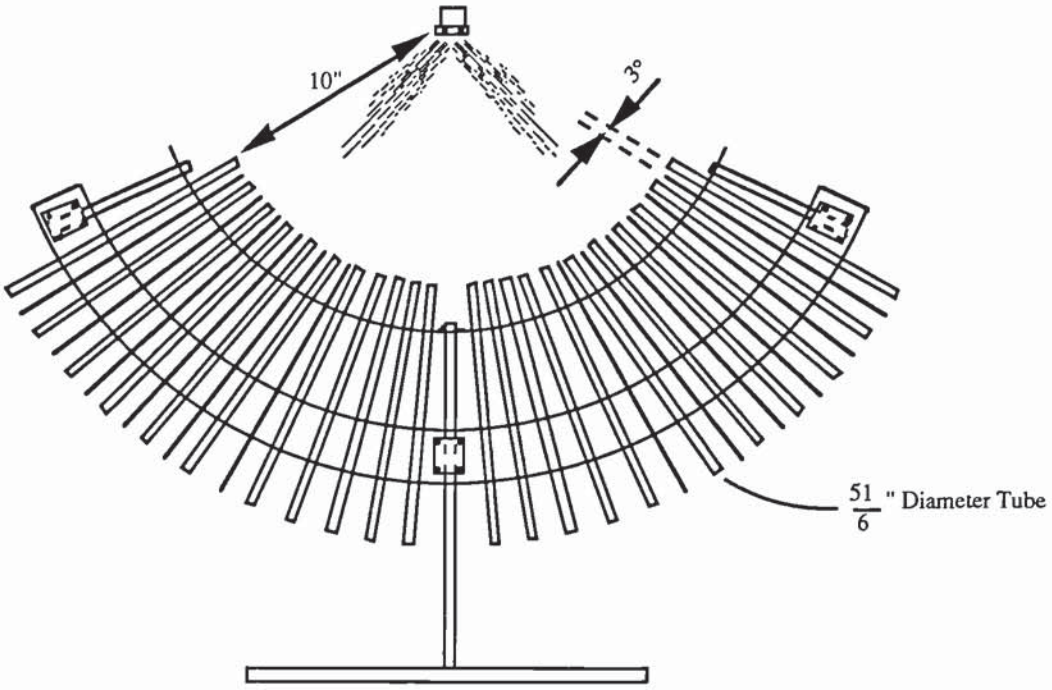

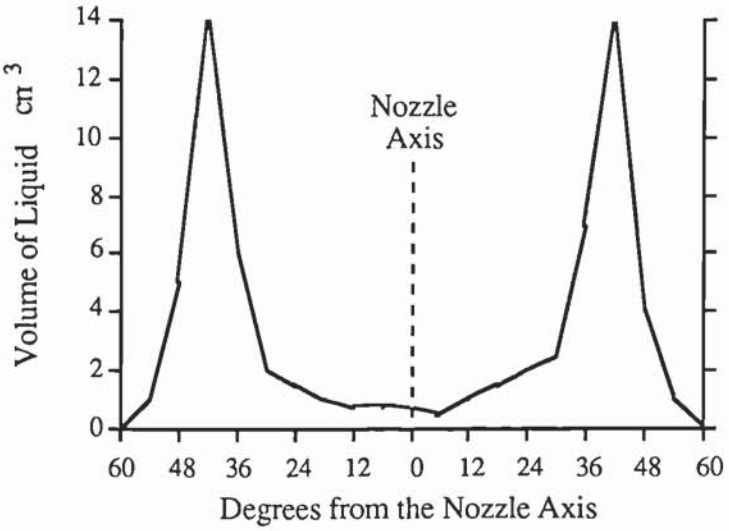

Figure 5.26: *Experimental Results for the Spray Cone Angle*

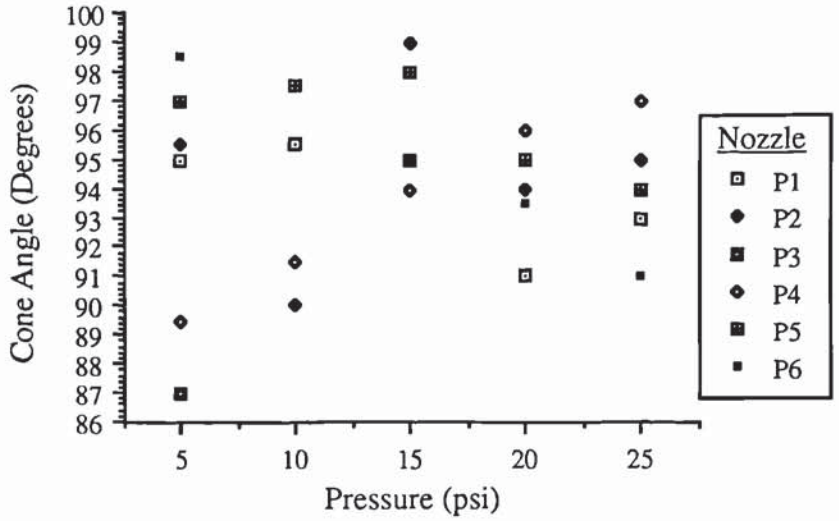

thrust (T) and mass flowrate (M) for each nozzle under specific conditions and determined the sheet velocity from the expression:

$$V_s = \frac{T}{M \rho_l \mathrm{Cos}\left(\frac{\theta}{2}\right)} \qquad - 5.73$$

where, θ is the spray cone angle.

An alternative method for measuring liquid sheet velocity is by the photographic technique of double flash photography. This method captures a double image of a disturbance on the surface of the sheet upon a photograph. It is possible to determine the velocity of the sheet from the knowledge of the time-delay between the two flashes and the distance between the two images.

The latter technique was used since the necessary equipment was available, having previously been used in work by Ashton [171]. The equipment is illustrated in Figure 5.27 and consisted of two argon jet lamps with a pulse generator in the circuit to provide the time-delay between successive flashes. The pulse generator was capable of producing time delays ranging from micro seconds up to several seconds but in practice a delay of 1ms was used on the basis of trial and error from

Figure 5.27: *Double Flash Photography Apparatus*

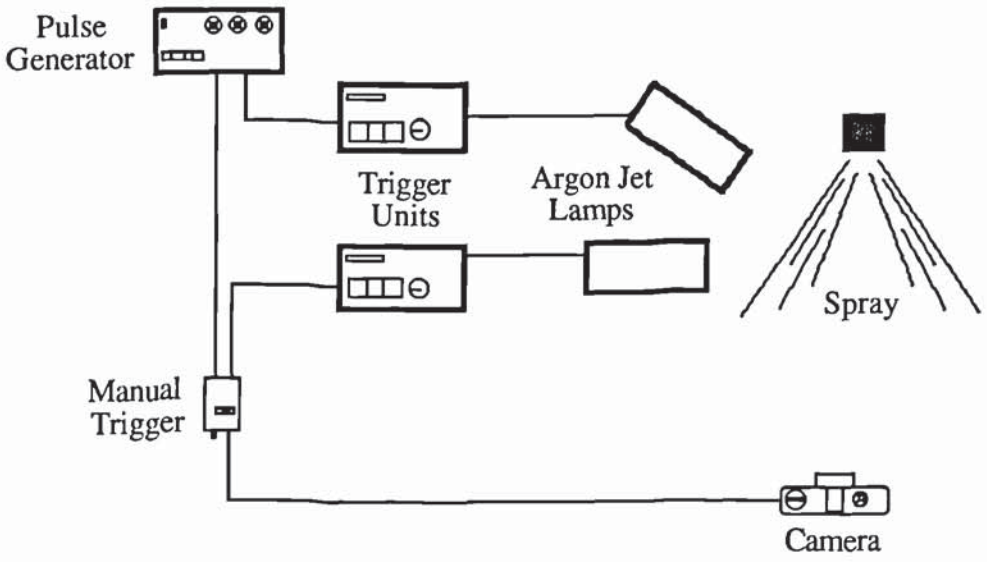

Figure 5.28: *Comparison of Theoretical Prediction and Experimental Results for the Liquid Sheet Velocities*

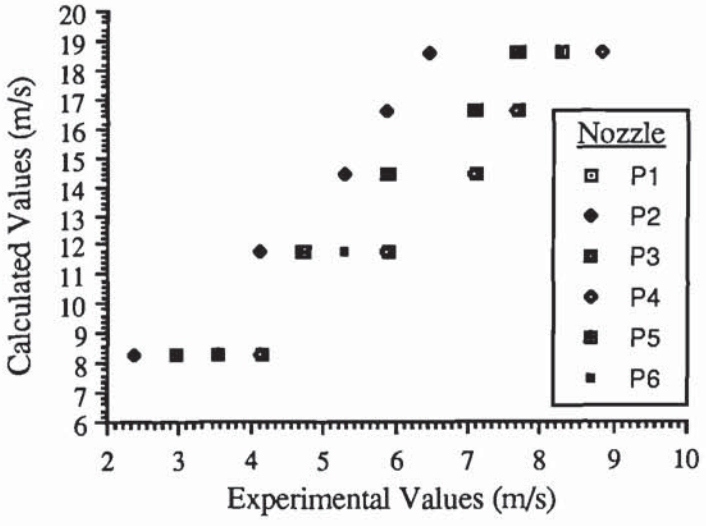

experimentation [200]. A comparison between experimental measurements and theoretical predictions is given in Figure 5.28 and typical photographs obtained using this technique are shown in Appendix 6.

Chapter 6: Experimental Work

Introduction

The main objective of this project was to investigate the atomisation characteristics of detergent slurries with a view to characterising atomisers and modelling the atomisation process. A selection of detergent slurries was therefore atomised using several centrifugal pressure nozzles supplied by Spraying Systems Co. Ltd. [187] upon the recommendation of Colgate-Palmolive. A selection of solutions and slurries was also studied using a range of centrifugal pressure nozzles including two nozzles supplied by Delevan Ltd. [188]. Details of all the nozzles used are given in Table 6.1 and both types of nozzle are illustrated in Plates 5 and 6.

Table 6.1: *Nozzle Dimensions*

Nozzle	Orifice Diameter (mm)	Swirlchamber Diameter (mm)	Area of Inlet (mm^2)
AAASTC 5-5	3.30	11.0	9.08
AAASTC 8-5	3.95	11.0	9.08
AAASTC 8-8	3.95	11.0	13.20
AAASTC 10-10	4.50	11.0	15.21
Delevan 2.0 SJ	2.00	12.0 (Av.)*	34.00*
Delevan 2.2 SJ	2.20	12.0 (Av.)*	34.00*

* Due to the nature of construction of the Delevan nozzles the values given for the Swirlchamber diameter represents an average of three measurements and the values of the inlet area are of the entrance into the region of swirl not the actual insert entrance.

Plate 5: *Spraying Systems Nozzles*

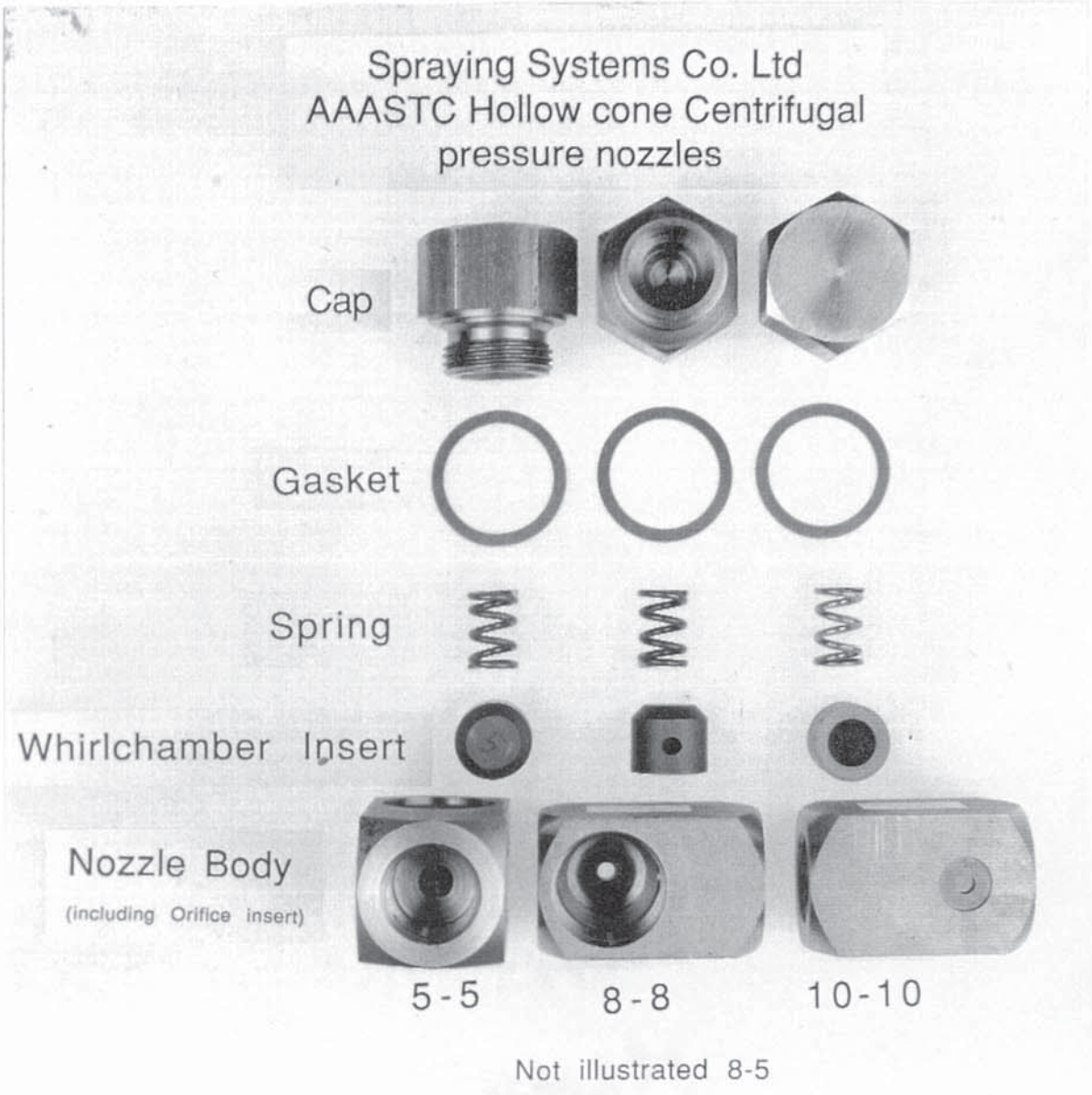

Plate 6: *Delevan Nozzles*

6.1 Experimental Apparatus

The experimental apparatus used throughout the project was similar to that used by Ashton for his atomisation studies with particulate slurries [171]. Ashton's original apparatus had been subsequently modified to enable a Malvern Particle Size Analyser to be used for measurements of spray-droplets within the tower. However, this original transparent tower section was considered unsuitable for a lengthy, science-based, project using the Particle Size Analyser, due to 'reflection' of the spray within the tower which could obscure the incident laser beam by up to 90%. Although it has been stated that reasonable accuracy can be obtained at these levels of obscuration [50], it was considered advisable to first physically reduce the obscuration of the laser beam within the tower. Only then would previously developed correction factors [108] be applied to amend the experimental results if necessary. The obscuration level had to be reduced prior to employing the correction factors because they can only be used between the range of 65 to 95% obscuration without causing experimental ambiguity.

Preliminary work with Ashton's rig failed to determine whether the majority of the obscuration in the tower was attributable to the actual spray cone or to impedance of the laser beam by a dense mist caused by the 'reflection' of the spray from the tower base (See Figure 6.1a). An attempt was made to arrest the production of this reflected mist by flooding the base of the tower with water but this was found to have a detrimental effect upon the obscuration levels recorded within the tower. Later work revealed that most of the obscuration was caused by the spray cone and that the obscuration level recorded in the tower was directly proportional to the cone angle (ie, narrow cone angle sprays produced the highest levels of obscuration.).

A replacement tower section was designed and constructed based upon the dimensions of the original design. This new tower included several recommendations from Lodge-Cottrel [107], who had used the Malvern Particle Size Analyser extensively in trials of this nature; it also had provision to alter the position of the Size Analyser relative to the spray in the tower (See Figure 6.1b). Lodge-Cottrel also recommended the use of two baffles to physically shield the incident laser beam and the resultant diffraction pattern from the mist in the tower.

Figure 6.1: *Transparent Tower Section with Particle Size Analyser*

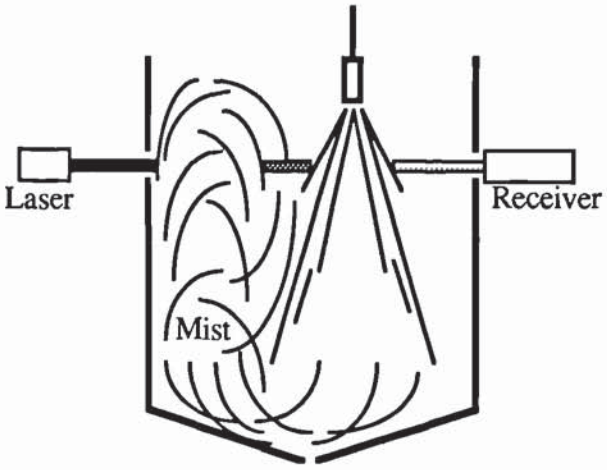

a) Before Modifications

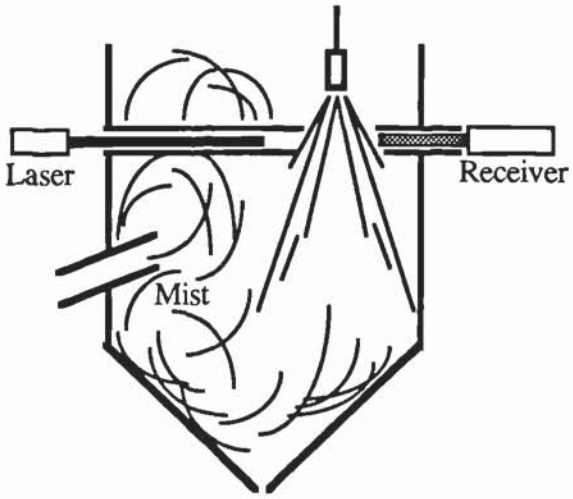

b) After Modifications

However, this generated the problem of incidental collection of the spraying medium in the baffle. This was quite serious at the receiver end, as the optical lens had to be kept clean to avoid further scattering of the beam (multi-scattering) and the production of unrepresentative results. The receiver could not be moved out of the range of the spray as the measuring area must always be kept within the focal length of the lens to avoid beam cut-off (ie, part of the diffraction pattern not being focused upon the detector elements). Partial solution of this problem was achieved by inducing

a flow of air through the baffles away from the receiver lens to blow the spray out of the open end of the baffle. However, in experiments when the spraying pressure was greater than 600 psi some of the spray still struck the receiver lens. Although this problem was not particularly serious, it would have required the apparatus to be frequently dismantled, to avoid any prolonged build-up of the spray upon the lens. This situation was avoided by placing a glass slide, to act as a window, in front of the receiver lens which could easily be removed for cleaning (See Figure 6.2).

Figure 6.2: *Obscuration Reduction by Baffles*

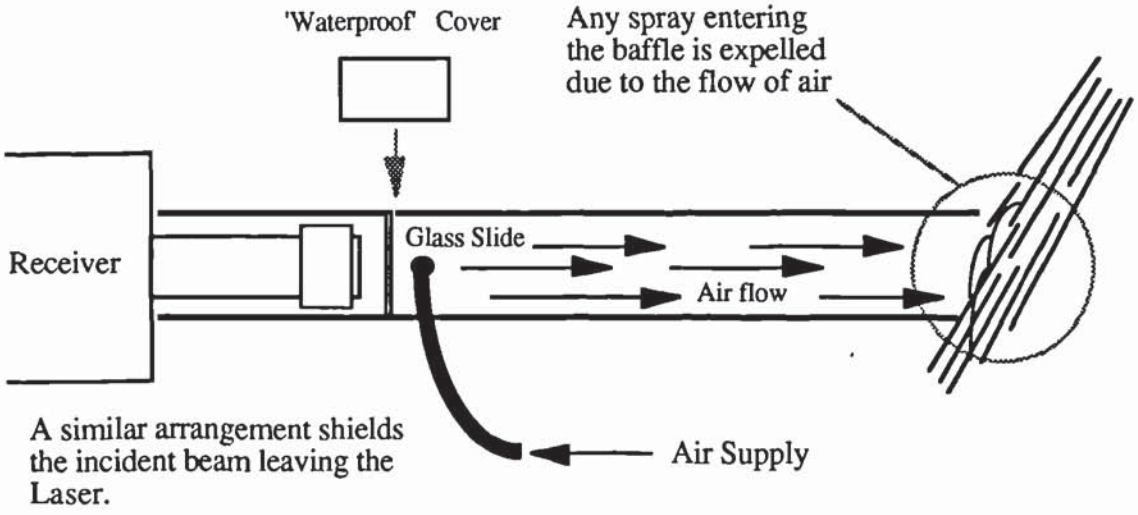

Initial experimentation with the new system determined that the droplet size distribution results obtained by the Size Analyser were not distorted by any abnormal air flow patterns in the region of the measuring area. In these, and in subsequent, experiments the obscuration of the laser beam was reduced to levels in the region of 40% to 50%. Under some conditions, however, the obscuration was recorded in excess of 65% which necessitated the use of Felton's correction factors, discussed in Chapter 3.

A triplex piston pump was initially used to supply the nozzles under test in the tower. However, this pump proved susceptible to significant pressure fluctuation when operated at high pressure. This pressure fluctuation was found to be more

noticeable as the viscosity of the feed increased until a situation was reached when the operating pressure could not be determined from the pressure gauge.

Figure 6.3: *Inert Gas Pumping System*

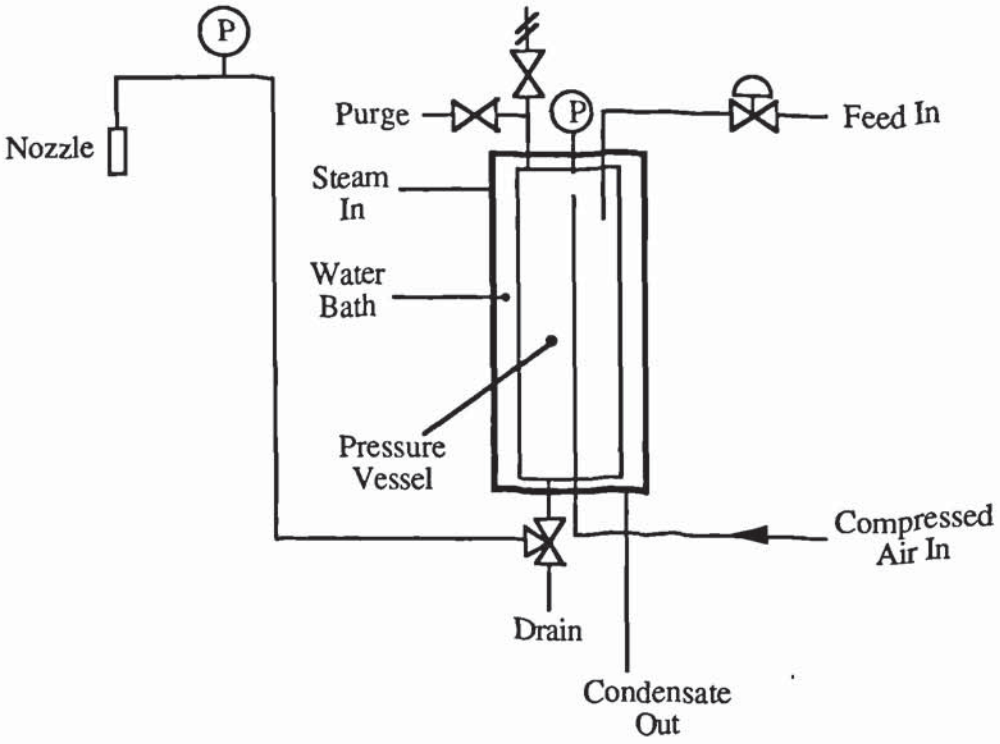

Several previous workers in this field [2][69][70][177][201] had used a pressurised reservoir as the basis for their atomisation test apparatus. A similar principle was adopted for further test work on the rig. For this purpose a double-ended stainless-steel pressure cylinder was incorporated into a system where the contents of the cylinder could be heated for temperature trials (See Figure 6.3). The capacity of the cylinder was approximately 37 litres, which was sufficient for three experiments, and it was rated with a maximum working pressure of 1500 psi (105 bar). This was sufficient to enable the vessel contents to be atomised through the nozzles at pressures of up to 1200 psi.

The feed reservoir was initially pressurised by gas from a compressed air cylinder. However, it proved difficult to maintain pressures over 800 psi for any length of time, particularly with the larger orifice Spraying Systems' nozzles. The

cause of this problem was identified as a restriction in the gas inlet pipe limiting the flow into the feed reservoir. The gas cylinder arrangement was therefore replaced by a Bristol four-stage air compressor, capable of delivering 340 litres of air per minute at pressures up to 2000 psi. Thus the feed reservoir could be pressurised up to 1500 psi for test purposes.

Figure 6.4: *Schematic Diagram of the Droplet Sizing Apparatus*

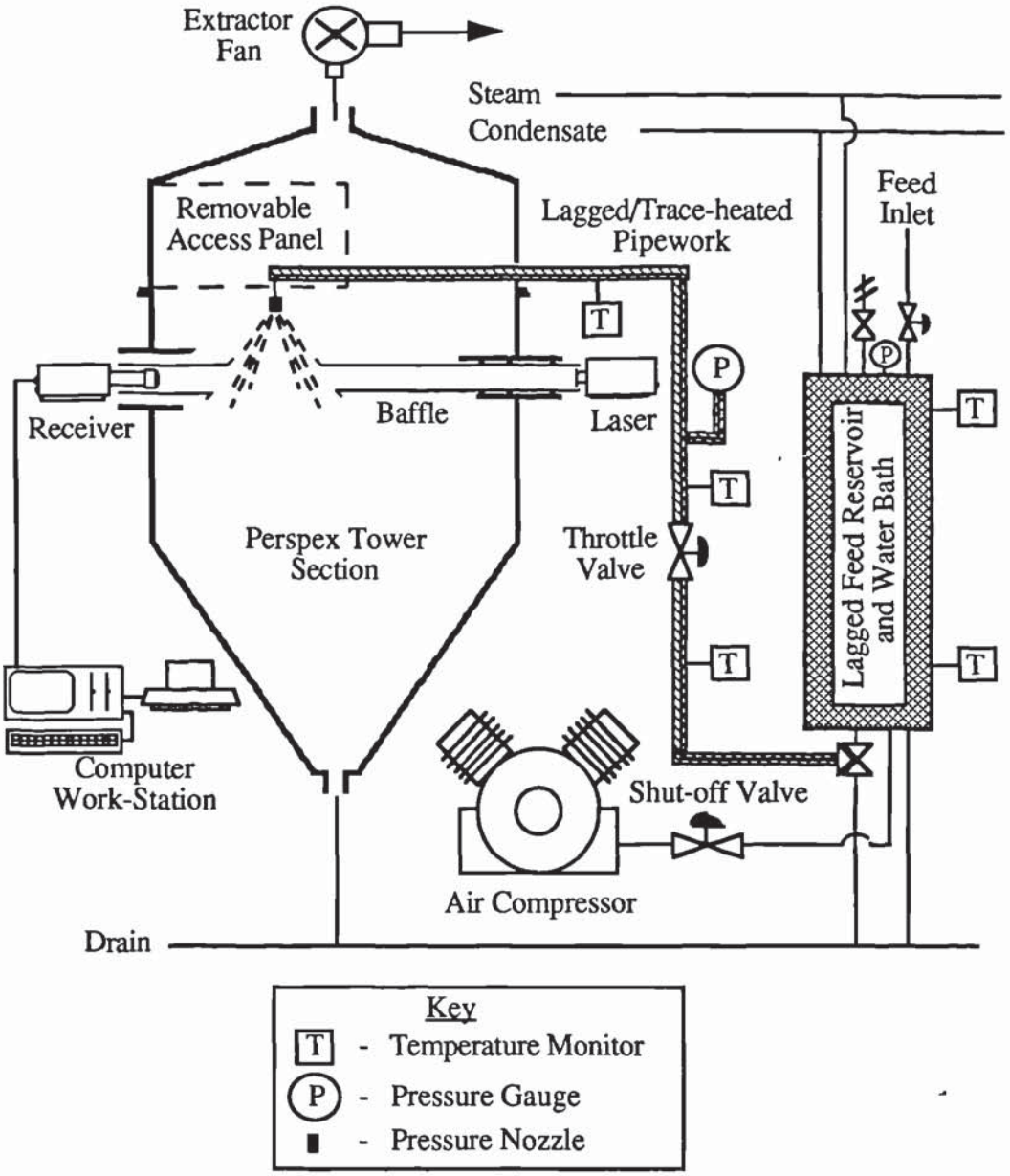

The final experimental apparatus is shown in Plate 7 and in the schematic diagram shown in Figure 6.4. The feed lines to the nozzle were trace-heated with

Plate 7: *Experimental Apparatus*

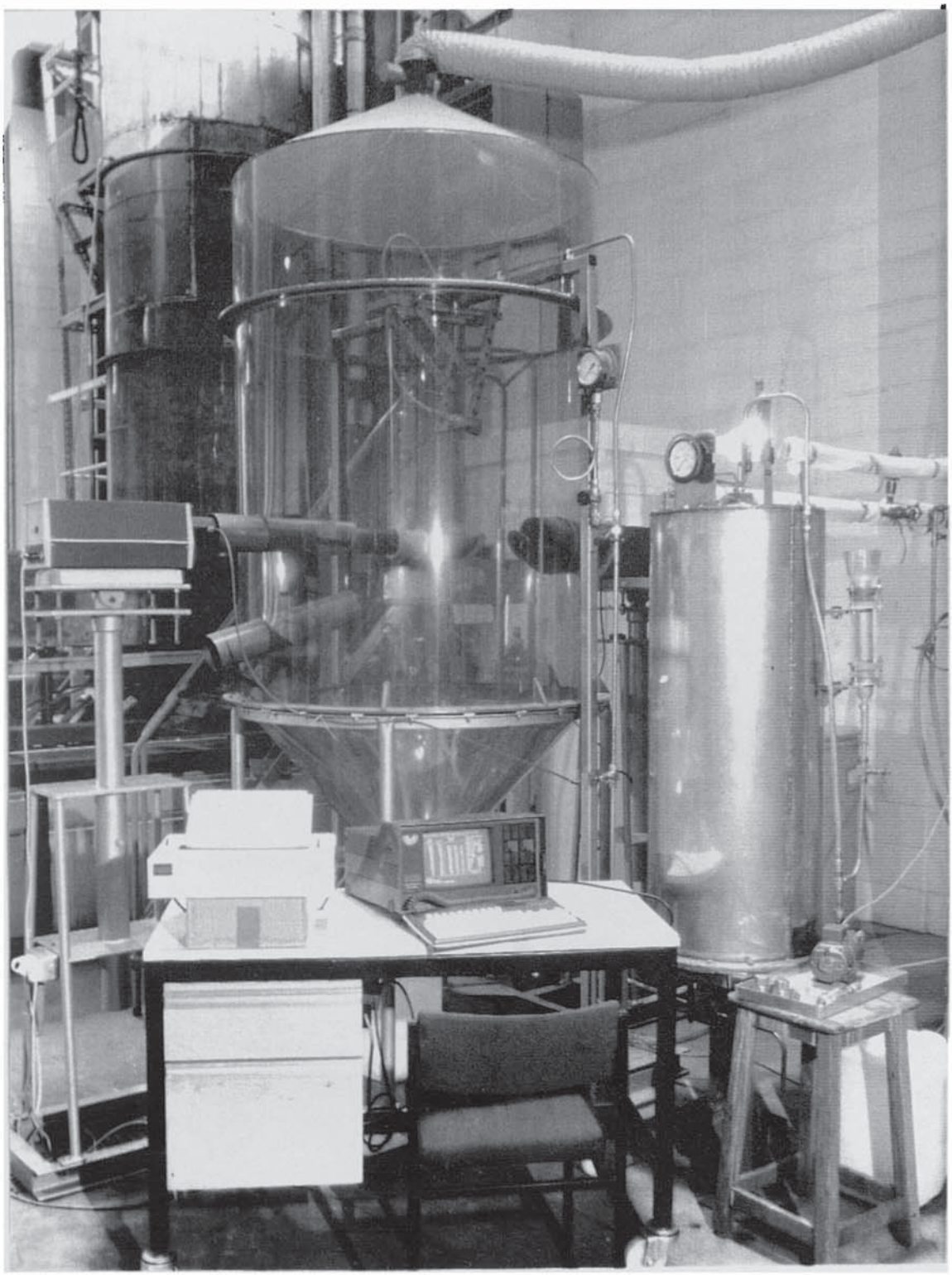

heating tape and lagged to avoid any significant drop in temperature. The main purpose of this was to avoid the possibility of any blockage of the feed line by the detergent slurry which could have been both problematic and detrimental to the safe operation of the apparatus.

6.2 Calibration of the Malvern Particle-Size Analyser

Although the Size Analyser is claimed not to require calibration prior to use [50], a series of calibration standards were employed to determine its accuracy. In addition, during a routine service of the equipment, the accuracy of each lens was checked and the maximum error in the system was found to be ±2%.

It was not possible to confirm the measurements obtained from a 'standard' spray since the facilities were not readily available. However, extensive use of this type of equipment for spray-droplet sizing is reported throughout the recent literature [51][202][203]. Therefore a similar degree of accuracy was assumed in the measurement of the sprays as in the measurement of the calibration standards.

Table 6.2: *Accuracy of the Particle-Size Analyser*

Sample	D(1,0)		Diff.	Error	D(v,0.5)		Diff.	Error
	Actual	Mea		(%)	Actual	Mea		(%)
F28	19.30	19.00	0.30	1.55	19.20	19.47	-0.27	1.44
G15	45.90	45.18	0.72	1.57	45.20	45.58	-0.38	0.84

The standards consisted of a series of P.V.D.B latex spheres within a defined size limit, but designed for use with a 'Coulter Counter' sizing device. Not all the sizes listed on the assay sheet for each standard could therefore be used with any degree of confidence. Nevertheless direct comparison of compatible measurements gave good agreement and a summary of the results from these experiments, shown in

Table 6.2, demonstrates that the accuracy of the equipment falls in to the region of 1 to 2%. This is well within the normal bounds of experimental error and is in line with the accuracy value determined during the routine servicing of the equipment.

Accuracy of Experimental Results

Discrepancy may also arise in the measurement of droplet size distribution from sprays due to evaporation of the spraying medium. Throughout this work the spray was always measured in exactly the same position relative to the nozzle. However, the major factors influencing spray evaporation are that of temperature and the humidity of the spraying atmosphere. The influence of the temperature difference between the spray and the atmosphere is a predominant effect and should therefore be maintained as low as possible.

Operating the apparatus at room temperature and spraying liquid at a similar temperature ensured that evaporation was kept to a minimum between injection from the nozzle and the measuring area. However, under some conditions the liquid sprayed was up to 60°C greater than room temperature. To account for such situations, when air temperatures cannot be raised as high, it is necessary to ensure that the measuring area is as close as possible to nozzle. Although this will reduce atomisation time, care must taken to ensure that the liquid sheet does not interfere with the laser beam. Therefore a clearance distance of between 15 to 20cm must be imposed to avoid beam interference by the sheet under any operating conditions.

Evaporation in sprays has been investigated by Pham & Keey [204], who presented a model of the evaporation of liquid spray in the jet zone of a nozzle, ie the region where the droplet sizing occurred. They drew their definition of jet zone from earlier work [21] which had shown the existence of two different aerodynamic zones around the spray: a jet zone and a subsequent principal zone where the spray-air mixing is complete. They noted that the jet zone had three main effects upon the liquid droplets:

i) The relative velocity between the droplets and air is higher than in the principal zone owing to the greater air-velocity gradient .

ii) The absolute velocity of the droplets will also be high, since the droplets are still decelerating.

iii) The confined geometry of the jet, and the limited amount of air in it, will restrict the maximum possible evaporation and hence diminish the effective driving force.

The first effect has a tendency to increase evaporation, whilst the other effects will decrease it. Therefore they concluded that evaporation was severely limited in the jet zone in comparison to the principle zone due to the high droplet velocities and limited air available.

It is therefore assumed that there is negligible evaporation of the droplets between their formation and subsequent measurement. Hence for modelling purposes it is possible to assume that the droplets measured by the size analyser are the same size as those produced from disintegration of the liquid sheet and/or ligaments.

6.3 Experimental Results

The Malvern Particle Size Analyser produces highly detailed results from each droplet sizing experiment and much of the data obtained during the atomisation trials were superfluous to the requirements of this project. It was therefore necessary to summarise the information obtained from the result print-outs (a typical print-out is illustrated in Figure 6.5) into a more compact tabulated form more relevant for the work-in-hand; these summarised results are presented in Appendix 1.

The experimental work covered in this chapter has been segregated into four sections, each described below, and the results presentation has been limited to conform with the main objective of the project (ie, determining the conditions under which the narrowest spray distribution (or most uniform droplet size) is produced.).

6.3.1 Water

The new apparatus was commissioned using water as the spraying medium. The work involved all six pressure nozzles being operated at a range of pressures between

Figure 6.5: *Typical Droplet Sizing Results*

Malvern Instruments MASTER Particle Sizer M3.0 Date 27-05-90 Time 15-22

Size microns	under	%in band	Size microns	under	%in band
564.0	100.0	0.2	53.1	8.6	2.4
487.0	99.8	0.5	45.8	6.2	1.7
420.0	99.3	0.7	39.5	4.4	1.3
362.0	98.7	0.7	34.1	3.2	0.9
312.0	98.0	0.6	29.4	2.3	0.6
270.0	97.4	2.8	25.4	1.6	0.5
233.0	94.6	7.9	21.9	1.2	0.3
201.0	86.7	11.5	18.9	0.8	0.3
173.0	75.2	13.2	16.3	0.5	0.1
149.0	62.0	12.5	14.1	0.4	0.1
129.0	49.5	10.3	12.1	0.3	0.1
111.0	39.2	8.9	10.5	0.3	0.1
95.9	30.3	8.2	9.5	0.1	0.0
82.7	22.1	5.9	7.8	0.1	0.0
71.4	16.2	4.3	6.7	0.1	0.0
61.6	12.0	3.3	5.8	0.1	0.0

Result source = Sample
Record No. = 0
Focal Length = 300 mm
Experiment type lds
Volume distribution
Beam length = 300.0 mm
Obscuration = 0.3130
Volume Conc. = 0.0076%
Log. Diff. = 5.13

Rosin-Rammler
X = 150.50 , N = 2.31
D(v,0.5) = 129.8 µm
D(v,0.9) = 211.9 µm
D(v,0.1) = 56.7 µm
D(4,3) = 135.3 µm
D(3,2) = 88.5 µm

Span = 1.2

Spec. surf. area
0.03 sq.m./cc.

Sample Details:- AAASSTC5-5 / Water / 200 psi

Malvern Instruments MASTER Particle Sizer M3.0 Date 27-05-90 Time 15-23

Particle diameters		Volume percentiles	
D(4,3)	135.30 µm	Dv.1	56.74 µm
D(4,2)	109.43 µm	Dv.2	78.88 µm
D(4,1)	73.06 µm	Dv.3	95.45 µm
D(4,0)	47.30 µm	Dv.4	112.47 µm
D(3,2)	88.51 µm	Dv.5	129.81 µm
D(3,1)	53.69 µm		
D(3,0)	33.32 µm	Dv.6	145.79 µm
		Dv.7	162.93 µm
D(2,1)	32.56 µm	Dv.8	183.41 µm
D(2,0)	20.45 µm	Dv.9	211.86 µm
D(1,0)	12.84 µm	Span	1.20
		Unif.	63.02

Distribution Moments

Distbn	Mean	Stan.Dev.	Skewness
Volume	135.30	69.00	1.20
Surface	88.51	64.35	0.93
Length	32.56	42.68	2.28
Number	12.84	15.91	6.24

Sample Details:- AAASSTC5-5 / Water / 200 psi

200 and 1200 psi. This pressure range was larger than that used subsequently as the main purpose of this work was to establish the maximum and minimum operating

limits of the apparatus in terms of obscuration levels and the maintenance of a constant pressure in the feed reservoir.

Obscuration was found to be affected by operating pressure and spray cone angle. Figure 6.6 demonstrates the general increase in obscuration with an increase in operating pressure with the highest obscuration levels being experienced with the two Delevan nozzles. It was observed in subsequent experiments that viscosity also influenced the obscuration levels; a general reduction in the obscuration occurred as viscosity was increased.

Figure 6.6: *Effect of Operating Pressure upon Laser Beam Obscuration*

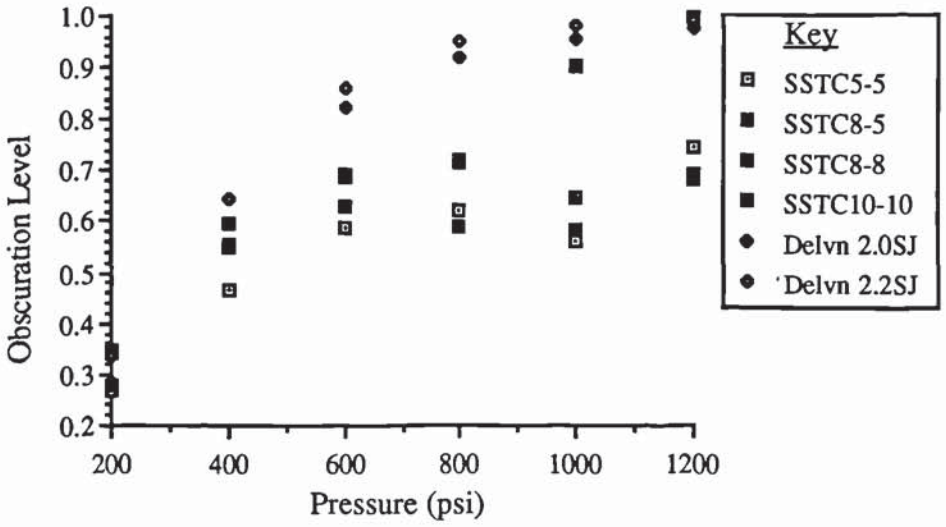

The problem experienced in maintaining a constant gas pressure, and its solution was noted in Section 6.1. The air compressor substantially reduced the pressure drop that occurred during operation of the apparatus, but there was still a slight reduction in the feed reservoir pressure, ie up to 100 psi. This problem was overcome by the inclusion of a throttle valve in the nozzle feed line and by ensuring that the feed reservoir pressure was kept in excess of the nozzle operating pressure by approximately 200 psi.

The results from this series of experiments are given in Tables A1.1 to A1.6 (See Appendix 1) and the relevant results are plotted in Figures 6.7 to 6.12.

Figure 6.7: *Nozzle AAASSTC5-5 with Water*

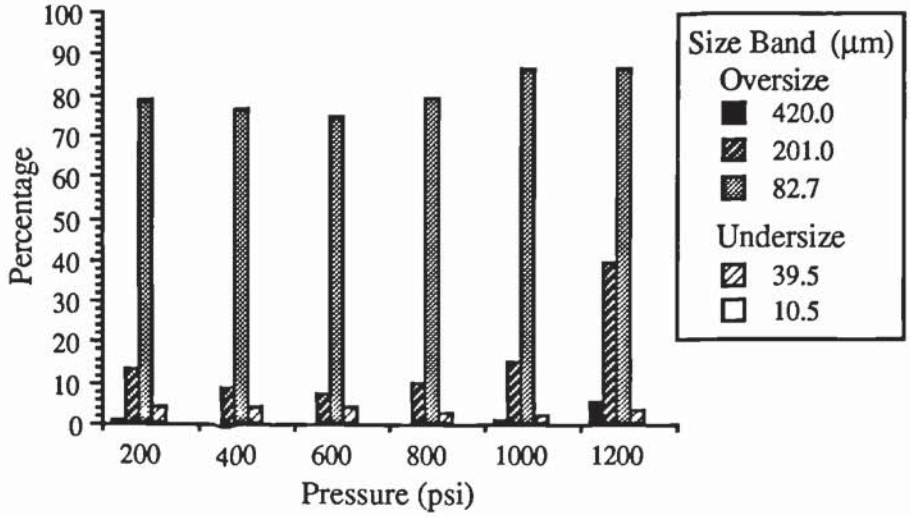

Figure 6.8: *Nozzle AAASSTC8-5 with Water*

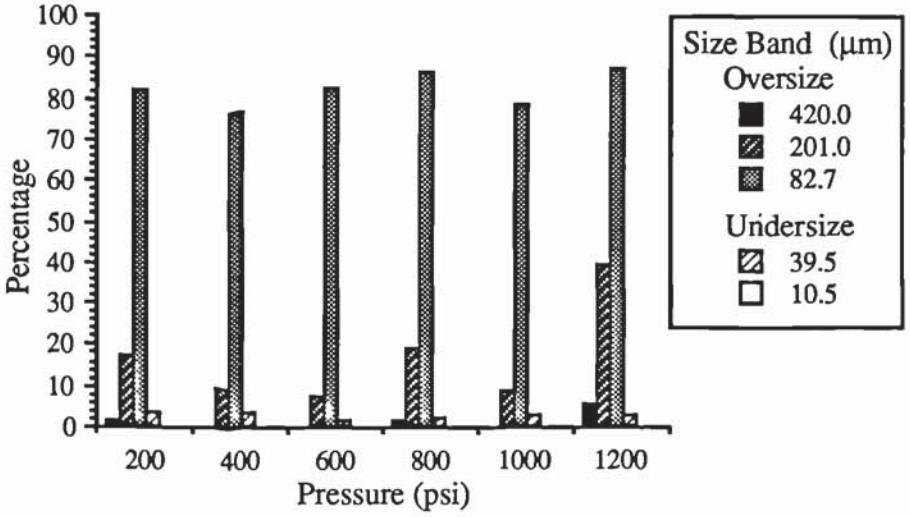

Figure 6.9: *Nozzle AAASSTC8-8 with Water*

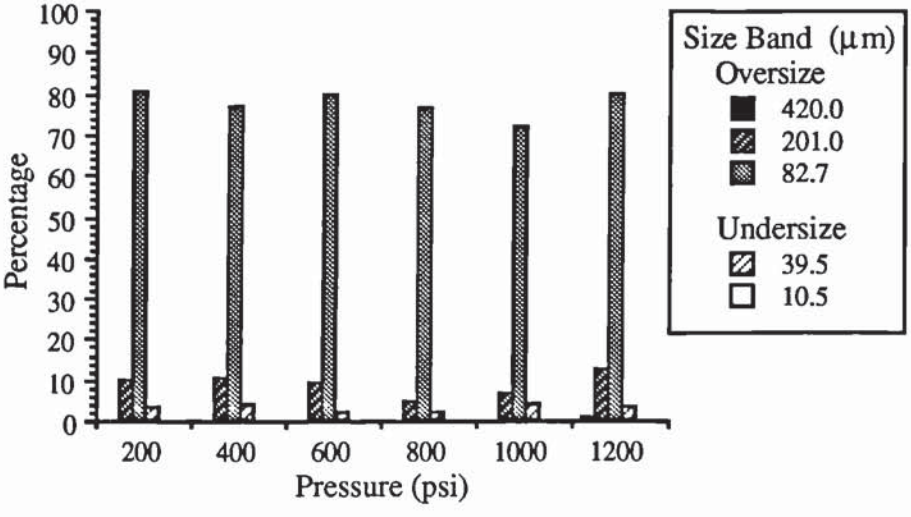

Figure 6.10: *Nozzle AAASSTC10-10 with Water*

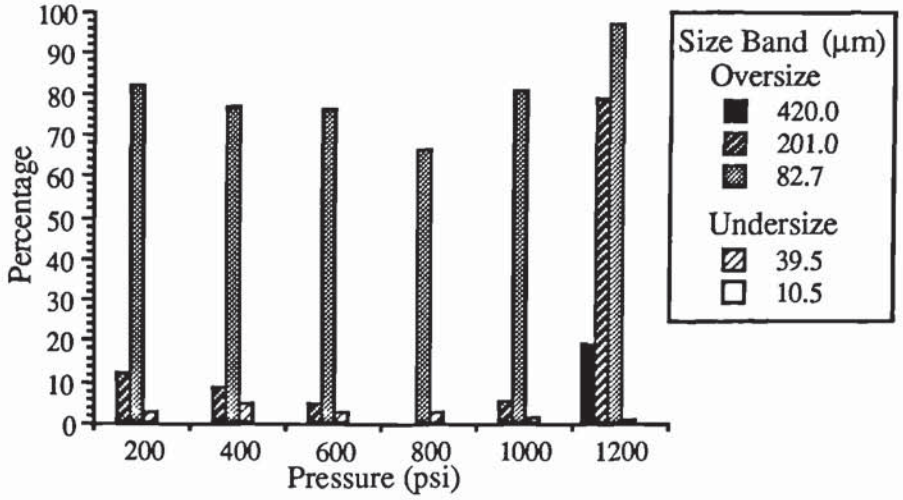

Figure 6.11: *Nozzle Delevan 2.0SJ with Water*

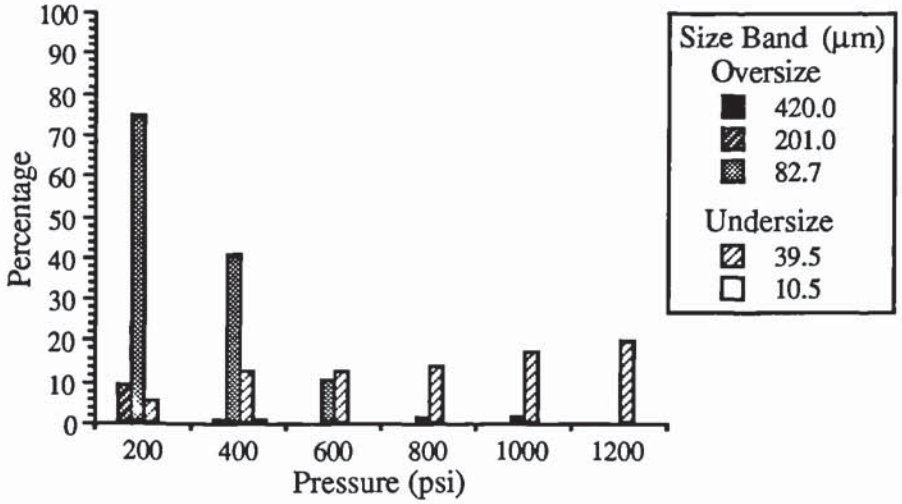

Figure 6.12: *Nozzle Delevan 2.2SJ with Water*

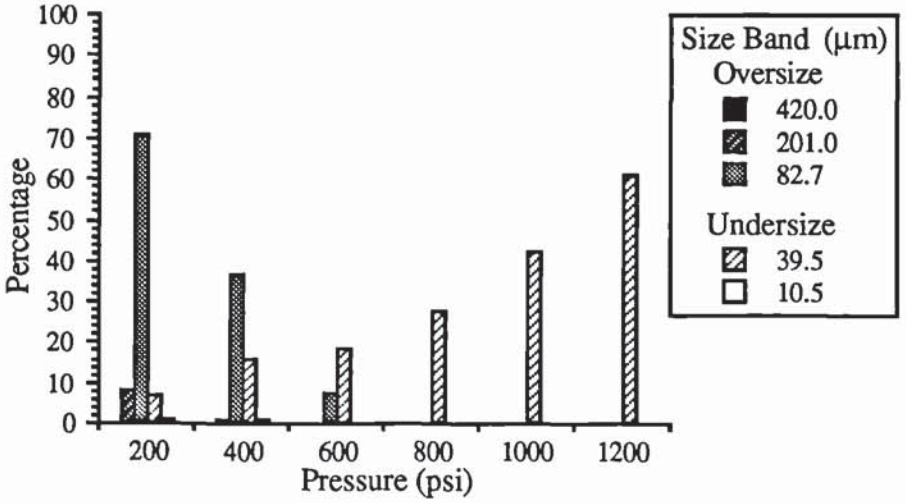

6.3.2 Sodium Sulphate Solutions

A series of experiments, using sodium sulphate solutions, was performed in cooperation with droplet drying/trajectory research within the Department. Three aqueous solutions of sodium sulphate (5%, 10% and 15%) were sprayed at a range of pressures between 400 and 1200 psi. These concentrations were chosen to produce a range of results over the limited conditions that sodium sulphate remains soluble in water. Although the maximum limit is approximately 22% at 20°C [205], concentrations were kept below this in order to avoid the possibility of any precipitation of sodium sulphate crystals at lower ambient temperature, since the solutions were often stored overnight prior to experimental use.

Table 6.3: *Physical Properties of Various Aqueous Solutions of Sodium Sulphate*

Concentration (% w/w)	5%	10%	15%
Temperature (°C)	20.0	20.0	20.0
Solution Density (kg/m^3) [1]	1053.6	1090.5	1140.2
Absolute Viscosity (cP) [2]	1.163	1.390	1.725
Surface Tension (dynes/cm) [1]	73.77	74.90	76.04

[1] Obtained from previously published data [205].
[2] Measured using a Haake Viscometer fitted with a Sensor system and NVST measuring head.

The physical properties of the aqueous solutions of sodium sulphate are given in Table 6.3 and the droplet sizing results from this series of experiments are given in Tables A1.7 to A1.24, with the relevant data plotted in Figures 6.13 to 6.18.

6.3.3 Calcium Carbonate Slurries

A range of calcium carbonate slurries were sprayed to test the ability of the apparatus to cope with viscous slurries. It was found that without constant agitation the calcium carbonate tended to gradually settle out. Since the pressure reservoir was not fitted

Figure 6.13: *Nozzle AAASSTC5-5*

a) *5% Sodium Sulphate*

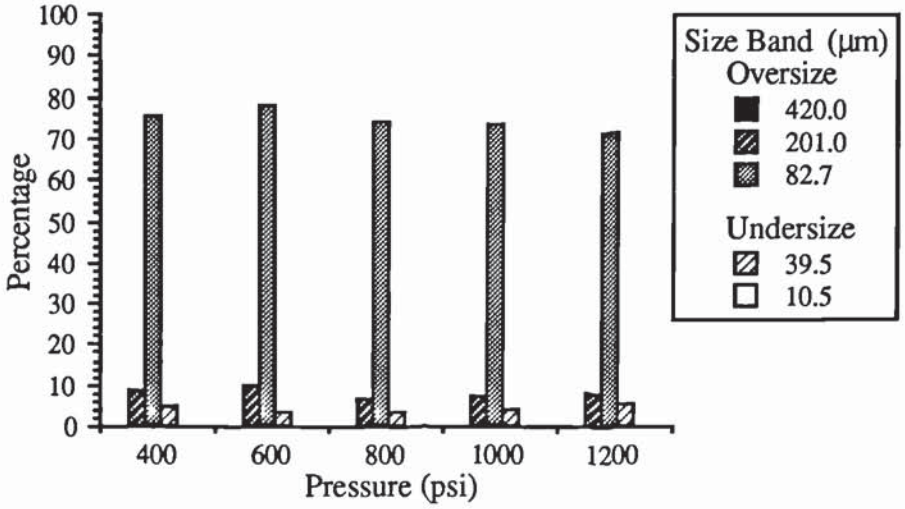

b) *10% Sodium Sulphate*

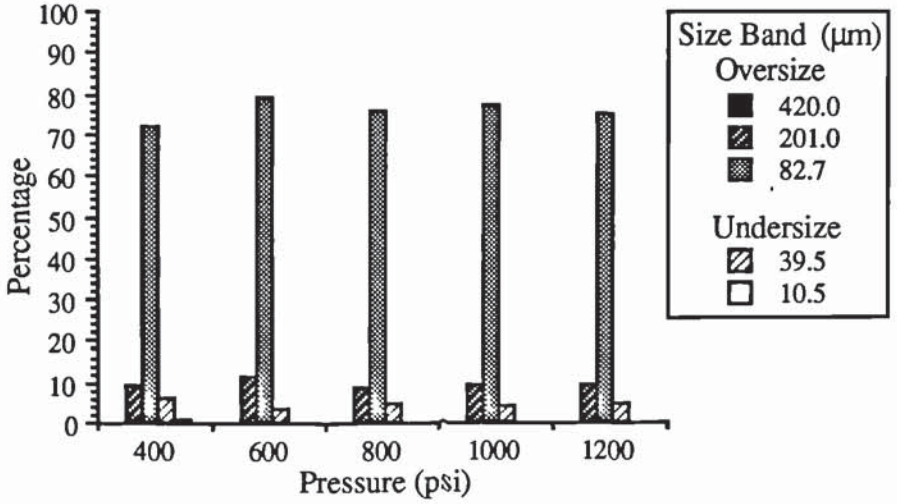

c) *15% Sodium Sulphate*

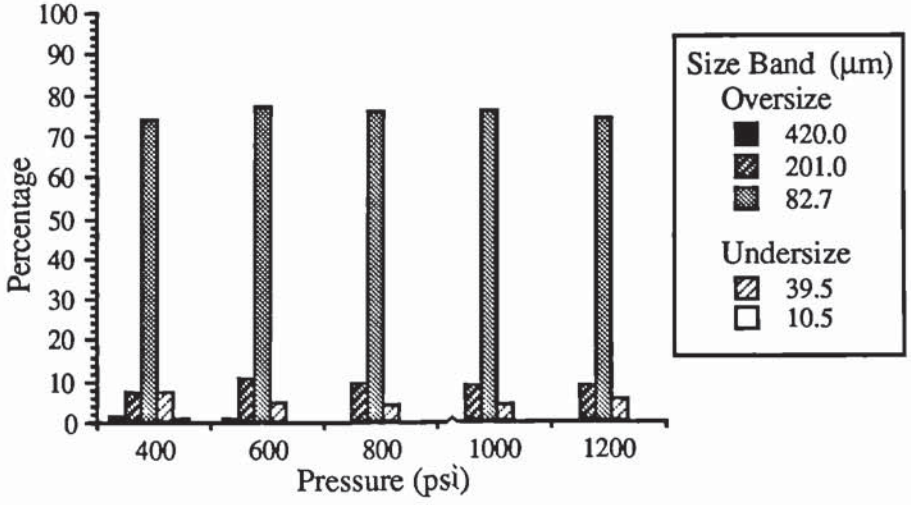

Figure 6.14: *Nozzle AAASSTC8-5*

a) *5% Sodium Sulphate*

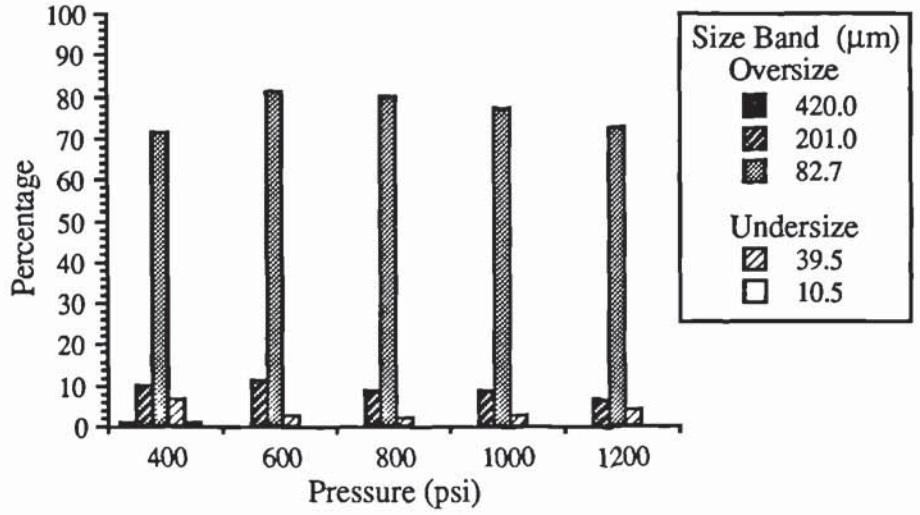

b) *10% Sodium Sulphate*

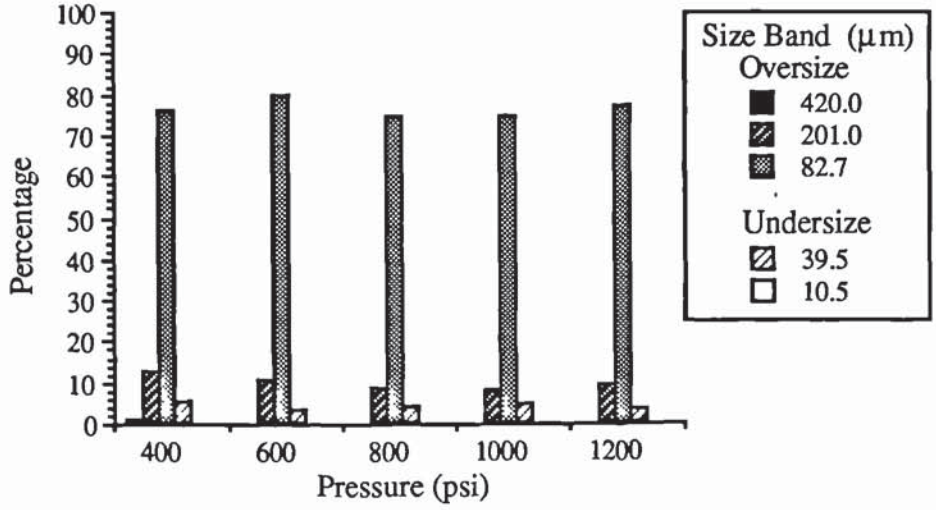

c) *15% Sodium Sulphate*

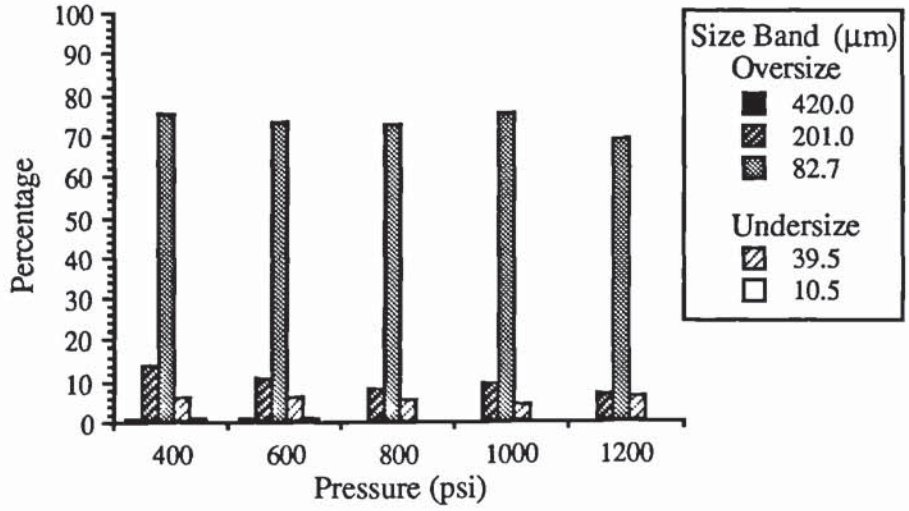

Figure 6.15: *Nozzle AAASSTC8-8*

a) *5% Sodium Sulphate*

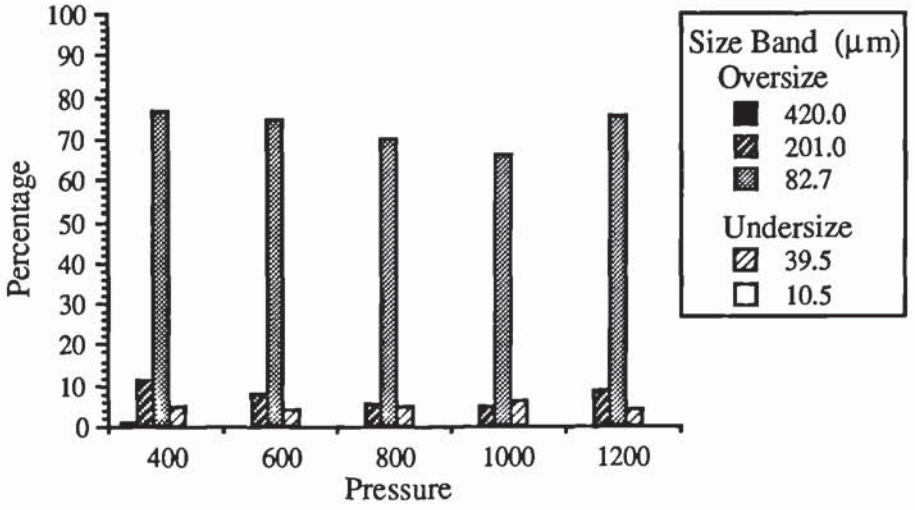

b) *10% Sodium Sulphate*

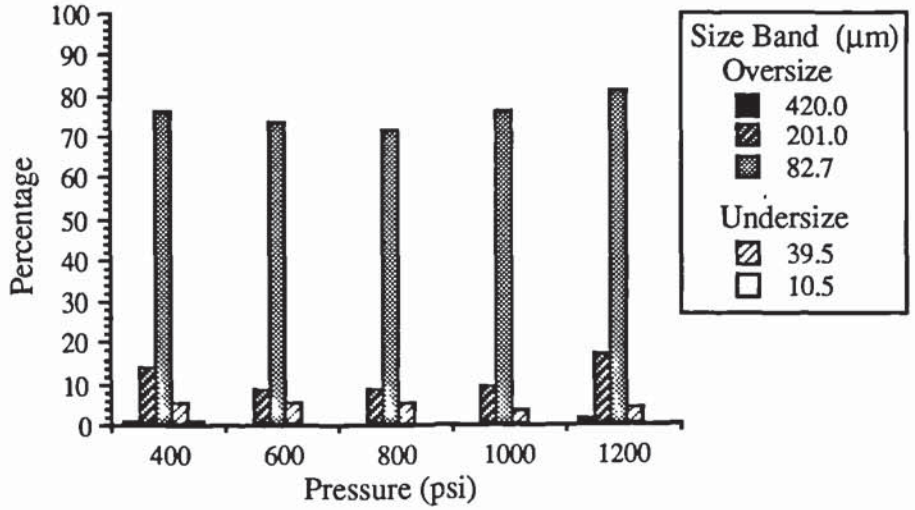

c) *15% Sodium Sulphate*

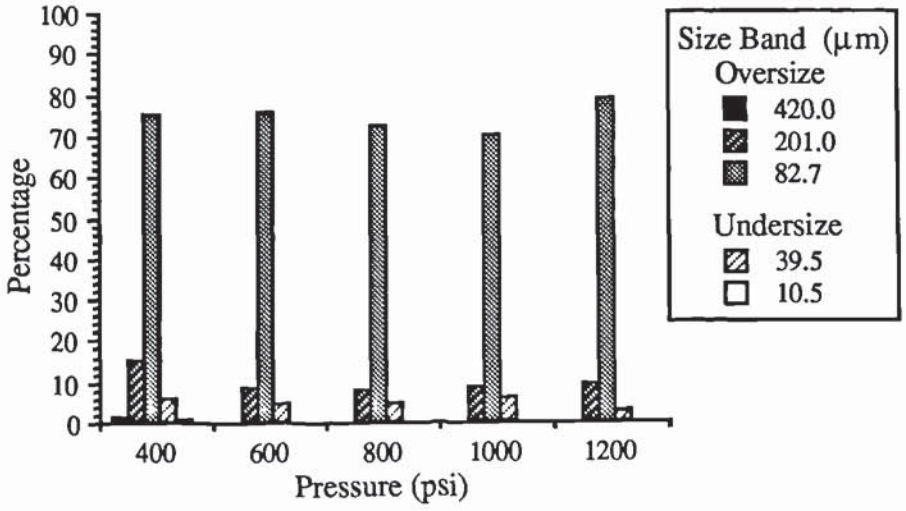

Figure 6.16: *Nozzle AAASSTC10-10*

a) *5% Sodium Sulphate*

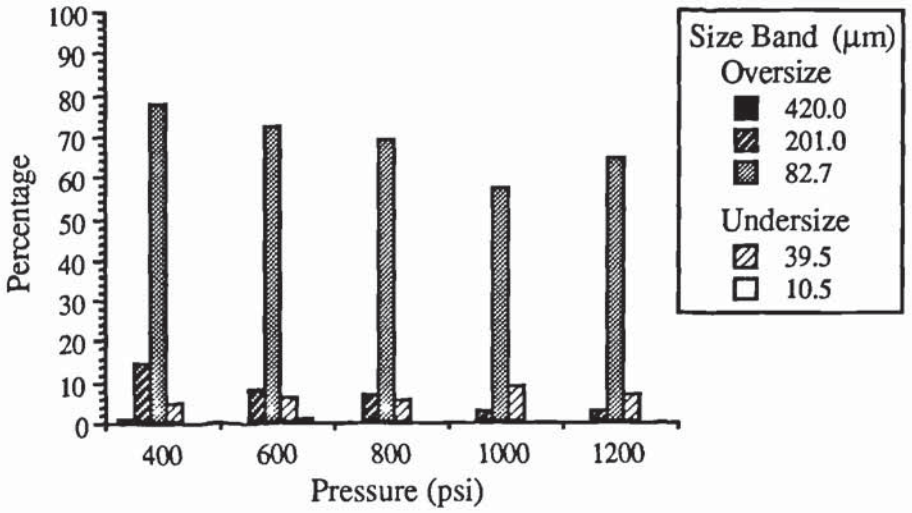

b) *10% Sodium Sulphate*

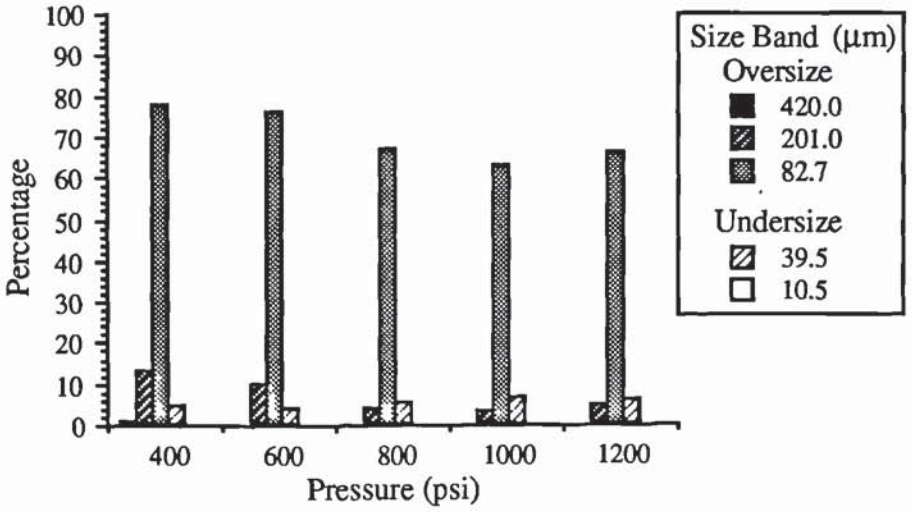

c) *15% Sodium Sulphate*

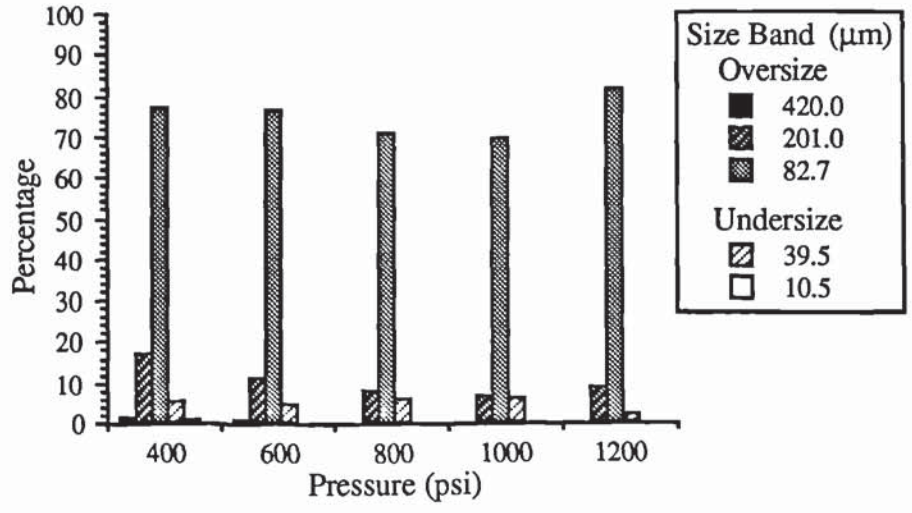

Figure 6.17: *Nozzle Delevan 2.0SJ*

a) *5% Sodium Sulphate*

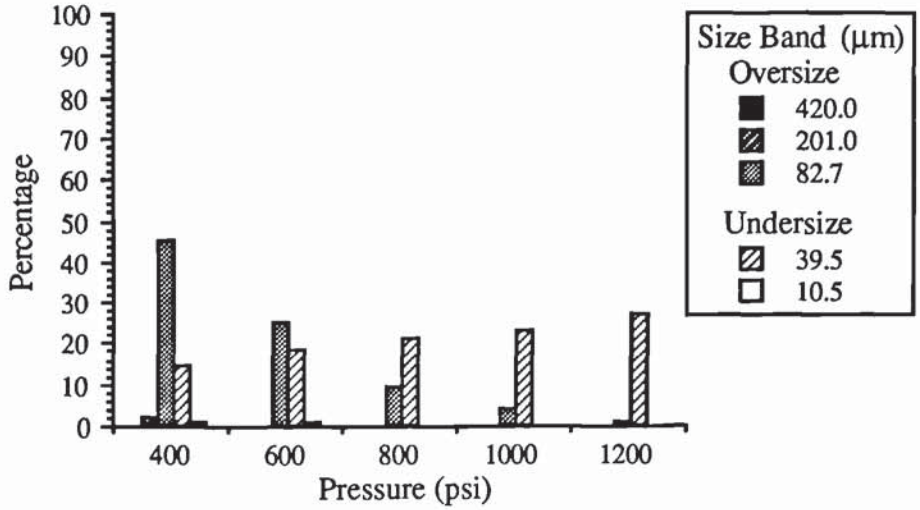

b) *10% Sodium Sulphate*

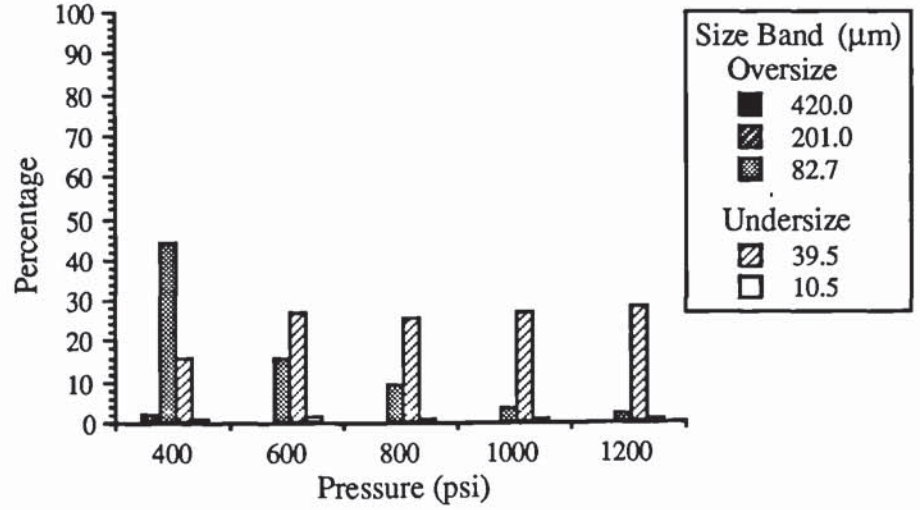

c) *15% Sodium Sulphate*

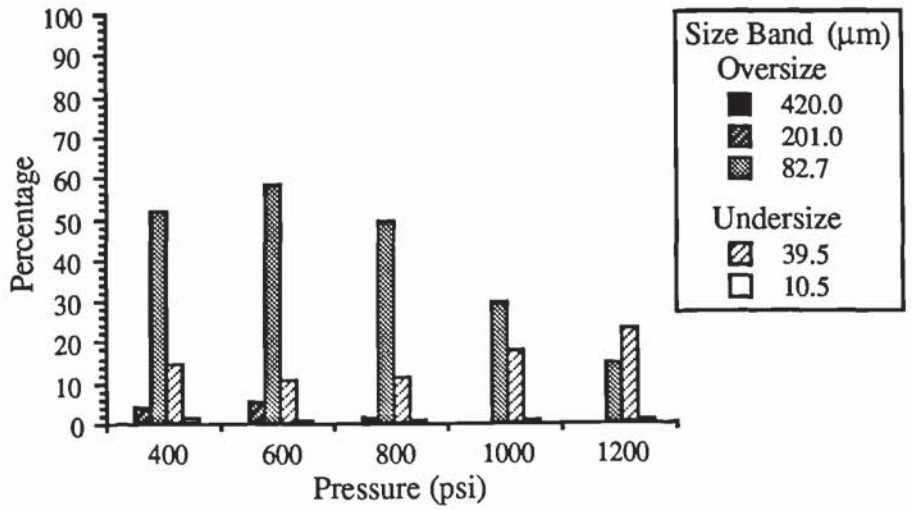

Figure 6.18: *Nozzle Delevan 2.2SJ*

a) *5% Sodium Sulphate*

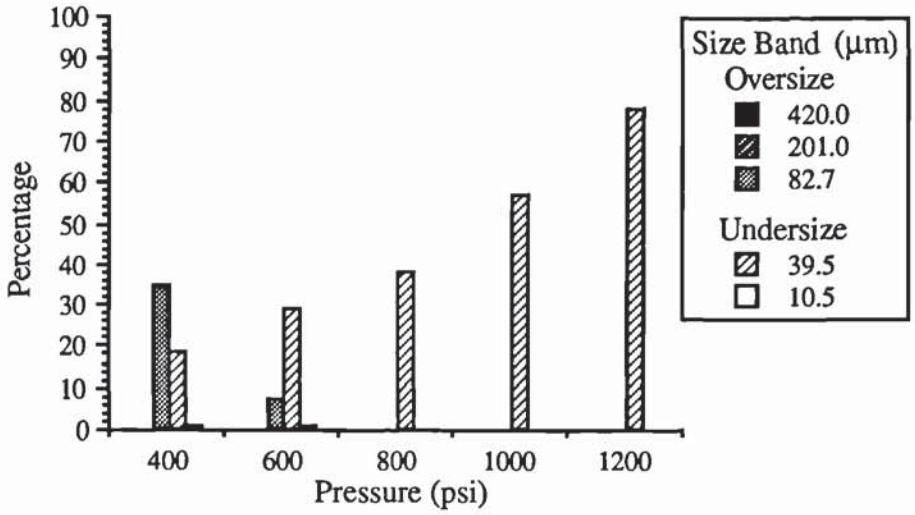

b) *10% Sodium Sulphate*

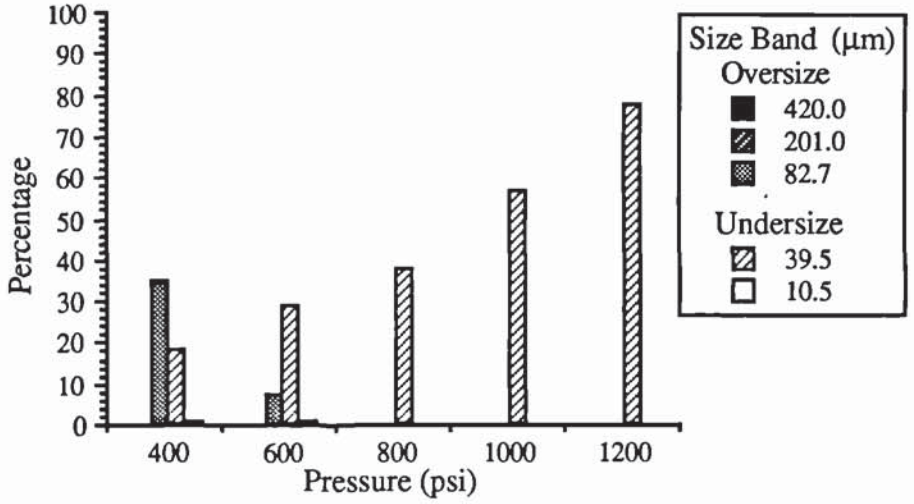

c) *15% Sodium Sulphate*

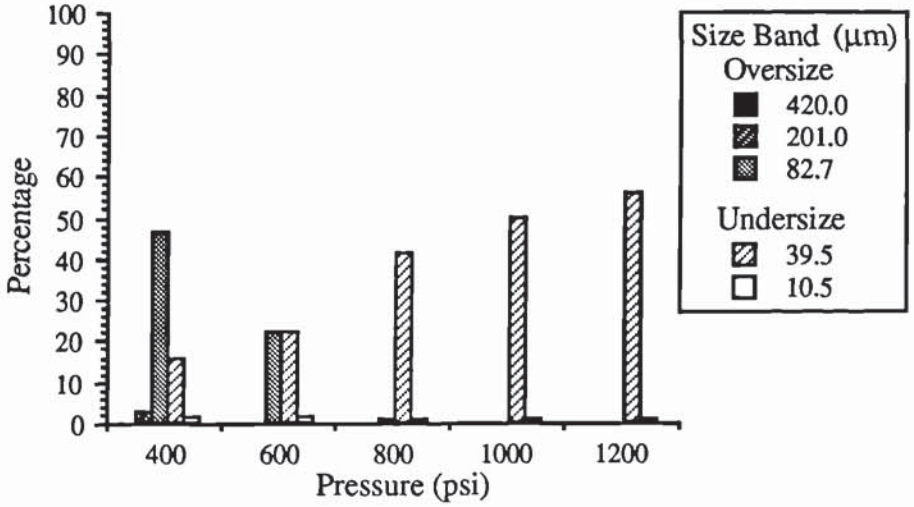

Figure 6.19: *Nozzle AAASSTC5-5*

a) *23% Calcium Carbonate*

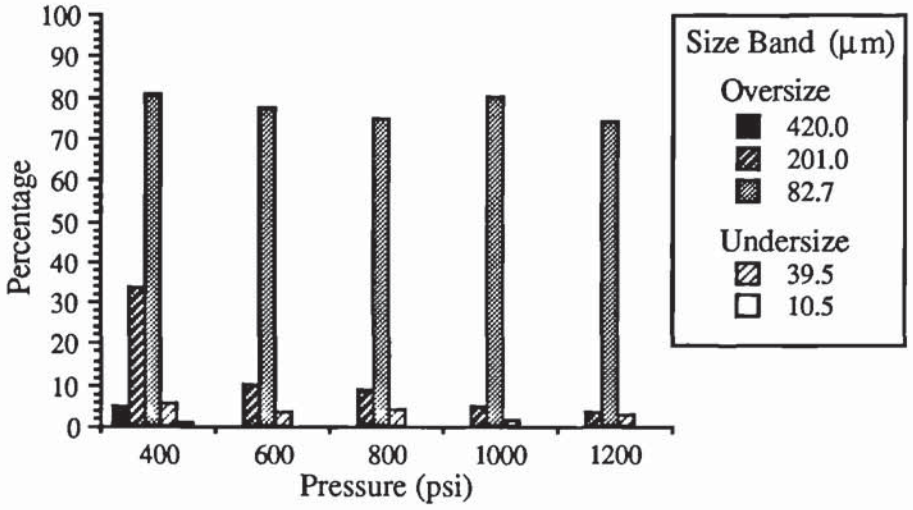

b) *35% Calcium Carbonate*

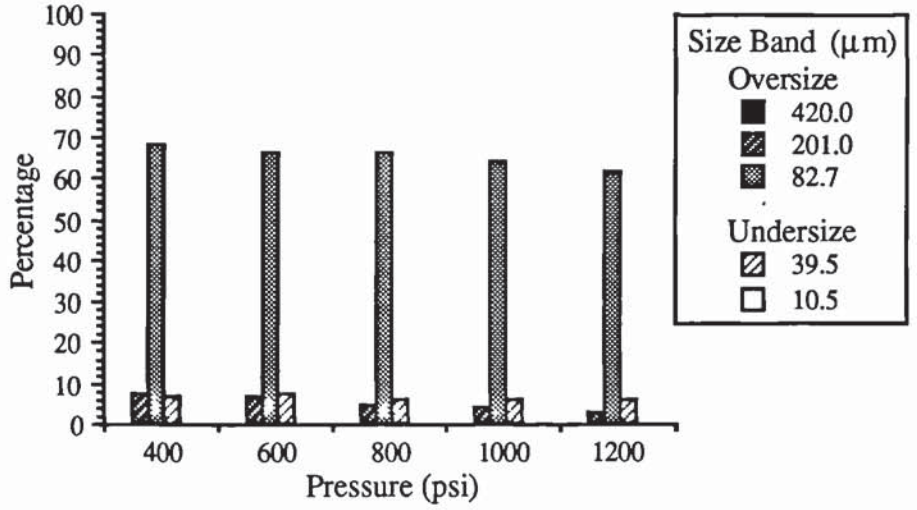

c) *45% Calcium Carbonate*

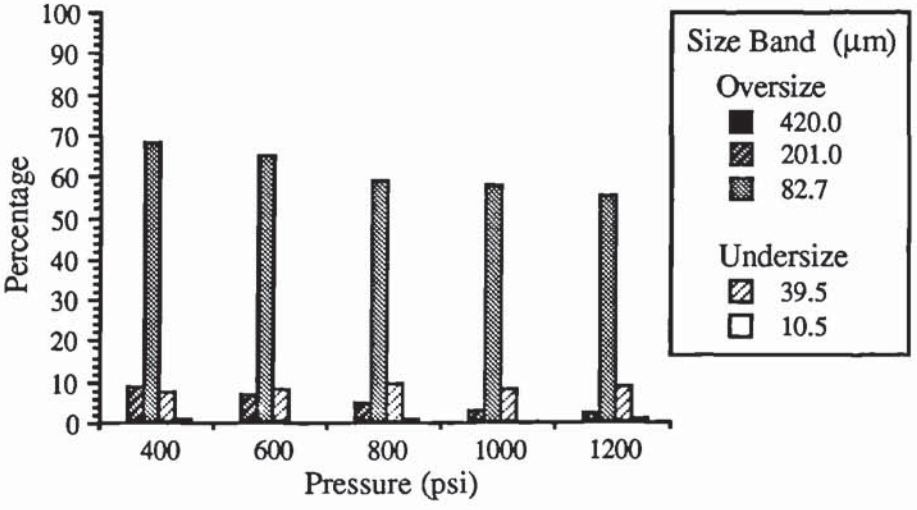

Figure 6.20: *Nozzle AAASSTC8-5*

a) *23% Calcium Carbonate*

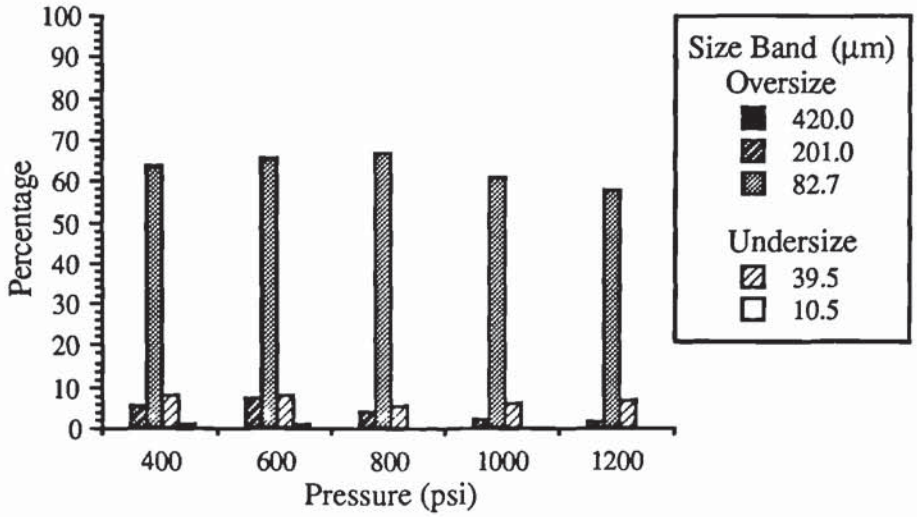

b) *35% Calcium Carbonate*

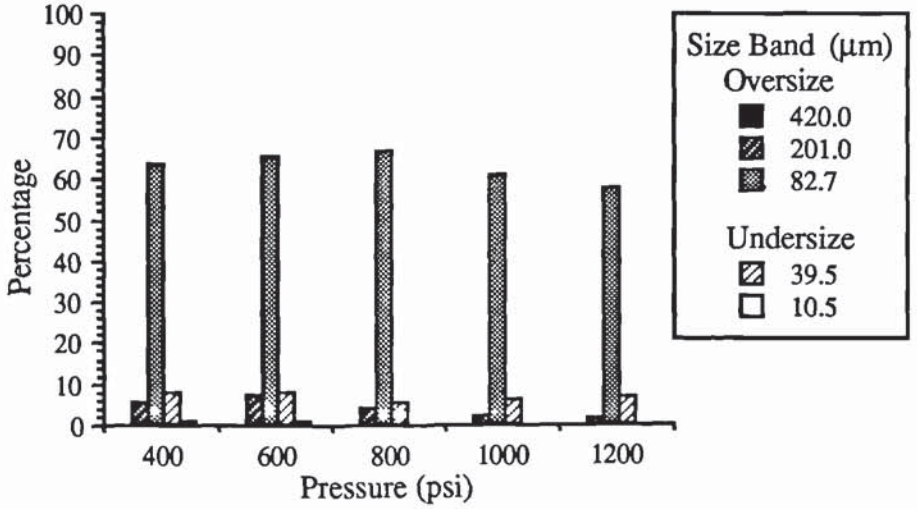

c) *45% Calcium Carbonate*

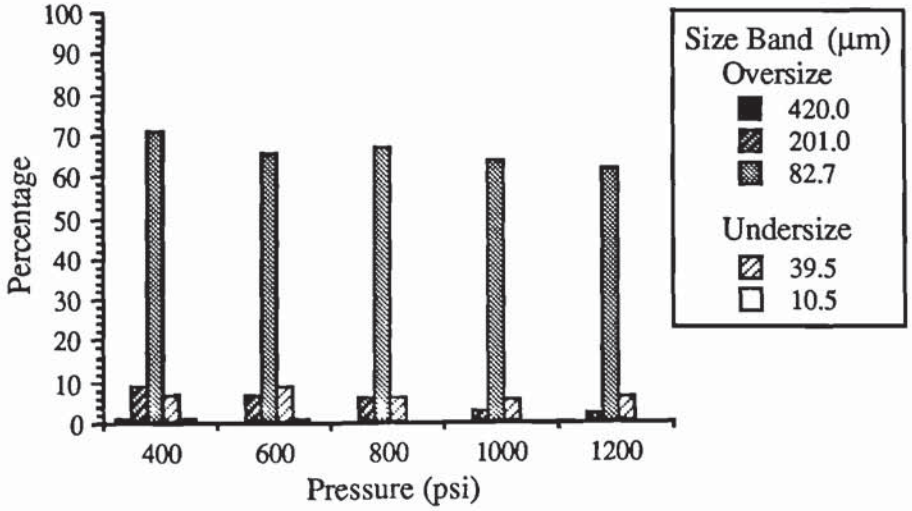

Figure 6.21: *Nozzle AAASSTC8-8*

a) *23% Calcium Carbonate*

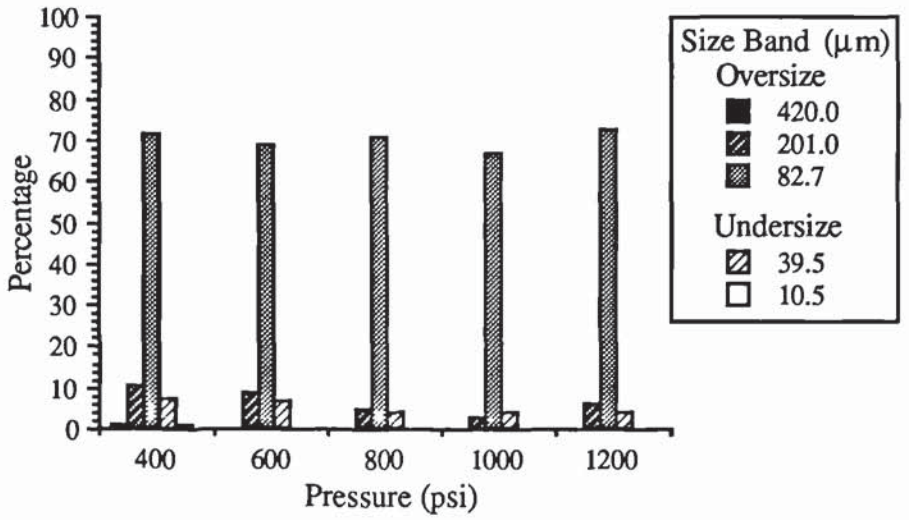

b) *35% Calcium Carbonate*

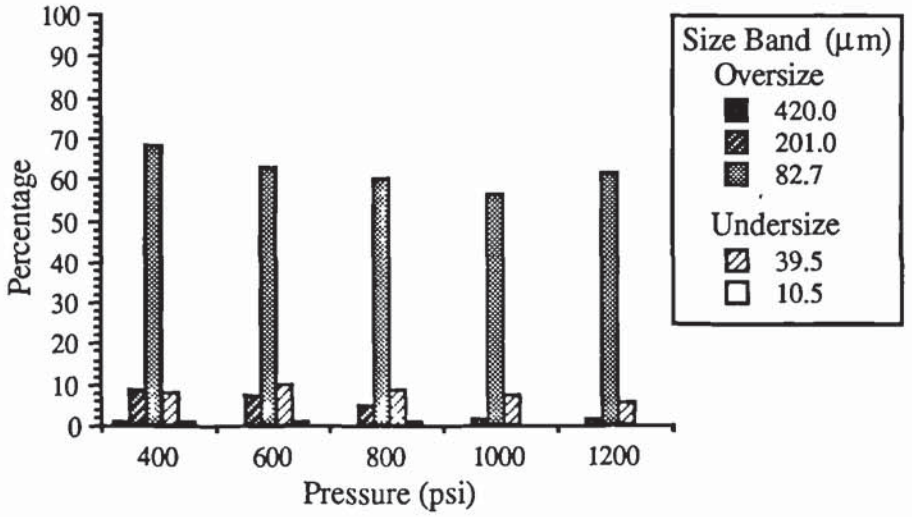

c) *45% Sodium Carbonate*

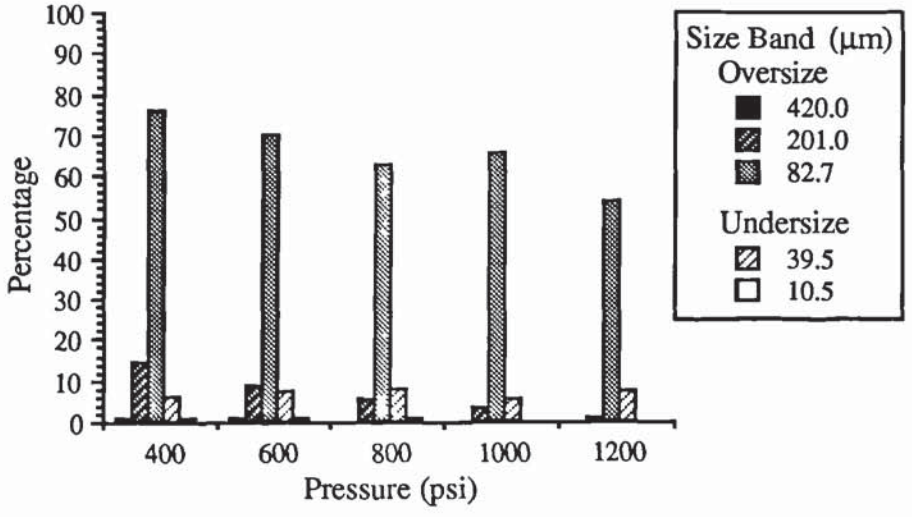

Figure 6.22: *Nozzle AAASSTC10-10*

a) *23% Calcium Carbonate*

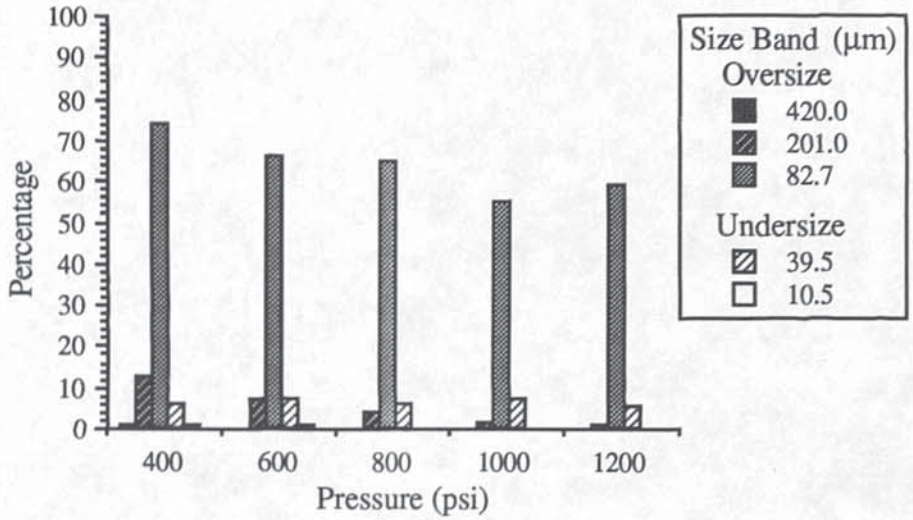

b) *35% Calcium Carbonate*

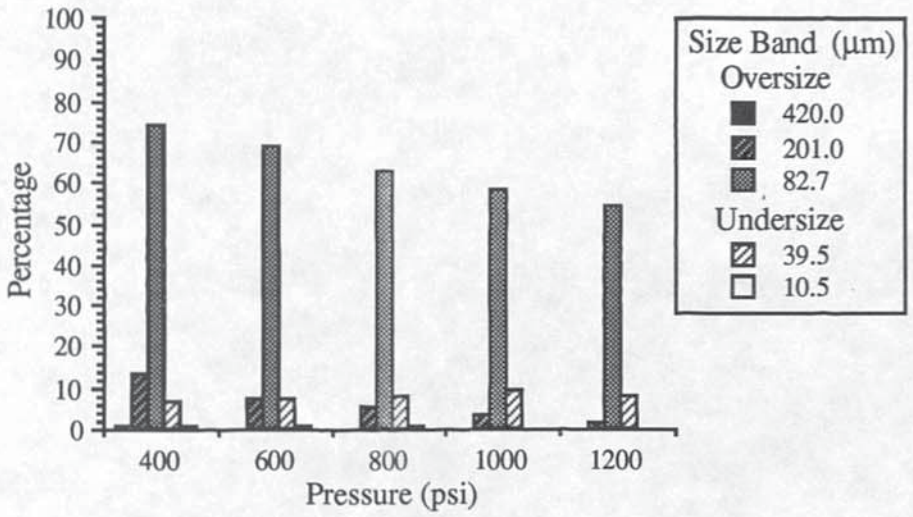

c) *45% Calcium Carbonate*

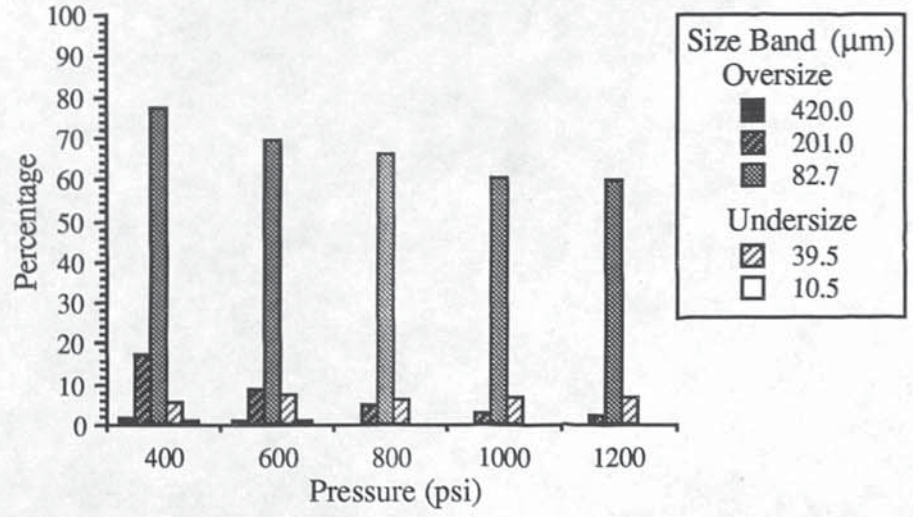

Figure 6.23: *Nozzle Delevan 2.0SJ*

a) *23% Calcium Carbonate*

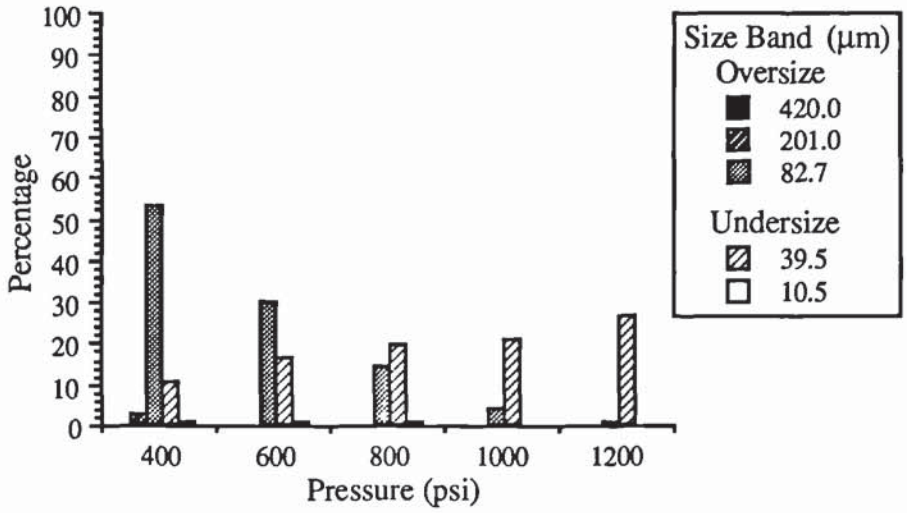

b) *35% Calcium Carbonate*

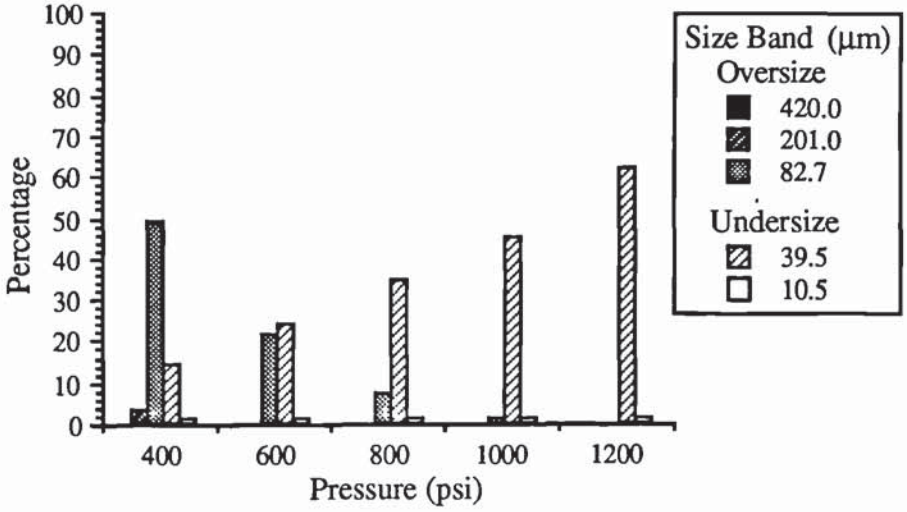

c) *45% Calcium Carbonate*

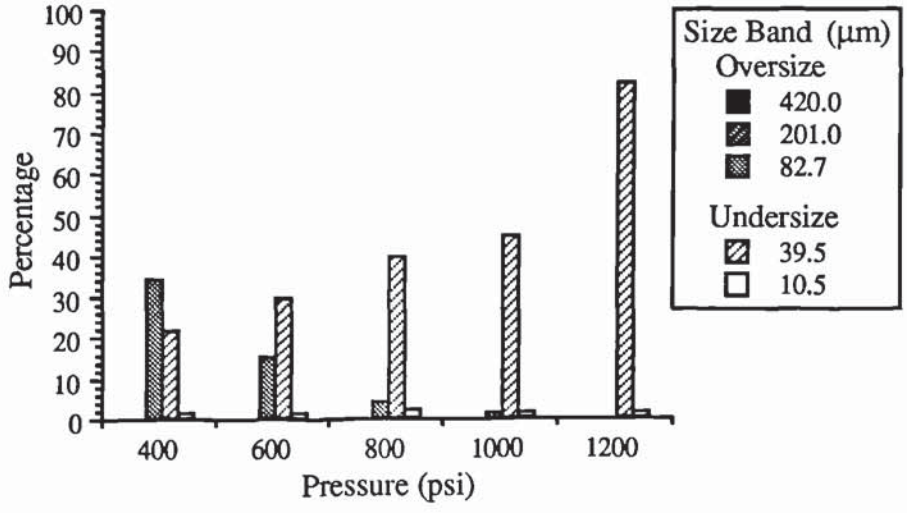

Figure 6.24: *Nozzle Delevan 2.2SJ*

a) *23% Calcium Carbonate*

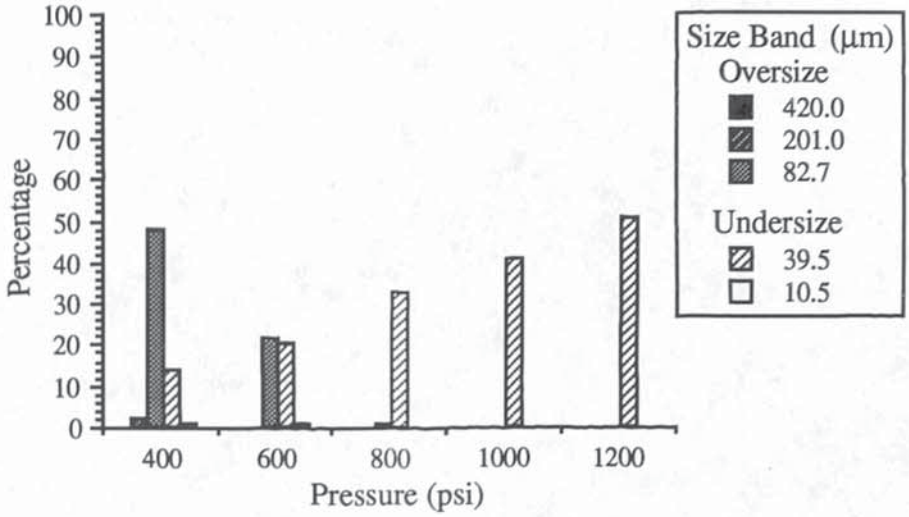

b) *35% Calcium Carbonate*

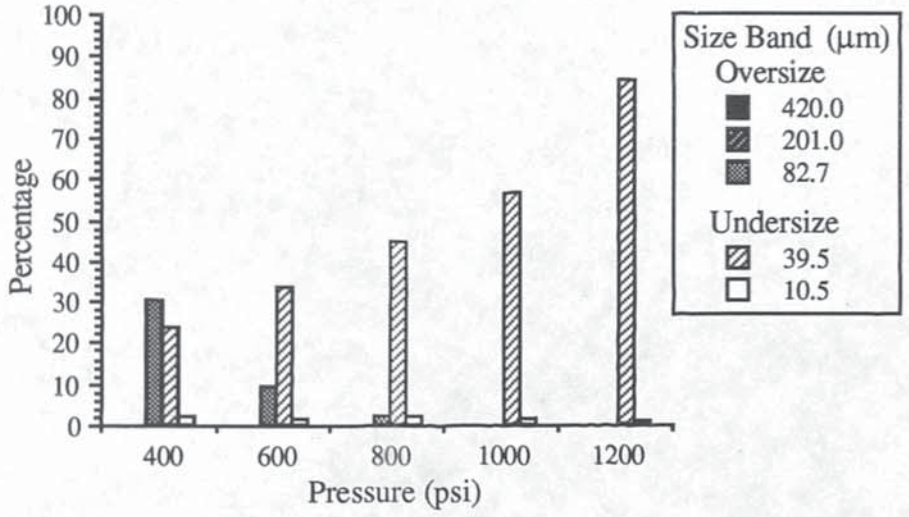

c) *45% Calcium Carbonate*

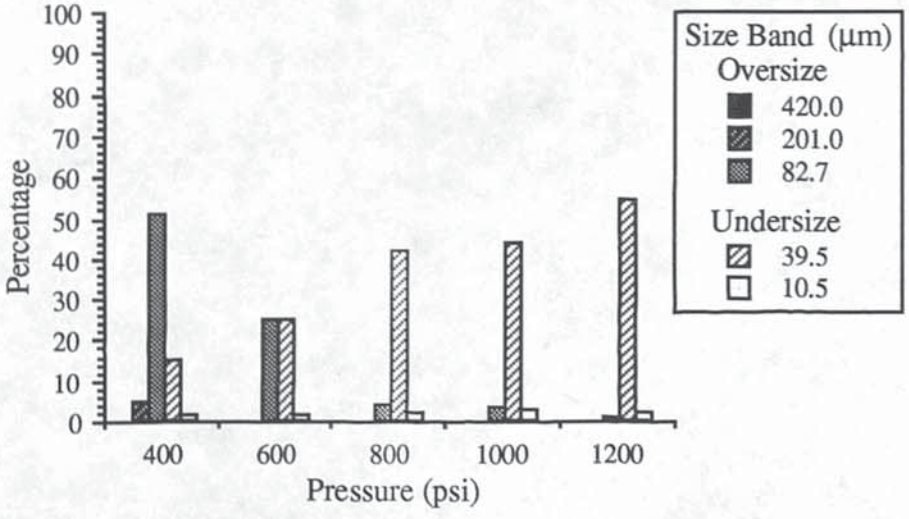

with an agitator and air agitation had to be avoided in order to reduce the possibility of aeration of the slurry mixture, the period of time that the slurry remained in the reservoir prior to each experiment was restricted to 15 minutes. This period allowed for pressurisation up to the maximum operating pressure. Additionally the measurement period was slightly reduced (ie, from 30 to 20 seconds) for this series of experiments to ensure that slurry viscosity did not vary significantly, ie the slurry sprayed was essentially of consistent properties.

The slurry viscosity was monitored by taking a sample of the spraying medium directly at the nozzle outlet and another sample at the reservoir drain prior to draining excess slurry from the reservoir. The two samples were then compared to ensure that there was no significant viscosity variation between the two sampling positions and an acceptable variation between both samples was set at $\pm$ 0.3 cP.

Table 6.4: *Physical Properties of Various Calcium Carbonate Slurries*

Concentration (% w/w)	23%	35%	45%
Temperature (°C)	20.0	20.0	20.0
Slurry Density (kg/m^3) [1]	1165.0	1265.0	1380.0
Apparent Viscosity (cP) [2]	2.250	2.700	3.375

1 Obtained from previously published data [171].
2 Measured using a Haake Viscometer fitted with a Sensor system and NVST measuring head.

The physical properties of the calcium carbonate slurries sprayed are given in Table 6.4 and the droplet sizing results from this series of experiments are given in Tables A1.25 to A1.42 and the relevant data plotted in Figures 6.19 to 6.24.

6.3.4 Detergent Slurries

The raw materials for the detergent slurries were supplied by Colgate-Palmolive. A range of slurries were made-up using a prescribed method. The concentrations, slurry formation and spraying conditions were predetermined from discussions with Colgate-

Palmolive and designed to represent common industrial practice. Unlike with the calcium carbonate slurries, the particulates within the detergent slurries did not settle out to any degree. The only problems forseen therefore were that the slurry might 'age', or that solidification could occur in either the pipework or the mixing vessel. Therefore it was only necessary to monitor the slurry viscosity in the mixing tank.

Storage of Raw Materials

Sodium Linear Tridecylbenzene Sulphonate (50%) - It was recommended that the sodium LTBS received in a drum was kept in a hot room for a period of several days in order to reduce its viscosity and make it easier to handle [39]. The temperature of the room was required to be about 49°C (120°F) and not to exceed 60°C (140°F) at which the base tends to form a gel.

Sodium LTBS is not a solution but a slurry and therefore, the solid tends to 'top separate' from the water after a certain period of storage. Gentle manual agitation with a long hand-paddle was thus required, to avoid aeration, but to obtain thorough mixing before use. To avoid evaporation of the water from the base material the lid of the drum was kept tightly closed.

Sodium Silicate (47.5%) - This is a clear solution and, as recommended, was stored in a hot room (38°C to 49°C) before mixing with the other ingredients [39]. The drum lid was kept tightly closed in order to avoid evaporation of water at high temperature. Since sodium silicate is a true solution, it did not require agitation before use.

Sodium Tripolyphosphate (99.5%) - As recommended the drum of sodium TPP was kept closed as it tends to hydrate and form cake and lumps when exposed to air [39]. Sodium TPP is a very fine, low density, powder and required sieving with a 20 to 40 mesh screen in order to segregate the lumps. During sieving, it was necessary to brush the powder to pass through the screen as it is very cohesive to the screen wire. Sodium TPP was, as recommended, stored at regular room temperature [39].

Sodium Sulphate - The drum lid was kept tightly closed as sodium sulphate also hydrates, albeit at a lower rate than sodium TPP. The sodium sulphate was easier to

screen than sodium TPP as it is crystalline and was, as recommended, stored at room temperature [39].

Table 6.5: *Composition of the Detergent Slurries*

Component	Percentage	Weight of Batch	
		200 lb	300 lb
Water	17.0	34.0	51.0
Steam*	4.4	8.8	13.2
Na+ LTBS	25.4	50.8	76.2
Na+ Silicate	11.4	22.8	34.2
Na+ TPP	20.3	40.6	60.9
Na+ Sulphate	21.5	43.0	64.5

* Approximate weight

Order of Addition and Preparation of the Slurry

The amount of raw materials and water necessary to make up a batch of the slurry was calculated from Table 6.5. The addition of water and steam to prepare the slurry mixture was an elaborate task in order to achieve:

i) the desired solids content of the slurry, and,

ii) the desired slurry temperature [39].

The mixing crutcher was located upon 400 lb (200 kg) weighing scales in order that the weight change on the addition and mixing of the raw materials could be determined. The mixer was filled with 17% by weight of water at a temperature between 38°C (100°F) and 60°C (140°F) , at which point the sodium LTBS would begin to gelatinise. The 24.4% of hot sodium LTBS was slowly added to the crutcher and gentle agitation was applied to avoid aeration, vortexing and splashing (The most commonly used agitation equipment is a paddle type agitator and Figure 6.25 illustrates the simple straight arm paddle with two flat vanes, as used by Colgate-

Palmolive, that was employed for mixing the slurry.). Once the sodium LTBS had been added to the mixture 11.4% of hot sodium silicate was slowly added into the crutcher using the gentle agitation as previously described. The temperature of the mixture was then increased to 71°C (160°F) by injecting steam into the mixture. When the mixture temperature reached 71°C, the weight of steam used was measured and the total percentage of water added to the mixture calculated from,

$$\text{Weight of Water Added} = 17\% + \frac{\text{Weight of Steam Injected}}{100} \qquad - 6.1$$

If the total water content was less than 21.4%, the difference was added to the mixture. The temperature of the additional water was also 71 °C.

Figure 6.25: *Slurry Mixing Crutcher*

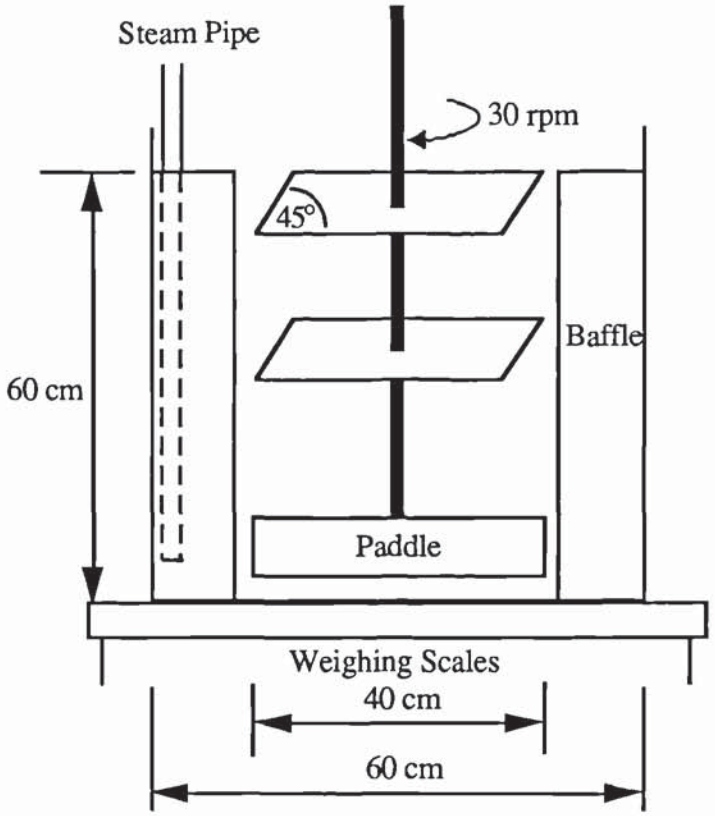

Figure 6.26: *Nozzle AAASSTC5-5*

a) *Detergent Slurry at 40℃*

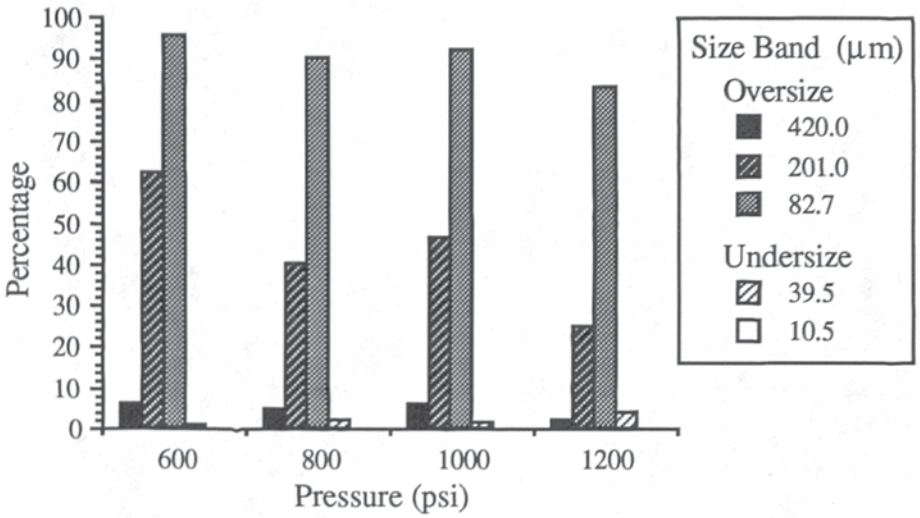

b) *Detergent Slurry at 60℃*

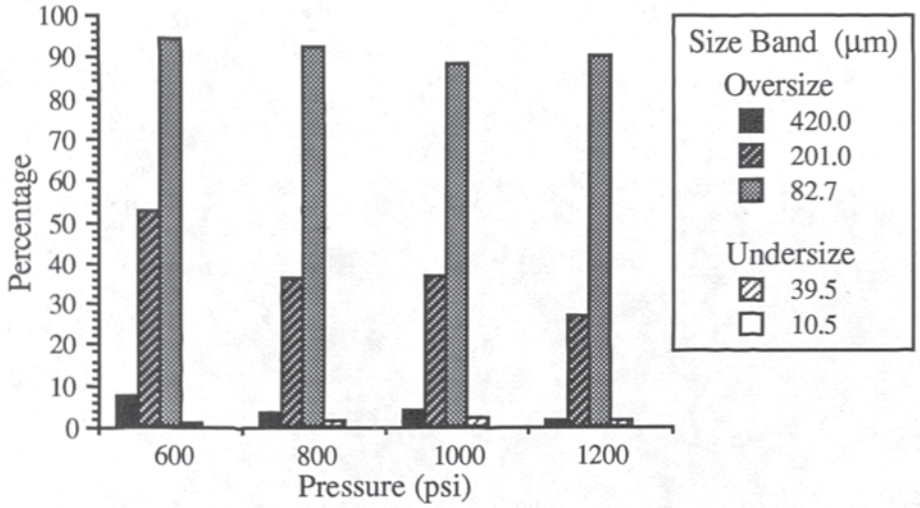

c) *Detergent Slurry at 80℃*

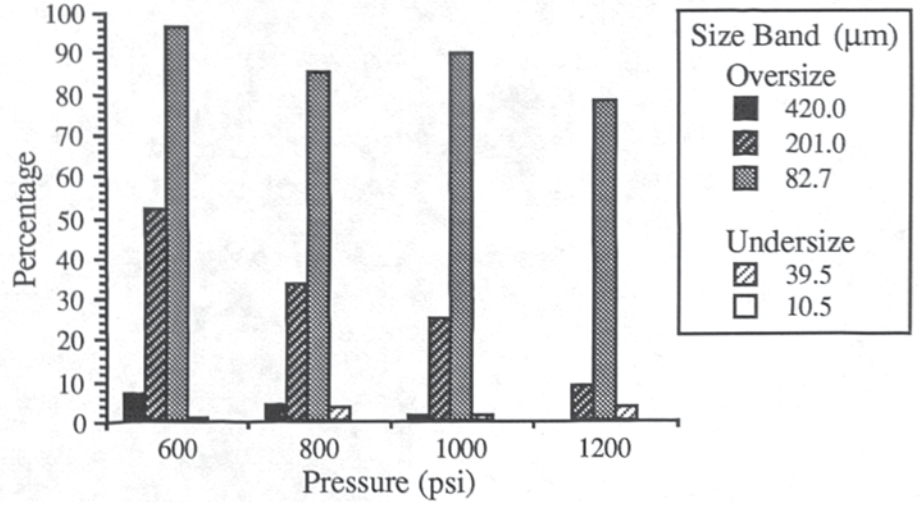

Figure 6.27: *Nozzle AAASSTC8-5*

a) *Detergent Slurry at 40℃*

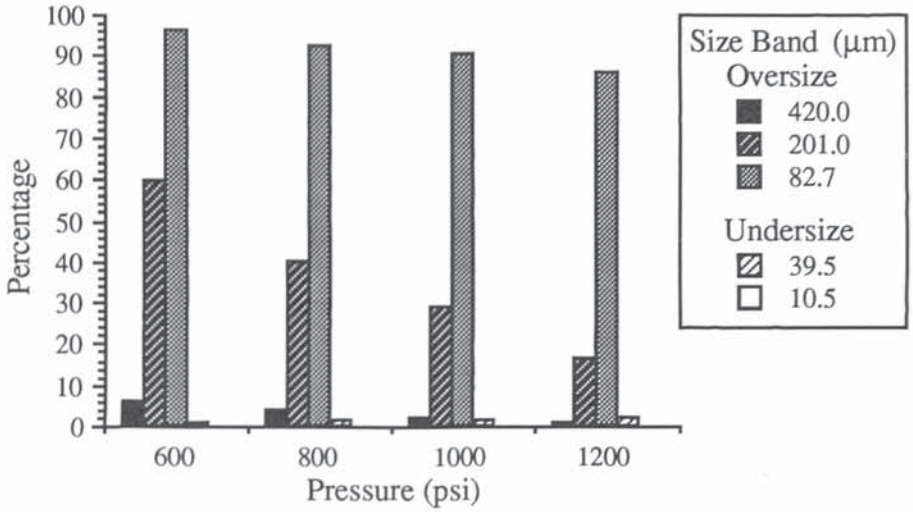

b) *Detergent Slurry at 60℃*

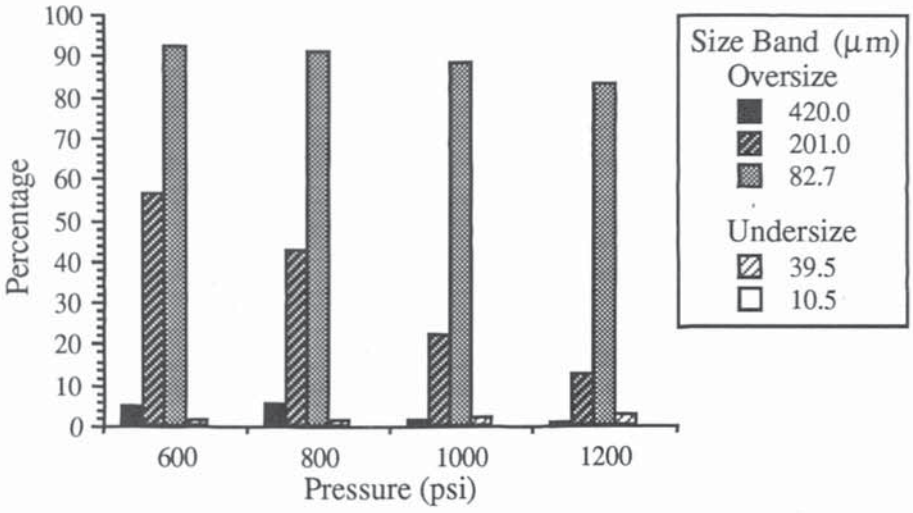

c) *Detergent Slurry at 80℃*

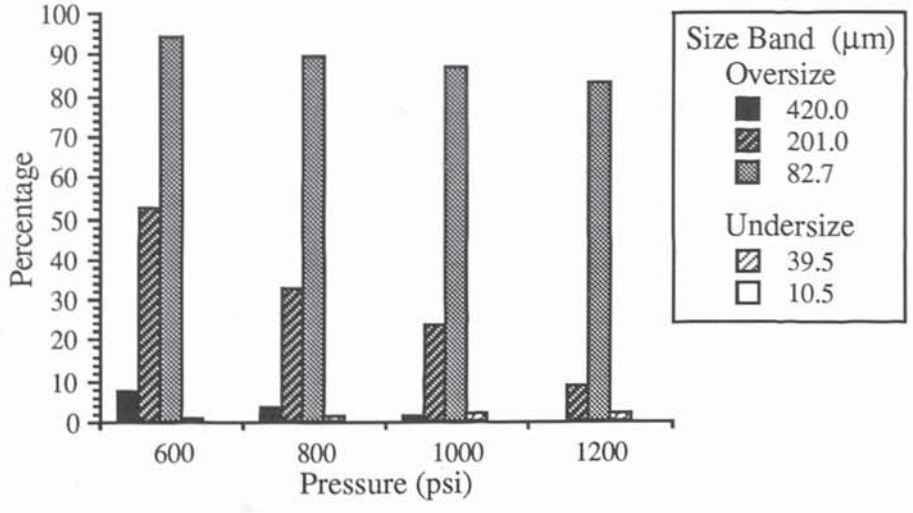

Figure 6.28: *Nozzle AAASSTC8-8*

a) *Detergent Slurry at 40°C*

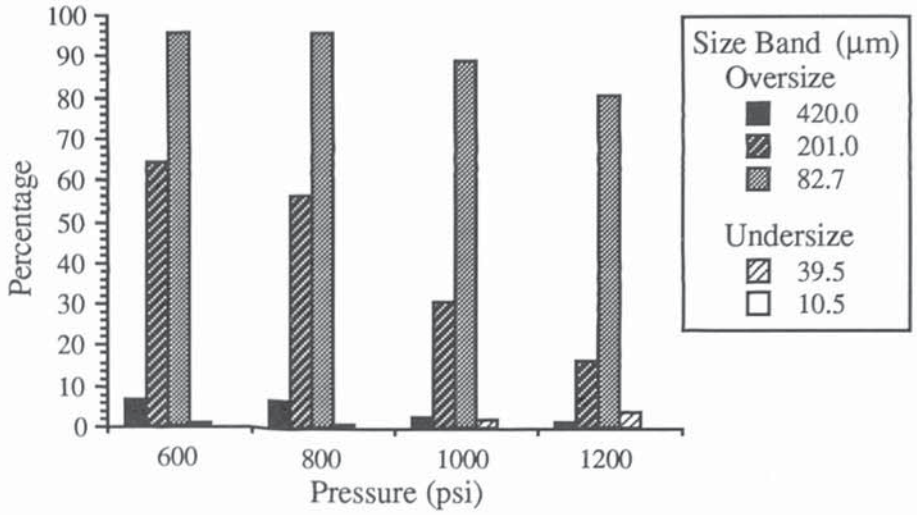

b) *Detergent Slurry at 60°C*

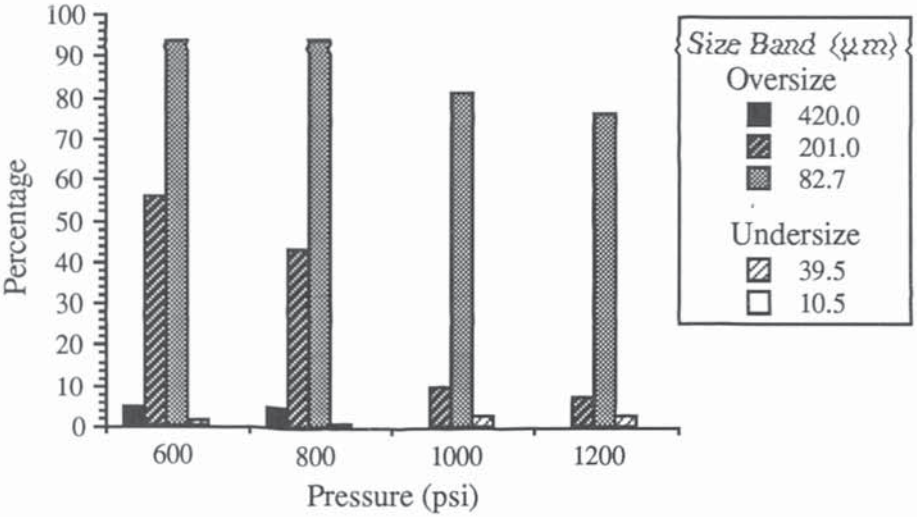

c) *Detergent Slurry at 80°C*

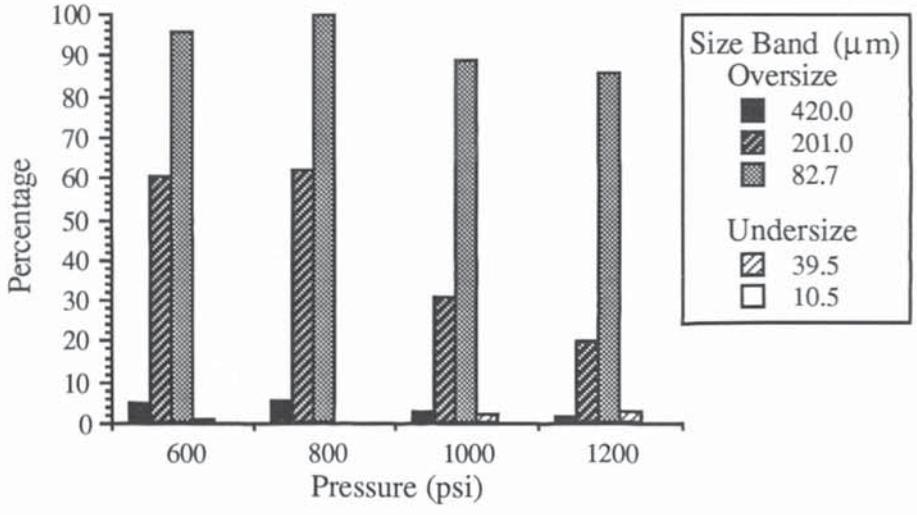

Figure 6.29: *Nozzle AAASSTC10-10*

a) *Detergent Slurry at 40℃*

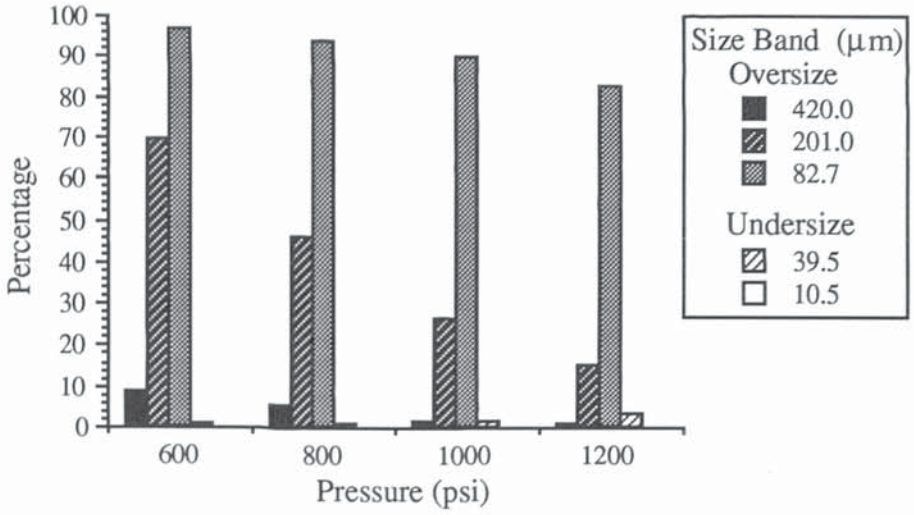

b) *Detergent Slurry at 60℃*

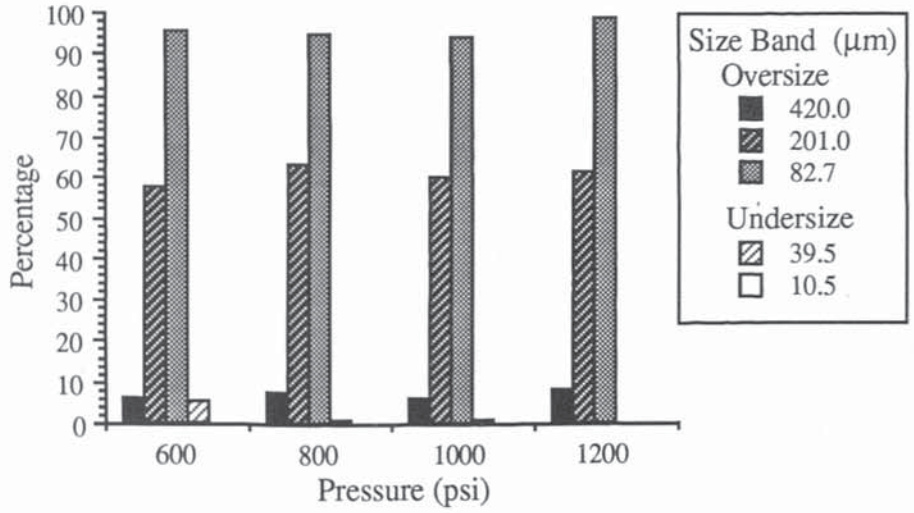

c) *Detergent Slurry at 80℃*

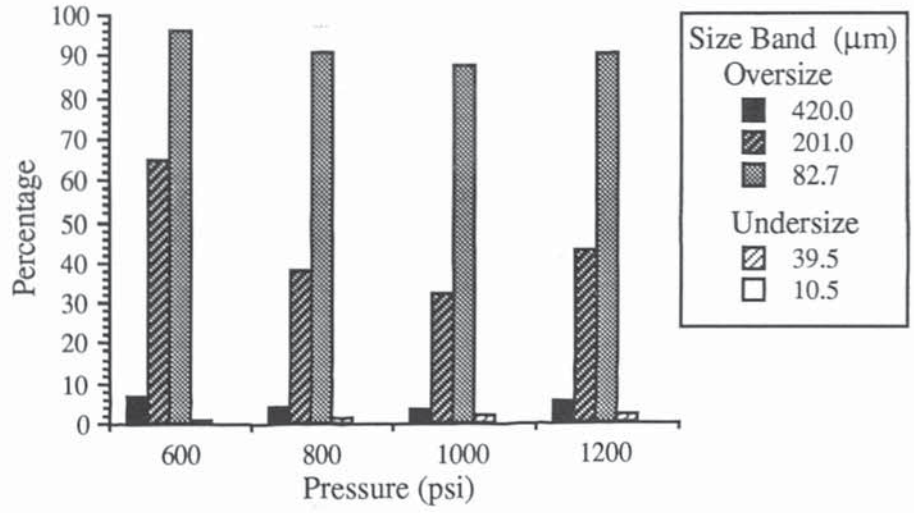

Experimental Procedure

It was not possible to measure the volumetric flowrate of the detergent slurry by the conventional method as the slurry tended to adhere to the walls of the tower section and no other convenient method could be employed. Therefore the volumetric flowrate was determined using the following empirical correlation, assuming that the coefficient of discharge (C_D) was 0.2 [1]:

$$Q = C_D r_o \sqrt{\frac{2P}{s_g \rho_w}} \qquad - 6.2$$

where s_g is the specific gravity of the slurry,

ρ_w is the density of water.

Table 6.6: *Physical Properties of Various Detergent Slurries*

Spraying Temperature (°C)	40.0	60.0	80.0
Relative Viscosity (cP) [1]	1186.0	947.0	210.5
Specific Gravity [2]	1.386	1.292	1.318
Solids Content (% w/w)	78.6	78.6	78.6

[1] Measured using a Haake Viscometer fitted with a Sensor system and NVST measuring head.
[2] Measured using a hydrometer.

The physical properties of the detergent slurries used in the experimental work are given in Table 6.6 and the droplet sizing results from this series of experiments are given in Tables A1.43 to A1.54, with the relevant data plotted in Figures 6.26 to 6.29.

Chapter 7: Discussion

It was not the objective of the experimental work merely to report upon the common trends associated with the process of liquid (fluid) atomisation (ie, a decrease in droplet size with an increase in pressure, an increase in droplet size with an increase in viscosity or orifice size, etc.). These have already been extensively recorded in the literature (for example, [1][2][4][71][72][84][96][111-113]) and, in particular, for the case of the nozzles currently under investigation, in the manufacturers' catalogues [187][188] (for example, the effect of nozzle dimensions upon spray cone angle.).

It is possible to confirm these trends from the experimental results summarised in Appendix 1. However the results presented graphically in Chapter 6 and those summarised in the following chapter are concerned with spray distribution, in particular distributions attaining to the idealised goal of a mono-dispersed or uniformly-sized spray distribution. The main purpose of the results obtained in this study was to enable generalised recommendations to be made towards achieving a uniformly-sized spray distribution for water, sodium sulphate solutions (both low viscosity fluids), calcium carbonate slurries (medium viscosity fluids) and detergent slurries (high viscosity fluids). The work also provides a data-base for the expansion of the computer simulation program into industrial applications.

An additional set of experimental results, presented in Appendix 2 and summarised in Chapter 5, has been generated merely for use in conjunction with the computer simulation program. This data was obtained using over-sized perspex nozzles which, although exhibiting the same performance trends as their industrial counter-parts, were not studied in anyway apart from providing the initial data-base for the computer simulation.

Consequently, as this project involved two distinctive areas of study, this chapter is divided into two sections which discuss the aspects of experimental work and mathematical modelling and computer simulation respectively.

7.1 Experimental Work

As previously mentioned the experimental work consisted of an investigation into the spray characteristics and nozzle performance of six centrifugal pressures nozzles using four different fluids. The behaviour of the nozzles with each fluid is discussed below prior to drawing conclusions.

7.1.1 Water

The results from these experiments are presented in Figures 6.7 to 6.12 and show that the two types of nozzle used in this investigation produce radically different spray distributions. Although they are both essentially centrifugal pressure nozzles, the Delevan nozzles have a noticeably narrower spray cone angle, smaller orifice size and different internal geometry to those manufactured by Spraying Systems Co. Ltd. (See Plates 5 and 6). This appears to have caused a substantially different distribution of the spray to be produced by the Delevan nozzles. There can obviously be no direct comparison between the two nozzles due to the large difference in orifice size but it would be expected that similar trends in the spray distributions would be produced by the two types of nozzle.

The results from this study are summarised in Figure 7.1, which shows the conditions when the best (most uniform or closest approach to mono-dispersed) and worst (most dispersed) spray distributions existed. High pressure (ie, 1200 psi) operation of the Delevan nozzles produced the most uniform spray distribution and low pressure (ie, 400 psi) operation produced the most dispersed spray. However, it would appear from Figures 6.11 and 6.12 that the spray distributions for 200 and 400 psi fall into similar size ranges. In these cases the definition of most dispersed spray has been attributed to conditions where the maximum frequency peak, in this case those droplets less than 82.7μm, is the lowest.

The results from Figure 7.1 are confirmed by Table 7.1, which shows the maximum and minimum values of the dispersion coefficient in the relevant Rosin-Rammler distribution (N) and the pressures where they occur. As a general rule, the larger the value of the dispersion coefficient the more uniform the spray distribution

and Table 7.1 shows that there is close agreement between the predictions made from graphical evidence and those obtained directly from experiment measurement.

Figure 7.1: *Comparison of Spraying Conditions for Water*

a) *Most Uniform Spray Distribution*

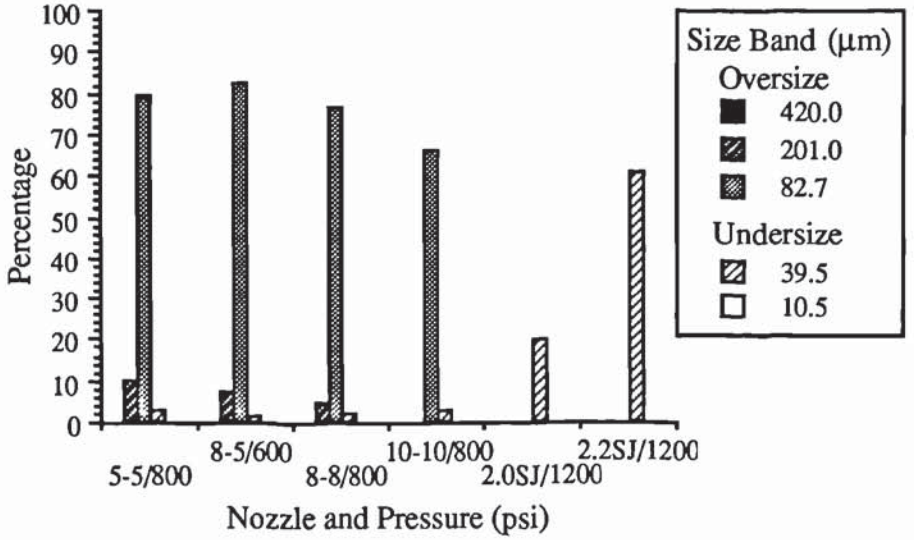

b) *Most Dispersed Spray Distribution*

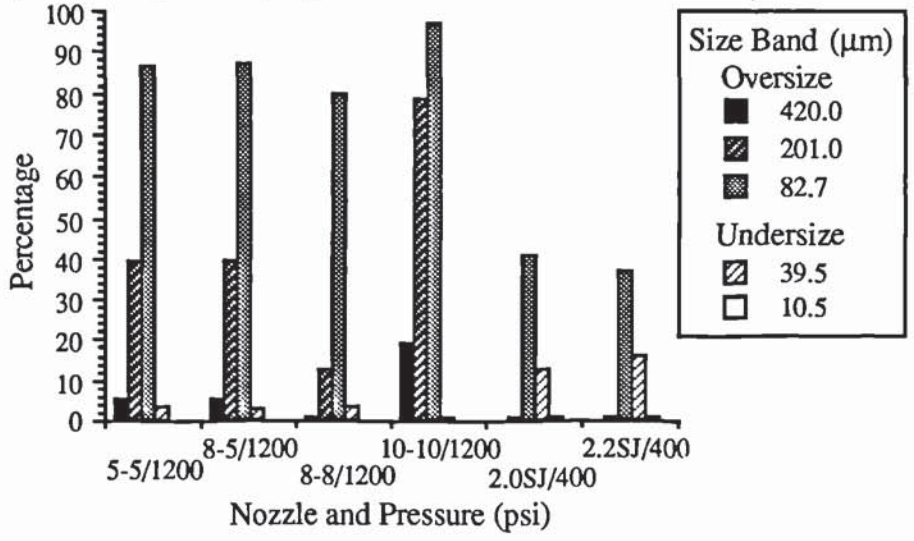

The trend with the Spraying Systems nozzles is for the most uniform spray distribution to occur in the middle of the pressure range (ie, 800 psi). The overall trend across the pressure range shows a slight initial increase in spray uniformity until the maximum point is reached then the spray rapidly becomes increasingly dispersed across the remainder of the pressure range.

Table 7.1: *Maximum and Minimum Values of Dispersion Coefficients for Water*

Nozzle	Dispersion Coefficient (N)		Distribution Type	
	Maximum	Minimum	Uniform	Disperse
5-5	800 psi	1200 psi	800 psi	1200 psi
8-5	600 psi	1200 psi	600 psi	1200 psi
8-8	800 psi	1200 psi	800 psi	1200 psi
10-10	800 psi	1200 psi	800 psi	1200 psi
2.0SJ	1200 psi	400 psi	1200 psi	400 psi
2.2SJ	1200 psi	400 psi	1200 psi	400 psi

This is virtually opposite to the trends described earlier for the Delevan nozzles which seems to indicate that, although both types of nozzle are essentially of similar design, different factors influence the spray distribution produced in each case. It is possible that differing nozzle geometry induces slightly different atomisation mechanisms which affects spray dispersion, although the underlying trend for both nozzles is for spray distribution uniformity to increase with an increase in orifice size under the conditions being investigated.

7.1.2 Sodium Sulphate Solutions

The results presented in Figures 6.13 to 6.18 show similar trends to those described above. These results are summarised in Figures 7.2 to 7.4 and show that the increase in solution concentration has little effect upon the spray distribution.

However, unlike with water, similar trends exist for both types of nozzle. Although the Spraying Systems nozzles still produced the most uniform spray distribution in the middle of the pressure range, the most dispersed spray was produced at low pressures. This would seem to indicate that the atomisation

mechanisms for both types of nozzle are similar and are not the critical factor influencing spray distribution uniformity.

Figure 7.2: *Comparison of Spraying Conditions for 5% Sodium Sulphate Solution*

a) *Most Uniform Spray Distribution*

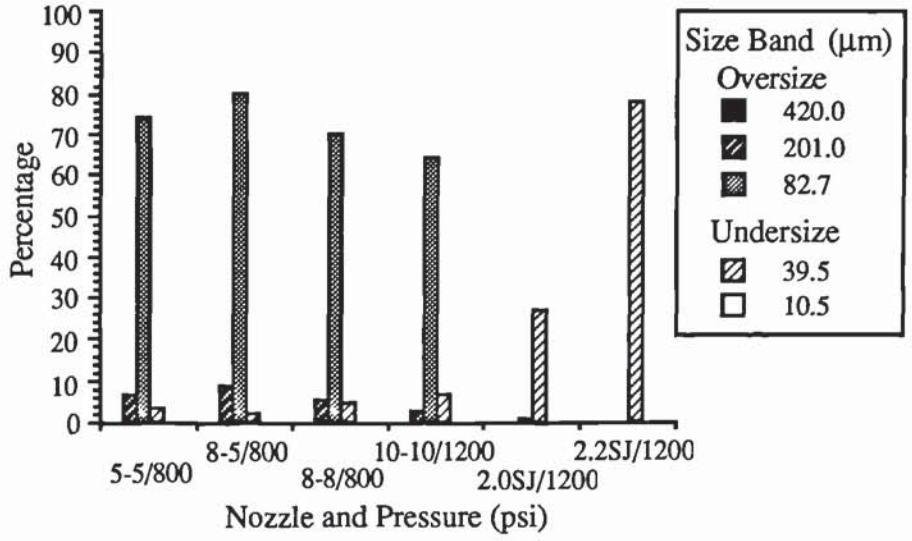

b) *Most Dispersed Spray Distribution*

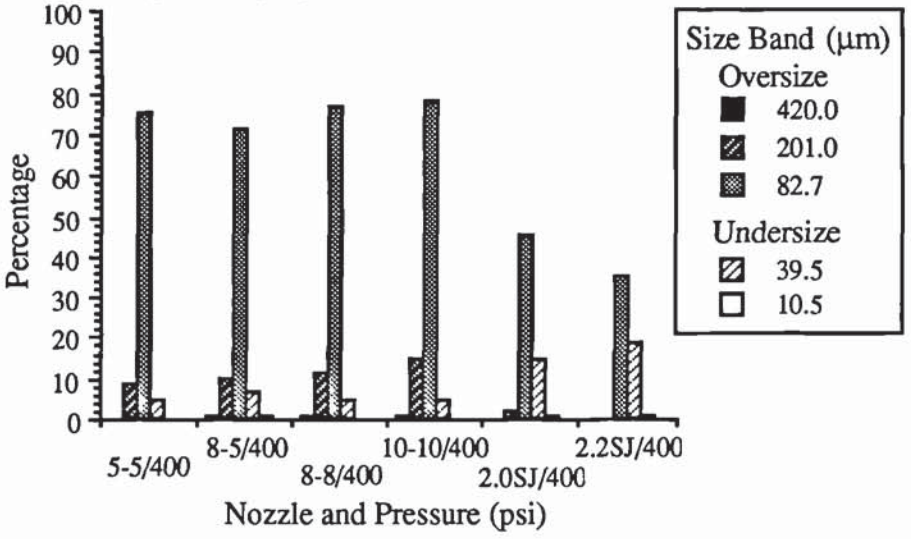

One possible explanation for the more dispersed spray distribution could be droplet instability, where further break-up of droplets occurred producing more stable smaller droplets. This could account for the differing conditions under which spray distribution uniformity occurred since droplet stability is determined by Reynolds number [206] and therefore spraying pressure. Hence the critical diameter for droplet

stability would vary depending upon the prevailing conditions and a slight change in viscosity could affect the internal droplet turbulence sufficiently to produce a significantly different spray distribution.

Figure 7.3: *Comparison of Spraying Conditions for 10% Sodium Sulphate Solution*

a) *Most Uniform Spray Distribution*

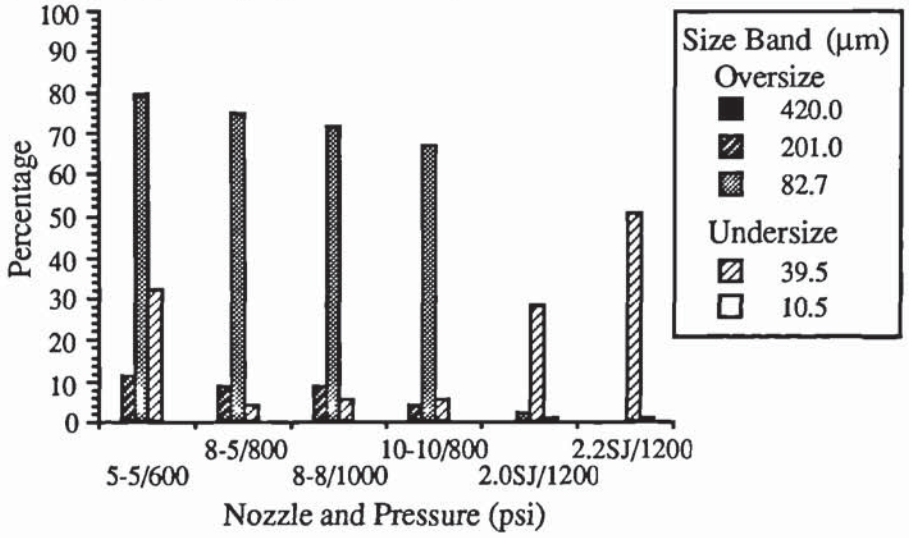

b) *Most Dispersed Spray Distribution*

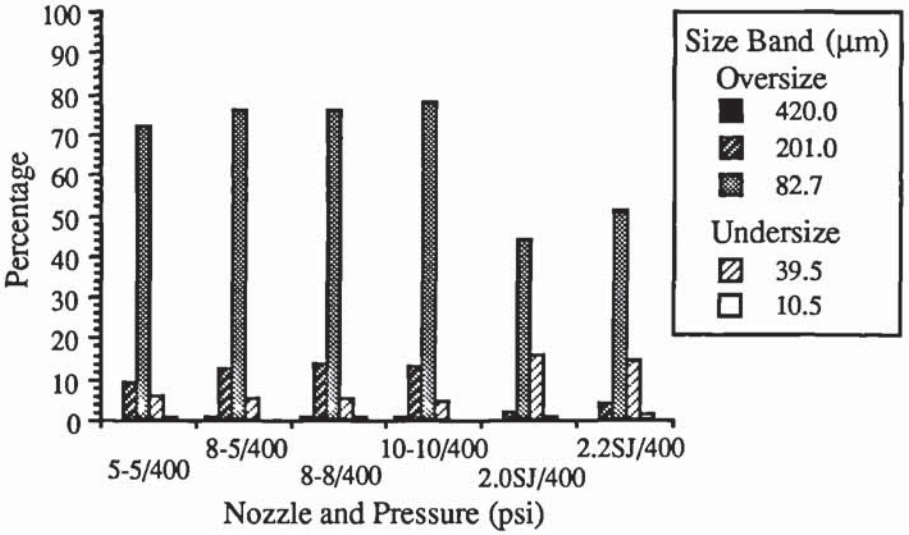

In order to determine the conditions which produced the most uniform and dispersed spray distributions for sodium sulphate the results of Figures 7.2 and 7.4, are summarised in Figure 7.5. Once again no definite trends are evident as the most

uniform spray distribution for the Delevan nozzles occurred under entirely different conditions to those for the Spraying Systems nozzles.

Figure 7.4: *Comparison of Spraying Conditions for 15% Sodium Sulphate Solution*

a) *Most Uniform Spray Distribution*

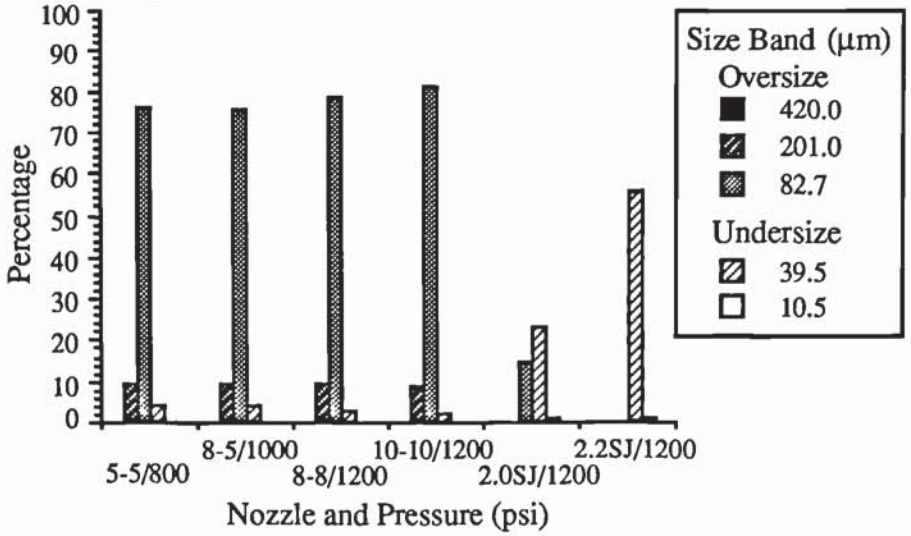

b) *Most Dispersed Spray Distribution*

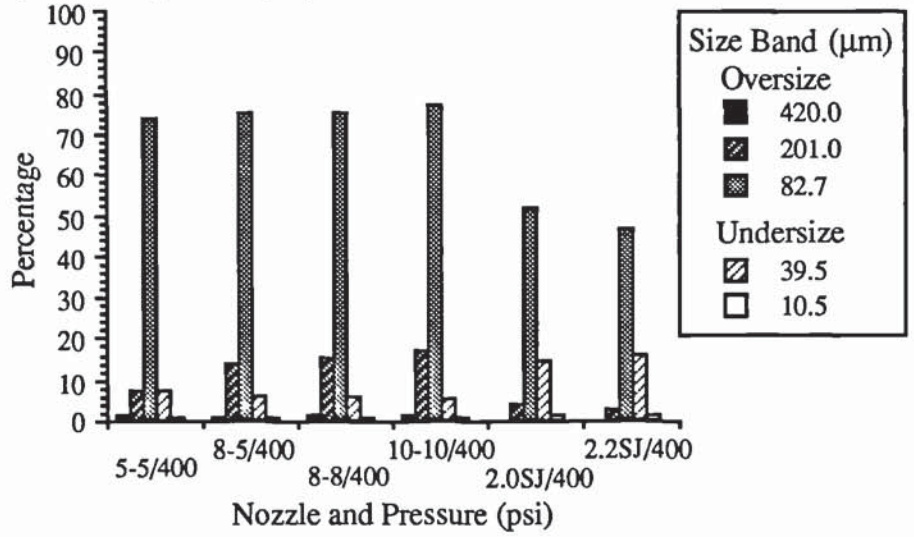

However, the most dispersed spray distribution for both types of nozzles, occurred at high concentrations, small orifice size and low pressure.

Figure 7.5: *Comparison of Spraying Conditions for Sodium Sulphate Solutions*

a) *Most Uniform Spray Distribution*

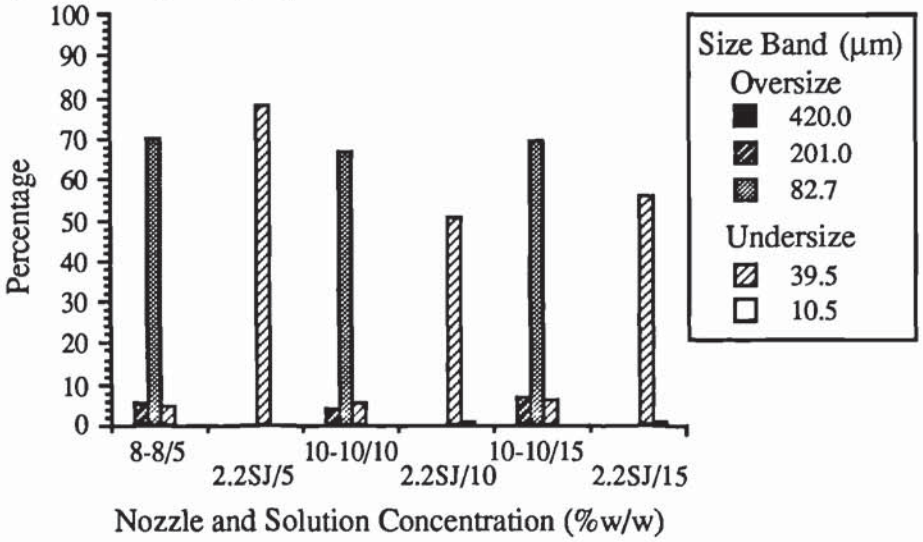

b) *Most Dispersed Spray Distribution*

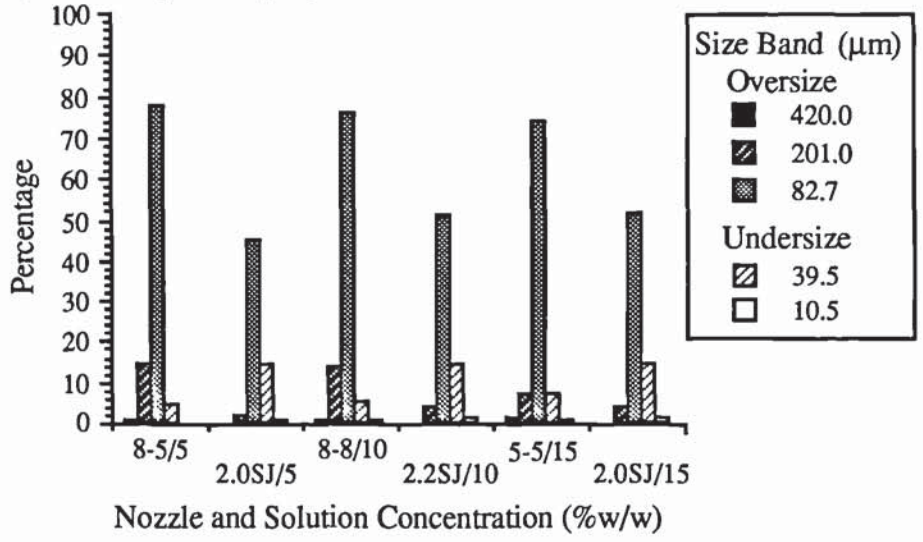

7.1.3 Calcium Carbonate Slurries

The graphs presented in Figures 6.19 to 6.23 show no significant differences in the performance of both types of nozzle whilst spraying calcium carbonate slurries. Only when these results are summarised as shown in Figures 7.6 to 7.8 do any trends appear. The most significant is that both types of nozzle exhibit similar characteristics whilst operating under similar conditions, ie dispersed spray distribution at low

pressure and uniform distribution at high pressure. There is a slight anomaly in the results for the Delevan nozzles as, at high slurry concentrations (See Figure 7.8), the 2.0SJ nozzle exhibits greater spray distribution uniformity than the 2.2SJ nozzle. There is no easily attributable reason for this.

Figure 7.6: *Comparison of Spraying Conditions for 23% Calcium Carbonate Slurry*

a) *Most Uniform Spray Distribution*

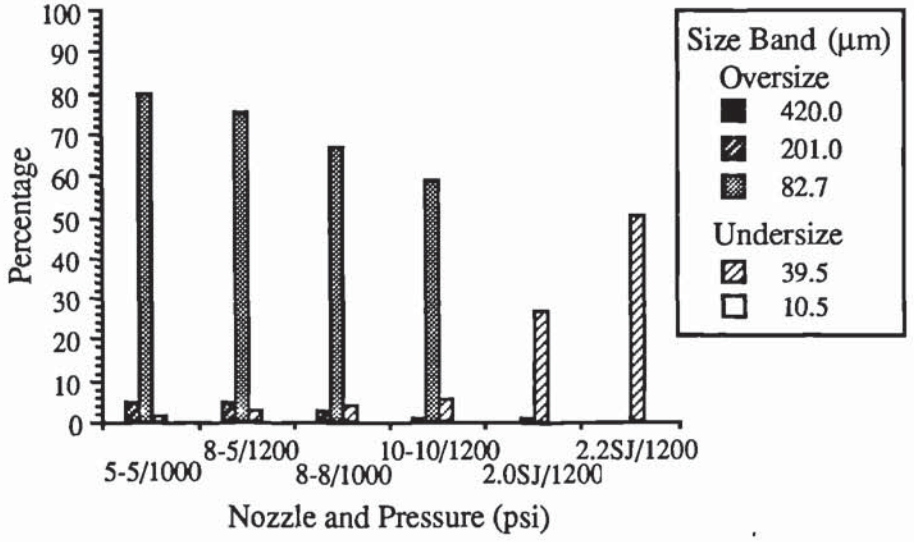

b) *Most Dispersed Spray Distribution*

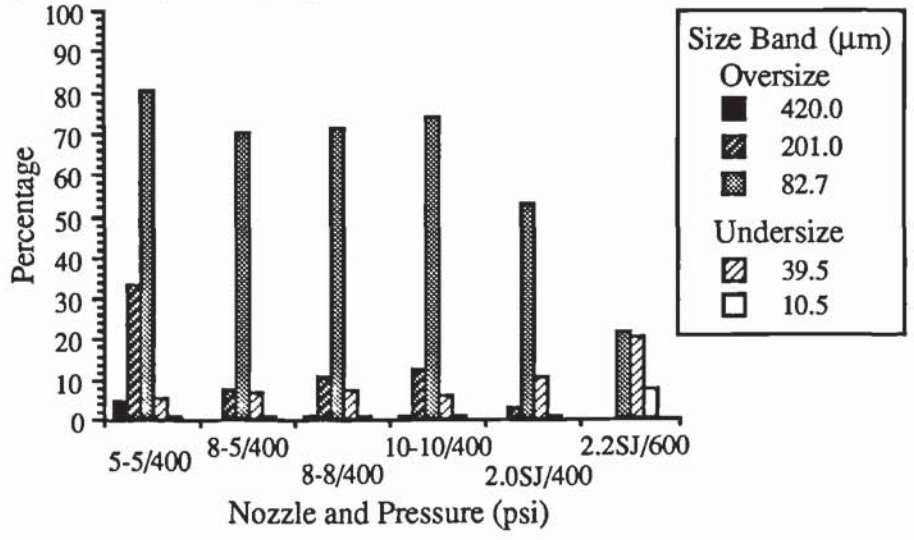

Figure 7.7: *Comparison of Spraying Conditions for 35% Calcium Carbonate Slurry*

a) *Most Uniform Spray Distribution*

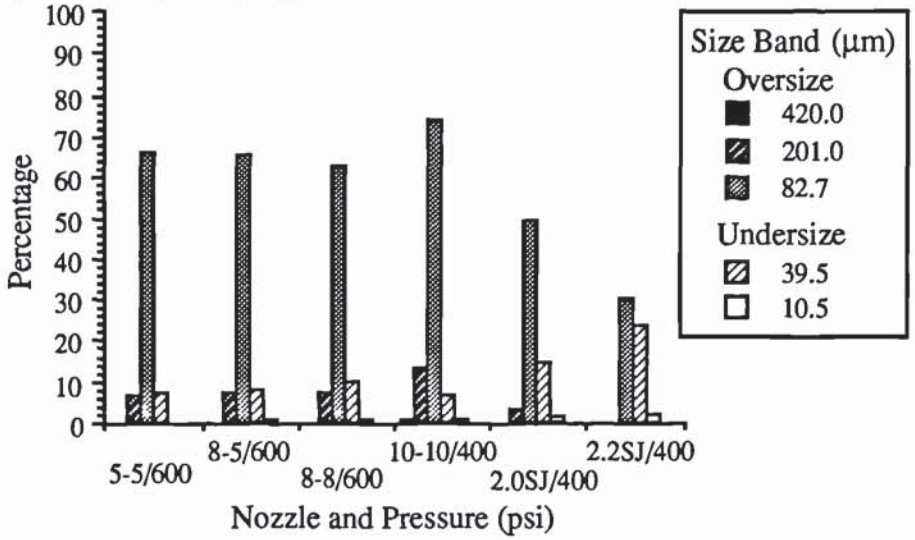

b) *Most Dispersed Spray Distribution*

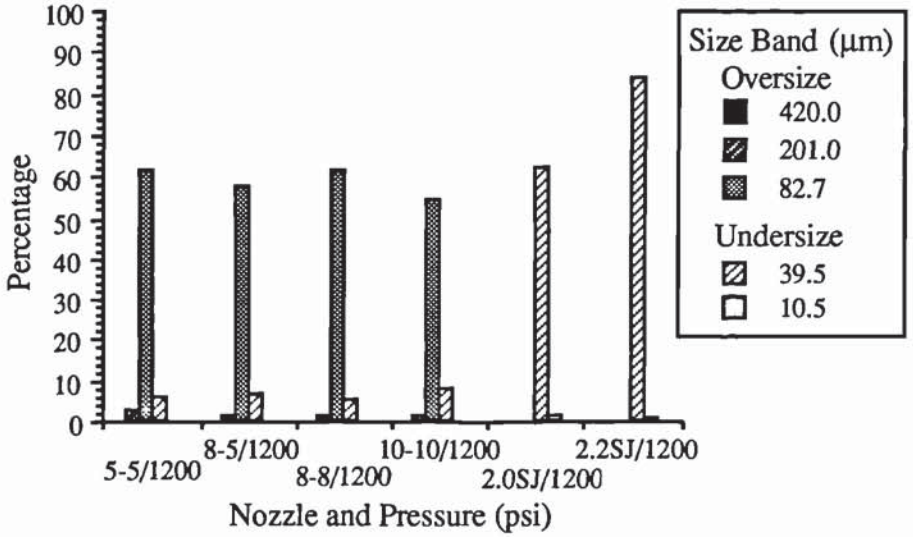

Overall fewer definite trends are exhibited by the results with the slurry than with the Newtonian liquids. This seems to indicate that viscosity has a significant influence upon spray distribution uniformity and that the effect of the high shear rates within the nozzle swirl-chamber upon slurry viscosity, and hence spray distribution uniformity, is, at present, unpredictable.

Another significant result demonstrated by Figures 7.6 to 7.7 is that the same nozzle exhibited the best and worse conditions for spray uniformity, albeit under

Figure 7.8: *Comparison of Spraying Conditions for 45% Calcium Carbonate Slurry*

a) *Most Uniform Spray Distribution*

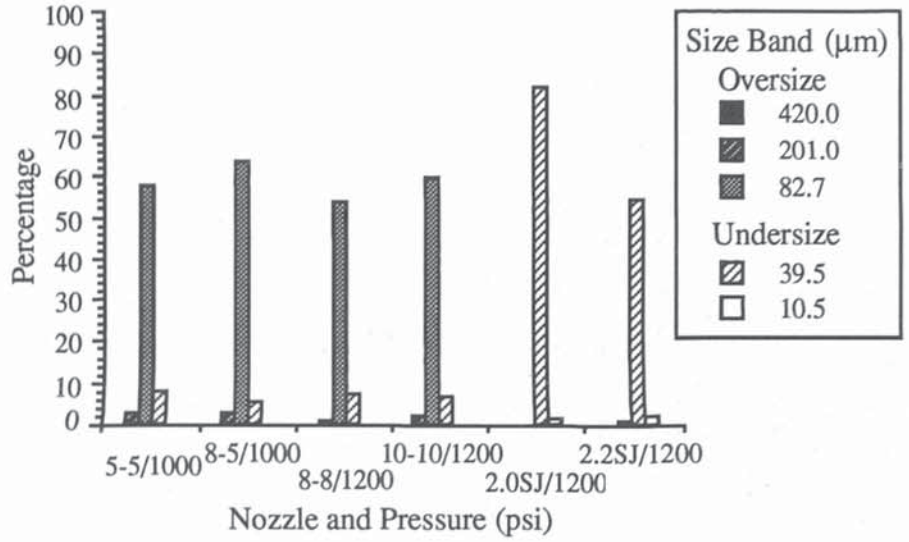

b) *Most Dispersed Spray Distribution*

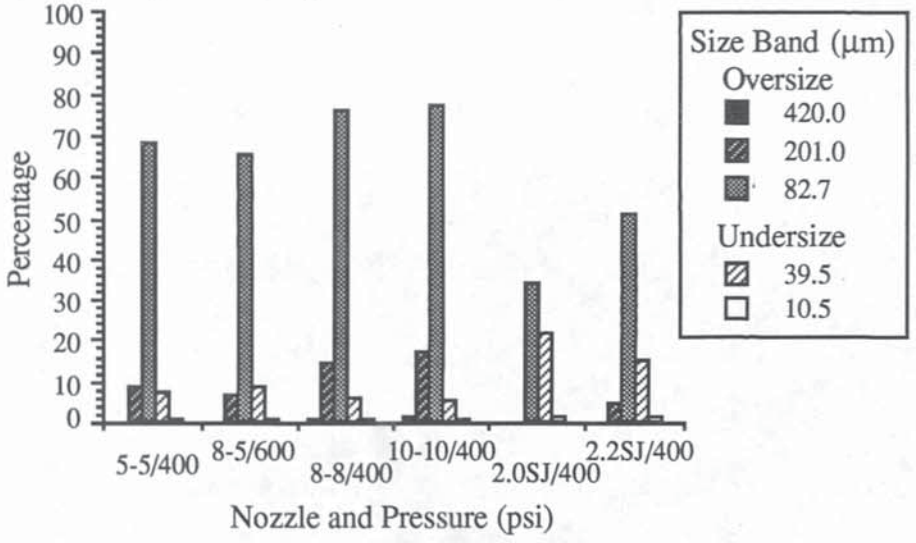

Table 7.2: Comparison of Results for Test Fluids with Both Nozzle Types

Spray Type	Nozzle	Water	NaSO4 Solution		CaCO3 Slurry	
			Conc	Pressure	Conc	Pressure
Uniform	AAASSTC	8-8/800	15%	10-10/1200	23%	5-5/1000
	Delevan	2.2/1200	5%	2.2/1200	35%	2.2/1200
Dispersed	AAASSTC	10-10/1200	15%	5-5/400	23%	5-5/400
	Delevan	2.2/400	15%	2.0/400	45%	2.2/400

extreme operating conditions. This did not appear with any other results and is an anomaly currently without explanation.

Figure 7.9: *Comparison of Spraying Conditions for Calcium Carbonate Slurries*

a) *Most Uniform Spray Distribution*

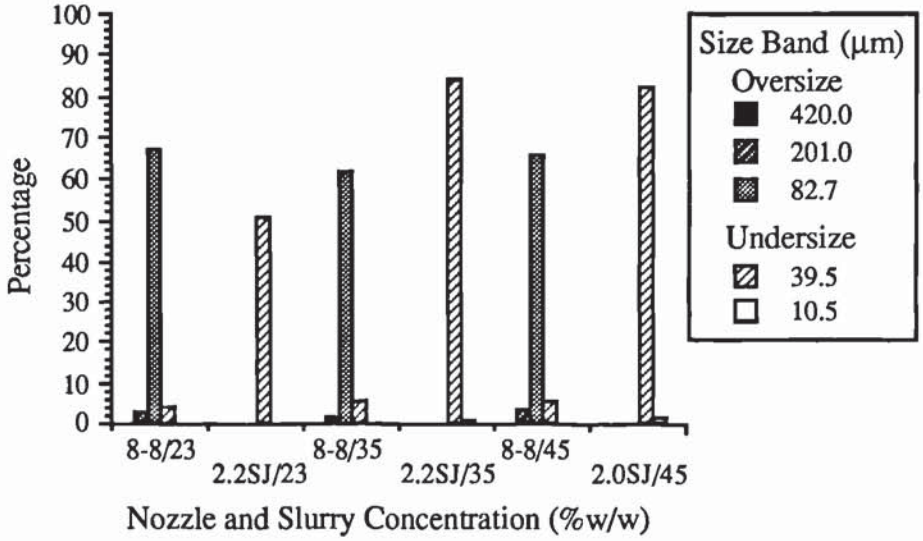

b) *Most Dispersed Spray Distribution*

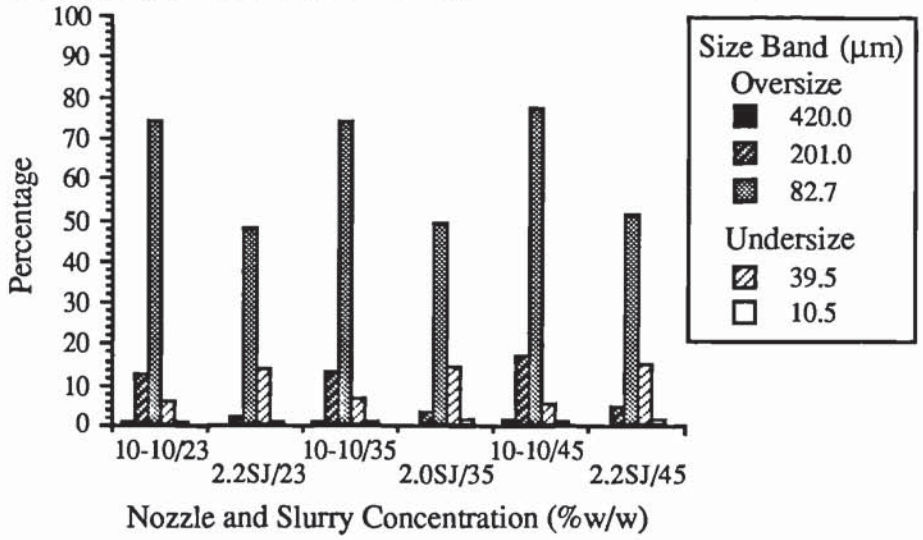

Figure 7.9 summarises the results from Figures 7.6 to 7.8 representing the best and worst conditions for spray uniformity for each slurry concentration. Once again both types of nozzle exhibit different characteristics and comparison of the results from each set of experiments (See Table 7.2) shows that it is impractical to predict the

conditions under which a particular nozzle will perform better than the rest. However, as a general rule high operating pressures favour better spray uniformity.

7.1.4 Detergent Slurries

Figures 6.25 to 6.28 show the results obtained when operating the Spraying Systems nozzles with detergent slurries. It was not practical to obtain a comparable set of results with the Delevan nozzles because they were susceptible to frequent blockage of

Figure 7.10: *Comparison of Spraying Conditions of the Detergent Slurry at 40°C*

a) *Most Uniform Spray Distribution*

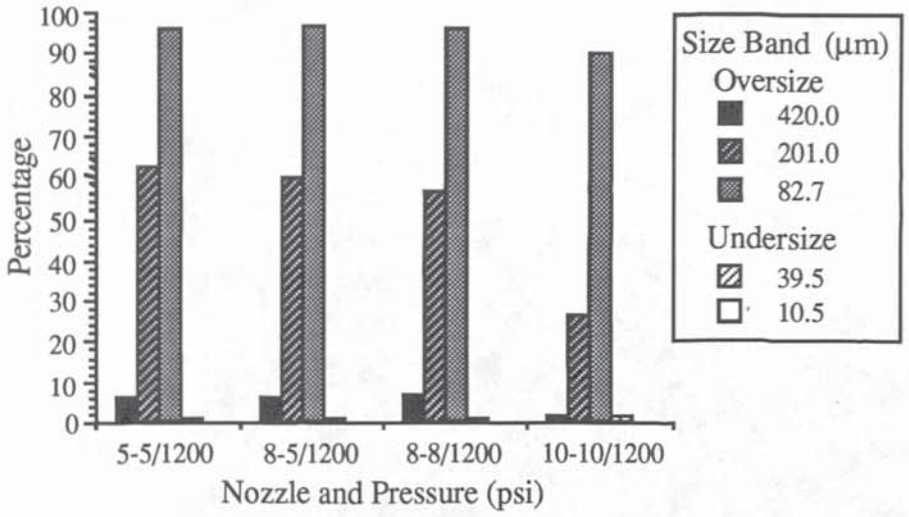

b) *Most Dispersed Spray Distribution*

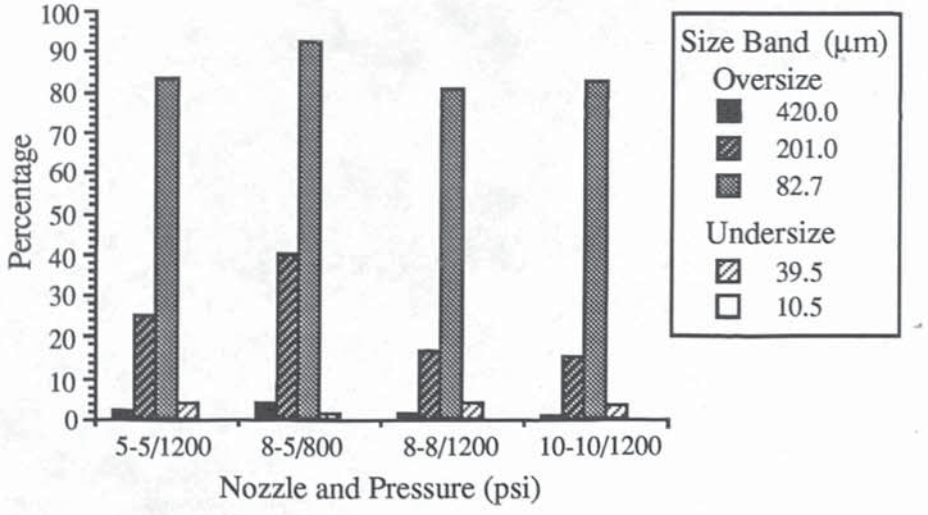

the nozzle orifice. This caused problems in reliably measuring the droplet size-distribution of the spray. Therefore no further tests were conducted using the Delevan nozzles.

Figure 7.11: *Comparison of Spraying Conditions of the Detergent Slurry at 60°C*

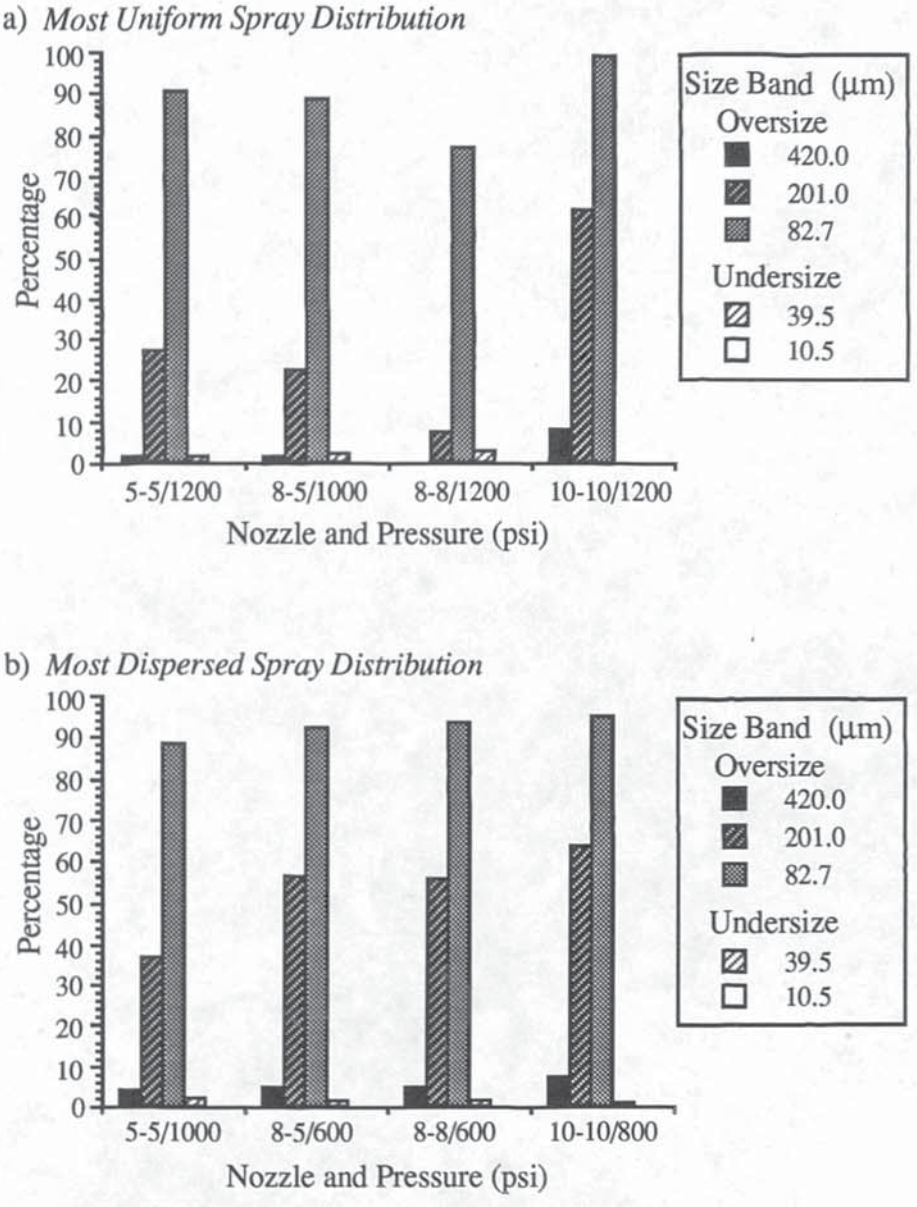

The results have been summarised into the format presented in Figures 7.10 to 7.12. However no significant trends are evident, although the 10-10 nozzle generally performed worst under most test conditions. As with the calcium carbonate slurry, the results confirm that the prediction of optimum spraying conditions for high viscosity

slurries is extremely unreliable as under certain conditions best and worst performance occurred within 200 psi (for example, 8-5 nozzle at 40°C and 5-5 nozzle at 80°C).

Figure 7.12: *Comparison of Spraying Conditions of the Detergent Slurry at 80°C*

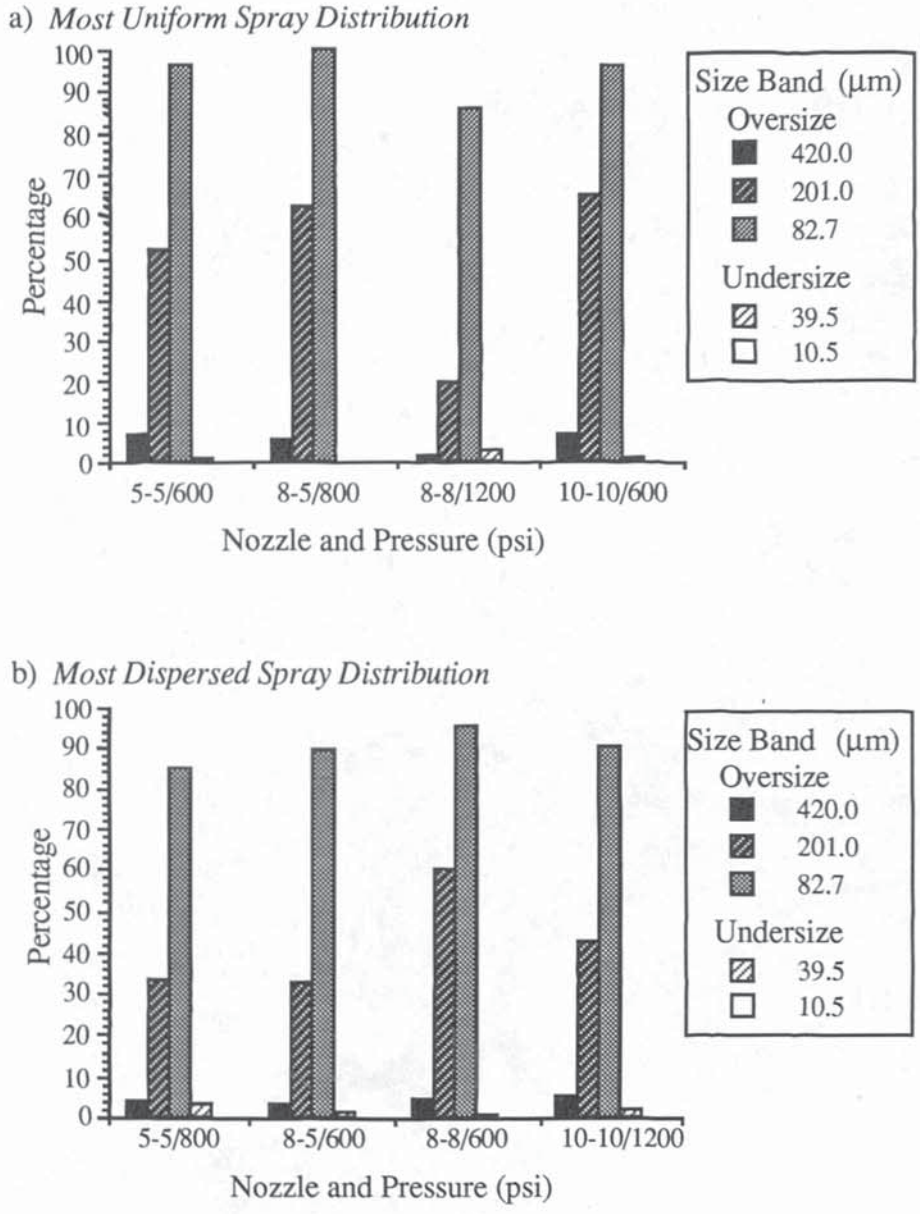

Figure 7.13 illustrates that, under most conditions, the 5-5 nozzle produced the most dispersed spray distribution. The only discrepancy occurred at 600 psi with a slurry temperature of 80°C; under these conditions the spray distribution was more uniform than with either the 10-10 or 8-5 nozzle. At low temperatures the large orifice 10-10 nozzle, and at high temperatures the 8-8 nozzle produced the most uniform spray distribution. Conversely each nozzle produced the most dispersed spray

distributions at high and low temperatures respectively. These results are summarised in Table 7.3 and demonstrate that the 8-8 nozzle operating at 800 psi with a slurry temperature of 80°C produced the most uniform spray distribution.

Figure 7.13: *Comparison of Spraying Conditions for Detergent Slurries*

a) *Most Uniform Spray Distribution*

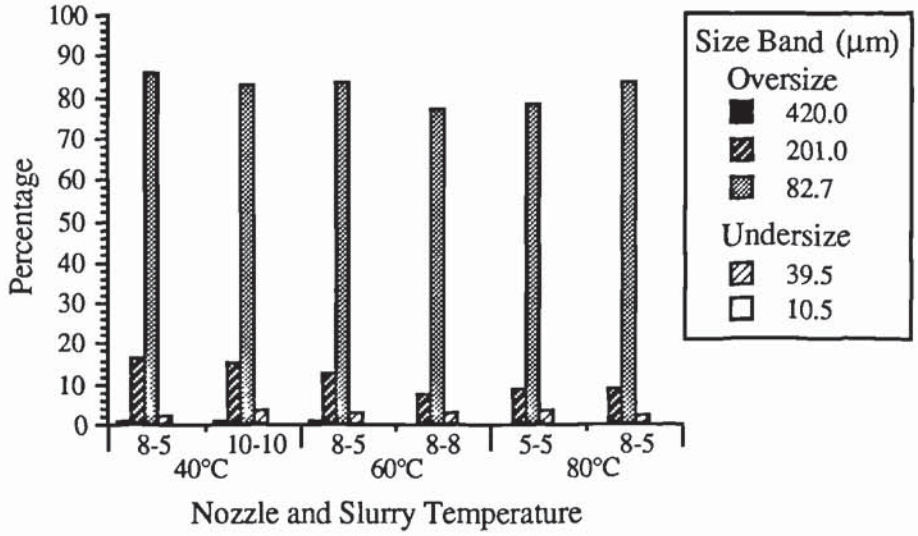

b) *Most Dispersed Spray Distribution*

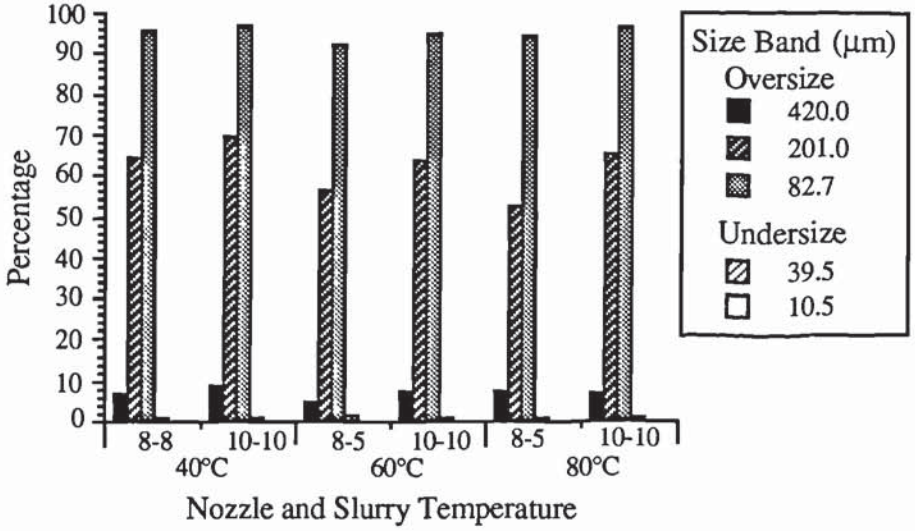

However, the results from the 8-8 nozzle operating at 800 psi have been amended using Felton's correction factors [108] applied at the upper limit of experimental obscuration (ie, in the region of 0.96 to 0.98). These results were discounted due to possible ambiguity in the corrected values, although the actual

measured value of the dispersion coefficient recorded during the experiment was 2.92 (ie, indicating a reasonably uniform spray distribution). Similarly the results obtained when the 10-10 nozzle was operated at 1200 psi with a slurry temperature of 60°C have been discounted; although in this case the actual measured value of the dispersion coefficient is 2.37 (ie, indicating a fairly dispersed spray distribution).

Table 7.3: *Dispersion Coefficients for Various Detergent Slurries*

Slurry Temp (°C)	Pressure (psi)	Nozzle	Spray Type	N - Value
40	600	8-8	Dispersed	2.35
40	1000	10-10	Uniform	2.82
60	1200	8-8	Uniform	2.98
60	1200	10-10	Uniform	3.79
80	800	8-8	Uniform	5.42
80	600	10-10	Dispersed	2.38

If these two results are discounted due to the fact that the original measurements were obtained at high levels of obscuration, then the most uniform spray distribution was obtained using 8-8 nozzle operating at 1200 psi with a slurry temperature of 60°C.

7.2 Mathematical Model

A comparison between experimental data and the predictions made by the mathematical model has already been presented in Chapter 5; this discussion will deal separately with each aspect of the computer simulation.

The main purpose of the mathematical model was to predict the droplet size distribution produced under known operating conditions and liquid properties for any given nozzle. This was achieved by the computer simulation, although the method

was limited due to the assumption that spray dispersion was constant (ie, the value of N in the Rosin-Rammler distribution remained constant) for all nozzle types, liquid properties and operating pressures. However, the simulation predicts droplet sizes significantly smaller (approximately 1/10th size) than the experimentally determined sizes despite the fact that the usual trends associated with swirlchamber nozzles (ie, a decrease in droplet size with an increase in pressure, etc) are displayed by the model. This seems to indicate that the inherent error in the size prediction is due to an inaccuracy in the original assumptions concerning the absence of wall friction in the swirlchamber. It is possible that over-simplification occurred in order to reduce the complexity of modelling three-dimensional liquid flow and to avoid the necessity of using second- or third-order partial differential equations. Alternatively, as noticed by Carlisle [174], the effect of a slight offset of the tangential entry into the swirlchamber may have affected the inlet velocity to a noteable degree. This, combined with an eliptical inlet hole (the model assumes it to be spherical), might have significantly reduced the inlet velocity and so produced larger droplets than predicted by the model.

In the model the most significant term involved in the various calculation stages is that of the sheet velocity. This is the controlling factor in the prediction of the break-up length, sheet thickness and spray cone angle. Figure 5.28 shows that the experimental values are approximately half those of the corresponding theoretical predictions. It would appear that a significant reduction occurs due to the effect of frictional drag caused by the boundary layer in the nozzle and air entrainment. The latter effect has not been accounted for in the original assumptions, as the model assumes that the sheet velocity remains constant along the length of the sheet [10]. If the sheet velocity is reduced, ie by taking its value relative to the localised air velocity then there is a marked increase in the droplet size and overall accuracy of the model.

7.2.1 Droplet Size Distribution

Figures 5.17 to 5.22 demonstrate that the model accurately predicts a decrease in droplet size with an increase in pressure but, as mentioned above, the size predicted is smaller than the comparable experimental result. There was also a noticeable

difference between the data obtained at 5 psi and that obtained at higher pressures for each nozzle. Reference to the Plate 5.1, presented in Appendix 5, and similar photographs [200] confirms that the liquid sheet is definitely 'bell-shaped'. It would appear that the spray cone has not formed properly, with break-up of the sheet occurring virtually vertically. This could lead to the supposition that sheet disintegration is significantly influenced by gravitational forces and a different break-up mechanism prevailing, as demonstrated by the absence of wave disturbances upon the sheet.

Although the objective of the mathematical model was to reduce empiricism in the prediction of droplet sizes and size distributions, it is possible to correlate experimental data and theoretical predictions in the form of 'best-line' equations from each graph. These results are presented in Table 7.4 and, if the data obtained at 5 psi are ignored due to the presence of a different break-up mechanism, the empirical factor is reasonably constant over the entire pressure range.

Table 7.4: *Empirical Correlations between Experimental and Predicted Size Results*

Pressure (psi)	**Correlation**
5	$D_{Exp} = 4.7\, D_{Cal} + 273.81$
10	$D_{Exp} = 9.3\, D_{Cal} - 52.28$
15	$D_{Exp} = 12.1\, D_{Cal} - 87.75$
20	$D_{Exp} = 12.5\, D_{Cal} - 52.42$
25	$D_{Exp} = 12.0\, D_{Cal} - 42.50$
Average*	$D_{Exp} = 11.5\, D_{Cal} - 58.74$

* This value ignores the 5 psi correlation in its computation.

The only discrepancy in the correlation factors presented in Table 7.4 is that obtained from the results at 10 psi, which could possibly be attributed to the fact that the spray cone has not fully opened out and is still slightly unstable. If the averaged

Table 7.5: *Improved Droplet Size Distribution Results*

Nozzle	Pressure	D_{Exp}	D_{Cal}	Accuracy	D_{Cor}	Accuracy
1	5	834.79	137.36	83.5	1520.90	82.8
	10	592.72	69.43	88.3	739.71	24.8
	15	460.90	46.69	89.9	478.20	3.8
	20	344.04	34.95	89.8	343.19	0.2
	25	280.52	28.00	90.0	263.26	6.2
2	5	906.29	136.92	84.9	1515.84	67.3
	10	613.61	69.21	88.7	737.18	20.1
	15	482.66	60.05	87.6	631.84	30.9
	20	362.96	34.84	90.4	341.92	5.8
	25	308.39	27.91	90.9	262.23	15.0
3	5	827.65	143.40	82.7	1590.36	92.1
	10	632.94	72.51	88.5	775.13	22.5
	15	533.72	48.56	90.9	499.70	6.4
	20	493.87	36.51	92.6	361.13	26.9
	25	443.89	29.25	93.4	277.64	37.5
4	5	823.73	141.41	82.8	1567.48	90.3
	10	629.18	71.49	88.6	763.40	21.3
	15	534.80	47.87	91.0	491.77	8.0
	20	524.54	35.99	93.1	355.15	32.3
	25	240.27	28.84	88.0	272.92	13.6
5	5	843.18	140.15	83.3	1552.99	84.2
	10	601.69	70.85	88.2	756.04	25.7
	15	504.42	47.44	90.6	486.82	3.5
	20	441.06	35.67	81.8	351.47	20.3
	25	343.82	28.58	87.3	269.93	21.5
6	5	756.46	138.05	81.8	1528.84	102.1
	10	548.67	69.78	87.3	743.73	35.6
	15	399.24	46.73	88.3	478.66	19.9
	20	293.20	35.13	88.0	345.26	17.8
	25	251.76	28.15	88.8	264.99	5.3

correlation factor is applied to the predicted values of the Volume Mean Diameters for each nozzle operating at each pressure, as illustrated in Table 7.5, then the overall accuracy of the model is increased. Nevertheless, in most cases, the accuracy of the model still does not fall within the normal bounds of experimental error; therefore, this is not the ideal method to employ in order to correlate the experimental data and predicted results. It is, however, the best correlation method that is available for use.

7.2.2 Air Core Diameter

Figure 5.23 demonstrates that there is good agreement between experimental data and theoretical predictions. It would appear that the formation of the air core is unaffected by the complexities of wall friction and the simplifications made in the initial assumptions seem to be valid. However, as in the original work by Nieukamp [167], no account has been made for viscosity in the flow model.

An increase in viscosity will cause a decrease in the air core diameter [167], due to a decrease in the rotational velocity caused by an increase in wall friction. In this type of case Taylor's boundary layer theory [170] would need to be applied to extend the work to allow for viscous and non-Newtonian fluids.

7.2.3 Liquid Sheet Length

There appears to be reasonable agreement between experimental data and theoretical predictions, as illustrated by Figure 5.23. Once again the anomaly of the 5 psi data-set is visible and if the graph is replotted without the 5 psi data-set, as in Figure 7.14, the results are noticeably dispersed. This factor is almost certainly due to the break-up length being controlled by sheet velocity.

The break-up length is determined by equation (5.33) which contains two velocity terms and an empirical term heavily influenced by Reynolds number, ie liquid velocity. Therefore, the factor of two difference between experimental data and theoretical predictions, reported above, is squared for the purpose of the calculation and a further inaccuracy is introduced by the presence of an empirically determined constant. However, equation (5.33) shows that an increase in surface tension will

increase the liquid sheet length and a decrease in ambient density will increase the liquid sheet length. This is in agreement with the work of Dombrowski & Fraser [6]; therefore most of the theory behind equation (5.33) appears to be correct.

Figure 7.14: *Modified Results for the Comparison between Experimental and Theoretical Values for the Liquid Sheet Length*

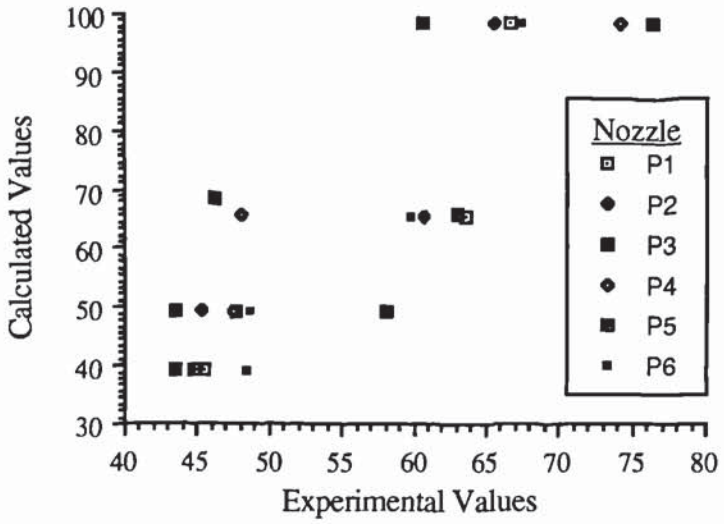

7.24 Spray Cone Angle

Figure 5.26 demonstrates no clear correlation of the experimental data for spray cone angle. Theoretical prediction, illustrated in Table 7.6, shows a constant value for the cone angle which is influenced by nozzle geometry but entirely independent of pressure and liquid properties. This is in agreement with the work of Doble & Halton [165] and other published data [187].

As mentioned in Chapter 5 the predicted values for the cone angle are generally larger than their corresponding experimental values. This is as expected due to the neglection of wall effects and frictional drag in the swirlchamber. There are a few discrepancies in the experimental data which is most probably due to error in the photographic measurement of the spray cone. This is most certainly attributable to parallax which also accounts for the spread of experimental data obtained during the experiments. There is a slight anomaly in the experimental data for P2, illustrated by Table 7.6, which shows that the average experimental value is greater than the

predicted value. This is clearly contrary to what would be expected and is due to fact that three data points have been obtained which fall within experimental error but are noticeably larger than the rest in the series.

Table 7.6 shows that, excluding the anomaly of the experimental data for P2, there is no clear correlation between experimental data and theoretical prediction. Therefore it is not possible to estimate the effect of viscous forces, frictional drag and wall effects upon the liquid flow from these experiments.

Table 7.6: *Theoretical Predictions for Spray Cone Angle*

Nozzle	Pressure (psi)					Exp Data
	5	10	15	20	25	(Av)
P1	95.99	95.99	95.99	95.99	95.99	89.9
P2	95.33	95.33	95.33	95.33	95.33	96.7
P3	101.69	101.69	101.69	101.69	101.69	83.0
P4	100.19	100.19	100.19	100.19	100.19	94.6
P5	99.11	99.11	99.11	99.11	99.11	95.7
P6	96.11	96.11	96.11	96.11	96.11	95.6

7.25 Liquid Sheet Velocity

As previously mentioned in Section 7.2 the main inaccuracy with the mathematical model lies in prediction of liquid sheet velocities approximately twice the value of those determined experimentally, as illustrated by Figure 5.28. This is contradictory to the good agreement between the theoretical predictions and experimental data for volumetric flowrate, as illustrated by Figure 7.15.

Since it has been shown above that the predicted values of the air core diameter are very close to those measured experimentally, then this knowledge combined with the results presented in Figure 7.15 would seem to indicate that the values of the sheet velocity should also hold some degree of accuracy. If reference is drawn to equation

(5.22), reproduced below, it can be seen that there should be more agreement between experimental and theoretical values.

$$Q_{Out} = V_o \pi \left(r_o^2 - r_{ac}^2 \right) \qquad - \ 5.22$$

or,

$$Q_{Out} = \sqrt{V_s^2 - U_o^2}\, \pi \left(r_o^2 - r_{ac}^2 \right) \qquad - \ 5.22a$$

Figure 7.15: *Comparison between the Theoretical and Experimental Values for the Volumetric Flowrate*

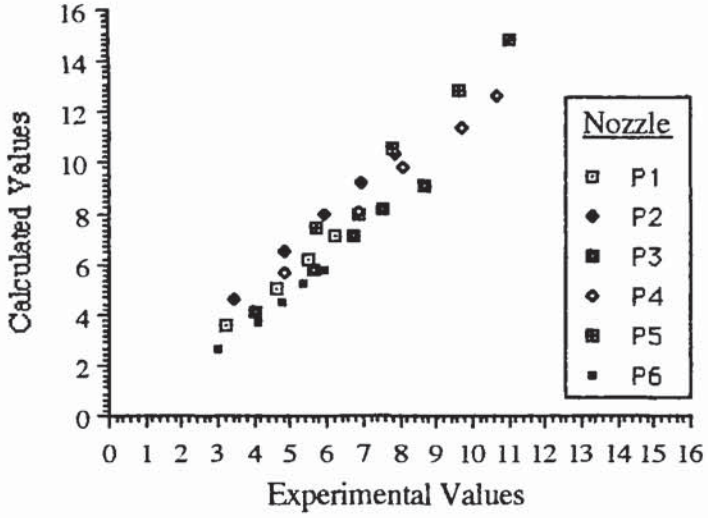

It would appear that the term V_s, used throughout the mathematical model, is slightly misleading and it should be interpreted as the resultant velocity. Unfortunately it is not possible to experimentally determine the liquid velocity at the nozzle outlet using the apparatus available. Thus the only direct comparison available for use is the sheet velocity as determined from the double-flash photography.

Therefore a considerable amount of frictional drag must be created by air entrainment into the spray cone which has not been accounted for in the mathematical model. The effect of the air entrainment is to significantly reduce the sheet velocity to approximately half of its initial value taken at the nozzle outlet. This essentially means that the assumption of constant sheet velocity based upon the work of Dombrowski &

Johns [10] is inaccurate and allowance should be made for velocity reduction along the length of the sheet.

7.26 Computer Simulation

Generally the mathematical model shows good agreement with experimental data. However, due to inaccuracies in assumptions made at various stages of the model it fails to provide an accurate prediction of droplet size and size distribution. It does however, predict sizes that can be empirically correlated into more useful, and accurate, distributions.

This problem could probably solved by the introduction of three-dimensional modelling into the simulation using packages like Phoenics [196]. This would best be achieved in the region of the swirlchamber where allowance could be made for boundary conditions and wall friction as discussed by Taylor [157]. Additionally the effects of frictional drag caused by air entrainment should also be included to allow for more accuracy in the modelling of liquid sheet break-up.

However, it is unlikely that a detailed simulation of this type of atomisation will be achieved until there is greater knowledge of the causes of sheet disturbances. Once these have been successfully identified (at present it would appear they are due to disturbances in the air core [186]) and a mathematical simulation of the process of their formation has been accomplished, then all forms of empiricism can be eliminated from the model.

Conclusions

8.1 Experimental Work

An experimental method has been developed which enables the accurate measurement of droplet sizes from sprays using a Malvern Particle Size Analyser.

The obscuration, that is normally associated with this type of size measurement was reduced to more acceptable levels by the use of baffles to stop the incident laser beam being impinged by mist and/or spray.

The problem of pumping viscous feeds was overcome by utilising a heated pressure vessel capable of supplying the atomising nozzles at pressures up to 1400 psi.

It was found that the Delevan 2.2SJ nozzle operating at 1200 psi produced the most uniform spray distribution with most types of feed. The AAASSTC5-5 nozzle operated at 400 psi produced the most dispersed spray for all feeds except water. In the case of water the most dispersed spray was obtained from the AAASSTC10-10 nozzle operating at 1200 psi.

The most uniform spray distribution for the detergent slurry was obtained at a slurry temperature of 60°C using the AAASSTC8-8 nozzle operating at 1200 psi. The most dispersed spray was obtained at a slurry temperature of 80°C using the AAASSTC8-5 nozzle operating at 600 psi.

8.2 Mathematical Model

A mathematical model has been developed that does not rely upon empirical expressions and is not limited to set conditions or nozzle types.

The model predicts air core diameter and volumetric flowrate but smaller droplet sizes are estimated than the corresponding experimentally determined sizes. This is

due to inaccuracies in the initial assumptions made in the development of the model, in particular the assumption of negligible wall friction in the swirlchamber.

There is good agreement between the predicted and experimental values for the air core diameter and good agreement between the predicted and experimental values for the volumetric flowrate.

There is reasonable agreement between the predicted and experimental values for the liquid sheet length. Over-sized values for the spray cone angle have been predicted due to the neglection of boundary layer and wall effects.

The predicted value of the liquid sheet velocity is higher than that determined experimentally due to the neglection of air entrainment and frictional drag in the model.

8.3 General Conclusions

This study has shown that the distribution of droplets from liquid feeds of widely varying physical properties can be accurately measured by the technique developed. The complexities of fluid hydrodynamics which lead to liquid dispersion have been confirmed, particularly with non-Newtonian feeds. Hence, whilst a definitive model leading to the prediction of droplet size distribution as a function of operating parameters, would be of practical value it seems likely that empirical correlations will remain in use until a better understanding is gained of the fundamentals of liquid flow, momentum transfer, the effects of liquid shear within the atomiser and surface wetting. It is entirely possible that identification of the effects of surface wetting and roughness upon liquid flow could lead to a better understanding of the break-up mechanisms of the liquid sheet.

Recommendations for Further Work

The following work would form a useful addition to this study:

a) Extension of the modelling work to include higher atomising pressures, ie up to those used in industrial applications (for example, between 800 to 1000 psi), and different nozzle designs, for example grooved core nozzles.

b) Expansion of the existing model to embrace three-dimensional flow within the swirlchamber, to account for the eliptical inlet port in the swirlchamber and include the effects of air friction/drag upon the liquid sheet. This would require the use of computer simulation packages such as Phoenics [196].

c) Extension of the work to allow the prediction of droplet size distributions from the atomisation of fluids exhibiting non-Newtonian properties. This would include the effects of wall friction, internal liquid shear and the increasing influence of viscosity.

d) Combination of the model with a spray dryer simulation model for design purposes to enable the prediction of spray dryer performance. The model developed by Sharma [23] is ideally suited for this purpose as it is based upon an experimentally determined droplet size distribution.

Nomenclature

a	–	Constant defined by $1 - (r_{ac}/r_o)^2$	
A	–	Experimentally determined constant from equation (4.45)	
A'	–	Uncorrected light absorption term	
A_i	–	Cross-sectional area of the inlet port	(m^2)
A_N	–	Internal surface area of the swirlchamber in contact with fluid	(m^2)
A_{sc}	–	Cross-sectional area of the swirlchamber	(m^2)
A_S	–	Cross-sectional area of the particles in size class S	(m^2)
A_1	–	Internal surface area of the nozzle orifice in contact with fluid	(m^2)
b	–	Constant in heat transfer equation	
B	–	Experimentally determined constant from equation (4.45)	
c	–	Width of light beam	(cm)
C	–	Empirical Constant	
C^*	–	Constant	
C'	–	Constant	
C''	–	Constant	
C_d	–	Correction factor for the discharge coefficient	
C_D	–	Discharge coefficient	
C_D'	–	Modified discharge coefficient	
C_N	–	Correction factor for the Rosin-Rammler dispersion coefficient	
C_p	–	Specific heat capacity	(J/kg/K)
C_t	–	Diameter of impact crater on measuring slide	(μm)
C_T	–	Droplet crust thickness	(μm)
C_X	–	Correction factor for the Rosin-Rammler characteristic diameter	
C_θ	–	Correction factor for the spray cone angle	
d	–	Unspecified dimension in general equations	(m)
d_l	–	Ligament diameter	(m)
d_{max}	–	Maximum (or upper limit) droplet diameter in the sample	(μm)
d_{min}	–	Minimum (or lower limit) droplet diameter in the sample	(μm)
d_p	–	Mean droplet diameter	(μm)
d_{si}	–	Inner diameter of the spray	(m)
d_{so}	–	Outer diameter of the spray	(m)
$d(N)$	–	Relative frequency at size, d	
D	–	Droplet or particle diameter	(μm)
$\overline{D}$	–	Mean droplet diameter determined by Turner & Moulton [87]	(μm)
D_{AM}	–	Arithmetic mean diameter	(μm)
D_f	–	Most frequent diameter	(μm)

$D(F,G)$	–	Statistical mean diameter where F and G are integers	(μm)
D_{GM}	–	Geometric mean diameter (size)	(μm)
D_i	–	Diameter of the inlet port of the swirlchamber	(m)
D_j	–	Diameter of the impactor jet	(cm)
D_m	–	Sample mean diameter	(μm)
D_M	–	Median diameter	(μm)
D_n	–	Diameter of the swirlchamber in the nozzle	(m)
D_o	–	Diameter of the outlet port of the nozzle (Jet orifice)	(m)
D_p	–	Diameter of the aerosol particle	(μm)
D_s	–	Diameter of the impactor slide	(cm)
D_{SM}	–	Surface mean diameter	(μm)
D_v	–	Molecular diffusivity	(m^2/s)
D_{VM}	–	Volume mean diameter	(μm)
D_{VS}	–	Volume-Surface or Sauter mean diameter	(μm)
D_{ws}	–	Distance from wall to slide in a cascade impactor	(cm)
E_{ij}	–	Light energy diffracted by a single particle on to detector ring ij	
$E(I)$	–	Matrix representing light energy distribution across all detector rings	
f	–	Index of fractional decay	
f	–	Amplitude ratio defined by $\ln(\alpha_b/\alpha_o)$	
F	–	Friction factor for swirlchamber (= 1 / 200)	
FN	–	Flow number	$((gal/h)/\sqrt{lb/in^2})$
g	–	Gravity term	(m/s^2)
G	–	Centrifugal potential	(m/s^4)
h'	–	Thickness of a liquid film at any point	(m)
h_b	–	Thickness of the liquid sheet at the break-up length	(m)
h_c	–	Heat transfer coefficient	(m/s)
h_i	–	Thickness of the liquid sheet at the nozzle outlet	(m)
h*	–	Height of 'weir' or liquid height at orifice	(m)
H'	–	Henry's Law constant for mass transfer	
i	–	Inside radius of the detector ring	(m)
I	–	Light energy transmitted by the sample to the detector	(W)
I_c	–	Impaction coefficient	
I_o	–	Incident light energy transmitted by the source (or laser)	(W)
$I(\theta)$	–	Light energy distribution	
j	–	Outside radius of the detector ring	(m)
J_o	–	Bessel function of the first kind of order 0	
J_1	–	Bessel function of the first order 1	
k	–	Sheet thickness parameter	(m^2)
k_c	–	Coefficient of mass transfer for the droplet crust	(m/s)
k_g	–	Mass transfer coefficient	(m/s)

k_i	–	Thermal conductivity	(W/m/K)
K_B	–	Constant in the Nukyama-Tanasawa equation	
K_C	–	Constant in the Nukyama-Tanasawa equation	
K_G	–	Overall mass transfer coefficient	(m/s)
K_{JO}	–	Constant in Joyce's empirical droplet size equation	
K_L	–	Constant in Longwell's empirical droplet size equation	
K_{MI}	–	Constant in McIrvine's empirical droplet size equation	
l_b	–	Break-up length of the liquid sheet	(m)
l_n	–	Length of the swirlchamber in the nozzle	(m)
l_o	–	Length of the outlet orifice	(m)
l_s	–	Length of the non-conical section of the swirlchamber	(m)
l'	–	The distance from the nozzle outlet to any point on the sheet	(m)
L	–	Optical path length	(m)
Ld	–	Log difference between calculated and measured values	
Le_{Cal}	–	Calculated light energy hitting the detector element	(W)
Le_{Mea}	–	Actual light energy hitting the detector element.	(W)
m	–	Maximum number in any distribution or series	
M	–	Mass flowrate of the spray	(kg/s)
n	–	Wave number $= 2\pi / \lambda$	(m^{-1})
n(D)	–	Number distribution	
n_T	–	Turbulence wave number	(m^{-1})
N	–	Dispersion coefficient in the Rosin-Rammler equation	
N_{App}	–	Apparent value of 'N' determined from the experiment	
N_k	–	Number of particles with diameter, d_k	
N_S	–	Number of droplets per unit volume	(m^{-3})
Ob	–	Obscuration of laser beam measured in the experiment	
P	–	Pressure drop across the nozzle	(N/m^2)
P_o	–	The porosity of the droplet crust	
q	–	Dispersion coefficient in the Nukyama-Tanasawa equation	
q	–	Growth rate of the wave disturbance	(1/s)
Q	–	Volumetric flowrate	(m^3/s)
Q_l	–	Volumetric flowrate passing through the plane of light beam	(m^3/s)
r	–	Distance	(m)
r_{ac}	–	Radius of the air core in the nozzle	(m)
r_d	–	Radial distance from the orifice to the centre of the perforation	(m)
r_e	–	External radius of the dried particle	(m)
r_i	–	Internal radius of the dried particle	(m)
r_n	–	Radius of the nozzle swirlchamber	(m)
r_o	–	Radius of the outlet port of the nozzle	(m)
r_p	–	Radius of the perforation	(m)

r_1	–	Radial distance from the orifice to the origin of the perforation	(m)
R_D	–	Dimensionless internal radius $= R_I / r_o$	
R_I	–	Radius of the swirlchamber inlet	(m)
R_J	–	Radius of the jet orifice	(m)
R_l	–	Distance along nozzle converging cone to swirlchamber inlet	(m)
S_g	–	Specific gravity of the slurry	
S_G	–	Geometric standard deviation	
S_N	–	Standard deviation of the particle sizes	
t	–	Time	(s)
T	–	Thrust developed by spray	(kg m/s^2)
T_a	–	Air temperature	(K)
T_{am}	–	Ambient air temperature	(K)
T_d	–	Droplet temperature	(K)
T(I,J)	–	Matrix defining the light energy distribution for each droplet	
U	–	Mean tangential velocity or horizontal component of velocity relative to the liquid sheet	(m/s)
U_I	–	Mean tangential inlet velocity	(m/s)
U_o	–	Mean exit spinning speed	(m/s)
U_s	–	Velocity due to the total pressure head defined by $\sqrt{\frac{2P}{\rho_l}}$	(m/s)
V	–	General velocity term	(m/s)
V_c	–	Velocity component normal to the liquid sheet	(m/s)
V_{ds}	–	Mean droplet velocity	(m/s)
V_D	–	Volume percent oversize in the Rosin-Rammler equation	
V_i	–	Mean inlet velocity	(m/s)
V_o	–	Mean outlet velocity	(m/s)
V_p	–	Relative velocity within the swirlchamber	(m/s)
V_r	–	Radial velocity component	(m/s)
V_s	–	Liquid sheet velocity	(m/s)
V_z	–	Axial velocity component	(m/s)
V_θ	–	Tangential velocity component	(m/s)
V*	–	Maximum velocity over a 'weir'	(m/s)
W(J)	–	Matrix representing the droplet weight (volume) distribution	
W_k	–	Weight (volume) fraction of droplets with diameter, d_k	
x	–	Radial distance	(m)
X	–	Rosin-Rammler diameter	(m)
y	–	Variable determined by $We\left(\frac{\rho_l Q V_s}{4 \sigma \pi}\right)$	
z	–	Variable in light energy equation determined by $(D \pi \theta) / \lambda_i$	

Greek Letters

α	–	Amplitude of a wave disturbance on the liquid sheet	(m)
α_b	–	Final amplitude of the wave disturbance on the liquid sheet	(m)
α_o	–	Initial amplitude of the wave disturbance on the liquid sheet	(m)
β	–	Parameter determined by equation (4.40)	
χ	–	Radial Proportionality Constant	
δ	–	Length of Sheet Segment	(m)
δ_1	–	Boundary layer thickness	(m)
δ_2	–	Constant in Taylor's equation (4.36)	
Δ	–	Nozzle Parameter	
Δ'	–	Modified nozzle parameter	
ϕ	–	Constant $= 1 - 1/N$	
Φ	–	Ratio of spinning speed at inlet radius and inlet velocity	
γ	–	Shear rate	(1/s)
Γ	–	Gamma Function	
η_w	–	Fraction of particles impacted on the wall of a cascade impactor	
φ	–	Constant in heat transfer equations	
λ	–	Wavelength of a sheet disturbance	(m)
λ_i	–	Wavelength of the incident light from laser	(m)
λ_{max}	–	Wavelength of the maximum sheet instability	(m)
λ_{opt}	–	Optimum wavelength of the sheet disturbance	(m)
λ'_{opt}	–	Optimum wavelength of the ligament disturbance	(m)
μ	–	General viscosity term	(kg/m s)
μ_a	–	Viscosity of the ambient air	(kg/m s)
μ_l	–	Viscosity of the liquid	(kg/m s)
θ	–	Angle at which the scattered light is observed by detector	(Degrees)
$\theta/2$	–	Semi-cone angle of the spray	(Degrees)
ρ_a	–	Density of the ambient air	(kg/m^3)
ρ_d	–	Density of the solid particle	(kg/m^3)
ρ_l	–	Density of the fluid	(kg/m^3)
ρ_w	–	Density of the water	(kg/m^3)
σ	–	Surface tension of the fluid	(kg/s^2)
τ	–	Shear stress	(Pa)
τ	–	Variable determined by $\pi D/V_s$	(Pa)
τ_o	–	Yield Stress	(Pa)
υ_l	–	Kinematic viscosity of the liquid $= \mu_a / \rho_a$	(m^2/s)
ϖ	–	Angle a radius vector makes with the axis	(Degrees)
ψ	–	Relative direction of flow within the swirlchamber	(Degrees)
Ω	–	Circulation constant	
Ω'	–	Modified circulation constant	

Dimensionless Groups

Nu	–	Nusselt number	= $(h_c\, d) / k$
Pr	–	Prandtl number	= $(C_p\, \mu_a) / k$
Re	–	Reynolds number	= $(\rho_l\, V\, d) / \mu$
Sc	–	Schmidt number	= $\mu_a / (\rho_a\, D_v)$
Sh	–	Sherwood number	= $(k_g\, d) / D_v$
We	–	Weber number	= $(\rho_l\, V^2\, h) / \sigma$
We_{ρ_a}	–	Modified Weber number (based on ρ_a)	= $(\rho_a\, V^2\, D_o) / \sigma$
We_{gl}	–	Modified Weber number	= $(\rho_a^2\, (U_a - U_\infty)\, h_i) / \sigma$
We*	–	Weber number of the sheet disturbance	= $(\rho_a\, V_a^2\, \lambda) / \sigma$
Z	–	Ohnesorge number	= $\mu_l / (\sigma\, \rho\, d)^{0.5}$

General Subscripts

g	–	Gas
l	–	Liquid
∞	–	Up-stream of nozzle
r	–	Radial Direction
z	–	Axial Direction
θ	–	Tangential Direction

Main Variables used in the Computer Program: Nozzle.For

AIN	–	Cross-sectional area of the inlet port	(m^2)
ADN	–	Density of the ambient air	(kg/m^3)
ANG	–	Semi-cone angle of the spray	(Degrees)
ACR	–	Radius of the air core in the nozzle	(m)
BLN	–	Break-up length of the liquid sheet	(m)
CAG	–	Cone angle of the spray	(Degrees)
CON	–	Sheet thickness parameter	(m^2)
DEN	–	Density of the fluid	(kg/m^3)
DIN	–	Diameter of the inlet port	(m)
DMA	–	Maximum droplet size	(m)
DMI	–	Minimum droplet size	(m)
DV	–	Droplet mean diameter	(m)
DVM	–	Mean volume diameter	(m)
DVS	–	Sauter mean diameter (Surface-Volume Mean Diameter)	(m)

Variables used in the Computer Program (continued)

EXT	–	Diameter of the outlet orifice	(m)
FER	–	Dimensionless amplitude ratio	
PIN	–	Pressure drop across the nozzle	(N/m^2)
QVF	–	Volumetric flowrate	(m^3/s)
REN	–	Reynolds number	
REO	–	Radius of the outlet orifice	(m)
RIN	–	Mean inlet radius of the spinning fluid	(m)
RN	–	Rosin-Rammler parameter	
RX	–	Rosin-Rammler diameter	(m)
SFT	–	Surface tension of the fluid	(kg/s^2)
SWC	–	Diameter of the swirlchamber in the nozzle	(m)
TBP	–	Thickness of the liquid sheet at the break-up length	(m)
TFF	–	Thickness of the liquid sheet at the nozzle outlet	(m)
TPF	–	Temperature of the liquid feed	(K)
UME	–	Mean exit spinning speed	(m/s)
VAE	–	Velocity at the nozzle outlet	(m/s)
VIN	–	Mean inlet velocity	(m/s)
VME	–	Mean exit velocity	(m/s)
VMF	–	Volume mass fraction of the spray	
VSC	–	Viscosity of the fluid	(kg/m s)
WEB	–	Weber number	

References

[1] K. Masters, "The Spray Drying Handbook", 4th Edition (1985), John Wiley & Sons (New York).

[2] J.D.B. McIrvine, "Atomisation of Viscous Liquids with Swirl-Chamber Pressure Nozzles", Ph.D. Thesis, University of Wisconsin, 1957.

[3] W.M. Herring, W.R. Marshall, "Performance of Vaned-Disk Atomisers", A.I.Ch.E.J., Vol. 1 (1955), No. 2, p200.

[4] N. Dombrowski, G. Munday, "Spray Drying", Chapter 16, p209, 'Biochemical and Biological Engineering Science', Vol. 2 (Ed. N. Blakeborough), Academic Press (London), 1968.

[5] J. Chen, V. Kevorkian, "Mass Production of 300 micron Water Droplets by Air-Water Two-Phase Nozzles", Ind. Eng. Chem. Process Design Development, Vol. 7 (168), No. 4, p586.

[6] N. Dombrowski, R.P. Fraser, "A Photographic Investigation into the Disintegration of Liquid Sheets", Phil. Trans. Royal Soc., Series A, Vol. 247 (1954), P101.

[7] N. Dombrowski, P.C. Hooper, "The Effect of Ambient Density on Drop Formation in Sprays", Chem. Eng Sci., Vol. 17 (1962), p291.

[8] R.P. Fraser, P. Eisenklam, N. Dombrowski, D. Hasson, "Drop Formation from Rapidly Moving Liquid Sheets", A.I.Ch.E.J., Vol 8, No. 5 (1962), p672.

[9] N. Dombrowski, P. Eisenklam, R.P. Fraser, "Flow and Disintegration of Thin Sheets of Visco-Elastic Fuels", J. Inst. Fuel, Vol. 30 (1957), p399.

[10] N. Dombrowski, W.E. Johns, "The Aerodynamic Instability and Disintegration of Viscous Liquid Sheet", Chem. Eng. Sci., Vol. 18 (1963), p203.

[11] R.L. Wilcox, R.W. Tate, "Liquid Atomisation in a High Intensity Sound Field", A.I.Ch E.J., Vol. 1 (1965), No. 1, p65.

[12] J. Litsios, "Industrial Application of Gas-Jet Sonic Generators", Inst. Elect. Electron. Eng. Trans. Ultrasonic Eng., No. 9 (1963), p91.

[13] 'Review of the International Chemical and Petrochemical Engineering Exhibition 1966', British Chem. Eng., Vol. 11 (1966), No. 9, p1049.

[14] A.G. Bailey, "Electrostatic Spraying of Liquids", Research Studies Press Ltd (John Wiley & Sons), 1988.

[15] J.H. Chaloud, J.B. Martin, J.S. Baker, "Fundamentals of Spray Drying Detergents", Chem. Eng. Prog., Vol. 53 (1957), No. 12, p593.

[16] C.E. Lapple, C.B. Shepherd, "Calculation of Particle Trajectories", Ind. Eng. Chem., Vol. 32 (1940), No. 5, p605

[17] K. Masters, "A Study of Centrifugal Atomisation and Spray Drying (Parts I & II)", British Chem. Eng., Vol. 13 (1968), No. 1, p88; No. 2, p242

[18] W.E. Ranz, W.R. Marshall, "Evaporation from Drops (Part I)", Chem. Eng. Prog., Vol. 48 (1952), No. 3, p141.

[19] F.A. Gluckert, "A Theoretical Correlation of Spray Dryer Performance", A.I.Ch.E.J., Vol. 8 (1962), No. 3, p460.

[20] S. Katta, W.H. Gauvin, "Some Fundamental Aspects of Spray Drying", A.I.Ch.E.J.,Vol. 21 (1975), No. , p143.

[21] W.H. Gauvin, S. Katta, F.H. Knelman, "Drop Trajectories and Their Importance in the Design of Spray Dryers", Int. J. Multiphase Flow, Vol. 1 (1975), p793.

[22] A.O. Ade-John, G.V. Jeffreys, "Flow Visualisation and Residence Time Studies in a Spray Dryer", Trans I. Ch. E., Vol. 56 (1978), p36.

[23] S. Sharma, "Spray Drier Simulation and Air Flow Pattern Studies", Ph.D Thesis, Aston University, 1990.

[24] N. Frössling, "On the Evaporation of Falling Drops", Beitr. Geophys., Vol. 52 (1938), p170 *(A.E.R.E., Harwell Translation August 1963).*

[25] Q.T. Pham, R.B. Keey, "Some Experiments on the Residence-Time Distribution of Droplets in a Co-Currently worked Spray Chamber", Can. J. Chem. Eng., Vol. 55 (1977), p466.

[26] D.M. Charlesworth, W.R. Marshall, "Evaporation from Drops containing Dissolved Solids", A.I.Ch.E.J., Vol. 6 (1960), No. 1, p9.

[27] T.O.K. Audu, "Studies of the Drying of Particulate Slurries", Ph.D Thesis, Aston University, 1973.

[28] H.H. Ali, "Drying of Droplets", Ph.D Thesis, Aston University, 1985.

[29] S. Akbar, "A Study of the Drying of Single Droplets in Free-Flight", Ph.D Thesis, Aston University, 1988.

[30] T. Audu, G.V. Jeffreys, "The Drying of Drops", Trans. I. Chem. E., Vol. 53 (1975), p165.

[31] J. Dlouhy, W.H. Gauvin, "Heat and Mass Transfer in Spray Drying", A.I.Ch.E.J., Vol. 6 (1960), No. 1, p29.

[32] S. Sharma, C.J. Mumford, E.L. Smith, "Scale-up and Modelling of Spray Drying", I. Chem. E. Annual Research Meeting, University of Nottingham, April 1987.

[33] G.S. Bains, C.J. Mumford, G.V. Jeffreys, "Mechanisms of Drying Particulate Slurries", I. Chem. E. Annual Research Meeting, University of Nottingham, April 1987.

[34] C.J. Stairmand, "Removal of Grit, Dust, and Fume from Exhaust Gases from Chemical Engineering Processes", The Chemical Engineer, No. 194 (1965), CE310.

[35] Business Ratio Report, "The Soap and Detergent Industry", 9th Edition (1988), ICC Information Group Ltd (London).

[36] "Detergents '89", Ed. H. Tilton, Chemical Market Reporter, 30th January 1989.

[37] Keynote Report: An Industry Sector Overview, "Soaps and Detergents", 7th Edition (1990), Keynote Publications Ltd..

[38] A. Davidsohn, B.M. Milwidsky, "Synthetic Detergents" (5th Edition), Leonard Hill (London), 1972.

[39] Internal Communication, Colgate-Palmolive, January 1988.

[40] A. Davidsohn, "Washing Powder Sans Spray Drying", Soap and Chemical Specialties, Vol. 36 (1960), No. 5, p215.

[41] A. Davidsohn, "Non-Spray Dried Wash Powder", Soap and Chemical Specialties, Vol. 36 (1960), No. 6, p151.

[42] M. Principi, C. Damasio, "Dry Granulation in Detergent Field: Comparison between Dry Granulation Plant and Traditional Spray Tower Plant", Comunicaciónes, Jornodos del Comité Español de la Detergencia, Vol. 21 (1990), p15.

[43] B.M. Milwidsky, "Spray Drying Detergents", Soap and Chemical Specialties, Vol. 38 (1962), No. 10, p59.

[44] B.M. Milwidsky, "Liquid Synthetic Detergents", Soap and Chemical Specialties, Vol. 39 (1963), No. 4, p53.

[45] A. Davidsohn, "Spray Drying and Dry Neutralisation of Powdered Detergents", J. American Oil Chemists' Soc., Vol. 55 (1978), p135.

[46] T.O.K. Audu, "Spray Drying Characteristics of Various Detergent Slurry Drops", Tenside Detergents, Vol. 15 (1978), No. 1, p13.

[47] R.A. Mugele, H.D. Evans, "Droplet Size Distribution in Sprays", Ind. Eng. Chem., Vol. 43 (1951), p1317. [33]

[48] S. Nukyama, Y. Tarasawa, "Experiment on the Atomisation of Liquid by means of an Air Stream; Part III: Distribution of the Size of Drops." Trans. Soc. Mech. Engrs. Japan, Vol. 4 (1938), No. 14, p86.

[49] P. Rosin, F. Rammler, "The Laws Governing the Fineness of Powdered Coal", J. Inst. Fuel, Vol. 26 (1953), p20.

[50] Malvern Instruments, "2600 Particle Sizer Manuals", Version 3.0, Oct 1985.

[51] P. Meyer, N. Chigier, "Drop Size Measurements using a Malvern 2200 Particle Sizer", Atomisation and Spray Technology, Vol. 2 (1986), p261.

[52] B.J. Azzopardi, "Drop Size Measurement", Int. J. Heat Mass Transfer, Vol. 22 (1979), p1245.

[53] W.R. Marshall, "Atomisation and Spray Drying", Chem. Eng. Prog. Monograph Series No. 2, Vol. 50 (1954).

[54] D.J. Ryley, "Analysis of a Polydisperse Aqueous Spray from a High-Speed Spinning Disk Atomizer", Br. J. Appl. Phys., Vol. 10 (1959), p180.

[55] J. Weberschinke, V. Vacek, Z. Halounova, "Some Effects of Liquid Atomisation on Distribution of Droplets in a Spray Dryer", Proceedings of 4th International Drying Symposium, Vol. 1, p378. [40]

[56] S.K. Som, "Drop Size Characteristics of the Atomised Spray from a Swirl Nozzle using Newtonian and Time-Dependent, Power Law non-Newtonian Liquids", Drying '84 (Ed. A.S. Mujumdar), McGraw-Hill (1984), p308. [177]

[57] I. Filkova, J. Weberschinke, "Drop Size Prediction of Pseudoplastic Fluids in a Spray Dryer", Drying '84 (Ed. A.S. Mujumdar), McGraw-Hill (1984), p302.

[58] K.R. May, "The Measurement of Airborne Droplets by the Magnesium Oxide Method", J. Scien. Instrum. Vol. 27 (1950), p128.

[59] S. Weinberg, "Heat Transfer to Low Pressure Sprays of Water in a Steam Atmosphere", Proc. Inst. Mech. Engrs., Vol. 1B (1952), p240.

[60] M. Bitron, "Atomisation of Liquids by Supersonic Air Jets", Ind. Eng. Chem., Vol. 47 (1955), p23.

[61] R.L. Pigford, C. Pyle, "Performance Characteristics of Spray-Type Absorption Equipment", Ind. Eng. Chem., Vol. 43 (1951), p1649.

[62] D.W. Lee, "The Effect of Nozzle Design and Operating Conditions on the Atomisation and Distribution of Fuel Sprays", N.A.C.A. Technical Report No. 425 (1932).

[63] R.L. Stoker, "A Method of Determining the Size of Droplets Dispersed in a Gas", J. Appl. Phys. Vol. 17 (1946), p243.

[64] K.R. May, "An 'Ultimate' Cascade Impactor for Aerosol Assessment", J. Scien. Instrum. Vol. 22 (1945), p187.

[65] R.I. Mitchell, J.M. Pilcher, "Measuring Aerosol Particles in Air Pollutants, Commercial Aerosols, Cigarette Smoke", Ind. Eng. Chem., Vol. 51 (1959), p1039.

[66] K.R. May, "The Cascade Impactor: An Instrument for Sampling Coarse Aerosols", J. Aerosol Sci. Vol. 6 (1975), p413.

[67] K.L. De Juhasz, O.F. Zahn, P.H. Schweitzer, "On the Formation and Dispersion of Oil Sprays", Pennsylvania State College, Engineering Experimental Station, Bulletin No. 40 (1932).

[68] J.H. Rupe, "A Technique for the Investigation of Spray Characteristics of Constant Flow Nozzles", Third Symposium on Combustion, Flame and Explosion Phenomena, University of Michigan, 1949.

[69] S.M. Doble,"Design of Spray Nozzles", Engineering, Vol. 159 (1945), p21; p61; p103.

[70] R.W. Tate, "Immersion Sampling of Droplets", A.I.Ch.E.J., Vol. 7 (1961), p574.

[71] W.H. Darnell, "Atomization by Centrifugal Pressure Nozzles", Ph.D. Thesis, University of Wisconsin, Madison, 1953.

[72] R.W. Tate, W.R. Marshall, "Atomisation by Centrifugal Pressure Nozzles", Chem. Eng. Prog., Vol. 49 (1953), No. 4, p169; No. 5, p226.

[73] R. Straus, "The Mechanism of Formation of Liquid Droplets in Sprays", Ph.D Thesis, London University, 1949.

[74] R.P. Fraser, P. Eisenklam, "Liquid Atomisation and the Drop Size of Sprays", Trans. Inst. Chem. Engrs., Vol. 34 (1956), p294.

[75] R.G. Dorman, "The Atomisation of Liquid in a Flat Spray", Br. J. Appl. Phys., Vol. 3 (1952), p189. [60]

[76] P.H. Schweitzer, "Mechanism of Disintegration of Liquid Jets", J. Appl. Phys., Vol. 8 (1937), p513.

[77] B.I. Leonchik, O.L. Danilon, E.K. Tynybekov, "Rapid Method for Determining the Dispersity of Droplets in Pure Liquids", Thermal Eng.,Vol. 17 (1970), No. 6, p101.

[78] C.A.A. van Passer, "Thermal Droplet-Size Measurement using a Thermocouple", Int. J. Heat Mass Transfer, Vol. 17.(1974), p1527.

[79] E.H. Taylor, D.B. Harmon, "Measuring Drop Sizes in Sprays", Ind. Eng. Chem., Vol. 46 (1954), p1455.

[80] P.A. Nelson, W.F. Stevens, "Size Distribution of Droplets from Centrifugal Spray Nozzles", A.I.Ch.E.J., Vol. 7 (1961), No. 1, p80.

[81] J.R. Joyce, "The Atomisation of Liquid Fuels for Combustion", J. Inst. Fuel, Vol. 22 (1949), p150.

[82] D. Hasson, J. Mizrahi, "The Drop Size of Fan Spray Nozzles: Measurements by the Solidifying Wax Method Compared with those obtained by other Sizing Techniques", Trans. Inst. Chem. Engrs., Vol. 39 (1961), p415.

[83] T. Gretzinger, W.R. Marshall, "Characteristics of Pneumatic Atomisers", A.I.Ch.E.J., Vol. 7 (1961), No. , p312.

[84] J.P. Longwell, "Fuel Oil Atomisation", D.Sc. Thesis, Massachusetts Institute of Technology, 1943.

[85] J.R. Joyce, "The Wax Method of Spray Particle-Size Measurement.", Shell Petroleum Co. Report No. I.C.T. 7 *(Reference cited by Joyce [81]).*

[86] H. Clare, A. Radcliffe, "An Air-Blast Atomiser for use with Viscous Fuels", J. Inst. Fuel, Vol. 27 (1954), p510.

[87] G.M. Turner, R.W. Moulton, "Drop-Size Distributions from Spray Nozzles", Chem. Eng. Prog., Vol. 49 (1953), No. 4, p185.

[88] E.F. Goedde, M.C. Yuen, "Experiments on Liquid Jet Instability", J. Fluid Mechanics, Vol. 40 (1970), p495.

[89] D.F. Rutland, G.J. Jameson, "Theoretical Prediction of the Sizes of Drops Formed in the Breakup of Capillary Jets", Chem. Eng. Sci., Vol. 25 (1970), p1689.

[90] F. Ruiz, N. Chigier, "The Mechanics of High Speed Atomisation", Proceedings of the Third International Conference on Liquid Atomisation and Spray Systems (ICLASS-85), London, (1985), Vol. 1, Paper VIB/3.

[91] C.J. Ashton, G.V. Jeffreys, "A Study of the Atomisation of Slurries in Swirl Spray Systems", Unpublished paper.

[92] E. Tyler, "Instability of Liquid Jets", Phil Mag. S. 7, Vol. 16 , No. 105, Suppl. August 1933, p504.

[93] J. Sauter, "Determining Size of Drops in Fuel Mixture of Internal Combustion Engine", Zeitschrift des Vereines deutscher Ingenieure, July 31,1926 *(Translation from N.A.C.A Report No. 390 (1926)).*

[94] R.P. Fraser, N. Dombrowski, J.H. Routley, "The Atomisation of a Liquid Sheet by an Impinging Air Stream", Chem. Eng. Sci., Vol. 18 (1963), p339.

[95] N. Dombrowski, D.L. Wolfsohn, "Measurement of the Surface-Volume Mean Diameter of Sprays", J. Aerosol Science, Vol. 2 (1971), p405.

[96] N. Dombrowski, D.L. Wolfsohn, "The Atomisation of Water by Swirl Spray Pressure Nozzles", Trans. I. Chem. E., Vol. 50 (1972), p259.

[97] G. Mie, "Contributions to the Optics of Turbid Media - Especially Colloidal Metal Solutions", Annin Physik, Vol. 25 (1908), p377 *(Reference cited by Azzopardi [52])*

[98] J. Swithenbank, J.M. Beer, D.S. Taylor, D. Abbot, G.C. McCreath, "A Laser Diagnostic Technique for the Measurement of Droplet and Particle Size Distribution", 'Experimental Diagnostics in Gas Phase Combustion Systems', Progress in Astronautics and Aeronautics (Ed. B. T. Zinn), Vol. 53 (1977).

[99] W.M. Farmer, "Observation of Large Particles with a Laser Interferometer", Appl. Optics, Vol. 13 (1974), p610.

[100] B.J. Thompson, W.R Zinky, "Holographic Detection of Submicron Particles", Appl. Optics, Vol. 7 (1968), p2426.

[101] B.J. Thompson, "Holographic Particle Sizing Techniques", J. Phys. E: Scien. Instrum., Vol. 7 (1974), p781.

[102] J.M. Webster, "A Technique for the size and Velocity Analysis of High-Velocity Droplets and Particles", Br. J. Photography, Vol. 34 (1971), p752.

[103] J.W. Pye, "Droplet Size Distribution in Sprays using a Pulse-Counting Technique", J. Inst. Fuel, Vol. 44 (1971), p253.

[104] C. Ramshaw, "A Technique for Drop-Size Measurement by Direct Photography and Electronic Image Size Analysis", J. Inst. Fuel, Vol 41 (1968), p288.

[105] Seescan Ltd, 'Solitaire Plus' Information Brochure, Cambridge, U.K.

[106] M.V. Klein, 'Optics', Wiley, New York, 1970.

[107] G. Guest, Lodge-Cottrell, Private Communication, Nov 1987.

[108] P.G. Felton, A.A. Hamidi, A.K. Aigal, "Measurement of Drop-size Distribution in Dense Sprays by Laser Diffraction", Proceedings of the Third International Conference on Liquid Atomisation and Spraying Systems (ICLASS-85), London, (1985), Vol. 2, Paper IVA/4.

[109] L.G. Dodge, "Change of Calibration of Diffraction-Based Particle Sizers", Optical Engineering, Vol. 23 (1984), No. 5, p626.

[110] C.E. Lapple, J.P. Henry, D.E. Blake, "Atomisation - A Survey and Critique of the Literature", Report No. AD821.314 (1967), Stanford Research Inst., Menlo Park, USA. [96]

[111] Proceedings of the First International Conference on Liquid Atomisation and Spray Systems (ICLAS '78), Tokyo, Japan (1978).

[112] Proceedings of the Second International Conference on Liquid Atomisation and Spray Systems (ICLASS-82), Madison, Wisconsin (1982).

[113] Proceedings of the Third International Conference on Liquid Atomisation and Spray Systems (ICLASS-85), London, (1985), Vol. 1 & 2.

[114] Lord Rayleigh (J.W. Strutt), "On the Instability of Jets", Proc. London Math. Soc., Vol. 10 (1879), p4.

[115] K.N. Murty, "Quick Estimate of Spray-Nozzle Mean Drop Size", Chem. Engng., Vol. 88 (1981), No. 15, p96.

[116] F. Savart, Ann. Chem, Vol. 53 (1833), p337, *(Reference cited by McCarthy & Molloy [121])*

[117] J.A.F. Plateau, "Statique Experimentale et Theorique des Liquides Soumis aux Seules Forces Molecularies", Paris (1873) *(Reference cited by Rayleigh [114]).*

[118] R.A. Castleman, "Mechanism of Atomisation of Liquids", J. U.S. National Bureau Standards, Vol. 6, RP281 (1931), p369.

[119] C.V. Weber, "Zum Zerfall eines Flussigkeitsstrahles (The Disintegration of Liquid Jets)", Z. Angew Math. Mech., Vol. 11 (1931), p136. [105]

[120] A. Haenlein, "Experiments on Jet Instabilities", Forsh. Gebiete Ingenium Forscungsheft, Vol. 2 (1931), p136 *(Translation from N.A.C.A. Tech. Report No. 659 (1932)).*

[121] M.J. McCarthy, N.A. Molloy, "Review of Stability of Liquid Jets and the Influence of Nozzle Design", Chem. Eng. J., Vol. 7 (1974), p1.

[122] S.W.J. Smith, H. Moss, "Experiments with Mercury Jets", Proc. Royal Soc. Series A, Vol. 93 (1916), p373.

[123] R.P. Grant, S. Middleman, "Newtonian Jet Stability", A.I.Chem.E. Journal, Vol. 12 (1966), p669.

[124] E. Tyler, E.G. Richardson, "The Characteristic Curves of Liquid Jets", Proc. Phys. Soc., Vol. 37 (1925), p297.

[125] R.W. Fenn, S. Middleman, "Newtonian Jet Stability - The Role of Air Resistance", A.I.Ch.E.J., Vol. 15 (1969), No. , p379.

[126] R.E. Phinney, "Stability of a Laminar Viscous Jet - The Influence of the Initial Disturbance Level", A.I.Ch.E.J., Vol. 18 (1972), No. , p432.

[127] R.E. Phinney, "Stability of a Laminar Viscous Jet - The Influence of an Ambient Gas", Physics of Fluids, Vol. 16 (1973), p193.

[128] W. Ohnesorge, "The Formation of Drops at Nozzles and the Disintegration of Fluid Jets", Z.V.D.I., Vol. 81 (1937), p465 *(Translation from J. Royal Aero. Soc., Vol. 48 (1944), p78).*

[129] C.C Miesse, "Correlation of Experimental Data on the Disintegration of Liquid Jets", Ind. Eng. Chem., Vol. 47 (1955), p1690.

[130] D.W. Lee, R.C. Spencer, "Photomicrographic Studies of Fuel Sprays", N.A.C.A. Technical Report No. 454 (1933).

[131] T. Sakai, N. Kito, M. Sato, M.J. Saito, "Transitions between Liquid Disintegration Mechanisms of Orifice-Type Pressure Nozzles", J. Inst. Fuel, Vol. 49 (1976), p398.

[132] H.B. Holroyd, "On the Atomisation of Liquid Jets", J. Franklin Inst., Vol. 215 (1933), p93.

[133] A.C. Merrington, E.G. Richardson, "The Break-up of Liquid Jets", Proc. Phys. Soc. London, Vol. 59 (1947), p1.

[134] J.A. Duffie, W.R. Marshall, "Factors Influencing the Properties of Spray Dried Materials", Part 1, Chem. Eng. Prog., Vol. 49 (1953), p417.

[135] J. MacDonald, Private Communication cited by Marshall [38].

[136] P. La France, "Non-Linear Break-up of a Laminar Liquid Jet", Phys. Fluids, Vol. 18 (1975), p428.

[137] R.J. Donnelly, W. Glaberson, "Experiments on the Capillary Instability of a Liquid Jet", Proc. Royal Soc. Series A, Vol. 290 (1966), p547.

[138] M. Goldin, M.J. Yerushalmi, R. Pfeffer, R. Shinnar, "Break-up of a Laminar Capillary Jet of Viscoelastic Fluid", J. Fluid Mech., Vol. 38 (1969), p689.

[139] M. Goldin, R. Pfeffer, R. Shinnar, "Break-up of a Capillary Jet of a Non-Newtonian Fluid having a Yield Stress", Chem. Eng. J., Vol. 4 (1972), p8.

[140] F.W. Krosser, S. Middleman, "Viscoelastic Jet Stability" A.I.Ch.E.J., Vol. 15 (1969), p383.

[141] M. Gordon, J. Yerushalmi, R. Shinnar, "Instability of Jets of Non-Newtonian Fluids", Trans. Soc. Rheology, Vol. 17 (1973), p303.

[142] L.O. Roth, J.G. Porterfield, "Spray Drop Size Control", Trans. A.S.A.E., Vol. 13 (1970), p779.

[143] T. Sakai, M. Sadakata, M. Saito, N. Hoshino, S. Senuma, "Uniform Size Droplets by Longitudinal Vibration of Newtonian and Non-Newtonian Fluids", Proceedings of the Second International Conference on Liquid Atomisation and Spray Systems (ICLASS-82), Madison, Wisconsin (1982), Paper 2-1.

[144] F.H. Garner, A.H. Nissan, G.F. Wood, "Thermodynamics and Rheological Behaviour of Elastoviscous Systems under Stress", Phil. Trans. Royal Soc. Series A, Vol. 243 (1950), p37.

[145] R.P. Fraser, N. Dombrowski, P. Eisenklam, "Vibrations as a Cause of Disintegration in Liquid Sheets", Nature, Vol. 173 (1954), p495.

[146] C.J. Clark, N. Dombrowski, "An Experimental Study of Thin Liquid Sheets in Hot Atmospheres", J. Fluid Mech., Vol. 64 (1974), p167.

[147] H.B. Squire, "Investigation of the Instability of a Moving Liquid Film", Br. J. Appl. Phys., Vol. 4 (1953), p167.

[148] Lamb, 'Hydrodynamics' 5th Edition (1932), Chapter 9, Cambridge University Press.

[149] W.W. Hagerty, J.F. Shea, "A Study of the Stability of Plane Fluid Sheets", Journal Appl. Mech., Vol 22 (1955), p509.

[150] C.J. Clark, N. Dombrowski, "Aerodynamic Instability and Disintegration of Inviscid Liquid Sheets", Proc. Royal Soc. London, Series A, Vol. 329 (1972), p467.

[151] C.J. Crapper, N. Dombrowski, W.P. Jepson, G.A.D. Pyott, "A Note on the Growth of Kelvin-Helmholtz Waves on Thin Liquid Sheets", J. Fluid Mech., Vol. 57 (1973), p671.

[152] C.J. Crapper, N. Dombrowski, G.A.D. Pyott, "Large Amplitude Kelvin-Helmholtz Waves on Thin Liquid Sheets", Proc. Royal Soc. London, Series A, Vol. 342 (1975), p209.

[153] C.J. Crapper, N. Dombrowski, W.P. Jepson, "Wave Growth on Thin Sheets of Non-Newtonian Liquids", Proc. Royal Soc. London, Series A, Vol. 342 (1975), p225.

[154] D. Weihs, "Stability of Thin Radially Moving Liquid Sheets", J. Fluid Mech., Vol. 87 (1978), p289.

[155] J.L. York, H.E. Stubbs, M.R. Tek, "The Mechanism of Disintegration of Liquid Sheets", Trans. A.S.M.E., Vol. 75 (1953), p1279.

[156] N. Dombrowski, D. Hasson, D.E. Ward, "Some Aspects of Liquid Flow Through Fan Spray Nozzles", Chem. Eng. Sci., Vol. 12 (1960), p35.

[157] G.I. Taylor, "The Dynamics of Thin Sheets of Fluid II - Waves on Fluid Sheets", p351, 'Scientific Papers of G.I. Taylor Vol. 4: Mechanics of Fluids' (Ed. G.K. Batchelor), Cambridge University Press (1971).

[158] F.E.J. Briffa, N. Dombrowski, "Entrainment of Air into a Liquid Spray", A.I.Ch.E.J., Vol. 12 (1966), p708.

[159] T. Arai, H. Hashimoto, "Disintegration of a Thin Liquid Sheet in a Co-Current Gas Stream", Proceedings of the Third International Conference on Liquid Atomisation and Spray Systems (ICLASS-85), London, (1985), Vol. 2, Paper VIB/1.

[160] R.W. Sellens, T.A. Brzustowski, "A Prediction of the Droplet-Size Distribution in a Spray from First Principles", Chem. Physical Processes in Combustion (1984), 17/1.

[161] G.D. Gordon, "Mechanism and Speed of Break-up of Drops", J. Appl. Phys., Vol. 30 (1959), p1759.

[162] E. Giffen, A. Muraszew, "Atomisation of Liquid Fuels", Chapman and Hall (London), 1953.

[163] H. Hayashi, S. Takeda, "Spray Drying Characteristics by a Centrifugal Pressure Nozzle with Large Orifice Diameter", Proc. 4th Int. Drying Symp. (1983), Vol. 1, p384.

[164] S.M. Doble, "Design of Centrifugal Nozzles for Output up to 1800 Gallons per Hour", Proc. Instn. Mech Eng., Vol. 157, (1947), p103.

[165] S.M. Doble, E.M. Halton, "The Application of Cyclone Theories to Centrifugal Spray Nozzles", Proc. Instn. Mech Eng., Vol. 157, (1947), p111.

[166] C.J. Stairmand, "Pressure Drop in Cyclone Separators", Engineering, Vol. 168 (1949), p409.

[167] W.C. Nieukamp, "Flow Analysis of a Hollow Cone Nozzle with Potential Flow Theory", ICLASS-85, Vol. 1, Paper IIIC/1.

[168] P. Sankarankutty, P., Narasimhan, M.V., Narayanaswamy, K., "Measurement of Air Core Size in Swirl Chamber Atomisers", Vol. 1 & Vol. 2, Inst. Petroleum (London), (1975).

[169] G.I. Taylor, "The Mechanics of Swirl Atomisers", p429, 'Scientific Papers of G.I. Taylor Vol. 3: Aerodynamics and the Mechanics of Projectiles and Explosives' (Ed. G.K. Batchelor), Cambridge University Press (1963).

[170] G.I. Taylor, "The Boundary Layer in the Converging Nozzle of a Swirl Atomiser", p522, 'Scientific Papers of G.I. Taylor Vol. 3: Aerodynamics and the Mechanics of Projectiles and Explosives' (Ed. G.K. Batchelor), Cambridge University Press (1963).

[171] C.J. Ashton, "A Study of Liquid Dispersions in a Spray Drying Tower", Ph.D Thesis, Aston University, 1980.

[172] M. Doumas, R. Laster, "Liquid-Film Properties for Centrifugal Pressure Nozzles", Chem. Eng. Prog., Vol. 49 (1953), p518.

[173] A. Radcliffe, "Performance of a Type of Swirl Atomiser", Proc. Instn. Mech. Eng., Vol. 169 (1955), p93.

[174] 'Communications', Proc. Instn. Mech. Eng., Vol. 169 (1955), p101.

[175] M.M. Elkotb, N.M. Rafat, M.A. Hanna, "The Influence of Swirl Atomiser Geometry on the Atomisation Performance", ICLASS-78, p109.

[176] N.K. Rizk, A.H. Lefebvre, "Prediction of Velocity Coefficient and Spray Cone Angle for Simplex Swirl Atomisers", ICLASS-85, Vol. 1, Paper IIIC/2.

[177] N. Dombrowski, D. Hasson, "The Flow Characteristics of Swirl (Centrifugal) Spray Pressure Nozzles with Low Viscosity Liquids", A.I.Ch.E.J., Vol. 15 (1969), p604.

[178] E. Giffen, B.S. Massey, "Some Observations on Flow in Spray Nozzles", Motor Industry Res. Assoc., Report No. 1950/5 (1950).

[179] K. Ranganadha Babu, M.V. Narasimhan, K. Narayanaswamy, "Correlations for Prediction of Discharge Rate, Cone Angle and Air Core Diameter of Swirl Spray Atomisers", ICLASS-82, Paper 3-3.

[180] K. Ranganadha Babu, M.V. Narasimhan, K. Narayanaswamy, "Prediction of Mean Drop Size of Fuel Sprays from Swirl Spray Atomisers", ICLASS-82, Paper 3-4.

[181] K. Ranganadha Babu, M.V. Narasimhan, K. Narayanaswamy, "Design of Swirl Chamber Atomisers", ICLASS-85, Vol. 1, Paper IIIC/3.

[182] Y. Kawase, T. Shirotsuka, "Atomisation of Viscoelastic Fluids", ICLASS-78, Paper 1-4.

[183] M. Nakamura, K. Nagoh, S. Matsumoto, "Spray Characteristics of Detergent Slurry using Swirl Type Pressure Nozzles", ICLASS-85, Vol. 1, Paper VB/1.

[184] T.G. Hodgkinson, "Control by Surface Tension of a Conical Fluid Sheet Jet", Porton Technical Paper No. 174 (1950).

[185] N. Dombrowski, M.A. Tahir, "Atomisation of Oils by Swirl Spray Pressure Nozzles", J. Inst. Fuel, Vol. 59 (1977), p59.

[186] T.A. Johnson, "Atomisation and Spray Drying Tower Simulations", Ph.D Thesis, Bradford University, 1972.

[187] Industrial Spray Products Catalog, 51M, Spraying Systema Co.

[188] SDX Nozzle Technical Instructions, Niro Atomizers Ltd.

[189] N. Dombrowski, D.L. Wolfsohn, "Some Aspects of Spray Formation from Swirl Spray Pressure Nozzles", J. Inst. Fuel, Vol. 54 (1972), p59.

[190] G.I. Taylor, "The Dynamics of Thin Sheets of Fluid III: Disintegration of Fluid Sheets", p368, Scientific Papers of G.I. Taylor, Vol. IV: Mechanics of Fluids (Ed. G.K. Batchelor), Cambridge University Press (1971).

[191] I.I. Novikov, "Atomisation of Liquids by Centrifugal Nozzles", J. Tech. Phys. (Russia), Vol. 18 (1948), p345 *(Translation: Engineers' Digest, Vol. 10 (1949), p72).*

[192] D. Hassan, Communication in R.P.Fraser, P. Eisenklam, "Liquid Atomisation and the Drop Size of Sprays", Trans. Instn. Chem. Eng., Vol. 34 (1956), p294.

[193] R.P. Fraser, P. Eisenklam, N. Dombrowski, "Liquid Atomisation in Chemical Engineering. Part 3: Pressure Nozzles", British Chem. Eng., Vol. 2 (1957), No. 10, p536.

[194] M. M.M. Abou-Ellail, M.M. Elkotb, N.M. Rafat, "Effect of Fuel Pressure, Air Pressure and Air Temperature on Droplet Size Distribution in Hollow-Cone Kerosene Sprays", (ICLAS '78), Tokyo, Japan (1978), Paper 4.2.

[195] N.K. Rizk, A.H. Lefebvre, "Influence of Liquid Properties on the Internal Flow Characteristics of Simplex Swirl Atomisers", Atomisation and Spray Technology, Vol. 2 (1986), p219.

[196] D.B. Spalding, "A General Purpose Computer Program for Multi-Dimensional One- and Two-Phase Flow", Mathematics and Computers in Simulation, Vol. 23 (1981), p267-276.

[197] O. Tietjens, Stromugslehre, Springer Verlag, 1960 *(Reference cited by Nieuwkamp [167]).*

[198] Y.H. Zhao, W.M. Li, S..Chin, "Experimental and Analytical Investigation on the Variation of Spray Characteristics Along the Radial Distance Downstream of a Pressure Swirl Atomizer", Journal Eng. Gas Turbines and Power, Vol. 108 (1986), p473.

[199] R.L. Burden, J.D. Faires, A.C. Reynolds, 'Numerical Analysis', 2nd Edition, Prindle, Weber & Schmidt (Boston), 1981, p40.

[200] Unbound Material, C.A. Sudlow, Ph.D. Thesis "Atomisation of Detergent Slurries", Dept. of Chemical Engineering and Applied Chemistry, Aston University, 1991.

[201] D.L. Wolfsohn, "Atomisation of Viscous Liquids by Swirl Spray Pressure Nozzles", Ph.D Thesis, University of Leeds, 1970.

[202] K.S. Robinson, C.J. Cusley, R.W.K. Allen, "The Spray Droplet Sizer: A Novel Technique for Droplet Size Analysis", A.E.R.E. Technical Report No. AERE-R 10823, March 1984.

[203] E.D. Hirleman, L.G. Dodge, "Performance Comparison of Malvern Instruments Laser Diffraction Drop Size Analyzers", ICLASS-85, Vol. 1, Paper IVA/3.

[204] Q.T. Pham, R.B. Keey, "Evaporation of A Spray in the Jet Zone from a Nozzle Atomiser", Trans. I.Chem.E., Vol. 55 (1977), p114.

[205] 'Handbook of Chemistry and Physics', 64th Edition (1983-1984), Ed. R.C. Weast, C.R.C. Press, Inc., Florida, USA.

[206] M.M.R.M Al Faize, "Mass Transfer Characteristics of Large Oscillating Drops:, Ph.D Thesis, Aston University, 1986.

Appendix 1

Drop-Size Distribution Results

Tables A1.1 to A2.6: Water

Tables A1.7 to A1.12: 5% Sodium Sulphate Solution

Tables A1.13 to A1.18: 10% Sodium Sulphate Solution

Tables A1.19 to A1.24: 15% Sodium Sulphate Solution

Tables A1.25 to A1.30: 23% Calcium Carbonate Slurry

Tables A1.31 to A1.36: 35% Calcium Carbonate Slurry

Tables A1.37 to A1.42: 45% Calcium Carbonate Slurry

Tables A1.43 to A1.47: Detergent Slurry at 40°C

Tables A1.48 to A1.51: Detergent Slurry at 60°C

Tables A1.52 to A1.54: Detergent Slurry at 80°C

Table A1.1: *Drop-Size Distribution Results for Water using the Nozzle AAASSTC5-5*

Pressure	Fluid	Obscuration	Log. Difference	Measured Values		Correction Factors		Corrected Values		Volumetric Flowrate (l/min)	Specific Surface Area (Sq.m/cc)
				X Parameter	N Parameter	X Parameter	N Parameter	X Parameter	N Parameter		
200 psi	Water	0.3130	5.13	150.50	2.31	-	-	-	-	6.16	0.03
		0.2597	5.08	150.81	2.39						0.03
		0.2381	5.08	150.81	2.39						0.03
				150.71	2.36						0.03
400 psi	Water	0.4880	4.66	135.80	2.65	-	-	-	-	8.82	0.03
		0.4426	4.69	135.73	2.66						0.04
		0.4832	4.59	135.73	2.66						0.04
				135.75	2.66						0.04
600 psi	Water	0.5776	4.28	128.80	2.81	-	-	-	-	11.12	0.04
		0.6109	4.40	128.17	2.71						0.04
		0.5733	4.80	128.13	2.82						0.04
				128.37	2.78						0.04
800 psi	Water	0.5884	4.95	137.54	2.88	-	-	-	-	12.76	0.04
		0.6326	4.46	137.13	2.84						0.04
		0.6378	5.04	137.94	2.84						0.04
				137.54	2.85						0.04
1000 psi	Water	0.7276	5.32	156.92	2.45	1.0375	1.1480	162.81	2.81	13.14	0.03
		0.7060	5.43	156.61	2.66	1.0344	1.1549	162.00	3.07		0.03
		0.7070	5.58	155.04	2.39	1.0365	1.1341	160.69	2.71		0.03
				156.19	2.50			161.83	2.86		0.03
1200 psi	Water	0.7053	5.46	201.29	1.86	1.0415	1.0946	209.63	2.04	16.76	0.02
		0.7812	5.73	200.39	1.86	1.0551	1.1204	211.43	2.08		0.02
		0.7427	5.51	200.84	1.89	1.0462	1.1076	210.13	2.09		0.02
				200.84	1.87			210.40	2.07		0.02

Fluid Temperature = 20.0 C Wet Bulb Temperature = 19 C Atmospheric Pressure = 748.6 mm Hg

Absolute Viscosity = 1.002 cP Dry Bulb Temperature = 20 C Air Density = 1.205 kg / Cu. m All Dimensions in microns

Density = 998.23 kg / Cu. m Relative Humidity = 91% Fluid Surface Tension = 72.75 Dynes / cm

Pressure	D(3,2)	D(2,1)	D(1,0)	D(v,0.9)	D(v,0.5)	D(v,0.1)	% > 420.0	% > 201.0	% > 82.7	% < 39.5	% < 10.5
200 psi	88.51	32.56	12.84	211.86	129.81	56.74	0.7	13.3	77.9	4.4	0.3
	95.47	47.60	21.80	210.46	130.77	58.72	0.6	12.9	78.9	4.0	0.2
	95.51	47.65	21.82	210.45	130.79	58.76	0.6	12.9	78.9	4.0	0.2
	93.16	42.60	18.82	210.92	130.46	58.07	0.6	13.0	78.6	4.1	0.2
400 psi	92.42	53.82	27.38	200.06	118.90	57.99	0.1	9.7	76.5	3.7	0.1
	92.54	54.06	27.55	199.87	118.90	58.14	0.0	9.7	76.6	3.7	0.1
	92.54	54.06	27.55	199.87	118.90	58.14	0.0	9.7	76.6	3.7	0.1
	92.50	53.98	27.49	196.93	118.90	58.09	0.0	9.3	76.4	3.7	0.1
600 psi	90.21	55.62	29.41	187.91	113.09	58.21	0.1	7.3	74.9	3.4	0.0
	88.41	52.90	27.53	188.62	111.83	56.19	0.1	7.5	74.6	3.9	0.0
	89.91	55.63	29.50	186.47	112.46	58.08	0.1	7.1	74.6	3.4	0.0
	89.51	54.72	28.81	187.67	112.46	57.49	0.1	7.3	74.7	3.6	0.0
800 psi	98.04	62.98	34.88	199.71	121.65	63.14	0.0	9.6	79.1	2.7	0.1
	97.16	61.86	34.07	199.60	121.09	62.34	0.0	9.6	78.6	2.9	0.1
	97.73	62.15	34.18	200.55	121.77	62.67	0.0	9.9	78.9	2.8	0.1
	97.64	62.33	34.38	199.95	121.50	62.72	0.0	9.7	78.8	2.8	0.1
1000 psi	113.78	70.24	37.04	216.26	143.91	73.62	0.5	15.7	86.2	1.9	0.1
	118.47	80.50	46.67	212.63	144.54	78.43	0.3	14.5	88.2	1.3	0.0
	110.45	66.44	34.52	215.49	141.52	70.39	0.6	15.2	84.8	2.2	0.1
	114.23	72.39	39.41	214.79	143.32	74.15	0.5	15.1	86.4	1.8	0.1
1200 psi	107.48	27.14	10.57	364.95	176.03	69.49	5.2	38.8	86.1	3.3	0.3
	98.34	16.32	6.69	366.45	178.04	71.56	5.3	39.5	86.8	3.0	0.2
	112.98	33.18	12.95	364.17	177.18	71.49	5.2	39.1	86.7	3.0	0.2
	106.27	25.55	10.07	365.19	177.08	70.85	5.2	39.1	86.5	3.1	0.2

Table A1.2: *Drop-Size Distribution Results for Water using the Nozzle AAASSTC8-5*

Pressure	Fluid	Obscuration	Log. Difference	Measured Values		Correction Factors		Corrected Values		Volumetric Flowrate (l/min)	Specific Surface Area (Sq.m/cc)
				X Parameter	N Parameter	X Parameter	N Parameter	X Parameter	N Parameter		
200 psi	Water	0.2628	5.17	162.78	2.31					6.65	0.03
		0.2822	5.21	161.37	2.39	-	-	-	-		0.03
		0.2907	5.05	161.37	2.39						0.03
				161.84	2.36						0.03
400 psi	Water	0.5724	4.91	135.73	2.66					10.88	0.04
		0.5582	4.81	135.86	2.63	-	-	-	-		0.03
		0.5419	4.76	134.45	2.60						0.04
				135.35	2.63						0.04
600 psi	Water	0.6855	4.34	130.30	2.95	1.0321	1.1677	134.75	3.44	13.46	0.04
		0.6998	4.55	130.64	2.90	1.0326	1.1708	134.91	3.40		0.04
		0.6668	4.19	128.82	3.00	1.0318	1.1627	132.92	3.49		0.04
				129.92	2.95			134.19	3.44		0.04
800 psi	Water	0.7094	5.33	163.12	2.39	1.0366	1.1351	169.09	2.71	15.59	0.03
		0.6975	5.24	163.12	2.31	1.0365	1.1246	169.07	2.60		0.03
		0.7282	5.53	162.36	2.39	1.0382	1.1432	168.55	2.73		0.03
				162.87	2.36			168.90	2.68		0.03
1000 psi	Water	0.6493	4.50	133.36	2.74	1.0000	1.0000	133.36	2.74	17.18	0.04
		0.6509	4.29	132.52	2.83	1.0327	1.1447	136.85	3.24		0.04
		0.6382	4.38	132.52	2.81	1.0000	1.0000	132.52	2.83		0.04
				132.80	2.79			134.24	2.94		0.04
1200 psi	Water	0.7007	5.43	202.80	1.94	1.0401	1.0991	210.93	2.13	18.67	0.02
		0.7035	5.39	202.82	1.88	1.0410	1.0956	211.14	2.06		0.02
		0.6717	5.29	202.87	1.92	1.0381	1.0914	210.61	2.10		0.02
				202.83	1.91			210.89	2.10		0.02

Fluid Temperature = 20.0 C | Wet Bulb Temperature = 19 C | Atmospheric Pressure = 748.6 mm Hg

Absolute Viscosity = 1.002 cP | Dry Bulb Temperature = 20 C | Air Density = 1.205 kg / Cu. m | All Dimensions in microns

Density = 998.23 kg / Cu. m | Relative Humidity = 91% | Fluid Surface Tension = 72.75 Dynes / cm

Pressure	D(3,2)	D(2,1)	D(1,0)	D(v,0.9)	D(v,0.5)	D(v,0.1)	% > 420.0	% > 201.0	% > 82.7	% < 39.5	% < 10.5
200 psi	100.61	47.65	21.35	226.13	140.31	61.37	1.2	18.0	81.2	3.7	0.2
	101.89	50.07	22.66	222.28	139.82	62.92	1.0	17.0	81.8	3.4	0.2
	101.85	50.02	22.64	222.31	139.81	62.88	1.0	17.0	81.7	3.4	0.2
	101.45	49.25	22.22	223.57	139.98	62.39	1.1	17.3	81.6	3.5	0.2
400 psi	92.50	53.99	27.50	199.90	118.88	58.09	0.0	9.7	76.6	3.7	0.1
	92.11	53.32	27.04	200.36	118.82	57.64	0.1	9.8	76.3	3.8	0.1
	93.81	61.80	25.03	187.91	115.48	61.05	0.1	7.4	76.8	2.8	0.0
	92.81	56.37	26.52	196.06	117.73	58.93	0.1	9.0	76.6	3.4	0.1
600 psi	104.00	78.64	52.67	188.91	121.82	69.17	0.1	7.5	82.8	1.3	0.0
	103.17	75.78	48.30	189.79	121.80	68.79	0.1	7.7	82.6	1.4	0.0
	103.06	78.57	53.12	183.98	120.46	68.90	0.1	6.7	82.5	1.3	0.0
	103.41	77.66	51.36	187.56	121.36	68.95	0.1	7.3	82.6	1.3	0.0
800 psi	115.97	69.15	35.54	224.18	148.61	74.22	0.9	18.7	86.7	1.9	0.1
	113.63	65.48	33.05	226.27	147.86	71.54	1.1	19.1	85.6	2.3	0.1
	116.03	69.62	35.93	223.27	148.29	74.44	0.9	18.4	86.7	1.9	0.1
	115.21	68.08	34.84	224.57	148.25	73.40	1.0	18.7	86.3	2.0	0.1
1000 psi	92.43	55.41	28.75	196.02	117.21	59.08	0.2	8.9	76.3	3.4	0.0
	102.83	73.29	45.20	195.17	122.75	67.76	0.1	8.7	82.1	1.6	0.0
	93.98	59.97	33.24	193.64	116.99	60.27	0.1	8.4	76.8	3.0	0.0
	96.41	62.89	35.73	194.94	118.98	62.37	0.1	8.7	78.4	2.7	0.0
1200 psi	122.37	49.36	21.01	364.19	178.38	73.21	5.2	39.4	87.3	2.8	0.2
	109.40	28.22	10.97	366.60	177.52	70.73	5.3	39.4	86.5	3.1	0.2
	113.05	32.57	12.67	364.61	177.70	72.02	5.2	39.3	86.9	2.9	0.2
	114.94	36.72	14.88	365.13	177.87	71.99	5.2	39.4	86.9	2.9	0.2

Table A1.3: *Drop-Size Distribution Results for Water using the Nozzle AAASSTC8-8*

Pressure	Fluid	Obscuration	Log. Difference	Measured Values		Correction Factors		Corrected Values		Volumetric Flowrate (l/min)	Specific Surface Area (Sq.m/cc)
				X Parameter	N Parameter	X Parameter	N Parameter	X Parameter	N Parameter		
200 psi	Water	0.3517	5.33	145.71	2.60	-	-	-	-	9.51	0.03
		0.3424	5.31	146.70	2.66						0.03
		0.3279	5.31	146.21	2.66						0.03
				146.21	2.64						0.03
400 psi	Water	0.5586	4.75	137.66	2.66	-	-	-	-	14.23	0.04
		0.5602	4.91	137.94	2.64						0.04
		0.5387	4.92	138.38	2.66						0.03
				137.99	2.65						0.04
600 psi	Water	0.6335	4.40	136.24	3.15	-	-	-	-	18.31	0.04
		0.6333	4.39	136.91	2.95						0.04
		0.6258	4.30	135.40	2.98						0.04
				136.18	3.03						0.04
800 psi	Water	0.5817	4.30	123.85	3.15	-	-	-	-	21.06	0.04
		0.5924	4.20	123.85	3.50						0.04
		0.5828	4.01	122.60	3.33						0.04
				123.43	3.33						0.04
1000 psi	Water	0.5841	5.00	126.43	2.66	-	-	-	-	23.34	0.04
		0.5822	4.34	124.03	2.72						0.04
		0.5798	4.57	124.38	2.82						0.04
				124.95	2.73						0.04
1200 psi	Water	0.6724	5.36	145.91	2.21	1.0360	1.1102	151.17	2.45	29.33	0.03
		0.6866	5.83	144.67	2.30	1.0360	1.1204	149.88	2.58		0.03
		0.6839	5.33	145.15	2.21	1.0365	1.1133	150.45	2.46		0.03
				145.24	2.24			150.50	2.50		0.03

Fluid Temperature = 19.5 C Wet Bulb Temperature = 19 C Atmospheric Pressure = 748.6 mm Hg

Absolute Viscosity = 1.015 cP Dry Bulb Temperature = 20 C Air Density = 1.205 kg / Cu. m All Dimensions in microns

Density = 998.23 kg / Cu. m Relative Humidity = 91% Fluid Surface Tension = 72.75 Dynes / cm

Pressure	D(3,2)	D(2,1)	D(1,0)	D(v,0.9)	D(v,0.5)	D(v,0.1)	% > 420.0	% > 201.0	% > 82.7	% < 39.5	% < 10.5
200 psi	97.71	55.50	27.57	200.72	127.92	61.23	0.2	9.9	79.6	3.3	0.1
	99.45	57.45	28.76	200.97	129.19	62.83	0.2	10.0	80.5	3.0	0.1
	99.18	57.38	28.76	200.33	128.77	62.67	0.2	9.8	80.4	3.0	0.1
	98.78	56.78	28.36	200.67	128.63	62.24	0.2	9.9	80.2	3.1	0.1
400 psi	93.77	54.57	27.71	202.04	120.55	58.91	0.1	10.3	77.3	3.6	0.1
	93.63	54.17	27.42	202.54	120.68	58.68	0.1	10.4	77.2	3.6	0.1
	94.29	54.87	27.84	202.78	121.18	59.27	0.1	10.5	77.6	3.5	0.1
	93.90	54.54	27.66	202.45	120.80	58.95	0.1	10.4	77.4	3.6	0.1
600 psi	101.37	71.29	43.48	195.18	121.88	66.42	0.1	8.7	81.2	1.8	0.0
	98.57	64.37	36.08	198.28	121.48	63.93	0.0	9.3	79.5	2.5	0.1
	98.16	64.42	36.41	196.03	120.36	63.75	0.2	8.9	79.4	2.3	0.0
	99.37	66.69	38.66	196.50	121.24	64.70	0.1	9.0	80.0	2.2	0.0
800 psi	91.67	63.59	37.77	163.80	109.92	61.04	0.1	4.8	75.4	2.6	0.0
	95.65	71.98	47.24	154.81	111.31	65.07	0.1	4.2	78.2	1.7	0.0
	93.14	68.47	43.91	155.26	109.43	62.65	0.1	4.3	76.1	2.2	0.0
	93.49	68.01	42.97	157.96	110.22	62.92	0.1	4.4	76.6	2.2	0.0
1000 psi	86.34	51.08	26.42	186.37	110.37	54.25	0.1	7.1	72.4	4.3	0.0
	85.62	51.97	27.28	179.77	108.92	54.53	0.1	6.2	71.6	4.2	0.0
	87.20	54.25	28.91	177.86	109.64	56.30	0.1	6.0	72.7	3.7	0.0
	86.39	52.43	27.54	181.33	109.64	55.03	0.1	6.4	72.2	4.1	0.0
1200 psi	97.08	49.59	22.88	209.66	131.58	60.24	0.5	12.7	79.7	3.7	0.2
	99.95	56.13	27.63	205.90	131.43	62.58	0.3	11.5	80.7	3.2	0.1
	96.85	49.75	23.01	208.66	131.03	60.17	0.5	12.4	79.6	3.7	0.2
	97.96	51.82	24.51	208.07	131.35	61.00	0.4	12.2	80.0	3.5	0.2

Table A1.4: *Drop-Size Distribution Results for Water using the Nozzle AAASSTC10-10*

Pressure	Fluid	Obscuration	Log. Difference	Measured Values		Correction Factors		Corrected Values		Volumetric Flowrate (l/min)	Specific Surface Area (Sq.m/cc)
				X Parameter	N Parameter	X Parameter	N Parameter	X Parameter	N Parameter		
200 psi	Water	0.3616	5.59	150.81	2.66	–	–	–	–	11.07	0.03
		0.3594	5.62	150.81	2.66						0.03
		0.3196	5.61	152.57	2.66						0.03
				151.40	2.66						0.03
400 psi	Water	0.5934	5.24	138.69	2.45	–	–	–	–	18.10	0.03
		0.6132	5.16	139.04	2.48						0.04
		0.5881	5.29	140.70	2.45						0.03
				139.48	2.46						0.03
600 psi	Water	0.6857	4.95	119.78	2.71	1.0334	1.1497	123.78	3.12	23.15	0.04
		0.6896	4.94	119.14	2.82	1.0328	1.1598	123.05	3.27		0.04
		0.6995	4.95	120.37	2.82	1.0327	1.1436	124.36	3.28		0.04
				119.76	2.78			123.73	3.22		0.04
800 psi	Water	0.7182	4.76	101.02	3.28	1.0311	1.2155	104.17	3.99	27.33	0.05
		0.7008	4.76	101.02	3.28	1.0307	1.2031	104.12	3.95		0.05
		0.7365	4.74	101.41	3.05	1.0334	1.2080	104.80	3.68		0.05
				101.15	3.20			104.36	3.87		0.05
1000 psi	Water	0.8897	5.92	118.94	2.48	1.0730	1.3326	127.62	3.30	31.87	0.04
		0.9298	5.76	117.89	2.64	1.0833	1.4865	127.71	3.92		0.04
		0.8813	5.60	119.98	2.48	1.0698	1.3151	128.36	3.26		0.04
				118.94	2.53			127.90	3.49		0.04
1200 psi	Water	0.9956	5.95	332.24	1.68	1.2322	1.3570	409.40	2.28	41.21	0.02
		0.9958	5.94	339.41	1.57	1.2578	1.3166	426.91	2.07		0.02
		0.9956	6.03	335.99	1.68	1.2322	1.3570	414.02	2.28		0.02
				335.88	1.64			416.78	2.21		0.02

Fluid Temperature = 19.6 C Wet Bulb Temperature = 19 C Atmospheric Pressure = 748.7 mm Hg

Absolute Viscosity = 1.015 cP Dry Bulb Temperature = 20 C Air Density = 1.205 kg / Cu. m All Dimensions in microns

Density = 998.23 kg / Cu. m Relative Humidity = 91% Fluid Surface Tension = 72.75 Dynes / cm

Pressure	D(3,2)	D(2,1)	D(1,0)	D(v,0.9)	D(v,0.5)	D(v,0.1)	% > 420.0	% > 201.0	% > 82.7	% < 39.5	% < 10.5
200 psi	102.11	58.75	29.26	205.72	132.76	64.66	0.3	11.5	81.7	2.8	0.1
	102.11	58.75	29.26	205.72	132.76	64.66	0.3	11.5	81.7	2.8	0.1
	103.31	59.42	29.56	207.63	134.29	65.52	0.3	12.2	82.3	2.7	0.1
	102.51	58.97	29.36	206.36	133.27	64.95	0.3	11.7	81.9	2.8	0.1
400 psi	89.51	46.60	21.86	194.76	120.40	55.37	0.2	8.3	75.6	4.5	0.2
	90.26	47.40	22.30	194.68	120.95	56.04	0.2	8.3	76.0	4.3	0.2
	91.96	47.58	22.19	199.77	124.11	56.95	0.3	9.6	77.0	4.2	0.2
	90.58	47.19	22.12	196.40	121.82	56.12	0.2	8.7	76.2	4.3	0.2
600 psi	91.25	62.85	37.08	165.04	109.72	60.58	0.1	4.9	75.1	2.7	0.0
	92.91	67.66	43.01	157.20	109.63	62.15	0.1	4.6	75.9	2.3	0.0
	93.93	68.44	43.46	160.39	110.95	62.87	0.1	4.6	76.7	2.2	0.0
	92.70	66.32	41.18	160.88	110.10	61.87	0.1	4.7	75.9	2.4	0.0
800 psi	84.32	69.30	51.98	135.03	94.87	58.00	0.0	0.1	66.7	2.0	0.0
	84.05	68.85	51.43	135.09	94.76	57.65	0.0	0.1	66.4	2.1	0.0
	82.46	64.38	44.52	136.40	94.79	55.82	0.0	0.4	65.4	2.7	0.0
	83.61	67.51	49.31	135.51	94.81	57.16	0.0	0.2	66.2	2.3	0.0
1000 psi	96.57	70.27	44.46	173.14	114.54	64.55	0.1	5.5	78.5	1.9	0.0
	102.44	82.37	59.38	155.92	117.15	70.60	0.1	4.3	83.1	0.9	0.0
	96.73	69.89	43.91	176.61	115.14	64.40	0.1	5.9	78.6	2.0	0.0
	98.58	74.18	49.25	168.56	115.61	66.52	0.1	5.2	80.1	1.6	0.0
1200 psi	225.37	106.62	46.13	459.97	321.30	140.18	19.1	79.1	97.0	0.6	0.0
	208.88	84.27	34.62	458.05	315.93	128.77	18.4	76.9	96.0	0.9	0.1
	226.86	107.33	46.40	460.54	322.71	141.31	19.3	79.4	97.1	0.5	0.0
	220.37	99.41	42.38	459.52	319.98	136.75	18.9	78.5	96.7	0.7	0.0

Table A1.5: *Drop-Size Distribution Results for Water using the Nozzle Delevan 2.0SJ*

Pressure	Fluid	Obscuration	Log. Difference	Measured Values		Correction Factors		Corrected Values		Volumetric Flowrate (l/min)	Specific Surface Area (Sq.m/cc)
				X Parameter	N Parameter	X Parameter	N Parameter	X Parameter	N Parameter		
200 psi	Water	0.2812	5.60	138.85	2.39	-	-	-	-	5.91	0.03
		0.2709	5.62	138.95	2.34						0.03
		0.2976	5.60	137.64	2.30						0.03
				138.48	2.34						0.03
400 psi	Water	0.5890	5.33	85.65	2.60	-	-	-	-	8.94	0.06
		0.6026	5.39	86.15	2.60						0.06
		0.6083	5.38	85.15	2.71						0.06
				85.65	2.64						0.06
600 psi	Water	0.8204	4.84	65.00	2.83	1.0458	1.2720	67.98	3.60	10.81	0.08
		0.8188	4.77	63.23	2.93	1.0441	1.2845	66.02	3.76		0.08
		0.8210	4.85	64.39	3.05	1.0429	1.3062	67.15	3.98		0.08
				64.21	2.94			67.05	3.78		0.08
800 psi	Water	0.9221	4.39	56.12	3.03	1.0672	1.5808	59.89	4.79	12.62	0.10
		0.9147	4.86	54.69	3.13	1.0624	1.5812	58.10	4.95		0.10
		0.9194	4.60	56.51	2.82	1.0727	1.5046	60.62	4.24		0.09
				55.77	2.99			59.54	4.66		0.10
1000 psi	Water	0.9553	4.39	51.31	2.83	1.0863	1.6627	55.74	4.71	15.61	0.10
		0.9532	4.40	52.19	2.83	1.0854	1.6522	56.65	4.68		0.10
		0.9532	4.63	54.54	2.54	1.0991	1.5408	59.94	3.91		0.09
				52.68	2.73			57.44	4.43		0.10
1200 psi	Water	0.9715	4.67	48.30	3.01	1.0855	1.8374	52.43	5.53	15.89	0.11
		0.9753	5.10	48.78	2.93	1.0905	1.8230	53.19	5.34		0.11
		0.9750	4.84	46.07	3.05	1.0852	1.8812	50.00	5.74		0.12
				47.72	3.00			51.87	5.54		0.11

Fluid Temperature = 20.5 C Wet Bulb Temperature = 18 C Atmospheric Pressure = 748.7 mm Hg

Absolute Viscosity = 0.990 cP Dry Bulb Temperature = 20 C Air Density = 1.205 kg / Cu. m All Dimensions in microns

Density = 998.23 kg / Cu. m Relative Humidity = 83% Fluid Surface Tension = 72.75 Dynes / cm

Pressure	D(3,2)	D(2,1)	D(1,0)	D(v,0.9)	D(v,0.5)	D(v,0.1)	% > 420.0	% > 201.0	% > 82.7	% < 39.5	% < 10.5
200 psi	88.27	44.91	20.92	196.33	120.01	54.11	0.2	8.7	74.9	4.8	0.3
	81.09	27.89	10.76	197.56	119.66	53.08	0.3	9.1	74.4	5.1	0.3
	79.15	26.32	10.13	197.88	117.33	51.75	0.3	9.2	73.4	5.5	0.3
	82.84	33.04	13.94	197.26	119.00	52.98	0.3	9.0	74.2	5.1	0.3
400 psi	54.34	23.10	9.26	121.78	74.63	36.04	0.0	0.4	40.3	12.5	0.4
	54.67	23.24	9.31	122.62	75.08	36.28	0.0	0.4	40.8	12.3	0.4
	55.35	24.79	10.06	118.83	74.61	37.09	0.0	0.3	39.8	11.7	0.3
	54.79	23.71	9.54	21.08	74.77	36.47	0.0	0.4	40.3	12.2	0.4
600 psi	53.03	41.11	28.10	87.41	61.75	36.65	0.0	0.0	12.4	13.3	0.2
	52.14	41.32	29.00	81.25	60.35	36.58	0.0	0.0	9.0	13.5	0.0
	54.08	44.47	33.10	81.73	61.60	38.28	0.0	0.0	9.4	11.4	0.0
	53.08	42.30	30.07	83.46	61.23	37.17	0.0	0.0	10.3	12.7	0.1
800 psi	50.69	44.82	37.58	73.68	55.51	36.72	0.0	0.0	1.0	12.4	0.0
	49.53	44.12	37.46	71.77	54.20	36.02	0.0	0.0	0.5	13.4	0.0
	49.70	42.00	32.67	75.01	55.66	34.86	0.0	0.0	2.2	14.7	0.1
	49.97	43.65	35.90	73.49	55.12	35.87	0.0	0.0	1.2	13.5	0.0
1000 psi	46.89	40.91	33.42	68.80	51.88	33.75	0.0	0.0	0.3	17.5	0.0
	47.59	41.44	33.75	70.39	52.73	34.17	0.0	0.0	0.4	16.5	0.0
	47.94	38.79	28.11	75.11	54.76	33.14	0.0	0.0	2.7	17.5	0.1
	47.47	40.38	31.76	71.43	53.12	33.69	0.0	0.0	1.1	17.2	0.0
1200 psi	45.55	41.71	36.76	60.13	49.16	33.97	0.0	0.0	0.2	18.3	0.0
	45.94	41.80	36.51	61.18	49.72	34.00	0.0	0.0	0.2	18.0	0.0
	43.69	40.08	35.37	57.82	47.06	33.61	0.0	0.0	0.0	22.2	0.0
	45.06	41.20	36.21	59.71	48.65	33.86	0.0	0.0	0.1	19.5	0.0

Table A1.6: *Drop-Size Distribution Results for Water using the Nozzle Delevan 2.2SJ*

Pressure	Fluid	Obscuration	Log. Difference	Measured Values		Correction Factors		Corrected Values		Volumetric Flowrate (l/min)	Specific Surface Area (Sq.m/cc)
				X Parameter	N Parameter	X Parameter	N Parameter	X Parameter	N Parameter		
200 psi	Water	0.3482	5.75	132.86	2.14	–	–	–	–	6.77	0.03
		0.3189	5.81	132.59	2.39						0.03
		0.3417	5.76	133.13	2.15						0.03
				132.86	2.23						0.03
400 psi	Water	0.6404	5.44	82.74	2.42	–	–	–	–	9.88	0.05
		0.6458	5.46	82.88	2.42						0.06
		0.6410	5.43	81.32	2.42						0.06
				82.27	2.42						0.06
600 psi	Water	0.8540	4.89	60.15	2.82	1.0532	1.3273	63.35	3.74	12.67	0.09
		0.8640	4.84	58.23	2.52	1.0628	1.2905	61.89	3.25		0.09
		0.8531	5.04	59.59	2.60	1.0576	1.2861	63.02	3.34		0.08
				59.32	2.65			62.75	3.44		0.09
800 psi	Water	0.9451	4.80	47.48	2.80	1.0833	1.6022	51.43	4.49	14.77	0.10
		0.9446	4.83	47.40	2.81	1.0826	1.6036	51.32	4.51		0.11
		0.9556	4.85	45.14	2.80	1.0881	1.6571	49.12	4.64		0.12
				46.67	2.80			50.62	4.55		0.11
1000 psi	Water	0.9786	4.74	39.79	3.05	1.0867	1.9069	43.24	5.82	17.74	0.13
		0.9779	4.75	40.48	3.10	1.0844	1.9282	43.89	5.98		0.11
		0.9734	4.87	40.24	3.36	1.0736	2.0318	43.20	6.83		0.14
				40.17	3.17			43.44	6.21		0.13
1200 psi	Water	0.9864	4.70	37.88	2.93	1.0954	1.8990	41.49	5.56	18.72	0.14
		0.9894	5.00	36.43	3.64	1.0699	2.3565	38.97	8.58		0.14
		0.9872	5.06	36.91	3.64	1.0692	2.3318	39.47	8.49		0.14
				37.07	3.40			39.98	7.54		0.15

Fluid Temperature = 20.5 C Wet Bulb Temperature = 18 C Atmospheric Pressure = 748.7 mm Hg

Absolute Viscosity = 0.990 cP Dry Bulb Temperature = 20 C Air Density = 1.205 kg / Cu. m All Dimensions in microns

Density = 998.23 kg / Cu. m Relative Humidity = 83% Fluid Surface Tension = 72.75 Dynes / cm

Pressure	D(3,2)	D(2,1)	D(1,0)	D(v,0.9)	D(v,0.5)	D(v,0.1)	% > 420.0	% > 201.0	% > 82.7	% < 39.5	% < 10.5
200 psi	72.45	22.02	8.53	195.78	111.95	46.44	0.4	8.7	69.6	7.2	0.4
	71.92	16.86	6.38	189.23	113.74	51.75	0.2	7.0	72.4	5.4	0.3
	72.90	22.29	8.63	195.79	112.29	46.81	0.4	8.7	69.8	7.0	0.5
	72.42	20.39	7.85	193.60	112.66	48.33	0.3	8.1	70.6	6.5	0.4
400 psi	50.45	20.15	8.05	119.74	71.28	32.65	0.0	0.5	37.0	15.4	0.6
	50.53	20.17	8.05	120.02	71.40	32.71	0.0	0.5	37.1	15.3	0.6
	49.69	19.96	8.00	116.69	70.02	32.09	0.0	0.2	35.6	15.7	0.5
	50.22	20.09	8.03	118.82	70.90	32.48	0.0	0.4	36.6	15.5	0.6
600 psi	49.98	39.61	27.87	77.82	57.97	34.06	0.0	0.0	6.1	15.4	0.1
	42.91	28.12	16.93	78.72	55.37	30.97	0.0	0.0	7.2	20.7	0.2
	43.99	28.84	17.24	79.63	56.57	32.14	0.0	0.0	7.9	18.9	0.3
	45.63	32.19	20.68	78.72	56.64	32.39	0.0	0.0	7.1	18.3	0.2
800 psi	42.84	37.22	30.30	60.92	47.65	31.43	0.0	0.0	0.2	25.9	0.1
	42.79	37.22	30.35	60.74	47.57	31.44	0.0	0.0	0.2	26.0	0.1
	41.23	36.20	29.96	58.22	45.73	30.17	0.0	0.0	0.1	30.0	0.1
	42.29	36.88	30.20	59.96	46.98	31.01	0.0	0.0	0.2	27.3	0.1
1000 psi	37.95	35.13	31.65	49.62	40.95	28.84	0.0	0.0	0.0	43.8	0.0
	38.67	35.86	32.36	51.14	41.67	29.96	0.0	0.0	0.0	40.4	0.0
	38.71	36.42	33.49	48.36	41.44	31.46	0.0	0.0	0.0	40.8	0.0
	38.44	35.80	32.50	49.71	41.35	30.09	0.0	0.0	0.0	41.7	0.0
1200 psi	36.07	33.05	29.17	47.45	38.86	26.94	0.0	0.0	0.0	53.6	0.1
	35.95	34.57	32.94	45.37	36.66	29.58	0.0	0.0	0.0	65.3	0.0
	36.36	35.01	33.36	44.81	37.66	30.20	0.0	0.0	0.0	62.8	0.0
	36.13	24.21	31.82	45.88	37.73	28.91	0.0	0.0	0.0	60.6	0.0

Table A1.7: *Drop-Size Distribution Results for 5% Sodium Sulphate Solution using the Nozzle AAASSTC5-5*

Pressure	Fluid	Obscuration	Log. Difference	Measured Values		Correction Factors		Corrected Values		Volumetric Flowrate (l/min)	Specific Surface Area (Sq. m/cc)
				X Parameter	N Parameter	X Parameter	N Parameter	X Parameter	N Parameter		
400 psi	5% NaSO4	0.4896	5.05	138.32	2.45	–	–	–	–	8.52	0.04
		0.4888	4.67	139.54	2.39						0.03
		0.4841	4.88	138.93	2.41						0.03
				138.93	2.42						0.03
600 psi	5% NaSO4	0.5241	4.88	136.75	2.62	–	–	–	–	9.97	0.03
		0.5226	4.68	136.24	2.84						0.04
		0.5289	4.80	137.01	2.71						0.04
				136.67	2.72						0.04
800 psi	5% NaSO4	0.5398	4.75	126.12	2.82	–	–	–	–	12.41	0.04
		0.5318	4.56	126.12	2.82						0.04
		0.5334	4.77	125.36	2.93						0.04
				125.87	2.86						0.04
1000 psi	5% NaSO4	0.5662	4.86	128.39	2.62	–	–	–	–	13.85	0.04
		0.5823	4.80	128.17	2.62						0.04
		0.5652	4.93	127.43	2.80						0.04
				128.00	2.68						0.04
1200 psi	5% NaSO4	0.5993	5.04	127.55	2.55	–	–	–	–	14.91	0.03
		0.5856	4.93	126.11	2.52						0.04
		0.5875	4.93	128.43	2.45						0.04
				127.36	2.51						0.04

All Dimensions in microns

Fluid Temperature = 19.9 C | Wet Bulb Temperature = 15 C | Atmospheric Pressure = 749.8 mm Hg

Absolute Viscosity = 1.163 cP | Dry Bulb Temperature = 19 C | Air Density = 1.209 kg / Cu. m

Density = 1043.6 kg / Cu. m | Relative Humidity = 65% | Fluid Surface Tension = 73.77 Dynes / cm

Pressure	D(3,2)	D(2,1)	D(1,0)	D(v,0.9)	D(v,0.5)	D(v,0.1)	% > 420.0	% > 201.0	% > 82.7	% < 39.5	% < 10.5
400 psi	89.20	46.40	21.77	194.37	120.02	55.14	0.2	8.2	75.4	4.5	0.2
	88.68	45.07	20.97	197.19	120.66	54.37	0.3	9.0	75.2	4.8	0.2
	88.74	45.47	21.22	196.00	120.26	54.56	0.2	8.6	75.2	4.7	0.2
	88.87	45.65	21.32	195.85	120.31	54.69	0.2	8.6	75.3	4.7	0.2
600 psi	92.51	53.32	26.96	201.46	119.53	57.83	0.1	10.1	76.6	3.8	0.1
	96.54	61.54	33.94	198.53	120.34	61.96	0.0	9.3	78.2	2.9	0.1
	94.24	55.76	28.58	200.78	120.33	59.61	0.0	9.9	77.6	3.4	0.1
	94.43	56.87	29.83	200.26	120.07	59.80	0.0	9.8	77.5	3.4	0.1
800 psi	88.43	54.93	29.21	182.01	111.01	57.15	0.1	6.5	73.6	3.6	0.0
	88.43	54.93	29.21	182.01	111.01	57.15	0.1	6.5	73.6	3.6	0.0
	90.11	59.57	33.97	177.15	110.34	58.57	0.1	5.9	74.3	3.2	0.0
	88.99	56.48	30.80	180.39	110.79	57.62	0.1	6.3	73.8	3.5	0.0
1000 psi	86.33	48.39	23.72	190.44	111.74	54.43	0.2	7.8	73.0	4.3	0.1
	86.19	48.31	23.68	190.09	111.56	54.34	0.1	7.7	72.9	4.4	0.1
	89.13	54.87	29.01	185.51	111.65	57.42	0.1	7.0	74.1	3.6	0.0
	87.22	50.52	25.47	188.68	111.65	55.40	0.1	7.5	73.3	4.1	0.1
1200 psi	84.52	46.18	22.34	190.39	110.67	52.80	0.2	7.8	71.9	4.8	0.1
	83.07	45.06	21.77	188.66	109.33	51.65	0.2	7.5	70.9	5.1	0.1
	83.25	43.93	20.96	193.52	110.77	51.27	0.2	8.3	71.2	5.3	0.2
	83.61	45.06	21.69	190.86	110.26	51.91	0.2	7.9	71.3	5.1	0.1

Table A1.8: *Drop-Size Distribution Results for 5% Sodium Sulphate Solution using the Nozzle AAASSTC8-5*

Pressure	Fluid	Obscuration	Log. Difference	Measured Values		Correction Factors		Corrected Values		Volumetric Flowrate (l/min)	Specific Surface Area (Sq. m/cc)
				X Parameter	N Parameter	X Parameter	N Parameter	X Parameter	N Parameter		
400 psi	5% NaSO4	0.5585	4.91	138.59	2.27						0.03
		0.5714	5.27	137.77	2.18	–	–	–	–	11.02	0.03
		0.6035	4.65	136.14	2.00						0.03
				137.50	2.15						0.03
600 psi	5% NaSO4	0.6720	4.85	136.12	2.45	1.0345	1.1262	140.82	2.76		0.03
		0.6749	4.78	137.35	2.67	1.0334	1.1462	141.93	3.05	13.07	0.03
		0.6627	4.81	136.94	2.60	1.0336	1.1334	141.54	2.95		0.03
				136.80	2.57			141.43	2.92		0.03
800 psi	5% NaSO4	0.6810	4.51	131.23	2.62	1.0338	1.1413	135.66	2.99		0.04
		0.6727	4.58	130.41	2.62	1.0336	1.1382	134.79	2.98	15.41	0.04
		0.6798	4.36	130.15	2.71	1.0332	1.1473	134.48	3.11		0.04
				130.60	2.65			134.98	3.03		0.04
1000 psi	5% NaSO4	0.6610	4.62	129.13	2.44	1.0344	1.1223	133.57	2.74		0.04
		0.6567	4.69	127.15	2.58	1.0337	1.1302	131.43	2.92	17.32	0.04
		0.6651	4.54	128.39	2.62	1.0335	1.1356	132.69	2.98		0.04
				128.22	2.55			132.56	2.88		0.04
1200 psi	5% NaSO4	0.6659	4.67	122.37	2.56	1.0338	1.1318	126.51	2.90		0.04
		0.6466	4.47	122.23	2.57	1.0000	1.0000	122.23	2.57	18.15	0.04
		0.6761	4.46	122.64	2.53	1.0342	1.1331	126.83	2.87		0.04
				122.41	2.55			125.19	2.78		0.04

All Dimensions in microns

Fluid Temperature = 20.1 C

Wet Bulb Temperature = 15 C

Atmospheric Pressure = 749.8 mm Hg

Absolute Viscosity = 1.163 cP

Dry Bulb Temperature = 19 C

Air Density = 1.209 kg / Cu. m

Density = 1043.6 kg / Cu. m

Relative Humidity = 65%

Fluid Surface Tension = 73.77 Dynes / cm

Pressure	D(3,2)	D(2,1)	D(1,0)	D(v,0.9)	D(v,0.5)	D(v,0.1)	% > 420.0	% > 201.0	% > 82.7	% < 39.5	% < 10.5
400 psi	78.85	25.63	9.86	199.74	117.89	51.44	0.3	9.7	73.4	5.6	0.4
	75.99	23.37	9.02	200.88	116.44	49.08	0.4	10.0	72.0	6.3	0.4
	70.39	19.77	7.75	203.91	113.36	44.22	0.6	10.7	69.2	8.1	0.6
	75.08	22.92	8.88	201.51	115.90	48.25	0.4	10.1	71.5	6.7	0.5
600 psi	97.72	58.59	30.26	204.33	123.77	62.23	0.1	11.0	79.5	2.9	0.1
	104.27	71.46	42.50	203.27	125.97	67.40	0.0	10.7	82.2	2.0	0.0
	101.88	66.15	36.81	203.56	125.21	65.83	0.0	10.8	81.2	2.3	0.1
	101.29	65.40	36.52	203.72	124.98	65.15	0.0	10.8	81.0	2.4	0.1
800 psi	98.48	64.76	36.65	196.29	120.63	64.00	0.2	9.0	79.5	2.3	0.0
	97.46	64.29	36.35	195.16	119.83	63.49	0.1	8.7	79.1	2.4	0.0
	99.57	69.66	42.36	192.89	120.20	65.15	0.1	8.2	80.1	2.0	0.0
	98.51	67.24	38.45	194.78	120.22	64.21	0.1	8.6	79.6	2.2	0.0
1000 psi	92.52	55.40	28.72	196.32	117.39	59.13	0.2	9.0	76.3	3.4	0.0
	94.28	61.66	34.73	190.71	116.44	61.15	0.1	7.8	77.1	2.8	0.0
	95.98	63.47	36.01	191.94	117.96	62.60	0.1	8.1	78.2	2.5	0.0
	94.26	60.18	33.15	192.99	117.26	60.96	0.1	8.3	77.2	2.9	0.0
1200 psi	90.53	59.34	33.60	180.88	111.30	58.63	0.1	6.3	74.6	3.2	0.0
	81.51	45.19	22.13	179.98	106.39	50.93	0.1	6.3	69.4	5.2	0.1
	89.76	56.57	30.46	182.35	111.45	58.30	0.1	6.5	74.5	3.3	0.0
	87.27	53.70	28.73	181.07	109.71	55.95	0.1	6.4	72.8	3.9	0.0

Table A1.9: *Drop-Size Distribution Results for 5% Sodium Sulphate Solution using the Nozzle AAASSTC8-8*

Pressure	Fluid	Obscuration	Log. Difference	Measured Values		Correction Factors		Corrected Values		Volumetric Flowrate (l/min)	Specific Surface Area (Sq. m/cc)
				X Parameter	N Parameter	X Parameter	N Parameter	X Parameter	N Parameter		
400 psi	5% NaSO4	0.5047	4.96	144.24	2.39					13.30	0.03
		0.5236	5.01	144.24	2.31	–	–	–	–		0.03
		0.5361	5.06	146.43	2.39						0.03
				144.97	2.36						0.03
600 psi	5% NaSO4	0.5932	4.68	130.71	2.62					17.00	0.04
		0.5923	4.74	128.17	2.81	–	–	–	–		0.04
		0.6055	4.80	129.66	2.64						0.04
				129.51	2.69						0.04
800 psi	5% NaSO4	0.5856	4.76	120.37	2.70					19.83	0.04
		0.6221	4.83	121.48	2.78	–	–	–	–		0.04
		0.5849	4.85	120.37	2.70						0.04
				120.74	2.73						0.04
1000 psi	5% NaSO4	0.5672	5.12	117.07	2.55					23.00	0.04
		0.6164	4.91	116.51	2.50	–	–	–	–		0.04
		0.5870	4.97	115.40	2.66						0.04
				116.33	2.57						0.04
1200 psi	5% NaSO4	0.7141	5.56	130.28	2.39	1.0370	1.1370	135.10	2.72	24.39	0.04
		0.7225	4.82	129.44	2.25	1.0390	1.1292	134.49	2.54		0.04
		0.7322	5.93	129.34	2.15	1.0411	1.1250	134.66	2.42		0.03
				129.69	2.26			134.75	2.56		0.04

All Dimensions in microns

Fluid Temperature = 20.0 C

Absolute Viscosity = 1.163 cP

Density = 1043.6 kg / Cu. m

Wet Bulb Temperature = 15 C

Dry Bulb Temperature = 19 C

Relative Humidity = 65%

Atmospheric Pressure = 750.6 mmHg

Air Density = 1.209 kg / Cu. m

Fluid Surface Tension = 73.77 Dynes / cm

Pressure	D(3,2)	D(2,1)	D(1,0)	D(v,0.9)	D(v,0.5)	D(v,0.1)	% > 420.0	% > 201.0	% > 82.7	% < 39.5	% < 10.5
400 psi	91.49	46.14	21.32	202.90	124.97	56.18	0.4	10.6	76.8	4.4	0.2
	83.22	27.89	10.74	204.63	124.26	54.40	0.5	11.0	75.9	4.9	0.3
	92.80	46.63	21.48	205.47	126.93	57.02	0.4	11.3	77.5	4.3	0.2
	89.17	40.22	17.85	204.33	125.39	55.87	0.4	11.0	76.7	4.5	0.2
600 psi	88.59	51.43	26.24	194.08	113.82	55.30	0.2	8.5	74.2	4.1	0.0
	89.78	55.39	29.31	186.74	112.44	57.93	0.1	7.2	74.6	3.5	0.0
	88.25	51.65	26.50	192.24	112.86	55.22	0.2	8.1	74.9	4.1	0.0
	88.87	52.82	27.35	191.02	113.04	56.15	0.2	7.9	74.6	3.9	0.0
800 psi	82.80	50.19	26.40	170.34	105.86	52.43	0.1	5.3	69.4	4.7	0.1
	84.70	52.40	27.88	170.70	107.15	54.31	0.1	5.3	70.8	4.2	0.0
	82.80	50.19	26.40	170.34	105.86	52.43	0.1	5.3	69.4	4.7	0.1
	83.43	50.93	26.89	170.46	106.29	53.06	0.1	5.3	69.9	4.5	0.1
1000 psi	77.69	43.49	21.38	166.01	101.81	48.43	0.1	5.0	66.3	6.0	0.2
	73.13	31.71	13.00	166.65	101.03	47.36	0.1	5.1	65.5	6.4	0.2
	78.29	45.36	22.78	155.70	100.91	49.52	0.1	4.6	66.3	5.5	0.1
	76.37	40.19	19.05	162.79	101.25	48.44	0.1	4.9	66.0	6.0	0.2
1200 psi	93.19	55.38	28.52	198.52	118.72	58.96	0.2	9.5	77.1	3.3	0.0
	88.78	47.82	22.87	199.89	116.95	55.38	0.1	9.7	74.8	4.4	0.2
	86.36	44.73	21.04	190.22	116.23	53.10	0.2	7.2	73.6	5.0	0.3
	89.44	49.31	24.14	196.21	117.30	55.81	0.2	8.8	75.2	4.2	0.2

Table A1.10: *Drop-Size Distribution Results for 5% Sodium Sulphate Solution using the Nozzle AAASSTC10-10*

Pressure	Fluid	Obscuration	Log. Difference	Measured Values		Correction Factors		Corrected Values		Volumetric Flowrate (l/min)	Specific Surface Area (Sq. m/cc)
				X Parameter	N Parameter	X Parameter	N Parameter	X Parameter	N Parameter		
400 psi	5% NaSO4	0.4988	5.29	151.80	2.22	–	–	–	–	17.96	0.03
		0.4923	5.18	150.81	2.39						0.03
		0.4869	5.20	152.79	2.15						0.03
				151.80	2.25						0.03
600 psi	5% NaSO4	0.6276	5.09	134.29	2.19	–	–	–	–	22.70	0.03
		0.6247	5.16	132.56	2.35						0.04
		0.6183	5.05	133.76	2.42						0.03
				133.54	2.32						0.03
800 psi	5% NaSO4	0.6499	5.05	121.44	2.60	–	–	–	–	26.47	0.04
		0.6448	5.04	122.04	2.66						0.04
		0.6259	4.82	122.64	2.36						0.04
				122.04	2.54						0.04
1000 psi	5% NaSO4	0.6471	5.11	103.74	2.55	–	–	–	–	29.46	0.04
		0.6366	4.99	101.56	2.55						0.05
		0.6476	4.89	103.93	2.55						0.05
				103.08	2.55						0.05
1200 psi	5% NaSO4	0.7382	5.42	103.15	2.26	1.0406	1.1368	107.34	2.57	32.58	0.04
		0.6889	5.42	103.15	2.28	1.0363	1.1197	106.89	2.55		0.06
		0.6772	5.02	104.99	2.55	1.0341	1.1349	108.57	2.89		0.04
				103.76	2.36			107.60	2.67		0.05

All Dimensions in microns

Fluid Temperature = 19.8 C

Wet Bulb Temperature = 15 C

Atmospheric Pressure = 749.9 mm Hg

Absolute Viscosity = 1.163 cP

Dry Bulb Temperature = 19 C

Air Density = 1.209 kg / Cu. m

Density = 1043.6 kg / Cu. m

Relative Humidity = 65%

Fluid Surface Tension = 73.77 Dynes / cm

Pressure	D(3,2)	D(2,1)	D(1,0)	D(v,0.9)	D(v,0.5)	D(v,0.1)	% > 420.0	% > 201.0	% > 82.7	% < 39.5	% < 10.5
400 psi	84.59	26.15	10.05	215.61	130.09	55.03	0.9	14.3	77.2	4.9	0.3
	95.47	47.60	21.80	210.46	130.77	58.72	0.6	12.9	78.9	4.0	0.2
	82.92	24.36	9.39	218.81	130.24	53.61	1.0	15.2	76.6	5.3	0.4
	85.66	32.70	13.75	214.96	130.37	55.79	0.8	14.1	77.6	4.7	0.3
600 psi	74.45	23.18	8.95	196.26	113.60	48.07	0.3	8.8	70.8	6.6	0.5
	77.65	26.90	10.38	190.14	113.41	50.88	0.2	7.3	71.9	5.6	0.3
	85.51	44.50	20.96	190.21	114.94	52.79	0.2	7.2	73.2	5.1	0.3
	79.20	31.53	13.43	192.20	113.98	50.58	0.2	7.8	72.0	5.8	0.4
800 psi	81.30	45.75	22.52	177.19	105.88	51.11	0.1	5.9	69.3	5.1	0.1
	82.67	47.49	23.63	176.75	107.01	52.49	0.1	5.9	70.0	4.7	0.1
	72.28	25.34	9.81	186.41	105.42	47.26	0.2	7.1	67.4	6.6	0.3
	78.75	39.53	18.65	180.12	106.10	50.29	0.1	6.3	68.9	5.5	0.2
1000 psi	64.70	26.17	10.33	140.97	89.92	42.92	0.1	2.5	57.1	8.1	0.3
	63.34	25.66	10.13	138.41	88.00	42.02	0.1	2.2	55.4	8.5	0.3
	64.82	26.22	10.35	141.19	90.09	43.00	0.1	2.6	57.3	8.1	0.3
	64.29	26.02	10.27	140.19	89.34	42.65	0.1	2.4	56.6	8.2	0.3
1200 psi	68.68	31.31	13.05	145.03	93.22	44.72	0.1	3.0	60.0	7.3	0.2
	66.68	26.99	10.66	144.85	92.72	44.23	0.1	3.1	59.5	7.5	0.3
	77.23	50.09	27.82	141.70	96.67	49.82	0.1	2.3	63.2	5.2	0.1
	70.86	36.13	17.18	143.86	94.20	46.26	0.1	2.8	64.2	6.7	0.2

Table A1.11: *Drop-Size Distribution Results for 5% Sodium Sulphate Solution using the Nozzle Delevan 2.0SJ*

Pressure	Fluid	Obscuration	Log. Difference	Measured Values		Correction Factors		Corrected Values		Volumetric Flowrate (l/min)	Specific Surface Area (Sq. m/cc)
				X Parameter	N Parameter	X Parameter	N Parameter	X Parameter	N Parameter		
400 psi	5% NaSO4	0.5345	5.43	90.75	2.25					9.13	0.05
		0.5379	5.47	91.64	2.25	-	-	-	-		0.05
		0.5252	5.56	93.18	2.15						0.05
				91.86	2.22						0.05
600 psi	5% NaSO4	0.7649	5.45	70.74	2.25	1.0445	1.1496	73.89	2.59	10.02	0.07
		0.7862	5.44	68.08	2.25	1.0484	1.1631	71.38	2.62		0.07
		0.7963	5.50	69.41	2.18	1.0519	1.1626	73.02	2.53		0.07
				69.41	2.23			72.76	2.58		0.07
800 psi	5% NaSO4	0.9105	5.56	57.81	2.36	1.0866	1.3518	62.82	3.19	11.74	0.08
		0.9078	5.58	57.81	2.36	1.0853	1.3454	62.74	3.18		0.08
		0.8983	5.55	57.94	2.25	1.0857	1.2997	62.91	2.92		0.08
				57.85	2.32			62.82	3.10		0.08
1000 psi	5% NaSO4	0.9484	5.82	53.25	2.38	1.1055	1.4664	58.87	3.49	12.53	0.06
		0.9268	5.68	54.15	2.34	1.0958	1.3881	59.34	3.25		0.09
		0.9354	5.68	52.35	2.42	1.0961	1.4368	57.38	3.48		0.09
				53.25	2.38			58.53	3.41		0.08
1200 psi	5% NaSO4	0.9518	5.76	48.30	2.52	1.0994	1.5279	53.10	3.85	13.37	0.10
		0.9509	5.74	48.82	2.54	1.0979	1.5316	53.60	3.89		0.10
		0.9562	5.79	46.40	2.82	1.0871	1.6632	50.44	4.69		0.11
				47.84	2.63			52.38	4.14		0.10

All Dimensions in microns

Fluid Temperature = 19.9 C

Absolute Viscosity = 1.163 cP

Density = 1043.6 kg / Cu. m

Wet Bulb Temperature = 15 C

Dry Bulb Temperature = 19 C

Relative Humidity = 65%

Atmospheric Pressure = 749.9 mm Hg

Air Density = 1.209 kg / Cu. m

Fluid Surface Tension = 73.77 Dynes / cm

Pressure	D(3,2)	D(2,1)	D(1,0)	D(v,0.9)	D(v,0.5)	D(v,0.1)	% > 420.0	% > 201.0	% > 82.7	% < 39.5	% < 10.5
400 psi	52.61	19.15	7.59	130.19	77.07	33.40	0.0	1.5	44.5	14.2	0.7
	53.09	19.26	7.62	131.30	77.83	33.72	0.0	1.6	45.2	13.9	0.7
	48.99	12.49	4.79	135.11	78.54	32.74	0.1	2.1	46.2	14.5	0.8
	51.56	16.97	6.67	132.20	77.81	33.29	0.0	1.7	45.3	14.2	0.7
600 psi	47.04	20.66	8.41	100.34	64.13	31.00	0.0	0.1	26.4	17.8	0.5
	45.80	20.52	8.40	97.01	62.04	30.24	0.0	0.1	23.1	19.1	0.6
	45.95	19.87	8.09	99.95	63.16	30.01	0.0	0.1	25.6	19.0	0.7
	46.26	20.35	8.30	99.10	63.11	30.42	0.0	0.1	25.0	18.6	0.6
800 psi	46.87	33.84	21.22	80.42	56.11	31.03	0.0	0.0	8.6	20.3	0.2
	41.79	23.88	12.56	80.38	56.01	30.92	0.0	0.0	8.5	20.5	0.2
	42.87	21.75	9.31	83.28	55.60	29.11	0.0	0.0	10.5	22.5	0.3
	43.84	26.49	14.36	81.36	55.91	30.35	0.0	0.0	9.2	21.1	0.2
1000 psi	45.33	34.39	22.73	74.17	52.91	30.81	0.0	0.0	3.4	21.7	0.3
	43.17	26.89	13.45	75.70	53.04	29.69	0.0	0.0	4.9	23.3	0.3
	44.18	33.56	22.29	74.00	51.46	30.09	0.0	0.0	2.6	23.6	0.2
	44.23	31.61	19.49	74.62	52.47	30.20	0.0	0.0	3.6	22.9	0.3
1200 psi	42.44	34.53	25.44	67.35	48.49	29.70	0.0	0.0	0.5	27.0	0.3
	42.94	35.03	25.86	68.14	48.94	30.10	0.0	0.0	0.5	25.9	0.2
	42.39	37.21	30.71	59.43	46.92	31.50	0.0	0.0	0.2	26.7	0.1
	42.59	35.59	27.34	64.97	48.12	30.43	0.0	0.0	0.4	26.5	0.2

Table A1.12: *Drop-Size Distribution Results for 5% Sodium Sulphate Solution using the Nozzle Delevan 2.2SJ*

Pressure	Fluid	Obscuration	Log. Difference	Measured Values		Correction Factors		Corrected Values		Volumetric Flowrate (l/min)	Specific Surface Area (Sq. m/cc)
				X Parameter	N Parameter	X Parameter	N Parameter	X Parameter	N Parameter		
400 psi	5% NaSO4	0.6007	5.53	82.02	2.22	-	-	-	-	10.10	0.06
		0.6232	5.54	79.74	2.18						0.06
		0.6187	5.63	79.88	2.34						0.06
				80.55	2.25						0.06
600 psi	5% NaSO4	0.8188	5.55	55.86	2.25	1.0562	1.1896	59.00	2.68	12.36	0.08
		0.8317	5.69	55.28	2.26	1.0596	1.2038	58.58	2.72		0.09
		0.8308	5.55	54.60	2.36	1.0569	1.2170	57.71	2.87		0.09
				55.25	2.29			58.43	2.76		0.09
800 psi	5% NaSO4	0.9507	5.78	43.59	2.82	1.0848	1.6360	47.28	4.61	14.13	0.12
		0.9497	5.66	43.47	2.54	1.0973	1.5269	47.70	3.88		0.12
		0.9383	5.62	42.19	2.82	1.0797	1.5794	45.55	4.45		0.12
				43.08	2.73			46.84	4.31		0.12
1000 psi	5% NaSO4	0.9778	5.77	36.40	3.13	1.0831	1.9434	39.43	6.08	16.23	0.15
		0.9768	5.75	37.69	2.91	1.0920	1.8228	41.16	5.30		0.14
		0.9651	5.83	38.76	2.93	1.0862	1.7595	42.10	5.16		0.14
				37.62	2.99			40.90	5.51		0.14
1200 psi	5% NaSO4	0.9861	5.80	35.23	3.37	1.0773	2.1505	37.95	7.25	18.12	0.16
		0.9822	5.83	32.92	3.74	1.0652	2.3405	35.07	8.75		0.17
		0.9812	5.48	35.69	3.35	1.0764	2.0936	38.42	7.01		0.17
				34.61	3.49			37.15	7.67		0.17

All Dimensions in microns

Fluid Temperature = 20.0 C

Wet Bulb Temperature = 15 C

Atmospheric Pressure = 749.7 mm Hg

Absolute Viscosity = 1.163 cP

Dry Bulb Temperature = 19 C

Air Density = 1.209 kg / Cu. m

Density = 1043.6 kg / Cu. m

Relative Humidity = 65%

Fluid Surface Tension = 73.77 Dynes / cm

Pressure	D(3,2)	D(2,1)	D(1,0)	D(v,0.9)	D(v,0.5)	D(v,0.1)	% > 420.0	% > 201.0	% > 82.7	% < 39.5	% < 10.3
400 psi	44.66	12.42	4.73	119.25	69.52	29.78	0.0	0.7	36.1	17.9	1.0
	48.16	23.09	10.76	117.05	67.40	28.43	0.0	0.1	34.0	19.3	1.1
	51.69	29.78	15.99	115.31	68.39	30.54	0.0	0.2	34.1	17.3	0.6
	48.17	21.76	10.49	117.20	68.44	29.58	0.0	0.3	34.7	18.2	0.9
600 psi	38.72	18.61	7.90	79.36	51.48	25.48	0.0	0.0	8.2	28.8	0.9
	38.73	18.86	8.03	78.38	51.21	25.61	0.0	0.0	7.5	28.9	0.8
	36.50	18.51	8.77	76.07	50.80	26.35	0.0	0.0	5.7	28.6	0.7
	37.98	18.66	8.23	77.94	51.16	25.81	0.0	0.0	7.1	28.8	0.8
800 psi	39.68	34.84	28.93	57.71	43.64	28.46	0.0	0.0	0.1	34.9	0.1
	38.05	30.73	22.18	58.35	43.84	26.22	0.0	0.0	0.2	37.8	0.3
	37.81	32.50	25.95	56.47	42.13	26.84	0.0	0.0	0.0	40.7	0.2
	38.51	32.69	25.69	57.51	43.20	27.17	0.0	0.0	0.1	37.8	0.2
1000 psi	34.74	32.13	28.67	45.24	37.19	26.88	0.0	0.0	0.0	63.6	0.0
	35.51	32.31	28.23	47.41	38.47	26.26	0.0	0.0	0.0	55.5	0.1
	36.17	32.67	28.30	49.04	39.29	26.55	0.0	0.0	0.0	50.7	0.1
	35.47	32.37	28.40	47.23	38.32	26.56	0.0	0.0	0.0	56.6	0.1
1200 psi	34.35	32.52	30.23	44.82	35.55	27.26	0.0	0.0	0.0	71.9	0.0
	32.33	31.24	29.93	38.23	33.71	26.53	0.0	0.0	0.0	92.4	0.0
	34.65	32.70	30.26	45.11	35.94	27.32	0.0	0.0	0.0	68.7	0.0
	33.78	32.15	30.14	42.72	35.07	27.04	0.0	0.0	0.0	77.7	0.0

Table A1.13: *Drop-Size Distribution Results for 10% Sodium Sulphate Solution using the Nozzle AAASSTC5-5*

Pressure	Fluid	Obscuration	Log. Difference	Measured Values		Correction Factors		Corrected Values		Volumetric Flowrate (l/min)	Specific Surface Area (Sq. m/cc)
				X Parameter	N Parameter	X Parameter	N Parameter	X Parameter	N Parameter		
400 psi	10% NaSO4	0.5524	4.67	136.46	2.27	–	–	–	–	8.45	0.03
		0.5070	4.51	135.73	2.22						0.03
		0.5140	4.64	136.20	2.23						0.03
				136.13	2.24						0.03
600 psi	10% NaSO4	0.5828	4.57	140.71	2.71	–	–	–	–	10.36	0.03
		0.5608	4.52	140.71	2.71						0.03
		0.5468	4.42	139.55	2.68						0.04
				140.32	2.70						0.03
800 psi	10% NaSO4	0.5659	5.01	139.59	2.45	–	–	–	–	11.91	0.04
		0.5711	5.07	140.14	2.47						0.03
		0.5853	4.94	138.49	2.45						0.03
				139.41	2.46						0.03
1000 psi	10% NaSO4	0.5757	5.01	141.82	2.39	–	–	–	–	13.44	0.03
		0.5740	5.20	144.06	2.47						0.03
		0.5976	5.04	140.70	2.52						0.04
				142.19	2.46						0.03
1200 psi	10% NaSO4	0.5922	5.13	141.52	2.37	–	–	–	–	16.05	0.03
		0.5409	5.13	140.61	2.37						0.03
		0.5249	5.10	139.69	2.37						0.03
				140.61	2.37						0.03

All Dimensions in microns

Fluid Temperature = 20.0 C

Absolute Viscosity = 1.390 cP

Density =1090.5 kg / Cu. m

Wet Bulb Temperature = 15 C

Dry Bulb Temperature = 19 C

Relative Humidity = 65%

Atmospheric Pressure = 750.4 mm Hg

Air Density = 1.205 kg / Cu. m

Fluid Surface Tension = 74.90 Dynes / cm

Pressure	D(3,2)	D(2,1)	D(1,0)	D(v,0.9)	D(v,0.5)	D(v,0.1)	% > 420.0	% > 201.0	% > 82.7	% < 39.5	% < 10.5
400 psi	77.68	25.31	9.74	197.08	116.09	50.64	0.3	9.0	72.6	5.8	0.4
	75.97	24.00	9.25	197.35	115.07	49.26	0.3	9.0	71.7	6.2	0.4
	77.01	24.77	9.54	197.22	115.71	50.11	0.3	9.0	72.2	6.0	0.4
	76.89	24.69	9.51	197.22	115.62	50.00	0.3	9.0	72.2	6.0	0.4
600 psi	96.72	56.96	29.05	204.67	123.40	61.23	0.1	11.1	79.0	3.1	0.1
	96.72	56.96	29.05	204.67	123.40	61.23	0.1	11.1	79.0	3.1	0.1
	95.41	55.76	28.33	203.79	122.28	60.16	0.1	10.8	78.3	3.3	0.1
	96.28	56.56	28.81	204.38	123.03	60.87	0.1	11.0	78.8	3.2	0.1
800 psi	89.98	46.71	21.87	195.99	121.21	55.64	0.2	8.6	75.8	4.4	0.2
	90.73	47.40	22.23	196.28	121.89	56.27	0.2	8.7	76.3	4.3	0.2
	89.30	46.44	21.78	194.59	120.18	55.21	0.2	8.2	75.4	4.5	0.2
	90.00	46.85	21.96	195.62	121.09	55.71	0.2	8.5	75.8	4.4	0.2
1000 psi	90.05	45.59	21.14	200.00	122.77	55.25	0.3	9.7	76.0	4.6	0.2
	93.14	48.40	22.58	201.09	125.47	57.83	0.3	10.0	77.6	4.0	0.2
	92.13	49.05	23.18	196.00	122.81	57.51	0.2	8.6	77.0	4.0	0.2
	91.77	47.68	22.30	199.03	123.68	56.86	0.3	9.4	76.9	4.2	0.2
1200 psi	89.43	44.97	20.83	200.06	122.32	54.70	0.3	9.7	75.6	4.7	0.3
	84.19	32.05	12.67	198.95	121.48	54.36	0.3	9.4	75.3	4.8	0.3
	83.80	32.19	12.77	197.81	120.62	54.00	0.3	9.1	75.0	4.9	0.3
	85.81	36.40	15.42	198.94	121.47	54.35	0.3	9.4	75.3	4.8	0.3

Table A1.14: *Drop-Size Distribution Results for 10% Sodium Sulphate Solution using the Nozzle AAASSTC8-5*

Pressure	Fluid	Obscuration	Log. Difference	Measured Values		Correction Factors		Corrected Values		Volumetric Flowrate (l/min)	Specific Surface Area (Sq. m/cc)
				X Parameter	N Parameter	X Parameter	N Parameter	X Parameter	N Parameter		
400 psi	10% NaSO4	0.5089	5.48	90.76	2.14	-	-	-	-	8.61	0.05
		0.5099	5.47	91.00	2.15						0.05
		0.5025	5.46	90.22	2.09						0.05
				90.66	2.13						0.05
600 psi	10% NaSO4	0.7989	5.35	61.96	2.09	1.0545	1.1543	65.34	2.41	9.96	0.07
		0.7828	5.33	60.55	2.09	1.0506	1.1441	63.61	2.39		0.07
		0.8027	5.30	60.55	2.09	1.0555	1.1570	63.91	2.42		0.07
				61.02	2.09			64.29	2.41		0.07
800 psi	10% NaSO4	0.9095	5.45	55.14	2.09	1.0999	1.2853	60.65	2.69	11.12	0.08
		0.9027	5.47	55.14	2.14	1.0933	1.2838	60.29	2.75		0.08
		0.9006	5.47	56.59	2.25	1.0868	1.3042	61.50	2.93		0.08
				55.62	2.16			61.81	2.79		0.08
1000 psi	10% NaSO4	0.9386	5.52	52.04	2.25	1.1077	1.3946	57.65	3.14	13.27	0.09
		0.9461	5.55	51.07	2.27	1.1111	1.4228	56.74	3.23		0.09
		0.9471	5.54	51.07	2.27	1.1117	1.4258	56.78	3.24		0.09
				51.39	2.26			57.06	3.20		0.09
1200 psi	10% NaSO4	0.9523	5.58	49.45	2.27	1.1151	1.4422	55.14	3.27	14.48	0.09
		0.9577	5.56	49.44	2.25	1.1201	1.4531	55.38	3.27		0.10
		0.9530	5.61	49.43	2.27	1.1155	1.4445	55.14	3.28		0.10
				49.44	2.26			55.52	3.27		0.10

All Dimensions in microns

Fluid Temperature = 19.9 C

Wet Bulb Temperature = 15 C

Atmospheric Pressure = 750.5 mm Hg

Absolute Viscosity = 1.390 cP

Dry Bulb Temperature = 19 C

Air Density = 1.205 kg / Cu. m

Density =1090.5 kg / Cu. m

Relative Humidity = 65%

Fluid Surface Tension = 74.90 Dynes / cm

Pressure	D(3,2)	D(2,1)	D(1,0)	D(v,0.9)	D(v,0.5)	D(v,0.1)	% > 420.0	% > 201.0	% > 82.7	% < 39.5	% < 10.5
400 psi	47.74	12.32	4.73	132.27	76.43	31.73	0.0	1.8	44.1	15.5	0.9
	55.64	29.28	14.99	132.37	76.70	31.97	0.0	1.8	44.3	15.3	0.9
	46.78	11.97	4.62	132.61	75.67	30.77	0.0	1.9	43.5	16.2	1.0
	50.05	17.89	8.11	132.42	76.27	31.49	0.0	1.8	44.0	15.7	0.9
600 psi	42.38	23.61	11.93	91.87	56.09	25.70	0.0	0.0	17.2	25.7	1.2
	37.12	12.28	4.67	89.88	54.54	24.82	0.0	0.0	15.4	27.4	1.3
	37.52	12.46	4.72	89.92	54.90	25.23	0.0	0.0	15.5	26.8	1.2
	39.01	16.12	7.11	90.56	55.18	25.25	0.0	0.0	16.0	26.6	1.2
800 psi	39.81	19.05	8.05	81.88	52.98	26.28	0.0	0.0	9.7	26.9	0.8
	40.01	19.50	8.28	80.58	52.82	26.60	0.0	0.0	8.9	26.7	0.7
	42.01	21.46	9.22	80.66	54.35	28.53	0.0	0.0	8.9	23.8	0.4
	40.61	20.00	8.52	81.04	53.38	27.14	0.0	0.0	9.2	25.8	0.6
1000 psi	40.65	22.46	10.03	74.38	51.31	28.16	0.0	0.0	4.2	26.3	0.4
	40.56	23.11	10.53	74.27	50.62	28.30	0.0	0.0	3.2	26.6	0.4
	40.64	23.25	10.62	74.27	50.66	28.38	0.0	0.0	3.2	26.5	0.4
	40.62	22.94	10.39	74.31	50.86	28.28	0.0	0.0	3.5	26.5	0.4
1200 psi	39.63	22.92	10.56	72.54	49.39	27.91	0.0	0.0	2.2	28.2	0.4
	39.81	23.03	10.61	72.79	49.58	28.03	0.0	0.0	2.3	27.9	0.4
	39.69	23.04	10.64	72.51	49.41	27.97	0.0	0.0	2.2	28.2	0.4
	39.71	23.00	10.60	72.61	49.46	27.97	0.0	0.0	2.2	28.1	0.4

Table A1.15: *Drop-Size Distribution Results for 10% Sodium Sulphate Solution using the Nozzle AAASSTC8-8*

Pressure	Fluid	Obscuration	Log. Difference	Measured Values		Correction Factors		Corrected Values		Volumetric Flowrate (l/min)	Specific Surface Area (Sq. m/cc)
				X Parameter	N Parameter	X Parameter	N Parameter	X Parameter	N Parameter		
400 psi	10% NaSO4	0.5310	5.06	146.75	2.36						0.04
		0.5495	5.22	146.50	2.36	–	–	–	–	10.03	0.04
		0.5752	4.62	145.23	2.00						0.03
				146.16	2.24						0.04
600 psi	10% NaSO4	0.6587	4.33	143.45	2.28	1.0352	1.1113	148.30	2.53		0.03
		0.6524	4.56	141.00	2.34	1.0348	1.1136	145.91	2.61	12.23	0.03
		0.6714	4.52	141.81	2.36	1.0350	1.1200	146.78	2.64		0.03
				142.09	2.33			147.00	2.59		0.03
800 psi	10% NaSO4	0.6675	4.78	128.69	2.43	1.0346	1.1235	133.14	2.73		0.03
		0.6559	4.69	126.74	2.29	1.0351	1.1113	131.19	2.54	14.63	0.03
		0.6757	5.16	126.74	2.39	1.0350	1.1233	131.17	2.68		0.04
				127.39	2.37			131.83	2.65		0.03
1000 psi	10% NaSO4	0.6430	4.81	134.29	2.44						0.03
		0.6408	4.92	135.52	2.54	–	–	–	–	16.72	0.03
		0.6494	4.51	134.41	2.44						0.03
				134.74	2.47						0.03
1200 psi	10% NaSO4	0.6794	4.77	131.87	2.54	1.0342	1.1350	136.38	2.88		0.04
		0.6575	5.57	133.37	2.28	1.0352	1.1110	138.07	2.53	19.47	0.02
		0.6661	4.94	131.87	2.36	1.0349	1.1185	136.48	2.64		0.03
				132.37	2.39			136.98	2.68		0.03

All Dimensions in microns

Fluid Temperature = 20.1 C

Wet Bulb Temperature = 15 C

Atmospheric Pressure = 750.5 mm Hg

Absolute Viscosity = 1.390 cP

Dry Bulb Temperature = 19 C

Air Density = 1.205 kg / Cu. m

Density =1090.5 kg / Cu. m

Relative Humidity = 65%

Fluid Surface Tension = 74.90 Dynes / cm

Pressure	D(3,2)	D(2,1)	D(1,0)	D(v,0.9)	D(v,0.5)	D(v,0.1)	% > 420.0	% > 201.0	% > 82.7	% < 39.5	% < 10.5
400 psi	86.85	32.08	12.61	206.90	126.78	56.02	0.5	11.7	77.1	4.5	0.3
	92.16	45.79	21.03	206.18	126.73	56.38	0.5	11.5	77.2	4.4	0.2
	74.68	20.47	8.01	215.10	120.99	47.17	1.0	13.8	72.3	7.1	0.5
	84.56	32.78	13.88	209.39	124.83	53.19	0.7	12.3	75.5	5.3	0.3
600 psi	97.92	54.20	26.54	204.95	129.69	60.84	0.3	11.2	79.7	3.5	0.2
	98.03	55.85	27.78	200.79	128.17	61.52	0.2	9.9	79.7	3.2	0.1
	99.17	56.97	28.44	201.34	129.14	62.51	0.2	10.1	80.3	3.1	0.1
	98.37	55.67	27.59	202.36	129.00	61.62	0.2	10.4	79.9	3.3	0.1
800 psi	92.07	55.01	28.48	195.88	116.93	58.76	0.2	8.9	76.0	3.4	0.0
	86.71	46.90	22.54	195.93	113.71	54.04	0.2	8.9	73.5	4.5	0.1
	89.92	53.13	27.38	193.84	114.72	56.56	0.2	8.4	75.0	3.8	0.0
	89.57	51.68	26.13	195.22	115.12	56.45	0.2	8.7	74.8	3.9	0.0
1000 psi	86.54	45.16	21.30	189.27	116.04	53.36	0.1	7.0	73.7	4.9	0.2
	89.44	48.11	22.98	201.05	117.89	55.80	0.1	10.0	75.3	4.3	0.2
	86.61	45.19	21.31	189.43	116.16	53.41	0.1	7.0	73.7	4.9	0.2
	87.53	46.15	21.86	193.25	116.70	54.19	0.1	8.0	74.2	4.7	0.2
1200 psi	97.22	62.56	34.71	198.29	120.67	62.66	0.0	9.3	78.7	2.8	0.1
	90.68	48.61	23.09	192.41	120.43	56.64	0.1	7.7	76.1	4.1	0.2
	92.69	53.77	27.29	200.94	119.43	58.09	0.1	10.0	76.7	3.7	0.1
	93.53	54.98	28.36	197.21	120.22	59.13	0.1	9.0	77.2	3.5	0.1

Table A1.16: *Drop-Size Distribution Results for 10% Sodium Sulphate Solution using the Nozzle AAASSTC10-10*

Pressure	Fluid	Obscuration	Log. Difference	Measured Values		Correction Factors		Corrected Values		Volumetric Flowrate (l/min)	Specific Surface Area (Sq. m/cc)
				X Parameter	N Parameter	X Parameter	N Parameter	X Parameter	N Parameter		
400 psi	10% NaSO4	0.5267	4.75	149.39	2.21	–	–	–	–	14.07	0.03
		0.5374	4.51	150.64	2.14						0.03
		0.5078	4.80	148.57	2.14						0.03
				149.53	2.16						0.03
600 psi	10% NaSO4	0.5927	4.53	134.95	2.36	–	–	–	–	17.84	0.03
		0.5805	4.56	133.97	2.36						0.04
		0.6014	4.37	133.49	2.44						0.03
				134.14	2.39						0.03
800 psi	10% NaSO4	0.6278	4.78	128.80	2.44	–	–	–	–	20.07	0.04
		0.6244	4.85	128.64	2.44						0.04
		0.6367	4.67	128.69	2.44						0.04
				128.44	2.44						0 04
1000 psi	10% NaSO4	0.6736	5.47	128.00	2.45	1.0346	1.1267	132.42	2.76	23.46	0.04
		0.6612	5.02	128.98	2.36	1.0348	1.1171	134.51	2.64		0.04
		0.6676	5.01	128.80	2.44	1.0345	1.1242	133.24	2.74		0.04
				128.59	2.42			133.39	2.71		0.04
1200 psi	10% NaSO4	0.8640	5.82	146.40	1.98	1.0813	1.1974	158.30	2.37	26.28	0.02
		0.8912	5.55	147.44	1.86	1.1028	1.2094	162.59	2.25		0.02
		0.8737	5.64	148.81	2.00	1.0851	1.2122	161.48	2.42		0.03
				147.55	1.95			160.79	2.35		0.02

All Dimensions in microns

Fluid Temperature = 20.2 C

Wet Bulb Temperature = 15 C

Atmospheric Pressure = 750.5 mm Hg

Absolute Viscosity = 1.390 cP

Dry Bulb Temperature = 19 C

Air Density = 1.205 kg / Cu. m

Density =1090.5 kg / Cu. m

Relative Humidity = 65%

Fluid Surface Tension = 74.90 Dynes / cm

Pressure	D(3,2)	D(2,1)	D(1,0)	D(v,0.9)	D(v,0.5)	D(v,0.1)	% > 420.0	% > 201.0	% > 82.7	% < 39.5	% < 10.5
400 psi	82.99	25.53	9.82	213.07	127.88	53.92	0.8	13.5	76.3	5.1	0.3
	81.49	23.88	9.22	217.19	127.03	52.64	0.9	14.7	75.8	5.5	0.4
	80.44	23.65	9.13	214.76	125.25	51.92	0.9	13.9	75.2	5.7	0.4
	81.64	24.35	9.39	215.01	126.72	52.83	0.9	14.0	75.8	5.4	0.4
600 psi	79.32	27.74	10.72	193.09	115.51	52.01	0.2	7.9	73.0	5.4	0.3
	78.74	27.52	10.63	191.78	114.68	51.63	0.2	7.6	72.6	5.4	0.3
	86.18	44.91	21.23	200.05	114.66	53.11	0.3	9.8	73.3	4.9	0.2
	81.41	33.39	14.19	194.97	114.95	52.25	0.2	8.4	73.0	5.2	0.3
800 psi	79.02	31.62	12.64	194.20	111.00	51.22	0.2	8.5	71.3	5.4	0.2
	78.95	31.65	12.66	193.98	110.88	51.16	0.2	8.4	71.2	5.4	0.2
	78.97	31.63	12.65	194.05	110.92	51.18	0.2	8.4	71.2	5.4	0.2
	78.98	31.63	12.65	194.08	110.93	51.19	0.2	8.4	71.2	5.4	0.2
1000 psi	92.07	55.54	28.95	194.49	116.44	58.97	0.2	8.6	76.0	3.3	0.0
	91.44	53.15	27.07	198.74	117.67	57.26	0.2	9.5	76.0	3.7	0.0
	92.30	55.30	28.68	195.88	117.08	58.98	0.2	8.9	76.2	3.4	0.0
	91.94	54.66	28.23	196.37	117.06	58.40	0.2	9.0	76.1	3.5	0.0
1200 psi	99.48	48.65	22.03	219.30	137.04	61.17	0.9	15.9	80.7	3.7	0.2
	93.65	32.90	12.92	227.75	139.59	59.72	1.3	18.2	80.4	4.1	0.3
	102.71	51.20	23.30	221.72	140.15	63.69	1.0	16.9	82.1	3.3	0.2
	98.61	44.25	19.42	222.92	138.93	61.53	1.1	17.0	81.1	3.7	0.2

Table A1.17: *Drop-Size Distribution Results for 10% Sodium Sulphate Solution using the Nozzle Delevan 2.0SJ*

Pressure	Fluid	Obscuration	Log. Difference	Measured Values		Correction Factors		Corrected Values		Volumetric Flowrate (l/min)	Specific Surface Area (Sq. m/cc)
				X Parameter	N Parameter	X Parameter	N Parameter	X Parameter	N Parameter		
400 psi	10% NaSO4	0.5858	5.32	150.73	2.39	–	–	–	–	18.53	0.03
		0.5714	5.29	149.31	2.39						0.03
		0.5884	5.33	150.68	2.15						0.03
				150.24	2.31						0.03
600 psi	10% NaSO4	0.6786	5.05	131.23	2.27	1.0359	1.1159	135.94	2.53	23.06	0.03
		0.6720	5.09	131.23	2.37	1.0350	1.1208	135.82	2.66		0.04
		0.6875	4.93	129.62	2.37	1.0355	1.1256	134.23	2.67		0.04
				130.69	2.34			135.33	2.62		0.04
800 psi	10% NaSO4	0.7210	4.58	111.56	2.25	1.0388	1.1286	115.89	2.54	28.19	0.04
		0.7164	5.00	110.62	2.55	1.0358	1.1510	114.58	2.93		0.04
		0.7361	5.08	110.46	2.39	1.0389	1.1470	114.76	2.74		0.04
				110.88	2.40			115.08	2.74		0.04
1000 psi	10% NaSO4	0.7122	4.93	105.70	2.39	1.0368	1.1362	109.59	2.72	29.60	0.04
		0.6974	4.90	107.45	2.31	1.0365	1.1246	111.37	2.60		0.04
		0.6841	4.96	107.45	2.31	1.0358	1.1203	111.30	2.59		0.04
				106.87	2.34			110.75	2.64		0.04
1200 psi	10% NaSO4	0.8497	5.71	107.47	2.00	1.0741	1.1852	115.43	2.37	32.46	0.03
		0.8574	5.51	107.52	2.07	1.0747	1.2041	115.55	2.49		0.04
		0.8642	5.05	108.13	2.37	1.0671	1.2636	115.39	2.99		0.04
				107.71	2.15			115.46	2.62		0.04

All Dimensions in microns

Fluid Temperature = 20.0 C

Wet Bulb Temperature = 15 C

Atmospheric Pressure = 750.4 mm Hg

Absolute Viscosity = 1.390 cP

Dry Bulb Temperature = 19 C

Air Density = 1.205 kg / Cu. m

Density =1090.5 kg / Cu. m

Relative Humidity = 65%

Fluid Surface Tension = 74.90 Dynes / cm

Pressure	D(3,2)	D(2,1)	D(1,0)	D(v,0.9)	D(v,0.5)	D(v,0.1)	% > 420.0	% > 201.0	% > 82.7	% < 39.5	% < 10.5
400 psi	95.42	47.58	21.79	210.37	130.70	58.69	0.6	12.9	78.9	4.0	0.2
	94.56	47.27	21.69	208.76	129.47	58.14	0.5	12.4	78.4	4.1	0.2
	81.82	24.12	9.30	216.27	128.40	52.88	0.9	14.4	76.0	5.5	0.4
	90.60	39.66	17.59	211.80	129.52	56.57	0.7	13.2	77.8	4.5	0.3
600 psi	89.50	47.94	22.84	201.63	118.20	55.78	0.1	10.2	75.3	4.3	0.2
	92.60	54.09	27.56	199.97	118.98	58.18	0.0	9.7	76.6	3.7	0.1
	91.77	53.83	27.55	198.04	117.61	57.68	0.2	9.4	76.2	3.6	0.0
	91.29	51.95	25.98	199.88	118.26	57.21	0.1	9.8	76.0	3.9	0.1
800 psi	76.78	42.85	21.14	161.87	100.71	47.78	0.1	4.8	65.5	6.2	0.2
	81.88	53.12	29.37	148.59	102.06	53.35	0.1	3.4	67.8	4.2	0.0
	79.08	47.26	24.24	152.37	101.38	50.49	0.1	4.1	66.4	5.1	0.1
	79.25	47.74	24.92	154.28	101.38	50.54	0.1	4.1	66.6	5.2	0.1
1000 psi	75.25	44.86	22.99	145.46	95.96	47.91	0.1	3.0	62.9	6.0	0.1
	74.78	42.87	21.51	150.07	96.99	46.86	0.1	3.8	63.1	6.4	0.2
	74.60	42.65	21.37	150.17	96.88	46.68	0.1	3.8	63.0	6.5	0.2
	74.88	43.46	21.96	148.57	96.61	47.15	0.1	3.5	63.0	6.3	0.2
1200 psi	68.36	24.37	9.46	169.74	99.28	44.66	0.1	5.3	63.6	7.5	0.3
	70.86	27.48	10.76	163.53	100.12	46.80	0.1	4.9	64.8	6.6	0.2
	83.71	56.83	33.30	148.80	102.99	54.65	0.1	3.4	68.9	3.9	0.0
	74.31	36.23	17.84	160.69	100.80	48.70	0.1	4.5	65.8	6.0	0.2

Table A1.18: *Drop-Size Distribution Results for 10% Sodium Sulphate Solution using the Nozzle Delevan 2.2SJ*

Pressure	Fluid	Obscuration	Log. Difference	Measured Values		Correction Factors		Corrected Values		Volumetric Flowrate (l/min)	Specific Surface Area (Sq. m/cc)
				X Parameter	N Parameter	X Parameter	N Parameter	X Parameter	N Parameter		
400 psi	10% NaSO4	0.5524	4.67	136.46	2.27	–	–	–	–	8.45	0.03
		0.5070	4.51	135.73	2.22						0.03
		0.5140	4.64	136.20	2.23						0.03
				136.13	2.24						0.03
600 psi	10% NaSO4	0.5828	4.57	140.71	2.71	–	–	–	–	10.36	0.03
		0.5608	4.52	140.71	2.71						0.03
		0.5468	4.42	139.55	2.68						0.04
				140.32	2.70						0.03
800 psi	10% NaSO4	0.5659	5.01	139.59	2.45	–	–	–	–	11.91	0.04
		0.5711	5.07	140.14	2.47						0.03
		0.5853	4.94	138.49	2.45						0.03
				139.41	2.46						0.03
1000 psi	10% NaSO4	0.5757	5.01	141.82	2.39	–	–	–	–	13.44	0.03
		0.5740	5.20	144.06	2.47						0.03
		0.5976	5.04	140.70	2.52						0.04
				142.19	2.46						0.03
1200 psi	10% NaSO4	0.5922	5.13	141.52	2.37	–	–	–	–	16.05	0.03
		0.5409	5.13	140.61	2.37						0.03
		0.5249	5.10	139.69	2.37						0.03
				140.61	2.37						0.03

All Dimensions in microns

Fluid Temperature = 20.0 C

Wet Bulb Temperature = 15 C

Atmospheric Pressure = 750.4 mm Hg

Absolute Viscosity = 1.390 cP

Dry Bulb Temperature = 19 C

Air Density = 1.205 kg / Cu. m

Density =1090.5 kg / Cu. m

Relative Humidity = 65%

Fluid Surface Tension = 74.90 Dynes / cm

Pressure	D(3,2)	D(2,1)	D(1,0)	D(v,0.9)	D(v,0.5)	D(v,0.1)	% > 420.0	% > 201.0	% > 82.7	% < 39.5	% < 10.5
400 psi	77.68	25.31	9.74	197.08	116.09	50.64	0.3	9.0	72.6	5.8	0.4
	75.97	24.00	9.25	197.35	115.07	49.26	0.3	9.0	71.7	6.2	0.4
	77.01	24.77	9.54	197.22	115.71	50.11	0.3	9.0	72.2	6.0	0.4
	76.89	24.69	9.51	197.22	115.62	50.00	0.3	9.0	72.2	6.0	0.4
600 psi	96.72	56.96	29.05	204.67	123.40	61.23	0.1	11.1	79.0	3.1	0.1
	96.72	56.96	29.05	204.67	123.40	61.23	0.1	11.1	79.0	3.1	0.1
	95.41	55.76	28.33	203.79	122.28	60.16	0.1	10.8	78.3	3.3	0.1
	96.28	56.56	28.81	204.38	123.03	60.87	0.1	11.0	78.8	3.2	0.1
800 psi	89.98	46.71	21.87	195.99	121.21	55.64	0.2	8.6	75.8	4.4	0.2
	90.73	47.40	22.23	196.28	121.89	56.27	0.2	8.7	76.3	4.3	0.2
	89.30	46.44	21.78	194.59	120.18	55.21	0.2	8.2	75.4	4.5	0.2
	90.00	46.85	21.96	195.62	121.09	55.71	0.2	8.5	75.8	4.4	0.2
1000 psi	90.05	45.59	21.14	200.00	122.77	55.25	0.3	9.7	76.0	4.6	0.2
	93.14	48.40	22.58	201.09	125.47	57.83	0.3	10.0	77.6	4.0	0.2
	92.13	49.05	23.18	196.00	122.81	57.51	0.2	8.6	77.0	4.0	0.2
	91.77	47.68	22.30	199.03	123.68	56.86	0.3	9.4	76.9	4.2	0.2
1200 psi	89.43	44.97	20.83	200.06	122.32	54.70	0.3	9.7	75.6	4.7	0.3
	84.19	32.05	12.67	198.95	121.48	54.36	0.3	9.4	75.3	4.8	0.3
	83.80	32.19	12.77	197.81	120.62	54.00	0.3	9.1	75.0	4.9	0.3
	85.81	36.40	15.42	198.94	121.47	54.35	0.3	9.4	75.3	4.8	0.3

Table A1.19: *Drop-Size Distribution Results for 15% Sodium Sulphate Solution using the Nozzle AAASSTC5-5*

Pressure	Fluid	Obscuration	Log. Difference	Measured Values		Correction Factors		Corrected Values		Volumetric Flowrate (l/min)	Specific Surface Area (Sq. m/cc)
				X Parameter	N Parameter	X Parameter	N Parameter	X Parameter	N Parameter		
400 psi	15% NaSO4	0.5794	4.81	152.39	2.05	–	–	–	–	9.10	0.03
		0.5652	4.69	153.76	1.94						0.03
		0.5757	4.54	153.30	1.80						0.02
				153.15	1.93						0.03
600 psi	15% NaSO4	0.5851	4.78	144.67	2.52	–	–	–	–	10.59	0.03
		0.5681	4.72	145.24	2.36						0.03
		0.5690	4.59	143.53	2.30						0.03
				144.48	2.39						0.03
800 psi	15% NaSO4	0.5970	4.68	134.29	2.52	–	–	–	–	12.04	0.04
		0.5770	4.89	133.92	2.62						0.04
		0.5985	4.74	133.74	2.82						0.04
				133.98	2.65						0.04
1000 psi	15% NaSO4	0.6067	4.67	135.60	2.44	–	–	–	–	14.14	0.03
		0.5832	4.88	135.36	2.71						0.04
		0.5863	4.96	135.44	2.74						0.03
				135.47	2.63						0.03
1200 psi	15% NaSO4	0.5880	5.06	136.05	2.32	–	–	–	–	15.77	0.03
		0.5630	5.20	137.03	2.30						0.03
		0.5679	5.03	139.07	2.39						0.03
				137.38	2.34						0.03

All Dimensions in microns

Fluid Temperature = 20.0 C

Wet Bulb Temperature = 12 C

Atmospheric Pressure = 749.9 mm Hg

Absolute Viscosity = 1.725 cP

Dry Bulb Temperature = 16 C

Air Density = 1.221 kg / Cu. m

Density = 1140.2 kg / Cu. m

Relative Humidity = 63%

Fluid Surface Tension = 76.04 Dynes / cm

Pressure	D(3,2)	D(2,1)	D(1,0)	D(v,0.9)	D(v,0.5)	D(v,0.1)	% > 420.0	% > 201.0	% > 82.7	% < 39.5	% < 10.5
400 psi	79.63	22.03	8.57	222.23	127.63	50.86	1.2	15.9	75.2	6.1	0.5
	76.79	19.97	7.87	228.54	127.55	48.23	1.5	17.2	74.1	6.9	0.5
	79.83	30.82	14.02	235.67	125.34	43.97	1.9	18.2	72.0	8.3	0.8
	78.75	24.27	10.15	228.81	126.84	47.69	1.5	7.1	73.8	7.1	0.6
600 psi	94.66	50.30	23.72	200.89	126.41	59.13	0.3	10.0	78.4	3.7	0.2
	91.41	45.51	20.94	204.71	125.61	55.90	0.4	11.1	76.8	4.5	0.2
	82.49	27.38	10.54	204.02	123.52	53.91	0.4	10.9	75.5	5.0	0.3
	89.52	41.06	18.40	203.21	125.18	56.31	0.4	10.7	76.9	4.4	0.2
800 psi	88.26	47.21	22.51	199.92	116.61	54.92	0.1	9.7	74.5	4.5	0.2
	90.70	52.44	26.64	198.28	116.99	56.64	0.2	9.4	75.6	3.9	0.0
	94.61	60.06	33.14	195.57	118.03	60.57	0.2	8.8	77.2	3.0	0.0
	91.19	59.24	27.43	197.92	117.21	57.38	0.2	9.3	75.8	3.8	0.1
1000 psi	87.34	45.48	21.40	191.03	117.33	53.87	0.2	7.4	74.2	4.8	0.2
	93.13	55.23	28.38	198.87	118.89	58.89	0.0	9.4	76.9	3.5	0.1
	93.78	56.03	28.97	198.70	119.07	59.93	0.2	9.5	77.1	3.2	0.0
	91.42	52.25	26.25	196.20	118.43	57.56	0.1	8.8	76.1	3.8	0.1
1200 psi	78.81	26.63	10.26	195.41	116.14	51.58	0.2	8.5	73.0	5.5	0.3
	78.81	26.22	10.09	197.11	116.81	51.52	0.3	9.0	73.1	5.6	0.3
	88.40	44.96	20.94	196.60	120.22	54.19	0.3	8.8	75.0	4.8	0.3
	82.01	32.60	13.76	196.37	117.72	52.43	0.3	8.8	73.7	5.3	0.3

Table A1.20: *Drop-Size Distribution Results for 15% Sodium Sulphate Solution using the Nozzle AAASSTC8-5*

Pressure	Fluid	Obscuration	Log. Difference	Measured Values		Correction Factors		Corrected Values		Volumetric Flowrate (l/min)	Specific Surface Area (Sq. m/cc)
				X Parameter	N Parameter	X Parameter	N Parameter	X Parameter	N Parameter		
400 psi	15% NaSO4	0.5014	5.08	149.31	2.15					9.85	0.03
		0.5123	4.45	148.23	2.15	-	-	-	-		0.03
		0.5299	4.91	149.31	2.15						0.03
				148.95	2.15						0.03
600 psi	15% NaSO4	0.6064	4.59	140.90	2.21					12.84	0.03
		0.6240	4.53	139.54	2.19	-	-	-	-		0.03
		0.6234	4.55	139.54	2.19						0.03
				139.99	2.20						0.03
800 psi	15% NaSO4	0.6461	4.65	133.27	2.42					14.39	0.03
		0.6201	4.49	133.21	2.36	-	-	-	-		0.03
		0.6432	4.52	133.30	2.40						0.04
				133.26	2.39						0.03
1000 psi	15% NaSO4	0.6597	4.52	129.62	2.37	1.0348	1.1174	134.13	2.65	16.88	0.04
		0.6622	4.76	128.43	2.30	1.0352	1.1135	132.95	2.56		0.04
		0.6599	4.72	129.03	2.36	1.0348	1.1168	133.52	2.64		0.04
				129.03	2.34			133.53	2.62		0.04
1200 psi	15% NaSO4	0.6830	4.71	117.53	2.34	1.0356	1.1221	121.81	2.63	21.99	0.04
		0.6534	4.84	117.59	2.21	1.0355	1.1057	121.77	2.44		0.03
		0.6718	4.74	118.61	2.18	1.0362	1.1081	122.91	2.42		0.04
				117.91	2.24			122.16	2.50		0.04

All Dimensions in microns

Fluid Temperature = 20.0 C

Absolute Viscosity = 1.725 cP

Density = 1140.2 kg / Cu. m

Wet Bulb Temperature = 12 C

Dry Bulb Temperature = 16 C

Relative Humidity = 63%

Atmospheric Pressure = 749.8 mm Hg

Air Density = 1.221 kg / Cu. m

Fluid Surface Tension = 76.04 Dynes / cm

Pressure	D(3,2)	D(2,1)	D(1,0)	D(v,0.9)	D(v,0.5)	D(v,0.1)	% > 420.0	% > 201.0	% > 82.7	% < 39.5	% < 10.5
400 psi	81.11	23.97	9.25	215.34	125.98	52.43	0.9	14.1	75.5	5.6	0.4
	80.56	23.85	9.20	214.08	125.05	52.06	0.8	13.8	75.2	5.7	0.4
	81.11	23.97	9.25	215.34	125.98	52.43	0.9	14.1	75.5	5.6	0.4
	80.93	23.93	9.23	214.92	125.67	52.31	0.9	14.0	75.4	5.6	0.4
600 psi	78.40	24.39	9.39	203.98	119.34	50.87	0.5	10.8	73.5	5.8	0.4
	77.17	23.79	9.17	202.80	118.02	49.95	0.5	10.5	72.8	6.1	0.4
	77.17	23.79	9.17	202.80	118.02	49.95	0.5	10.5	72.8	6.1	0.4
	77.58	23.99	9.24	203.19	118.46	50.26	0.5	10.6	73.0	6.0	0.4
800 psi	85.64	44.34	20.92	200.09	114.37	52.61	0.3	9.8	73.0	5.1	0.2
	78.30	27.36	10.57	190.80	114.04	51.34	0.3	7.4	72.3	5.5	0.3
	80.95	32.16	12.86	190.02	114.41	52.20	0.2	7.2	72.8	5.3	0.3
	81.63	34.62	14.78	193.64	114.27	52.05	0.3	8.1	72.7	5.3	0.3
1000 psi	91.37	53.29	27.20	198.16	117.39	57.28	0.2	9.4	76.0	3.7	0.0
	88.21	47.95	23.07	197.88	115.63	55.13	0.2	9.3	74.5	4.3	0.1
	90.79	52.85	26.95	197.53	116.75	56.84	0.2	9.2	75.6	3.8	0.0
	90.12	51.36	25.74	197.86	116.59	56.42	0.2	9.3	75.4	3.9	0.0
1200 psi	82.03	46.60	23.04	177.15	106.37	51.78	0.1	5.9	69.8	4.9	0.1
	73.64	27.39	10.67	182.69	105.22	48.41	0.1	6.6	67.8	6.1	0.2
	73.85	27.02	10.51	185.39	106.05	48.50	0.1	7.0	68.2	6.1	0.2
	76.51	33.67	14.74	181.74	105.88	49.56	0.1	6.5	68.6	5.7	0.2

Table A1.21: *Drop-Size Distribution Results for 15% Sodium Sulphate Solution using the Nozzle AAASSTC8-8*

Pressure	Fluid	Obscuration	Log. Difference	Measured Values		Correction Factors		Corrected Values		Volumetric Flowrate (l/min)	Specific Surface Area (Sq. m/cc)
				X Parameter	N Parameter	X Parameter	N Parameter	X Parameter	N Parameter		
400 psi	15% NaSO4	0.5400	5.06	150.83	2.00	–	–	–	–	11.99	0.03
		0.5200	4.88	151.26	2.08						0.03
		0.5137	4.98	151.48	2.15						0.03
				151.19	2.08						0.03
600 psi	15% NaSO4	0.6150	4.48	139.98	2.36	–	–	–	–	15.70	0.03
		0.5970	4.64	139.73	2.60						0.03
		0.6014	4.77	140.23	2.36						0.03
				139.98	2.44						0.03
800 psi	15% NaSO4	0.5879	4.70	128.45	2.62	–	–	–	–	16.49	0.04
		0.6314	4.83	128.80	2.44						0.04
		0.5823	4.92	128.10	2.64						0.04
				128.45	2.57						0.04
1000 psi	15% NaSO4	0.6277	4.81	128.23	2.27	–	–	–	–	21.62	0.03
		0.6024	4.88	127.54	2.34						0.03
		0.6373	4.77	127.21	2.55						0.04
				127.66	2.39						0.03
1200 psi	15% NaSO4	0.7065	4.57	128.65	2.75	1.0338	1.1624	133.00	3.20	27.50	0.04
		0.6893	5.82	131.18	2.45	1.0351	1.1320	135.78	2.77		0.03
		0.6864	5.29	131.57	2.39	1.0354	1.1267	136.22	2.69		0.03
				130.47	2.53			135.00	2.89		0.03

All Dimensions in microns

Fluid Temperature = 20.0 C

Absolute Viscosity = 1.725 cP

Density = 1140.2 kg / Cu. m

Wet Bulb Temperature = 12 C

Dry Bulb Temperature = 16 C

Relative Humidity = 63%

Atmospheric Pressure = 749.8 mm Hg

Air Density = 1.221 kg / Cu. m

Fluid Surface Tension = 76.04 Dynes / cm

Pressure	D(3,2)	D(2,1)	D(1,0)	D(v,0.9)	D(v,0.5)	D(v,0.1)	% > 420.0	% > 201.0	% > 82.7	% < 39.5	% < 10.5
400 psi	77.34	20.90	8.18	222.10	125.75	48.98	1.2	15.7	74.0	6.6	0.5
	80.00	22.57	8.76	219.80	126.97	51.29	1.1	15.3	75.2	5.9	0.5
	82.29	24.22	9.34	217.35	129.19	53.19	1.0	14.7	76.3	5.4	0.4
	79.88	22.56	8.76	219.75	127.30	51.15	1.1	15.2	75.2	6.0	0.5
600 psi	83.89	32.39	12.88	198.39	120.80	53.90	0.3	9.3	75.0	4.9	0.3
	93.88	53.75	26.95	193.23	122.52	58.70	0.1	7.8	77.5	3.7	0.1
	84.01	32.37	12.87	198.70	121.04	54.00	0.3	9.4	75.1	4.9	0.3
	87.26	39.50	17.57	196.77	123.85	55.53	0.2	8.8	75.9	4.5	0.2
800 psi	86.37	48.41	23.73	190.53	111.79	54.46	0.2	7.8	73.0	4.3	0.1
	79.02	31.62	12.64	194.20	111.00	51.22	0.2	8.5	71.3	5.4	0.2
	87.16	51.16	26.30	189.61	111.62	54.67	0.1	7.6	73.1	4.3	0.0
	84.18	43.73	20.89	191.45	111.47	53.45	0.2	8.0	72.5	4.7	0.1
1000 psi	73.30	24.11	9.31	196.56	109.38	47.58	0.3	9.0	69.1	6.6	0.4
	74.61	25.67	9.92	194.32	109.33	48.75	0.2	8.5	69.6	6.2	0.3
	84.30	46.09	22.31	189.85	110.40	52.66	0.3	7.7	71.7	4.8	0.1
	77.40	31.96	13.85	193.58	119.70	49.66	0.3	8.4	70.1	5.9	0.3
1200 psi	99.53	70.82	43.75	188.95	119.32	65.66	0.1	7.5	80.2	1.9	0.0
	94.44	57.03	29.65	198.70	119.54	60.60	0.0	9.4	77.4	3.2	0.1
	93.38	54.98	28.13	200.10	119.52	58.90	0.0	9.8	77.1	3.5	0.1
	95.78	60.94	33.84	195.92	119.46	61.72	0.0	8.9	78.2	2.9	0.1

Table A1.22: *Drop-Size Distribution Results for 15% Sodium Sulphate Solution using the Nozzle AAASSTC10-10*

Pressure	Fluid	Obscuration	Log. Difference	Measured Values		Correction Factors		Corrected Values		Volumetric Flowrate (l/min)	Specific Surface Area (Sq. m/cc)
				X Parameter	N Parameter	X Parameter	N Parameter	X Parameter	N Parameter		
400 psi	15% NaSO4	0.5435	5.07	156.30	2.07	-	-	-	-	19.93	0.03
		0.5380	5.05	157.07	2.08						0.03
		0.5416	5.14	156.30	2.15						0.03
				156.56	2.10						0.03
600 psi	15% NaSO4	0.6688	4.74	139.54	2.15	1.0363	1.1054	144.61	2.38	22.49	0.03
		0.6605	4.67	139.54	2.15	1.0360	1.1035	144.57	2.37		0.03
		0.6817	4.74	138.69	2.05	1.0377	1.1019	143.91	2.26		0.03
				139.26	2.12			144.36	2.34		0.03
800 psi	15% NaSO4	0.6874	4.68	122.32	2.09	1.0377	1.1060	126.93	2.31	25.62	0.03
		0.6934	4.72	122.76	2.25	1.0367	1.1190	127.27	2.52		0.04
		0.7287	4.74	121.44	2.18	1.0404	1.1260	126.34	2.45		0.04
				122.17	2.17			126.85	2.43		0.04
1000 psi	15% NaSO4	0.8042	5.58	117.58	2.00	1.0580	1.1478	124.40	2.30	27.29	0.04
		0.7859	5.04	117.97	2.10	1.0511	1.1470	124.00	2.41		0.04
		0.7930	5.04	116.30	2.36	1.0479	1.1805	121.87	2.79		0.04
				117.28	2.15			123.42	2.50		0.04
1200 psi	15% NaSO4	0.9079	5.93	124.16	2.45	1.0815	1.3679	134.28	3.35	35.21	0.03
		0.9072	5.89	125.18	2.09	1.0986	1.2810	137.52	2.68		0.03
		0.9094	5.73	124.49	2.52	1.0794	1.3896	134.38	3.50		0.03
				124.61	2.35			135.39	3.18		0.03

All Dimensions in microns

Fluid Temperature = 19.9 C

Wet Bulb Temperature = 12 C

Atmospheric Pressure = 749.6 mm Hg

Absolute Viscosity = 1.725 cP

Dry Bulb Temperature = 16 C

Air Density = 1.221 kg / Cu. m

Density = 1140.2 kg / Cu. m

Relative Humidity = 63%

Fluid Surface Tension = 76.04 Dynes / cm

Pressure	D(3,2)	D(2,1)	D(1,0)	D(v,0.9)	D(v,0.5)	D(v,0.1)	% > 420.0	% > 201.0	% > 82.7	% < 39.5	% < 10.5
400 psi	82.16	22.81	8.85	226.48	131.21	52.72	1.4	17.2	76.5	5.6	0.5
	82.86	23.11	8.96	227.11	131.98	53.25	1.4	17.4	76.9	5.5	0.4
	84.74	24.76	9.54	223.12	133.26	54.83	1.2	16.5	77.6	5.1	0.4
	83.25	23.56	9.12	225.57	132.15	53.60	1.3	17.0	77.0	5.4	0.4
600 psi	91.49	45.94	21.19	203.55	125.21	56.10	0.4	10.7	76.8	4.5	0.2
	91.24	45.65	21.04	203.71	125.09	55.87	0.4	10.8	76.7	4.5	0.2
	81.50	26.17	10.06	205.40	123.49	53.14	0.5	11.3	75.2	5.2	0.3
	88.08	39.25	17.43	204.22	124.60	55.04	0.4	10.9	76.2	4.7	0.2
800 psi	73.54	24.83	9.59	194.08	108.62	47.91	0.2	8.4	69.0	6.5	0.3
	83.81	45.36	21.87	190.52	110.27	52.13	0.2	7.8	71.4	5.0	0.1
	77.91	31.73	12.76	190.45	109.08	50.43	0.2	7.8	71.2	5.5	0.2
	78.42	33.97	14.74	191.68	109.32	50.16	0.2	8.0	70.5	5.7	0.2
1000 psi	71.91	24.23	9.37	190.67	106.47	46.76	0.2	7.8	67.7	6.8	0.2
	74.25	26.95	10.47	187.53	106.90	48.74	0.2	7.3	68.7	6.1	0.2
	85.10	52.76	28.10	171.57	107.51	54.66	0.1	5.4	71.1	4.1	0.0
	77.09	34.65	15.98	183.26	106.96	50.05	0.2	6.8	69.2	5.7	0.1
1200 psi	102.11	74.28	46.81	189.25	121.08	67.96	0.1	7.6	82.0	1.5	0.0
	94.07	55.13	28.10	201.66	120.58	59.28	0.1	10.2	77.5	3.5	0.1
	104.28	79.47	53.66	187.23	121.74	69.65	0.1	7.2	83.1	1.2	0.0
	100.15	69.63	42.86	192.71	121.13	65.63	0.1	8.3	80.9	2.1	0.0

Table A1.23: *Drop-Size Distribution Results for 15% Sodium Sulphate Solution using the Nozzle Delevan 2.0SJ*

Pressure	Fluid	Obscuration	Log. Difference	Measured Values		Correction Factors		Corrected Values		Volumetric Flowrate (l/min)	Specific Surface Area (Sq. m/cc)
				X Parameter	N Parameter	X Parameter	N Parameter	X Parameter	N Parameter		
400 psi	15% NaSO4	0.5663	5.56	101.16	2.08	–	–	–	–	8.62	0.04
		0.5620	5.60	100.97	1.95						0.04
		0.5474	5.56	101.56	1.95						0.04
				101.23	1.99						0.04
600 psi	15% NaSO4	0.7757	5.49	104.68	1.94	1.0520	1.1255	110.12	2.18	11.88	0.04
		0.7668	5.50	105.11	1.86	1.0516	1.1141	110.53	2.07		0.04
		0.7670	5.52	104.46	1.90	1.0508	1.1178	109.77	2.12		0.04
				104.75	1.90			110.14	2.12		0.04
800 psi	15% NaSO4	0.8727	5.50	87.84	2.11	1.0798	1.2300	94.85	2.60	13.49	0.05
		0.8884	5.50	87.17	2.09	1.0883	1.2492	94.87	2.61		0.05
		0.8523	5.45	86.34	1.95	1.0772	1.1805	93.00	2.30		0.05
				87.12	2.05			94.24	2.50		0.05
1000 psi	15% NaSO4	0.9078	5.37	67.75	1.95	1.1077	1.2513	75.04	2.44	15.06	0.06
		0.9117	5.41	69.46	1.99	1.1076	1.2667	76.93	2.52		0.06
		0.9155	5.47	68.32	2.01	1.1087	1.2781	75.75	2.57		0.06
				68.51	1.98			75.91	2.51		0.06
1200 psi	15% NaSO4	0.9349	5.38	58.30	2.04	1.1200	1.3252	65.29	2.70	17.26	0.08
		0.9170	5.44	58.97	1.95	1.1139	1.2669	65.69	2.47		0.08
		0.9471	5.48	56.98	2.09	1.1250	1.3693	64.10	2.86		0.08
				58.08	2.03			65.03	2.68		0.08

All Dimensions in microns

Fluid Temperature = 20.2 C

Wet Bulb Temperature = 12 C

Atmospheric Pressure = 749.9 mm Hg

Absolute Viscosity = 1.725 cP

Dry Bulb Temperature = 16 C

Air Density = 1.221 kg / Cu. m

Density = 1140.2 kg / Cu. m

Relative Humidity = 63%

Fluid Surface Tension = 76.04 Dynes / cm

Pressure	D(3,2)	D(2,1)	D(1,0)	D(v,0.9)	D(v,0.5)	D(v,0.1)	% > 420.0	% > 201.0	% > 82.7	% < 39.5	% < 10.5
400 psi	51.54	12.34	4.78	147.68	84.84	34.32	0.1	3.8	51.9	13.1	0.8
	55.44	21.87	9.57	152.08	83.68	31.89	0.1	4.4	50.9	14.7	1.1
	57.93	27.38	13.60	153.22	84.17	32.07	0.1	4.5	51.3	14.5	1.1
	54.97	20.53	9.32	150.99	84.23	32.76	0.1	4.2	51.4	14.1	1.0
600 psi	61.74	20.31	7.94	162.95	93.32	39.24	0.1	4.8	58.6	10.1	0.5
	55.53	12.60	4.90	171.10	92.83	37.29	0.1	5.4	57.8	11.1	0.7
	60.38	19.38	7.61	165.84	92.57	37.99	0.1	5.0	57.8	10.8	0.6
	59.22	17.43	6.82	166.63	92.91	38.17	0.1	5.1	58.1	10.7	0.6
800 psi	59.95	25.16	10.01	129.96	82.37	39.92	0.0	1.1	49.7	9.7	0.4
	60.11	25.38	10.11	129.86	82.43	40.06	0.0	1.1	49.7	9.6	0.4
	54.56	20.05	7.91	132.11	79.27	34.97	0.0	1.6	46.6	13.0	0.6
	58.21	23.53	9.34	130.64	81.36	38.21	0.0	1.3	48.7	10.8	0.5
1000 psi	46.25	19.21	7.78	103.75	64.38	29.85	0.0	0.1	28.3	18.8	0.7
	48.20	20.40	8.24	105.25	66.55	31.50	0.0	0.1	30.3	16.9	0.5
	48.01	20.77	8.42	102.93	65.70	31.56	0.0	0.1	28.7	17.0	0.5
	47.49	20.13	8.15	103.98	65.61	30.97	0.0	0.1	29.1	17.6	0.6
1200 psi	42.75	20.14	8.41	90.99	57.16	28.37	0.0	0.0	14.6	22.7	0.7
	44.05	27.55	15.83	91.64	56.60	26.42	0.0	0.0	17.2	24.7	1.0
	43.22	21.44	9.09	87.14	56.53	29.18	0.0	0.0	12.2	22.0	0.4
	43.34	23.04	11.11	89.92	56.76	27.99	0.0	0.0	14.7	23.1	0.7

Table A1.24: *Drop-Size Distribution Results for 15% Sodium Sulphate Solution using the Nozzle Delevan 2.2SJ*

Pressure	Fluid	Obscuration	Log. Difference	Measured Values		Correction Factors		Corrected Values		Volumetric Flowrate (l/min)	Specific Surface Area (Sq. m/cc)
				X Parameter	N Parameter	X Parameter	N Parameter	X Parameter	N Parameter		
400 psi	15% NaSO4	0.5632	5.69	94.28	2.07	-	-	-	-	9.25	0.05
		0.5581	5.67	94.34	2.00						0.05
		0.5471	5.62	94.34	2.00						0.04
				94.32	2.02						0.05
600 psi	15% NaSO4	0.7866	5.46	65.78	2.09	1.0515	1.1464	69.17	2.40	13.15	0.07
		0.8139	5.50	65.78	2.09	1.0586	1.1653	69.64	2.44		0.07
		0.8055	5.49	65.96	2.09	1.0562	1.1590	69.67	2.42		0.07
				65.84	2.09			69.49	2.42		0.07
800 psi	15% NaSO4	0.9237	5.40	42.54	2.33	1.0946	1.3770	46.57	3.21	16.59	0.11
		0.9336	5.34	44.74	2.04	1.1190	1.3223	50.07	2.70		0.10
		0.9240	5.54	43.99	2.52	1.0858	1.4313	47.76	3.61		0.11
				43.76	2.30			48.13	3.17		0.11
1000 psi	15% NaSO4	0.9670	5.60	39.62	2.42	1.1142	1.5514	44.14	3.75	19.31	0.12
		0.9618	5.56	39.76	2.42	1.1110	1.5302	44.17	3.70		0.12
		0.9690	5.52	38.39	2.36	1.1197	1.5357	42.98	3.62		0.13
				39.26	2.40			43.76	3.69		0.12
1200 psi	15% NaSO4	0.9728	5.45	37.52	2.40	1.1193	1.5679	41.99	3.76	21.46	0.12
		0.9729	5.45	38.13	2.16	1.1389	1.4721	43.43	3.18		0.12
		0.9803	5.52	36.29	2.34	1.1289	1.5750	40.97	3.69		0.13
				37.31	2.30			42.13	3.54		0.12

All Dimensions in microns

Fluid Temperature = 20.1 C

Absolute Viscosity = 1.725 cP

Density = 1140.2 kg / Cu. m

Wet Bulb Temperature = 12 C

Dry Bulb Temperature = 16 C

Relative Humidity = 63%

Atmospheric Pressure = 749.7 mm Hg

Air Density = 1.221 kg / Cu. m

Fluid Surface Tension = 76.04 Dynes / cm

Pressure	D(3,2)	D(2,1)	D(1,0)	D(v,0.9)	D(v,0.5)	D(v,0.1)	% > 420.0	% > 201.0	% > 82.7	% < 39.5	% < 10.5
400 psi	56.19	28.47	14.41	138.27	78.94	31.82	0.1	2.6	46.7	15.1	1.0
	53.00	22.00	9.75	140.11	78.50	30.66	0.1	2.9	46.4	16.0	1.1
	53.00	22.00	9.75	140.11	78.50	30.66	0.1	2.9	46.4	16.0	1.1
	54.06	24.16	11.30	139.50	78.65	31.05	0.1	2.8	46.5	15.7	1.1
600 psi	45.61	27.72	15.60	96.75	59.34	27.10	0.0	0.1	21.7	22.9	1.0
	46.29	28.37	15.98	96.85	59.89	27.70	0.0	0.1	22.0	22.1	0.9
	46.12	28.12	15.81	97.13	59.84	27.50	0.0	0.1	22.1	22.3	1.0
	46.01	28.07	15.80	96.91	59.69	27.43	0.0	0.1	21.9	22.4	1.0
800 psi	31.20	17.70	8.94	59.52	41.58	23.10	0.0	0.0	0.3	44.5	0.8
	34.81	22.43	12.75	69.48	43.82	21.76	0.0	0.0	2.0	40.9	1.4
	37.35	29.39	20.62	59.24	43.58	25.29	0.0	0.0	0.2	39.2	0.4
	34.45	23.17	14.10	62.41	42.99	23.38	0.0	0.0	0.8	41.5	0.9
1000 psi	34.96	28.13	20.37	56.27	39.90	24.13	0.0	0.0	0.1	48.5	0.4
	33.91	23.99	13.73	56.40	39.87	23.98	0.0	0.0	0.1	48.6	0.5
	32.22	20.61	10.29	55.38	38.86	23.16	0.0	0.0	0.1	52.4	0.6
	33.70	24.24	14.80	56.02	39.54	23.76	0.0	0.0	0.1	49.8	0.5
1200 psi	32.49	23.46	13.83	53.78	38.19	23.16	0.0	0.0	0.0	55.1	0.5
	31.05	18.16	8.53	57.05	38.72	21.42	0.0	0.0	0.1	52.4	1.1
	30.98	20.22	10.32	52.28	37.30	22.42	0.0	0.0	0.0	58.5	0.7
	31.51	20.61	10.89	54.37	38.07	22.33	0.0	0.0	0.0	55.3	0.8

Table A1.25: *Drop-Size Distribution Results for 23% Calcium Carbonate Slurry using the Nozzle AAASSTC5-5*

Pressure	Fluid	Obscuration	Log. Difference	Measured Values		Correction Factors		Corrected Values		Volumetric Flowrate (l/min)	Specific Surface Area (Sq. m/cc)
				X Parameter	N Parameter	X Parameter	N Parameter	X Parameter	N Parameter		
400 psi	23% CaCO3	0.6532	4.65	186.11	1.72	1.0387	1.0763	193.32	1.85	8.83	0.02
		0.6817	4.57	186.06	1.68	1.0411	1.0781	193.71	1.81		0.03
		0.6552	4.65	186.06	1.66	1.0400	1.0744	193.50	1.78		0.02
				186.08	1.69			193.51	1.81		0.02
600 psi	23% CaCO3	0.7014	5.67	132.37	2.42	1.0359	1.1343	137.12	2.74	11.18	0.03
		0.6832	4.65	131.76	2.36	1.0354	1.1235	136.43	2.65		0.03
		0.7051	4.96	131.92	2.36	1.0366	1.1311	136.75	2.67		0.03
				132.02	2.38			136.77	2.69		0.03
800 psi	23% CaCO3	0.6638	5.20	127.49	2.22	1.0357	1.1087	132.04	2.46	14.03	0.04
		0.6591	5.28	127.81	2.22	1.0356	1.1076	132.36	2.46		0.04
		0.6774	4.52	126.70	2.64	1.0336	1.1414	130.95	3.01		0.04
				127.33	2.36			131.78	2.64		0.04
1000 psi	23% CaCO3	0.7276	5.30	123.08	2.96	1.0335	1.1930	127.20	3.53	17.02	0.04
		0.6837	5.25	123.08	2.96	1.0320	1.1676	127.02	3.46		0.04
		0.6858	4.48	122.63	3.03	1.0317	1.1740	126.52	3.56		0.04
				122.93	2.98			126.91	3.52		0.04
1200 psi	23% CaCO3	0.6915	4.54	116.63	2.93	1.0323	1.1692	120.40	3.43	19.10	0.04
		0.6806	5.10	114.98	2.84	1.0326	1.1572	118.73	3.29		0.04
		0.6788	4.73	114.31	2.84	1.0326	1.1564	118.03	3.28		0.04
				115.31	2.87			119.05	3.33		0.04

All Dimensions in microns

Slurry Temperature = 20.0 C

Apparent Viscosity = 2.250 cP

Density = 1165.0 kg / Cu. m

Wet Bulb Temperature = 12 C

Dry Bulb Temperature = 16 C

Relative Humidity = 63%

Atmospheric Pressure = 751.3 mm Hg

Air Density = 1.221 kg / Cu. m

Pressure	D(3,2)	D(2,1)	D(1,0)	D(v,0.9)	D(v,0.5)	D(v,0.1)	% > 420.0	% > 201.0	% > 82.7	% < 39.5	% < 10.5
400 psi	90.88	20.54	8.22	345.58	158.24	57.31	4.4	33.1	81.2	5.2	0.5
	89.22	19.71	7.94	348.39	157.80	55.90	4.5	33.3	80.7	5.5	0.5
	87.74	19.09	7.73	349.55	156.98	54.68	4.5	33.3	80.2	5.7	0.5
	89.28	19.78	7.96	347.84	157.67	55.96	4.5	33.2	80.7	5.5	0.5
600 psi	94.83	56.61	29.18	200.59	120.60	60.20	0.0	9.9	77.9	3.2	0.1
	92.83	54.01	27.45	200.78	119.45	58.25	0.1	9.9	76.8	3.7	0.1
	93.39	54.63	27.84	200.91	119.85	58.76	0.1	10.0	77.1	3.6	0.1
	93.68	55.08	28.16	200.76	119.97	59.07	0.1	9.9	77.3	3.5	0.1
800 psi	85.68	45.07	21.40	198.05	113.67	52.92	0.2	9.3	72.9	4.9	0.2
	85.87	45.15	21.43	198.43	113.92	53.05	0.2	9.4	73.1	4.9	0.2
	95.10	63.46	36.29	188.09	116.48	62.28	0.1	7.4	77.7	2.5	0.0
	95.55	51.23	26.37	194.86	114.69	56.08	0.2	8.7	74.6	4.1	0.1
1000 psi	98.97	76.31	52.35	163.10	115.12	66.81	0.1	4.8	80.1	1.3	0.0
	97.37	72.27	46.63	166.49	114.48	65.71	0.1	5.0	79.3	1.7	0.0
	98.74	76.41	52.67	159.27	114.50	66.81	0.1	4.9	80.0	1.5	0.0
	98.36	75.00	50.55	162.95	114.70	66.44	0.1	4.9	79.8	1.6	0.0
1200 psi	92.27	69.09	45.09	149.90	108.67	62.74	0.1	3.4	75.6	2.1	0.0
	89.78	66.05	42.44	149.31	106.85	60.35	0.1	3.4	73.5	2.6	0.0
	89.17	65.55	42.11	148.51	106.23	59.89	0.1	3.2	73.0	2.6	0.0
	90.41	66.90	43.21	19.24	107.25	62.98	0.1	3.3	74.0	2.4	0.0

Table A1.26: *Drop-Size Distribution Results for 23% Calcium Carbonate Slurry using the Nozzle AAASSTC8-5*

Pressure	Fluid	Obscuration	Log. Difference	Measured Values		Correction Factors		Corrected Values		Volumetric Flowrate (l/min)	Specific Surface Area (Sq. m/cc)
				X Parameter	N Parameter	X Parameter	N Parameter	X Parameter	N Parameter		
400 psi	23% CaCO3	0.4618	5.13	130.71	2.31	-	-	-	-	10.88	0.03
		0.4924	5.00	128.90	2.22						0.04
		0.4451	5.11	127.93	2.34						0.04
				129.18	2.29						0.04
600 psi	23% CaCO3	0.6873	4.83	129.62	2.45	1.0350	1.1313	134.16	2.77	13.92	0.04
		0.6819	4.86	129.62	2.45	1.0348	1.1295	134.13	2.77		0.04
		0.6923	4.75	130.71	2.15	1.0375	1.1115	135.61	2.39		0.03
				129.98	2.35			134.63	2.64		0.04
800 psi	23% CaCO3	0.6749	5.71	118.07	2.77	1.0329	1.1497	121.95	3.18	16.59	0.04
		0.6707	4.61	117.83	2.73	1.0330	1.1452	121.72	3.13		0.04
		0.6652	4.63	117.83	2.73	1.0330	1.1431	121.72	3.12		0.04
				117.91	2.74			121.80	3.14		0.04
1000 psi	23% CaCO3	0.6963	4.49	119.78	2.62	1.0342	1.1474	123.88	3.01	18.31	0.04
		0.6863	4.51	120.11	2.65	1.0337	1.1455	124.16	3.04		0.04
		0.6825	4.56	118.55	2.62	1.0338	1.1419	122.56	2.99		0.04
				119.48	2.63			123.53	3.01		0.04
1200 psi	23% CaCO3	0.6840	4.44	119.57	2.64	1.0337	1.1439	123.60	3.02	20.59	0.04
		0.7031	4.70	118.41	2.93	1.0326	1.1753	122.27	3.44		0.04
		0.6919	4.71	119.78	2.62	1.0341	1.1456	123.86	3.00		0.04
				119.25	2.73			123.24	3.15		0.04

All Dimensions in microns

Slurry Temperature = 20.0 C

Apparent Viscosity = 2.250 cP

Density = 1165.0 kg / Cu. m

Wet Bulb Temperature = 12 C

Dry Bulb Temperature = 16 C

Relative Humidity = 63%

Atmospheric Pressure = 751.3 mm Hg

Air Density = 1.221 kg / Cu. m

Pressure	D(3,2)	D(2,1)	D(1,0)	D(v,0.9)	D(v,0.5)	D(v,0.1)	% > 420.0	% > 201.0	% > 82.7	% < 39.5	% < 10.5
400 psi	75.56	25.45	9.81	188.54	111.54	49.35	0.2	6.9	70.7	6.1	0.4
	72.38	23.16	8.95	188.32	109.30	46.79	0.3	7.0	68.8	7.0	0.5
	74.83	25.74	9.95	194.84	109.64	48.90	0.2	8.6	69.8	6.1	0.3
	74.26	24.78	9.57	190.58	110.16	48.35	0.2	7.5	69.8	6.4	0.4
600 psi	93.42	56.40	29.38	196.73	118.11	59.90	0.2	9.1	76.9	3.2	0.0
	93.40	56.39	29.38	196.69	118.08	59.89	0.2	9.0	76.9	3.2	0.0
	81.99	32.14	12.81	192.15	116.91	52.86	0.2	7.7	73.6	5.1	0.3
	89.60	41.64	23.86	195.19	117.70	57.55	0.2	8.6	75.8	3.8	0.1
800 psi	90.54	63.35	37.94	156.46	109.14	60.51	0.1	4.6	74.6	2.6	0.0
	89.81	62.19	36.87	157.12	108.77	59.74	0.1	4.7	74.0	2.8	0.0
	89.70	61.99	36.69	157.37	108.74	59.60	0.1	4.7	73.9	2.8	0.0
	90.02	62.51	37.17	156.98	108.88	56.95	0.1	4.7	74.2	2.7	0.0
1000 psi	89.97	60.69	35.15	169.96	110.05	59.07	0.1	5.3	74.2	3.0	0.0
	90.52	61.41	35.72	169.83	110.39	59.64	0.1	5.3	74.6	2.9	0.0
	88.80	59.76	34.59	165.73	108.92	58.15	0.1	5.0	73.3	3.2	0.0
	89.76	60.62	35.15	168.51	109.79	58.95	0.1	5.2	74.0	3.0	0.0
1200 psi	89.89	60.78	35.28	168.55	109.87	59.09	0.1	5.2	74.1	3.0	0.0
	93.86	70.11	45.67	153.22	109.51	63.71	0.1	3.9	76.8	1.9	0.0
	89.84	60.48	34.97	170.27	110.00	58.92	0.1	5.3	74.1	3.1	0.0
	91.20	63.79	38.64	164.01	109.79	60.57	0.1	4.8	75.0	2.7	0.0

Table A1.27: *Drop-Size Distribution Results for 23% Calcium Carbonate Slurry using the Nozzle AAASSTC8-8*

Pressure	Fluid	Obscuration	Log. Difference	Measured Values		Correction Factors		Corrected Values		Volumetric Flowrate (l/min)	Specific Surface Area (Sq. m/cc)
				X Parameter	N Parameter	X Parameter	N Parameter	X Parameter	N Parameter		
400 psi	23% CaCO3	0.5203	5.01	138.20	2.08	–	–	–	–	14.45	0.02
		0.5274	5.40	137.87	2.08						0.02
		0.5325	5.09	136.88	2.17						0.03
				137.65	2.11						0.02
600 psi	23% CaCO3	0.6035	5.03	125.49	2.25	–	–	–	–	18.41	0.04
		0.6051	4.82	126.73	2.36						0.04
		0.6085	5.03	126.73	2.36						0.04
				126.32	2.32						0.04
800 psi	23% CaCO3	0.6668	4.67	118.55	2.62	1.0335	1.1362	122.53	2.98	21.48	0.04
		0.6663	4.58	116.72	2.62	1.0335	1.1360	120.63	2.98		0.04
		0.6445	4.65	115.40	2.66	1.0000	1.0000	115.40	2.66		0.04
				116.89	2.63			119.52	2.87		0.04
1000 psi	23% CaCO3	0.6808	4.61	106.78	2.95	1.0320	1.1655	110.20	3.44	23.89	0.05
		0.6692	4.61	108.43	2.45	1.0345	1.1254	112.17	2.76		0.05
		0.6890	4.74	108.55	2.62	1.0340	1.1444	112.55	3.00		0.04
				107.92	2.67			111.64	2.93		0.05
1200 psi	23% CaCO3	0.6839	4.90	118.85	2.66	1.0336	1.1453	122.84	3.05	27.80	0.04
		0.6891	4.81	118.28	2.55	1.0344	1.1393	122.35	2.91		0.04
		0.7270	4.64	119.41	2.31	1.0388	1.1360	124.05	2.62		0.04
				118.85	2.51			123.08	2.86		0.04

All Dimensions in microns

Slurry Temperature = 19.8 C

Wet Bulb Temperature = 12 C

Atmospheric Pressure = 751.4 mm Hg

Apparent Viscosity = 2.250 cP

Dry Bulb Temperature = 16 C

Air Density = 1.221 kg / Cu. m

Density = 1165.0 kg / Cu. m

Relative Humidity = 63%

Pressure	D(3,2)	D(2,1)	D(1,0)	D(v,0.9)	D(v,0.5)	D(v,0.1)	% > 420.0	% > 201.0	% > 82.7	% < 39.5	% < 10.5
400 psi	73.56	21.39	8.32	204.08	115.88	46.86	0.6	10.8	70.9	7.1	0.4
	73.39	21.36	8.30	203.67	115.60	46.75	0.5	10.7	70.8	7.2	0.4
	75.27	23.05	8.91	200.04	115.60	48.54	0.4	9.7	71.5	6.5	0.5
	74.07	21.93	8.51	202.60	115.69	47.38	0.5	10.4	71.1	6.9	0.4
600 psi	71.35	23.33	9.02	193.34	107.00	46.16	0.2	8.3	67.6	7.1	0.4
	74.63	26.06	10.08	192.81	108.81	48.84	0.2	8.2	69.4	6.1	0.3
	74.63	26.06	10.08	192.81	108.81	48.84	0.2	8.2	69.4	6.1	0.3
	73.54	25.15	9.73	192.99	108.21	47.95	0.2	8.2	68.8	6.4	0.3
800 psi	88.66	59.55	34.41	166.07	108.86	57.99	0.1	5.0	73.2	3.3	0.0
	87.34	58.78	34.08	158.54	107.32	57.08	0.1	4.8	72.1	3.4	0.0
	78.29	45.36	22.78	155.70	100.91	49.52	0.1	4.6	66.3	5.5	0.1
	84.76	54.56	30.42	160.10	105.70	54.86	0.1	4.8	70.5	4.1	0.0
1000 psi	84.69	64.25	42.83	138.61	99.97	57.79	0.0	1.3	68.5	2.9	0.0
	77.59	46.79	24.17	148.01	99.25	49.61	0.1	3.4	64.8	5.4	0.1
	81.28	53.88	30.37	145.03	100.59	53.36	0.1	2.8	67.0	4.2	0.0
	81.19	54.97	32.46	143.88	99.94	53.59	0.1	2.5	66.8	4.2	0.0
1200 psi	89.69	61.08	35.66	164.09	109.38	59.16	0.1	4.9	73.9	3.0	0.0
	87.10	55.85	30.51	168.41	108.42	56.83	0.1	5.2	72.5	3.5	0.0
	83.52	46.95	23.12	182.57	108.20	52.57	0.1	6.6	70.9	4.8	0.1
	86.77	54.63	29.76	171.69	108.74	56.19	0.1	5.6	72.4	3.8	0.0

Table A1.28: *Drop-Size Distribution Results for 23% Calcium Carbonate Slurry using the Nozzle AAASSTC10-10*

Pressure	Fluid	Obscuration	Log. Difference	Measured Values		Correction Factors		Corrected Values		Volumetric Flowrate (l/min)	Specific Surface Area (Sq. m/cc)
				X Parameter	N Parameter	X Parameter	N Parameter	X Parameter	N Parameter		
400 psi	23% CaCO3	0.5274	5.40	144.66	2.14	-	-	-	-	19.15	0.03
		0.5236	5.33	145.66	2.15						0.03
		0.5040	5.42	144.66	2.14						0.03
				144.99	2.14						0.03
600 psi	23% CaCO3	0.6408	5.20	121.44	2.25	-	-	-	-	23.29	0.03
		0.6450	5.24	121.44	2.25						0.03
		0.6403	5.24	122.84	2.30						0.03
				121.91	2.27						0.03
800 psi	23% CaCO3	0.7105	5.13	109.22	2.39	1.0367	1.1355	113.23	2.71	26.88	0.04
		0.7477	5.19	108.83	2.32	1.0411	1.1467	113.30	2.66		0.04
		0.7188	5.16	109.30	2.34	1.0378	1.1350	113.43	2.66		0.04
				109.45	2.35			113.32	2.68		0.04
1000 psi	23% CaCO3	0.7615	5.15	94.69	2.34	1.0427	1.1563	98.74	2.71	29.57	0.05
		0.7831	5.17	94.69	2.60	1.0426	1.1995	98.73	3.12		0.05
		0.7645	5.39	94.53	2.42	1.0421	1.1661	98.51	2.82		0.05
				94.64	2.45			98.66	2.88		0.05
1200 psi	23% CaCO3	0.8763	5.93	94.62	2.38	1.0712	1.2856	101.36	3.06	31.67	0.05
		0.8812	5.64	95.83	2.38	1.0731	1.2945	102.84	3.08		0.05
		0.8711	5.57	95.83	2.38	1.0693	1.2767	102.47	3.04		0.05
				95.43	2.38			102.22	3.06		0.05

All Dimensions in microns

Slurry Temperature = 19.9 C

Apparent Viscosity = 2.250 cP

Density = 1165.0 kg / Cu. m

Wet Bulb Temperature = 12 C

Dry Bulb Temperature = 16 C

Relative Humidity = 63%

Atmospheric Pressure = 751.4 mm Hg

Air Density = 1.221 kg / Cu. m

Pressure	D(3,2)	D(2,1)	D(1,0)	D(v,0.9)	D(v,0.5)	D(v,0.1)	% > 420.0	% > 201.0	% > 82.7	% < 39.5	% < 10.5
400 psi	78.45	23.24	8.98	210.17	121.91	50.56	0.7	12.6	73.9	6.0	0.4
	79.25	23.57	9.10	211.07	122.85	51.15	0.7	12.8	74.4	5.9	0.4
	78.45	23.24	8.98	210.17	121.91	50.56	0.7	12.6	73.9	6.0	0.4
	78.72	23.35	9.02	210.47	122.22	50.76	0.7	12.7	74.1	6.0	0.4
600 psi	69.18	22.82	8.84	187.21	103.63	44.67	0.2	7.2	65.7	7.6	0.4
	69.18	22.82	8.84	187.21	103.63	44.67	0.2	7.2	65.7	7.6	0.4
	71.04	24.01	9.29	188.24	105.17	46.17	0.2	7.4	66.9	7.0	0.4
	69.80	23.22	8.99	187.55	104.14	45.17	0.2	7.3	66.1	7.4	0.4
800 psi	77.57	45.82	23.30	150.51	99.93	49.32	0.1	3.8	65.1	5.5	0.1
	76.90	44.72	22.54	151.82	99.03	48.62	0.1	4.0	64.9	5.8	0.1
	76.98	44.76	22.55	152.03	99.14	48.67	0.1	4.1	65.0	5.8	0.1
	77.15	45.09	22.80	151.45	99.37	48.87	0.1	4.0	65.0	5.7	0.1
1000 psi	67.93	41.19	21.58	133.18	86.25	43.04	0.0	1.3	53.9	8.0	0.3
	72.75	50.17	29.60	133.57	88.20	48.22	0.0	0.7	56.0	5.5	0.1
	68.98	43.09	22.96	131.72	86.50	44.36	0.0	1.1	54.3	7.3	0.2
	69.89	44.82	24.71	132.82	86.98	45.21	0.0	1.2	54.7	6.9	0.2
1200 psi	73.93	50.30	29.17	132.10	90.75	48.52	0.0	0.8	58.2	5.4	0.1
	75.17	51.29	29.78	133.57	92.23	49.50	0.0	1.0	59.7	5.1	0.1
	74.52	50.41	29.07	133.51	91.72	48.83	0.0	1.0	59.1	5.3	0.1
	74.54	50.67	29.34	133.06	91.57	48.95	0.0	0.9	59.0	5.3	0.1

Table A1.29: *Drop-Size Distribution Results for 23% Calcium Carbonate Slurry using the Nozzle Delevan 2.0SJ*

Pressure	Fluid	Obscuration	Log. Difference	Measured Values		Correction Factors		Corrected Values		Volumetric Flowrate (l/min)	Specific Surface Area (Sq. m/cc)
				X Parameter	N Parameter	X Parameter	N Parameter	X Parameter	N Parameter		
400 psi	23% CaCO3	0.4830	5.49	99.70	2.39	–	–	–	–	8.27	0.05
		0.4606	5.60	100.82	2.28						0.04
		0.4706	5.53	99.70	2.39						0.05
				100.07	2.35						0.05
600 psi	23% CaCO3	0.7020	5.44	74.75	2.25	1.0373	1.1217	77.54	2.52	10.69	0.06
		0.7254	5.44	73.01	2.30	1.0388	1.1345	75.84	2.61		0.06
		0.7067	5.42	74.75	2.25	1.0376	1.1233	77.56	2.53		0.06
				74.17	2.27			76.98	2.55		0.06
800 psi	23% CaCO3	0.8798	5.46	61.05	2.36	1.0733	1.2880	65.52	3.04	12.34	0.08
		0.8839	5.47	61.54	2.28	1.0779	1.2793	66.33	2.92		0.08
		0.8552	5.48	62.94	2.25	1.0676	1.2302	67.20	2.77		0.07
				61.84	2.30			66.35	2.91		0.08
1000 psi	23% CaCO3	0.9349	5.45	54.82	2.42	1.0959	1.4352	60.07	3.47	14.82	0.09
		0.9322	5.44	54.64	2.36	1.0976	1.4090	59.97	3.33		0.09
		0.9262	5.50	53.79	2.52	1.0868	1.4381	58.46	3.62		0.10
				54.42	2.40			59.50	3.47		0.09
1200 psi	23% CaCO3	0.9529	5.44	49.77	2.42	1.1057	1.4962	55.03	3.62	16.40	0.10
		0.9583	5.74	48.77	2.42	1.1089	1.5165	54.08	3.67		0.11
		0.9542	5.47	48.30	2.43	1.1059	1.5046	53.41	3.66		0.10
				48.95	2.42			54.17	3.65		0.10

All Dimensions in microns

Slurry Temperature = 20.0 C

Wet Bulb Temperature = 12 C

Atmospheric Pressure = 751.4 mm Hg

Apparent Viscosity = 2.25 cP

Dry Bulb Temperature = 16 C

Air Density = 1.221 kg / Cu. m

Density = 1165.0 kg / Cu. m

Relative Humidity = 63%

Pressure	D(3,2)	D(2,1)	D(1,0)	D(v,0.9)	D(v,0.5)	D(v,0.1)	% > 420.0	% > 201.0	% > 82.7	% < 39.5	% < 10.5
400 psi	59.68	22.31	8.74	138.69	85.54	38.89	0.1	2.3	52.8	10.3	0.4
	58.52	20.77	8.14	142.14	85.88	37.59	0.1	2.9	53.0	11.1	0.5
	59.68	22.31	8.74	138.69	85.54	38.89	0.1	2.3	52.8	10.3	0.4
	59.29	21.80	8.54	139.84	85.65	38.46	0.1	2.5	52.9	10.6	0.4
600 psi	48.56	20.50	8.27	106.16	67.09	31.75	0.0	0.1	31.0	16.6	0.5
	48.47	21.26	8.64	102.55	65.92	32.02	0.0	0.1	28.7	16.6	0.5
	48.67	20.62	8.32	106.03	67.15	31.87	0.0	0.1	31.0	16.5	0.5
	48.57	20.79	8.41	104.91	66.72	31.88	0.0	0.1	30.2	16.6	0.5
800 psi	45.48	24.06	10.48	87.83	58.25	31.26	0.0	0.0	12.6	19.3	0.3
	45.10	22.74	9.67	90.47	58.69	30.70	0.0	0.0	14.4	19.7	0.4
	44.48	21.25	8.87	92.96	59.05	29.82	0.0	0.0	16.4	20.5	0.5
	45.02	22.68	9.67	90.42	58.66	30.59	0.0	0.0	14.5	19.8	0.4
1000 psi	46.14	34.84	22.87	75.52	53.96	31.24	0.0	0.0	4.4	20.5	0.3
	45.46	33.71	21.75	76.01	53.75	30.51	0.0	0.0	5.0	22.0	0.2
	45.57	35.23	23.85	74.57	52.49	31.23	0.0	0.0	2.8	21.2	0.3
	45.72	34.59	22.82	75.37	53.40	30.99	0.0	0.0	4.1	21.2	0.3
1200 psi	42.94	33.32	22.73	71.19	49.79	29.66	0.0	0.0	1.2	25.7	0.3
	42.40	33.14	22.83	69.80	49.08	29.43	0.0	0.0	0.9	26.7	0.3
	41.85	32.72	22.57	68.85	48.53	29.05	0.0	0.0	0.7	27.9	0.2
	42.40	33.06	22.71	69.95	49.13	29.38	0.0	0.0	0.9	26.8	0.3

Table A1.30: *Drop-Size Distribution Results for 23% Calcium Carbonate Slurry using the Nozzle Delevan 2.2SJ*

Pressure	Fluid	Obscuration	Log. Difference	Measured Values		Correction Factors		Corrected Values		Volumetric Flowrate (l/min)	Specific Surface Area (Sq. m/cc)
				X Parameter	N Parameter	X Parameter	N Parameter	X Parameter	N Parameter		
400 psi	23% CaCO3	0.4888	5.79	95.08	2.22	-	-	-	-	10.67	0.05
		0.5215	5.67	94.34	2.15						0.05
		0.4712	5.73	95.44	2.22						0.05
				94.95	2.59						0.05
600 psi	23% CaCO3	0.7462	5.54	66.10	2.30	1.0411	1.1441	68.82	2.63	12.62	0.07
		0.7553	5.55	66.52	2.25	1.0430	1.1443	69.38	2.57		0.07
		0.7241	5.54	68.74	2.25	1.0391	1.1299	71.43	2.54		0.07
				67.12	2.27			69.88	2.58		0.07
800 psi	23% CaCO3	0.8998	5.48	48.98	2.42	1.0792	1.3414	52.86	3.25	14.94	0.11
		0.8895	5.45	47.30	2.71	1.0658	1.3842	50.41	3.75		0.11
		0.8671	5.49	47.30	2.71	1.0590	1.3327	50.09	3.61		0.11
				47.86	2.61			51.12	3.54		0.11
1000 psi	23% CaCO3	0.9490	5.43	42.19	2.82	1.0836	1.6231	45.72	4.58	16.60	0.12
		0.9482	5.43	42.19	2.82	1.0837	1.6240	45.72	4.58		0.12
		0.9363	5.47	41.67	2.82	1.0790	1.5708	44.96	4.43		0.12
				41.29	2.82			45.47	4.53		0.12
1200 psi	23% CaCO3	0.9672	5.45	39.21	2.88	1.0892	1.7492	42.71	5.04	20.74	0.13
		0.9539	5.45	38.99	2.72	1.0905	1.6121	42.52	4.39		0.14
		0.9701	5.43	39.06	2.60	1.1048	1.6403	43.15	4.26		0.13
				39.09	2.73			42.79	4.56		0.13

All Dimensions in microns

Slurry Temperature = 20.0 C

Wet Bulb Temperature = 12 C

Atmospheric Pressure = 751.4 mm Hg

Apparent Viscosity = 2.250 cP

Dry Bulb Temperature = 16 C

Air Density = 1.221 kg / Cu. m

Density = 1165.0 kg / Cu. m

Relative Humidity = 63%

Pressure	D(3,2)	D(2,1)	D(1,0)	D(v,0.9)	D(v,0.5)	D(v,0.1)	% > 420.0	% > 201.0	% > 82.7	% < 39.5	% < 10.5
400 psi	54.47	19.27	7.61	136.10	80.58	34.52	0.1	2.2	48.1	13.2	0.7
	57.56	29.99	15.20	136.57	79.52	33.14	0.1	2.3	47.1	14.2	0.8
	54.66	19.32	7.62	136.54	80.89	34.65	0.1	2.2	48.4	13.1	0.7
	55.56	22.86	10.14	136.40	80.33	34.10	0.1	2.2	47.9	13.5	0.7
600 psi	44.34	20.16	8.31	93.86	59.83	29.25	0.0	0.0	19.9	20.7	0.7
	44.15	19.64	8.07	95.13	60.12	28.91	0.0	0.0	20.9	20.9	0.7
	45.10	19.70	8.05	97.90	61.80	- 29.46	0.0	0.1	23.6	19.8	0.7
	44.53	19.83	8.14	95.63	60.58	29.21	0.0	0.0	21.5	20.5	0.7
800 psi	37.91	21.80	10.01	69.98	47.51	26.64	0.0	0.0	1.3	31.9	0.5
	36.84	25.87	16.18	62.09	46.12	27.91	0.0	0.0	0.4	32.6	0.2
	39.13	30.68	21.35	62.28	45.68	27.09	0.0	0.0	0.5	34.2	0.3
	37.99	26.12	15.85	64.78	46.44	27.21	0.0	0.0	0.7	32.9	0.3
1000 psi	38.20	33.09	26.73	56.46	42.36	27.31	0.0	0.0	0.0	39.6	0.2
	38.20	33.09	26.73	56.46	42.36	27.31	0.0	0.0	0.0	39.6	0.2
	37.30	32.02	25.54	56.00	41.62	26.45	0.0	0.0	0.0	42.6	0.2
	37.90	32.73	26.33	56.31	42.11	27.02	0.0	0.0	0.0	40.6	0.2
1200 psi	36.51	32.83	28.25	50.81	39.93	26.62	0.0	0.0	0.0	48.5	0.1
	35.22	30.28	24.22	52.78	39.10	25.11	0.0	0.0	0.0	51.8	0.3
	35.50	30.26	23.91	54.17	39.51	25.10	0.0	0.0	0.0	50.0	0.2
	35.74	31.12	25.46	52.59	39.51	25.61	0.0	0.0	0.0	50.1	0.2

Table A1.31: *Drop-Size Distribution Results for 35% Calcium Carbonate Slurry using the Nozzle AAASSTC5-5*

Pressure	Fluid	Obscuration	Log. Difference	Measured Values		Correction Factors		Corrected Values		Volumetric Flowrate (l/min)	Specific Surface Area (Sq. m/cc)
				X Parameter	N Parameter	X Parameter	N Parameter	X Parameter	N Parameter		
400 psi	35% CaCO3	0.4118	5.03	123.67	2.35					8.45	0.04
		0.4553	5.04	123.67	2.42	-	-	-	-		0.04
		0.4890	4.66	123.77	2.36						0.04
				123.70	2.38						0.04
600 psi	35% CaCO3	0.4426	4.94	121.94	2.25					9.71	0.04
		0.4485	4.84	120.27	2.34	-	-	-	-		0.04
		0.4844	4.74	120.27	2.42						0.04
				120.83	2.34						0.04
800 psi	35% CaCO3	0.5385	5.09	115.77	2.65					11.94	0.04
		0.5449	4.59	114.87	2.65	-	-	-	-		0.04
		0.5110	4.85	114.24	2.66						0.04
				114.96	2.65						0.04
1000 psi	35% CaCO3	0.5772	4.73	111.34	2.66					14.06	0.04
		0.5486	4.74	111.50	2.85	-	-	-	-		0.04
		0.5653	4.71	111.81	2.55						0.04
				111.55	2.69						0.04
1200 psi	35% CaCO3	0.6108	4.93	107.82	2.66					15.61	0.05
		0.5828	4.95	106.75	2.66	-	-	-	-		0.05
		0.5703	4.99	106.75	2.95						0.05
				107.11	2.76						0.05

All Dimensions in microns

Slurry Temperature = 20.0 C

Wet Bulb Temperature = 14 C

Atmospheric Pressure = 751.7 mm Hg

Apparent Viscosity = 2.700 cP

Dry Bulb Temperature = 17 C

Air Density = 1.217 kg / Cu. m

Density = 1265.0 kg / Cu. m

Relative Humidity = 72%

Pressure	D(3,2)	D(2,1)	D(1,0)	D(v,0.9)	D(v,0.5)	D(v,0.1)	% > 420.0	% > 201.0	% > 82.7	% < 39.5	% < 10.5
400 psi	72.64	25.27	9.78	188.39	106.22	47.46	0.2	7.4	67.9	6.5	0.3
	74.30	27.19	10.57	186.73	106.69	48.80	0.2	7.2	68.6	6.0	0.2
	72.93	25.53	9.88	188.32	106.37	47.69	0.2	7.4	68.0	6.4	0.3
	73.29	26.00	10.08	187.81	106.43	47.98	0.2	7.3	68.2	6.3	0.3
600 psi	69.45	22.88	8.86	188.03	104.05	44.85	0.2	7.4	65.9	7.5	0.4
	70.49	24.49	9.49	182.60	103.28	45.97	0.1	6.6	66.0	7.0	0.3
	72.26	26.45	10.28	180.17	103.81	47.45	0.1	6.3	66.8	6.4	0.3
	70.73	24.61	9.54	183.60	103.71	46.09	0.1	6.8	66.2	7.0	0.3
800 psi	78.39	45.24	22.67	156.82	101.19	49.52	0.1	4.7	66.5	5.5	0.1
	77.79	44.97	22.57	154.90	100.38	49.13	0.1	4.5	65.9	5.6	0.1
	77.52	45.00	22.64	153.44	99.87	49.02	0.1	4.3	65.6	5.6	0.1
	77.90	45.07	22.63	155.05	100.48	49.22	0.1	4.5	66.0	5.6	0.1
1000 psi	75.60	44.11	22.31	148.82	97.26	47.78	0.1	3.6	63.6	6.1	0.1
	78.79	50.38	27.64	145.71	99.07	50.65	0.1	3.0	65.0	5.0	0.1
	70.94	31.29	12.85	151.95	97.12	46.26	0.1	4.2	63.0	6.7	0.2
	75.11	41.93	20.93	148.83	97.82	48.23	0.1	3.6	63.9	5.9	0.1
1200 psi	73.28	43.06	21.94	144.18	94.09	46.27	0.1	2.8	61.1	6.6	0.2
	72.58	42.73	21.82	142.88	93.13	45.81	0.1	2.6	60.3	6.8	0.2
	76.62	50.51	28.44	139.02	95.29	49.76	0.0	1.8	62.2	5.1	0.1
	74.16	45.43	24.07	142.03	94.17	47.28	0.1	2.4	61.2	6.2	0.2

Table A1.32: *Drop-Size Distribution Results for 35% Calcium Carbonate Slurry using the Nozzle AAASSTC8-5*

Pressure	Fluid	Obscuration	Log. Difference	Measured Values		Correction Factors		Corrected Values		Volumetric Flowrate (l/min)	Specific Surface Area (Sq. m/cc)
				X Parameter	N Parameter	X Parameter	N Parameter	X Parameter	N Parameter		
400 psi	35% CaCO3	0.4302	5.20	115.84	2.30						0.04
		0.4404	5.14	116.15	2.42	–	–	–	–	11.24	0.04
		0.4599	5.20	115.84	2.30						0.04
				115.94	2.34						0.04
600 psi	35% CaCO3	0.5687	4.87	121.44	2.25						0.04
		0.5852	4.79	120.95	2.16	–	–	–	–	13.83	0.04
		0.5965	4.92	121.38	2.25						0.04
				121.26	2.22						0.04
800 psi	35% CaCO3	0.6731	4.66	111.77	2.39	1.0349	1.1225	115.67	2.68		0.04
		0.6747	4.94	111.88	2.31	1.0355	1.1175	115.85	2.58	15.31	0.04
		0.6715	5.09	110.01	2.66	1.0334	1.1406	113.68	3.03		0.04
				111.22	2.45			115.07	2.76		0.04
1000 psi	35% CaCO3	0.6688	4.82	101.06	2.37	1.0349	1.1199	104.59	2.65		0.05
		0.6647	4.68	101.94	2.55	1.0339	1.1307	105.39	2.88	16.56	0.04
		0.6730	4.75	102.82	2.66	1.0334	1.1411	106.25	3.04		0.05
				101.94	2.53			105.41	2.86		0.05
1200 psi	35% CaCO3	0.6695	4.66	98.08	2.55	1.0339	1.1323	101.41	2.89		0.05
		0.6970	4.76	98.08	2.55	1.0347	1.1424	101.49	2.91	18.99	0.05
		0.6865	4.67	97.45	2.54	1.0344	1.1376	100.80	2.89		0.05
				97.87	2.55			101.23	2.93		0.05

All Dimensions in microns

Slurry Temperature = 20.0 C

Wet Bulb Temperature = 14 C

Atmospheric Pressure = 751.6 mm Hg

Apparent Viscosity = 2.700 cP

Dry Bulb Temperature = 17 C

Air Density = 1.217 kg / Cu. m

Density = 1265.0 kg / Cu. m

Relative Humidity = 72%

Pressure	D(3,2)	D(2,1)	D(1,0)	D(v,0.9)	D(v,0.5)	D(v,0.1)	% > 420.0	% > 201.0	% > 82.7	% < 39.5	% < 10.5
400 psi	67.18	23.04	8.94	174.09	99.17	43.55	0.1	5.7	63.1	8.0	0.4
	69.85	25.62	9.97	169.53	100.23	45.83	0.1	5.3	64.5	7.0	0.3
	67.18	23.04	8.94	174.09	99.17	43.55	0.1	5.7	63.1	8.0	0.4
	68.07	23.90	9.28	172.57	99.52	44.31	0.1	5.4	63.6	7.7	0.4
600 psi	69.18	22.82	8.84	187.21	103.63	44.67	0.2	7.2	65.7	7.6	0.4
	66.94	21.13	8.23	188.82	102.51	42.68	0.2	7.5	64.4	8.5	0.4
	69.15	22.81	8.84	187.11	103.58	44.65	0.2	7.2	65.6	7.6	0.4
	68.42	22.25	8.64	187.71	103.24	44.00	0.2	7.3	65.2	7.9	0.4
800 psi	78.77	45.90	23.12	155.63	101.86	49.94	0.1	4.6	66.4	5.3	0.1
	77.40	43.70	21.67	159.69	100.89	48.42	0.1	5.1	65.9	5.9	0.1
	82.93	56.92	33.70	146.04	101.68	54.36	0.1	2.9	68.0	3.9	0.0
	79.70	48.84	26.16	153.79	101.48	50.91	0.1	4.2	66.8	5.0	0.1
1000 psi	71.04	41.89	21.47	140.49	91.15	44.74	0.1	2.2	58.5	7.2	0.2
	74.92	48.73	27.21	138.26	93.76	48.18	0.0	1.7	60.6	5.7	0.1
	77.22	51.99	29.78	137.60	95.19	50.71	0.0	1.5	62.4	4.8	0.1
	74.39	47.54	26.15	138.78	93.37	47.88	0.0	1.8	60.5	5.9	0.1
1200 psi	72.27	47.42	26.75	134.24	89.32	46.55	0.0	1.1	57.5	6.3	0.1
	72.54	47.82	27.06	134.14	89.47	46.84	0.0	1.1	57.7	6.2	0.1
	71.85	47.19	26.65	133.57	88.78	46.27	0.0	1.1	56.9	6.4	0.2
	72.22	47.48	26.82	133.98	89.19	46.55	0.0	1.1	57.4	6.3	0.1

Table A1.33: *Drop-Size Distribution Results for 35% Calcium Carbonate Slurry using the Nozzle AAASSTC8-8*

Pressure	Fluid	Obscuration	Log. Difference	Measured Values		Correction Factors		Corrected Values		Volumetric Flowrate (l/min)	Specific Surface Area (Sq. m/cc)
				X Parameter	N Parameter	X Parameter	N Parameter	X Parameter	N Parameter		
400 psi	35% CaCO3	0.4460	5.02	130.71	2.15	–	–	–	–	12.82	0.03
		0.4049	5.21	130.60	2.07						0.03
		0.4386	5.16	131.14	2.08						0.03
				130.82	2.10						0.03
600 psi	35% CaCO3	0.5650	4.86	119.68	2.09	–	–	–	–	16.30	0.04
		0.6088	4.64	119.68	2.02						0.03
		0.5822	4.99	119.68	2.09						0.04
				119.68	2.07						0.04
800 psi	35% CaCO3	0.6054	4.84	111.85	2.25	–	–	–	–	20.08	0.04
		0.5994	4.71	110.46	2.31						0.04
		0.6101	4.82	109.33	2.39						0.04
				110.55	2.32						0.04
1000 psi	35% CaCO3	0.6614	4.59	99.56	2.55	1.0338	1.1297	102.93	2.88	22.09	0.05
		0.6455	4.68	98.33	2.55	1.0000	1.0000	98.33	2.55		0.05
		0.6785	4.77	98.08	2.55	1.0341	1.1354	101.42	2.90		0.05
				98.66	2.55			100.89	2.78		0.05
1200 psi	35% CaCO3	0.6988	4.79	100.08	2.55	1.0348	1.1431	103.56	2.91	24.24	0.05
		0.6862	4.97	101.96	2.68	1.0335	1.1477	105.38	3.08		0.05
		0.7469	4.91	102.82	2.63	1.0377	1.1751	106.69	3.09		0.05
				101.62	2.62			105.21	3.03		0.05

All Dimensions in microns

Slurry Temperature = 20.2 C

Apparent Viscosity = 2.700 cP

Density = 1265.0 kg / Cu. m

Wet Bulb Temperature = 14 C

Dry Bulb Temperature = 17 C

Relative Humidity = 72%

Atmospheric Pressure = 751.7 mm Hg

Air Density = 1.217 kg / Cu. m

Pressure	D(3,2)	D(2,1)	D(1,0)	D(v,0.9)	D(v,0.5)	D(v,0.1)	% > 420.0	% > 201.0	% > 82.7	% < 39.5	% < 10.5
400 psi	71.61	21.99	8.52	192.67	110.23	45.91	0.4	8.0	68.8	7.3	0.4
	69.55	20.53	8.01	194.79	109.41	44.06	0.4	8.5	67.8	8.1	0.5
	70.07	20.75	8.08	195.21	109.96	44.47	0.4	8.6	68.2	7.9	0.5
	70.41	21.09	8.20	194.22	109.87	44.81	0.4	8.4	68.3	7.8	0.5
600 psi	64.72	19.85	7.77	188.78	100.86	40.79	0.2	7.5	63.0	9.4	0.6
	58.44	12.56	4.93	181.07	99.81	39.31	0.2	5.8	62.3	10.1	0.7
	64.72	19.85	7.77	188.78	100.86	40.79	0.2	7.5	63.0	9.4	0.6
	62.63	17.42	6.82	186.21	100.51	40.30	0.2	6.9	62.8	9.6	0.6
800 psi	64.02	21.63	8.42	164.57	95.33	41.15	0.1	4.9	60.3	9.1	0.4
	64.34	22.50	8.75	156.85	94.51	41.70	0.1	4.8	60.0	8.8	0.3
	65.19	23.82	9.27	151.93	94.01	42.64	0.1	4.3	59.9	8.3	0.4
	64.52	22.65	8.81	157.78	94.62	41.83	0.1	4.7	60.1	8.7	0.4
1000 psi	73.22	47.82	26.84	136.00	90.63	47.12	0.0	1.4	58.7	6.1	0.1
	61.36	24.93	9.85	134.68	85.17	40.69	0.0	1.7	52.6	9.3	0.4
	72.39	47.61	26.90	134.16	89.37	46.68	0.0	1.1	57.5	6.3	0.1
	68.99	40.12	21.20	134.95	88.39	44.83	0.0	1.4	56.3	7.2	0.2
1200 psi	73.98	48.59	27.37	135.94	92.20	47.72	0.0	1.4	59.2	5.8	0.1
	77.03	52.44	30.38	136.32	94.56	50.79	0.0	1.3	61.9	4.7	0.1
	78.53	55.02	33.33	137.62	95.78	51.59	0.0	1.5	63.1	4.5	0.1
	76.51	52.03	30.36	136.63	94.18	50.03	0.0	1.4	61.4	5.0	0.1

Table A1.34: *Drop-Size Distribution Results for 35% Calcium Carbonate Slurry using the Nozzle AAASSTC10-10*

Pressure	Fluid	Obscuration	Log. Difference	Measured Values		Correction Factors		Corrected Values		Volumetric Flowrate (l/min)	Specific Surface Area (Sq. m/cc)
				X Parameter	N Parameter	X Parameter	N Parameter	X Parameter	N Parameter		
400 psi	35% CaCO3	0.4768	5.32	145.25	2.00	–	–	–	–	16.74	0.03
		0.3664	5.12	143.45	2.15						0.03
		0.3502	5.17	147.55	2.15						0.03
				145.42	2.10						0.03
600 psi	35% CaCO3	0.5240	4.99	128.42	2.25	–	–	–	–	21.97	0.03
		0.5457	5.12	130.14	2.15						0.03
		0.5020	5.03	128.61	2.25						0.04
				129.06	2.22						0.03
800 psi	35% CaCO3	0.6415	4.91	114.60	2.25	–	–	–	–	25.29	0.04
		0.5985	4.87	116.15	2.34						0.04
		0.6099	4.93	113.50	2.34						0.04
				114.75	2.31						0.04
1000 psi	35% CaCO3	0.6450	5.04	104.73	2.25	1.0000	1.0000	104.73	2.25	28.42	0.04
		0.6673	4.91	105.70	2.39	1.0348	1.1281	109.38	2.68		0.04
		0.6473	4.85	104.32	2.30	1.0000	1.0000	104.32	2.30		0.04
				104.92	2.31			106.14	2.41		0.04
1200 psi	35% CaCO3	0.6642	4.92	95.32	2.37	1.0348	1.1186	98.64	2.65	34.16	0.05
		0.6780	5.30	96.24	2.42	1.0349	1.1261	99.60	2.73		0.05
		0.6523	5.00	95.78	2.38	1.0346	1.1161	99.10	2.66		0.05
				95.78	2.39			99.11	2.68		0.05

All Dimensions in microns

Slurry Temperature = 20.1 C

Wet Bulb Temperature = 14 C

Atmospheric Pressure = 751.6 mm Hg

Apparent Viscosity = 2.700 cP

Dry Bulb Temperature = 17 C

Air Density = 1.217 kg / Cu. m

Density = 1265.0 kg / Cu. m

Relative Humidity = 72%

Pressure	D(3,2)	D(2,1)	D(1,0)	D(v,0.9)	D(v,0.5)	D(v,0.1)	% > 420.0	% > 201.0	% > 82.7	% < 39.5	% < 10.5
400 psi	74.69	20.47	8.01	215.12	121.00	47.17	1.0	13.8	72.3	7.1	0.5
	78.12	23.33	9.01	208.48	120.97	50.38	0.6	12.1	73.6	6.1	0.4
	80.21	23.77	9.18	213.28	124.47	51.82	0.8	13.5	75.0	5.7	0.4
	77.67	22.52	8.73	212.29	122.15	49.79	0.8	13.1	73.6	6.3	0.4
600 psi	72.84	23.73	9.16	186.85	109.13	47.25	0.2	6.6	69.0	6.8	0.4
	71.32	21.93	8.50	191.91	109.75	45.71	0.4	7.8	68.6	7.4	0.4
	72.94	23.75	9.17	187.12	109.29	47.32	0.2	6.7	69.1	6.8	0.4
	72.37	23.14	8.94	188.63	109.39	46.76	0.3	7.0	68.9	7.0	0.4
800 psi	65.50	21.97	8.54	173.05	97.74	42.16	0.1	5.6	61.9	8.6	0.4
	68.16	23.86	9.26	173.20	99.71	44.40	0.1	5.6	63.7	7.6	0.4
	66.67	23.47	9.12	164.89	97.39	43.39	0.1	5.0	62.1	8.0	0.4
	66.78	23.10	8.97	170.38	98.28	43.32	0.1	5.4	62.6	8.1	0.4
1000 psi	60.13	20.79	8.13	148.30	89.09	38.53	0.1	3.8	55.6	10.4	0.4
	74.58	43.93	22.38	145.82	95.58	47.23	0.1	3.1	62.4	6.2	0.2
	60.78	21.52	8.40	146.44	89.04	39.22	0.1	3.5	55.7	10.1	0.4
	65.16	28.75	12.97	146.85	91.24	41.66	0.1	3.5	57.9	8.9	0.3
1200 psi	64.38	30.82	13.09	133.77	85.91	42.20	0.0	1.5	53.5	8.4	0.3
	68.73	41.82	21.92	133.93	87.09	43.68	0.0	1.4	54.8	7.7	0.2
	64.65	30.67	12.93	134.17	86.35	42.53	0.0	1.5	53.9	8.3	0.3
	65.92	34.44	15.98	133.96	86.45	42.80	0.0	1.5	54.1	8.1	0.3

Table A1.35: *Drop-Size Distribution Results for 35% Calcium Carbonate Slurry using the Nozzle Delevan 2.0SJ*

Pressure	Fluid	Obscuration	Log. Difference	Measured Values		Correction Factors		Corrected Values		Volumetric Flowrate (l/min)	Specific Surface Area (Sq. m/cc)
				X Parameter	N Parameter	X Parameter	N Parameter	X Parameter	N Parameter		
400 psi	35% CaCO3	0.4655	5.77	97.83	2.20	-	-	-	-	7.76	0.04
		0.4327	5.44	96.98	2.00						0.04
		0.4349	5.47	96.98	2.00						0.04
				97.26	2.07						0.04
600 psi	35% CaCO3	0.6749	5.37	65.42	2.09	1.0370	1.1030	67.84	2.31	9.10	0.07
		0.6794	5.36	65.78	2.09	1.0372	1.1040	68.23	2.31		0.07
		0.6834	5.38	66.86	2.09	1.0374	1.1050	69.36	2.31		0.07
				66.02	2.09			68.48	2.31		0.07
800 psi	35% CaCO3	0.8281	5.28	52.63	2.09	1.0630	1.1772	55.95	2.46	10.85	0.09
		0.7977	5.32	52.09	2.09	1.0542	1.1535	54.91	2.41		0.09
		0.8171	5.31	53.89	2.16	1.0578	1.1766	57.01	2.54		0.09
				52.87	2.11			55.96	2.47		0.09
1000 psi	35% CaCO3	0.9020	5.29	42.04	2.25	1.0875	1.3070	45.72	2.94	11.30	0.11
		0.8993	5.28	43.04	2.18	1.0895	1.2863	46.89	2.80		0.11
		0.9222	5.25	44.46	2.09	1.1078	1.3106	49.25	2.74		0.09
				43.18	2.17			47.29	2.83		0.10
1200 psi	35% CaCO3	0.9505	5.23	35.86	2.28	1.1132	1.4398	39.92	3.28	13.02	0.13
		0.9424	5.23	35.88	2.27	1.1088	1.4416	39.78	3.20		0.13
		0.9273	5.37	36.31	2.34	1.0960	1.3894	39.80	3.25		0.13
				36.02	2.30			39.83	3.24		0.13

All Dimensions in microns

Slurry Temperature = 19.9 C

Apparent Viscosity = 2.700 cP

Density = 1265.0 kg / Cu. m

Wet Bulb Temperature = 14 C

Dry Bulb Temperature = 17 C

Relative Humidity = 72%

Atmospheric Pressure = 751.8 mm Hg

Air Density = 1.217 kg / Cu. m

Pressure	D(3,2)	D(2,1)	D(1,0)	D(v,0.9)	D(v,0.5)	D(v,0.1)	% > 420.0	% > 201.0	% > 82.7	% < 39.5	% < 10.5
400 psi	55.61	19.32	7.62	139.96	82.80	35.19	0.1	2.7	30.2	12.6	0.7
	56.41	27.61	13.87	143.82	80.71	31.52	0.1	3.4	48.4	15.2	1.1
	56.41	27.61	13.87	143.82	80.71	31.52	0.1	3.4	48.4	15.2	1.1
	56.48	24.85	11.79	142.53	81.41	32.74	0.1	3.2	49.0	14.3	1.0
600 psi	38.61	12.13	4.62	96.23	57.85	25.63	0.0	0.1	20.7	24.9	1.3
	38.81	12.16	4.63	96.72	58.18	25.77	0.0	0.1	21.1	24.6	1.2
	40.91	21.47	11.31	98.14	59.14	26.20	0.0	0.1	22.4	23.8	1.2
	39.44	15.25	6.85	97.03	58.39	25.87	0.0	0.1	21.4	24.4	1.2
800 psi	36.95	21.51	11.31	77.37	48.18	22.43	0.0	0.0	7.1	34.5	1.5
	32.71	11.69	4.51	76.50	47.14	21.60	0.0	0.0	6.6	36.3	1.7
	38.30	22.92	12.24	77.98	49.34	23.51	0.0	0.0	7.4	32.4	1.2
	35.99	18.71	9.35	77.28	48.22	22.51	0.0	0.0	7.0	34.4	1.5
1000 psi	31.03	20.35	12.77	59.85	40.38	21.27	0.0	0.0	0.6	47.8	1.3
	33.26	22.21	13.08	62.51	41.18	20.99	0.0	0.0	1.0	46.1	1.5
	34.52	22.53	12.97	68.05	43.17	21.67	0.0	0.0	1.9	42.0	1.4
	32.94	21.76	12.94	66.80	41.58	21.31	0.0	0.0	1.2	45.3	1.4
1200 psi	28.97	17.56	8.49	52.39	35.80	20.12	0.0	0.0	0.0	62.1	1.2
	29.91	22.24	14.69	52.56	35.58	19.70	0.0	0.0	0.0	62.5	1.4
	28.79	17.37	8.37	52.33	35.66	19.93	0.0	0.0	0.0	62.4	1.3
	29.22	19.06	10.52	52.43	35.68	19.92	0.0	0.0	0.0	62.3	1.3

Table A1.36: *Drop-Size Distribution Results for 35% Calcium Carbonate Slurry using the Nozzle Delevan 2.2SJ*

Pressure	Fluid	Obscuration	Log. Difference	Measured Values		Correction Factors		Corrected Values		Volumetric Flowrate (l/min)	Specific Surface Area (Sq. m/cc)
				X Parameter	N Parameter	X Parameter	N Parameter	X Parameter	N Parameter		
400 psi	35% CaCO3	0.4810	5.46	75.66	2.04	-	-	-	-	9.66	0.06
		0.4963	5.49	74.78	2.04						0.06
		0.4875	5.56	75.87	2.01						0.06
				75.44	2.03						0.06
600 psi	35% CaCO3	0.7209	5.34	55.03	2.09	1.0405	1.1160	57.26	2.33	13.18	0.08
		0.6973	5.32	56.16	2.18	1.0369	1.1122	58.23	2.42		0.08
		0.7051	5.54	55.60	2.14	1.0385	1.1146	57.74	2.39		0.10
				55.60	2.14			57.74	2.38		0.09
800 psi	35% CaCO3	0.7869	5.18	46.16	2.14	1.0506	1.1518	48.49	2.46	14.10	0.10
		0.8428	5.30	44.79	2.18	1.0654	1.2044	47.72	2.63		0.10
		0.8334	5.42	45.70	2.34	1.0581	1.2171	48.36	2.85		0.11
				45.55	2.22			48.19	2.65		0.10
1000 psi	35% CaCO3	0.9307	5.24	37.18	2.25	1.1030	1.3732	41.01	3.09	16.51	0.13
		0.9221	5.26	37.94	2.25	1.0981	1.3515	41.66	3.04		0.13
		0.9167	5.43	37.51	2.44	1.0859	1.3881	40.73	3.39		0.13
				37.54	2.31			41.13	3.17		0.13
1200 psi	35% CaCO3	0.9603	5.13	30.47	2.62	1.0985	1.6021	33.47	4.20	19.14	0.17
		0.9773	5.09	30.47	2.62	1.1075	1.6862	33.75	4.42		0.17
		0.9696	5.18	31.06	2.44	1.1144	1.5706	34.61	3.83		0.15
				30.67	2.56			33.94	4.15		0.16

All Dimensions in microns

Slurry Temperature = 19.9 C

Apparent Viscosity = 2.700 cP

Density = 1265.0 kg / Cu. m

Wet Bulb Temperature = 14 C

Dry Bulb Temperature = 17 C

Relative Humidity = 72%

Atmospheric Pressure = 751.7 mm Hg

Air Density = 1.217 kg / Cu. m

Pressure	D(3,2)	D(2,1)	D(1,0)	D(v,0.9)	D(v,0.5)	D(v,0.1)	% > 420.0	% > 201.0	% > 82.7	% < 39.5	% < 10.5
400 psi	43.63	19.47	8.94	113.90	63.23	25.15	0.0	0.1	30.2	23.2	1.7
	40.44	18.52	9.13	112.55	62.50	24.85	0.0	0.1	29.4	23.7	1.7
	43.25	18.95	8.67	114.94	63.24	24.81	0.0	0.1	30.5	23.5	1.7
	42.44	18.98	8.91	113.80	62.99	24.94	0.0	0.1	30.0	23.5	1.7
600 psi	36.59	20.09	10.21	81.00	48.91	21.82	0.0	0.0	9.3	34.2	1.8
	34.55	12.01	4.60	81.32	50.05	22.99	0.0	0.0	9.4	32.2	1.4
	37.45	21.08	10.84	80.92	49.53	22.54	0.0	0.0	9.2	33.1	1.6
	36.20	17.73	8.55	81.08	49.50	22.45	0.0	0.0	9.3	33.2	1.6
800 psi	32.15	19.20	10.38	68.13	41.77	19.44	0.0	0.0	2.5	45.3	2.3
	32.82	20.81	11.75	66.15	41.57	20.29	0.0	0.0	1.7	45.5	1.8
	34.55	23.29	13.80	64.92	42.60	21.96	0.0	0.0	1.3	42.9	1.2
	33.17	21.10	11.98	66.40	41.98	20.56	0.0	0.0	1.8	44.6	1.8
1000 psi	30.39	22.08	14.20	54.76	36.52	19.81	0.0	0.0	0.1	59.1	1.5
	30.67	22.02	13.97	55.70	37.02	19.89	0.0	0.0	0.1	57.4	1.5
	29.89	18.42	8.98	53.22	36.80	21.14	0.0	0.0	0.0	59.6	1.0
	30.32	20.84	12.38	54.56	36.78	20.28	0.0	0.0	0.1	56.0	1.3
1200 psi	26.87	20.96	13.78	42.10	30.63	19.38	0.0	0.0	0.0	85.8	0.7
	28.01	24.11	19.35	42.11	31.23	19.93	0.0	0.0	0.0	85.7	0.5
	26.53	17.95	9.51	43.88	31.31	19.10	0.0	0.0	0.0	80.3	1.0
	27.14	21.01	14.21	42.70	31.06	19.47	0.0	0.0	0.0	83.9	0.7

Table A1.37: *Drop-Size Distribution Results for 45% Calcium Carbonate Slurry using the Nozzle AAASSTC5-5*

Pressure	Fluid	Obscuration	Log. Difference	Measured Values		Correction Factors		Corrected Values		Volumetric Flowrate (l/min)	Specific Surface Area (Sq. m/cc)
				X Parameter	N Parameter	X Parameter	N Parameter	X Parameter	N Parameter		
400 psi	45% CaCO3	0.3933	5.19	125.18	2.25	–	–	–	–	8.55	0.04
		0.3774	5.00	125.49	2.25						0.04
		0.3620	5.01	126.91	2.25						0.04
				125.86	2.25						0.04
600 psi	45% CaCO3	0.5253	4.82	119.42	2.25	–	–	–	–	12.22	0.04
		0.5335	4.67	117.40	2.25						0.04
		0.5155	4.64	118.61	2.25						0.04
				118.48	2.25						0.04
800 psi	45% CaCO3	0.5928	4.48	109.22	2.39	–	–	–	–	14.63	0.04
		0.5903	4.49	110.46	2.15						0.04
		0.5878	4.43	107.45	2.39						0.04
				109.04	2.31						0.04
1000 psi	45% CaCO3	0.5907	4.54	103.93	2.55	–	–	–	–	15.91	0.05
		0.6109	4.50	103.93	2.55						0.05
		0.6309	4.50	104.53	2.57						0.05
				104.13	2.56						0.05
1200 psi	45% CaCO3	0.6376	4.53	101.56	2.47	–	–	–	–	19.83	0.05
		0.6421	4.61	101.29	2.66						0.05
		0.6334	4.59	101.56	2.47						0.05
				101.47	2.53						0.05

All Dimensions in microns

Slurry Temperature = 20.0 C

Wet Bulb Temperature = 12 C

Atmospheric Pressure = 752.3 mm Hg

Apparent Viscosity = 3.375 cP

Dry Bulb Temperature = 16 C

Air Density = 1.221 kg / Cu. m

Density = 1380.0 kg / Cu. m

Relative Humidity = 63%

Pressure	D(3,2)	D(2,1)	D(1,0)	D(v,0.9)	D(v,0.5)	D(v,0.1)	% > 420.0	% > 201.0	% > 82.7	% < 39.5	% < 10.5
400 psi	71.19	23.29	9.01	192.91	106.75	46.04	0.2	8.2	67.5	7.1	0.4
	71.35	23.33	9.02	193.34	107.00	46.16	0.2	8.3	67.6	7.1	0.4
	72.11	23.51	9.09	195.25	108.16	46.68	0.3	8.7	68.3	6.9	0.4
	71.55	23.38	9.04	193.83	107.30	46.29	0.2	8.4	67.8	7.0	0.4
600 psi	68.09	22.57	8.75	183.66	101.91	43.93	0.2	6.7	64.6	7.9	0.3
	67.01	22.31	8.66	179.65	100.17	43.19	0.1	6.2	64.5	8.2	0.3
	67.66	22.46	8.72	182.11	101.22	43.63	0.2	6.5	64.2	8.0	0.3
	67.59	22.45	8.71	181.81	101.10	43.58	0.2	6.5	64.4	8.0	0.3
800 psi	65.12	23.80	9.27	151.74	93.91	42.60	0.1	4.2	59.9	8.3	0.4
	61.33	19.89	7.79	166.20	93.39	38.80	0.1	5.0	58.5	10.3	0.5
	64.11	23.52	9.17	148.89	92.34	41.91	0.1	3.8	58.7	8.6	0.4
	63.52	22.40	8.74	155.61	91.21	41.10	0.1	4.3	59.0	9.1	0.4
1000 psi	64.82	26.22	10.35	141.19	90.09	43.00	0.1	2.6	57.3	8.1	0.3
	64.82	26.22	10.35	141.19	90.09	43.00	0.1	2.6	57.3	8.1	0.3
	65.57	26.91	10.66	141.61	90.72	43.55	0.1	2.6	57.9	7.8	0.3
	65.07	26.45	10.45	141.33	90.30	43.18	0.1	2.6	57.5	8.0	0.3
1200 psi	62.03	24.01	9.42	139.61	87.59	40.84	0.1	2.4	54.8	9.2	0.4
	69.01	41.08	21.25	136.65	88.28	43.47	0.0	1.8	55.9	7.8	0.3
	62.03	24.01	9.42	139.61	87.59	40.84	0.1	2.4	54.8	9.2	0.4
	64.36	29.70	13.36	138.62	87.82	41.72	0.1	2.2	55.2	8.7	0.4

Table A1.38: *Drop-Size Distribution Results for 45% Calcium Carbonate Slurry using the Nozzle AAASSTC8-5*

Pressure	Fluid	Obscuration	Log. Difference	Measured Values		Correction Factors		Corrected Values		Volumetric Flowrate (l/min)	Specific Surface Area (Sq. m/cc)
				X Parameter	N Parameter	X Parameter	N Parameter	X Parameter	N Parameter		
400 psi	45% CaCO3	0.4556	4.91	133.21	2.22	-	-	-	-	11.85	0.03
		0.4350	5.10	132.63	2.30						0.03
		0.4539	4.90	134.38	2.15						0.03
				133.41	2.22						0.03
600 psi	45% CaCO3	0.5854	4.90	124.36	2.09	-	-	-	-	14.08	0.03
		0.5843	4.90	124.36	2.09						0.03
		0.5946	4.96	123.95	2.14						0.03
				124.22	2.11						0.03
800 psi	45% CaCO3	0.6662	4.68	114.63	2.25	1.0356	1.1113	118.71	2.50	16.06	0.04
		0.6600	4.64	114.63	2.25	1.0354	1.1097	118.69	2.50		0.04
		0.6760	4.69	114.46	2.20	1.0362	1.1105	118.61	2.44		0.04
				114.57	2.23			118.67	2.48		0.04
1000 psi	45% CaCO3	0.7354	4.62	105.02	2.66	1.0363	1.1707	108.84	3.11	17.01	0.04
		0.7118	4.53	106.13	2.47	1.0426	1.1763	110.65	2.91		0.04
		0.6784	4.64	104.94	2.28	1.0358	1.1166	108.70	2.55		0.04
				105.36	2.47			109.40	2.86		0.04
1200 psi	45% CaCO3	0.7084	4.40	102.82	2.39	1.0366	1.1347	106.58	2.71	18.81	0.03
		0.7242	4.64	103.97	2.45	1.0372	1.1464	107.84	2.81		0.04
		0.6776	4.38	102.82	2.54	1.0341	1.1343	106.33	2.88		0.05
				103.20	2.46			106.92	2.80		0.05

All Dimensions in microns

Slurry Temperature = 20.0 C

Apparent Viscosity = 3.375 cP

Density = 1380.0 kg / Cu. m

Wet Bulb Temperature = 12 C

Dry Bulb Temperature = 16 C

Relative Humidity = 63%

Atmospheric Pressure = 752.4 mm Hg

Air Density = 1.221 kg / Cu. m

Pressure	D(3,2)	D(2,1)	D(1,0)	D(v,0.9)	D(v,0.5)	D(v,0.1)	% > 420.0	% > 201.0	% > 82.7	% < 39.5	% < 10.5
400 psi	74.65	23.69	9.14	194.15	112.94	48.35	0.4	8.3	70.7	6.5	0.4
	76.37	25.50	9.83	191.42	113.09	49.86	0.3	7.6	71.4	6.0	0.4
	73.47	22.38	8.66	197.41	113.32	47.20	0.4	9.1	70.3	6.9	0.5
	74.83	23.86	9.21	194.33	113.12	48.47	0.4	8.2	70.8	6.5	0.4
600 psi	66.98	20.30	7.92	185.62	104.36	42.39	0.3	6.5	65.3	8.7	0.5
	66.98	20.30	7.92	185.62	104.36	42.39	0.3	6.5	65.3	8.7	0.5
	67.94	21.11	8.21	183.53	104.44	43.32	0.2	6.1	65.7	8.3	0.5
	67.30	20.57	8.02	184.92	104.39	42.90	0.3	6.4	65.4	8.6	0.5
800 psi	74.38	31.48	12.80	173.58	102.95	48.25	0.1	5.6	66.8	6.1	0.2
	74.21	31.54	12.81	173.52	102.94	48.24	0.1	5.6	66.7	6.1	0.2
	71.71	26.66	10.39	175.61	102.50	47.16	0.1	5.8	66.1	6.5	0.2
	73.43	29.89	12.00	174.24	102.80	47.88	0.1	5.7	66.5	6.2	0.2
1000 psi	80.27	56.31	34.09	139.73	97.76	52.97	0.0	1.8	65.0	4.1	0.0
	78.90	51.23	28.43	143.87	98.58	51.11	0.1	2.6	64.9	4.8	0.1
	62.57	16.99	6.30	147.25	94.33	44.97	0.1	3.5	60.8	7.2	0.2
	73.91	41.51	22.94	143.62	96.89	49.68	0.1	2.6	63.6	5.4	0.1
1200 psi	73.12	43.67	22.47	141.98	93.20	46.45	0.1	2.4	60.5	6.5	0.2
	75.80	48.25	26.48	141.83	95.66	48.36	0.1	2.4	62.0	5.7	0.1
	75.56	49.08	27.35	139.30	94.62	48.62	0.0	1.9	61.3	5.6	0.1
	74.83	47.00	25.43	141.04	94.49	47.81	0.1	2.2	61.3	5.9	0.1

Table A1.39: *Drop-Size Distribution Results for 45% Calcium Carbonate Slurry using the Nozzle AAASSTC8-8*

Pressure	Fluid	Obscuration	Log. Difference	Measured Values		Correction Factors		Corrected Values		Volumetric Flowrate (l/min)	Specific Surface Area (Sq. m/cc)
				X Parameter	N Parameter	X Parameter	N Parameter	X Parameter	N Parameter		
400 psi	45% CaCO3	0.3974	5.24	150.22	2.10	–	–	–	–	13.17	0.03
		0.3626	5.18	150.86	2.15						0.03
		0.3679	5.29	148.23	2.15						0.03
				149.77	2.13						0.03
600 psi	45% CaCO3	0.5584	5.34	134.56	2.16	–	–	–	–	18.56	0.03
		0.5349	4.75	132.25	2.16						0.03
		0.5525	4.72	132.90	2.16						0.03
				133.24	2.16						0.03
800 psi	45% CaCO3	0.6008	4.41	114.78	2.42	–	–	–	–	20.12	0.04
		0.6132	4.40	113.50	2.34						0.04
		0.6143	4.49	114.66	2.25						0.04
				114.31	2.34						0.04
1000 psi	45% CaCO3	0.7479	5.21	108.67	2.55	1.0386	1.1682	112.86	2.98	23.70	0.04
		0.6881	4.66	108.91	2.39	1.0354	1.1273	112.77	2.69		0.04
		0.7176	5.16	107.49	2.37	1.0374	1.1369	111.51	2.69		0.04
				108.34	2.44			112.38	2.79		0.04
1200 psi	45% CaCO3	0.6288	4.78	98.33	2.86	–	–	–	–	24.50	0.05
		0.6326	4.72	96.04	2.73						0.05
		0.6336	4.79	98.33	3.03						0.05
				97.57	2.87						0.05

All Dimensions in microns

Slurry Temperature = 19.9 C

Apparent Viscosity = 3.375 cP

Density = 1380.0 kg / Cu. m

Wet Bulb Temperature = 12 C°

Dry Bulb Temperature = 16 C

Relative Humidity = 63%

Atmospheric Pressure = 752.4 mm Hg

Air Density = 1.221 kg / Cu. m

Pressure	D(3,2)	D(2,1)	D(1,0)	D(v,0.9)	D(v,0.5)	D(v,0.1)	% > 420.0	% > 201.0	% > 82.7	% < 39.5	% < 10.5
400 psi	80.07	22.91	8.87	217.90	126.28	51.46	1.0	14.8	75.2	5.9	0.5
	81.92	24.14	9.31	216.49	128.56	52.95	0.9	14.5	76.0	5.4	0.4
	80.56	23.85	9.20	214.08	125.05	52.06	0.8	13.8	75.2	5.7	0.4
	80.85	23.63	9.13	216.16	126.63	52.16	0.9	14.4	75.5	5.7	0.4
600 psi	73.82	22.60	8.74	197.38	113.56	47.49	0.4	9.1	70.5	6.8	0.5
	72.65	22.35	8.65	194.44	111.62	46.67	0.4	8.4	69.6	7.1	0.5
	72.98	22.42	8.68	195.29	112.17	46.90	0.4	8.6	69.8	7.0	0.5
	73.15	22.46	8.69	195.70	112.45	47.02	0.4	8.7	70.0	7.0	0.5
800 psi	68.91	25.40	9.88	164.79	99.02	45.29	0.1	5.0	63.7	7.2	0.3
	66.67	23.47	9.12	164.89	97.39	43.39	0.1	5.0	62.1	8.0	0.4
	65.53	21.98	8.54	173.21	97.79	42.18	0.1	5.6	62.0	8.6	0.4
	67.04	23.62	9.18	167.63	98.07	43.62	0.1	5.2	62.6	7.9	0.4
1000 psi	81.26	53.33	30.00	145.66	100.78	53.23	0.1	2.9	67.1	4.2	0.0
	76.97	45.22	22.93	150.34	98.69	48.85	0.1	3.8	64.9	5.7	0.1
	76.13	44.82	22.78	148.50	97.55	48.30	0.1	3.5	64.0	5.9	0.1
	78.12	47.86	25.24	148.17	99.01	50.13	0.1	3.4	65.3	5.3	0.1
1200 psi	69.31	43.78	23.53	131.11	86.50	44.77	0.0	1.0	54.4	7.1	0.2
	66.34	40.68	21.52	129.82	83.97	42.12	0.0	1.0	51.5	8.4	0.3
	71.58	48.55	28.22	133.70	86.83	46.84	0.0	0.8	55.5	6.1	0.1
	69.08	44.34	24.42	131.54	85.77	44.58	0.0	0.9	53.8	7.2	0.2

Table A1.40: *Drop-Size Distribution Results for 45% Calcium Carbonate Slurry using the Nozzle AAASSTC10-10*

Pressure	Fluid	Obscuration	Log. Difference	Measured Values		Correction Factors		Corrected Values		Volumetric Flowrate (l/min)	Specific Surface Area (Sq. m/cc)
				X Parameter	N Parameter	X Parameter	N Parameter	X Parameter	N Parameter		
400 psi	45% CaCO3	0.4299	5.34	155.69	2.15	–	–	–	–	18.02	0.03
		0.3648	5.41	156.66	2.05						0.03
		0.4190	5.36	156.30	2.07						0.03
				156.22	2.09						0.03
600 psi	45% CaCO3	0.5752	5.15	132.98	2.09	–	–	–	–	22.23	0.03
		0.5893	5.20	132.93	2.16						0.03
		0.5950	5.25	132.93	2.16						0.03
				132.95	2.14						0.03
800 psi	45% CaCO3	0.6894	5.01	111.85	2.25	1.0365	1.1177	115.93	2.51	28.33	0.04
		0.7071	4.97	111.85	2.25	1.0377	1.1235	116.06	2.53		0.04
		0.6605	4.91	113.50	2.42	1.0345	1.1208	117.42	2.71		0.04
				112.40	2.31			116.47	2.58		0.04
1000 psi	45% CaCO3	0.7019	4.94	101.06	2.37	1.0363	1.1307	104.73	2.68	33.13	0.05
		0.7065	4.89	102.59	2.37	1.0366	1.1324	106.34	2.68		0.05
		0.7166	4.91	103.67	2.34	1.0376	1.1341	107.57	2.65		0.05
				102.44	2.36			106.21	2.67		0.05
1200 psi	45% CaCO3	0.8077	5.67	99.63	2.29	1.0525	1.1845	104.86	2.71	36.48	0.05
		0.8025	5.34	100.58	2.38	1.0496	1.1909	105.57	2.83		0.05
		0.8115	5.70	99.50	2.23	1.0547	1.1805	104.94	2.63		0.05
				99.90	2.30			105.12	2.72		0.05

All Dimensions in microns

Slurry Temperature = 20.1 cC

Apparent Viscosity = 3.375 cP

Density = 1380.0 kg/Cu. m

Wet Bulb Temperature = 12 C

Dry Bulb Temperature = 16 C

Relative Humidity = 63%

Atmospheric Pressure = 752.1 mm Hg

Air Density = 1.221 kg/Cu. m

Pressure	D(3,2)	D(2,1)	D(1,0)	D(v,0.9)	D(v,0.5)	D(v,0.1)	% > 420.0	% > 201.0	% > 82.7	% < 39.5	% < 10.5
400 psi	84.43	24.69	9.52	222.36	132.74	54.62	1.2	16.2	77.4	5.1	0.4
	81.70	22.40	8.71	227.74	131.31	52.28	1.4	17.5	76.4	5.8	0.5
	82.16	22.81	8.85	226.48	131.21	52.72	1.4	17.2	76.5	5.6	0.5
	82.76	23.30	9.03	225.53	131.75	53.21	1.3	17.0	76.8	5.5	0.5
600 psi	71.23	21.10	8.21	197.32	111.60	45.33	0.5	9.1	69.0	7.6	0.5
	72.99	22.42	8.68	195.33	112.19	46.91	0.4	8.6	69.9	7.0	0.5
	72.99	22.42	8.68	195.33	112.19	46.91	0.4	8.6	69.9	7.0	0.5
	72.40	21.98	8.52	195.99	111.26	46.38	0.4	8.8	69.6	7.2	0.5
800 psi	72.87	31.61	12.95	163.84	100.57	47.29	0.1	4.9	65.2	6.4	0.2
	76.73	42.68	21.02	163.15	100.80	47.68	0.1	4.9	65.5	6.2	0.2
	80.42	47.32	23.98	158.93	103.48	51.23	0.1	4.9	67.8	5.0	0.1
	76.67	40.54	19.32	161.97	101.17	48.73	0.1	4.9	66.2	5.9	0.2
1000 psi	71.51	42.51	21.86	140.25	91.41	45.23	0.1	2.2	58.8	7.0	0.2
	72.57	43.00	22.04	142.11	92.85	45.92	0.1	2.5	60.1	6.7	0.2
	72.99	42.78	21.78	144.02	93.82	46.01	0.1	2.8	60.8	6.7	0.2
	72.36	42.76	21.89	142.13	92.69	45.72	0.1	2.5	59.9	6.8	0.2
1200 psi	71.97	43.13	22.27	140.01	91.66	45.71	0.1	2.1	59.2	6.8	0.2
	74.46	47.84	26.47	139.39	92.80	47.66	0.0	1.9	60.6	6.0	0.1
	71.01	41.61	21.26	141.17	91.37	44.60	0.1	2.4	58.6	7.3	0.2
	72.48	44.19	23.33	140.06	91.94	45.99	0.1	2.1	59.5	6.7	0.2

Table A1.41: *Drop-Size Distribution Results for 45% Calcium Carbonate Slurry using the Nozzle Delevan 2.0SJ*

Pressure	Fluid	Obscuration	Log. Difference	Measured Values		Correction Factors		Corrected Values		Volumetric Flowrate (l/mnn)	Specific Surface Area (Sq. m/cc)
				X Parameter	N Parameter	X Parameter	N Parameter	X Parameter	N Parameter		
400 psi	45% CaCO3	0.5985	5.48	79.11	2.03					7.54	0.05
		0.5851	5.61	79.35	1.95	-	-	-	-		0.05
		0.5704	5.40	79.11	2.09						0.05
				79.19	2.02						0.05
600 psi	45% CaCO3	0.7187	5.37	60.42	2.09	1.0403	1.1153	62.85	2.33	11.16	0.07
		0.7538	5.30	59.77	2.09	1.0450	1.1290	62.46	2.36		0.07
		0.7654	5.27	59.45	1.95	1.0495	1.1216	62.39	2.19		0.07
				59.70	2.04			62.57	2.29		0.07
800 psi	45% CaCO3	0.8902	5.34	47.83	2.09	1.0892	1.2520	52.10	2.62	13.14	0.10
		0.8806	5.23	47.92	2.09	1.0844	1.2375	51.96	2.59		0.10
		0.8547	5.19	48.05	1.95	1.0782	1.1828	51.81	2.31		0.09
				47.93	2.04			51.96	2.51		0.10
1000 psi	45% CaCO3	0.9497	5.35	42.54	2.09	1.1269	1.3762	47.94	2.88	15.11	0.11
		0.9560	*5.31*	42.54	2.09	1.1318	1.3937	*48.15*	2.91		0.11
		0.9497	5.16	41.06	1.97	1.1376	1.3397	46.71	2.64		0.11
				42.05	2.05			47.60	2.81		0.11
1200 psi	45% CaCO3	0.9639	5.55	30.65	2.84	1.0896	1.7125	33.39	4.86	16.05	0.17
		0.9610	5.42	30.47	2.62	1.0989	1.6053	33.48	4.21		0.17
		0.9639	5.18	32.65	2.09	1.1381	1.4169	37.16	2.96		0.14
				31.26	2.52			34.68	4.01		0.16

All Dimensions in microns

Slurry Temperature = 20.0 C

Apparent Viscosity = 3.375 cP

Density = 1380.0 kg / Cu. m

Wet Bulb Temperature = 12 C

Dry Bulb Temperature = 16 C

Relative Humidity = 63%

Atmospheric Pressure = 752.1 mm Hg

Air Density = 1.221 kg / Cu. m

Pressure	D(3,2)	D(2,1)	D(1,0)	D(v,0.9)	D(v,0.5)	D(v,0.1)	% > 420.0	% > 201.0	% > 82.7	% < 39.5	% < 10.5
400 psi	45.35	19.93	9.08	119.52	66.06	26.15	0.0	0.1	33.6	21.6	1.5
	41.35	17.81	8.58	121.98	65.77	25.08	0.0	0.1	33.9	22.5	1.8
	46.36	21.12	9.71	118.08	66.40	26.99	0.0	0.1	33.5	20.8	1.3
	44.35	19.62	9.12	119.86	66.08	26.07	0.0	0.1	33.7	21.6	1.5
600 psi	37.40	20.07	10.77	90.05	53.70	23.94	0.0	0.0	15.1	28.7	1.5
	36.27	12.04	4.59	89.06	53.47	24.09	0.0	0.0	14.4	28.7	1.4
	34.76	11.09	4.30	91.46	52.78	22.36	0.0	0.0	15.7	30.7	2.0
	36.14	14.40	6.55	90.19	5.32	23.46	0.0	0.0	15.1	29.4	1.6
800 psi	32.45	12.42	4.77	71.15	45.27	22.08	0.0	0.0	3.3	38.3	1.5
	32.20	12.28	4.72	71.21	45.07	21.80	0.0	0.0	3.3	38.8	1.5
	33.03	18.34	9.46	74.44	44.21	19.58	0.0	0.0	5.3	41.4	2.4
	32.56	14.35	6.32	72.27	44.85	21.15	0.0	0.0	4.0	39.5	1.8
1000 psi	31.35	13.04	5.03	63.68	42.28	21.95	0.0	0.0	1.1	43.3	1.2
	35.13	25.34	16.62	63.81	42.52	22.22	0.0	0.0	1.1	42.9	1.1
	32.21	20.55	11.68	63.74	40.69	19.92	0.0	0.0	1.3	47.3	1.9
	32.90	19.64	11.11	63.74	41.83	21.36	0.0	0.0	1.2	44.6	1.4
1200 psi	28.30	24.93	20.70	40.58	31.13	20.51	0.0	0.0	0.0	88.7	0.3
	25.54	15.21	6.79	42.10	30.64	19.40	0.0	0.0	0.0	85.8	0.7
	25.59	17.62	11.41	48.81	32.88	17.38	0.0	0.0	0.0	69.9	2.3
	26.48	19.25	12.97	43.83	31.55	19.10	0.0	0.0	0.0	81.5	1.1

Table A1.42: *Drop-Size Distribution Results for 45% Calcium Carbonate Slurry using the Nozzle Delevan 2.2SJ*

Pressure	Fluid	Obscuration	Log. Difference	Measured Values		Correction Factors		Corrected Values		Volumetric Flowrate (l/min)	Specific Surface Area (Sq. m/cc)
				X Parameter	N Parameter	X Parameter	N Parameter	X Parameter	N Parameter		
400 psi	45% CaCO3	0.4693	5.53	100.94	1.92	-	-	-	-	9.87	0.04
		0.4598	5.57	100.94	1.92						0.04
		0.4628	5.53	100.38	2.00						0.04
				100.75	1.95						0.04
600 psi	45% CaCO3	0.6777	5.39	67.91	1.99	1.0379	1.0971	70.48	2.18	12.31	0.07
		0.6702	5.33	67.36	1.95	1.0378	1.0929	69.91	2.13		0.06
		0.6840	5.32	68.19	1.95	1.0386	1.0958	70.83	2.14		0.06
				67.82	1.96			70.41	2.15		0.06
800 psi	45% CaCO3	0.8445	5.24	47.80	2.12	1.0679	1.1974	51.04	2.54	14.01	0.10
		0.8431	5.21	46.84	2.09	1.0683	1.1916	50.04	2.49		0.10
		0.8168	5.19	48.09	2.00	1.0619	1.1567	51.07	2.31		0.09
				47.58	2.07			50.72	2.45		0.10
1000 psi	45% CaCO3	0.9210	5.18	44.48	1.95	1.1168	1.2741	49.68	2.48	16.84	0.10
		0.9002	5.10	45.52	1.95	1.1028	1.2394	50.20	2.42		0.10
		0.8792	5.15	45.01	1.95	1.0905	1.2104	49.08	2.36		0.10
				45.00	1.95			49.65	2.42		0.10
1200 psi	45% CaCO3	0.9637	5.14	37.48	2.04	1.1428	1.3991	42.83	2.85	18.21	0.12
		0.9667	5.06	36.96	1.95	1.1550	1.3769	42.69	2.68		0.12
		0.9542	5.41	38.85	2.08	1.1312	1.3854	43.95	2.88		0.12
				37.76	2.02			43.16	2.80		0.12

All Dimensions in microns

Slurry Temperature = 20.0 C

Apparent Viscosity = 3.375 cP

Density = 1380.0 kg / Cu. m

Wet Bulb Temperature = 12 C

Dry Bulb Temperature = 16 C

Relative Humidity = 63%

Atmospheric Pressure = 752.1 mm Hg

Air Density = 1.221 kg / Cu. m

Pressure	D(3,2)	D(2,1)	D(1,0)	D(v,0.9)	D(v,0.5)	D(v,0.1)	% > 420.0	% > 201.0	% > 82.7	% < 39.5	% < 10.5
400 psi	54.70	21.13	9.23	153.37	83.40	31.31	0.1	4.6	50.7	15.1	1.2
	54.70	21.13	9.23	153.37	83.40	31.31	0.1	4.6	50.7	15.1	1.2
	58.32	28.20	14.04	149.08	83.57	32.62	0.1	4.0	50.8	14.2	1.0
	55.91	23.49	10.83	151.94	83.46	31.75	0.1	4.4	50.7	14.8	1.1
600 psi	42.80	20.98	9.97	101.61	59.54	25.13	0.0	0.1	24.5	24.5	1.4
	41.78	19.96	9.42	101.70	58.82	24.34	0.0	0.1	24.1	25.5	1.6
	42.45	20.34	9.59	102.82	59.65	24.78	0.0	0.1	25.1	24.8	1.5
	42.34	20.43	9.69	102.04	59.34	24.75	0.0	0.1	24.6	24.9	1.5
800 psi	34.37	20.95	11.43	70.47	44.15	21.06	0.0	0.0	3.1	40.6	1.7
	30.54	11.63	4.52	69.62	43.17	20.28	0.0	0.0	2.8	42.6	2.0
	32.58	18.13	9.39	73.39	43.58	19.30	0.0	0.0	4.8	42.4	2.5
	32.50	16.90	8.45	71.16	43.63	20.21	0.0	0.0	3.6	41.9	2.1
1000 psi	33.06	19.80	10.71	69.65	42.85	20.06	0.0	0.0	2.9	43.2	2.1
	32.94	19.25	10.25	70.98	43.14	19.83	0.0	0.0	3.5	42.9	2.2
	29.22	10.93	4.30	69.98	42.02	18.93	0.0	0.0	3.3	45.1	2.6
	31.74	16.66	8.42	70.20	42.67	19.61	0.0	0.0	3.2	43.7	2.3
1200 psi	28.14	12.30	4.85	56.82	37.65	19.45	0.0	0.0	0.3	54.8	1.8
	28.00	17.93	10.91	57.59	37.22	18.44	0.0	0.0	0.5	55.6	2.3
	27.30	12.14	5.11	57.99	38.70	20.12	0.0	0.0	0.3	52.0	1.6
	27.81	14.12	6.96	57.50	37.90	19.34	0.0	0.0	0.4	54.1	1.9

Table A1.43: *Drop-Size Distribution Results for Detergent Slurry at 40°C using the Nozzle AAASSTC5-5*

Pressure	Fluid	Obscuration	Log. Difference	Measured Values		Correction Factors		Corrected Values		Volumetric Flowrate* (l/min)	Specific Surface Area (Sq.m/cc)
				X Parameter	N Parameter	X Parameter	N Parameter	X Parameter	N Parameter		
600 psi	Detergent	0.2102	4.54	261.38	2.75	–	–	–	–	31.85	0.02
		0.2049	4.56	261.38	2.75						0.02
		0.2410	4.72	261.12	2.64						0.02
				261.29	2.71						0.02
800 psi	Detergent	0.2604	4.67	210.38	2.28	–	–	–	–	36.79	0.02
		0.2808	4.93	209.54	2.54						0.02
		0.3295	5.12	211.00	2.54						0.02
				210.31	2.45						0.02
1000 psi	Detergent	0.6876	5.69	219.12	2.09	1.0377	1.1053	227.38	2.31	41.13	0.02
		0.6714	5.25	218.23	2.28	1.0355	1.1146	225.99	2.54		0.02
		0.6928	5.28	218.23	2.28	1.0365	1.1209	226.19	2.56		0.02
				218.53	2.22			226.52	2.47		0.02
1200 psi	Detergent	0.8100	6.08	164.00	1.96	1.0608	1.1472	173.98	2.25	45.05	0.02
		0.8216	5.56	163.79	1.84	1.0686	1.1410	175.02	2.10		0.02
		0.8108	5.33	165.58	2.02	1.0595	1.1547	175.43	2.33		0.02
				164.46	1.94			174.81	2.23		0.02

All Dimensions in microns

Slurry Temperature = 40.1 C

Wet Bulb Temperature = 18 C

Atmospheric Pressure = 749.9 mm Hg

Apparent Viscosity = 1186.0 cP

Dry Bulb Temperature = 22 C

Air Density = 1.197 kg / Cu. m

Solid Content of Slurry = 78.6%

Relative Humidity = 68%

Specific Gravity = 1.386

* Determined from empirical correlation

Pressure	D(3,2)	D(2,1)	D(1,0)	D(v,0.9)	D(v,0.5)	D(v,0.1)	% > 420.0	% > 201.0	% > 82.7	% < 39.5	% < 10.5
600 psi	181.88	109.36	56.94	379.12	228.45	114.93	5.5	62.3	95.8	0.6	0.0
	181.88	109.36	56.94	379.12	228.45	114.93	5.5	62.3	95.8	0.6	0.0
	178.00	103.87	53.18	380.52	227.25	111.50	5.7	61.4	95.3	0.7	0.0
	180.59	107.53	55.69	379.59	228.05	113.79	5.6	62.0	95.6	0.6	0.0
800 psi	129.45	59.46	26.50	358.37	179.76	78.80	4.9	39.3	88.8	2.2	0.1
	138.86	74.47	35.77	344.27	182.22	86.14	4.3	39.4	91.1	1.4	0.1
	139.82	74.86	35.92	347.80	183.32	86.67	4.5	40.0	91.2	1.4	0.1
	136.04	69.60	32.73	350.15	181.77	83.87	4.6	39.6	90.4	1.7	0.1
1000 psi	140.75	64.22	28.35	383.16	193.02	85.90	6.3	46.0	90.8	1.7	0.1
	149.83	79.22	37.69	377.60	194.07	92.03	6.0	46.2	92.6	1.2	0.1
	151.81	84.15	41.82	377.55	194.38	92.67	6.0	46.4	92.7	1.1	0.0
	147.46	75.86	35.95	379.44	193.82	90.20	6.1	46.2	92.0	1.3	0.1
1200 psi	105.58	47.76	21.06	245.94	147.38	63.98	2.0	24.2	82.9	3.5	0.2
	92.67	25.42	9.83	258.52	146.62	59.86	2.4	25.3	81.3	4.3	0.3
	108.81	50.91	22.59	244.70	149.33	66.89	2.0	24.6	84.1	3.0	0.2
	102.35	41.36	17.83	249.72	147.78	63.58	2.1	24.7	82.8	3.6	0.2

Table A1.44: *Drop-Size Distribution Results for Detergent Slurry at 40°C using the Nozzle AAASSTC8-5*

Pressure	Fluid	Obscuration	Log. Difference	Measured Values		Correction Factors		Corrected Values		Volumetric Flowrate* (l/min)	Specific Surface Area (Sq.m/cc)
				X Parameter	N Parameter	X Parameter	N Parameter	X Parameter	N Parameter		
600 psi	Detergent	0.1682	5.05	252.12	2.75	-	-	-	-	45.64	0.02
		0.1599	4.96	254.20	2.96						0.02
		0.1728	4.84	252.36	2.84						0.02
				252.89	2.85						0.02
800 psi	Detergent	0.1992	5.23	210.67	2.74	-	-	-	-	45.64	0.02
		0.2735	5.36	209.57	2.65						0.02
		0.2295	5.12	209.23	2.65						0.02
				209.49	2.68						0.02
1000 psi	Detergent	0.2932	5.52	188.07	2.66	-	-	-	-	58.93	0.02
		0.3022	4.89	187.88	2.76						0.02
		0.2808	4.93	186.21	2.76						0.03
				187.39	2.73						0.02
1200 psi	Detergent	0.3874	5.62	163.66	2.57	-	-	-	-	64.55	0.03
		0.3208	4.93	161.39	2.95						0.03
		0.3842	5.22	163.24	2.61						0.03
				162.76	2.71						0.03

All Dimensions in microns

Slurry Temperature = 39.9 C

Wet Bulb Temperature = 18 C

Atmospheric Pressure = 752.9 mm Hg

Apparent Viscosity = 1186.0 cP

Dry Bulb Temperature = 22 C

Air Density = 1.197 kg / Cu. m

Solid Content of Slurry = 78.6%

Relative Humidity = 68%

Specific Gravity = 1.386

* Determined from empirical correlation

Pressure	D(3,2)	D(2,1)	D(1,0)	D(v,0.9)	D(v,0.5)	D(v,0.1)	% > 420.0	% > 201.0	% > 82.7	% < 39.5	% < 10.5
600 psi	175.56	106.37	55.87	364.06	220.85	111.43	4.4	59.3	95.4	0.6	0.0
	185.87	121.15	69.43	407.62	217.49	117.82	8.5	59.0	96.4	0.4	0.0
	178.40	110.59	58.92	362.29	221.76	114.04	4.2	60.0	95.9	0.5	0.0
	179.94	112.70	61.41	377.99	220.03	114.43	5.7	59.4	95.9	0.5	0.0
800 psi	146.20	87.07	45.18	337.57	184.82	91.45	4.1	41.2	92.6	1.0	0.0
	143.21	83.24	42.66	339.14	183.29	88.92	4.1	39.6	91.9	1.2	0.0
	142.98	83.14	42.62	338.22	183.04	88.80	4.1	39.4	91.9	1.2	0.0
	144.13	84.48	43.49	338.31	183.72	89.72	4.1	40.1	92.1	1.1	0.0
1000 psi	127.75	73.27	36.63	252.94	164.65	81.05	2.2	29.6	89.4	1.6	0.1
	130.94	80.58	43.03	248.67	165.46	83.27	2.0	29.4	90.2	1.3	0.0
	129.79	80.03	42.82	246.05	163.71	82.61	1.9	28.5	90.0	1.4	0.0
	129.49	77.96	40.83	249.22	164.61	82.31	2.0	28.5	89.9	1.4	0.0
1200 psi	108.54	59.73	28.86	220.95	143.11	68.39	0.9	17.0	84.2	2.6	0.1
	116.11	77.03	43.83	213.20	143.45	75.88	0.4	14.6	87.1	1.6	0.0
	109.21	61.09	29.79	219.76	143.04	69.18	0.8	16.7	84.5	2.4	0.1
	111.29	65.95	34.16	217.91	143.20	71.15	0.7	16.1	85.3	2.2	0.1

Table A1.45: *Drop-Size Distribution Results for Detergent Slurry at 40℃ using the Nozzle AAASSTC8-8*

Pressure	Fluid	Obscuration	Log. Difference	Measured Values X Parameter	Measured Values N Parameter	Correction Factors X Parameter	Correction Factors N Parameter	Corrected Values X Parameter	Corrected Values N Parameter	Volumetric Flowrate* (l/min)	Specific Surface Area (Sq.m/cc)
600 psi	Detergent	0.3569	4.49	270.13	2.57	-	-	-	-	45.64	0.02
		0.1722	4.85	269.71	2.63						0.02
		0.2056	5.00	268.23	2.74						0.02
				269.36	2.65						0.02
800 psi	Detergent	0.2458	4.61	246.23	2.76	-	-	-	-	52.7	0.02
		0.2245	4.99	248.34	2.66						0.02
		0.2349	4.56	246.12	2.84						0.02
				246.90	2.75						0.02
1000 psi	Detergent	0.5524	5.26	190.55	2.55	-	-	-	-	58.93	0.02
		0.5145	5.23	190.55	2.55						0.02
		0.5040	4.99	189.63	2.60						0.02
				190.24	2.57						0.02
1200 psi	Detergent	0.3936	5.06	159.26	2.28	-	-	-	-	64.55	0.03
		0.4324	5.28	158.77	2.30						0.03
		0.4700	5.31	159.34	2.46						0.03
				159.12	2.35						0.03

All Dimensions in microns

Slurry Temperature = 40.0 C

Wet Bulb Temperature = 18 C

Atmospheric Pressure = 753.0 mm Hg

Apparent Viscosity = 1186.0 cP

Dry Bulb Temperature = 22 C

Air Density = 1.197 kg/Cu. m

Solid Content of Slurry = 78.6%

Relative Humidity = 68%

Specific Gravity = 1.386

* Determined from empirical correlation

Pressure	D(3,2)	D(2,1)	D(1,0)	D(v,0.9)	D(v,0.5)	D(v,0.1)	% > 420.0	% > 201.0	% > 82.7	% < 39.5	% < 10.5
600 psi	179.87	97.54	46.78	392.88	234.04	112.52	6.8	63.4	95.3	0.7	0.0
	183.24	106.01	53.81	391.83	234.33	114.34	6.7	63.8	95.6	0.6	0.0
	185.15	111.07	57.38	388.87	234.14	117.16	6.4	64.3	96.1	0.5	0.0
	182.75	104.87	52.66	391.19	234.17	114.70	6.6	63.8	95.7	0.6	0.0
800 psi	173.02	104.36	55.37	400.37	210.22	109.42	7.7	55.0	95.2	0.6	0.0
	168.80	96.09	47.64	359.82	217.05	107.22	4.1	57.4	94.8	0.8	0.0
	175.29	107.82	57.94	399.90	210.65	111.62	7.7	55.4	95.6	0.6	0.0
	172.37	102.76	53.65	386.70	212.64	109.42	6.5	55.9	95.2	0.7	0.0
1000 psi	126.63	69.79	34.19	273.20	165.96	79.28	2.6	30.8	88.8	1.8	0.1
	126.63	69.79	34.19	273.20	165.96	79.28	2.6	30.8	88.8	1.8	0.1
	127.29	71.42	35.28	260.72	165.59	80.20	2.5	30.4	89.1	1.7	0.1
	126.85	70.33	34.55	269.04	165.84	79.59	2.6	30.7	89.0	1.8	0.1
1200 psi	92.33	32.32	12.63	222.74	137.07	59.27	1.1	16.8	80.0	4.1	0.2
	97.99	46.53	20.93	221.61	136.83	59.59	1.0	16.5	80.1	4.0	0.2
	103.30	54.93	26.24	218.45	138.65	63.80	0.8	15.8	82.0	3.2	0.2
	97.87	44.59	19.93	220.93	137.52	60.89	1.0	16.4	80.7	3.8	0.2

Table A1.46: *Drop-Size Distribution Results for Detergent Slurry at 40°C using the Nozzle AAASSTC10-10*

Pressure	Fluid	Obscuration	Log. Difference	Measured Values		Correction Factors		Corrected Values		Volumetric Flowrate* (l/min)	Specific Surface Area (Sq.m/cc)
				X Parameter	N Parameter	X Parameter	N Parameter	X Parameter	N Parameter		
600 psi	Detergent	0.2049	4.56	284.38	2.75	–	–	–	–	59.24	0.02
		0.2410	4.72	285.20	2.75						0.02
		0.2197	4.42	286.71	2.84						0.02
				285.43	2.78						0.02
800 psi	Detergent	0.2808	4.93	224.65	2.68	–	–	–	–	68.4	0.02
		0.3295	5.12	223.20	2.87						0.02
		0.2975	4.93	224.12	2.56						0.02
				223.99	2.70						0.02
1000 psi	Detergent	0.3499	4.77	182.94	2.84	–	–	–	–	76.48	0.02
		0.3842	5.22	180.86	2.64						0.02
		0.3927	5.01	181.52	2.97						0.02
				181.77	2.82						0.02
1200 psi	Detergent	0.2427	5.41	157.75	2.45	–	–	–	–	83.78	0.03
		0.3816	5.22	158.66	2.57						0.03
		0.4407	5.22	158.66	2.57						0.03
				158.36	2.53						0.03

All Dimensions in microns

Slurry Temperature = 40.0 C

Wet Bulb Temperature = 18 C

Atmospheric Pressure = 750.1 mm Hg

Apparent Viscosity = 1186.0 cP

Dry Bulb Temperature = 22 C

Air Density = 1.197 kg / Cu. m

Solid Content of Slurry = 78.6%

Relative Humidity = 68%

Specific Gravity = 1.386

* Determined from empirical correlation

Pressure	D(3,2)	D(2,1)	D(1,0)	D(v,0.9)	D(v,0.5)	D(v,0.1)	% > 420.0	% > 201.0	% > 82.7	% < 39.5	% < 10.5
600 psi	197.19	117.00	59.83	406.99	248.34	123.36	8.3	68.8	96.7	0.4	0.0
	197.73	117.29	59.95	407.76	249.07	123.67	8.3	69.0	96.7	0.4	0.0
	203.55	128.32	69.88	409.16	251.44	127.00	8.5	70.2	97.1	0.3	0.0
	199.49	120.87	63.22	407.96	249.62	124.68	8.4	69.3	96.8	0.4	0.0
800 psi	154.33	88.90	45.05	371.32	194.28	95.38	5.6	46.1	93.4	0.9	0.0
	159.58	100.85	55.55	363.80	194.68	99.88	5.2	46.0	94.4	0.7	0.0
	150.40	83.56	41.60	373.18	192.92	91.91	5.7	45.5	92.5	1.2	0.0
	154.77	91.10	47.40	369.43	193.96	95.72	5.5	45.9	93.4	0.9	0.0
1000 psi	129.19	81.59	44.38	239.71	160.90	83.01	1.5	26.8	90.1	1.3	0.0
	122.45	70.33	35.29	241.94	156.95	77.63	1.7	26.2	88.2	1.8	0.0
	130.71	85.33	47.57	235.74	160.47	84.98	1.2	26.0	90.8	1.1	0.0
	127.45	79.08	42.41	239.13	159.44	81.87	1.5	26.3	89.7	1.4	0.0
1200 psi	101.22	51.44	23.65	216.91	137.23	62.90	0.8	15.2	81.5	3.3	0.2
	105.37	58.31	28.33	215.61	138.88	66.18	0.6	15.0	83.0	2.8	0.1
	105.37	58.31	28.33	215.61	138.88	66.18	0.6	15.0	83.0	2.8	0.1
	103.99	56.02	26.77	216.04	138.33	65.09	0.7	15.1	82.5	3.0	0.1

Table A1.47: *Drop-Size Distribution Results for Detergent Slurry at 60℃ using the Nozzle AAASSTC5-5*

Pressure	Fluid	Obscuration	Log. Difference	Measured Values		Correction Factors		Corrected Values		Volumetric Flowrate* (l/min)	Specific Surface Area (Sq.m/cc)
				X Parameter	N Parameter	X Parameter	N Parameter	X Parameter	N Parameter		
600 psi	Detergent	0.3120	4.59	241.22	2.66	-	-	-	-	33.00	0.02
		0.1777	4.99	241.92	2.64						0.02
		0.2410	4.72	241.37	2.58						0.02
				241.50	2.63						0.02
800 psi	Detergent	0.2254	4.91	202.59	2.95	-	-	-	-	38.10	0.02
		0.2102	5.19	201.62	2.84						0.02
		0.2973	4.93	200.35	2.76						0.02
				201.52	2.85						0.02
1000 psi	Detergent	0.4037	5.25	203.34	2.37	-	-	-	-	42.60	0.02
		0.4148	5.28	202.20	2.21						0.02
		0.4616	5.19	202.77	2.46						0.02
				202.77	2.35						0.02
1200 psi	Detergent	0.5256	5.56	182.59	2.84	-	-	-	-	46.66	0.02
		0.5233	5.33	182.34	2.95						0.03
		0.5040	5.42	181.23	2.92						0.03
				182.05	2.90						0.03

All Dimensions in microns

Slurry Temperature = 60.2 C

Wet Bulb Temperature = 16 C

Atmospheric Pressure = 753.1 mm Hg

Apparent Viscosity = 947.0 cP

Dry Bulb Temperature = 20 C

Air Density = 1.205 kg / Cu. m

Solid Content of Slurry = 78.6%

Relative Humidity = 66%

Specific Gravity = 1.292

* Determined from empirical correlation

Pressure	D(3,2)	D(2,1)	D(1,0)	D(v,0.9)	D(v,0.5)	D(v,0.1)	% > 420.0	% > 201.0	% > 82.7	% < 39.5	% < 10.5
600 psi	165.04	93.22	46.53	395.60	205.90	104.34	7.3	52.6	94.3	0.8	0.0
	164.83	92.40	45.90	396.48	206.26	103.98	7.4	52.8	94.3	0.8	0.0
	162.44	89.36	43.97	396.28	205.40	101.75	7.4	52.3	93.9	0.9	0.0
	164.10	91.66	45.47	396.12	205.85	103.36	7.4	52.6	94.2	0.8	0.0
800 psi	146.41	96.34	54.96	294.12	180.52	92.96	2.9	36.7	93.2	0.8	0.0
	142.31	88.02	46.90	298.99	178.83	90.26	3.0	36.1	92.4	1.0	0.0
	139.59	84.61	44.53	300.13	177.08	88.04	3.1	35.5	91.7	1.1	0.0
	142.77	89.66	48.80	297.75	178.81	90.42	3.0	36.1	92.4	1.0	0.0
1000 psi	128.27	61.87	27.99	337.30	175.28	79.08	4.1	36.5	88.9	2.0	0.1
	120.62	51.22	22.02	343.34	172.33	73.42	4.3	36.1	87.1	2.7	0.2
	132.01	69.36	33.13	330.48	175.83	81.51	3.8	36.3	89.6	1.8	0.1
	126.97	60.82	27.71	337.04	174.48	78.00	4.1	36.3	88.5	2.2	0.1
1200 psi	128.94	81.47	44.33	239.29	160.51	82.86	1.5	26.7	90.1	1.3	0.0
	130.89	84.96	47.12	236.94	161.21	84.93	1.3	26.4	90.8	1.1	0.0
	129.54	83.54	46.13	236.25	159.74	83.92	1.3	26.9	90.4	1.2	0.0
	129.79	83.32	45.86	237.49	160.49	83.90	1.4	26.7	90.4	1.2	0.0

Table A1.48: *Drop-Size Distribution Results for Detergent Slurry at 60℃ using the Nozzle AAASSTC8-5*

Pressure	Fluid	Obscuration	Log. Difference	Measured Values		Correction Factors		Corrected Values		Volumetric Flowrate* (l/min)	Specific Surface Area (Sq.m/cc)
				X Parameter	N Parameter	X Parameter	N Parameter	X Parameter	N Parameter		
600 psi	Detergent	0.3846	5.92	249.73	2.42	–	–	–	–	47.27	0.02
		0.3569	4.80	249.58	2.39						0.02
		0.3329	5.00	249.17	2.39						0.02
			5.21	249.49	2.40						0.02
800 psi	Detergent	0.2398	5.21	215.99	2.30	–	–	–	–	54.59	0.02
		0.2687	4.63	217.05	2.65						0.02
		0.2805	4.93	217.11	2.34						0.02
				216.72	2.43						0.02
1000 psi	Detergent	0.2811	4.96	172.06	2.84	–	–	–	–	61.03	0.03
		0.2864	5.82	174.32	2.85						0.03
		0.2971	5.06	173.21	2.66						0.02
				173.20	2.78						0.03
1200 psi	Detergent	0.3876	5.16	155.73	2.64	–	–	–	–	66.86	0.02
		0.3381	5.26	153.21	2.66						0.03
		0.3234	5.03	153.43	2.71						0.03
				154.12	2.67						0.03

All Dimensions in microns

Slurry Temperature = 60.0 C

Wet Bulb Temperature = 16 C

Atmospheric Pressure = 753.2 mm Hg

Apparent Viscosity = 947.0 cP

Dry Bulb Temperature = 20 C

Air Density = 1.205 kg / Cu. m

Solid Content of Slurry = 78.6%

Relative Humidity = 66%

Specific Gravity = 1.292

* Determined from empirical correlation

Pressure	D(3,2)	D(2,1)	D(1,0)	D(v,0.9)	D(v,0.5)	D(v,0.1)	% > 420.0	% > 201.0	% > 82.7	% < 39.5	% < 10.5
600 psi	159.35	79.14	36.07	368.64	215.74	99.28	4.8	56.2	93.3	1.1	0.1
	158.02	77.50	35.17	369.21	215.26	98.03	4.9	56.0	93.1	1.2	0.1
	157.77	77.40	35.13	368.61	214.94	97.87	4.8	55.8	93.1	1.2	0.1
	158.38	78.01	35.46	368.82	215.31	98.39	4.8	56.0	92.2	1.2	0.1
800 psi	133.54	61.46	27.33	367.36	184.20	81.45	5.4	41.5	89.6	2.0	0.1
	148.30	85.44	43.44	357.29	188.72	91.69	4.9	42.8	92.6	1.1	0.0
	135.77	63.51	28.34	368.16	185.76	83.11	5.4	42.2	90.1	1.8	0.1
	139.20	70.14	33.04	364.27	186.23	85.42	5.2	42.2	90.8	1.6	0.1
1000 psi	121.66	77.76	42.87	228.03	150.46	78.45	0.9	21.4	88.3	2.3	0.0
	123.42	78.88	43.44	230.17	152.51	79.63	1.0	22.5	88.8	1.4	0.0
	117.83	68.72	34.88	232.24	150.22	74.86	1.2	22.5	87.0	1.9	0.1
	120.97	75.12	40.40	230.15	151.06	77.65	1.0	22.1	88.0	1.9	0.0
1200 psi	104.93	59.76	29.51	211.35	136.86	66.50	0.5	13.5	82.9	2.6	0.1
	103.73	59.63	29.66	208.33	134.83	65.81	0.4	12.4	82.4	2.7	0.1
	105.65	64.07	33.62	207.84	135.34	67.01	0.3	12.3	83.0	2.5	0.1
	104.77	61.15	30.93	209.17	135.68	66.44	0.4	12.7	82.8	2.6	0.1

Table A1.49: *Drop-Size Distribution Results for Detergent Slurry at 60°C using the Nozzle AAASSTC8-8*

Pressure	Fluid	Obscuration	Log. Difference	Measured Values		Correction Factors		Corrected Values		Volumetric Flowrate* (l/min)	Specific Surface Area (Sq.m/cc)
				X Parameter	N Parameter	X Parameter	N Parameter	X Parameter	N Parameter		
600 psi	Detergent	0.2056	5.00	248.21	2.52	–	–	–	–	47.27	0.02
		0.2187	5.00	248.19	2.36						0.02
		0.2132	5.26	247.45	2.42						0.02
				247.85	2.43						0.02
800 psi	Detergent	0.2914	5.03	216.78	2.95	–	–	–	–	54.59	0.02
		0.2906	5.06	215.88	3.08						0.02
		0.2716	5.00	214.67	2.84						0.02
				215.78	2.96						0.02
1000 psi	Detergent	0.4910	5.15	148.18	2.74	–	–	–	–	61.03	0.03
		0.3534	5.01	148.18	2.93						0.03
		0.4761	5.12	147.86	2.64						0.03
				148.07	2.77						0.03
1200 psi	Detergent	0.2401	4.73	129.75	2.95	–	–	–	–	66.86	0.03
		0.3700	5.31	129.18	3.03						0.04
		0.4324	5.28	128.22	2.95						0.03
				129.05	2.98						0.03

All Dimensions in microns

Slurry Temperature = 60.1 C

Apparent Viscosity = 947.0 cP

Solid Content of Slurry = 78.6%

Wet Bulb Temperature = 16 C

Dry Bulb Temperature = 20 C

Relative Humidity = 66%

Atmospheric Pressure = 753.2 mm Hg

Air Density = 1.205 kg / Cu. m

Specific Gravity = 1.292

* Determined from empirical correlation

Pressure	D(3,2)	D(2,1)	D(1,0)	D(v,0.9)	D(v,0.5)	D(v,0.1)	% > 420.0	% > 201.0	% > 82.7	% < 39.5	% < 10.5
600 psi	163.77	88.75	42.90	363.57	215.61	102.43	4.4	56.4	93.9	1.0	0.0
	155.95	75.65	34.24	367.99	213.79	96.27	4.8	55.3	92.8	1.3	0.1
	157.95	78.59	35.86	365.21	213.92	98.37	4.6	55.5	93.2	1.2	0.1
	159.22	81.00	37.67	365.59	214.44	99.02	4.6	55.7	93.3	1.2	0.1
800 psi	156.74	101.54	57.01	345.85	190.84	99.03	4.4	43.4	94.4	0.7	0.0
	158.88	106.31	61.39	337.97	191.08	101.84	4.1	43.3	95.0	0.5	0.0
	152.74	96.73	53.51	344.49	188.57	95.45	4.3	42.2	93.6	0.8	0.0
	156.12	101.53	57.30	342.76	190.16	98.77	4.3	43.0	94.3	0.7	0.0
1000 psi	102.74	63.16	33.56	201.46	131.01	65.21	0.2	10.1	81.8	2.6	0.1
	105.94	68.35	37.55	198.86	132.10	69.04	0.1	9.3	83.5	2.1	0.1
	99.86	57.30	28.56	202.61	130.08	62.99	0.3	10.5	80.7	3.0	0.1
	102.85	62.94	33.22	200.98	131.06	65.75	0.2	10.0	82.0	2.6	0.1
1200 psi	93.47	61.69	35.02	186.83	114.94	60.87	0.1	7.2	76.6	2.8	0.0
	94.09	63.19	36.37	184.06	114.81	61.78	0.1	6.8	77.0	2.6	0.0
	92.39	61.10	34.78	183.64	113.33	60.18	0.1	6.7	75.9	2.9	0.0
	93.32	61.99	35.39	184.84	114.36	60.94	0.1	6.9	76.5	2.8	0.0

Table A1.50: *Drop-Size Distribution Results for Detergent Slurry at 60℃ using the Nozzle AAASSTC10-10*

Pressure	Fluid	Obscuration	Log. Difference	Measured Values		Correction Factors		Corrected Values		Volumetric Flowrate* (l/min)	Specific Surface Area (Sq.m/cc)
				X Parameter	N Parameter	X Parameter	N Parameter	X Parameter	N Parameter		
600 psi	Detergent	0.2422	4.84	251.71	2.74	–	–	–	–	61.36	0.02
		0.2101	5.02	250.83	2.66						0.02
		0.2351	5.23	251.49	2.84						0.02
				251.34	2.75						0.02
800 psi	Detergent	0.3274	4.86	275.15	2.35	–	–	–	–	70.85	0.02
		0.3042	5.17	275.76	2.37						0.02
		0.3425	4.93	274.23	2.37						0.02
				275.05	2.43						0.02
1000 psi	Detergent	0.4207	5.26	262.32	2.37	–	–	–	–	79.21	0.02
		0.4874	5.91	261.56	2.65						0.02
		0.4310	5.72	262.46	2.41						0.02
				262.11	2.48						0.02
1200 psi	Detergent	0.9742	5.44	222.27	2.36	1.1231	1.5572	249.64	3.67	86.77	0.02
		0.9879	5.71	221.03	2.46	1.1248	1.6663	248.61	4.10		0.02
		0.9884	5.21	222.73	2.28	1.1402	1.5841	253.95	3.61		0.02
				222.01	2.37			250.73	3.79		0.02

All Dimensions in microns

Slurry Temperature = 60.0 C

Wet Bulb Temperature = 16 C

Atmospheric Pressure = 753.2 mm Hg

Apparent Viscosity = 947.0 cP

Dry Bulb Temperature = 20 C

Air Density = 1.205 kg / Cu. m

Solid Content of Slurry = 78.6%

Relative Humidity = 66%

Specific Gravity = 1.292

* Determined from empirical correlation

Pressure	D(3,2)	D(2,1)	D(1,0)	D(v,0.9)	D(v,0.5)	D(v,0.1)	% > 420.0	% > 201.0	% > 82.7	% < 39.5	% < 10.5
600 psi	174.98	105.78	55.50	363.59	220.44	110.98	4.4	59.1	95.4	0.6	0.0
	170.52	97.05	48.12	364.11	219.05	108.20	4.4	58.3	94.9	0.7	0.0
	179.09	109.69	58.65	405.28	214.67	113.71	8.2	57.3	95.8	0.5	0.0
	174.84	104.17	54.09	377.66	218.05	110.96	5.7	57.6	95.4	5.0	0.0
800 psi	181.90	97.78	46.56	398.48	238.03	113.63	7.3	64.6	95.4	0.7	0.0
	172.50	82.56	36.81	400.01	236.12	107.06	7.5	63.1	94.4	1.0	0.1
	171.62	82.17	36.66	398.60	234.88	106.52	7.4	62.7	94.3	1.0	0.1
	175.34	87.50	40.01	399.03	236.34	109.07	7.4	63.5	94.7	0.9	0.1
1000 psi	164.71	79.32	35.60	386.19	225.23	102.16	6.2	59.6	93.7	1.1	0.1
	178.65	104.54	53.60	380.98	227.71	111.99	5.7	61.6	95.4	0.7	0.0
	166.67	81.85	37.01	385.79	225.86	103.82	6.2	59.9	94.0	1.0	0.1
	170.01	88.57	42.07	384.32	226.27	105.99	6.0	60.4	94.4	0.9	0.1
1200 psi	199.84	154.28	109.40	399.69	216.87	130.80	7.7	60.7	98.3	0.1	0.0
	205.17	165.61	124.59	395.78	217.14	138.15	7.3	61.9	98.9	0.1	0.0
	202.60	154.86	108.57	406.42	220.13	131.71	8.3	62.2	98.2	0.1	0.0
	202.54	158.25	114.19	400.63	218.05	133.55	7.8	61.6	98.5	0.1	0.0

Table A1.51: *Drop-Size Distribution Results for Detergent Slurry at 80°C using the Nozzle AAASSTC5-5*

Pressure	Fluid	Obscuration	Log. Difference	Measured Values		Correction Factors		Corrected Values		Volumetric Flowrate* (l/min)	Specific Surface Area (Sq.m/cc)
				X Parameter	N Parameter	X Parameter	N Parameter	X Parameter	N Parameter		
600 psi	Detergent	0.1777	4.99	236.82	3.03	–	–	–	–	32.67	0.02
		0.2100	5.01	234.17	2.97						0.02
		0.1923	5.17	235.65	2.97						0.02
				235.55	2.99						0.02
800 psi	Detergent	0.3329	5.19	194.18	2.05	–	–	–	–	37.72	0.02
		0.2710	5.21	195.89	2.11						0.02
		0.2832	5.03	195.72	2.23						0.02
				195.26	2.13						0.02
1000 psi	Detergent	0.3197	5.42	178.67	2.84	–	–	–	–	42.18	0.03
		0.3478	5.46	179.84	2.84						0.03
		0.3519	5.23	178.32	2.84						0.03
				178.94	2.84						0.03
1200 psi	Detergent	0.4616	5.72	141.90	2.68	–	–	–	–	46.20	0.04
		0.4894	5.21	140.76	2.64						0.04
		0.4999	5.00	140.21	2.52						0.04
				140.62	2.61						0.04

All Dimensions in microns

Slurry Temperature = 80.0 C

Wet Bulb Temperature = 17 C

Atmospheric Pressure = 750.6 mm Hg

Apparent Viscosity = 210.5 cP

Dry Bulb Temperature = 20 C

Air Density = 1.205 kg / Cu. m

Solids Content = 78.6%

Relative Humidity = 74%

Specific Gravity = 1.318

* Determined from empirical correlation

Pressure	D(3,2)	D(2,1)	D(1,0)	D(v,0.9)	D(v,0.5)	D(v,0.1)	% > 420.0	% > 201.0	% > 82.7	% < 39.5	% < 10.5
600 psi	174.77	117.27	69.26	385.58	204.90	112.63	6.5	52.4	96.0	0.4	0.0
	170.10	109.12	60.74	382.15	202.75	108.61	6.3	51.1	95.6	0.5	0.0
	171.23	109.79	61.10	384.53	203.77	109.52	6.4	51.7	95.7	0.5	0.0
	172.03	112.06	63.70	384.09	203.81	110.25	6.4	51.7	95.8	0.5	0.0
800 psi	100.25	25.84	10.05	335.71	162.75	64.79	4.1	33.1	84.0	3.7	0.3
	104.10	28.43	11.00	334.47	165.31	67.55	4.0	33.6	85.1	3.3	0.2
	117.60	50.91	22.01	325.70	166.92	71.68	3.7	33.4	86.4	2.8	0.2
	107.32	35.06	14.35	331.96	164.99	68.01	3.9	33.4	85.2	3.3	0.2
1000 psi	126.25	80.10	43.80	234.87	156.48	81.26	1.3	24.7	89.5	1.4	0.0
	127.05	80.51	43.96	236.15	157.64	81.74	1.3	25.3	89.6	1.3	0.0
	126.01	79.98	43.76	234.49	156.14	81.11	1.1	24.6	89.4	1.4	0.0
	126.44	80.20	43.84	235.17	156.75	81.37	1.2	24.9	89.5	1.4	0.0
1200 psi	96.74	56.58	28.62	194.62	125.07	61.18	0.1	8.2	79.1	3.2	0.1
	95.28	55.14	27.77	193.84	123.76	59.91	0.1	8.0	78.3	3.4	0.1
	91.82	48.91	23.13	195.38	122.36	57.31	0.2	8.4	76.8	4.0	0.2
	94.61	53.54	26.51	194.61	123.73	59.47	0.1	8.2	78.1	3.5	0.1

Table A1.52: *Drop-Size Distribution Results for Detergent Slurry at 80°C using the Nozzle AAASSTC8-5*

Pressure	Fluid	Obscuration	Log. Difference	Measured Values		Correction Factors		Corrected Values		Volumetric Flowrate* (l/min)	Specific Surface Area (Sq.m/cc)
				X Parameter	N Parameter	X Parameter	N Parameter	X Parameter	N Parameter		
600 psi	Detergent	0.1826	5.13	240.86	2.64	–	–	–	–	46.81	0.02
		0.1971	5.12	239.21	2.64						0.02
		0.1778	5.23	238.97	2.71						0.02
				239.68	2.66						0.02
800 psi	Detergent	0.2973	5.55	195.75	2.55	–	–	–	–	54.05	0.02
		0.2523	5.45	195.19	2.57						0.02
		0.2223	5.27	194.87	2.61						0.02
				195.27	2.58						0.02
1000 psi	Detergent	0.5040	5.46	176.89	2.57	–	–	–	–	60.43	0.02
		0.5123	5.37	174.65	2.57						0.02
		0.5117	5.23	174.82	2.59						0.02
				175.45	2.58						0.02
1200 psi	Detergent	0.4228	5.68	148.36	3.05	–	–	–	–	66.19	0.04
		0.3616	5.62	146.61	2.95						0.03
		0.4334	5.57	146.10	2.84						0.03
				147.02	2.95						0.03

All Dimensions in microns

Slurry Temperature = 80.0 C

Apparent Viscosity = 210.5 cP

Solids Content = 78.6%

Wet Bulb Temperature = 17 C

Dry Bulb Temperature = 20 C

Relative Humidity = 74%

Atmospheric Pressure = 750.5 mm Hg

Air Density = 1.205 kg / Cu. m

Specific Gravity = 1.318

* Determined from empirical correlation

Pressure	D(3,2)	D(2,1)	D(1,0)	D(v,0.9)	D(v,0.5)	D(v,0.1)	% > 420.0	% > 201.0	% > 82.7	% < 39.5	% < 10.5
600 psi	164.12	92.08	45.78	395.34	205.50	103.54	7.3	52.4	94.2	0.8	0.0
	163.01	91.58	45.59	393.51	204.33	102.86	7.1	51.8	94.1	0.9	0.0
	165.28	95.25	48.22	392.64	204.47	102.31	7.1	51.9	94.6	0.8	0.0
	164.14	92.97	46.53	393.83	204.77	102.90	7.2	52.0	94.3	0.8	0.0
800 psi	130.02	71.20	34.70	299.22	170.84	81.30	3.1	33.2	89.5	1.7	0.1
	130.19	71.82	35.12	294.82	170.55	81.60	3.0	32.9	89.6	1.6	0.1
	131.03	73.32	36.10	289.18	170.68	82.49	2.9	32.8	89.9	1.5	0.1
	130.47	72.18	35.31	294.41	170.69	81.80	3.0	33.0	89.7	1.6	0.1
1000 psi	118.20	66.68	33.23	238.66	152.70	74.18	1.6	24.5	86.9	2.1	0.1
	116.71	66.02	32.96	235.88	150.76	73.22	1.4	23.4	86.4	2.2	0.1
	117.30	66.81	33.48	235.61	151.06	73.81	1.4	23.4	86.7	2.1	0.1
	117.40	66.50	33.22	236.72	151.51	73.74	1.5	23.4	86.7	2.1	0.1
1200 psi	108.61	74.21	43.64	197.69	132.74	70.04	0.1	9.0	84.3	1.8	0.0
	105.17	68.31	37.77	196.61	130.85	68.64	0.1	8.6	83.2	2.1	0.1
	103.05	65.12	35.28	197.48	129.80	66.24	0.1	8.9	82.1	2.4	0.1
	105.61	69.21	38.90	197.26	131.13	68.31	0.1	8.8	83.2	2.1	0.1

Table A1.53: *Drop-Size Distribution Results for Detergent Slurry at 80°C using the Nozzle AAASSTC8-8*

Pressure	Fluid	Obscuration	Log. Difference	Measured Values		Correction Factors		Corrected Values		Volumetric Flowrate* (l/min)	Specific Surface Area (Sq.m/cc)
				X Parameter	N Parameter	X Parameter	N Parameter	X Parameter	N Parameter		
600 psi	Detergent	0.3100	5.07	255.95	2.65	-	-	-	-	46.81	0.02
		0.3413	5.03	256.32	2.84						0.02
		0.3267	5.00	256.09	2.71						0.02
				256.12	2.73						0.02
800 psi	Detergent	0.9851	5.21	220.63	2.94	1.0943	1.8951	241.44	5.57	54.05	0.02
		0.9859	5.34	221.21	2.97	1.0932	1.9173	241.84	5.69		0.02
		0.9721	5.46	221.56	2.84	1.0932	1.7596	242.21	5.00		0.02
				221.13	2.92			241.83	5.42		0.02
1000 psi	Detergent	0.4804	5.06	189.26	2.46	-	-	-	-	60.43	0.02
		0.3718	5.21	190.18	2.64						0.02
		0.3923	4.94	190.73	2.67						0.02
				190.06	2.59						0.02
1200 psi	Detergent	0.4248	5.66	170.91	2.57	-	-	-	-	66.19	0.03
		0.4370	5.23	169.23	2.64						0.03
		0.4557	5.71	169.82	2.48						0.03
				169.99	2.56						0.03

All Dimensions in microns

Slurry Temperature = 80.0 C

Wet Bulb Temperature = 17 C

Atmospheric Pressure = 750.7 mm Hg

Apparent Viscosity = 210.5 cP

Dry Bulb Temperature = 20 C

Air Density = 1.205 kg / Cu. m

Solids Content = 78.6%

Relative Humidity = 74%

Specific Gravity = 1.318

* Determined from empirical correlation

Pressure	D(3,2)	D(2,1)	D(1,0)	D(v,0.9)	D(v,0.5)	D(v,0.1)	% > 420.0	% > 201.0	% > 82.7	% < 39.5	% < 10.5
600 psi	174.92	102.74	52.91	372.66	223.10	109.87	5.0	59.1	95.1	0.7	0.0
	181.19	111.99	59.48	369.32	224.98	115.54	4.8	61.3	96.0	0.5	0.0
	177.02	105.78	55.02	371.63	223.74	111.77	5.0	60.3	95.4	0.6	0.0
	177.71	106.84	55.80	371.20	223.94	112.39	4.9	60.2	95.5	0.6	0.0
800 psi	210.01	186.90	162.28	364.06	213.47	162.21	5.2	62.1	99.7	0.0	0.0
	210.84	188.17	163.97	363.99	213.76	165.33	5.2	62.6	99.8	0.0	0.0
	208.19	181.91	154.65	373.69	213.68	150.19	5.7	61.4	99.5	0.0	0.0
	209.71	185.66	160.30	367.25	213.64	159.24	5.4	62.0	99.7	0.0	0.0
1000 psi	122.24	62.36	28.91	278.50	163.62	76.30	2.7	30.4	87.8	2.1	0.1
	128.66	73.13	36.35	259.42	166.57	81.41	2.4	30.6	89.6	1.6	0.1
	129.79	74.53	37.27	259.01	167.42	82.34	2.4	30.8	89.9	1.5	0.1
	126.90	70.01	34.18	265.64	165.87	80.02	2.5	30.6	89.1	1.7	0.1
1200 psi	113.24	61.91	29.75	229.04	149.17	71.59	1.2	20.0	85.7	2.3	0.1
	114.62	66.91	34.01	225.63	148.27	72.60	1.0	19.0	86.1	2.1	0.1
	110.33	58.31	27.60	229.99	147.59	68.75	1.3	20.0	84.6	2.6	0.1
	112.73	62.38	30.45	228.22	148.34	70.98	1.2	19.7	85.5	2.3	0.1

Table A1.54: *Drop-Size Distribution Results for Detergent Slurry at 80°C using the Nozzle AAASSTC10-10*

Pressure	Fluid	Obscuration	Log. Difference	Measured Values		Correction Factors		Corrected Values		Volumetric Flowrate* (l/min)	Specific Surface Area (Sq.m/cc)
				X Parameter	N Parameter	X Parameter	N Parameter	X Parameter	N Parameter		
600 psi	Detergent	0.3479	5.00	271.42	2.75	–	–	–	–	60.75	0.02
		0.3216	5.01	269.57	2.61						0.02
		0.3334	4.97	270.24	2.84						0.02
				270.41	2.73						0.02
800 psi	Detergent	0.4077	5.12	205.72	2.54	–	–	–	–	70.15	0.02
		0.4128	5.07	205.72	2.54						0.02
		0.3997	5.01	204.32	2.62						0.02
				205.25	2.57						0.02
1000 psi	Detergent	0.6252	5.37	193.15	2.39	–	–	–	–	78.43	0.02
		0.6128	5.46	193.15	2.39						0.02
		0.6035	5.47	192.69	2.46						0.02
				193.00	2.41						0.02
1200 psi	Detergent	0.8849	5.60	200.78	1.91	1.0959	1.2105	220.03	2.31	85.91	0.02
		0.8280	5.61	200.24	2.36	1.0562	1.2138	211.49	2.60		0.02
		0.8973	5.97	201.93	1.84	1.1081	1.2136	223.77	2.23		0.02
				200.98	2.04				2.38		0.02

All Dimensions in microns

Slurry Temperature = 80.1 C

Apparent Viscosity = 210.5 cP

Solids Content = 78.6%

Wet Bulb Temperature = 17 C

Dry Bulb Temperature = 20 C

Relative Humidity = 74%

Atmospheric Pressure = 750.5 mm Hg

Air Density = 1.205 kg / Cu. m

Specific Gravity = 1.318

* Determined from empirical correlation

Pressure	D(3,2)	D(2,1)	D(1,0)	D(v,0.9)	D(v,0.5)	D(v,0.1)	% > 420.0	% > 201.0	% > 82.7	% < 39.5	% < 10.5
600 psi	188.63	112.61	58.11	392.84	236.97	118.62	6.8	65.3	96.2	0.5	0.0
	182.39	104.88	53.06	391.85	234.00	113.64	6.7	63.6	95.5	0.7	0.0
	192.36	122.35	67.58	390.54	236.76	120.75	6.5	65.7	96.6	0.4	0.0
	124.92	113.28	59.58	391.74	235.91	117.67	6.7	64.9	96.1	0.5	0.0
800 psi	136.35	73.46	35.41	334.19	179.28	84.76	4.0	37.8	90.6	1.5	0.1
	136.35	73.46	35.41	334.19	179.28	84.76	4.0	37.8	90.6	1.5	0.1
	137.74	76.64	37.57	325.29	178.97	86.27	3.7	37.2	91.1	0.9	0.1
	136.81	74.85	36.13	331.22	178.18	83.93	3.9	37.6	90.8	1.3	0.1
1000 psi	122.60	60.44	27.65	303.92	166.61	75.80	3.2	32.2	87.7	2.2	0.1
	122.60	60.44	27.65	303.92	166.61	75.80	3.2	32.2	87.7	2.2	0.1
	124.43	63.27	29.27	295.04	167.01	77.66	3.0	31.9	88.3	2.0	0.1
	123.21	61.38	28.19	300.96	166.74	76.42	3.1	32.1	87.9	2.1	0.1
1200 psi	136.40	62.72	27.83	373.33	187.55	83.18	5.7	43.2	90.1	1.9	0.1
	142.06	78.06	38.00	346.40	184.26	88.38	4.4	40.3	91.7	1.3	0.0
	135.31	59.78	26.26	379.91	189.18	81.47	6.1	44.3	89.7	2.1	0.1
	137.92	66.85	30.70	366.55	187.00	84.34	5.4	42.6	90.5	1.8	0.1

Appendix 2

Mathematical Model Results

Tables A2.1 to A2.6: Experimental Data

Tables A2.7 to A2.12: Theoretical Predictions

Table A2.1: *Drop-Size Distribution Results using the Perspex Nozzle P1*

Pressure	Fluid	Obscuration	Log. Difference	X Parameter	N Parameter	D(3,2)	D(v,0.5)	Specific Surface Area (Sq.m/cc)	Volumetric Flowrate (l/min)	Cone Angle (Degrees)	Liquid Sheet Velocity (m/s)	Liquid Sheet Length (mm)	Air Core Diameter (mm)
5 psi	Water	0.1304	3.43	1164.06	1.99	534.60	836.83	0.01	3.20	95.0	4.14	98.88	9.02
		0.1871	3.85	1164.95	1.99	534.79	837.06	0.01					
		0.1697	4.08	1164.51	1.95	523.27	830.47	0.01					
				1164.69	1.98	530.89	834.79	0 01					
10 psi	Water	0.2088	4.30	723.43	1.89	332.74	592.99	0.01	4.58	85.5	5.92	66.59	9.21
		0.1962	4.32	723.34	1.92	340.18	595.53	0.01					
		0.1810	4.29	723.51	1.85	324.15	589.63	0.01					
				723.43	1.89	332 36	592.72	0 01					
15 psi	Water	0.2235	4.90	558.98	1.86	261.97	460.85	0 01	5.48	95.0	7.10	63.65	9.21
		0.2252	4.87	559.61	1.86	262.57	461.67	0.01					
		0.2312	4.81	558.04	1.86	261.79	460.18	0.01					
				558.88	1.86	262.11	460 90	0 01					
20 psi	Water	0.3087	4.97	415.18	1.92	205.39	343.89	0.01	6.21	91.0	7.69	47.65	9.21
		0.2982	4.92	416.04	1.90	204.44	344.12	0.01					
		0.2877	4.98	416.04	1.90	204.44	344.12	0.01					
				415.74	1.91	204.76	344 04	0 01					
25 psi	Water	0.3564	4.90	337.66	1.95	135.24	279.93	0.01	6.86	83.0	8.28	45.39	9.21
		0.3544	4.90	339.96	1.95	135.71	281.70	0.01					
		0.3572	4.93	337.66	1.95	135.24	279.93	0.01					
				338.43	1.95	135.40	280.52	0.01					

All Dimensions in microns

Fluid Temperature = 18.0 C | Wet Bulb Temperature = 17 C | Atmospheric Pressure = 749.8 mm Hg | Swirlchamber Diameter = 43.71 mm

Absolute Viscosity = 1.053 cP | Dry Bulb Temperature = 20 C | Air Density = 1.205 kg / Cu. m | Inlet Diameter = 4.0 mm

Density = 997.21 kg / Cu. m | Relative Humidity = 74% | Fluid Surface Tension = 73.05 Dynes / cm | Outlet Diameter = 10.0 mm

Pressure	D(v,0.9)	D(v,0.8)	D(v,0.7)	D(v,0.6)	D(v,0.5)	D(v,0.4)	D(v,0.3)	D(v,0.2)	D(v,0.1)	% > 965.3	% > 344.0	% < 105.5	% < 37.5
5 psi	1219.43	1100.53	1006.01	921.03	836.83	736.49	602.26	490.66	331.97	34.7	89.2	1.0	0.1
	1219.52	1100.65	1006.16	921.21	837.06	736.82	602.50	490.85	332.10	34.7	89.2	1.0	0.1
	1217.10	1097.22	1001.87	915.98	830.47	725.89	593.70	482.01	324.11	34.2	88.7	1.1	0.2
	1218.68	1099.47	1004.65	919.41	834.79	733.01	599.49	487.84	329.39	34.5	89.0	1.0	0.1
10 psi	1061.90	898.78	779.24	680.60	592.99	508.45	411.62	321.53	217.52	15.4	77.4	2.6	0.4
	1061.75	899.00	780.01	682.13	595.53	512.23	416.82	325.87	222.43	15.4	77.9	2.5	0.4
	1061.97	898.36	778.12	678.52	589.63	503.48	405.19	315.98	211.40	15.4	76.7	2.9	0.5
	1061.87	898.71	779.12	680.42	592.72	508.05	411.21	321.13	217.12	15.4	77.3	2.7	0.4
15 psi	986.98	746.86	600.37	526.79	460.85	385.28	319.51	249.98	166.66	10.8	66.2	4.4	0.6
	988.04	748.90	601.28	527.56	461.67	386.04	320.14	250.57	167.10	10.9	66.3	4.4	0.6
	985.69	744.30	599.35	526.06	460.18	384.75	319.16	249.73	166.56	10.8	66.1	4.4	0.6
	986.90	746.69	600.33	526.80	460.90	385.36	319.60	250.09	166.77	10.8	66.2	4.4	0.6
20 psi	619.54	521.05	455.07	397.84	343.89	292.54	242.59	190.19	128.68	3.3	50.0	6.9	1.0
	623.00	522.75	456.20	398.54	344.12	292.34	242.07	189.42	127.77	3.4	50.0	7.0	1.0
	623.00	522.75	456.20	398.54	344.12	292.34	242.07	189.42	127.77	3.4	50.0	7.0	1.0
	621.85	522.18	455.82	398.31	344.04	292.41	242.24	189.68	128 07	3.4	50.0	7.0	1.0
25 psi	514.86	430.72	371.38	322.94	279.93	239.93	199.33	156.83	106.89	0.9	35.5	9.8	1.3
	518.40	433.89	374.03	325.11	281.70	240.89	200.42	157.59	107.30	0.9	36.0	9.7	1.3
	514.86	430.72	371.38	322.94	279.93	239.93	199.33	156.83	106.89	0.9	35.5	9.8	1.3
	516.04	431.78	372.26	323.66	280.52	240.25	199.69	157.12	107.08	0.9	35.7	9.8	1.3

Table A2.2: *Drop-Size Distribution Results using the Perspex Nozzle P2*

Pressure	Fluid	Obscuration	Log. Difference	X Parameter	N Parameter	D(3,2)	D(v,0.5)	Specific Surface Area (Sq.m/cc)	Volumetric Flowrate (l/min)	Cone Angle (Degrees)	Liquid Sheet Velocity (m/s)	Liquid Sheet Length (mm)	Air Core Diameter (mm)
5 psi	Water	0.1842	3.23	1424.75	2.19	645.02	906.31	0.01	3.40	95.5	2.35	122.40	11.49
		0.1205	3.28	1426.75	2.19	644.68	906.26	0.01					
		0.1444	3.49	1424.75	2.19	645.02	906.31	0.01					
				1425.42	2.19	644.91	906.29	0 01					
10 psi	Water	0.2264	4.10	746.56	1.94	361.56	605.37	0.01	4.84	90.0	4.12	65.48	11.12
		0.2248	4.06	745.59	1.99	396.38	616.56	0.01					
		0.1708	4.20	744.61	2.03	403.68	618.89	0.01					
				745.59	1.99	387.21	613.61	0 01					
15 psi	Water	0.2286	4.36	578.76	1.92	278.52	483.20	0.01	5.91	99.0	5.29	60.67	11.12
		0.2661	4.41	576.83	1.92	277.67	481.57	0.01					
		0.2074	4.29	578.76	1.92	278.52	483.20	0.01					
				578.12	1.92	278 24	482.66	0.01					
20 psi	Water	0.2961	4.76	439.87	1.86	210.77	362.77	0.01	6.92	94.0	5.88	45.31	11.12
		0.3317	4.73	440.14	1.86	211.03	363.06	0.01					
		0.3717	4.74	440.14	1.86	211.03	363.06	0.01					
				440.05	1.86	210.94	362.96	0.01					
25 psi	Water	0.3967	4.66	371.43	1.95	188.27	308.01	0.01	7.91	105.0	6.47	44.96	11.12
		0.3755	4.78	371.43	1.95	188.27	308.01	0.01					
		0.3664	4.75	372.96	1.95	188.59	309.14	0.01					
				371.94	1.95	188.38	308.39	0.01					

All Dimensions in microns

Fluid Temperature = 18.2 C | Wet Bulb Temperature = 17 C | Atmospheric Pressure = 749.8 mm Hg | Swirlchamber Diameter = 43.87 mm

Absolute Viscosity = 1.053 cP | Dry Bulb Temperature = 20 C | Air Density = 1.205 kg / Cu. m | Inlet Diameter = 4.0 mm

Density = 997.21 kg / Cu. m | Relative Humidity = 74% | Fluid Surface Tension = 73.05 Dynes / cm | Outlet Diameter = 12.0 mm

Pressure	D(v,0.9)	D(v,0.8)	D(v,0.7)	D(v,0.6)	D(v,0.5)	D(v,0.4)	D(v,0.3)	D(v,0.2)	D(v,0.1)	% > 965.3	% > 344.0	% < 105.5	% < 37.5
5 psi	1246.60	1138.88	1053.69	978.27	906.31	831.59	734.17	578.06	421.74	41.8	93.3	0.5	0.1
	1246.58	1138.85	1053.66	978.23	906.26	831.52	734.02	577.89	421.37	41.8	93.3	0.5	0.1
	1246.60	1138.88	1053.69	978.27	906.31	831.59	734.17	578.06	421.74	41.8	93.3	0.5	0.1
	1246.59	1138.87	1053.68	978.26	906.29	831.57	734.18	578.00	421.62	41.8	93.3	0.5	0.1
10 psi	1100.69	940.70	815.65	701.87	605.37	523.54	434.37	336.28	231.33	18.2	79.1	2.3	0.3
	1076.74	917.55	800.25	703.03	616.56	533.86	442.63	342.85	239.11	16.6	79.9	2.1	0.3
	1076.29	917.42	800.67	704.25	618.89	537.62	448.76	347.94	245.29	16.6	80.4	1.9	0.2
	1084.57	925.22	805.52	703.05	613.61	531.67	441.92	342.36	238.58	16.8	79.8	2.1	0.3
15 psi	904.20	740.58	637.19	556.62	483.20	404.75	335.57	266.09	179.45	7.5	68.7	3.7	0.4
	901.22	738.10	635.19	554.87	481.57	403.30	334.55	265.21	178.86	7.4	68.6	3.7	0.5
	904.20	740.58	637.19	556.62	483.20	404.75	335.57	266.09	179.45	7.5	68.7	3.7	0.5
	903.21	739.75	636.52	556.04	482.66	404.27	335.23	265.80	179.25	7.5	68.7	3.7	0.5
20 psi	678.90	550.73	479.76	420.21	362.77	306.71	252.48	196.53	131.29	4.8	53.3	6.8	1.0
	679.18	550.92	479.98	420.47	363.06	307.00	252.74	196.78	131.50	4.8	53.4	6.7	1.0
	679.18	550.92	479.98	420.47	363.06	307.00	252.74	196.78	131.50	4.8	53.4	6.7	1.0
	679.09	550.86	479.91	420.38	362.96	306.90	252.65	196.70	131.43	4.8	53.4	6.7	1.0
25 psi	558.09	471.68	408.82	355.59	308.01	263.33	219.27	172.51	117.57	1.6	42.4	8.2	1.1
	558.09	471.68	408.82	355.59	308.01	263.33	219.27	172.51	117.57	1.6	42.4	8.2	1.1
	560.45	473.68	410.60	357.05	309.14	264.18	219.88	172.88	117.71	1.6	42.4	8.2	1.1
	558.88	472.35	409.41	356.08	308.39	263.61	219.47	172.63	117.62	1.6	42.4	8.2	1.1

Table A2.3: *Drop-Size Distribution Results using the Perspex Nozzle P3*

Pressure	Fluid	Obscuration	Log. Difference	X Parameter	N Parameter	D(3,2)	D(v,0.5)	Specific Surface Area (Sq.m/cc)	Volumetric Flowrate (l/min)	Cone Angle (Degrees)	Liquid Sheet Velocity (m/s)	Liquid Sheet Length (mm)	Air Core Diameter (mm)
5 psi	Water	0.2011	3.08	1076.40	2.16	565.70	837.08	0.01	4.05	87.0	2.96	65.48	7.290
		0.2063	3.60	1078.97	1.97	510.20	808.80	0.01					
		0.2156	3.95	1076.40	2.16	565.70	837.08	0.01					
				1077.26	2.10	547.20	827.65	0.01					
10 psi	Water	0.3346	4.15	800.04	1.85	351.15	630.85	0.01	5.61	83.5	4.73	60.66	7.290
		0.3431	4.12	800.20	1.86	354.27	632.35	0.01					
		0.2390	3.98	800.08	1.89	362.28	635.62	0.01					
				800.11	1.87	355.90	632.94	0.01					
15 psi	Water	0.3183	4.76	640.57	1.94	307.68	534.03	0.01	6.71	77.0	5.92	46.26	7.290
		0.4695	4.86	639.16	1.94	307.56	533.10	0.01					
		0.2811	4.81	640.57	1.94	307.68	534.03	0.01					
				640.10	1.94	307.64	533.72	0.01					
20 psi	Water	0.3206	5.02	599.07	1.75	260.95	488.51	0.01	7.51	83.5	7.10	43.48	7.290
		0.3160	4.94	600.70	1.86	278.59	497.64	0.01					
		0.3075	4.96	598.04	1.86	277.51	495.47	0.01					
				599.27	1.82	272.35	493.87	0.01					
25 psi	Water	0.4485	5.02	533.41	1.94	260.81	443.27	0.01	8.73	84.0	7.69	43.47	7.290
		0.4530	5.06	533.90	1.94	261.40	443.86	0.01					
		0.4711	4.88	534.66	1.94	261.75	444.54	0.01					
				533.99	1.94	261.32	443.89	0.01					

All Dimensions in microns

Fluid Temperature = 18.0 C | Wet Bulb Temperature = 17 C | Atmospheric Pressure = 749.8 mm Hg | Swirlchamber Diameter = 43.51 mm

Absolute Viscosity = 1.053 cP | Dry Bulb Temperature = 20 C | Air Density = 1.205 kg / Cu. m | Inlet Diameter = 6.0 mm

Density = 997.21 kg / Cu. m | Relativee Humidity = 74% | Fluid Surface Tension = 73.05 Dynes / cm | Outlet Diameter = 8.0 mm

Pressure	D(v,0.9)	D(v,0.8)	D(v,0.7)	D(v,0.6)	D(v,0.5)	D(v,0.4)	D(v,0.3)	D(v,0.2)	D(v,0.1)	% >965.3	% >344.0	% <105.5	% <37.5
5 psi	1218.95	1099.98	1005.53	920.74	837.08	738.85	609.37	503.28	349.23	34.7	90.3	0.8	0.1
	1208.63	1085.39	987.24	898.45	808.80	691.46	574.14	466.04	314.66	32.4	87.9	1.2	0.2
	1218.95	1099.98	1005.53	920.74	837.08	738.85	609.37	503.28	349.23	34.7	90.3	0.8	0.1
	1215.51	1095.12	999.43	913.31	827.65	723.05	597.63	490.87	337.71	33.9	89.5	0.9	0.1
10 psi	1128.92	976.53	855.30	742.17	630.85	541.01	449.77	342.32	231.54	20.9	79.8	2.4	0.4
	1129.45	977.30	856.31	743.55	632.35	542.69	452.12	344.29	233.71	20.9	80.0	2.4	0.4
	1130.49	978.83	858.35	746.41	635.62	546.43	457.40	348.90	238.87	21.0	80.5	2.2	0.3
	1129.62	977.55	856.65	744.04	632.94	543.38	453.10	345.17	234.71	20.9	80.1	2.3	0.4
15 psi	986.27	816.48	701.20	612.05	534.03	455.66	370.01	294.83	199.61	11.0	73.5	3.0	0.4
	984.42	814.69	699.71	610.87	533.10	454.87	369.54	294.57	199.54	10.9	73.4	3.0	0.4
	986.27	816.48	701.20	612.05	534.03	455.66	370.01	294.83	199.61	11.0	73.5	3.0	0.4
	985.65	815.88	700.70	611.66	533.72	455.40	369.85	294.74	199.59	11.0	73.5	3.0	0.4
20 psi	954.40	779.27	662.15	570.67	488.51	403.09	328.70	253.57	164.75	9.5	67.8	4.7	0.8
	944.06	773.32	661.53	575.08	497.64	415.73	341.16	268.55	178.75	9.1	69.6	3.9	0.6
	940.51	770.03	658.79	572.71	495.47	413.69	339.78	267.39	177.99	8.9	69.4	3.9	0.6
	946.32	774.21	660.82	572.82	493.87	410.84	336.55	263.17	173.83	9.2	68.9	4.2	0.7
25 psi	942.34	670.27	572.80	507.06	443.27	373.11	312.45	246.41	166.98	9.2	64.7	4.2	0.6
	942.85	670.81	573.19	507.50	443.86	373.64	312.95	246.94	167.42	9.2	64.8	4.2	0.6
	944.15	672.22	573.92	508.13	444.54	374.16	313.36	247.30	167.66	9.3	64.9	4.2	0.6
	943.11	671.10	573.30	507.56	443.89	373.64	312.92	246.88	167.35	9.2	64.0	4.2	0.6

Table A2.4: *Drop-Size Distribution Results using the Perspex Nozzle P4*

Pressure	Fluid	Obscuration	Log. Difference	X Parameter	N Parameter	D(3,2)	D(v,0.5)	Specific Surface Area (Sq.m/cc)	Volumetric Flowrate (l/min)	Cone Angle (Degrees)	Liquid Sheet Velocity (m/s)	Liquid Sheet Length (mm)	Air Core Diameter (mm)
5 psi	Water	0.1880	4.49	979.74	2.39	592.81	823.96	0.01	4.81	89.5	4.12	98.14	8.46
		0.2188	4.18	978.77	2.39	592.72	823.62	0.01					
		0.2241	4.29	978.77	2.39	592.72	823.62	0.01					
				979.09	2.39	592.75	823.73	0.01					
10 psi	Water	0.3131	4.03	798.38	1.87	356.87	632.61	0.01	6.84	101.5	5.88	74.13	8.82
		0.3721	4.05	799.71	1.78	334.90	622.50	0.01					
		0.2954	3.78	800.33	1.86	354.31	632.43	0.01					
				799.47	1.84	348.69	629.18	0.01					
15 psi	Water	0.3809	4.61	660.05	1.73	279.90	533.86	0.01	8.12	94.0	7.06	47.95	8.82
		0.3489	4.75	662.72	1.73	280.81	535.81	0.01					
		0.3877	4.65	661.39	1.73	280.13	534.73	0.01					
				661.39	1.73	280.28	534.80	0.01					
20 psi	Water	0.3964	4.60	649.32	1.69	269.22	522.29	0.01	9.69	96.0	7.65	47.53	9.00
		0.4442	4.36	648.16	1.73	275.62	524.98	0.01					
		0.4665	4.25	647.72	1.75	278.89	526.35	0.01					
				648.40	1.72	274.58	524.54	0.01					
25 psi	Water	0.5663	5.94	294.31	1.80	149.83	240.18	0.01	10.68	91.0	8.82	44.66	9.00
		0.5650	5.82	295.75	1.77	148.05	240.49	0.01					
		0.5629	5.93	294.31	1.80	149.72	240.14	0.01					
				294.79	1.79	149.20	240.27	0.01					

All Dimensions in microns

Fluid Temperature = 18.1 C | Wet Bulb Temperature = 17 C | Atmospheric Pressure = 749.8 mm Hg | Swirlchamber Diameter = 43.76 mm

Absolute Viscosity = 1.053 cP | Dry Bulb Temperature = 20 C | Air Density = 1.205 kg / Cu. m | Inlet Diameter = 6.0 mm

Density = 997.21 kg / Cu. m | Relative Humidity = 74% | Fluid Surface Tension = 73.05 Dynes / cm | Outlet Diameter = 10.0 mm

Pressure	D(v,0.9)	D(v,0.8)	D(v,0.7)	D(v,0.6)	D(v,0.5)	D(v,0.4)	D(v,0.3)	D(v,0.2)	D(v,0.1)	% >965.3	% >344.0	% <105.5	% <37.5
5 psi	1212.87	1091.68	995.56	909.26	823.96	722.08	604.60	507.93	362.67	33.4	91.2	0.5	0.0
	1212.72	1091.48	995.32	909.00	823.62	721.59	604.34	507.79	362.61	33.4	91.2	0.5	0.0
	1212.72	1091.48	995.32	909.00	823.62	721.59	604.34	507.79	362.61	33.4	91.2	0.5	0.0
	1212.77	1091.55	995.40	909.09	823.73	721.75	604.43	507.84	362.63	33.4	91.2	0.5	0.0
10 psi	1129.05	976.84	855.87	743.30	632.61	543.39	453.44	345.61	235.40	20.9	80.2	2.3	0.4
	1126.08	972.40	849.83	734.56	622.50	531.55	435.91	331.34	219.62	20.5	78.7	2.8	0.5
	1129.51	977.38	856.40	743.65	632.43	542.75	452.19	344.33	233.75	20.9	80.0	2.4	0.4
	1128.21	975.54	854.03	740.50	629.18	539.23	447.18	340.43	229.59	20.8	79.6	2.5	0.4
15 psi	1016.85	844.31	721.16	621.89	533.86	445.43	356.13	275.73	178.28	12.5	71.5	4.1	0.7
	1019.06	846.79	723.59	624.08	535.81	447.32	357.40	276.75	178.94	12.7	71.7	4.1	0.7
	1018.01	845.58	722.37	622.93	534.73	446.20	356.61	276.06	178.44	12.6	71.6	4.1	0.7
	1017.97	845.56	722.37	622.97	534.80	446.32	356.71	276.18	178.55	12.6	71.6	4.1	0.7
20 psi	1009.37	835.09	711.06	611.17	522.29	431.86	345.85	265.59	170.06	12.1	70.2	4.6	0.8
	1006.63	832.96	710.20	612.02	524.98	436.63	350.32	270.96	175.15	12.0	70.8	4.3	0.7
	1005.27	831.93	709.83	612.50	526.35	439.06	352.59	273.67	177.74	11.9	71.1	4.1	0.7
	1007.09	833.33	710.36	611.90	524.54	435.85	349.59	270.07	174.32	12.0	70.7	4.3	0.7
25 psi	467.35	383.49	326.39	280.38	240.18	202.80	166.18	128.14	84.59	0.5	26.6	14.5	2.4
	473.18	387.24	328.62	281.52	240.49	202.46	165.32	126.89	83.16	0.6	27.1	14.8	2.5
	467.52	383.58	326.42	280.37	240.14	202.74	166.10	128.05	84.50	0.5	26.6	14.5	2.4
	469.35	384.77	327.14	280.76	240.27	202.67	165.87	127.69	84.08	0.5	26.8	14.6	2.4

Table A2.5: *Drop-Size Distribution Results using the Perspex Nozzle P5*

Pressure	Fluid	Obscuration	Log. Difference	X Parameter	N Parameter	D(3,2)	D(v,0.5)	Specific Surface Area (Sq.m/cc)	Volumetric Flowrate (l/min)	Cone Angle (Degrees)	Liquid Sheet Velocity (m/s)	Liquid Sheet Length (mm)	Air Core Diameter (mm)
5 psi	Water	0.2410	3.45	1156.27	2.05	555.74	844.09	0.01	5.67	97.0	3.53	90.25	11.42
		0.2330	3.37	1155.40	2.07	559.99	846.38	0.01					
		0.3071	3.45	1154.34	2.02	547.28	839.07	0.01					
				1155.34	2.05	554.34	843.18	0.01					
10 psi	Water	0.2664	3.88	734.44	1.90	339.23	601.65	0.01	7.83	97.5	4.71	76.29	10.96
		0.2659	3.75	735.18	1.85	328.66	597.93	0.01					
		0.3106	3.84	735.71	1.94	348.82	605.48	0.01					
				735.11	1.90	338.90	601.69	0.01					
15 psi	Water	0.3434	4.40	610.68	1.80	273.43	501.65	0.01	9.64	98.0	5.88	62.95	11.32
		0.3412	4.56	610.70	1.86	282.91	505.81	0.01					
		0.3369	4.71	610.70	1.86	282.91	505.81	0.01					
				610.69	1.84	279.75	504.42	0.01					
20 psi	Water	0.4094	4.78	547.45	1.68	172.82	440.19	0.01	11.06	95.0	7.06	58.02	11.32
		0.3852	4.96	548.65	1.68	173.10	441.24	0.01					
		0.4486	4.72	549.63	1.68	172.86	441.74	0.01					
				548.58	1.68	172.93	441.06	0.01					
25 psi	Water	0.5305	5.12	423.54	1.75	147.72	344.66	0.01	12.48	91.0	7.65	44.80	11.14
		0.5232	5.21	425.78	1.68	142.90	343.51	0.01					
		0.5312	5.17	425.78	1.68	142.54	343.30	0.01					
				425.03	1.70	144.39	343.82	0.01					

All Dimensions in microns

Fluid Temperature = 18.0 C | Wet Bulb Temperature = 17 C | Atmospheric Pressure = 749.8 mm Hg | Swirlchamber Diameter = 43.89 mm

Absolute Viscosity = 1.053 cP | Dry Bulb Temperature = 20 C | Air Density = 1.205 kg / Cu. m | Inlet Diameter = 6.0 mm

Density = 997.21 kg / Cu. m | Relative Humidity = 74% | Fluid Surface Tension = 73.05 Dynes / cm | Outlet Diameter = 12.0 mm

Pressure	D(v,0.9)	D(v,0.8)	D(v,0.7)	D(v,0.6)	D(v,0.5)	D(v,0.4)	D(v,0.3)	D(v,0.2)	D(v,0.1)	% >965.3	% >344.0	% <105.5	% <37.5
5 psi	1222.08	1104.29	1010.74	926.80	844.09	748.01	612.91	501.29	342.50	35.3	89.9	0.9	0.1
	1222.94	1105.50	1012.25	928.62	846.38	751.50	616.28	504.45	345.69	35.5	90.1	0.9	0.1
	1220.21	1101.64	1007.42	922.78	839.07	740.24	605.97	494.83	336.35	34.9	89.5	1.0	0.1
	1221.74	1103.81	1010.14	926.07	843.18	746.58	611.72	500.19	341.51	35.2	89.8	0.9	0.1
10 psi	1069.16	907.53	788.51	689.76	601.65	516.71	420.01	326.91	222.13	16.0	78.0	2.5	0.4
	1069.33	907.20	787.40	687.56	597.93	511.07	412.13	320.35	214.75	16.0	77.3	2.8	0.4
	1070.10	909.07	790.65	692.64	605.48	521.77	427.06	332.26	228.10	16.1	78.7	2.3	0.3
	1069.53	907.93	788.85	689.99	601.69	516.52	419.73	326.51	221.66	16.0	78.0	2.5	0.4
15 psi	962.93	789.38	672.96	582.40	501.65	417.08	340.11	265.35	174.37	9.9	69.5	4.2	0.6
	956.84	785.43	671.81	583.99	505.81	423.70	346.46	273.09	181.80	9.6	70.3	3.7	0.5
	956.84	785.43	671.81	583.99	505.81	423.70	346.46	273.09	181.80	9.6	70.3	3.7	0.5
	958.77	786.75	671.53	583.46	504.42	421.49	344.34	270.51	179.32	9.7	70.0	3.9	0.5
20 psi	895.68	722.21	610.80	522.38	440.19	362.98	295.80	223.68	143.27	7.3	62.8	6.1	1.1
	897.39	723.70	612.04	523.48	441.24	363.73	296.40	224.17	143.58	7.4	62.9	6.1	1.1
	899.52	725.34	613.16	524.23	441.74	363.93	296.39	223.99	143.29	7.5	62.9	6.1	1.1
	897.53	723.75	612.00	523.36	441.06	363.55	296.20	223.95	143.38	7.4	62.9	6.1	1.1
25 psi	668.37	540.38	466.72	404.16	344.66	288.41	234.99	179.89	117.25	4.6	50.1	8.4	1.4
	701.58	548.13	470.56	405.44	343.51	285.30	230.57	174.52	111.78	5.0	49.9	9.1	1.6
	704.08	548.50	470.68	405.39	343.30	284.98	230.19	174.09	111.37	5.1	49.9	9.2	1.7
	691.34	545.67	469.32	405.00	343.82	286.23	231.92	176.17	113.47	4.9	50.0	8.9	1.6

Table A2.6: *Drop-Size Distribution Results using the Perspex Nozzle P6*

Pressure	Fluid	Obscuration	Log. Difference	X Parameter	N Parameter	D(3,2)	D(v,0.5)	Specific Surface Area (Sq.m/cc)	Volumetric Flowrate (l/min)	Cone Angle (Degrees)	Liquid Sheet Velocity (m/s)	Liquid Sheet Length (mm)	Air Core Diameter (mm)
5 psi	Water	0.1073	4.74	856.21	2.80	598.73	767.22	0.01	3.00	98.5	2.35	108.76	7.50
		0.1164	4.82	854.90	2.66	576.27	755.67	0.01					
		0.1322	4.86	855.90	2.53	559.28	746.48	0.01					
				855.67	2.66	578.09	756.46	0.01					
10 psi	Water	0.1541	5.46	687.55	1.68	279.45	548.50	0.01	4.11	90.0	5.29	67.32	7.68
		0.1573	5.46	687.40	1.68	280.07	548.76	0.01					
		0.1573	5.47	687.40	1.68	280.07	548.76	0.01					
				687.45	1.68	279.86	548.67	0.01					
15 psi	Water	0.2286	5.69	485.32	1.94	239.00	399.24	0.01	4.73	95.0	5.88	59.65	7.68
		0.2138	5.70	485.32	1.94	239.00	399.24	0.01					
		0.2355	5.71	485.32	1.94	239.00	399.24	0.01					
				485.32	1.94	239.00	399.24	0.01					
20 psi	Water	0.2436	5.79	350.24	2.04	184.39	292.66	0.01	5.30	93.5	7.06	48.60	7.68
		0.2535	5.77	352.95	2.00	182.86	293.85	0.01					
		0.2554	5.52	349.53	2.08	186.81	293.10	0.01					
				350.91	2.04	184.69	293.20	0.01					
25 psi	Water	0.3255	5.44	303.27	2.00	126.39	253.34	0.01	5.90	101.0	8.24	48.42	7.50
		0.2986	5.17	300.16	2.00	125.35	250.68	0.01					
		0.2931	4.92	301.72	1.97	124.39	251.26	0.01					
				301.72	1.99	125.38	251.76	0.01					

All Dimensions in microns

Fluid Temperature = 18.1 C
Absolute Viscosity = 1.053 cP
Density = 997.21 kg / Cu. m

Wet Bulb Temperature = 17 C
Dry Bulb Temperature = 20 C
Relative Humidity = 74%

Atmospheric Pressure = 749.8 mm Hg
Air Density = 1.205 kg / Cu. m
Fluid Surface Tension = 73.05 Dynes / cm

Swirlchamber Diameter = 43.59 mm
Inlet Diameter = 4.0 mm
Outlet Diameter = 8.0 mm

Pressure	D(v,0.9)	D(v,0.8)	D(v,0.7)	D(v,0.6)	D(v,0.5)	D(v,0.4)	D(v,0.3)	D(v,0.2)	D(v,0.1)	% > 965.3	% > 344.0	% < 105.5	% < 37.5
5 psi	1186.16	1055.44	952.28	859.73	767.22	662.86	579.54	501.64	372.05	28.7	91.9	0.3	0.0
	1181.83	1049.40	944.78	850.65	755.67	651.20	568.83	488.76	356.08	27.9	90.9	0.4	0.0
	1178.72	1045.00	939.23	843.77	746.48	641.83	559.34	476.18	342.43	27.4	89.9	0.5	0.0
	1182.24	1049.95	945.43	851.38	756.46	651.69	569.24	488.86	356.85	28.0	90.9	0.4	0.0
10 psi	1038.70	868.41	743.90	640.92	548.50	456.61	361.84	278.00	177.52	13.8	72.1	4.3	0.7
	1038.56	868.31	743.89	641.03	548.76	457.06	362.28	278.51	178.00	13.8	72.2	4.3	0.7
	1038.56	868.31	743.89	641.03	548.76	457.06	362.28	278.51	178.00	13.8	72.2	4.3	0.7
	1038.61	868.34	743.89	640.99	548.67	456.91	362.13	278.34	177.84	13.8	72.2	4.3	0.7
15 psi	832.74	602.78	527.82	465.48	399.24	340.98	285.52	223.76	151.99	6.7	59.5	5.1	0.7
	832.74	602.78	527.82	465.48	399.24	340.98	285.52	223.76	151.99	6.7	59.5	5.1	0.7
	832.74	602.78	527.82	465.48	399.24	340.98	285.52	223.76	151.99	6.7	59.5	5.1	0.7
	832.74	602.78	527.82	465.48	399.24	340.98	285.52	223.76	151.99	6.7	59.5	5.1	0.7
20 psi	524.37	442.19	383.62	335.52	292.66	251.94	211.33	167.94	116.29	0.9	38.1	8.3	1.0
	531.19	447.52	387.43	337.89	293.85	252.19	210.81	166.74	114.60	1.1	38.7	8.5	1.1
	520.25	439.38	382.05	335.06	293.10	253.06	212.99	170.01	118.56	0.8	38.0	7.9	0.9
	525.27	443.03	384.37	336.16	293.20	252.40	211.71	168.23	116.48	0.9	38.3	8.2	1.0
25 psi	483.81	376.15	329.43	290.95	253.34	216.70	181.15	143.44	98.62	0.4	26.5	11.3	1.5
	477.65	372.37	326.45	288.10	250.68	214.45	179.31	141.96	97.61	0.3	25.8	11.6	1.5
	484.21	375.77	328.41	289.34	251.26	214.41	178.77	141.00	96.37	0.4	26.3	11.8	1.6
	481.89	374.76	328.10	289.46	251.76	215.19	179.74	142.13	97.53	0.4	26.2	11.6	1.5

Table A2.7: *Mathematical Model Results for the Perspex Nozzle P1*

Pressure (psi)	Volumetric Flowrate (l/h)	Sheet Velocity (m/s)	Cone Angle (Degrees)	Air Core Diameter (mm)	Break-up Length (mm)	Distribution Parameters		Sauter Mean Diameter	Volume Mean Diameter
						X	N		
5	3.57	8.32	95.99	9.30	196.21	163.15	2.13	97.53	137.36
10	5.05	11.76	95.99	9.30	98.10	82.47	2.13	49.30	69.43
15	6.17	14.40	95.99	9.30	65.40	55.22	2.13	33.01	46.69
20	7.13	16.63	95.99	9.30	49.05	41.51	2.13	24.81	34.95
25	7.97	18.59	95.99	9.30	39.24	33.26	2.13	19.88	28.00

Pressure (psi)	D(v,0.9)	D(v,0.8)	D(v,0.7)	D(v,0.6)	D(v,0.5)	D(v,0.4)	D(v,0.3)	D(v,0.2)	D(v,0.1)
5	241.33	203.98	178.00	156.59	137.36	119.03	100.56	80.69	56.73
10	121.98	103.11	89.97	79.15	69.43	60.16	50.83	40.78	28.68
15	81.68	69.04	60.24	53.00	46.69	40.28	34.03	27.31	19.20
20	61.40	51.90	45.29	39.84	34.95	30.28	25.59	20.53	14.43
25	49.20	41.59	36.29	31.92	28.00	24.27	20.50	16.45	11.57

All dimensions in microns unless otherwise stated

Table A2.8: *Mathematical Model Results for the Perspex Nozzle P2*

Pressure (psi)	Volumetric Flowrate (l/h)	Sheet Velocity (m/s)	Cone Angle (Degrees)	Air Core Diameter (mm)	Break-up Length (mm)	Distribution Parameters		Sauter Mean Diameter	Volume Mean Diameter
						X	N		
5	4.61	8.32	95.33	11.25	196.18	162.62	2.13	97.21	136.92
10	6.52	11.76	95.33	11.25	98.09	82.20	2.13	49.14	69.21
15	7.98	14.40	95.33	11.25	65.39	55.04	2.13	32.90	60.05
20	9.22	16.63	95.33	11.25	49.04	41.38	2.13	24.73	34.84
25	10.31	18.59	95.33	11.25	39.24	33.15	2.13	19.82	27.91

Pressure (psi)	D(v,0.9)	D(v,0.8)	D(v,0.7)	D(v,0.6)	D(v,0.5)	D(v,0.4)	D(v,0.3)	D(v,0.2)	D(v,0.1)
5	240.55	203.33	177.43	156.08	136.92	118.64	100.23	80.43	56.55
10	121.59	102.77	89.68	78.89	69.21	59.97	50.66	40.65	28.58
15	81.41	68.81	60.05	52.82	60.05	52.82	33.92	27.22	19.14
20	61.20	51.73	45.14	39.71	34.84	30.19	25.50	20.46	14.39
25	49.04	41.45	36.17	31.82	27.91	24.19	20.43	16.40	11.53

All dimensions in microns unless otherwise stated

Table A2.9: *Mathematical Model Results for the Perspex Nozzle P3*

Pressure (psi)	Volumetric Flowrate (l/h)	Sheet Velocity (m/s)	Cone Angle (Degrees)	Air Core Diameter (mm)	Break-up Length (mm)	Distribution Parameters		Sauter Mean Diameter	Volume Mean Diameter
						X	N		
5	4.08	8.32	101.69	6.89	196.70	170.32	2.13	101.82	143.40
10	5.77	11.76	101.69	6.89	98.35	86.12	2.13	51.48	72.51
15	7.07	68.57	101.69	6.89	68.57	57.67	2.13	34.47	48.56
20	8.16	16.63	101.69	6.89	49.17	43.36	2.13	25.92	36.51
25	9.13	18.59	101.69	6.89	39.34	34.74	2.13	20.77	29.25

Pressure (psi)	D(v,0.9)	D(v,0.8)	D(v,0.7)	D(v,0.6)	D(v,0.5)	D(v,0.4)	D(v,0.3)	D(v,0.2)	D(v,0.1)
5	251.94	212.96	185.83	163.48	143.4	124.26	104.98	84.24	59.23
10	127.39	107.68	93.96	82.66	72.51	62.83	53.08	42.59	29.95
15	85.31	72.11	62.92	55.35	48.56	42.07	35.55	28.52	20.05
20	64.14	54.21	47.31	41.62	36.51	31.63	26.73	21.44	15.08
25	51.39	43.44	37.91	33.35	29.25	25.35	21.41	17.18	12.08

All dimensions in microns unless otherwise stated

Table A2.10: *Mathematical Model Results for the Perspex Nozzle P4*

Pressure (psi)	Volumetric Flowrate (l/h)	Sheet Velocity (m/s)	Cone Angle (Degrees)	Air Core Diameter (mm)	Break-up Length (mm)	Distribution Parameters		Sauter Mean Diameter	Volume Mean Diameter
						X	N		
5	5.69	8.32	100.19	8.79	196.53	167.96	2.13	100.40	141.41
10	8.05	11.76	100.19	8.79	98.26	84.91	2.13	50.76	71.49
15	9.86	14.40	100.19	8.79	65.51	56.86	2.13	33.99	47.87
20	11.39	16.63	100.19	8.79	49.13	42.75	2.13	25.55	35.99
25	12.68	18.59	100.19	8.79	39.31	34.25	2.13	20.48	28.84

Pressure (psi)	D(v,0.9)	D(v,0.8)	D(v,0.7)	D(v,0.6)	D(v,0.5)	D(v,0.4)	D(v,0.3)	D(v,0.2)	D(v,0.1)
5	248.44	210	183.25	161.2	141.41	122.53	103.52	83.06	58.4
10	125.6	106.17	92.64	81.5	71.49	61.95	52.34	41.99	29.53
15	84.11	71.09	62.04	54.57	47.87	41.48	35.05	28.12	19.77
20	63.24	53.45	46.64	41.03	35.99	31.19	26.35	21.14	14.87
25	50.67	42.83	37.37	32.88	28.84	24.99	21.11	16.94	11.91

All dimensions in microns unless otherwise stated

Table A2.11: *Mathematical Model Results for the Perspex Nozzle P5*

Pressure (psi)	Volumetric Flowrate (l/h)	Sheet Velocity (m/s)	Cone Angle (Degrees)	Air Core Diameter (mm)	Break-up Length (mm)	Distribution Parameters		Sauter Mean Diameter	Volume Mean Diameter
						X	N		
5	7.45	8.32	99.11	10.71	196.42	166.46	2.13	99.51	140.15
10	10.54	11.76	99.11	10.71	98.21	84.15	2.13	50.30	70.85
15	12.90	14.40	99.11	10.71	65.47	56.35	2.13	33.68	47.44
20	14.90	16.63	99.11	10.71	49.11	42.36	2.13	25.32	35.67
25	16.66	18.59	99.11	10.71	39.28	33.94	2.13	20.29	28.58

Pressure (psi)	D(v,0.9)	D(v,0.8)	D(v,0.7)	D(v,0.6)	D(v,0.5)	D(v,0.4)	D(v,0.3)	D(v,0.2)	D(v,0.1)
5	246.23	208.13	181.62	159.77	140.15	121.44	102.6	82.32	57.88
10	124.48	105.22	91.81	80.77	70.85	61.39	51.87	41.62	29.26
15	83.35	70.45	61.48	54.08	47.44	41.11	34.73	27.87	19.59
20	62.67	52.97	46.22	40.66	35.67	30.91	26.11	20.95	14.73
25	50.21	42.44	37.04	32.58	28.58	24.76	20.92	16.79	11.80

All dimensions in microns unless otherwise stated

Table A2.12: *Mathematical Model Results for the Perspex Nozzle P6*

Pressure (psi)	Volumetric Flowrate (l/h)	Sheet Velocity (m/s)	Cone Angle (Degrees)	Air Core Diameter (mm)	Break-up Length (mm)	Distribution Parameters		Sauter Mean Diameter	Volume Mean Diameter
						X	N		
5	2.59	8.32	96.91	7.35	196.26	163.97	2.13	98.02	138.05
10	3.67	11.76	96.91	7.35	98.13	82.88	2.13	49.55	69.78
15	4.49	14.40	96.91	7.35	65.42	55.50	2.13	33.17	46.73
20	5.19	16.63	96.91	7.35	49.06	41.72	2.13	24.94	35:13
25	5.80	18.59	96.91	7.35	39.25	33.43	2.13	19.98	28.15

Pressure (psi)	D(v,0.9)	D(v,0.8)	D(v,0.7)	D(v,0.6)	D(v,0.5)	D(v,0.4)	D(v,0.3)	D(v,0.2)	D(v,0.1)
5	242.55	205.01	178.9	157.38	138.05	119.63	101.06	81.09	57.02
10	122.6	103.63	90.43	79.55	69.78	60.47	51.09	40.99	28.82
15	82.09	69.39	60.55	53.27	46.73	40.49	34.21	27.45	19.3
20	61.72	52.17	45.52	40.05	35.13	30.44	25.72	20.63	14.51
25	49.45	41.80	36.47	32.09	28.15	24.39	20.60	16.53	11.62

All dimensions in microns unless otherwise stated

Appendix 3

Computer Programs:

a) **Nozzle.for**

b) **Rrparco.for**

a) NOZZLE.FOR

```
C ***************************************************************
C ***                                                         ***
C *** This program  models the  Particle Size Distribution  ***
C *** from a centrifugal  pressure type, hollow cone spray  ***
C *** nozzle. Experimental  data  for  use in the  program  ***
C *** was obtained  using a  Malvern  Instruments'  Series  ***
C *** 3600 Particle Size Analyser.  It is assumed that the  ***
C *** fluid used is Inviscid (1.0 cP) and Newtonian.         ***
C ***                                                         ***
C ***          Atomisation of Detergent Slurries            ***
C ***                                                         ***
C ***                                                         ***
C ***          Author:    Colin Sudlow                      ***
C ***                                                         ***
C ***          Date:      1987 - 1991                       ***
C ***                                                         ***
C ***************************************************************
C18
C ***************************************************************
C **                                                           **
C **                 DEFINITION OF VARIABLES                   **
C **                                                           **
C ** AIN - Cross sectional Area of the Inlet Port    (Sq M)    **
C ** ADN - Density of the Ambient Air              (Kg/Cu M)   **
C ** ANG - Semi-cone angle of the spray            (Degrees)   **
C ** ACR - Air-Core radius                             (M)     **
C ** BLN - Break-up Length of the Liquid Sheet         (M)     **
C ** CAG - Cone angle of the spray                 (Degrees)   **
C ** CON - Sheet Thickness Parameter              (Constant)   **
C ** DEN - Density of the fluid                    (Kg/Cu M)   **
C ** DIN - Diameter of the inlet port                 (M)     **
C ** DMA - Maximum Droplet Size                  (M - micron)  **
C ** DMI - Minimum Droplet Size                  (M - micron)  **
C ** DV  - Droplet Mean Diameter                 (M - micron)  **
C ** DVM - Volume Mean Diameter                  (M - micron)  **
C ** DVS - Sauter Mean Diameter                  (M - micron)  **
C ** EXT - Diameter of the nozzle outlet              (M)     **
C ** FER - Dimensionless Amplitude Ratio                      **
C ** PIN - Pressure Drop across the nozzle        (Kg/Sq M)   **
C ** QVF - Volumetric Flowrate                     (Cu M/S)    **
C ** REN - Reynolds Number                                    **
C ** REO - Radius of the outlet orifice               (M)     **
C ** RIN - Mean inlet radius of spinning fluid         (M)     **
C ** RN  - Rosin-Rammler parameter                             **
C ** RX  - Rosin-Rammler diameter                              **
C ** SFT - Surface Tension of the fluid           (Kg/Sq S)   **
C ** SWC - Diameter of swirlchamber                    (M)     **
C ** TBP - Thickness of liquid sheet at break-up       (M)     **
C ** TFF - Thickness of liquid sheet at outlet orifice (M)     **
C ** TPF - Temperature of the liquid feed              (K)     **
C ** UME - Mean exit spinning speed                  (M/S)     **
C ** VAE - Velocity at nozzle exit                   (M/S)     **
C ** VIN - Mean inlet velocity                       (M/S)     **
C ** VME - Mean exit velocity                        (M/S)     **
C ** VMF - Volume Mass Fraction of spray                      **
C ** VSC - Viscosity of the fluid                  (Kg/M S)    **
C ** WEB - Weber Number                                       **
C **                                                           **
C ***************************************************************
```

```
C58
C
C     ***************************************************
C     ***                                             ***
C     ***                   NOTICE                    ***
C     ***                                             ***
C     ***  In the  subroutine 'ROSRAM' is the special  ***
C     ***  function S14AAF. This is included in order  ***
C     ***  to calculate the Gamma  Function of one of  ***
C     ***  the variables in that subroutine.          ***
C     ***      This function will not work unless the  ***
C     ***  program is linked to the Nag library using  ***
C     ***  the following command (on the Vax Cluster)  ***
C     ***          LINK NOZZLE,NAG14/LIB              ***
C     ***                                             ***
C     ***************************************************
C
C C    INITIALISE CONSTANTS AND VARIABLES
C76
      IMPLICIT REAL*8(a-h,p-z)
      DIMENSION dv(10)
      CHARACTER fle*6 , oid*6 , odm*7
      COMMON /a     / i , itt , pi , tol
      l = 0
C
C C     ****    Enter the data for the program     ****
C
      CALL dtntry(adn,den,din,fle,oid,pin,reo,sft,swc,tpf,vsc)
C
C C    CREATE INPUT DATA FILE (UNIT=10, FILENAME=FLE)
C
      OPEN (10,FILE=fle,STATUS='UNKNOWN',FORM='FORMATTED')
      WRITE (*,99002)
      WRITE (*,99003) fle
      WRITE (*,99002)
C
C C     ****    Transfer to calculation section    ****
C99
      CALL atomize(den,din,pin,reo,swc,ang,qvf,ume,vae,tff,l)
      IF ( l.EQ.1 ) THEN
         odm = 'Atomize'
         CALL fail(odm)
         CLOSE (10)
         STOP
      ENDIF
C
      CALL sheet(adn,ang,den,sft,tff,ume,vae,vsc,bln,dma,dmi,
     & dvm,dvs,l)
      IF ( l.EQ.1 ) THEN
         odm = ' Sheet '
         CALL fail(odm)
         CLOSE (10)
         STOP
      ENDIF
C117
      CALL droplet(dvm,dvs,dv,rn,rx,l)
      IF ( l.EQ.1 ) THEN
         CALL fail(odm)
         odm = 'Droplet'
         CLOSE (10)
```

```
         STOP
       ENDIF
C
       CALL rsltfle(adn,ang,bln,den,din,dma,dmi,dv,dvm,dvs,
      & fle,oid,pin,qvf,reo,rn,rx,sft,swc,tff,tpf,vae,vsc)
       WRITE (*,99002)
       WRITE (*,99001)
       WRITE (*,99002)
       STOP
99001 FORMAT (20X,4('-'),2(' '),'END OF PROGRAM',2(' '),
     & 4('-'))
99002 FORMAT (1X,' ')
99003 FORMAT (22X,'Opened Data File: ',A6)
       END
C
C C     BLOCK DATA
C3
       BLOCKDATA
       IMPLICIT REAL*8(a-h,p-z)
       COMMON /a      / i , itt , pi , tol
       DATA i , itt , pi , tol/2 , 50 , 3.1416 , 1.0D-12/
       END
C
C C          ****    SUBROUTINE ATOMIZE    ****
C
C C     To determine the Nozzle's operating conditions
C5
       SUBROUTINE atomize(den,din,pin,reo,swc,ang,qvf,ume,
      & vae,tff,l)
       IMPLICIT REAL*8(a-h,p-z)
       DIMENSION b(10) , p(10)
       COMMON /a      / i , itt , pi , tol
       b(1) = reo - (0.1*reo)
       b(2) = reo - (0.2*reo)
       rin = (swc-din)/2.0D0
C
C  C  To determine the value of the initial film thickness
C16
       zn = 4.0D0*rin/(din**2.0D0)
       DO 100 n = 1 , i
          p(n) = (zn/b(n))*sqrt((reo-b(n))/b(n))
      &    *((reo**2.0D0)-(b(n)**2.0D0)) - 1.0D0
 100   CONTINUE
       DO 200 no = i , itt
          pf = b(2) - p(2)*(b(2)-b(1))/(p(2)-p(1))
          err = abs(pf-b(2))
          IF ( err.LT.tol ) THEN
             acr = b(2)
             tff = reo - b(2)
             a1 = ((reo**2.0D0)-(acr**2.0D0))
             a2 = (acr**2.0D0)/((reo**2.0D0)-(acr**2.0D0))
C
C  C  Determine the values of the Nozzle outlet parameters
C32
             vae = sqrt(2.0D0*pin/den)
             um = sqrt(((2.0D0*pin)/den)*a2)
             qvf = pi*a1*um*sqrt((reo-acr)/reo)
             vme = qvf/(pi*a1)
             ume = sqrt((vae**2.0D0)-(vme**2.0D0))
             ang = (180.0D0/pi)*atan(ume/vme)
```

```
            RETURN
         ENDIF
         b(1) = b(2)
         b(2) = pf
         p(1) = p(2)
         p(2) = (zn/pf)*sqrt((reo-pf)/pf)*((reo**2.0D0) -
     &   (pf**2.0D0)) - 1.0D0
 200  CONTINUE
      l = 1
      RETURN
      END
C
C C            ****    SUBROUTINE SHEET    ****
C
C  C    To determine the dimensions of the liquid sheet
C5
      SUBROUTINE sheet(adn,ang,den,sft,tff,ume,vae,vsc,bln,
     & dma,dmi,dvm,dvs,l)
      IMPLICIT REAL*8(a-h,p-z)
      DIMENSION d(10) , p(10) , z(10)
      COMMON /a     / i , itt , pi , tol
      ant = (pi/180.0D0)*ang
      ren = den*vae*tff/vsc
      IF ( ren.GE.9000.0 ) THEN
         fer = 12.0D0
      ELSEIF ( ren.LT.9000.0 ) THEN
         fer = 50.0D0
      ENDIF
C
C  C    To determine the Sheet Thickness at Break-up
C20
      zn = (3.0D0/2.0D0)*((sft*fer)/(adn*vae))
      bl1 = zn/(ume*cos(ant))
      con = (sft*bl1)/(den*((ume*cos(ant))**2.0D0))
      tb1 = con/bl1
      web = (den*(vae**2.0D0)*tb1)/sft
      wb2 = sqrt(web)*((web+1.0D0)/((web-1.0D0)**2.0D0))
      bln = sqrt(1.50D0*(den/adn)*con*fer*wb2)
      tbp = con/bln
C
C  C     To determine the ligament diameter
C
      d(1) = tbp
      d(2) = 1.50D0*tbp
      DO 100 n = 1 , i
         z(n) = 1.0D0 + ((3.0D0*vsc)/sqrt(den*sft*d(n)))
         p(n) = d(n) - sqrt(32.0D0*(tbp**2.0D0)/z(n))
 100  CONTINUE
C34
      DO 200 no = i , itt
         pf = d(2) - p(2)*(d(2)-d(1))/(p(2)-p(1))
         err = abs(pf-d(2))
         IF ( err.LT.tol ) THEN
            dlg = d(2)
            dma = dlg*((3.0D0*pi)/(4.0D0*tbp))**(1.0D0/3.0D0)
            zn = (1.0D0/2.0D0) + ((3.0D0*vsc)/(2.0D0*
     &      sqrt(den*sft*tbp)))
            dmi = tbp*((3.0D0*pi)/sqrt(zn))**(1.0D0/3.0D0)
            dvm = 0.40D0*(dma-dmi) + dmi
            dvs = 0.710D0*dvm
```

```
            RETURN
         ENDIF
         d(1) = d(2)
         d(2) = pf
         p(1) = p(2)
         z(2) = 1.0D0 + ((3.0D0*vsc)/sqrt(den*sft*pf))
         p(2) = pf - sqrt(32.0D0*(tbp**2.0D0)/z(2))
 200  CONTINUE
      l = 1
      RETURN
      END
C
C C        ****    SUBROUTINE DROPLET   . ****
C
C C     To determine the Rosin-Rammler parameters
C5
      SUBROUTINE droplet(dvm,dvs,dv,rn,rx,l)
      IMPLICIT REAL*8(a-h,p-z)
      DIMENSION gf(10) , p(10) , xt(10)
      DIMENSION dv(10) , vf(10) , rr(10)
      COMMON /a     / i , itt , pi , tol
      vmf = 0.50D0
      xt(1) = 0.3
      xt(2) = 0.6
      zn = log(log(1.0D0/(1.0D0-vmf)))
      DO 100 n = 1 , i
         ifail = 1
         gf(n) = s14aaf(xt(n),ifail)
          p(n) = zn - (1.0D0/(1.0D0-xt(n)))*
     &    log(dvm/(dvs*gf(n)))
 100  CONTINUE
C20
      DO 200 no = i , itt
         ifail = 1
         pf = xt(2) - p(2)*(xt(2)-xt(1))/(p(2)-p(1))
         err = abs(pf-xt(2))
         IF ( err.LT.tol ) THEN
            rn = 1.0D0/(1.0D0-xt(2))
            x1 = (log(1.0D0/(1.0D0-vmf)))**(1.0D0/rn)
            rx = dvm/x1
C
C   C     To determine the Drop-size Distribution
C31
            DO 120 k = 1 , 9
               vf(k) = k/10.0D0
               rr(k) = (log(1.0D0/(1.0D0-vf(k))))**(1.0D0/rn)
               dv(k) = rx*rr(k)
 120        CONTINUE
            RETURN
         ENDIF
         ifail = 1
         xt(1) = xt(2)
         xt(2) = pf
         p(1) = p(2)
         gf(2) = s14aaf(pf,ifail)
         p(2) = zn - (1.0D0/(1.0D0-pf))*log(dvm/(dvs*gf(2)))
 200  CONTINUE
      l = 1
      RETURN
      END
```

```
C
C C     **      SUBROUTINE DTNTRY     **
C
C C      To enter the data for the program
C5
      SUBROUTINE dtntry(adn,den,din,fle,oid,pin,reo,sft,swc,
     & tpf,vsc)
      IMPLICIT REAL*8(a-h,p-z)
      COMMON /a     / i , itt , pi , tol
      CHARACTER fle*6 , oid*6
C
C C            ************************************
C
C C     INPUT INITIAL DATA FOR THE NOZZLE AND SLURRY
C43
      WRITE (*,99001)
      WRITE (*,99002)
      WRITE (*,99005)
      WRITE (*,99003)
      WRITE (*,99005)
      WRITE (*,99004)
      WRITE (*,99005)
      WRITE (*,99006)
      WRITE (*,99007)
      READ (*,99008) oid
      WRITE (*,99005)
      WRITE (*,99009)
      WRITE (*,99010)
      WRITE (*,99005)
 100  WRITE (*,99011)
      READ * , ext
      IF ( ext.LE.0.0 ) GOTO 100
      reo = ext/2000.0D0
 200  WRITE (*,99012)
      READ * , swc
      IF ( swc.LE.0.0 ) GOTO 200
      IF ( ext.GT.swc ) THEN
         WRITE (*,99013)
         GOTO 100
      ENDIF
      swc = swc/1000.0D0
 300  WRITE (*,99014)
      READ * , din
      IF ( din.LE.0.0 ) GOTO 300
      din = din/1000.0D0
      WRITE (*,99005)
C72
      WRITE (*,99015)
      WRITE (*,99016)
 400  WRITE (*,99017)
      READ * , den
      IF ( den.LE.0.0 ) GOTO 400
 500  WRITE (*,99018)
      READ * , sft
      IF ( sft.LE.0.0 ) GOTO 500
      sft = sft*(1.019716D-04*9.806)
 600  WRITE (*,99019)
      READ * , vsc
      IF ( vsc.LE.0.0 ) GOTO 600
```

```
      vsc = 0.10D0*vsc
      WRITE (*,99020)
      WRITE (*,99021)
 700  WRITE (*,99022)
      READ * , pin
      IF ( pin.LE.0.0 ) GOTO 700
      pin = pin*703.069*9.806
 800  WRITE (*,99023)
      READ * , adn
      IF ( adn.LE.0.0 ) GOTO 800
 900  WRITE (*,99024)
      READ * , tpf
      IF ( tpf.LT.0.0 ) GOTO 900
      tpf = tpf + 273.0D0
C92
      WRITE (*,99005)
      WRITE (*,99016)
      WRITE (*,99005)
      WRITE (*,99025)
      WRITE (*,99007)
      READ (*,99026) fle
      RETURN
C
C C  Format Statements for the the data input
C13
99001 FORMAT (16X,'Prediction of the Drop-Size Distribution
     & Result')
99002 FORMAT (16X,47('-'))
99003 FORMAT (32X,'Inviscid Newtonian Fluid')
99004 FORMAT (12X,'(Dimensions in millimetres unless
     & otherwise stated)')
99005 FORMAT (1X,' ')
99006 FORMAT (2X,'Enter the Nozzle name or Identification
     & number')
99007 FORMAT (14X,'(Max. 6 Characters)')
99008 FORMAT (A6)
99009 FORMAT (25X,'Nozzle Specifications:')
99010 FORMAT (25X,22('-'))
99011 FORMAT (2X,'Outlet Orifice Diameter')
99012 FORMAT (2X,'Swirl Chamber Diameter')
99013 FORMAT (6X,'Incorrect Nozzle Geometry')
99014 FORMAT (2X,'Diameter of the Inlet port')
99015 FORMAT (25X,'Slurry Characteristics:')
99016 FORMAT (25X,23('-'))
99017 FORMAT (2X,'Density (Kg/Cu.M)')
99018 FORMAT (2X,'Surface Tension (Dynes/Cm)')
99019 FORMAT (2X,'Viscosity (cP)')
99020 FORMAT (25X,'Operating Conditions:')
99021 FORMAT (25X,21('-'))
99022 FORMAT (2X,'Pumping Pressure (PSI)')
99023 FORMAT (2X,'Density of Ambient Air (Kg/Cu.M)')
99024 FORMAT (2X,'Ambient Air Temperature (C)')
99025 FORMAT (1X,'Please name the output file')
99026 FORMAT (A6)
      END
C
C C     **      SUBROUTINE RSLTFLE     **
C
C C      To enter the data for the program
C5
```

```
      SUBROUTINE rsltfle(adn,ang,bln,den,din,dma,dmi,dv,dvm,
     & dvs,fle,oid,in,qvf,reo,rn,rx,sft,swc,tff,tpf,vae,vsc)
      IMPLICIT REAL*8(a-h,p-z)
      CHARACTER fle*6 , oid*6
      DIMENSION dv(10)
      COMMON /a     / i , itt , pi , tol
C
C C    ****    Convert variables into write format    ****
C59
      acr = (reo-tff)*2000.0D0
      ext = reo*2000.0D0
      bln = bln*1000.0D0
      swc = swc*1000.0D0
      din = din*1000.0D0
      tff = tff*1000.0D0
      sft = sft/(1.019716D-04*9.806)
      pin = pin/(703.069*9.806)
      cag = 2.0D0*ang
      dvm = dvm*1.0D+06
      dvs = dvs*1.0D+06
      dma = dma*1.0D+06
      dmi = dmi*1.0D+06
      rx = rx*1.0D+06
      vsc = vsc*10.0D0
C
C C          Write the Results into output file
C75
      WRITE (*,99001)
      WRITE (10,99001)
      WRITE (10,99002) fle
      WRITE (10,99001)
      WRITE (10,99003)
      WRITE (10,99004)
      WRITE (10,99005)
      WRITE (10,99001)
      WRITE (10,99006)
      WRITE (10,99001)
      WRITE (10,99007) oid
      WRITE (10,99001)
      WRITE (10,99008)
      WRITE (10,99009)
      WRITE (10,99010)
      WRITE (10,99011) ext , din , swc
      WRITE (10,99001)
      WRITE (10,99012)
      WRITE (10,99013)
      WRITE (10,99014)
      WRITE (10,99015) den , vsc , sft
      WRITE (10,99001)
C98
      WRITE (10,99016)
      WRITE (10,99017)
      WRITE (10,99018)
      WRITE (10,99019) pin , qvf
      WRITE (10,99001)
      WRITE (10,99020)
      WRITE (10,99021) tpf , bln , adn
      WRITE (10,99001)
      WRITE (10,99022)
      WRITE (10,99023) acr , vae , cag
```

```
      WRITE (10,99001)
      WRITE (10,99001)
      WRITE (10,99024)
      WRITE (10,99001)
      WRITE (10,99025)
      WRITE (10,99026)
C115
      WRITE (10,99001)
      WRITE (10,99027)
      WRITE (10,99001)
      WRITE (10,99028)
      WRITE (10,99029) dvm , dvs
      WRITE (10,99001)
      WRITE (10,99030)
      WRITE (10,99031) dmi , dma
      WRITE (10,99001)
      WRITE (10,99032)
      WRITE (10,99033)
      WRITE (10,99034) rx , rn
      WRITE (10,99001)
      WRITE (10,99035)
      DO 100 k = 1 , 9
         d = k/10.0D0
         dv(k) = dv(k)*1.0D+06
         WRITE (10,99036) d , dv(k)
 100  CONTINUE
      CLOSE (10)
      RETURN
C
C C  Format Statements for the data file
C13
99001 FORMAT (1X)
99002 FORMAT (1X,'Filename:',1X,A6)
99003 FORMAT (14X,'Prediction of the Drop-Size Distribution
     & Result')
99004 FORMAT (14X,47('-'))
99005 FORMAT (30X,'Inviscid Newtonian Fluid')
99006 FORMAT (10X,'(Dimensions in millimetres unless
     & otherwise stated)')
99007 FORMAT (2X,'Nozzle ID: ',1X,A6)
99008 FORMAT (23X,'Nozzle Specifications:')
99009 FORMAT (23X,22('-'))
99010 FORMAT (2X,'Outlet Orifice',12X,'Inlet Orifice',11X,
     & 'Swirl Chamber Diameter')
99011 FORMAT (5X,F6.2,20X,F6.2,20X,F8.2)
99012 FORMAT (23X,'Slurry Characteristics:')
99013 FORMAT (23X,23('-'))
99014 FORMAT (2X,'Slurry Density (Kg/Cu.M)',4X,'Viscosity
     & (cP)',4X,'Surface Tension (Dynes/Cm)')
99015 FORMAT (9X,F8.3,15X,F6.3,17X,F7.2)
99016 FORMAT (24X,'Operating Conditions:')
99017 FORMAT (24X,21('-'))
99018 FORMAT (2X,'Pumping Pressure (PSI)',22X,'Volumetric
     & Flowrate (Cu.M/S)')
99019 FORMAT (6X,F8.2,39X,E11.5)
99020 FORMAT (2X,'Air Temperature (K)',7X,'Break-up Length',
     & 7X,'Density of Air (Kg/Cu.M)')
9021 FORMAT (7X,F6.1,17X,F9.2,20X,F7.4)
99022 FORMAT (2X,'Air Core Diameter',8X,'Exit Velocity (M/S)',
     & 8X,'Cone Angle (Degrees)')
```

```
99023 FORMAT (6X,F9.4,17X,F7.3,19X,F8.2)
99024 FORMAT (31X,18('*'))
99025 FORMAT (24X,'Drop-Size Distribution Results')
99026 FORMAT (24X,30('-'))
99027 FORMAT (27X,'All Dimensions in Microns')
99028 FORMAT (7X,'Mean Droplet Size',21X,'Sauter Mean
     & Diameter')
99029 FORMAT (11X,F9.2,30X,F9.2)
99030 FORMAT (7X,'Min Droplet Diameter',18X,'Max Droplet
     & Diameter')
99031 FORMAT (11X,F9.2,30X,F9.2)
99032 FORMAT (26X,'Rosin-Rammler Parameters')
99033 FORMAT (31X,'X',11X,'N')
99034 FORMAT (26X,F10.2,5X,F7.2)
99035 FORMAT (20X,'Volume Mean Percentile Diameters')
99036 FORMAT (26X,'D(v,',F3.1,') = ',F10.2)
      END
C
C C    **    SUBROUTINE FAIL    **
C
C C         FAILURE   ROUTINE
C5
      SUBROUTINE fail(odm)
      IMPLICIT REAL*8(a-h,p-z)
      CHARACTER odm*7
      COMMON /a     / i , itt , pi , tol
C13
      WRITE (*,99005)
      WRITE (*,99001)
      WRITE (*,99002)
      WRITE (*,99003) odm
      WRITE (*,99004)
      WRITE (*,99002)
      WRITE (*,99001)
      WRITE (10,99005)
      WRITE (10,99001)
      WRITE (10,99002)
      WRITE (10,99003) odm
      WRITE (10,99004)
      WRITE (10,99002)
      WRITE (10,99001)
      RETURN
99001 FORMAT (6X,59('*'))
99002 FORMAT (6X,8('*'),43(' '),8('*'))
99003 FORMAT (6X,8('*'),1X,'Calculation Failure in Subroutine'
     & ,1X,A7,1X,8('*'))
99004 FORMAT (6X,8('*'),14X,'EXITING PROGRAM',14X,8('*'))
99005 FORMAT (1X,' ')
      END
```

b) RRPARCO.FOR

```
C ***************************************************
C ****                                           ****
C ****  This is a program for computing Felton's ****
C ****  correction factors for the Rosin-Rammler ****
C ****  distribution when measuring dense sprays ****
C ****    The factors are valid between 0.65 and ****
C ****  0.98 obscuration.                        ****
C ****                                           ****
C ****   Colin Sudlow   26th February 1991       ****
C ****                                           ****
C ***************************************************
C
C13
      CHARACTER ans*1 , id*5 , fle*6 , fld*9 , pin*4
      REAL n , ncor , obs
      WRITE (*,99020)
      READ (*,99021) fle
      OPEN (11,FILE=fle,STATUS='UNKNOWN',FORM='FORMATTED')
 100  WRITE (*,99001)
      READ * , inp
      IF ( inp.LT.1 ) THEN
         WRITE (*,99002)
         GOTO 100
      ENDIF
      WRITE (11,99017)
      WRITE (11,99022) fle
      WRITE (11,99017)
      WRITE (11,99003)
C24
      DO 200 i = 1 , inp
         WRITE (*,99004)
         READ (*,99005) id
         WRITE (*,99006)
         READ (*,99007) fld
         WRITE (*,99008)
         READ (*,99009) pin
         WRITE (*,99010)
         READ * , x
         WRITE (*,99011)
         READ * , n
 150     WRITE (*,99012)
         READ * , obs
         IF ( obs.GT.0.9999 .OR. obs.LT.0.50D0 ) GOTO 150
C39
         a = 1.9D0 - 3.437*obs
         cx = 1.0D0 + ((0.036+0.4947*(obs**8.997))*(n**a))
         b = 0.35D0 + 1.45*obs
         cn = 1.0D0 + ((0.035+0.1099*(obs**8.650))*(n**b))
         xcor = cx*x
         ncor = cn*n
         WRITE (11,99013) id , fld , pin , obs , xcor , ncor ,
     &   cx , cn
         IF ( i.LT.inp ) THEN
            WRITE (*,99017)
            WRITE (*,99017)
            WRITE (*,99014)
            READ (*,99015) ans
            IF ( ans.EQ.'y' .OR. ans.EQ.'Y' ) THEN
               CLOSE (11)
```

```
                WRITE (*,99017)
                WRITE (*,99016)
                WRITE (*,99017)
                GOTO 300
              ENDIF
            ENDIF
            WRITE (*,99017)
 200    CONTINUE
        CLOSE (11)
        WRITE (*,99017)
        WRITE (*,99018)
        WRITE (*,99017)
        WRITE (*,99017)
 300    WRITE (*,99019) fle
        WRITE (*,99017)
        STOP
99001 FORMAT (1X,'How many values do you wish to compute ?')
99002 FORMAT (6X,'Incorrect value! Please try again.')
99003 FORMAT (4X,'ID',5X,'Fluid',6X,'P',4X,'Obs'4X,'X Value',
     & 3X,'N Value',3X,'X Factor',3X,'N Factor')
99004 FORMAT (1X,'Enter the Nozzle Identifying Number')
99005 FORMAT (A5)
99006 FORMAT (1X,'Enter details of the test')
99007 FORMAT (A9)
99008 FORMAT (1X,'Enter the operating pressure')
99009 FORMAT (A4)
99010 FORMAT (1X,'Enter the value of the X parameter')
99011 FORMAT (1X,'Enter the value of the N paramter')
99012 FORMAT (1X,'Enter the value of the obscuration')
99013 FORMAT (2X,A5,2X,A9,2X,A4,1X,F6.4,3X,F7.2,3X,F5.2,
     & 6X,F6.4,5X,F6.4)
99014 FORMAT (1X,'Do you want to quit the program ?')
99015 FORMAT (A1)
99016 FORMAT (6X,'****    User Terminated Program    ****')
99017 FORMAT (1X)
99018 FORMAT (6X,'*******      End of Program      *******')
99019 FORMAT (2X,'Results may be found in the data file: ',A6)
99020 FORMAT (1X,'Please name the output file')
99021 FORMAT (A6)
99022 FORMAT (2X,A6)
      END
```

Appendix 4

Typical Photographs of the Air Core in the Perspex Nozzles

Plate 4.1: Perspex Nozzle P1 at 5 psi

Plate 4.2: Perspex Nozzle P1 at 10 psi

Plate 4.3: Perspex Nozzle P1 at 15 psi

Plate 4.4: Perspex Nozzle P1 at 20 psi

Plate 4.5: Perspex Nozzle P1 at 25 psi

Plate 4.1: *Air Core in Perspex Nozzle P1 at 5 psi*

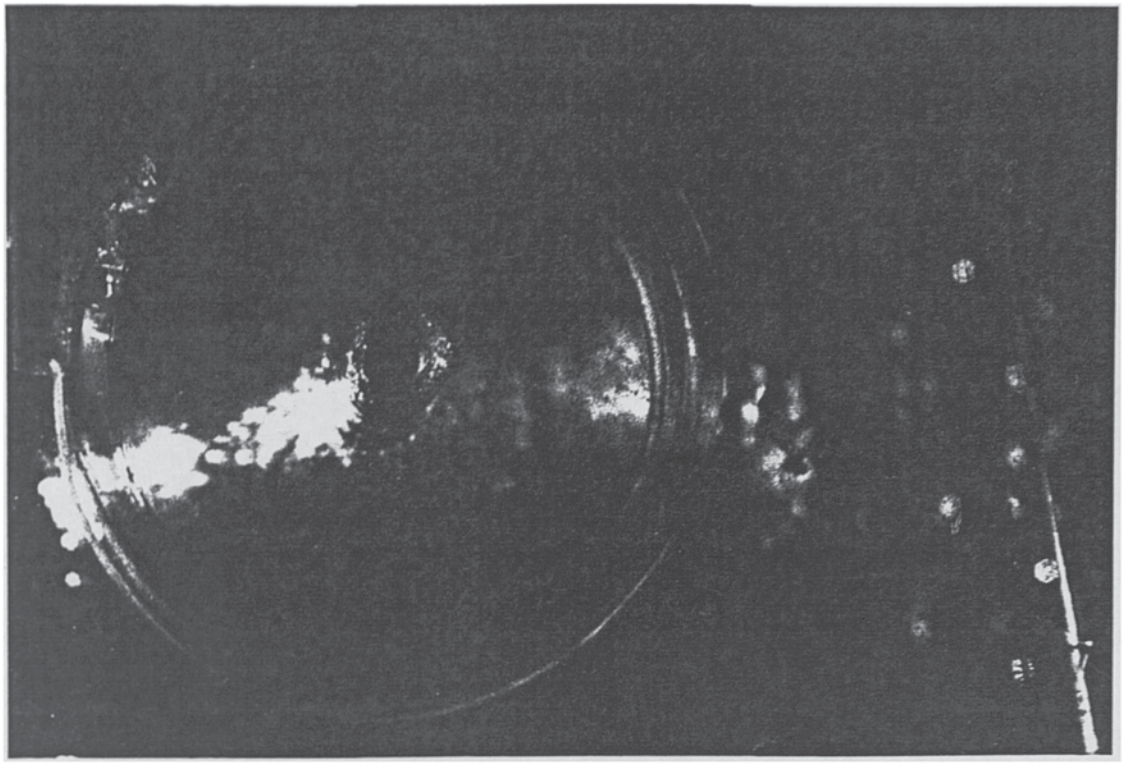

Plate 4.2: *Air Core in Perspex Nozzle P1 at 10 psi*

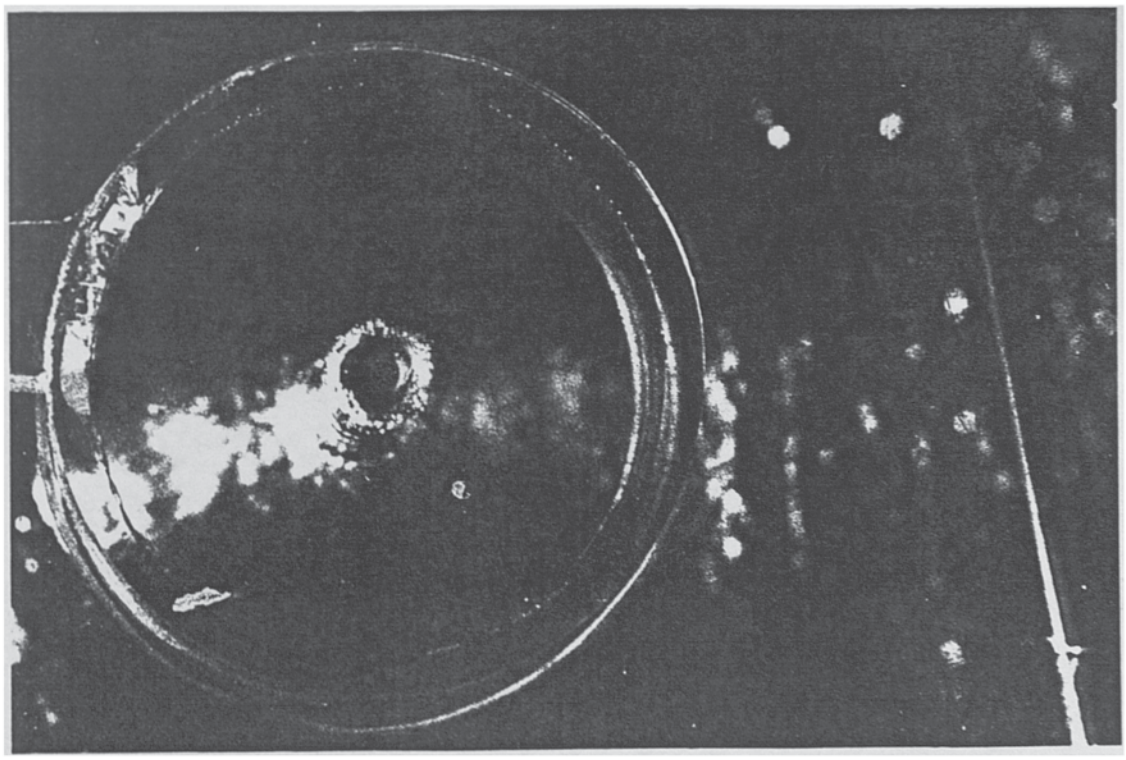

Plate 4.1: *Air Core in Perspex Nozzle P1 at 5 psi*

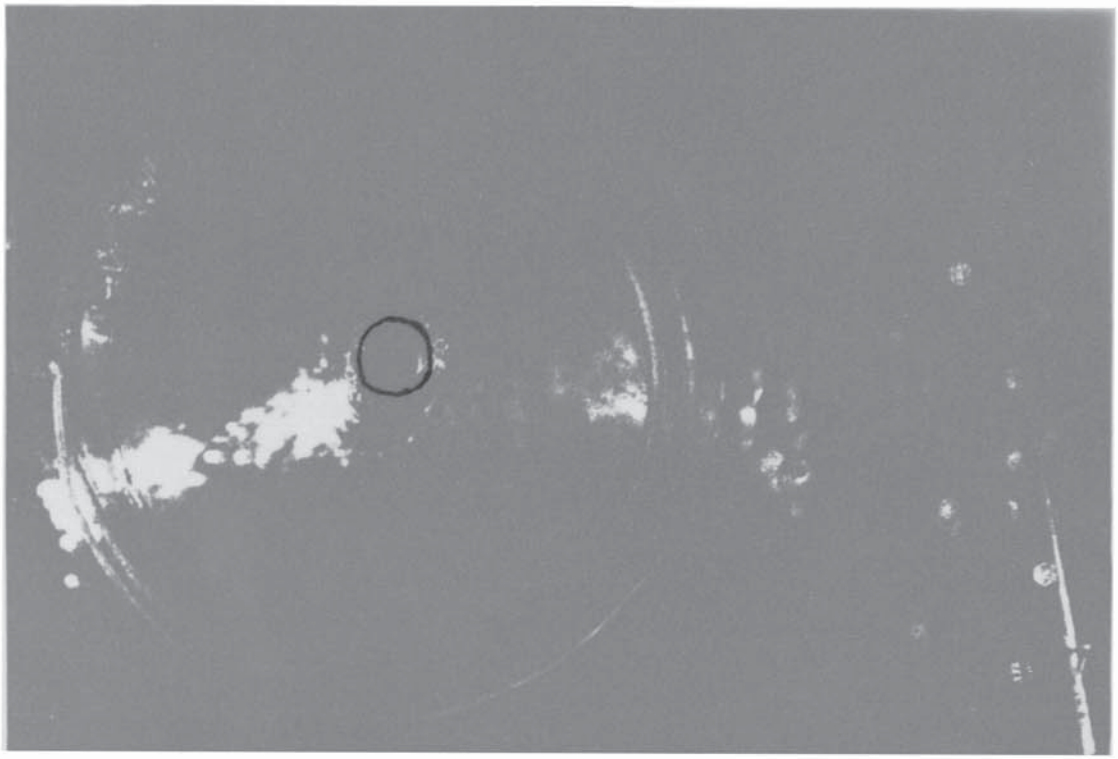

Plate 4.2: *Air Core in Perspex Nozzle P1 at 10 psi*

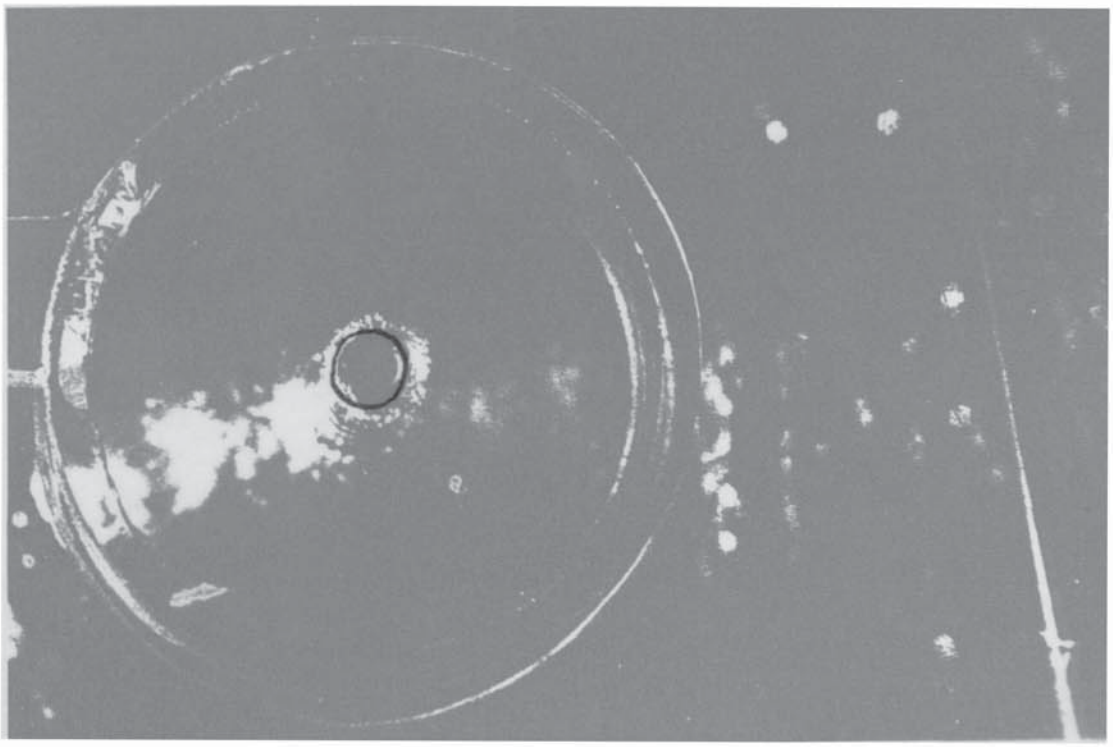

Plate 4.3: *Air Core in Perspex Nozzle P1 at 15 psi*

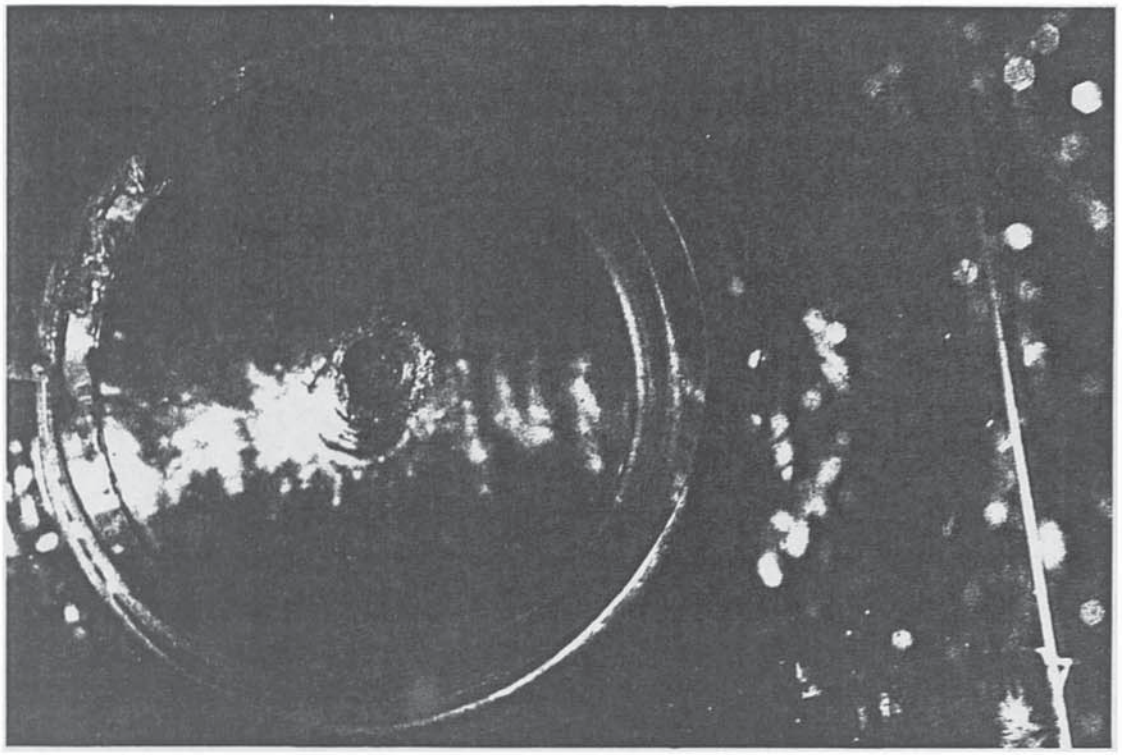

Plate 4.4: *Air Core in Perspex Nozzle P1 at 20 psi*

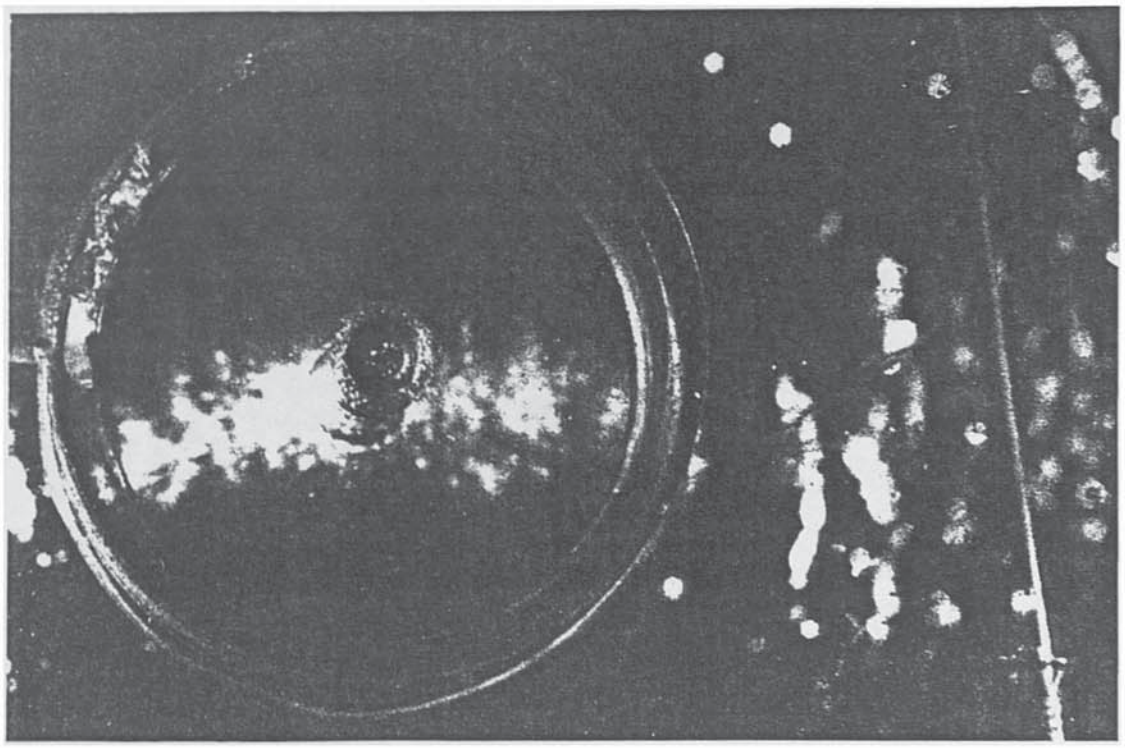

Plate 4.3: *Air Core in Perspex Nozzle P1 at 15 psi*

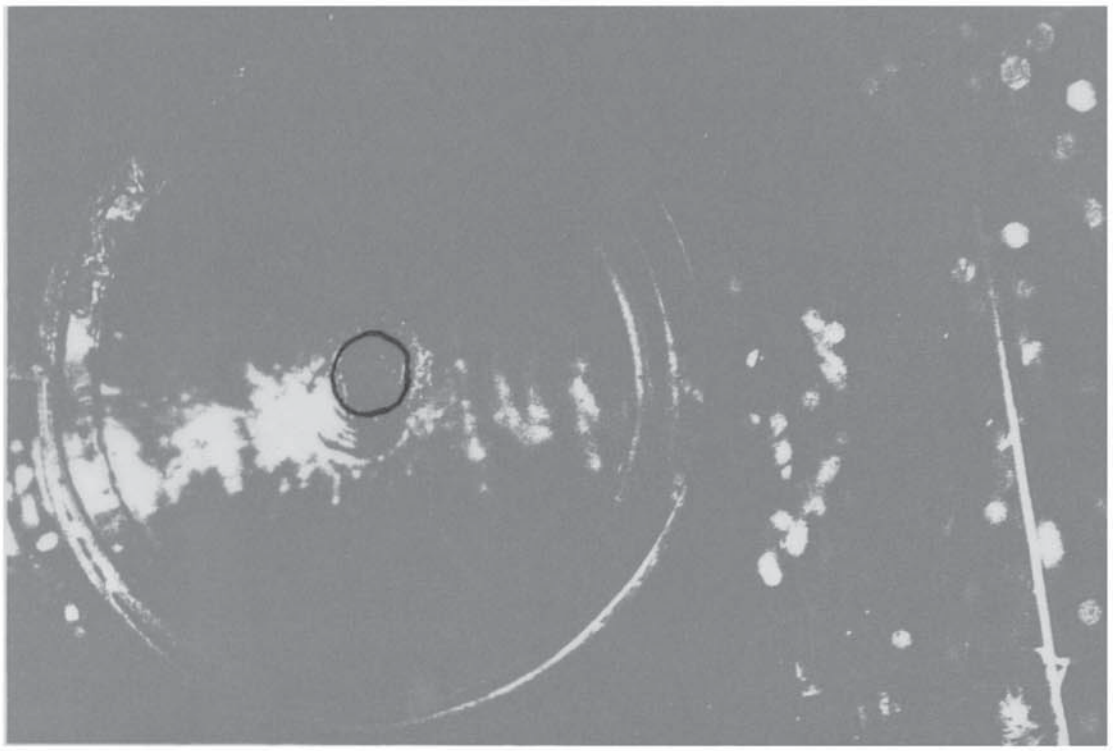

Plate 4.4: *Air Core in Perspex Nozzle P1 at 20 psi*

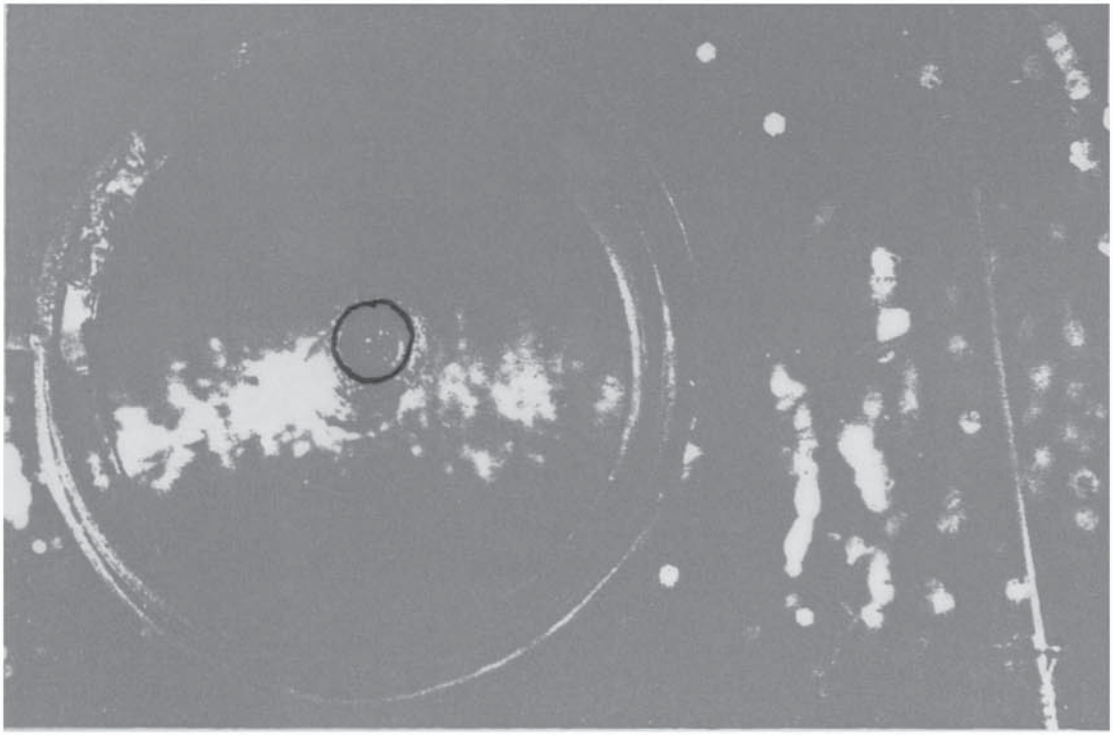

Plate 4.5: *Air Core in Perspex Nozzle P1 at 25 psi*

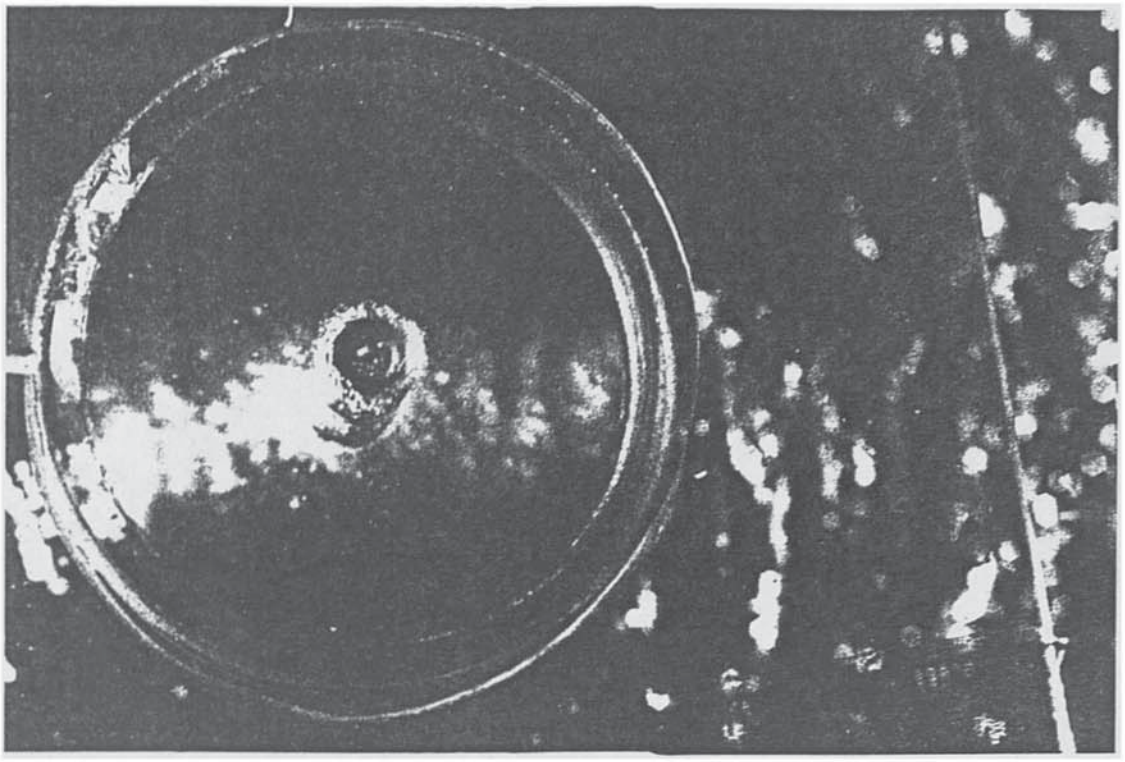

Plate 4.5: *Air Core in Perspex Nozzle P1 at 25 psi*

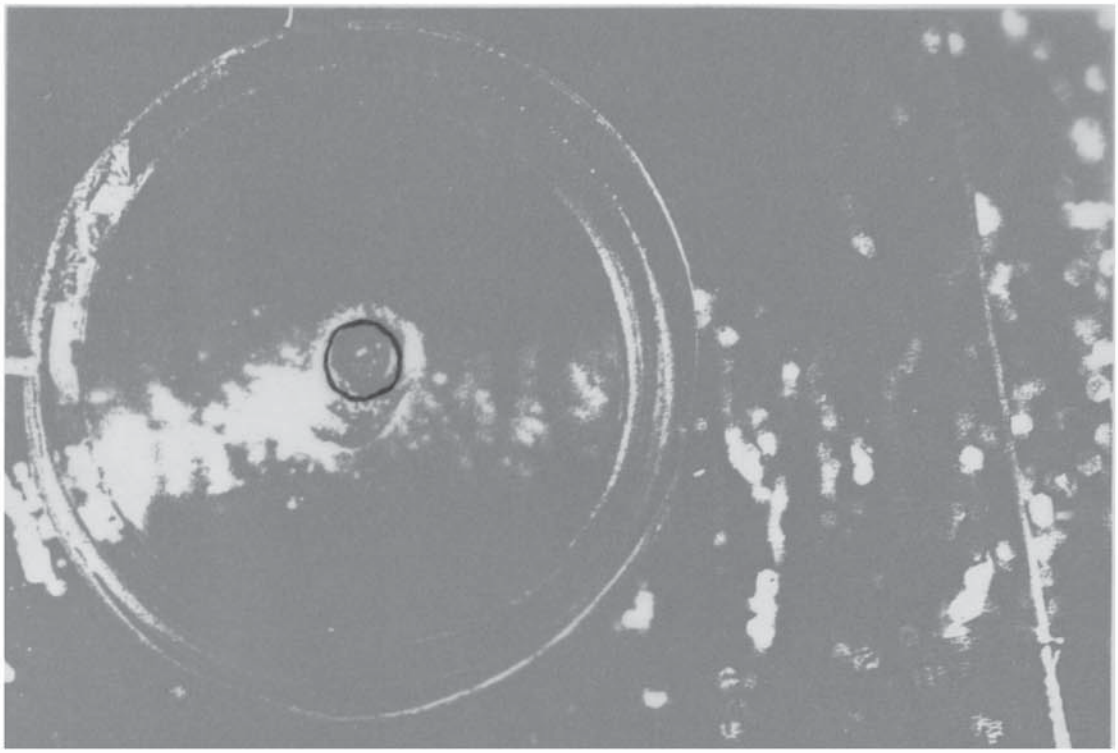

Appendix 5

Typical Photographs of Conical Liquid Sheets

Plate 5.1: Perspex Nozzle P1 at 5 psi

Plate 5.2: Perspex Nozzle P1 at 10 psi

Plate 5.3: Perspex Nozzle P1 at 15 psi

Plate 5.4: Perspex Nozzle P1 at 20 psi

Plate 5.5: Perspex Nozzle P1 at 25 psi

Plate 5.6: Photographic Scale at 0.6 x Full Size

Plate 5.1: *Conical Sheet Produced by Perspex Nozzle P1 at 5 psi*

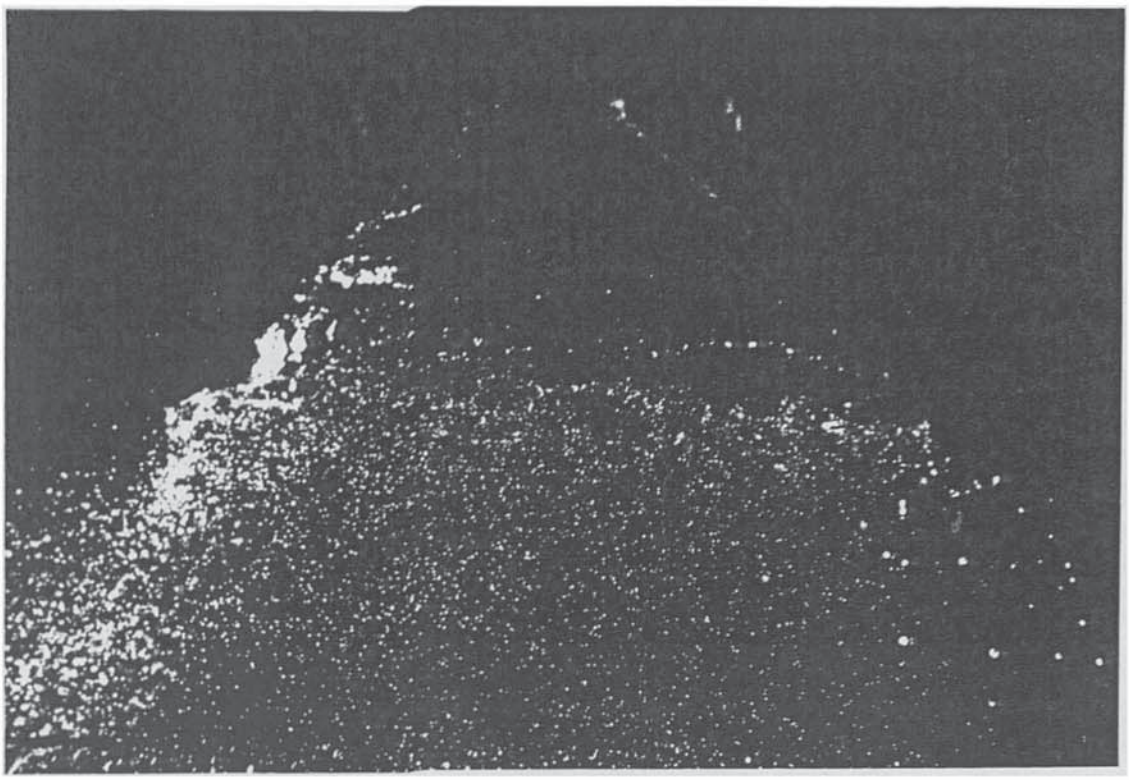

Plate 5.2: *Conical Sheet Produced by Perspex Nozzle P1 at 10 psi*

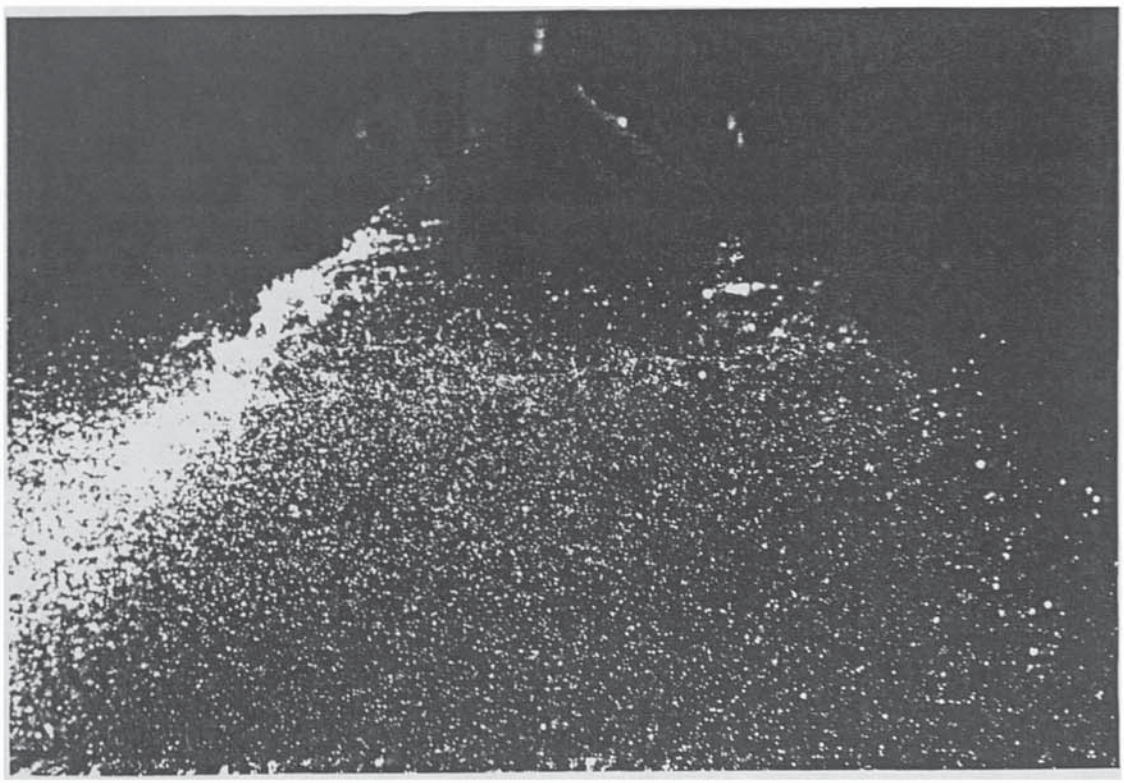

Plate 5.3: *Conical Sheet Produced by Perspex Nozzle P1 at 15 psi*

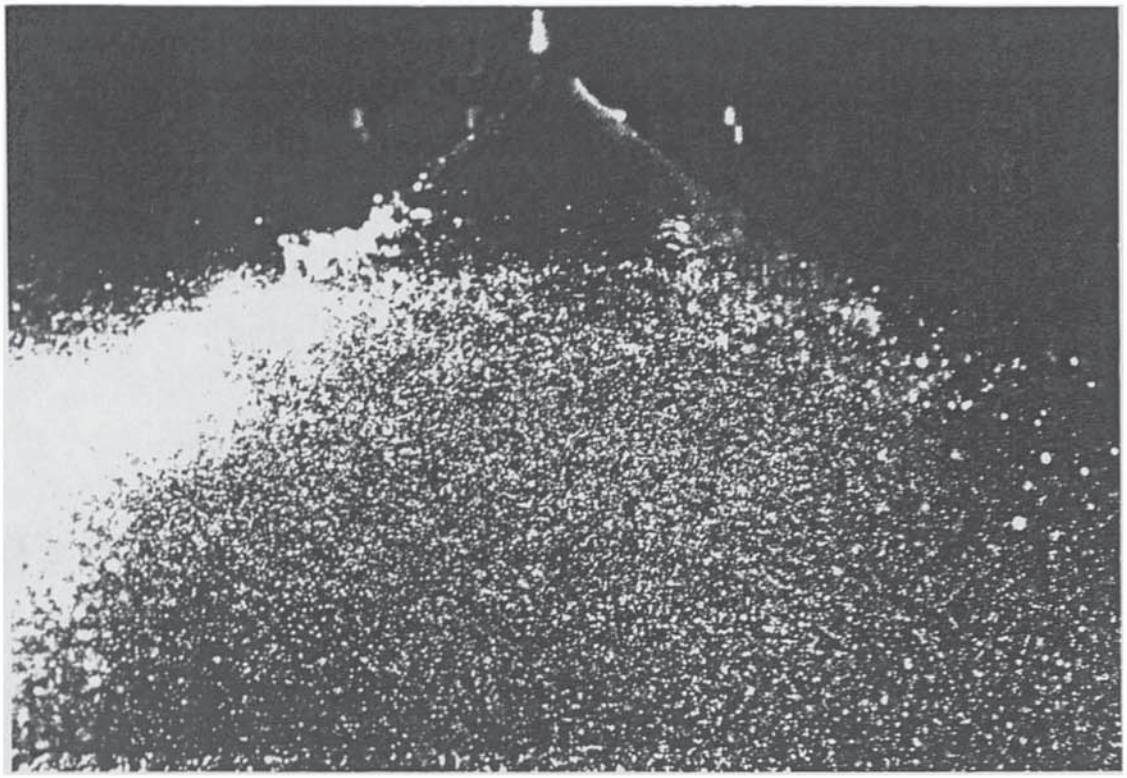

Plate 5.4: *Conical Sheet Produced by Perspex Nozzle P1 at 20 psi*

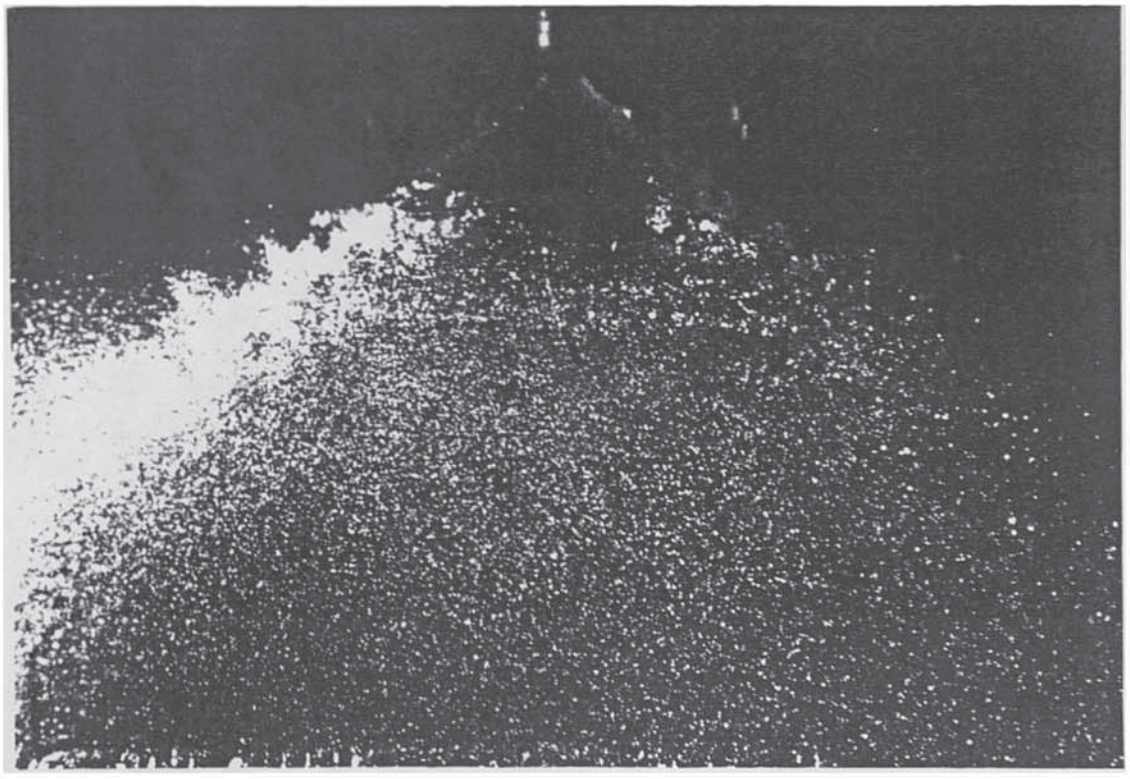

Plate 5.5: *Conical Sheet Produced by Perspex Nozzle P1 at 25 psi*

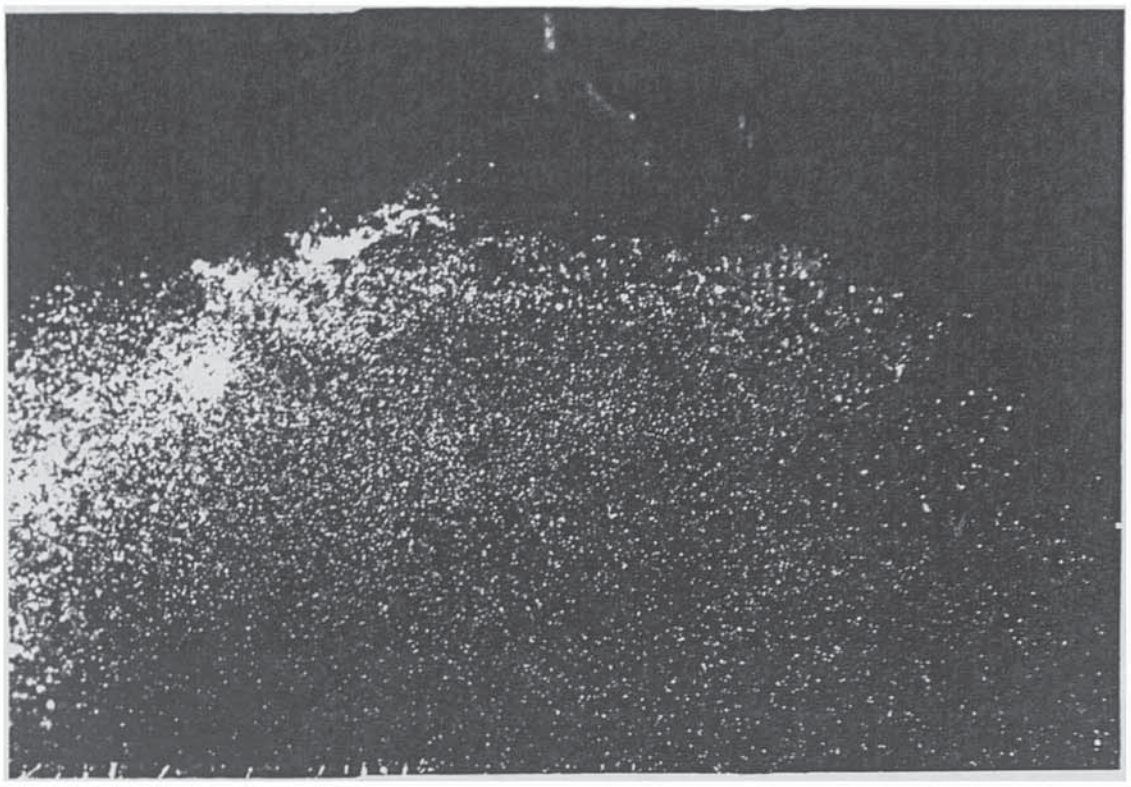

Plate 5.6: *Photographic Scale at 0.6 x Full Size*

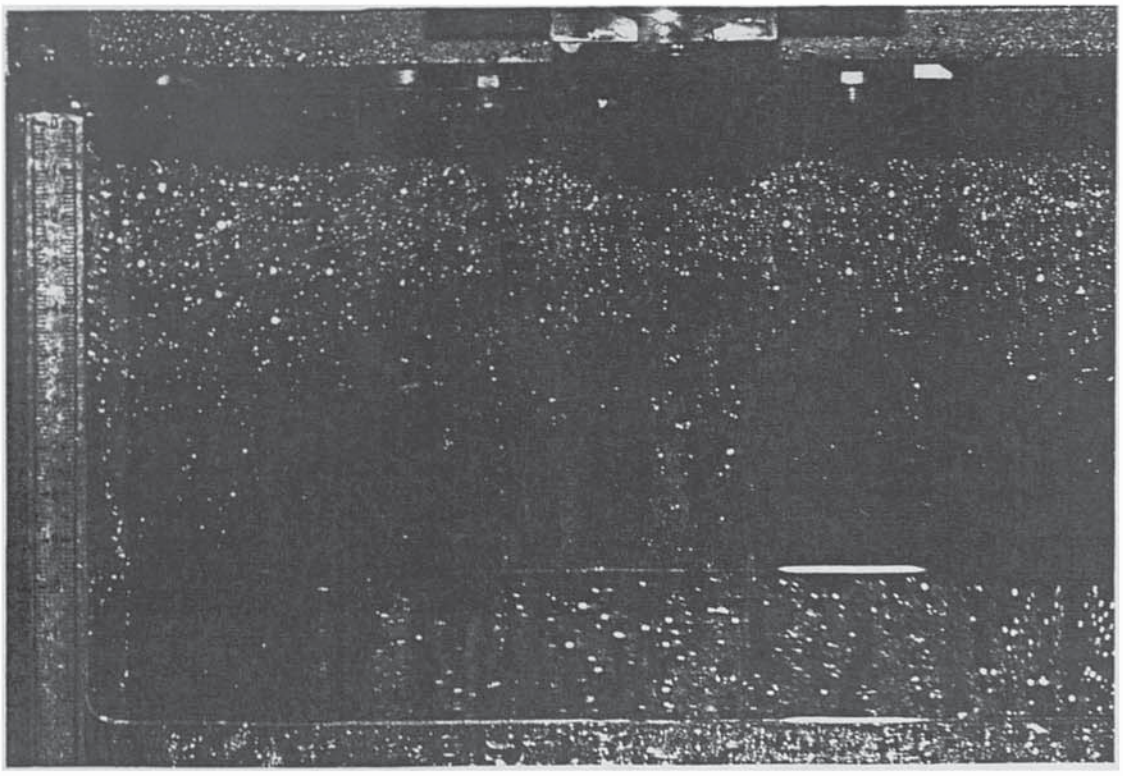

Appendix 6

Typical Double-Flash Photographs of Sheet Disturbances

Plate 6.1: Perspex Nozzle P1 at 5 psi

Plate 6.2: Perspex Nozzle P1 at 10 psi

Plate 6.3: Perspex Nozzle P1 at 15 psi

Plate 6.4: Perspex Nozzle P1 at 20 psi

Plate 6.5: Perspex Nozzle P1 at 25 psi

Plate 6.1: *Liquid Sheet Disturbances from Perspex Nozzle P1 at 5 psi*

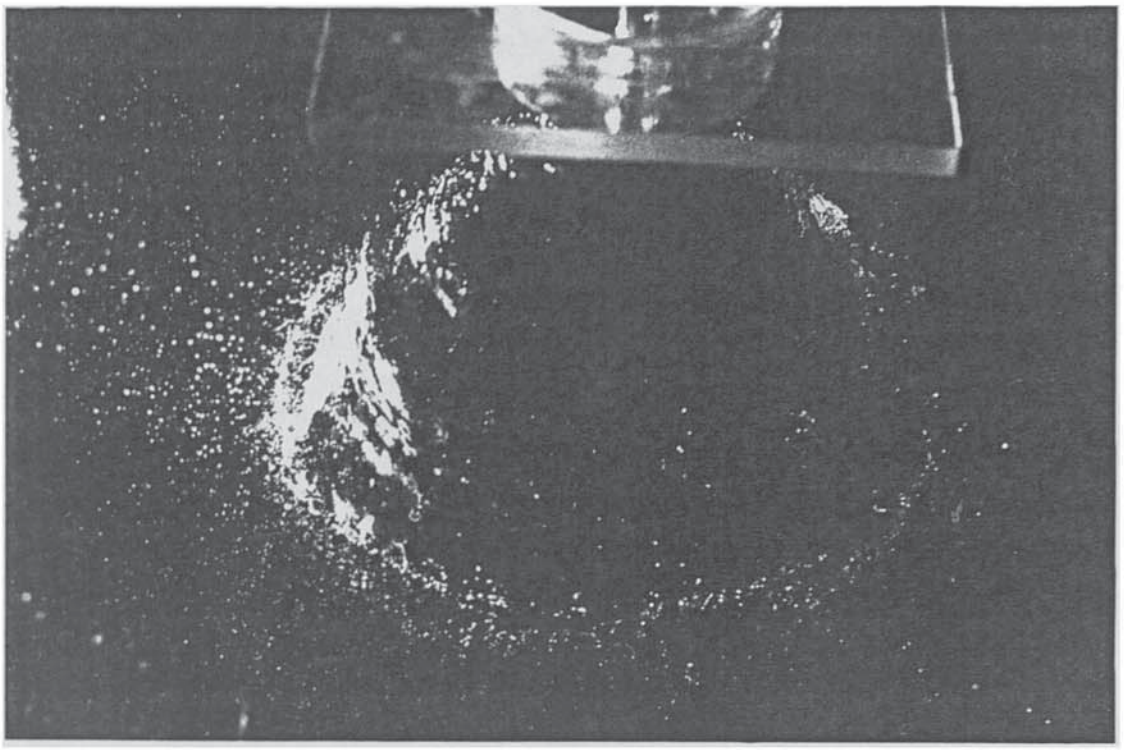

Plate 6.2: *Liquid Sheet Disturbances from Perspex Nozzle P1 at 10 psi*

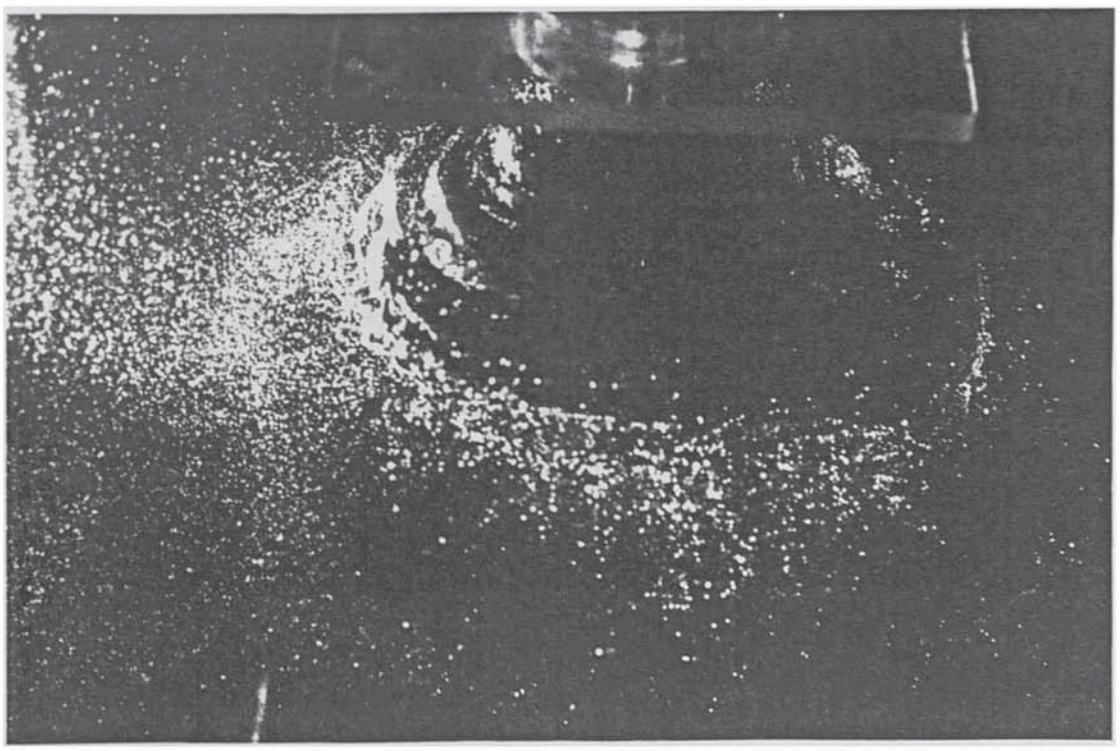

Plate 6.3: *Liquid Sheet Disturbances from Perspex Nozzle P1 at 15 psi*

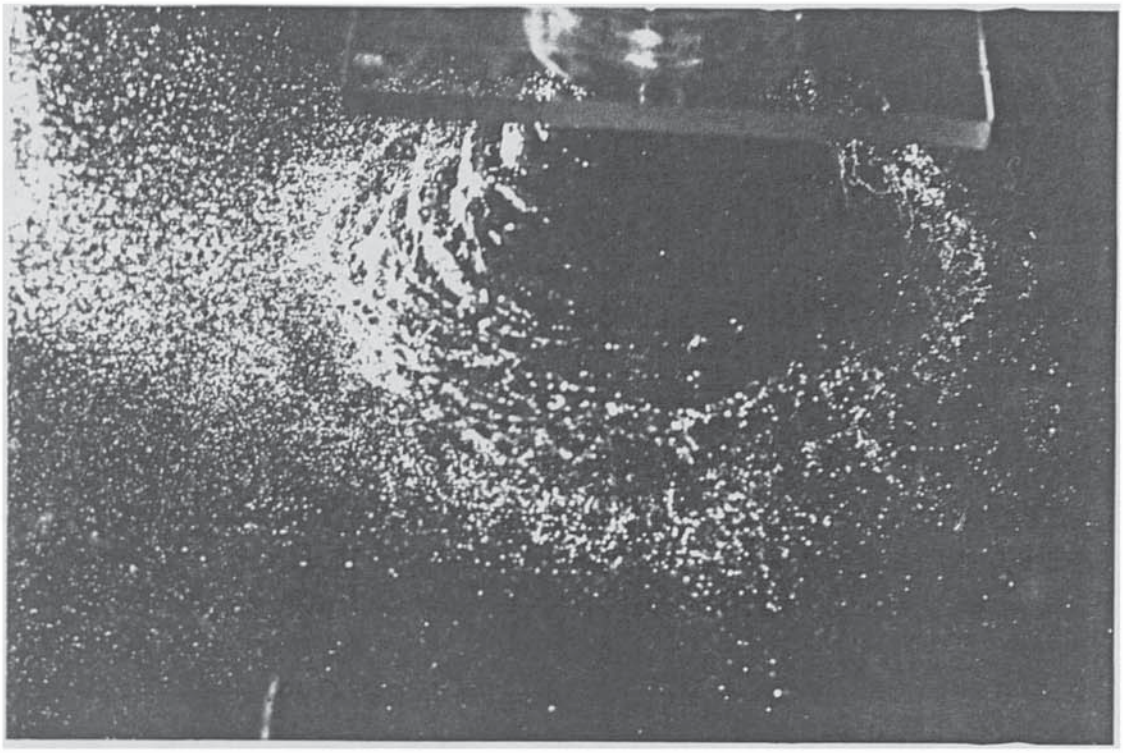

Plate 6.4: *Liquid Sheet Disturbances from Perspex Nozzle P1 at 20 psi*

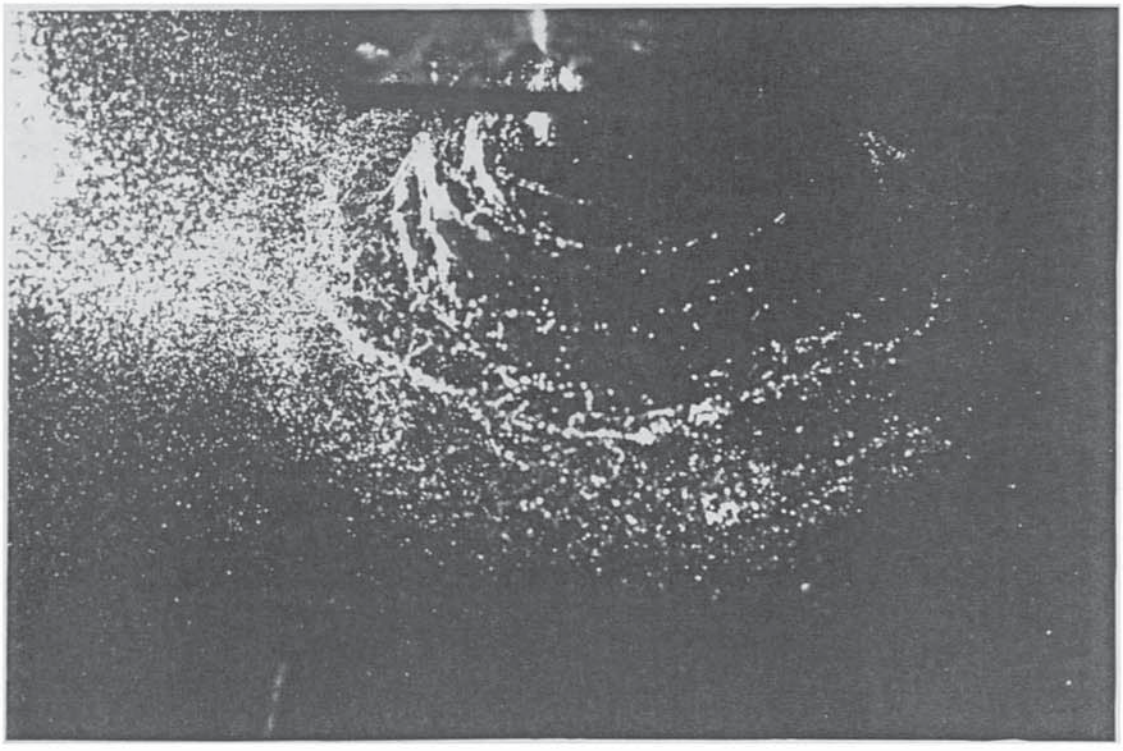

Plate 6.5: *Liquid Sheet Disturbances from Perspex Nozzle P1 at 25 psi*